UNIVERSITY OF NAPLES FEDERICO II

DEPARTMENT OF PHARMACY

SCHOOL OF MEDICINE AND SURGERY

Ph.D. course in
NUTRACEUTICALS, FUNCTIONAL FOODS AND HUMAN HEALTH

Ph.D. Thesis

Identification and development of new nutraceuticals in support to the antiaging approaches

VINCENZO PICCOLO

Ph.D. TUTOR
PROF. VINCENZO SUMMA

Ph.D. COORDINATOR:
PROF. ANGELO A. IZZO

XXXVI CYCLE (2020-2023)

Preface

The Ph.D. thesis is submitted as a requirement for obtaining the Ph.D. Degree in "Nutraceuticals, Functional Foods, and Human Health" at the University of Naples Federico II (Italy). It is written based on three-years research conducted by the author, Vincenzo Piccolo, at the Department of Pharmacy in Naples, under the supervision of Prof. Vincenzo Summa, and for a 5-month secondment period at the I.C.S.N – C.N.R.S. in Gif-Sur-Yvette (Paris), under the supervision of Prof. David Touboul.

Vincenzo Piccolo

Naples, October 2023

INDEX

Abstract 15

1. Introduction 18

1.1. Aging and aging-related diseases 19

1.2. Sarcopenia: definitions and pathogenesis 21

1.3 Skin and skin aging-related diseases 25

1.4 Aging-related diseases: nutraceuticals approach for the prevention 27

1.5 Background and aim of the project 30

2. Unripe tomatoes: features from literature 31

2.1. *Solanum lycopersicum* L.: botanical features 32

2.2 Chemistry of glycoalkaloids 35

2.3 Unripe tomatoes as a source of glycoalkaloids 41

2.3.1. Glycoalkaloids extraction methods 41

2.3.2. Glycoalkaloids analysis methods 44

2.4. Glycoalkaloids beneficial effects on human health 48

2.4.1. Anticancer activity 48

2.4.2. Chemotherapic activity 49

2.4.3. Anti-inflammatory activity 51

2.4.4. Anti-aging activity 53

2.4.5. Neuroprotective activity 53

2.4.6. Cardioprotective and anti-obesity activity 54

2.4.7. α-tomatine and green tomato extract: toxicological aspects 56

3. Phytochemical investigation of unripe tomato cultivars **57**

3.1. Introduction of the project **58**

3.2. Materials and Methods **59**

3.2.1. Reagents **59**

3.2.2. Cultivars selection and extraction **59**

3.2.3. Qualitative glycoalkaloids analysis **60**

3.2.4. Quantitative glycoalkaloids analysis **62**

3.2.5. Qualitative polyphenols analysis **63**

3.2.6. Quantitative polyphenols analysis **65**

3.2.7. Total phenolic content (TPC) **66**

3.2.8. DPPH assay **66**

3.2.9. ABTS assay **67**

3.2.10. FRAP assay **68**

3.2.11. Method validation according to ICH guidelines **68**

3.2.12. Statistical analysis **69**

3.3. Results and discussion **70**

3.3.1. Preparation of the matrix and extraction method **70**

3.3.2. Chemical profile of green tomato extracts **73**

3.3.2.1. Glycoalkaloids profile of green tomatoes **73**

3.3.2.2. Polyphenolic profile of green tomatoes **78**

3.3.3. Development of glycoalkaloids and polyphenols HPLC methods **93**

3.3.3.1. Development of glycoalkaloids HPLC-HESI-MS/MS method **93**

3.3.3.2. Development of polyphenols HPLC-DAD-FLD method **100**

3.3.4. HPLC method validation **103**

3.3.4.1. Method validation according to ICH guidelines 103

3.3.4.2. Validation of glycoalkaloids method 104

3.3.4.3. Validation of polyphenolic method 108

3.3.5. Quantitative analysis of green tomato extracts 110

3.3.5.1. Glycoalkaloids quantitative analysis 110

3.3.5.2. Polyphenols quantitative analysis 112

3.3.5.3. Green tomato extracts metabolomics analysis 113

3.3.6. Green tomatoes: a rich source of antioxidants 118

3.3.6.1. Antioxidant properties of green tomatoes 118

3.3.6.2. Statistical correlation between antioxidant properties and polyphenols content 126

3.4. Summary of cultivar selection 128

4. Datterini green tomatoes efficacy study: nutraceutical effects in sarcopenia prevention 129

4.1. Introduction of the project 130

4.2. Materials and methods 131

4.2.1. Animal experiments 131

4.2.2. Reagents 131

4.2.3. Chow preparation for LGT diet 132

4.2.4. LGT diet extraction 132

4.2.5. LGT diet qualitative analysis by HPLC-HESI-MS/MS 133

4.2.6. α-tomatine quantitative analysis of LGT diet by HPLC-HESI-MS/MS 135

4.2.7. Rutin quantitative analysis of LGT diet by HPLC-HESI-MS/MS 136

4.2.8. Linearity and sensitivity of α-tomatine and rutin HPLC-HESI-MS/MS analysis 138

4.2.9. Precision and accuracy of α-tomatine and rutin extraction 139

4.2.10. Matrix effect and recovery of α-tomatine and rutin extraction 139

4.2.11. Simulated gastro-intestinal digestion protocol 140

4.2.12. Cell lines and culture conditions 141

4.2.13. MTT assay 142

4.2.14. Measurement of mitochondrial activity 142

4.2.15. Measurement of glucose uptake 143

4.2.16. Real time qRT-PCR of myoblast cells 143

4.2.17. Measurement of total protein synthesis 144

4.2.18. NMR data acquisition and processing 145

4.2.19. Treadmill exercise running 145

4.2.20. Real time qRT-PCR of gastrocnemius muscles 146

4.2.21. Histology, MHC, and Pax7 immunostaining 147

4.2.22. GC-MS analysis of myoblast cells 147

4.2.23. Statistical analysis 148

4.3. Results and discussion 149

4.3.1. Design of the experimental study 149

4.3.2. α-tomatine metabolism 151

4.3.3. Preparation of LGT diet 152

4.3.4. Qualitative analysis of LGT diet 153

4.3.5. Development of α-tomatine HPLC-HESI-MS/MS method for LGT diet analysis 154

4.3.6. Development of rutin HPLC-HESI-MS/MS method for LGT diet analysis 156

4.3.7. HPLC-HESI-MS/MS method validation 159

4.3.7.1. Validation of α-tomatine method 159

4.3.7.2. Validation of rutin method 161

4.3.8. Validation and extraction of LGT diet 164

4.3.8.1. Development of LGT diet extraction 164

4.3.8.2. Validation of α-tomatine extraction 164

4.3.8.3. Validation of rutin extraction 166

4.3.8.4. Quality control of LGT diet 168

4.3.9. LGT gastro-intestinal digestion 170

4.3.10. Green tomatoes: a valuable healthy matrix for muscle cells 172

4.3.10.1. Tomatidine activity on muscle cells metabolism 172

4.3.10.2. Tomatidine modifies aminoacidic composition of muscle cells 177

4.3.10.3. Green tomatoes represent a safe product in chronical treatments 183

4.3.10.4. Green tomatoes improve the muscle performance 187

4.4. Summary of green tomatoes efficacy study 198

5. Chemical and microbiological approaches to improve green tomatoes nutraceutical properties 199

5.1. Metabolome of *Solanum lycopersicum* L. plant 201

5.1.1. Metabolomic profile of green tomato fruits 202

5.1.2. Metabolomic profile of green tomato leaves 206

5.1.3. Metabolomic profile of green tomato roots and stem 208

5.2. A PDO tomato variety: Vesuvian Piennolo tomatoes 212

5.3. Biological roles and benefits of *Trichoderma* spp. in agriculture 216

5.3.1. Taxonomic and biological features of *Trichoderma* spp. 216

5.3.2. Current and potential uses of *Trichoderma* spp. in eco-sustainable agriculture **221**

5.4. Chemical hydrolysis of α-tomatine **223**

5.5. Materials and methods **227**

5.5.1. Reagents **227**

5.5.2. Cultivar selection and matrix preparation **227**

5.5.3. Samples extraction **232**

5.5.4. Recovery experiments **232**

5.5.4.1. α-tomatine recovery experiments **232**

5.5.4.2. Tomatidine recovery experiments **233**

5.5.4.3. Polyphenols recovery experiments **233**

5.5.5. Matrix effect experiments **234**

5.5.5.1. α-tomatine matrix effect experiments **234**

5.5.5.2. Tomatidine matrix effect experiments **235**

5.5.5.3. Chlorogenic acid and rutin matrix effect experiments **235**

5.5.6. HPLC-HESI-MS/MS method validation **236**

5.5.6.1. Linearity and sensitivity of the HPLC-HESI-MS/MS method **236**

5.5.6.2. Precision and accuracy of the HPLC-HESI-MS/MS method **236**

5.5.7. HPLC-DAD method validation **237**

5.5.7.1. Linearity and sensitivity of the HPLC-DAD method **237**

5.5.7.2. Precision and accuracy of the HPLC-DAD method **237**

5.5.8. Qualitative glycoalkaloids analysis **238**

5.5.9. Qualitative polyphenols analysis **239**

5.5.10. Quantitative glycoalkaloids analysis **241**

5.5.11. Quantitative polyphenols analysis 242

5.5.12. Total phenolic content (TPC) 243

5.5.13. DPPH assay 244

5.5.14. FRAP assay 245

5.5.15. α-tomatine acid hydrolysis 246

5.5.16. α-tomatine hydrolysis in green tomatoes matrix 246

5.5.17. Statistical analysis 247

5.6. Results and discussion 248

5.6.1. Samples collection 248

5.6.2. Development of glycoalkaloids and polyphenols HPLC methods 249

5.6.2.1. Development of glycoalkaloids HPLC-HESI-MS/MS method 249

5.6.2.2. Development of polyphenols HPLC-DAD method 254

5.6.3. Method validation 255

5.6.3.1. Validation of glycoalkaloids method 255

5.6.3.2. Validation of polyphenols method 260

5.6.4. Validation of the extraction procedure 262

5.6.4.1. Preparation of the matrix and extraction method 262

5.6.4.2. Recovery and matrix effect of glycoalkaloids method 263

5.6.4.3. Recovery and matrix effect of polyphenols method 266

5.6.5. Metabolomics analysis of Piennolo tomato plants 268

5.6.5.1. Qualitative profile of Piennolo tomato plants 268

5.6.5.2. Quantitative profile of Piennolo tomato plants 269

5.6.5.2.1. Comparison of different green tomato cultivars 270

5.6.5.2.2. Evaluation of harvesting time 274

5.6.5.2.3. Evaluation of Trichoderma spp. treatment on green tomato fruits 282

5.6.5.2.4. Evaluation of Trichoderma spp. treatment on roots 288

5.6.5.2.5. Metabolomic comparison between botanical parts 292

5.6.6. Antioxidant activity of Piennolo tomato plant extracts 299

5.6.7. Development of a tomatidine-enriched food matrix: α-tomatine hydrolysis assay 305

5.7. Summary of chemical and microbiological effects on Piennolo tomato plant metabolome 312

6. Development of an innovative oil formulation for the prevention of aging-related skin diseases 314

6.1. Oleolytes: old remedies for modern diseases 315

6.2. Annurca apple as a promising food matrix for nutracosmeceutic applications 317

6.2.1. Triterpenoids: chemistry and botanical distribution 319

6.2.2. Triterpenoids: biological properties 322

6.3. Materials and methods 332

6.3.1. Reagents 332

6.3.2. Annurca apple collection and oleolyte preparation 332

6.3.2.1. Oleolyte preparation and experimental design 332

6.3.2.2. Deacidification procedure of sunflower oil 333

6.3.2.3. Oil samples acidity determination 333

6.3.3. Triterpenoid analysis of Annurca apple oleolytes 334

6.3.3.1. Ursolic acid extraction of oil formulation 334

6.3.3.2. Quantitative analysis of ursolic acid by HPLC-DAD 334

6.3.4. HPLC-DAD method validation for ursolic acid analysis 335

6.3.4.1. Linearity and sensitivity of ursolic acid HPLC-DAD analysis 335

6.3.4.2. Precision and accuracy of ursolic acid HPLC-DAD analysis 336

6.3.5. Matrix effect and recovery of ursolic acid extraction from oil formulation 336

6.3.6. Polyphenols analysis of Annurca apple oleolyte 337

6.3.6.1. Polyphenols extraction of Annurca apple oleolyte 337

6.3.6.2. Quantitative analysis of polyphenols by HPLC-DAD 338

6.3.7. Qualitative analysis of Annurca apple oleolyte 338

6.3.8. Total phenolic content (TPC) 341

6.3.9. DPPH assay 341

6.3.10. ABTS assay 342

6.3.11. FRAP assay 343

6.3.12. Statistical analysis 343

6.4. Results and discussion 344

6.4.1. Experimental design of oleolyte prepartion 344

6.4.2. Optimization and validation of oleolyte extraction 345

6.4.3. HPLC-DAD method validation 347

6.4.3.1. Development of ursolic acid HPLC-DAD method 347

6.4.3.2. Validation of ursolic acid method 347

6.4.4. Ursolic acid quantification in oil formulations 351

6.4.5. Polyphenols quantification in oil formulations 355

6.4.6. Qualitative analysis of oil formulations 357

6.4.7. Antioxidant properties of Annurca apple oleolytes 361

6.5. Summary of Annurca apple oleolytes formulation 363

7. Annurca apple oleolytes efficacy study for nutracosmeceutic applications **364**

7.1. Introduction of the project **365**

7.2. Materials and methods **366**

7.2.1. Reagents **366**

7.2.2. Franz's cell diffusion system **366**

7.2.3. Ursolic acid quantitative analysis in Franz's cell diffusion system **367**

7.2.4. Tyrosinase inhibition assay **369**

7.2.5. HPLC-FLD assisted tyrosinase assay **370**

7.2.6. HPLC-FLD method validation **371**

7.2.6.1. Linearity and sensitivity of L-tyrosine HPLC-FLD method **371**

7.2.6.2. Precision and accuracy of L-tyrosine HPLC-FLD method **372**

7.2.7. Ultrafiltration assisted tyrosinase assay **372**

7.2.8. Elastase inhibition assay **373**

7.2.9. Cell culture **374**

7.2.10. MTT assay **374**

7.2.11. Measurement of melanin content **374**

7.2.12. RNA extraction and real time qPCR analysis **375**

7.2.13. Flow cytometry analysis **375**

7.2.14. Preparation of a cosmetical OAAO cream for topical formulation **376**

7.2.15. Study design and partecipants selection **376**

7.2.16. Randomization and masking **378**

7.2.17. Skin tolerability test **379**

7.2.18. Statistical analysis **379**

7.3. Results and discussion **381**

7.3.1. Melanogenesis inhibition properties of Annurca apple oleolytes **381**

7.3.1.1. Validation of the spectrophotometric tyrosinase inhibition assay **383**

7.3.1.2. Development and validation of the HPLC-FLD assisted tyrosinase assay **386**

7.3.1.3. HPLC-FLD assisted tyrosinase assay: analysis of real samples **388**

7.3.1.4. Ultrafiltration assisted tyrosinase assay **391**

7.3.1.5. Annurca apple oleolytes activity on melanogenesis **392**

7.3.1.6. Antioxidant properties of Annurca apple oleolytes on human melanoma cells **396**

7.3.2. Ursolic acid skin permeation **398**

7.3.3. Elastase inhibition properties of Annurca apple oleolytes **401**

7.3.3.1. Validation of the spectrophotometric elastase inhibition assay **401**

7.3.3.2. Elastase inhibition assay: analysis of the real samples **403**

7.3.4. Efficacy study of OAAO cream for topical applications **405**

7.3.4.1. Study design and skin tolerability test **405**

7.3.4.2. Skin visco-elasticity test **406**

7.3.4.3. Skin hydration and film repairing activity **407**

7.3.4.4. Evaluation of wrinkles and fine lines **409**

7.4. Summary of Annurca apple oleolytes efficacy study **411**

8. General conclusion **412**

9. External project contributions **415**

Supplementary Materials **419**

Abbreviation and acronyms **456**

List of publications **464**

Bibliography **467**

ABSTRACT

Aging is the progressive loss of body function over time, with a gradual decline of physical function of the organism. Recognizing aging as a significant risk factor for chronic diseases becomes crucial for the identification of new targets and the development of future therapeutic approaches. The aging process is associated with an increased susceptibility to some diseases, like Parkinson's and Alzheimer's diseases, metabolic syndrome, sarcopenia, and some skin diseases. The emerging role of the aging-related diseases represents a challenging for the national health system. Despite extensive studies on the pathophysiological mechanisms of aging, effective treatments remain ineffective. Today, the most effective approach is the prevention, mainly with dietary modifications and the physical exercise. Nutraceuticals could represent a valid strategy in aging-related diseases prevention for the health benefits related to the natural compounds of the food matrix. In this context, this thesis work is focused on the development of new nutraceutical formulations for the prevention of sarcopenia and the skin aging-relating diseases.

In order to develop an innovative nutraceutical product for sarcopenia prevention, our resarch was focused on the identification of natural compounds active on the targets involved in muscle atrophy. These include the mammalian target of rapamycin complex 1 (mTORC1) and the Activating transcription factor 4 (ATF4). These mediators are modulated by tomatidine (TD), a natural alkaloid isolated from *Solanum lycopersicum* L. plant which represents the aglycone component of the glycoalkaloid α-tomatine (α-TM). Therefore, according to the aims of the doctoral project, I focused on the study of anti-sarcopenic properties of green tomatoes.

In Chapter 3, the screening of 7 green tomato cultivars was performed to identify the food matrix with the higher α-TM content. The chemical composition and the evaluation of the antioxidant properties were assessed to evaluate the nutraceutical potential of the matrix. The matrix selection allowed to identify the “Datterini” tomatoes as the most promising tomato cultivar for further biological investigation. After that, in Chapter 4 the evaluation of the anti-sarcopenic properties of TD and the “Datterini” tomatoes was assessed. These results demonstrated the potential of this food matrix for the development of new nutraceutical for sarcopenia prevention.

For the relevance of the tomato production in the Italian economy, and in particular in the Campania region (Southern Italy), an agronomic study was carried out and described in Chapter 5, investigating the chemical composition of a regional tomato variety called “Piennolo”. Agronomic parameters (e.g., harvest time), botanical parameters (e.g.,

anatomical part of tomato plant), and microbiological parameters (e.g., the treatment with beneficial microorganisms as *Trichoderma* spp.) were taken into account in this study. The research represented the most extensive metabolomic characterization of "Piennolo" tomato plant, providing interesting information on the *Trichoderma* spp. effects to influence metabolite production in tomato plant. In addition, a new food-grade approach to chemically convert α-TM to TD was investigated in Chapter 5, obtaining a new food matrix with a high TD content that could be employed for the development of an innovative nutraceutical for sarcopenia prevention.

As second line of my thesis work, the development of an innovative cosmeceutical formulation for the prevention and the treatment of some skin aging-related diseases, as age spots, fine wrinkles, and hyperpigmentation, was performed. For this goal, we focused on ursolic acid, another natural compound of nutraceutical interest. Although this compound is present in several food matrices, the study was carried out using the apples of "Annurca" variety, typical of the Campania region in Southern Italy. In addition, to develop an ursolic acid enriched formulation for topical and cosmeceutical application, ursolic acid was delivered by the preparation of an oleolyte, an oil formulation obtained by maceration of the plant matrix in oil.

In Chapter 6, an oleolyte obtained by the "Annurca" apples was developed and optimized using sunflower seed oil as oil vehicle. The oleolyte was chemically characterized for the evaluation of the qualitative and quantitative profile and the assessment of the antioxidant properties. After that, the skin-lighting properties of "Annurca" apple oleolyte and ursolic acid were evaluated in the Chapter 7. These results demonstrated the potential of this oleolyte for the development of new cosmeceutical formulations for the skin aging-related diseases prevention and treatment.

Although my research work was focused on the development of new potential treatments for the prevention of aging-related diseases, during my Ph.D. thesis I work to other projects for the chemical analysis of other food matrices with a nutraceutical interest. In Chapter 8, I summarized the extraction contributions to other projects.

CHAPTER 1

INTRODUCTION

1. Introduction

1.1. Aging and aging-related diseases

Aging is a universal biological process characterized by a gradual and irreversible decline of physical function across all organ systems. This decline is attributed to the accumulation of damages resulting from various stress factor. Aging process plasticity plays a critical role in promoting longevity. Approximately three decades ago, researchers isolated the first long-lived strain in *C. elegans*, marking a milestone in aging (J. Guo et al., 2022). For many years, biologists have speculated about an intricate connection between aging and numerous chronic human disorders. Aging significantly increases the susceptibility to common diseases, such as Parkinson's disease, Alzheimer's disease, cardiovascular conditions, diabetes, chronic obstructive pulmonary disorders, osteoarthritis, osteoporosis, sarcopenia, and some skin diseases (J. Guo et al., 2022). Furthermore, comorbidities become more prevalent in the elderly, particularly after the age of 60 years, necessitating a combination of therapies for long-term therapeutic benefits. Additionally, it's worth noting that various therapeutic options for age-related diseases may interact generating some side-effects (Bettonte et al., 2022). Given that aging ranks among the foremost risk factors for most chronic diseases, the comprehension of aging process promises to uncover potential therapeutic targets and the development of future-approved pharmacological agents and prevention approaches. Cellular senescence, a central player in maintaining normal tissue homeostasis and contributing to pathological conditions, represent the main cause of the aging process and the onset of aging-related diseases. Cellular senescence manifests as a gradual reduction in cell proliferation, differentiation, and physiological functionality over time. In 1956, Denham Harman proposed the free radical theory of aging, suggesting that age-related degeneration stems from the harmful effects of free radicals generated by the physiological cellular metabolism (Harman, n.d.). In 1961, in continuous human diploid cell culture, the lifespan of fibroblasts was found to be limited (Hayflick & Moorhead, 1961). Since then, many molecular mechanisms governing aging have been unveiled, including genomic instability, mitochondrial dysfunction, telomere dysfunction, stem cell depletion, cellular senescence, nutrient sensing deregulation, epigenetic modifications, proteostasis loss, autophagy dysregulation, and intercellular communication (J. Guo et al., 2022). A timeline of the main outbreaks in the study of aging and aging-related diseases processes is reported in the **Figure 1** (J. Guo et al., 2022).

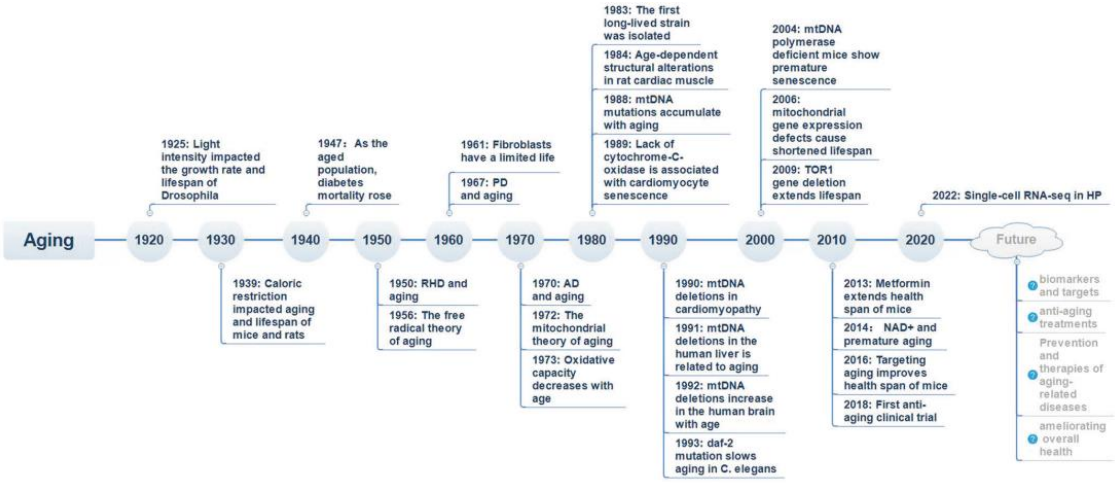


Figure 1. Research timeline on aging and aging related diseases. RHD: rheumatic heart disease; PD: Parkinson's disease; AD: Alzheimer's disease; mtDNA: mitochondrial DNA; NAD^+: Nicotinamide adenine dinucleotide; HP: heterochronic parabiosis. Picture adapted by (J. Guo et al., 2022).

The aging process results from intricate pathways, with many of these pathways closely linked to chronic oxidative stress arising from elevated reactive oxygen species (ROS) (Mossad et al., 2022). Aging itself is influenced by a complex interplay of physical, environmental, and social factors, rendering the elucidation of molecular aging triggers a formidable effort. Human lifespan correlates with diminishing tissue and organ repair and regenerative capabilities. Genetic, epigenetic, and environmental factors contribute to a dwindling organismal physiological reserve in response to stress though different molecular mechanisms that collectively promote aging and the aging-related diseases. Several mechanisms, such as telomere shortening, DNA damage accumulation, metabolic alterations, and excessive ROS production, intricately connect various factors with the pace of aging. These mechanisms hinder cell proliferation, alter metabolic pathways and gene expression profiles, and foster heightened ROS production, maintaining the phenotype in the state of cellular senescent (J. Guo et al., 2022). Among the alternations associated with the aging, autophagy dysregulations represent a key factor. Autophagy is a process highly conserved in mammalian species and degrades the cellular components in lysosomes, including misfolded proteins and defective organelles (Aman et al., 2021). One of the key factors for the activation of autophagy process is represented by the mammalian target of rapamycin (mTOR). The autophagic process decreases with the age in different tissues,

exacerbating cellular damages and promoting the development of the aging-related diseases. Since aging process and the aging-related diseases represent a complex and system involving different pathological states, our attention in this Ph.D. thesis was focused on the study of two aging-related diseases, the sarcopenia and the skin aging-related pathologies.

1.2. Sarcopenia: definitions and pathogenesis

The term "sarcopenia" was used for the first time in the 1988 and was introduced to describe the loss of muscle tissue in the elderly (Rosenberg, n.d.). Despite its significance, sarcopenia remains unfamiliar to many clinicians and researchers. Recognizing and addressing sarcopenia has gained importance due to research findings linking low muscle mass to functional and cognitive impairments (Baumgartner et al., 1998; Janssen et al., 2002). The loss of motor mobility is associated with an increment of adverse outcomes, which include functional decline, falls, frailty, and mortality. Studies indicate an annual muscle mass decline of 1-2% after the age of 50 (Buford et al., 2010), resulting in a 50% reduction in muscle mass among those aged 80 and older (Baumgartner et al., 1998). Over representing a public health problem, sarcopenia is a challenging for the national health system. For example, it's estimated that reducing sarcopenia prevalence by 10.5% could lead to a $1.1 billion reduction in healthcare costs annually in the United States (Janssen et al., 2004). However, the prevalence and impact of sarcopenia depend significantly on its definition. A clear and accurate definition is essential for clinical diagnosis and tailored treatment. Over time, the term "sarcopenia" has been used interchangeably to describe both low muscle mass and low muscle strength and physical performance. However, loss of muscle mass alone cannot fully explain the loss of muscle strength (Goodpaster et al., 2006). While some propose defining sarcopenia as the presence of low muscle mass combined with low muscle strength or function (Fielding et al., 2011), other authors used the term "sarcopenia" for low muscle mass and introducing a separate term, "dynapenia," for low muscle strength (Clark & Manini, 2008). The prevalence of sarcopenia in elderly populations varies significantly, primarily due to differences in diagnostic criteria for sarcopenia, leading to challenges in comparing different cohorts and individual patients. In 1988, Rosenberg coined the term "sarcopenia," which literally translates from Greek to "deficiency of muscle mass" (milestone 1: coining of a term, Fig. 1) (Rosenberg, n.d.). Since its introduction, the medical community's attention to sarcopenia has grown. Although the techniques to measure muscle

mass were available at the time the term was coined, there was initially little application, as the clinical consequences were unknown. Baumgartner et al. (1998) proposed a formula for the diagnosis of sarcopenia as the appendicular lean mass divided by height squared, with values more than two standard deviations below the mean of a young reference population classified as sarcopenia. The introduction of diagnostic criteria contributed to understanding the implications of low muscle mass. There is growing evidence linking muscle mass to self-reported physical disability and functional impairment (Baumgartner et al., 1998; Delmonico et al., 2007; Janssen et al., 2004). Sarcopenia has also been defined by muscle strength, including knee extension isometric torque, handgrip strength, lower extremity muscle power, or physical performance, such as gait speed (Lauretani et al., 2003). Some have proposed defining sarcopenia by combining muscle mass with muscle strength or function, such as low muscle mass coupled with low gait speed (Cruz-Jentoft et al., 2010; Fielding et al., 2011; Muscaritoli et al., 2010). However, one of the most recent and internationally recognized criteria for sarcopenia diagnosis are given by the European Working Group on Sarcopenia in Older People (EWGSOP) in January, 2019 (Cruz-Jentoft et al., 2010). In clinical practice, a person with low muscle strength and low muscle mass or quality can be diagnosed with sarcopenia.

Currently, the cellular mechanisms involved in the development of sarcopenia have been poorly elucidated in literature. This pathology is mainly due to processes of altered protein turnover and mitochondrial function and inflammatory, oxidative, and hormonal processes (Damiano et al., 2019; Liguori et al., 2018). Furthermore, muscle atrophy is related to various pathophysiological processes, such as malnutrition, ageing, physical inactivity (Moro et al., 2016) and metabolic syndrome (Rubio-Ruiz et al., 2019). Two important mediators involved in the regulation of protein turnover are mammalian target of rapamycin complex 1 (mTORC1) (Liguori et al., 2018) and activating transcription factor 4 (ATF4) (Adams et al., 2017). The mTORC1 complex is a second messenger of the IR-IP3K-Akt-mTORC1 anabolic signal transduction pathway and his activation leads to an increase in protein synthesis resulting in an increasing of muscle mass. Indeed, the Akt factor (called also “protein kinase B” PKB) is a kinase capable of phosphorylating and inactivating the transcription factor FOXO1 (“Forkhead box protein O1”), which is necessary for the transcription of a group of genes known as “atrogens”. The main genes belonging to this class are the E3 ubiquitin-ligase atrogin-1 (MAFbx), the muscle RING-finger protein-1 (MuRF-1) (Liguori et al., 2018), and the Gadd45a factor (“Growth Arrest and DNA Damage 45-α”) (Adams et al., 2017). In fact, these factors are actively involved in muscle atrophy

processes and represent the main components of the ubiquitin-proteasome system (Perry et al., 2016). In contrast, the mTORC1 complex is a kinase that promotes the phosphorylation of several factors that stimulate protein synthesis by activating S6 kinase 1 (S6K1) and inhibiting 4E binding protein 1 (4EBP1) (Yoon, 2017). S6K1 is a kinase able to phosphorylate and activate the ribosomal protein S6, while 4EBP1 is a translational repressor that promotes inhibition of ribosomal activity (Schiaffino & Mammucari, 2011). ATF4 is a transcriptional factor that stimulates the transcription of several genes that inhibit protein synthesis, such as Gadd45a. This factor interacts with the MAP kinase MEKK4, forming a multi-protein complex actively involved in muscle atrophy processes (Adams et al., 2017). The balance of mTORC1 and ATF4 factor activity controls protein turnover, thus determining the processes of atrophy or hypertrophy. The control role of mTORC1 and ATF4 in muscle atrophy processes is summarized in **Figure 2** (Adams et al., 2017).

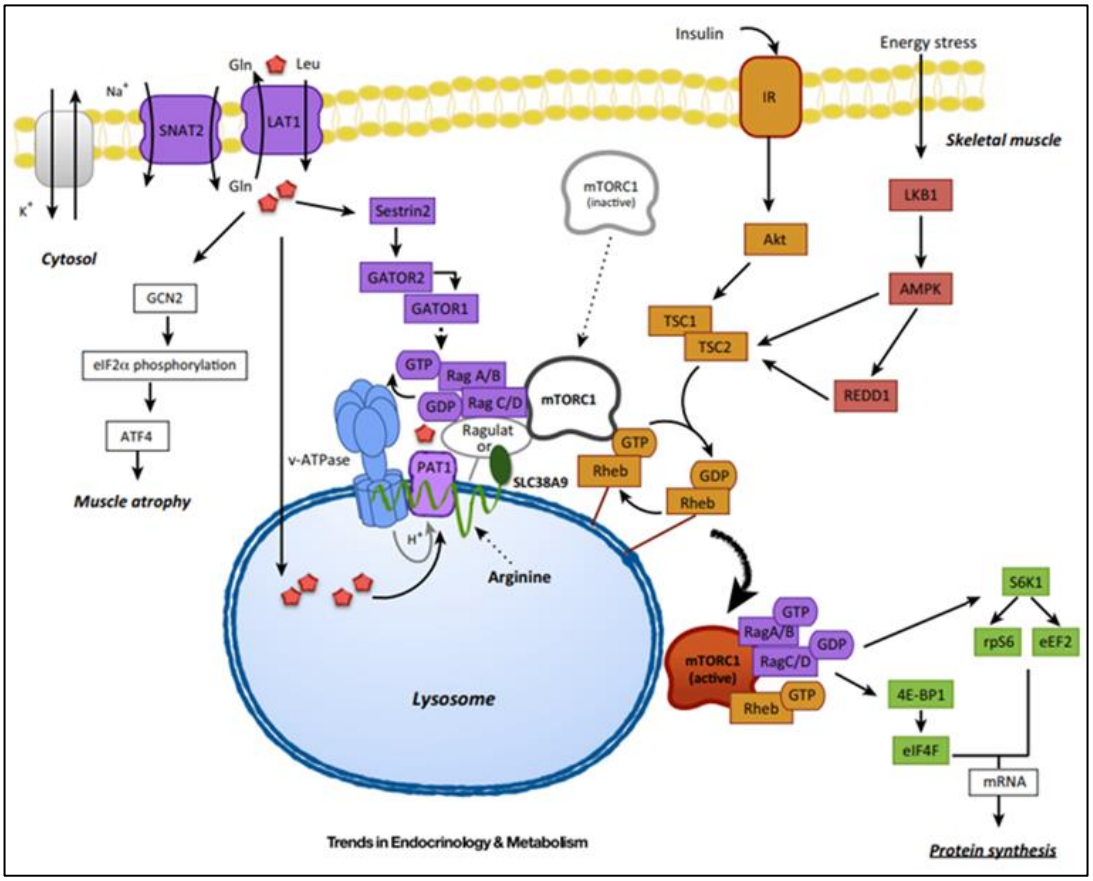


Figure 2. Summary of mTORC1 and ATF4 activities in the control of protein muscular turnover (Adams et al., 2017).

In addition to protein metabolism dysregulation, sarcopenia has an important inflammatory and oxidative component. Indeed, in chronic inflammatory diseases there is an increase of proinflammatory cytokines plasma levels, such as tumour necrosis factor-alpha (TNF-α), interleukin-1 (IL-1) and interleukin-6 (IL-6) (Scalabrin et al., 2020). For example, TNF-α results in the activation of the NF-κB factor, a transcriptional factor which stimulates the transcription of certain genes that code for both inflammatory factors leading to muscle inflammation, such as inducible nitric oxide synthase (iNOS) and cyclooxygenase-2 (COX2), and for factors involved in the ubiquitin-proteasome system, such as the MuRF-1 factor (Chiu & Lin, 2008; Scalabrin et al., 2020). Sarcopenia differs from other forms of muscular atrophy by an increase of oxidative stress, generally due to decreased levels of endogenous antioxidants, with production of ROS and Reactive nitrogen species (RNS) at both systemic and muscular levels. Reactive species (RONS) represent one of the predominant causes of age-related forms of sarcopenia, in which there is a marked dysfunction of mitochondrial function and energy metabolism (Gomes et al., 2017). However, recent studies have indicated that mitochondria play a secondary function in muscle oxidative stress and that the production of ROS is mainly due to enzymes of the NADPH oxidase class (NOXs), particularly the Nox2 isoform (Damiano et al., 2019; Hord & Lawler, 2017). RONS react directly with proteins, usually through oxidation or carbonylation reactions, modifying their activity and reducing their half-life due to their increased susceptibility to the action of cellular proteases (Brioche & Lemoine-Morel, 2016). In particular, the oxidation of cysteine residues of the Akt factor interferes with the Akt-mTORC1 anabolic pathway (Damiano et al., 2019), directly inhibiting protein synthesis and resulting in the activation of FOXO1, MAFbx and MuRF-1 factors, which lead to muscle atrophy processes (Hord & Lawler, 2017). In addition, RONS activate cellular proteases such as caspases, promotes autophagy processes, and stimulate NF-κB factor activity, correlating oxidative processes with inflammatory processes (Gomes et al., 2017; Rubio-Ruiz et al., 2019).

1.3. Skin and skin aging-related diseases

The skin is body's largest organ and serves multiple vital functions. It acts as a protective shield against mechanical and chemical threats, hosts innate and adaptive immune defenses, facilitates thermoregulation and the production of vitamin D, and represents our sensory touch organ (Chuong et al., 2002). Similar to other complex biological systems, the skin undergoes growth, maturation, and aging processes. Skin aging involves a decline in functional capacity, increasing vulnerability to cutaneous issues, dermatoses, and skin cancers. Beyond changes in its structure and function, skin aging is also evident in its appearance, serving as a visible marker of the overall aging process. Skin aging comprises two interconnected processes: intrinsic aging, which is a time-dependent phenomenon resulting in specific age-related changes to the skin's appearance and function, and extrinsic aging, driven by environmental factors. Lifestyle choices significantly impact skin appearance and function, with chronic sun exposure (ultraviolet radiation [UVR]) recognized as a major environmental factor influencing skin biology. Emerging evidence also suggests that factors like smoking, hormonal status, and environmental pollution contribute to skin aging (Bolognia et al., n.d.; Brincat et al., 1983; Daniell, 1971; Emmerson & Hardman, 2012; Kadunce et al., 1991; Krutmann et al., 2014; Martires et al., 2009). Both intrinsic and extrinsic aging ultimately lead to a decline in skin's physiological function, with extrinsic aging often accelerating intrinsic aging processes. Clinically, intrinsic aging signs typically appear after the age of 70 years, manifesting as dry skin with fine wrinkles. In contrast, areas exposed to chronic UV radiation display a different clinical appearance, featuring roughened, sallow skin with hypopigmented and hyperpigmented lesions, called age spots, and pronounced wrinkles, particularly in dynamic facial expression regions like "crow's feet." Nevertheless, it's important to note that the effects of aging are inevitable to varying degrees for all individuals. Skin comprises two primary, functionally distinct layers: the outer epidermis and the inner dermis (Blume-Peytavi et al., 2016). The epidermis, rich in cells and devoid of blood vessels, primarily consists of keratinocytes and acts as a physical barrier, preventing water loss and protecting against infections. The dermis, comparatively cell-poor, primarily consists of an extracellular matrix (ECM) that provides the skin with strength and resilience while housing vascular, lymphatic, and neural systems. The dermal-epidermal junction (DEJ) between these layers plays a crucial role in intercellular communication and cohesion. With age, all skin layers undergo structural and functional changes. The aging epidermis becomes atrophic with diminished rete pegs and ridges,

resulting in reduced barrier function and diminished repair capacity following injuries (Choi et al., 2007). Age-related lipid processing decline affects the production of ceramides vital for epidermal barrier function (J-m et al., n.d.). Epidermal CD44, a transmembrane glycoprotein affecting keratinocyte proliferation and hyaluronic acid regulation, decreases with age (Kaya et al., 2006; Kaya & Saurat, 2007), contributing to epidermal thinning and decreased viscoelasticity. Another parameter strictly connected to the aging is represented by the transepidermal water loss (TEWL). This factor is reduced with the age due to the reduction of the water content in the aged skin and a loss of skin perspiration capacity (Harvell & Maibach, 1994).

The appearance of aging skin has significant psychological and social implications, impacting self-esteem and interactions. Perceptions of aging are influenced by cultural and ethnic factors, although wrinkled and mottled skin is generally not socially preferred anywhere. Pigmentary irregularities, particularly in individuals with darker skin, can be a significant source of psychological concern (Verma, 2011)

In summary, aging affects the skin both intrinsically and extrinsically, leading to changes in appearance and function. These changes can have profound effects on an individual's self-esteem and social interactions. It's important to distinguish between physiological aging and pathological conditions, recognizing that cosmetic and cosmeceutical products are aimed at enhancing life quality rather than saving lives.

1.4. Aging-related diseases: nutraceuticals approach for the prevention

The pathophysiological basis of aging has been much studied in recent years. However, despite the efforts of the scientific community, there are not available effective treatments for the prevention and treatment of aging. The most studied approaches to prevent the aging related diseases include dietary modifications, exercise and calorie restriction. In addition, innovative therapeutic approaches as the stem cell transplantation, the senescent cell removal open and promise a new avenue for the treatment of aging and the aging-related diseases. Nowadays, a valid approach in the prevention of the aging is represented by the dietary supplementation and the use of nutraceutical products. Nutraceuticals are products derived from food matrices sources which offer additional health benefits beyond the basic nutritional value found in food. Depending on the regulations in a particular region, these products may make claims related to the prevention of chronic diseases, enhancement of overall health, slowing down the aging process, extending lifespan, or supporting the body's structure and functions. Many definitions are currently used to explain the word "nutraceuticals", whose meaning depends on the institution, the country, the commercial companies and the consumers. The first definition of nutraceuticals was obtained with the union of the words "nutrition" and "pharmaceutical" by De Felice in 1989, for which "a nutraceutical is any substance that is a food or a part of a food and provides medical or health benefits, including the prevention and treatment of disease. Such products may range from isolated nutrients, dietary supplements and specific diets, to genetically engineered designer foods, herbal products, and processed foods such as cereals, soups and beverages" (Santini & Novellino, 2013). This definition includes dietay not-nutrient compounds and clarify the direct link between nutraceuticals and foods. The definition was suddenly modified by the Health Canada Minister, for which "a nutraceutical is a product isolated or purified from foods, and generally sold in medicinal forms not usually associated with food and demonstrated to have a physiological benefit or provide protection against chronic disease". Therefore, this new definition clarifies the difference between nutraceuticals and foods. Another interesting definition is given by the European Food Safety Authority (EFSA), which commonly uses the definition of food supplement in relation to concentrated nutrients sources or other matrices with physiological and nutritional effects that can supplement the normal diet. This definition includes both nutraceuticals and botanicals (i.e., Ginkgo, Ginseng, St. John's Wort), which are not-food products from plant origin

commonly marked as nutraceuticals (González-Sarrías et al., 2013). As matter of fact, the European Commission approved a list of the foods and the plant matrices approved for the development of functional foods and nutraceuticals products. This list is generally called BELFRIT since it has been developed by Belgium, France, and Italy, representing the first tentative to arrive at a common discipline on the use of plants and derivatives in food supplement field and to promote a harmonization of this discipline in Europe.

Nutraceuticals are characterised by active compounds administered through specific pharmaceutical forms that can guarantee a beneficial action in the prevention and/or treatment of a given pathology. The contrast between nutraceuticals and drugs is not only limited to the characteristics of the active ingredient but is linked to a different way of conceiving clinical practice. In fact, drugs are part of the general framework of "watchful medicine", a classical approach focused on the symptomatic treatment of an ongoing pathology. Nutraceuticals, on the other hand, fall within the scope of "Initiative Medicine", a dynamic approach focused on preventing the disease state before the development of symptoms, acting mainly in pre-pathological states (Santini & Novellino, 2013). The clinical use of nutraceuticals is described by two main, closely related endpoints, health promotion and disease prevention. Health promotion represents the ability of the nutraceutical to ensure a beneficial effect on individual's health, regardless of the risk of developing a certain pre-pathological or pathological state. An example is represented by nutraceuticals able to improve muscle performance, with potential in muscle supplementation and sports medicine. Instead, disease prevention represents the ability of nutraceuticals to prevent and reduce the complications of a given disease state by restoring normal homeostasis and improving the body's functionality (Dutta et al., 2018). The main field of application of nutraceuticals is the prevention of chronic multifactorial diseases, such as type 2 diabetes mellitus (T2DM), cardiovascular diseases and inflammatory-based diseases, and related risk factors, such as obesity, hypertension and hyperglycaemia (Bergamin et al., 2019). Multifactorality makes pharmacological intervention with a single drug unsuccessful, requiring the combined administration of several drugs. Moreover, the dysregulation of the different metabolic pathways involved means that these diseases can be controlled but not effectively treated. From a clinical point of view, nutraceuticals have clear similarities with combination therapy, a polypharmacological approach involving the administration of several different drugs to treat a certain pathology. In fact, nutraceuticals consist of a complex mixture of food-derived compounds with weak or moderate biological activities capable of interacting with different cellular targets. The use of the whole extract often

guarantees a synergic action, with pharmacological effects greater than those of the individual components. This effect is particularly effective in multifactorial diseases, where a multi-target action enables the body's homeostasis to be restored (Lötsch & Geisslinger, 2011). Indeed, the use of low doses of active components, as observed in food matrices, guarantees a partial action in the metabolic pathways concerned while maintaining normal physiological functions and reducing the risk of side effects (Lötsch & Geisslinger, 2011). Moreover, the different components of natural origin are often characterised by a high structural promiscuity that guarantees their interaction with different biological targets, further extending the spectrum of action.

1.5. Background and aim of the project

The lack of pharmacological treatment for the prevention of some aging-related diseases, as the sarcopenia and the skin related diseases, represent a significant gap in the initiative medicine for two widespread diseases. Therefore, this Ph.D. thesis was focused on the development of innovative nutraceuticals with beneficial effects in the prevention of these two aging-related disorders. The development of a nutraceutical product is divided into several phases (**Figure 3**), which can be resumed as follows (Santini et al., 2018):

1) Selection of the food matrix.
2) Qualitative and quantitative chemical characterization of the matrix.
3) *In vitro* assay and evaluation of mechanism of action determined by the active ingredient or by the phytocomplex.
4) Technological development of the formulation.
5) Dose assessment and *in vivo* study.
6) Market release.

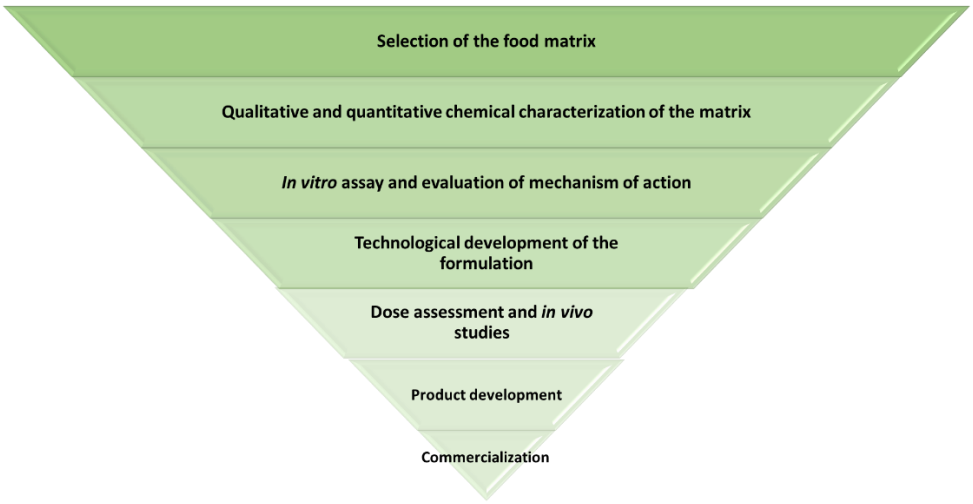


Figure 3. Summary of stages of nutraceutical development.

During this Ph.D. thesis, a detail study about the different development stages of two different nutraceutical products was performed. In addition, a great attention was given on the chemical analysis of two food matrices of interest, unripe tomatoes from *Solanum lycopersicum* L. and apple fruits from *Malus pumila* Miller named "Annurca", and the preliminary *in vitro* studies for the confirmation of the nutraceutical potential of the matrix.

CHAPTER 2

UNRIPE TOMATOES: FEATURES FROM LITERATURE

2.1. *Solanum lycopersicum* L.: botanical features

Tomato is the berry fruit of the vegetable plant *Solanum lycopersicum* L. (Solanaceae), originated in Western South America. This tomato plant has been cultivated in Europe since the XVII century and is considered one of the most worldwide vegetables, not only as an edible food, but also as a source of many bioactive compounds (Kimura & Sinha, 2008). According to the botanical classification of Carolus Linnaeus (1753), it belongs to the genus Solanum as *Solanum lycopersicum* L. (where *lyco* means "wolf" and *persicum* means "peach") and to the large family of Solanaceae, together with other commercially important plants, such as potato, eggplant, peppers, and tobacco. There are 13 recognized wild tomato species with a great diversity of phenotypes that can be crossed with cultivated tomatoes (Kimura & Sinha, 2008). Tomato plants are characterized by fleshy berries, a sympodial shoot, and compound leaves (**Figure 4**).

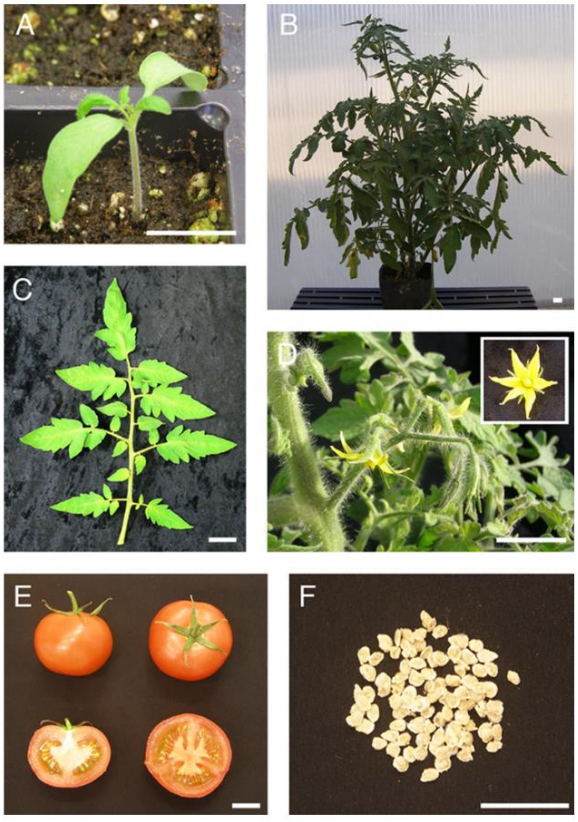


Figure 4: *Solanum lycopersicum* L. and its anatomical parts: A) seedling; (B) 40-days-old plant; (C) leaves; (D) flowers; (E) fruit; (F) seeds. Bar, 2 cm (picture from (Kimura & Sinha, 2008)).

Solanum pimpinellifolium is the ancestor of the modern cultivated tomato and is characterized by tiny fruits that weighed only few grams each. Nowadays, thanks to domestication and breeding, the cultivated tomatoes are more than 10 cm in diameter and 500 g in weight, with a fruit shape and a color controlled by several genetic loci that have been identified and characterized (Tanksley, 2004). The fruit color is controlled by multiple genetic loci that encode regulators and enzymes involved in the carotenoid biosynthetic pathways. The color is another important agricultural feature, which varies from green and yellow to orange and red, according to the quantities of chlorophylls and carotenoids, such as lycopene and β-carotene. In fact, red and orange tomatoes display a higher lycopene and β-carotene content, respectively, while green tomatoes contain chlorophylls, which is degraded during the ripening process (Kimura & Sinha, 2008).

Tomato is the most important and cultivated vegetable in the world, second only to potato cultivation. According to the "Food and Agriculture Organization of the United Nations" (FAO STAT Report), China is the world leader in tomato production, surpassing the USA in the 90s, with over 67 million tons produced in 2021, followed by India (20 million tons) and Turkey (13 million tons). Actually, Italy is the 6th world tomato productor. Moreover, according to FAO statistics updated in December 2022, total world tomato production for both processing and fresh consumption in 2021 amounted to just over 189,1 million metric tons, higher than 184,8 of 2020 (FAO STAT Report). The great production of tomato industry generates approximately 15 million tons of waste, which include pre-processing and post-processing wastes. Pre-processing waste, which range between the 1% and the 6% of the total tomato production, consists of damaged and unripe green tomatoes (Carillo et al., 2018). During the harvesting of ripe red tomatoes, a color-sorting machine is employed to separate green tomatoes, which are subsequently discarded. During the red tomatoes processing to obtain the products for sale, a post-processing waste is produced. The main post-processing waste is known as tomato pomace, a blend of seeds, peels, fibrous components, and a small portion of pulp (Matei et al., 2021). This waste constitutes around 2 million tons of organic material and represents about 5% of the weight of processed tomatoes (P. A. Silva et al., 2019). The disposal of tomato agricultural by-products represents supplementary costs for industries and has a negative impact on the environment. Consequently, the recovery of these wastes represents an appealing research field and governments promote the recycling of these agricultural wastes with the aim of obtaining new products with potential beneficial actions on the environment or human health.

Green tomato waste is mainly recycled for the production of snacks, cocktail sauces, and other food products (Patel et al., 2023). Green tomato juice if also used as substitute for sugar-rich juices in beverage preparation (El Mashad et al., 2019) and for the enrichment of animal feed. The tomato crop is used to obtain several processed products (such as paste, sauce puree, soup, juice, ketchup, and canned tomatoes) and takes an important place in the human diet for its beneficial health properties against chronic diseases (Kiralan & Ketenoglu, 2022). In addition to these applications, the nutraceutical properties of tomato waste allowed to consider it for the isolation of natural compounds for the preparation of supplements, additives, and pharmaceuticals. While red tomatoes have been extensively used for lycopene extraction (Lu et al., 2022), green tomatoes are only beginning to be considered for pharmaceutical or nutraceutical purposes. This is noteworthy since both unripe and ripe tomatoes exhibit interesting nutraceutical properties (P. A. Silva et al., 2019). The primary compositional disparities between green and red tomatoes are related to specific classes of secondary metabolites, including glycoalkaloids (SGAs), polyphenols, carotenoids, ascorbic acid, and chlorophylls. The polyphenol content varies significantly between green and red tomatoes. Anton et al. (2017a) observed a high polyphenol content in green tomatoes, mainly for chlorogenic acid and rutin. This content decreases as the fruits ripen but increase in ripe red tomatoes, where the main polyphenols are naringenin and homovanillic acid. Another distinctive secondary metabolite class of tomatoes is represented by carotenoids, which exhibit qualitative and quantitative variations depending on fruits ripeness. In immature tomatoes, lutein is the most abundant carotenoid, constituting approximately 45% of the total carotenoid content, although violaxanthin, neoxanthin, and β-carotene are also reported. Instead, lycopene is completely absent in green unripe tomatoes. In ripe red tomatoes, lycopene represents the main carotenoid, ranging from 59% and 91% of total carotenoid content, leading to the characteristic red color (Periago et al., 2008). However, β-carotene and lutein are also relevant. The high lycopene content in the ripe red tomatoes justifies the use of the waste of tomato pomace as a source for the extraction of carotenoids. Green tomatoes are rich in essential nutrients, such as vitamins (C, K, and B-complex vitamins), minerals (magnesium, potassium), and dietary fibers, all contributing to a balanced diet. Ascorbic acid, known as vitamin C, is a potent antioxidant with several health benefits. Vitamin C content in tomatoes depends on the ripeness fruit (Patel et al., 2023). Green tomatoes display an ascorbic acid content about 25 mg per 100 grams of fresh fruit. This amount increases with the fruit ripeness, but slightly decreases in the red ripe tomatoes around 10-20 mg per 100 grams of fresh fruit (Chaudhary et al., 2018).

2.2. Chemistry of glycoalkaloids

SGAs are a group of secondary metabolites widely spread in the Solanaceae family and sporadically in Liliaceae, including tomatoes, potatoes, and eggplants. There compounds are found in different botanical parts, including fruits, leaves, stems, flowers, and roots (Bishal & Keith, 2019). They are characterized by a nitrogen steroidal aglycone and a glycoside moiety, generally located in the C3 position. In particular, the aglycone unit is a hydrophobic 27-carbon skeleton of cholestane with nitrogen incorporated into the F-ring. Instead, the carbohydrate side chain is made up of 1-4 carbohydrates, attached at the 3-hydroxyl position on the A ring of the aglycone or at other locations, such as C-6, C-7, C-23, C-25, and C-27 (D. K. Zhao et al., 2021). However, each Solanaceous is characterized by its own unique assortment of steroidal SGAs. Some examples include dehydrotomatine and α-TM in tomatoes (*Solanum lycopersicum* L.), α-solanine and α-chaconine in potatoes (*Solanum tuberosum*), α-solasonine and α-solamargine in eggplants (*Solanum melogena*), whose structures are provided in the following picture (**Figure 5**). Although the chemical differences between these compounds, they share the general role of antiherbivore agents and phytoanticipins, which are low molecular weight antimicrobial compounds, present in their biologically active form in plants before the attack of phytopathogens (Dzakovich et al., 2020; González-Lamothe et al., 2009).

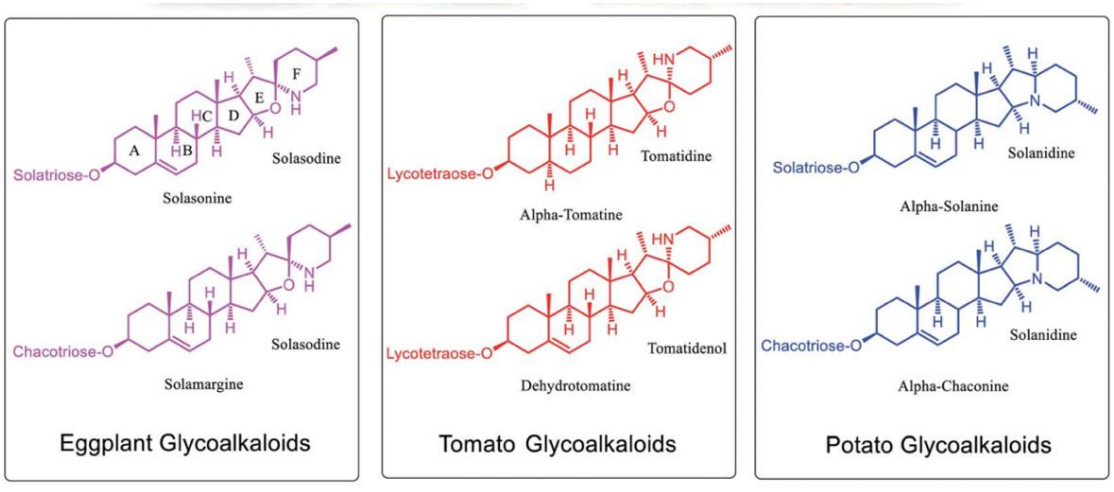


Figure 5: Chemical structures of the main SGA from eggplant, tomato and potato (picture from Zhao et al., 2021a).

The two typical aglycones of these triterpene-derived metabolites are solanidane and spirosolane (**Figure 6**). Solanidane is the aglycone characterized by an indazolidine ring and it is typical of potato-type SGAs. This aglycone is characteristic of two SGAs: solanidine and demissidine, that differ from each other only by the addition of the B-ring double-bond in position C5-C6. On the other hand, spirosolane is the aglycone characterized by a 1-oxa-6-azaspirodecane ring system in the ring E. Tomatidenol, TD, solasodine and soladulcine are the main four compounds that belong to this group, and they differ from each other only by the stereochemistry of C-22 (α or β N) and for the presence or absence of the B-ring double bond in position C5-C6.

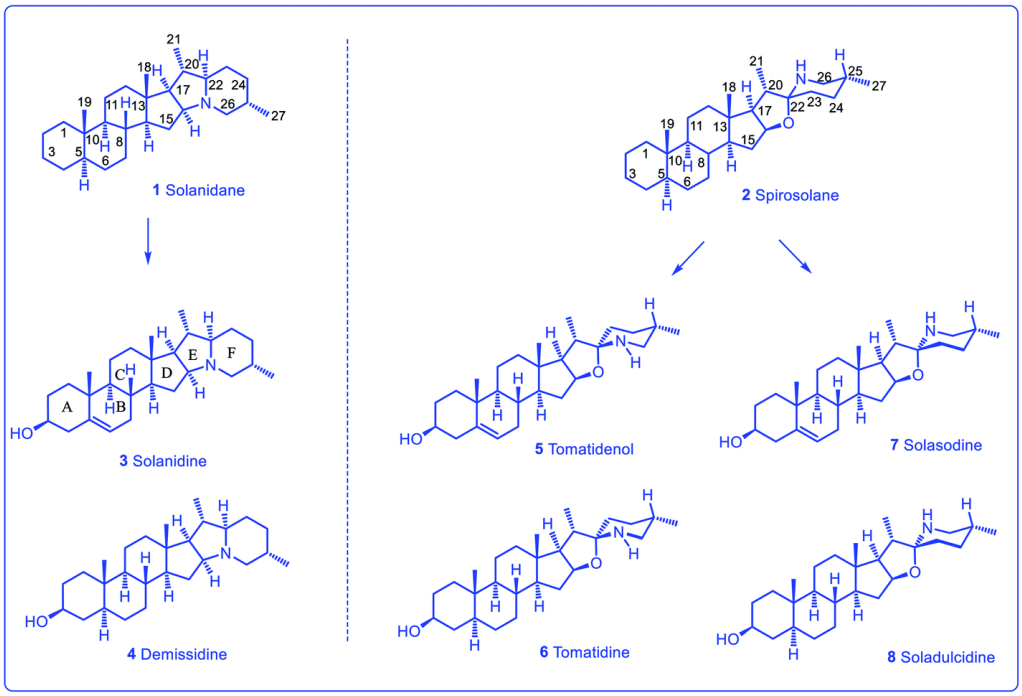


Figure 6: Structure of solanidane and spirosolane and typical aglycone units of *Solanum lycopersicum* L. steroidal SGAs (picture fromZhao et al., 2021a).

Tomatidenol (or dehydrotomatidine) is a type of seco-cholestane alkaloid with 11 stereocenters and a unique 1-oxa-6-azaspirodecane ring system. The configuration observed for the rings A-E is the same of solanidine analogues. In particular, the C-22 is in the *S* configuration with a 22-β N in ring F, and methyl-21 and methyl-25 are in α orientation. In addition, there is a double bond between C-5 and C-6 in ring B. TD shares the same chemical structure and stereochemistry in rings A-F of tomatidenol, but it is saturated

between C-5 and C-6. Furthermore, these two compounds are the main aglycones produced by *Solanum lycopersicum* L. (**Figure 7**) (D. K. Zhao et al., 2021).

The glycosidic units of natural SGA consist of 1-4 carbohydrates, generally attached to the hydroxyl group in position 3 of the A ring. Among trisaccharides, solatriose is the most common carbohydrate side-chain of *Solanum* SGAs, while chacotriose, commertetraose, and lycotetraose are the most common among the tetrasaccharides (D. K. Zhao et al., 2021). In particular, chacotriose is made up of two L-rhamnoses and one D-glucose; solatriose is characterized by D-glucose, D-galactose, and L-rhamnose; lycotetraose has two D-glucose, a D-xylose, and D-galactose; commertetraose has the same structure of lycotetraose except that one of the D-glucose is replaced by another D-xylose (**Figure 8**). According to the literature, half of these glycosidic said chains are linked to the aglycon through a glucose unit, while the other half is linked through galactose. The only exception is represented by ravifoline, which is linked through a xylose. Although most SGAs link the polysaccharide portion to the hydroxyl group at C3 there are other accessory positions on the aglycone moiety. In these positions, other secondary sugar moieties can be linked, and they include the C6, C7, C23 (e.g. lycoperoside G), C25 (e.g. esculeoside A) and C27 (e.g. esculeoside B, C and D).

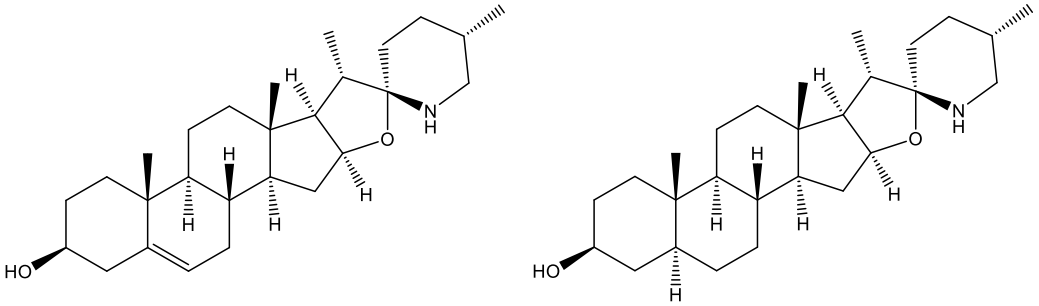


Figure 7: Tomatidenol (left) and TD (right) chemical structures.



Figure 8: Chemical structures of SGA glycosidic moieties (Zhao et al., 2021a).

In conclusion, the chemical structures of the more common *Solanum lycopersicum* L. SGAs can be summarized as follows:

- α-solanine and α-chaconine in the potato, which are both characterized by the aglycone solanidine (i.e., a solanidane with an indazolidine ring) and by the polysaccharide side chain, which is the trisaccharide solatriose and the tetrasaccharide chacotriose, respectively;

- Solasonine and Solamargine in eggplant, which are both characterized by the aglycone solasodine (a spirosolane with a 1-oxa-6-aza-spirodecan ring system) and by the polysaccharide side chain, which is solatriose and chacotriose, respectively;

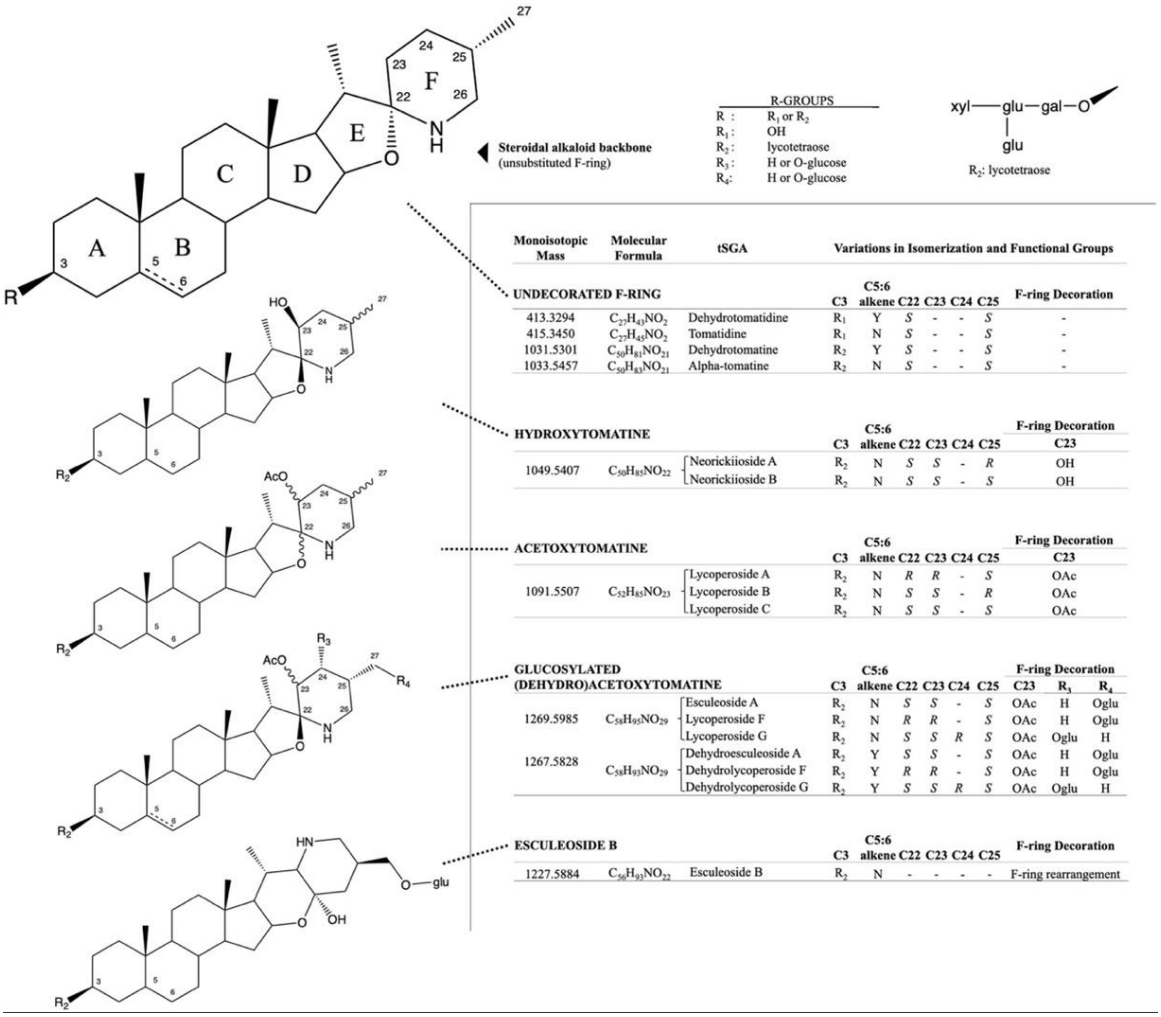
- α-TM and dehydrotomatine in the tomato, which are made up of TD and tomatidenol, respectively. Instead, the glycosidic unit is the tetrasaccharide β-lycotetraose for both compounds (**Figure 7**). α-TM and dehydrotomatine were initially isolated by Fontaine et al. in 1948 as a mixture 10:1 of the two compounds called as tomatine.

Other steroidal SGAs found in tomatoes include hydroxytomatine, acetoxytomatine, acetoxy-hydroxytomatine, Esculeoside A, δ-tomatine (δ-TM), β1-tomatine (β1-TM), β2-tomatine (β2-TM) and γ-tomatine (γ-TM). They are spirosolane-type saponins with variations in a singular double bond (C5-C6), F-ring decorations (C22-C27), F-ring rearrangements (resulting a change in stereochemistry at C22) and C3 glycosylation (Dzakovich et al., 2020). In particular, hydroxytomatine, acetoxytomatine, acetoxy-hydroxytomatine, and Esculeoside A derive from α-TM catabolism, which occurs during the ripening process in the fruit. On the other hand, β1-TM and β2-TM are the biosynthetic precursors of α-TM in the SGA pathway, lacking the terminal glucose or xylose, respectively. γ-TM is the precursor of β1-TM and β2-TM, lacking both two-terminal sugars, and δ-TM is the precursor of γ-TM, characterized by the aglycone TD with only a galactose unit attached to the hydroxyl group at C3. Although α-TM is the most abundant SGA in unripe tomatoes, several other secondary SGAs have been identified, both as biosynthetic precursors and products of α-TM metabolism in the plant. α-TM chemical diversity derived from various chemical modifications, including isomerization, hydroxylation, acetylation, and glycosylation (Iijima et al., 2013). The most important secondary SGAs in unripe tomatoes include dehydrotomatine, hydroxytomatine, acetoxytomatine, and esculeoside A (Iijima et al., 2013). The main possible structural and isomeric variations in selected tomato steroidal alkaloids, along with the monoisotopic mass, the molecular formula, and the common name are displayed in the following picture (**Figure 9**). α-TM is a distinctive compound in the entire tomato plant and its concentration in the fruit depends on the stage of maturity. Specifically, α-TM accumulates in unripe tomatoes, but its level significantly decreases as the fruit ripens (Friedman, 2002). During the tomato maturation, it is metabolized into esculeoside A, which represents the not bitter and less toxic primary SGA in red ripe tomatoes (Iijima et al. 2013). In fact, the major change in SGAs composition

during fruit ripening results in the accumulation of Esculeoside A, increasing the palatability of the fruit for consumption and favoring seed dispersal. The metabolic conversion of α-TM to Esculeoside A can be summarized with the following metabolism reactions:

1) α-TM is oxidated to hydroxytomatine by a reaction of hydroxylation;
2) hydroxytomatine is acetylated to acetoxytomatine;
3) acetoxytomatine is oxidated to acetoxyhydroxytomatine;
4) aceroxyhydroxytomatine is acetylated to esculeoside A.

The same process also affects dehydrotomatine, which is converted into the final product dehydroesculeoside A.



Monoisotopic Mass	Molecular Formula	tSGA	C3	C5:6 alkene	C22	C23	C24	C25	F-ring Decoration		
UNDECORATED F-RING											
413.3294	$C_{27}H_{43}NO_2$	Dehydrotomatidine	R_1	Y	*S*	-	-	*S*	-		
415.3450	$C_{27}H_{45}NO_2$	Tomatidine	R_1	N	*S*	-	-	*S*	-		
1031.5301	$C_{50}H_{81}NO_{21}$	Dehydrotomatine	R_2	Y	*S*	-	-	*S*	-		
1033.5457	$C_{50}H_{83}NO_{21}$	Alpha-tomatine	R_2	N	*S*	-	-	*S*	-		
HYDROXYTOMATINE									**F-ring Decoration**		
			C3	**alkene**	**C22**	**C23**	**C24**	**C25**	**C23**		
1049.5407	$C_{50}H_{83}NO_{22}$	Neorickiioside A	R_2	N	*S*	*S*	-	*R*	OH		
		Neorickiioside B	R_2	N	*S*	*S*	-	*S*	OH		
ACETOXYTOMATINE									**F-ring Decoration**		
			C3	**alkene**	**C22**	**C23**	**C24**	**C25**	**C23**		
1091.5507	$C_{52}H_{85}NO_{23}$	Lycoperoside A	R_2	N	*R*	*R*	-	*S*	OAc		
		Lycoperoside B	R_2	N	*S*	*S*	-	*R*	OAc		
		Lycoperoside C	R_2	N	*S*	*S*	-	*S*	OAc		
GLUCOSYLATED (DEHYDRO)ACETOXYTOMATINE									**F-ring Decoration**		
			C3	**alkene**	**C22**	**C23**	**C24**	**C25**	**C23**	**R_3**	**R_4**
1269.5985	$C_{58}H_{95}NO_{29}$	Esculeoside A	R_2	N	*S*	*S*	-	*S*	OAc	H	Oglu
		Lycoperoside F	R_2	N	*R*	*R*	-	*S*	OAc	H	Oglu
		Lycoperoside G	R_2	N	*S*	*S*	*R*	*S*	OAc	Oglu	H
1267.5828	$C_{58}H_{93}NO_{29}$	Dehydroesculeoside A	R_2	Y	*S*	*S*	-	*S*	OAc	H	Oglu
		Dehydrolycoperoside F	R_2	Y	*R*	*R*	-	*S*	OAc	H	Oglu
		Dehydrolycoperoside G	R_2	Y	*S*	*S*	*R*	*S*	OAc	Oglu	H
ESCULEOSIDE B									**F-ring Decoration**		
			C3	**alkene**	**C22**	**C23**	**C24**	**C25**			
1227.5884	$C_{56}H_{93}NO_{22}$	Esculeoside B	R_2	N	-	-	-	-	F-ring rearrangement		

Figure 9: Structural and isomeric variations of SGA of tomatoes. In order, from top to bottom: steroidal alkaloid backbon (with unsubstituted F-ring), hydroxytomatine, acetoxytomatine, glucosylated(dehydro)acetoxytomatine and Esculeoside B (picture from Dzakovich et al., 2020).

2.3. Unripe tomatoes as a source of glycoalkaloids

2.3.1. Glycoalkaloids extraction methods

α-TM extraction is a critical process for an accurate quantification in unripe tomato extracts. Generally, SGAs from tomatoes are extracted by grinding the samples using a mortar and pestle or a blender, followed by the extraction of analytes using polar solvents (Dzakovich et al., 2020). The extraction protocols for unripe tomatoes requires the addition of the extraction solvents to an amount of fresh tomatoes or lyophilized tomato powder, stirring the mixture at a controlled temperature for a certain amount of time. Commonly used extraction solvents include acidic aqueous solutions or organic solvents, such as methanol, acetonitrile, chloroform, and tetrahydrofuran. These solvents are often used in a pure form or as mixture, as combination of acetonitrile-methanol or methanol-chloroform. α-TM solubility in water is influenced by the pH of the solution, with values of 6 mM at pH = 5, 1 mM at pH = 6, 0.04 mM at pH = 7, and 0.03 mM at pH = 8 (Nepal & Stine, 2019). The addition of acetic acid enhances α-TM extraction by protonating the nitrogen atom, thereby increasing water solubility. However, acetic acid is primarily used in dried samples, whereas organic solvents like methanol or chloroform are preferred for fresh tomatoes. In fact, fresh samples contain a sufficient water content to solubilize the alkaloids during the extraction with organic solvents (Monteiro & Pinheiro, 2013). Following extraction, the solution can undergo one of three processes:

1) Centrifugation to remove precipitated components (Friedman et al., 1994; Friedman & Levin, 1995, 1998; Itkin et al., 2011; Taveira et al., 2012, 2014; Tamasi et al., 2019; Koh et al., 2013; Steinert et al., 2020; Marcolongo et al., 2020; Pardini et al., 2021; Trung Huy Ngo et al., 2022; Abbasi-Parizad et al., 2023);
2) Concentration under vacuum followed by acidification with a hydrochloric acid solution (Kozukue et al., 1994, 2004; Vaananen 2000; Kozukue & Friedman, 2003; Silva-Beltran et al., 2015);
3) A combination of both procedures (Friedman et al., 2009; S.-H. Choi et al., 2010, 2013).

The resulting samples can be directly analyzed (Marcolongo et al., 2020; Steinert et al., 2020; Pardini et al., 2021; Trung Huy Ngo et al., 2022) or subjected to partial purification procedures. Common methods of partial purification include:

1) Clean-up by solid-phase extraction (SPE) (Friedman et al., 1994; Friedman & Levin, 1995, 1998; Leonardi et al., 2000; Vaananen 2000; Taveira et al., 2012, 2014; Koh et al., 2013; Caprioli 2014; Abbasi-Parizad et al., 2023);

2) Precipitation and centrifugation of SGAs in a basic environment through the addition of an ammonium solution (Kozukue et al., 2004, 1994; Kozukue & Friedman, 2003; Friedman et al., 2009; S.-H. Choi et al., 2010; Choi et al., 2013; Silva-Beltran et al., 2015; Abbasi-Parizad et al., 2023);

3) Liquid-liquid extraction (LLE) with organic solvents (Friedman et al., 1994).

The ammonium hydroxide purification approach purified SGAs, although the precipitation is not quantitative and exhibits a low recovery rate (Monteiro & Pinheiro, 2013). Instead, the SPE purification offers greater reproducibility but necessitates validation of recovery parameters for an accurate quantification (Vaananen et al., 2000). Commercially available SPE cartridges utilize different sorbent types. The most common type is the octadecyl phase (C_{18}), but other SPE cartridges are the macro porous copolymer (Oasis HLB), the sulphonic acid cation exchanger (SCX), the aminopropyl bonded silica (NH2), the polar cyanopropyl (CN), the mixed sorbent phases as a combined octyl and SCX (Certify), and the combined packings (CN/SiOH; NH_2/C_{18}) (Taveira et al., 2012; Vaananen et al., 2000). SPE clean-up procedures involve three steps: the SGAs absorption to the sorbent, the washing of the impurities off the phase, and the SGAs elution with an organic solvent, typically methanol. Impurity washing can be performed with water to remove fibers and sugars or with basic ammonium mixtures to elute acidic interferents like polyphenols (Friedman et al., 1994; Friedman & Levin, 1995). The C_{18} SPE requires the loading of only aqueous extracts to adsorb the SGAs in the hydrophobic phase. Therefore, C_{18} SPE is commonly used for acidic aqueous extracts requiring clean-up or interference elimination in samples analysis (Bushway et al., 1994; Friedman et al., 1994; Friedman & Levin, 1995, 1998; Väänänen et al., 2000; Taveira et al., 2012; Koh et al., 2013; Kim et al., 2014: Abbasi-Parizad et al., 2023). Extracts obtained with organic solvents need the evaporation and the subsequent solubilization in water before loading on the SPE cartridge. Heptanesulphonic acid can be added as ion-pairing reagent to ensure SGAs solubility and cartridge loading (Bushway et al., 1994). α-TM recoveries using many types of SPE are high, approaching 100%. However, the use of SCX sorbent phases ensures greater selectivity in SGAs purification, reducing matrix effects during analysis. The sulphonic acid group in SCX strongly interacts with basic species, such as the nitrogen group in SGAs, enhancing purification efficiency (Taveira et al., 2012; Vaananen et al., 2000).

Another sample clean-up method includes liquid-liquid extraction (LLE) of the aqueous ammonia solution with a water-saturated 1-butanol solution, recovering the 1-butanol layer enriched with SGAs. The 1-butanol layer can be following subjected to a C_{18} SPE clean-up to achieve robust sample purification by removing matrix interferents (Friedman, 2013; Friedman & Levin, 1995).

Ultrasound-assisted extraction (UAE) is often integrated with other extraction steps to enhance extraction yields. UAE is a flexible, cost-effective, simple, and scalable not-conventional technique based on the cavitation principle, which allows the cell wall disruption and the bioactive compound extraction. The extraction process can also be conducted in high throughput to reduce analysis times and maximize extraction yields. (Dzakovich et al., 2020) reported an α-TM and TD extraction method with an approximate preparation time of 1.25 minutes per samples, achieving close to 100% α-TM without the need for clean-up procedures. α-TM extraction procedures for extraction and quantification of other tomato SGAs have also been described (Dzakovich et al., 2020; Itkin et al., 2011). These procedures rely on the use of pH modifiers (e.g., formic acid, acetic acid, ammonium hydroxide) to control the solubility of compounds for the ionization of nitrogen atom, which is common to all α-TM analogues. Some protocols have been established for the extraction of acetoxytomatine (Dzakovich et al., 2020; Itkin et al., 2011) and TD (Caprioli et al, 2013; Silva-Beltran et al., 2015; Nirmala et al., 2020; Dzakovich et al., 2020; Fujimaki et al., 2022). **Table 1** summarized the extraction method conditions applied over the years for α-TM extraction.

In the analytical validation of an extraction, an essential aspect is the recovery study of the active ingredient from the matrix. While several papers have described α-TM extraction methods, few authors have provided comprehensive recovery studies. Nevertheless, it appears that the use of acidified solvents ensures very high recovery and analytical accuracy (Bushway et al., 1994; Pardini et al., 2021; Taveira et al., 2012). More rigorous clean-up procedures significantly reduce extraction recovery, making the samples suitable for qualitative analysis but not for quantitative purposes. For example, (Friedman et al. (1994) described an extraction procedure involving two consecutive clean-ups with C_{18} SPE and 1-butanol LLE. However, this method resulted in a very clean sample with a low α-TM recovery. Since an independent study reported high recovery with C_{18} SPE (Vaananen et al., 2000), it is reasonable to conclude that the low recovery is attributed to the 1-butanol LLE clean-up.

The structural similarities between α-TM and secondary SGAs allows to hypothesize that they are effectively extracted under the same α-TM extraction conditions. However, the absence of analytical standards for most secondary tomato SGAs avoids the extraction and the analysis methods validation.

Sample	Total volume of extraction	Extraction features	Clean-up	Reference
Lyophilized sample (0.1 g)	10 ml acetic acid 1% in aqueous EtOH 80% (v/v)	UAE (10 min), centrifugation (5 min, 4000 rpm) for 2 cycles of extraction		Pardini et al., 2021 Tamasi et al., 2019
Fresh sample (10 g)	10 ml methanol	UAE (1 h), centrifugation (10 min, 12000 rpm)		Trung Huy Ngo et al., 2022
Lyophilized sample (0.1 g)	10 ml acetic acid 1% in aqueous EtOH 70% (v/v)	UAE (15 min), centrifugation (5 min, 4000 rpm) for 2 cycles of extraction		Marcolongo et al., 2020
Hot air dried sample (35 g)	Acetic acid 5% in EtOH; volume not reported	UAE (20 min)	$(NH_4)OH$ 5% (*w/v*) solution	Silva-Beltran et al., 2015
Fresh sample	H_2O Chloroform/MeOH 2:1 (v/v)	UAE, centrifugation (10 min, 9800 g)	$(NH_4)OH$ 2% (*w/v*) solution	Choi et al., 2013
Fresh sample (1-20 g)	$CHCl_3$/MeOH 2:1 (v/v)		$(NH_4)OH$ 2% (*w/v*) solution	Kozukue & Friedman, 2003 Kozukue & Friedman, 2004
Lyophilized sample (0.5 g)	100 ml acetic acid 5%	UAE (10 min)	Different SPE sorbents (C_{18}, CN, SCX, Oasis HLB)	Vaananen 2000
Fresh sample (2 g)	10 ml formic acid 1% in aqueous MeOH 70% (v/v)	Centrifugation (10 min, 2588 g)		Steinert et al., 2020
Lyophilized sample (0.16 g)	2 ml acetic acid 5%	UAE (60 min), centrifugation (5 min, 12000 rpm)	SPE (SCX)	Taveira et al., 2012 Taveira et al., 2014 Abbasi-Parizad et al., 2023 Nirmala et al., 2020
Air dried sample (0.25 g)	10 ml acetic acid 1%	Centrifugation (15 min)	SPE (C_{18})	Koh et al., 2013
Lyophilized samples (1 g)	30 ml acetic acid 1%	Centrifugation (10 min, 13300 rpm) for 2 cycles of extraction	SPE (C_{18}), LLE with 1-butanol	Friedman et al., 1994 Friedman & Levin, 1995
Lyophilized samples (1 g)	30 ml acetic acid 1%	Centrifugation (10 min, 13300 rpm) for 2 cycles of extraction	SPE (C_{18})	Friedman & Levin, 1998
Fresh sample (1-22 g)	100 ml acetic acid 2% in MeOH	Centrifugation (10 min, 18000 g)	$(NH_4)OH$ 2% (*w/v*) solution	S.-H. Choi et al., 2010
Fresh sample (3-41 g)	100 ml acetic acid 2% in MeOH	Centrifugation (5 min, 18000 g)	$(NH_4)OH$ 2% (*w/v*) solution	Friedman et al., 2009
Fresh sample	45 ml methanol	Centrifugation (5 min, 3000 rpm) for 3 cycles of extraction	SPE (C_{18})	Caprioli et al., 2014
Lyophilized sample (1 g)	20 ml acetic acid 1%		SPE (C_{18})	Leonardi et al., 2000
Lyophilized sample (0.5 g)	5 ml acetic acid 2% in MeOH	Centrifugation (15 min, 8000 rpm) for 2 cycles of extraction	$(NH_4)OH$ 25% (w/w) solution	Abbasi-Parizad et al., 2023
Fresh sample (55 g)	50 ml of THF/H_2O/ACN/acetic acid (50/30/20/1)		SPE (C_{18})	Bushway et al., 1994
Lyophilized sample (0.05 g)	15 ml MeOH	Centrifugation (5 min, 3000 g)		Dzakovich et al., 2020
Fresh sample (0.2 g)	20 ml formic acid 0.1% in aqueous MeOH 80% (v/v)	Centrifugation (10 min, 20000 g)		Itkin et al., 2011

Table 1. Different conditions reported for α-TM extraction. UAE: Ultrasound Assisted Extraction; LLE: Liquid-Liquid Extraction; SPE: Solid-Phase Extraction; H_2O: water; $(NH_4)OH$: ammonium hydroxide; MeOH: methanol; EtOH: ethanol; ACN: acetonitrile; $CHCl_3$: chloroform; THF: tetrahydrofuran.

2.3.2. Glycoalkaloids analysis methods

Over the years, different techniques have been used for α-TM identification and the quantification. High-performance liquid chromatography (HPLC) has been the most widely employed analytical approach. Initially, gas chromatography (GC) was the first detector coupled with HPLC for α-TM analysis. However, due to the compound polarity, it could not be directly analyzed in its intact form and required hydrolysis reactions of the sugar moiety and functionalization to enhance volatility. This analysis could be performed on lycotetraose sugars or on the aglycone. For example, (Friedman et al., 1998) described a protocol

involving SGAs hydrolysis, the monosaccharide reduction to alditols, and the subsequent acetylation reaction. While GC is a fairly sensitive technique, it has many disadvantages. SGAs, which often share the same aglycone but differ in the tetrasaccharide group, can generate the same aglycone during hydrolysis, leading to errors in identification and quantification in real samples (Faria-Silva et al., 2022). Another issue is the use of hydrolysis and derivatization steps, which require rigorous validation for quantitative goals. In addition, glycolkaloids with TD-type aglycons can generate not-specific GC fragmentation patterns, which are difficult to monitor for quantitative purposes. For this reason, (Laurila et al., 1999) proposed a protocol involving trimethylsilylation and pentafluoropropionylation steps of TD. Although this protocol improved the clarity of GC fragmentation spectra for the identification, the reactions were not always complete, and the authors reported the products of both reactions and the products of silylation reaction. The incomplete aglycone reaction could interfere with a correct quantification.

The most common approach for α-TM analysis involves liquid-chromatography coupled with mass spectrometry techniques, such as quadrupole time-of-flight mass spectrometer (Q-TOF MS), with electron spray ionisation mass spectrometer (LC/ESI-MS), and Fourier transform ion cyclotron resonance mass spectrometry (FTICR-MS) (Caprioli et al., 2014; Iijima et al., 2013; Kozukue et al., 2023; Moco et al., 2006). These techniques employ soft ionization methods that allow the analysis of high molecular weight, high polarity and thermally unstable compounds in their intact form (Faria-Silva et al., 2022). Furthermore, the presence of a nitrogen atom in SGAs makes the analysis highly sensitive in positive acquisition mode. For example, (Dzakovich et al., 2020) reported a limit of quantification (LOQ) for α-TM of 1.1 femtomoles. Qualitative experiments, such as full MS, MS/MS, and data-dependent acquisition (DDA), are commonly used for the SGAs identification in food matrices (Itkin et al., 2011) and biological samples (Cichon et al., 2017; Cooperstone et al., 2017; Dzakovich et al., 2023). Additionally, the application of more sensitive experiments for quantitative purposes, such as the multiple reaction monitoring (MRM), along with chromatographic separation, allows samples to be injected without needing partial purification procedures like SPE or LLE, which are time-consuming and unsuitable for quantitative analysis (Koh et al., 2013; Tamasi et al., 2019; Marcolongo et al., 2020; Steinert et al., 2020; Dzakovich et al., 2020; Pardini et al., 2021). However, one of the main disadvantages of these techniques is their dependence on ionization step, which can alter molecule response over time, be influenced by ion suppression effects, and requires frequent

instrument calibration (Taveira et al., 2012). Nevertheless, unlike GC, several studies have reported comprehensive validation of α-TM analysis by mass spectrometry.

Despite the use of GC and MS in α-TM analysis, these methods are not always available in laboratories. Consequently, some analysis methods have been developed using reverse-phase high-pressure liquid chromatography (RP-HPLC) coupled with alternative detectors, including ultraviolet (UV), pulsed amperometry detector (PAD), diode array detector (DAD), evaporative light scattering (ELS), and refractive index (RI). The pulsed amperometry detector (PAD) was among the first techniques used for α-TM analysis. It was employed for the quantification of α-TM in tomatoes (Friedman et al., 1994), different botanical parts of *Solanum lycopersicum* L. plant (Friedman, 1998), and processed tomatoes products (Friedman et al., 1995). Although PAD is more sensitive than other detectors based on spectroscopic properties (e.g., DAD and UV), HPLC analysis can result in a not-linear response due to the overloaded of the detector cell at high analyte concentrations (Friedman, 1998). Ultraviolet (UV) and diode array (DAD) detectors are the most used techniques due to their simplicity and cost-effectiveness (Vaananen et al., 2000; Yamanaka et al., 2008; Taveira et al., 2012; Choi et al., 2013; Taveira et al., 2014; Silva-Beltran et al., 2015; Nirmala et al., 2020; Abbasi-Parizad et al., 2023). However, α-TM detection requires a wavelength around 200 nm due to the lack of UV-visible functional groups, resulting in low specificity. Therefore, there detectors often require the use of cleanup techniques (e.g., SPE) to eliminate potential interferents and is characterized by low sensitivity. For example, (Friedman et al., 1998) reported a limit of detection (LOD) value of 2.5 µg for α-TM analysis by HPLC-UV. Additionally, this analysis can only be performed using mobile phases with low UV cut-offs (e.g., acetonitrile and phosphate buffer) (Ghisalberti, 2006). Due to the low sensitivity of UV and DAD in α-TM analysis, some researchers described the use of these detectors more commonly for SGAs preparative separation from natural matrices and the subsequent analysis of the fractions using other detectors (Friedman et al., 1998). The evaporative light-scattering detector (ELSD) is easy to use but does not yield a linear response for quantitative analysis (Wolfender, 2009). Therefore, it has mainly been used for identification and purity analysis of α-TM and other SGAs (Yamanaka et al., 2008; Steinert et al., 2020; Trung Huy Ngo et al., 2022). The refractive index detector (RID) is an easy-to-use detector and responds independently of parameters such as UV-visibility, volatility, or the presence of ionizable functional groups. However, RID lacks sensitivity, can’t be used for elution gradients, and is sensitive to variations in pressure, flow, and

temperature (Wolfender, 2009). Consequently, RID use in α-TM analysis is limited to SGAs preparative separation from natural matrices (Rial et al., 2018).

Although RP-HPLC is the main approach for α-TM and secondary SGAs analysis, many alternative methods have been developed over the years for the purification, the identification, and the quantification of these compounds. Thin-layer chromatography (TLC) is a direct-phase chromatography technique that separates SGAs based on their different polarities due to the sugar moieties. It is used to provide an estimation of the number of molecules in a mixture and to monitor fractions during chromatographic separation. Therefore, TLC is used mainly for qualitative purposes and cannot be used to obtain quantitative information. Nonetheless, some published paper reported the use of preparative TLC or high-pressure thin-layer chromatography (HPTLC) for α-TM isolation from plant matrices (Bachmann et al., 2013; Rial et al., 2018). A different approach for SGAs separation is represented by capillary electrophoresis (CE), a cost-effective and rapid technique that separates compounds based on their ion mobilities. CE has often been employed for the separation of ionizable basic compounds like alkaloids (Altria et al., 2006). Bianco et al. (2002) reported a not-aqueous CE method coupled with electrospray ionization mass spectrometry for α-TM separation and identification. The use of methanol as not-aqueous solvent enhances SGAs solubility and eliminates the need for salt buffers that can be often incompatible with mass spectrometry detectors (Altria et al., 2006). However, to our knowledge, papers about CE separation using real samples from *Solanum lycopersicum* L. are not reported in literature. An innovative approach involves the application of attenuated total reflectance infrared spectroscopy and thermogravimetric analysis to estimate α-TM content in tomato samples. The effectiveness of these approaches was validated by statistical techniques, such as multiple linear regression and partial least square regression (Tamasi et al., 2021).

2.4. Glycoalkaloids beneficial effects on human health

2.4.1. Anticancer activity

Regarding the anticancer properties, it's interesting to note that α-TM is more active than dehydromatine in all cell lines and the entire tetrasaccharide portion of the α-TM is essential for this bioactivity (Bailly, 2021). In fact, the removal of one, two, or three sugar residues (to produce respectively β1-TM, β2-TM, γ-TM and δ-TM) is associated with the formation of compounds with a significantly reduced anticancer activity (Friedman, 2013). However, these properties seem to be not equal in all cell lines. For example, P53 prostate cancer cells are 5-10 more sensitive to α-TM than KATO-III gastric adenocarcinoma cells (Bailly, 2021). Other investigators as Shin et al. (2009), have studied the mechanism of α-TM antimetastatic effect and have highlighted the implication of NF-kB/ERK signaling pathway and the inhibition of matrix metalloproteinases, notably MMP-2, -7 and -9, involved in the anti-invasion and anti-metastatic activity (Bailly, 2021). In particular, it was seen that this compound can inhibit the phosphorylation of Akt factor and extracellular signal-regulated kinase 1 and 2 (ERK1/2). Another important mechanism includes the decrease in the nuclear levels of nuclear factor kappa B (NF-kB) by blocking its nuclear translocation, and its binding ability (Friedman, 2013). In addition, α-TM may repress the expression of prosurvival proteins such as Bcl-2, Bcl-xl, c-IAP2, XIAP, and survivin. Huang et al. have also hypothesized that α-T dependent mechanisms for modulating apoptosis could be the result of cell membrane disruption due to the interaction between α-TM and cholesterol.

Thanks to several *in vitro* studies it was seen that, in highly metastatic A549 lung cancer cells, α-TM reduced the oncogenic properties of the cells via the inactivation of the phosphoinositide 3-kinase/protein kinase B (PI3K/Akt) and of the extracellular signal-regulated kinase 1 and 2 (ERK1/2) signaling pathways, both master regulators of cell metabolism and key role players in cancer progression (Shih et al., 2009). In addition, α-TM exerts antimetastatic effects in melanoma. Specifically, the combination of the two SGAs inhibits the invasion and viability of BRAF and V600BRAF-positive metastatic melanoma cells. In this context, α-TM has been shown to induce autophagy, increasing the LC3II/LC3I ratio and endoplasmic reticulum stress in metastatic melanoma.

Moreover, the anticarcinogenic effect of α-TM has been studied *in vivo*, using a rainbow trout model. The long-term study has demonstrated that the oral intake of a solution 2000

ppm of α-TM and 224 ppm of the multiorgan carcinogen dibenzo [*a,l*] pyrene (DBP) lead to a reduced incidence of liver and stomach tumors by 41.3 and 36.3% respectively.

Another important study, conducted by Lee et al. (2013) and performed with the PC3 xenograft model of human androgen-independent prostate cancer, has demonstrated an α-TM dose-dependent activity, with a low effect at 5 mg/kg and a complete inhibition of cell growth at 10 mg/kg, quite like that shown by docetaxel at the same dose, but with better tolerance (Bailly, 2021).

Although TD shows a higher IC_{50} value, which results in a lower anticancer effect, it may contribute to the overall bioactivity. As reported by Lavie et al., TD can play a key role as a chemosensitizer in multidrug-resistant tumor cells, and so it could be used in combination chemotherapy with cytotoxic drugs for treating multidrug-resistant cancers (Friedman, 2013).

A short summary of SGAs anticancer properties in summarized in **Table 2**.

2.4.2. Chemotherapic activity

SGAs are known historically as phytoalexins, which display a protection role of the plant against bacteria, fungi, insects, and animals, thanks to their recognized antibiotic activities (Friedman, 2002). Among them, α-TM has displayed citotoxicity by inhibiting the growth of both human colon and liver cancer cell lines. As demonstrated in microculture tetrazolium (MTT) *in vitro* assays, the anticarcinogenic activity against human liver cancer cells at an α-TM concentration of 1 μg/ml was higher than the reference compound doxorubicin, a compound with a well-known antitumoral activity (Friedman, 2013). α-TM induces a decrease in blood cholesterol and triglycerides levels, mainly thanks to the molecular affinity and the consequent possibility to form complexes with cholesterol, thus decreasing its absorption and bioavailability. α-TM can also offer protection against virulent bacteria and protozoa, also enhancing the immune system against pathogens and tumors. For example, Friedman (2013a) reported an α-TM activity in the induction of T-cell mediated regression of murine lymphoid experimental tumors.

SGAs display a large spectrum of activity against strains of *Cacillus*, *Listeria*, and *Staphylococcus*, thanks to a strong inhibition of bacterial protein synthesis (Bailly, 2021). Mitchell et al. have also found that TD can inhibit the *Staphylococcus aureus* small-colony variants (SCVs) and improve the antibiotic effect of aminoglycosides against multi-drug resistant forms of *S. aureus*, by preventing the expression of virulence microbial genes.

Another synergic effect between TD and ampicillin or ciprofloxacin against standard strains of *Enterococcus faecalis* and *P.aeruginasa* have been found as well (Mitchell et al., 2012). Leaves extracts from unripe tomatoes obtained by Californian *Solanum lycopersicum* L. displayed antimicrobial activity against *Staphylococcus aureus*, *Salmonella enterica*, and *Escherichia coli*. Interesting, the extracts didn't inhibit the growth of some beneficial bacteria, such as *Lactobacillus rhamnosus*, *Lactobacillus acidophilus*, and *Lactobacillus reuteri*, which constitute the intestinal bacterial flora (Tam et al., 2021).

On the other hand, both TD and α-TM have been found to be active against some varieties of fungi. In particular, α-TM displayed a greater activity than its aglycon against *Aspergillus nidulans*, *Fusarium moniliforme*, *Botrytis cinerea*, and other species. On the other hand, there are some varieties where TD seems to be more active. α-TM showed a strong anti-fungal activity against several pathogens, such as *Fusarium caereleum* (IC_{50} = 0.44 mM), and *Fusarium oxisporum* (IC_{50} = 40 µM). Moreover, the active ingredient inhibits also the spore germination of other fungal strains, such as *Paecilomyces Fumosoreus* (IC_{50} = 500 µM) and *Beauveria brassiana* (IC_{50} = 1 mM) (K McKEE, 1959; Poprawski et al., 2000).

Mechanistically, α-TM increases the membrane permeabilization by sequestering ergosterol. Ergosterol sequestration disrupts the membrane bilayer, ultimately causing leakage of cell components, osmotic stress, and the programmed cell-death process. Differently, TD is involved in the inhibition of ergosterol synthesis, by inhibiting the sterol methyltransferase enzyme Erg6 implicated in the transformation of zymosterol to fecosterol, in the presence of the cofactor S-adenosyl-L-methionine (SAM), converted into S-adenosyl-L-homocysteine (SAH), as shown in **Figure 10** (Sandrock et al., 1998). Moreover, α-TM can damage fungal pathogens *Fusarium* by increasing ROS production and leading to fungal programmed cell death (Ito et al., 2007).

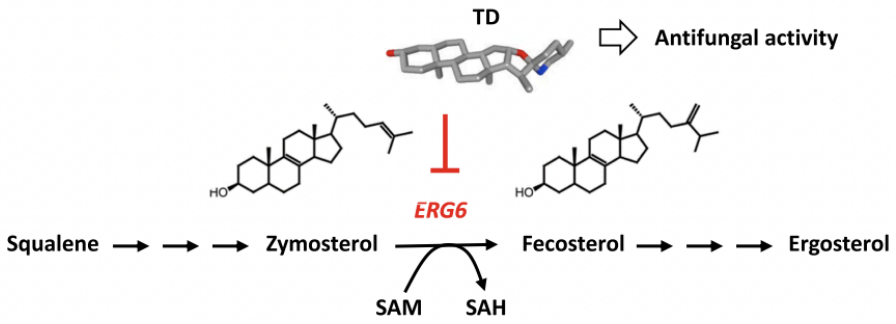


Figure 10: TD inhibition of ergosterol synthesis by the inhibition of ERG6 enzyme that transforms zymosterol into fecosterol (picture form Bailly (2021a)).

SGAs represent an important defense for the plant against pest agents. Therefore, it should not surprising that α-TM, together with other alkaloids extracted from Solonaceae, displays an insecticidal and antiparasitic activity against a variety of pests. They include *Schizaphis gramimum*, the red flour beetle *Tribolium castaneum* and the wasp *Hyposoter exiguae*, but also flower thrips and trypanosomatids (Bailly, 2021). Another *in vitro* study has demonstrated that α-TM can inhibit the flagellate growth of *T. Cruzi*. Both α-TM and TD have been demonstrated to be active against protozoa that infect humans such as *Trichomonas vaginalis* and *Thricomonas Foetus* (specific for animal farms), with an IC_{50} value in the micromolar range, representing a valid therapeutic alternative to metronidazole. α-TM is also effective against Chagas Disease caused by *Trypanosoma cruzi* parasites and has been shown to possess anti-ciliate activity (IC_{50} = 10.14 μM), and potent effects against *Philasterides dicentrarchi*, a scuticociliate colonizing farmed fishes (Sueiro et al., 2022).

Tomato plant SGAs can also exert antiviral activity. For example, α-TM can inactivate the herpes simplex virus (HSV) by perturbing the viral envelope, but its aglycone TD has no activity against this virus. However, TD has shown potent antiviral activity against different viruses, including the porcine epidemic diarrhea virus (PEDV), the Zike virus (ZIKV), the dengue virus (DENV), the chikungunya virus (CHIKV), probably by inhibiting the 3CL viral protease and upregulating ATF4 transcription factor, but the specific mechanism needs to be clarified (Bailly, 2021). A short summary of SGAs chemotherapic properties in summarized in **Table 2**.

2.4.3. Anti-inflammatory activity

Another important α-TM and TD health benefit includes the anti-inflammatory effects in LPS-stimulated macrophages, thanks to a decrease in the inducible nitric oxide synthase and cyclooxygenase-2 expression (Friedman, 2013). In particular, both compounds may block the NF-kB/JNK signaling pathway in macrophages stimulated by LPS. In this way, the phosphorylation with the consequent degradation of ikB and the nuclear translocation of NF-kB is inhibited. This causes the reduction in the transcription of inflammatory mediators, such as iNOS/NO and COX-2/ prostaglandin E2 (PGE2), and inflammatory cytokines such as TNF-α, IL-1, and IL-6 (B. Zhao et al., 2015). α-TM and TD anti-inflammatory effects are summarized in **Figure 11**. Some authors reported anti-inflammatory activities of unripe

tomatoes extracts. For example, extracts obtained from locular gel and serum of *Lycopersicum esculentum* L. var. "Camone" (55 µg α-TM/kg dried extract) significantly reduce inflammation by decreasing blood inflammatory cytokines count, heart rate, systolic pressure and aorta thickness (Marcolongo et al., 2020).

Furthermore, α-TM exhibits a powerful antihistaminic effect. In particular, α-TM intramuscular administration of 1-10 mg/kg (i.v.) or 15-30 mg/kg (p.o.) significantly reduces paw-induced edema in rats (Barbosa-Filho et al., n.d.). TD has been shown to exert anti-inflammatory activity also in lung tissues where, by modulating cytokine expressions in bronchoalveolar lavage fluid, attenuates neutrophil infiltration, increases superoxide dismutase activity and glutathione levels while reducing myeloperoxidase expression. Finally, in a rat model of osteoarthritis, TD inhibits the expression of IL-1β-induced metalloproteinases, the degradation of aggrecan and collagen-II, thus ameliorating the inflammatory condition of the animals (Barbosa-Filho et al., n.d.). In addition, TD suppresses NF-κB activation with a dose dependent manner and by inhibiting IkB-α degradation in a model of LPS-stimulated RAW 264.7 macrophages (Chiu & Lin, 2008).

A short summary of SGAs anti-inflammatory properties in summarized in **Table 2**.

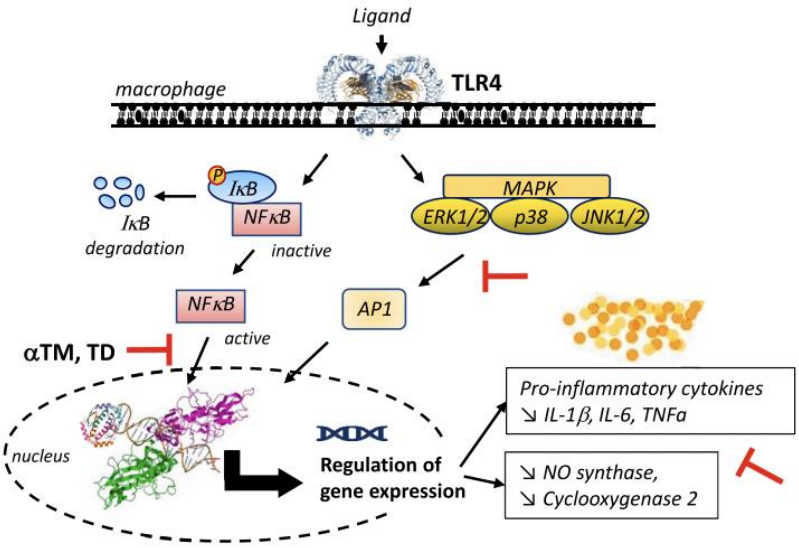


Figure 11: Molecular pathways and targets involved in α-TM and TD anti-inflammatory activity (picture from Bailly (2021a)).

2.4.4. Anti-aging activity

Interestingly, the great benefits against musculoskeletal disorders are shown only by the compound TD, while α-TM seems to be inactive. TD beneficial effect against skeletal muscle weakness and atrophy has been investigated in some recent studies. TD can inhibit age-related skeletal muscle atrophy in mice through mTORC1 activation, which leads to the stimulation of anabolic processes, the promotion of skeletal muscle hypertrophy and the associated loss of fat, as demonstrated in animal models of aging (Dyle et al., 2014). TD can also reduce the expression of activating transcription factor 4 (ATF4), a regulator with a key role in age-related muscle atrophy, whose upregulation is caused by several factors, such as the pro-inflammatory cytokine TNF-α (Adams et al., 2017). In addition, using an animal model of aging (the worm *Caenorhabditis elegans*) it was found that TD can activate the SNK-1/Nrf2 pathway, a classical antioxidant response involved in the induction of mitochondrial biogenesis. Moreover, TD can reduce osteoclast formation/differentiation and osteoclastic bone resorption, by a mechanism that has not been fully elucidated, but that probably involves modulation of p53 and MAPK signaling pathways (Bailly, 2021). A diet supplementation with unripe tomatoes extracts from "Korean Chal tomato" (1.06 ± 0.11 mg of TD/100 g dry extract) improves bone mineral density and overall bone quality in a model of post-menopausal osteoporosis of ovariectomizes rats (Nirmala et al., 2020). Moreover, the consumption of fresh tomatoes and tomato products in the Japanese population has been associated with a reduced decline in muscle strength, thanks to the protective action against the decline in skeletal muscle and the downregulation of the inflammatory and oxidative stress associated with aging (Bailly, 2021). A short summary of SGAs anti-aging properties in summarized in **Table 2**.

2.4.5. Neuroprotective activity

Regarding the neuroprotective action, displayed both by α-TM and TD, it was found a modest neuroprotective effect against glutamate-induced toxicity in SH-SY5Y neuroblastoma cells *in vitro*. In particular, α-TM can attenuate the cytotoxic effect of hydrogen peroxide (H_2O_2) in SH-SY5Y cells, with a dose-dependent effect, restoring the activity of superoxide dismutase and the level of the antioxidant compound GSH. In addition, this compound exhibits anti-acetylcholinesterase and anti-butyrylcholinesterase activities, making it eligible for the treatment of neurodegenerative diseases, such as

Alzheimer's disease (Bailly, 2021). However, α-TM seems to be cytotoxic at higher concentrations (1-4 μM), causing damage to the cell membrane, till the entire disruption of plasma membrane integrity at a concentration of 10 μM, while the aglycone TD is safer because it doesn't display these toxic effects. Recent studies have demonstrated that TD at a concentration in a range of 1-10 μM can protect mouse neuroblastoma N2A cells and primary cultured mice cortical neurons from the damages caused by the ischemic injury, in particular from the oxygen-glucose deprivation followed by reperfusion (Bailly, 2021).

A short summary of SGAs neuroprotective properties in summarized in **Table 2**.

2.4.6. Cardioprotective and anti-obesity activity

In addition to the ability to lower blood cholesterol levels shown by α-TM, TD may also have a cardioprotective and anti-obesity effect. This compound reduces the formation and accumulation of cholesterol induced by acetylated-LDL in human monocyte-derived macrophages. In addition, TD was found to reduce levels of serum cholesterol, LDL-cholesterol, and atherosclerotic lesions in a mice model. Mechanistically, TD regulates the sirtuin 1 (sirt1)/AMPK signaling pathway, in particular by acting as an agonist for vitamin D receptor and inducing an AMPK-dependent suppression of lipid accumulation, increasing lipolysis and β-oxidation in fatty liver cells (Bailly, 2021).

A short summary of SGAs cardioprotective and anti-obesity properties in summarized in **Table 2**.

Activity	Models	Extracts/pure molecule	EC_{50}
Antimicrobial	Escherichia Coli K12	Green leaves extract	10% w/V
	Salmonella enterica	Green leaves extract	10% w/V
	Beauveria brassiana	α-TM	1 mg/mL
	Fusarium caereleum	α-TM	460 mg/mL
	Paecilomyces Fumosoreus	α-TM	0.5 mg/mL
	Trichomonas Vaginalis	α-TM	<1 μM range
	Trichomonas Foetus	α-TM	< 1 μM range
	Trypansoma cruzi	α-TM	10.14 μM
Anti-inflammatory	*In vivo* rat models	Locular gel and serum extract of *Lycopersicum esculentum* L. var. "Camone"	55 μg/kg in α-TM
	In vivo rabbit models	Dried green tomatoes extract	
	In vivo rat models	α-TM	1-10 mg/kg (i.v.)
	In vivo rat models	TD	
	In vitro coltures of murine macrophages	α-TM	
Anti-aging	*In vivo* rat models	Green tomatoes extract	1 mg/100g in TD
	In vitro primary cultures from rat models	TD	
	In vitro coltures of neuronal cells	Leaves of green tomatoes (*Solanum Licopersicum* "Cherry") extract	640 μg/mL
	In vitro coltures of neuronal cells	Leaves of green tomatoes (Solanum Licopersicum "Bull's heart") extract	402 μg/mL
	In vivo mouse model	TD	
Antitumoral	*In vitro* breast cancer cell	Green tomatoes extract (5,75 - 31,40 mg of α-TM/100 g of extract)	18.7 μg/mL
	In vitro colon cancer. cell	Green tomatoes extract (5,75 - 31,40 mg of α-TM/100 g of extract)	5.4 μg/mL
	In vitro liver cancer cell	Green tomatoes extract (5,75 - 31,40 mg of α-TM/100 g of extract)	12.3 μg/mL
	In vitro stomach cancer cells	Green tomatoes extract (5,75 - 31,40 mg of α-TM/100 g of extract)	11.4 μg/mL
	In vitro Hepatocarcinoma cell lines	α-TM	1 μM
	In vitro Hepatocarcinoma cells	α-TM	30 μM
	In vitro lung cancer cells	α-TM	
	In vitro human breast cancer cells	α-TM	
	In vitro not-small lung cancer cells	α-TM	
	In vitro prostate cancer cells	α-TM	
	In vitro melanoma cells	Mixture of α-TM and dehydrotomatine	87.1 ± 1.6% 13.0 ± 0.8%
	In vitro leukemic cell lines	α-TM	

Table 2. Summary of the biological effects of *Solanum lycopersicum* L. extracts, α-TM and TD.

2.4.7. α-tomatine and green tomato extract: toxicological aspects

Tomatoes and tomato extracts, including those with high levels of α-TM, are typically consumed without any harmful effects (Friedman, 2002). For instance, Peruvian populations have a tradition of consuming a tomato variant (var. cerasiforme) that is particularly rich in α-TM (0.5–5 mg/g dry weight), and there have been no reports of toxicity associated with this practice (Rick et al., 1994). However, it's important to note that the excessive SGAs consumption, including α-TM, can have adverse effects on the human body, leading to a range of side effects such as low blood pressure, gastrointestinal and neurological issues, and even coma. Among SGAs, α-TM exhibits moderate toxicity. Harmful effects can become apparent at doses ranging from 2 to 5 mg/kg/day of SGAs, which could be reached either by using pure SGAs or as a result of massive daily consumption of green tomatoes (Nepal & Stine, 2019; Yamashoji & Onoda, 2016). In mice studies, oral administration of α-TM standard had an LD_{50} (lethal dose for 50% of population) of 500 mg/kg body weight (Schrenk et al., 2020). Intravenous administration resulted in an LD_{50} of 18 mg/kg body weight and caused symptoms such as low blood pressure, changes in respiratory rate, and impacts on red blood cells (Schrenk et al., 2020). When administered subcutaneously in mice, the LD_{50} of α-TM was greater than 1000 mg/kg body weight (Schrenk et al., 2020). However, via intraperitoneal administration, the LD_{50} of α-TM was in the range of 25-33 mg/kg body weight, which led to reduced urine output in rats, along with changes in the Na^+/K^+ serum ratio and increases in neutrophils and corticosteroids (Friedman, 2002). Interestingly, topical application of α-TM appears to be not-toxic. An ointment containing 5% α-TM, when applied to the skin of rabbits and rats, did not result in erythema (skin redness) and had no significant impact on hemoglobin or red blood cell counts. However, when applied topically to the eye, this ointment caused conjunctivitis with an inflammation of the conjunctiva (Wilson et al., 1961).

CHAPTER 3

PHYTOCHEMICAL INVESTIGATION OF UNRIPE TOMATO CULTIVARS

3.1. Introduction of the project

The first point to be considered in the development of a nutraceutical formulation is the selection of the matrix under investigation. With the aim of developing a potentially useful nutraceutical for the prevention of sarcopenia, attention was turned to the green tomato. As reported in the paragraph **2.4.4. Anti-aging activity**, the aglycone TD isolated in the plant of *Solanum lycopersicum* L. showed anti-aging activity that could be useful for the prevention of sarcopenia. Therefore, the first step was to analyse different cultivars of green tomatoes to identify those with the highest α-TM content for further pharmacological investigation. The analysis was performed using both green tomatoes obtained as waste subproduct during mature fruits harvesting and green tomatoes for food consumption. The analysis on the green tomatoes produced as agrifood waste represent an appealing research topic for the possibility to recover a by-product for a pharmaceutical and a nutraceutical application (Madia et al., 2021). The results of this screening were published as a scientific research article entitled "Phytochemical investigation and antioxidant properties of unripe tomato cultivars (*Solanum lycopersicum* L.)" in the international journal Food Chemistry (Piccolo et al., 2023).

In this context, the goals of the first part of the thesis are as follows:

1) To analyze the SGAs and polyphenols composition by agrifood waste green tomatoes from different Italians cultivars;
2) To provide a complete qualitative and quantitative profile of the phytochemicals in unripe tomatoes used for human consumptions;
3) To assess whether agrifood waste green tomatoes display a different metabolomic profiles than green tomatoes for human consumptions;
4) Investigate the relationship between the antioxidant properties and the polyphenols content in green tomatoes.

3.2. Materials and Methods

3.2.1. Reagents

All chemicals, reagents, and standards used were of analytical or LC-MS grade reagents. The water was treated in a Milli-Q water purification system (Millipore, Bedford, MA, USA) before use. Gallic acid (purity ≥ 98% HPLC), procyanidin B1 (purity ≥ 90% HPLC), procyanidin B2 (purity ≥ 90% HPLC), procyanidin B3 (purity ≥ 95% HPLC), procyanidin C1 (purity ≥ 90% HPLC), catechin (purity ≥ 98% HPLC), chlorogenic acid (purity ≥ 95% HPLC), neochlorogenic acid (purity ≥ 98% HPLC), caffeic acid (purity ≥ 98% HPLC), vanillic acid (purity ≥ 97% HPLC), syringic acid (purity ≥ 98% HPLC), *p*-coumaric acid (purity ≥ 98% HPLC), epicatechin (purity ≥ 98% HPLC), rutin (purity ≥ 94% HPLC), naringenin (purity ≥ 95% HPLC), quercetin 3-*O*-glucoside (purity ≥ 98% HPLC), and quercetin (purity ≥ 98% HPLC) were purchased from Sigma-Aldrich (Milan, Italy). α-TM (purity ≥ 95% HPLC) was obtained from Phytolab (Vestenbergsgreuth, Germany).

3.2.2. Cultivars selection and extraction

Seven tomato cultivars have been selected and used for the proposed study. The samples have been selected between the vegetal matrices considered as a waste in the processing being in their unripe growth stage and analysed. Green tomatoes (GT) were collected at fruit thinning stage from local farmers in Campania and Sicilia Regions (Italy). Avellino tomatoes (AT) were harvested by a local farmer (Montemarano, Avellino, Italy, 40°54'58"32 N - 14°59'54"60 E) in March 2021. The varieties “Cuore di Bue” (CT) and “Sorrento” tomatoes (ST) were harvested by a local farmer (Positano, Salerno, Italy, 40°37’40’’N – 14°28’55’’E) in August 2021. Agro-food waste “Tondi” tomatoes (TT) and “Datterini” (DT) tomatoes were harvested by a local farmer (Licata, Sicily, 37°6'29"52 N) in March 2021. The genotype of unripe E42 tomatoes (ET) were harvested by a local farmer (Acerra, Napoli, Italy, 40°96′52″ N, 14°42′86″ E, 13°56'48"84 E) in May 2021. Agri-food waste “San Marzano” tomatoes (MT) were harvested by a local farmer (Acerra, Naples, Italy, 40°96′52″ N, 14°42′86″ E) in July 2021. AT, CT, ST were green tomatoes used for human consumption while TT, DT, ET and MT were produced as agri-food wastes during mature tomatoes harvesting.

As a first step, tomatoes were cut, frozen at -80 °C, lyophilized, and stored in 15 ml plastic tubes at -20 °C until use. The extraction process was performed as follows: 1.5 g of lyophilized sample were homogenized with 10 ml of 80% aqueous methanol containing 1% formic acid, treated with a vortex mixer for 1 min, and sonicated (Branson Fisher Scientific 150E Sonic Dismembrator) for 10 min. After centrifugation for 10 min at 9000 rpm, the supernatant was transferred into another plastic tube. The pellet was re-extracted with 5 ml of the extraction mixture as previously reported. The supernatants were combined, filtered with a 0.22 µm nylon filter (CellTreat, Shirley, MA), and stored at -20 °C until analysis. Hydroalcoholic extracts were used for the analysis of SGAs and polyphenols content and the antioxidant assays. A purification protocol for qualitative analysis was performed using a SPE C_{18}, as described by Caprioli et al. (2014a) with slight modifications. 10 ml of the supernatant was evaporated and reconstituted with 10 ml of water. The SPE tube was conditioned with methanol (5 ml) followed by water (5 ml). Samples were loaded on each cartridge using a vacuum pump, washed with water (5 ml), and eluted using methanol (10 ml). The eluted solution was evaporated to dryness under a gentle stream of nitrogen, reconstituted in 50% methanol (*v/v*), filtered with a 0.22 µm nylon filter, and stored at -20°C until analysis.

3.2.3. Qualitative glycoalkaloids analysis

A HPLC DIONEX UltiMate 3000 (Thermo Fisher Scientific, Waltam, MA, USA) equipment, coupled with an autosampler, a binary solvent pump, and a LTQ XL mass spectrometer (Thermo Fisher Scientific, Waltam, MA, USA), was used for the analysis. The chromatographic analysis was performed according to the method proposed by Caprioli et al. (2014a), with slight modifications. Elution was performed on a Kinetex® C18 column (75 mm × 2.1 mm, 2.6 µm; Phenomenex, Torrance, CA, USA). The mobile phases were water at 0.01% formic acid (A) and methanol at 0.01% formic acid (B). After 2 min hold at 20% solvent B, elution was performed with a linear gradient to 95% solvent B in 10 min, then the column was equilibrated to the initial conditions for the remaining 4 min. The separation conditions were as follows: column temperature was set at 30°C, inject volume was 10 µl, and the flow rate was set at 0.35 ml/min. The source was a heated electrospray interface (HESI), operated in positive ionization with multiple scanning modes. Full scan (FS) and data dependent acquisition (DDA) were used for the qualitative analysis. Collision-induced fragmentation was made using argon, with a collision energy of 35 eV. α-TM identification was based on external standard addition to the samples. The ion source was set using the

following parameters: sheath gas flow rate: 35 l/min; auxiliary gas flow rate: 5 l/min; capillary temperature: 320 °C; source heated temperature: 200 °C; source voltage: 3.5 kV; source current: 100 µA; capillary voltage: 49 V; tube lens: 205 V. The separation conditions and the source parameters are summarized in the **Tables 3** and **4**, respectively.

Time (min)	% B
0	20
2	20
12	95
12.1	20
16	20

Table 3. Summary of the gradient condition of the HPLC-HESI-MS/MS qualitative SGAs method.

Column	Kinetex® C18 column (75 mm x 2.1 mm; 2.6 µm)
Phase A	Water at 0.01% HCOOH
Phase B	Methanol at 0.01% HCOOH
Column Temperature	30 °C
Injection volume	10 µl
Flow rate	0.35 ml/min
Collision Energy	35 eV
Sheath gas flow rate	35 l/min
Auxiliary gas flow rate	5 l/min
Capillary temperature	320 °C
Source heated temperature	200 °C
Source voltage	3.5 kV
Source current	100 µA
Capillary voltage	49 V
Tube lens	205 V

Table 4. Summary of the chromatographic and source parameters of the HPLC-HESI-MS/MS qualitative SGAs method.

3.2.4. Quantitative glycoalkaloids analysis

A HPLC Agilent 1200, coupled with an Agilent Technologies 6470-triple quadrupole mass spectrometer (Agilent Technologies, Palo Alto, CA, USA), was used for the analysis. The separation was performed adopting the same chromatographic condition described in **Section 3.2.3. Qualitative SGAs analysis** and in **Table 3**. The source was a heated electrospray interface (HESI) operated in positive ionization with a multiple reaction monitoring (MRM) scanning mode. One MRM transition was used as a quantifier transition and a second MRM transition served as a qualifier transition. The first transition (1034.4 – 1034.4) was made with a collision energy of 10 eV, while the second transition (1034.4 – 416.2) was performed with a collision energy of 40 eV. Argon was used as gas for collision-induced fragmentation. The MRM and the source parameters were optimized using an α-TM methanolic solution at the concentration of 1 ppm, which is the only commercial analytical standard available. α-TM was quantified according to a calibration curve ($R_2 \geq 0.99$) made with eight different concentrations prepared in a hydroalcoholic solution at the 50% of methanol in a range of 1.5 ppm – 0.001 ppm and triplicate injections at each concentration. α-TM stock solution was prepared as a methanolic solution a concentration of 1 mg/ml. Secondary SGAs quantification was based on α-TM calibration curve. The ion source was set using the following parameters: gas flow rate: 8 l/min; gas temperature: 300°C; sheath gas flow rate: 12 l/min; gas temperature: 400°C; nebulizer pressure: 35 psi; capillary voltage: 3500 V; nozzle voltage: 500 V. The source parameters are summarized in the **Tables 5**.

Column	Kinetex® C18 column (75 mm x 2.1 mm; 2.6 µm)
Phase A	Water at 0.01% HCOOH
Phase B	Methanol at 0.01% HCOOH
Column Temperature	30 °C
Injection volume	10 µl
Flow rate	0.35 ml/min
Collision energy transition quantifier	10 eV
Collision energy transition qualifier	40 eV
Gas flow rate	8 ml/min
Gas temperature	300 °C
Sheath gas flow rate	12 l/min
Gas temperature	400 °C
Nebulizer pressure	35 psi
Capillary voltage	3500 V
Nozzle voltage	500 V

Table 5. Summary of the chromatographic and source parameters of the HPLC-HESI-MS/MS quantitative SGAs method.

3.2.5. Qualitative polyphenols analysis

A HPLC DIONEX UltiMate 3000 (Thermo Fisher Scientific, Walton, MA, USA) equipment, coupled with an autosampler, a binary solvent pump, and an LTQ XL mass spectrometer (Thermo Fisher Scientific, Walton, MA, USA), was used for the analysis. The chromatographic analysis was performed according to the method proposed by Maisto et al. (2022a), with slight modifications. Elution was performed on a Kinetex® C18 column (250 mm × 4.6 mm, 5 µm; Phenomenex, Torrance, CA, USA). The mobile phases were: water with 2% formic acid (A) and 0.5% formic acid in acetonitrile and water 50:50, *v/v*. The elution gradient was performed according to the following conditions: 0-2, isocratic on 10% phase B; 2-52, linear gradient from 10 to 55% B; 52-62, linear gradient from 55 to 95% B; 62-70, isocratic on 10% B for column recondition. The separation parameters were as follows: column temperature was set at 30 °C, injected volume was 10 µl, and the flow rate was set at 1 ml/min. The source was a heated electrospray interface (HESI), operated in

negative ionization with full scanning (FS) and data dependent acquisition (DDA). Collision-induced fragmentation was made using argon gas, with a collision energy of 35.0 eV. The ion source was set using the following parameters: sheath gas flow rate: 30 ml/min; auxiliary gas flow rate: 10 ml/min; capillary temperature: 320 °C; source heated temperature: 150 °C; source voltage: 3 kV; source current: 3.20 µA; capillary voltage: -20 V; tube lens: -106.40 V. The separation conditions and the source parameters are summarized in the **Tables 6** and **7**, respectively.

Time (min)	% B
0	10
2	10
52	55
62	95
62.1	10
70	10

Table 6. Summary of the gradient condition of the HPLC-HESI-MS/MS qualitative polyphenols method.

Column	Kinetex® C18 column (250 mm x 4.6 mm; 5.0 µm)
Phase A	Water at 2% HCOOH
Phase B	Water/Acetonitrile (50:50 *v/v*) at 0.5% HCOOH
Column Temperature	30 °C
Injection volume	10 µl
Flow rate	1.00 ml/min
Collision Energy	35 eV
Sheath gas flow rate	30 l/min
Auxiliary gas flow rate	10 l/min
Capillary temperature	320 °C
Source heated temperature	150 °C
Source voltage	3.0 kV
Source current	3.20 µA
Capillary voltage	-20 V
Tube lens	-106.4 V

Table 7. Summary of the chromatographic and source parameters of the HPLC-HESI-MS/MS qualitative polyphenols method.

3.2.6. Quantitative polyphenols analysis

A HPLC Jasco Extrema LC-4000 system (Jasco Inc., Easton, MD, USA), coupled with an autosampler, a binary solvent pump, a diode-array detector (DAD), and a fluorometric detector (FLD) was used for the analysis. The chromatographic analysis was performed as previously described by (Maisto et al. (2022a). Phenolic acids, hydroxycinnamic acids, flavanols, and flavanones were monitored at 280 nm, while flavonols were monitored at 360 nm. Procyanidins were monitored by a fluorescence detector, using an excitation wavelength of 272 nm and an emission wavelength of 312 nm. Peak identifications were based on standard addition to the samples and were quantified according to a calibration curve ($R^2 \geq 0.99$) generated with six different concentrations prepared in a hydroalcoholic solution at the 50% of methanol in a range of 1000 ppm and 0.1 ppm and triplicate injections at each point. For procyanidin B1 and B2 the lower point of the concentration range was set at 0.5 ppm. Every polyphenol was analyzed by preparing a methanolic stock solution at a concentration

of 1 mg/ml. Quantification of quercetin-*O*-(pentosylrutinoside) and neochlorogenic acid was based on rutin and chlorogenic acid calibration curve, respectively.

3.2.7. Total phenolic content (TPC)

The Folin-Ciocalteau method was used to determine the total phenolic content (TPC). The assay was performed according to Maisto et al. (2022a), with slight modifications. Briefly, 0.125 ml of each sample hydroalcoholic extracts were diluted to the final volume of 3 ml by addition of 0.125 ml of Folin-Ciocalteau's reagent, 1.25 ml of an aqueous solution of Na_2CO_3 7.5 (*w/v*), and 1.5 ml of water. After mixing for 10 seconds, the samples were kept in the dark for 90 min. After the reaction time, the absorbance was measured at 760 nm with a V-730 UV-visible/NIR spectrophotometer operated by Spectra Manager™ Suite (Jasco Inc., Easton, MD, USA). Calibration curve was obtained using seven concentrations of gallic acid, in a concentration range from 7.5 to 250 ppm with a dilution factor of 4 and three replicates were performed at each concentration. Gallic acid stock solution was obtained by dissolving the analytical standard in methanol at a concentration of 1 mg/ml. The hydroalcoholic extracts were analysed in triplicate and the total phenolic content was calculated as mg gallic acid equivalents (GAE)/g dry weight (DW).

3.2.8. DPPH assay

The antioxidant activity of GE samples was measured using DPPH (radical 2,2-diphenyl-1-picrylhydrazyl) assay. The assay was performed according to (Iannuzzo et al., 2022), with slight modifications. Briefly, 200 µl of GT hydroalcoholic extracts were added to 1000 µl of a methanol solution of DPPH 0.05 mM. After mixing, the solutions were kept in the dark for 10 min. After the reaction period, a decrease in the absorbance was measured at 517 nm with a V-730 UV-visible/NIR spectrophotometer operated by Spectra Manager™ Suite (Jasco Inc., Easton, MD, USA). The absorbance of methanolic solution of DPPH radical without sample, e.g., the control, was used as blank. Inhibition was calculated according to the following equation:

$$\% \, \boldsymbol{inhibition} = \left[\frac{\left(\boldsymbol{A_i} - \boldsymbol{A_f}\right)}{\boldsymbol{A_c}}\right] \boldsymbol{x} \, \mathbf{100}$$

where Ai is the absorbance of the sample at time zero, Af is the absorbance after 10 min, and Ac is the absorbance of the control at time zero. 6-hydroxy-2,5,7,8-tetramethylchroman-2-carboxylic acid (Trolox) was used as antioxidant standard. Calibration curve was performed using eight concentrations, with a concentration range of 5 – 250 µM with two dilution factors of 2 and 5 and three replicates at each concentration. Trolox stock solution was obtained by dissolving the analytical standard in methanol at a concentration of 1 mM. Hydroalcoholic extracts were analysed in triplicate and the results were expressed in µmol Trolox equivalent (TE)/g DW.

3.2.9. ABTS assay

The antioxidant activity of GE samples was measured using ABTS (2,20-azinobis(3-ethylbenzotiazoline-6-sulfonate)] assay. The assay was performed according to (Maisto et al., 2023), with slight modifications. ABTS solution was prepared by adding 2.5 ml of ABTS 7.0 mM solution to 44 µl of potassium persulfate 140 mM solution, and kept 7 h, at 5°C in the dark to react. The mixture was diluted with ethanol until an absorbance value of 0.70 ± 0.05 at 754 nm (Jasco Inc., Easton, MD). 100 µl of GT hydroalcoholic extracts was added to 1000 µl of ABTS ethanolic solution. After mixing, the solutions were kept in the dark for 2.5 min. After the reaction period, a decrease in the absorbance was measured at 517 nm (Jasco Inc., Easton, MD, USA). The control ABTS ethanolic solution absorbance was used as blank. Inhibition was calculated according to the following equation:

$$\% \, \boldsymbol{inhibition} = \left[\frac{\left(\boldsymbol{A_i} - \boldsymbol{A_f}\right)}{\boldsymbol{A_c}}\right] \boldsymbol{x} \, \mathbf{100}$$

where Ai is the absorbance of the sample at time zero, Af is the absorbance after 10 min, and Ac is the absorbance of the control at time zero. Trolox was used as antioxidant standard. The calibration curve was performed with eight different concentrations, with a concentration range of 5 – 200 µM with two dilution factors of 2 and 5 and three replicates at each concentration. Trolox stock solution was obtained by dissolving the analytical

standard in methanol at a concentration of 1 mg/ml. GT hydroalcoholic extracts were analysed in triplicate and the results were expressed in µmol TE/g DW.

3.2.10. FRAP assay

Ferric reducing activity of GE samples was measured using the ferric reducing antioxidant power (FRAP) assay. The assay was performed according to the methods proposed by Schiano et al. (2022a). To prepare the FRAP reactive, a solution of 10 mM TPTZ (2,4,6-tris(2-pyridyl)-s-triazine) was prepared by dissolving 33.5 mg of the reagent in 10 ml of 40 mM HCl solution. FRAP working solution was prepared by mixing 1 ml of TPTZ solution with 10 ml of 0.3 M pH 3.6 acetate buffer and 1 ml of 20 mM ferric chloride solution. The mixture was pre-warmed at 37°C. 0.15 ml of GT hydroalcoholic extracts was added to 2.85 ml of FRAP working solution. After mixing, the solutions were incubated at 37°C for 4 min. After the reaction period, an increase in the absorbance was measured at 593 nm with a V-730 UV-visible/NIR spectrophotometer operated by Spectra Manager™ Suite (Jasco Inc., Easton, MD, USA). The absorbance of FRAP control solution without samples was used as blank and was subtracted from the absorbances of the samples. Trolox was used as antioxidant standard, and the results were expressed in µmol TE/g DW. Trolox calibration curve was performed with eight different concentrations, with a concentration range of 5 – 200 µM with two dilution factors of 2 and 5 and three replicates at each concentration. Trolox stock solution was obtained by dissolving the analytical standard in methanol at a concentration of 1 mg/ml.

3.2.11. Method validation according to ICH guidelines

Two HPLC analytical methods were validated for the SGAs and polyphenols quantitative analysis, respectively. The validations were performed according to the ICH validation guideline (ICH.Q2[R2], 2022). The first method was an HPLC-MS/MS analysis in positive mode acquisition for the quantification of α-TM while the second method was an HPLC-DAD-FLD analysis for the quantification of polyphenols. In the last method, eight polyphenols (catechin, epicatechin, procyanidins B1 and B2, gallic acid, chlorogenic acid, rutin, and quercetin) were selected for HPLC-DAD-FLD method development and validation. To assess these parameters, the calibration curves of the nine selected compounds were prepared in triplicate. In the methods validation process, we evaluated the

linearity, the limit of detection (LOD), the limit of quantification (LOQ), the accuracy, and the precision. LOD and LOQ were calculated using the following equations: LOD = 3.3 SD/S and LOQ = 10 SD/S, where SD is the standard deviation of the intercept of the regression line and S is the slope of the calibration curve. The accuracy of the methods was assessed as percentage bias while precision was evaluated through the percentage coefficient of variation (CV%). The intra-day precision and accuracy were assessed with three concentration levels in one day. The inter-day precision and accuracy were evaluated with three concentration levels over three consecutive days.

3.2.12. Statistical analysis

Quantitative analyses were carried out using the SPSS 27.0 software (IBM Corporation, NY, USA) by using one-way ANOVA followed by Tukey's post-hoc test. Significant differences were accepted at the 95% confidence level. All analyses were performed in triplicates. The principal component analysis (PCA), the heat map, and the hierarchical clustering map were performed using polyphenols and SGAs quantitative data. The Pearson correlation plot was obtained using polyphenols and SGAs quantitative data and antioxidant assays results. PCA, Pearson correlation coefficient, and Pearson correlation plot was generated using OriginPro 2021b (OriginLab Corporation, Northampton, MA, USA). Variables were normalized using an auto-scaling of data. Hierarchical clustering heatmap was performed based on the "ward" method and conducted using MetaboAnalystTM online software (https://www.metaboanalyst.ca/).

3.3. Results and discussion

3.3.1. Preparation of the matrix and extraction method

All vegetable matrices have been cut, frozen, lyophilized, reduced to powder by grinding, and finally stored in the dark, protected from light. According to the literature, it is possible to prevent the degradation of SGAs and polyphenols compounds by respecting these conditions of pre-treatment and storage. Lyophilization is a crucial step that allows the removal of water from the plant matrix and therefore the inactivation of all those enzymes that could modify the metabolic profile of the sample. The grinding step provides a powder, characterized by particles with a high surface area, thus increasing the solid-liquid contact volume and therefore the extraction speed and yield. Finally, by considering the presence of photosensitive compounds, such as polyphenols, it is necessary to store the samples in the dark, to maintain the profile and content of the starting metabolites over time. The extraction mixture was a hydroalcoholic solvent at 80% methanol and 1% formic acid, which provided a suitable extraction yield and solubility for both classes of compounds. To select a suitable extraction approach, a screening of 5 extraction protocols previously reported in literature for α-TM and polyphenols extraction was performed (Caprioli et al., 2014; Pardini et al., 2021; Silva-Beltrán et al., 2015; Tamasi et al., 2021). The screening was conducted on 3 unripe tomato varieties (e.g., AT, TT, DT). For the evaluation of polyphenols extraction, the FOLIN assay was used for the estimation of the total polyphenol content. The extraction protocols differed for the nature of extraction solvent (e.g., water, methanol, and ethanol), for the use and the nature of pH modifiers (e.g., formic acid, acetic acid), and for the contact time matrix/solvent in a range of 10 and 120 minutes. The results of the quantification are summarized in **Table 8**.

Extraction method	Extraction solvent	Extraction time	mg GAE/g DW			mg α-TM/g DW		
			AT	TT	DT	AT	TT	DT
1	EtOH/H_2O 80:20 *v/v* + 1% CH_3COOH	10 min	1.91 ± 0.13	1.71 ± 0.07	6.40 ± 0.56	2.38 ± 0.16	10.04 ± 0.22	28.24 ± 1.18
2	MeOH/H_2O 80:20 *v/v* + 1% HCOOH	10 min	1.86 ± 0.10	1.49 ± 0.04	6.74 ± 0.54	2.61 ± 0.42	11.05 ± 1.10	34.70 ± 1.36
3	MeOH	10 min	1.12 ± 0.13	0.92 ± 0.04	5.26 ± 0.03	1.87 ± 0.25	8.53 ± 1.03	19.19 ± 1.29
4	H_2O + 1% CH_3COOH	10 min	1.52 ± 0.14	0.95 ± 0.08	4.53 ± 0.03	2.03 ± 0.43	9.75 ± 0.58	24.14 ± 1.42
5	H_2O + 1% CH_3COOH	120 min	1.26 ± 0.07	1.20 ± 0.11	4.76 ± 0.20	2.31 ± 0.48	10.12 ± 0.75	28.12 ± 1.04

Table 8. Setup of the extraction methods used for α-TM and polyphenols extraction.

A difference in the use of aqueous solvents compared to alcoholic or hydroalcoholic solvents was observed, which confirmed the use of alcohols for α-TM and polyphenols quantification. In addition, the use of pH acid modifiers significantly improved α-TM extraction. As a matter of fact, methanol represents a good solvent that allows both polyphenols and SGAs to be solubilized, both as glycosylated and aglycone derivatives. It was preferred to ethanol, although it is a "food-grade" solvent suitable for the development of a nutraceutical product. However, methanol alone is insufficient for extracting purposes, thus requiring the use of a hydroalcoholic solution instead of the pure organic solvent. Moreover, both polyphenols and SGAs required the addition of acids to improve their solubility in the extracting solvent. In fact, SGAs are greatly more soluble in an acid-aqueous solution rather than in water, by considering their basic nature due to the presence of a nitrogen atom in the spirostanoic ring. For the same reason, they are not soluble in a basic aqueous solution. On the other hand, polyphenols greatly improve their solubility in the presence of an acidic aqueous solution, because they break the ester and ether bonds that keep them bound to other structural components of the plant cell, thus being released more easily. Therefore, the hydroalcoholic mixture was acidified to 1% with formic acid and used as extracting solvent. Unfortunately, this solvent does not provide a selective extraction of SGAs and polyphenols of interest, but it may also solubilize many other medium-high and high polarity compounds, including sugars, amino acids, fibers, and chlorophyll, depending on the anatomical part of the plant used for extraction. All these compounds represent interferents that may affect the HPLC-DAD and HPLC-MS/MS methods, thus increasing

the matrix effect in the analysis of both polyphenols and SGAs. The extraction procedure is already described in the previous paragraph **3.2.2. Cultivar selection and extraction**. As the first step, 10 ml of the hydroalcoholic solvent at the 80% of methanol was added to 1.5 g of the dried matrix, in order to ensure a good solvent-matrix contact. Then, the suspension was placed in an ultrasonic bath and sonicated for 10 minutes to enhance the extraction by the disruption of biological membranes of cells and organelles in which polyphenols and SGAs are stored. After sonication, the extraction procedure was carried out by putting the sample in an orbital shaker, which shook at a speed of 600 rpm for 10 minutes at room temperature, to provide a larger contact surface between the matrix and the extracting solvents. Then, samples were centrifuged at 9000 rpm for 10 minutes and at room temperature to separate supernatants, enriched by the first extraction cycle, from the pellets settled on the bottom due to centrifugal force. Therefore, supernatants have been collected and stored at 4 °C, protected from the light while pellets have been re-suspended with another 5 ml of extraction solvent to undergo a second cycle of extraction. This second cycle of extraction, using the same extraction procedure composed of sonication, shaking, and centrifugation, was performed to enhance the extraction yield from the matrix. The supernatants obtained after centrifugation of this second cycle of extraction have been added to the previous ones. These hydroalcoholic extracts were first evaporated at 37 °C with a rotavapor to remove the methanolic fraction of the extraction mixture solution. As a matter of fact, the hydroalcoholic solution used as an extracting solvent could not be directly frozen because of methanol's low melting point (-97.8 °C). After the methanolic part was removed by evaporation, the extracts derived from the hydroalcoholic extraction method were frozen and then freeze-dried. Once the freeze-drying procedure was completed and all the water was removed, the dried extracts were weighed up to a constant value to perform a proper difference in weight with tare masses. The extraction procedure was performed in triplicate for each sample. As shown in this procedure, all steps were carried out at room temperature, to preserve the compounds of interest from oxidation or hydrolysis reactions that could be enhanced under heating.

3.3.2. Chemical profile of green tomato extracts

The analysis of green tomato extracts by HPLC-HESI-MS/MS allowed to putatively identify 76 compounds by comparison with literature data. The qualitative screening was preliminary to the quantitative analysis to elucidate the chemical distinctive features of polyphenols and SGAs of green tomato cultivars of the current study. The retention time, the quasi-molecular ion, the molecular formula, and the fragment ions were listed in the **Tables 9** and **10**. These compounds include SGAs, polyphenols, phytohormones, organic acids, and oxylipins. SGAs chemical analysis is reported in **Table 9** while the characterization of the other compounds is reported in **Table 10**. The molecular identity of 18 compounds (numbered as: 13: α-TM; 21: gallic acid; 30: vanillic acid; 33: procyanidins B1+B3; 37: syringic acid; 38: catechin; 42 chlorogenic acid; 43: epicatechin; 46: caffeic acid; 53: *p*-coumaric acid; 55: neochlorogenic acid; 57: procyanidin B2; 59: procyanidin C1; 64: rutin; 67: quercetin 3-*O*-glucoside; 69: naringenin; 76: quercetin) was confirmed by comparison with analytical standards.

3.3.2.1. Glycoalkaloids profile of green tomatoes

SGAs are peculiar compounds of the genus *Solanum* which different pharmacological activities, previously described at the paragraph **2.4. Glycoalkaloids beneficial effects on human health** (Friedman, 2002, 2013; Roddick, 1989). Their tandem mass spectra display a prominent fragment ion due to the loss of water (-18 Da) and a characteristic fragmentation pattern due to the neutral losses of sugars of a tetrasaccharide moiety. Therefore, a diagnostic fragment for SGAs identification is represented by the aglycone ion. The two main aglycones of green tomato SGAs are represented by TD and dehydrotomatidine, with a molecular ion of *m/z* 416.5 and *m/z* 414.5, respectively. These ions represent the aglycon component of α-TM and dehydrotomatine, the most common SGAs identified in the green tomatoes, which differ for a double bond between C5 and C6 in the aglycon group. However, a different value for the aglycone fragment ion can be detected due to a different degree of substitution on steroid scaffold, classifying SGAs in different chemical groups. The most abundant compounds are represented by undecorated derivatives, as α-TM and dehydrotomatine. However, other important analogues include the acetoxytomatine, the glucosylated acetoxytomatine, and the hydroxytomatine, which differ in the substitution an acetoxy group, a sugar moiety, and a hydroxy group, respectively (Dzakovich et al., 2020). In these chemical moieties, the aglycone fragment ions were produced by the loss of the

tetrasaccharide group and the substituents of the steroid component, which include the neutral losses of water (-18 Da), acetic acid (-60 Da) and a sugar not directly linked to the tetrasaccharide. These fragmentations produce aglycone fragment ions with a molecular ion of *m/z* 414.5 and *m/z* 412.5, depending on the presence of a double bond on the sterol scaffold. The expression of tomato SGAs appeared to be influenced by fruit development. Indeed, in the first phases of fruit ripening, there is a greater expression of α-TM and its analogues. On the opposite, when the fruit is mature, there is a change in SGAs content, with a reduction of α-TM derivatives and an increase of esculeoside B and glucosylated-acetoxytomatine analogues (Dzakovich et al., 2020). In agreement with literature data, the HPLC-MS/MS analysis of the selected matrices showed the typical expression pattern of SGAs of the unripe tomatoes (Itkin et al., 2011), with a greater amount of undecorated derivatives than compounds functionalized on the sterol scaffold. In fact, SGAs fragmentation pattern allowed to identify 20 compounds, 17 of them have been previously reported in literature. Compounds **1** and **11** displayed a $[M+H]^+$ ion at *m/z* 1032 and the fragment ion at *m/z* 414 $[M+H\text{-}Pent\text{-}3Hex]^+$, suggesting the presence of dehydrotomatidine and lycotetraose as aglycone and sugar components, respectively. This fragmentation pattern allowed identifying the molecules as dehydrotomatine isomers, those were previously reported in GT extract (Itkin et al., 2011). Compound **2** showed a $[M+H]^+$ ion at *m/z* 916 and diagnostic fragment ions at *m/z* 430 $[M+H\text{-}3Hex]^+$ and *m/z* 412 $[M+H\text{-}3Hex\text{-}3H_2O]^+$. The fragment ion at *m/z* 430 referred to the dehydrotomatidine aglycone component for the loss of the hexoside trisaccharide moiety (-162 Da) while the ion at *m/z* 412 displayed the typical hydroxytomatine fragmentation pattern, with an additional neutral loss of water on the sterol scaffold. Therefore, this compound was identified as hydroxy-dehydrotomatidine trihexoside (Casarrubias-Castillo et al., 2020). Compound **3**, with a $[M+H]^+$ ion at *m/z* 918 and fragment ions at *m/z* 432 $[M+H\text{-}3Hex]^+$ and *m/z* 414 $[M+H\text{-}3Hex\text{-}3H_2O]^+$, was labelled as hydroxytomatidine trihexoside (Shinde et al., 2017). According to the similar structure, compounds **2** and **3** produced the same fragmentation pattern, which differed for the absence of the double bond in the aglycone group. Compound **4** displayed a $[M+H]^+$ ion at m/z 1050 was identified and two diagnostic fragment ions at *m/z* 918 $[M+H\text{-}Pent]^+$, which indicated the loss of a pentose group, and *m/z* 414 $[M+H\text{-}Pent\text{-}3Hex\text{-}H_2O]^+$, due to the loss of water and lycotetraose moieties. Based on this fragmentation pattern and the similarity with the fragmentation pattern of compound **3**, compound **4** was identified as hydroxytomatine, which was previously reported in GT extracts (Dzakovich et al., 2020). Compound **5** displayed a $[M+H]^+$ ion at *m/z* 1270 and was identified as a glucosylated acetoxytomatine

derivative, such as lycoperoside G/F or esculeoside A. It showed some diagnostic fragment ions at *m/z* 1210 $[M+H-AcOH]^+$, corresponding to the loss of an acetoxy group, and at *m/z* 412 $[M+H-Pent-4Hex-AcOH-H_2O]^+$, for the subsequent loss of the tetrasaccharide group (Dzakovich et al., 2020). Two acetoxydehydrotomatine isomers (compounds **7** and **20**) with a $[M+H]^+$ ion at *m/z* 1090 were detected. In the tandem spectra of these compounds, the fragment ions at *m/z* 1030 $[M+H-AcOH]^+$ and *m/z* 412 $[M+H-Pent-3Hex-AcOH]^+$ indicated the loss of an acetoxy group and the lycotetraose cleavage (Itkin et al., 2011). The mass spectrum of the analyte **9** showed a $[M+H]^+$ ion at *m/z* 1108 and a product ion at *m/z* 412 $[M+H-Pent-3Hex-H_2O-AcOH]^+$, which represented the aglycone scaffold ion for the simultaneous elimination of the acetoxy and hydroxy groups and the tetrasaccharide moiety. In agreement with literature data (Itkin et al., 2011), compound **9** was identified as acetoxyhydroxytomatine. Tomatidine tetrahexoside (**12**) displayed a $[M+H]^+$ ion at *m/z* 1064 and three product ions at *m/z* 902 $[M+H-Hex]^+$, *m/z* 740 $[M+H-2Hex]^+$, and *m/z* 416 $[M+H-4Hex]^+$, due to the hexoside tetrasaccharide cleavage (Itkin et al., 2011). Compounds **13** and **15** showed a $[M+H]^+$ ion at *m/z* 1034 and three diagnostic fragment ions at *m/z* 902 $[M+H-Xyl]^+$, *m/z* 740 $[M+H-Xyl-Glu]^+$, *m/z* 578 $[M+H-Xyl-2Glu]^+$, and *m/z* 416 $[M+H-Pent-3Hex]^+$. These fragmentation patterns indicated the presence of TD and lycotetraose as aglycone and sugar components, respectively. Therefore, these compounds were identified as α-TM and as a putative regioisomer (Caprioli et al., 2014). α-TM identity was confirmed by the comparison with the analytical external standard. α-TM represents the main SGA of unripe tomatoes and the only one on which extensive pharmacological studies have been carried out. α-TM isomer can't be unequivocal identified due to the absence of significative differences in the fragmentation pattern. However, based on the retention time difference and the literature data, compound **15** could be represented by filotomatine (Cataldi et al., 2005). Compound **14** showed a $[M+H]^+$ ion at *m/z* 1092 and diagnostic ions at *m/z* 1032 $[M+H-AcOH]^+$, due to the loss of an acetoxy group, and *m/z* 414 $[M+H-Pent-3Hex-AcOH]^+$, which indicated the lycotetraose cleavage. Therefore, this compound was identified as acetoxytomatine (Itkin et al., 2011). Compound **16** produced a $[M+H]^+$ ion at *m/z* 1062 and a diagnostic fragment at *m/z* 414 $[M+H-4Hex]^+$. Compounds **12** and **16** displayed the same fragmentation pattern and a difference of 2 Da for the aglycone ion moiety, which corresponded to a single double bond. Therefore, this was identified as dehydrotomatidine tetrahexoside (Itkin et al., 2011). Compound **17** showed a $[M+H]^+$ ion at *m/z* 1048 and a fragment ion at *m/z* 412 $[M+H-Pent-3Hex-H_2O]^+$. The similarity with the fragmentation of compound **4** suggested the presence of hydroxy-dehydrotomatine, in

according to literature data (Casarrubias-Castillo et al., 2020). Several unknown SGAs have been detected (**8**, **10**, **18, 19**): these compounds showed the typical fragmentation pattern of know SGAs and diagnostic fragment ions of the aglycone component with *m/z* 416, *m/z* 414, *m/z* 412, and *m/z* 410. Compound **8**, which was previously reported by (Itkin et al., 2011) produced a $[M+H]^+$ ion at *m/z* 1046 and fragment ions at *m/z* 914 $[M+H\text{-}Pent]^+$, corresponding to the loss of a pentose group, and *m/z* 410 $[M+H\text{-}Pent\text{-}3Hex\text{-}H_2O]^+$, which indicated the loss of water and a lycotetraose cleavage. This aglycone component agreed with solaspiralidine, a compound previously reported in Solanum species (Ripperger, 1996). Compounds **10**, **18** and **19**, which have never been reported in literature to our knowledge, were three acetoxytomatine derivatives, as suggested by the neutral loss of an acetoxy group. Compound **10** and **18** showed a $[M+H]^+$ ion at *m/z* 1132 and *m/z* 1120, respectively, and a fragment at *m/z* 414 $[Agl+H]^+$, that was referred to dehydrotomatidine aglycone for the elimination of acetoxy moiety. Instead, compound **19** showed a $[M+H]^+$ ion at *m/z* 1132 and a fragment at *m/z* 416 $[Agl+H]^+$, that represented TD aglycone component. This data suggested that the acetoxy group is bound at sugar group instead the most common acetoxytomatine derivative.

No.	Putatively compound	R_t	Precursor ion $[M+H]^+$	Characteristic fragment ions
1	Dehydrotomatine isomer 1	6.83	1032.62	1014.55 $[M+H\text{-}H_2O]^+$, 900.64 $[M+H\text{-}Pent]^+$, 870.56 $[M+H\text{-}Hex]^+$, 576.54 $[M+H\text{-}Pent\text{-}2Hex]^+$, 414.38 $[M+H\text{-}Pent\text{-}3Hex]^+$
2	Hydroxy-dehydrotomatidine trihexoside	7.12	916.76	898.49 $[M+H\text{-}H_2O]^+$, 754.49 $[M+H\text{-}Hex]^+$, 592.34 $[M+H\text{-}2Hex]^+$, 430.45 $[M+H\text{-}3Hex]^+$, 412.51 $[M+H\text{-}3Hex\text{-}H_2O]^+$
3	Hydroxytomatidine trihexoside	7.27	918.67	900.56 $[M+H\text{-}H_2O]^+$, 756.57 $[M+H\text{-}Hex]^+$, 594.59 $[M+H\text{-}2Hex]^+$, 432.44 $[M+H\text{-}3Hex]^+$, 414.50 $[M+H\text{-}3Hex\text{-}H_2O]^+$
4	Hydroxytomatine	7.48	1050.60	1032.57 $[M+H\text{-}H_2O]^+$, 918.71 $[M+H\text{-}Pent]^+$, 756.60 $[M+H\text{-}Pent\text{-}Hex]^+$, 576.48 $[M+H\text{-}Pent\text{-}2Hex\text{-}H_2O]^+$, 414.50 $[M+H\text{-}Pent\text{-}3Hex\text{-}H_2O]^+$
5	Lycoperoside G/F or esculeoside A	7.51	1270.75	1210.64 $[M+H\text{-}AcOH]^+$, 1048.62 $[M+H\text{-}Hex\text{-}AcOH]^+$, 754.54 $[M+H\text{-}Pent\text{-}2Hex\text{-}AcOH]^+$, 592.93 $[M+H\text{-}Pent\text{-}3Hex\text{-}AcOH]^+$, 412.51 $[M+H\text{-}Pent\text{-}4Hex\text{-}AcOH\text{-}H_2O]^+$
6	Unknown SGA	7.64	1044.68	1026.62 $[M+H\text{-}H_2O]^+$, 912.61 $[M+H\text{-}Pent]^+$, 750.44 $[M+H\text{-}Pent\text{-}Hex]^+$, 588.40 $[M+H\text{-}Pent\text{-}2Hex]^+$, 408.35 $[M+H\text{-}Pent\text{-}3Hex\text{-}H_2O]^+$

7	Acetoxydehydrotomatine isomer 1	7.68	1090.61	1030.57 $[M+H-AcOH]^+$, 958.61 $[M+H-Pent]^+$, 616.57 $[M+H-Pent-2Hex-H_2O]^+$, 574.39 $[M+H-Pent-2Hex-AcOH]^+$, 412.54 $[M+H-Pent-3Hex-AcOH]^+$
8	Unknown SGA	7.74	1046.66	1028.67 $[M+H-H_2O]^+$, 1017.58 $[M+H-CH_3N]^+$, 914.58 $[M+H-Pent]^+$, 572.51 $[M+H-Pent-2Hex-H_2O]^+$, 410.46 $[M+H-Pent-3Hex-H_2O]^+$
9	Acetoxyhydroxytomatine	7.87	1108.54	1048.57 $[M+H-AcOH]^+$, 1030.62 $[M+H-H_2O-AcOH]^+$, 1001.65 $[M+H-H_2O-AcOH-CH_3N]^+$, 652.64 $[M+H-Pent-2Hex]^+$, 412.43 $[M+H-Pent-3Hex-H_2O-AcOH]^+$
10	Unknown SGA	7.98	1132.72	1114.58 $[M+H-H_2O]^+$, 1072.58 $[M+H-AcOH]^+$, 910.62 $[M+H-Hex-AcOH]^+$, 778.56 $[M+H-Pent-Hex-AcOH]^+$, 414.47 $[Agl+H]^+$
11	Dehydrotomatine isomer 2	8.31	1032.54	1014.61 $[M+H-H_2O]^+$, 900.61 $[M+H-Pent]^+$, 738.55 $[M+H-Pent-Hex]^+$, 576.53 $[M+H-Pent-2Hex]^+$, 414.46 $[M+H-Pent-3Hex]^+$
12	Tomatidine tetrahexoside	8.38	1064.70	1046.63 $[M+H-H_2O]^+$, 902.66 $[M+H-Hex]^+$, 740.65 $[M+H-2Hex]^+$, 578.41 $[M+H-3Hex]^+$, 416.37 $[M+H-4Hex]^+$
13	α-Tomatine*	8.47	1034.46	1016.61 $[M+H-H_2O]^+$, 902.51 $[M+H-Xyl]^+$, 740.58 $[M+H-Xyl-Glu]^+$,578.66 $[M+H-Xyl-2Glu]^+$, 416.46 $[M+H-Xyl-2Glu-Gal]^+$
14	Acetoxytomatine	8.69	1092.63	1032.58 $[M+H-AcOH]^+$, 900.64 $[M+H-Pent-AcOH]^+$, 738.67 $[M+H-Pent-Hex-AcOH]^+$, 576.63 $[M+H-Pent-2Hex-AcOH]^+$, 414.53 $[M+H-Pent-3Hex-AcOH]^+$
15	Filotomatine	8.82	1034.77	1016.61 $[M+H-H_2O]^+$, 902.56 $[M+H-Pent]^+$, 740.54 $[M+H-Pent-Hex]^+$, 578.60 $[M+H-Pent-2Hex]^+$, 416.46 $[M+H-Pent-3Hex]^+$
16	Dehydrotomatidine tetrahexoside	8.90	1062.62	1044.54 $[M+H-H_2O]^+$, 900.56 $[M+H-Hex]^+$, 738.66 $[M+H-2Hex]^+$,576.56 $[M+H-3Hex]^+$, 414.41 $[M+H-4Hex]^+$
17	Hydroxy-dehydrotomatine	8.97	1048.74	1030.65 $[M+H-H_2O]^+$, 916.74 $[M+H-Pent]^+$, 724.64 $[M+H-2Hex]^+$, 592.53 $[M+H-Pent-2Hex]^+$, 412.47 $[M+H-Pent-3Hex-H_2O]^+$
18	Unknown SGA	9.00	1120.48	1060.60 $[M+H-AcOH]^+$, 898.52 $[M+H-Hex-AcOH]^+$, 766.41 $[M+H-Pent-Hex-AcOH]^+$, 604.50 $[M+H-Pent-2Hex-AcOH]^+$, 414.42 $[Agl+H]^+$
19	Unknown SGA	10.15	1132.63	1072.61 $[M+H-AcOH]^+$, 1000.67 $[M+H-Pent]^+$, 970.59 $[M+H-Hex]^+$,

				838.51 [M+H-Pent-Hex]$^+$, 416.46 [Agl+H]$^+$
20	Acetoxydehydrotomatine isomer 2	10.73	1090.72	1030.60 [M+H-AcOH]$^+$, 928.61 [M+H-Hex]$^+$, 910.64 [M+H-Hex-H_2O]$^+$, 766.57 [M+H-2Hex]$^+$, 412.52 [M+H-Pent-3Hex-AcOH]$^+$

Table 9. SGAs putatively identified in green tomato extracts by their MS/MS spectra in agreement with literature by HPLC-MS analysis in positive acquisition mode. * The identification of this molecule was confirmed using commercial standard. Agl, Glu, Hex, Pent, Xyl, and AcOH indicate aglycone, glucose, hexoside, pentoside, xylose, and acetoxy moieties, respectively.

3.3.2.2. Polyphenolic profile of green tomatoes

Phenolic acids are the most known chemical group of polyphenols. They include different compounds with a phenolic group and a carboxylic acid moiety. Phenolic acids are divided into two large families, hydroxycinnamic acids and hydroxybenzoic acids, which are derivatives of hydroxycinnamic acid and benzoic acid, respectively. Phenolic acid fragmentation pattern is characterized by a prominent base peak ion due to the loss of CO_2 (-48 Da), due to the carboxylic acid neutral loss. Therefore, the phenolic group exhibits other two diagnostic fragment ions for the neutral losses of water (-18 Da) and CO (-28 Da) (F. Sheng et al., 2021). Based on this fragmentation profile, 16 hydroxycinnamic acids (numbered as: **23**: hydroxycaffeic acid; **31**: coumaric acid *O*-hexoside isomer 1; **32**: coumaric acid *O*-hexoside isomer 2; **35**: caffeoylquinic acid *O*-hexoside isomer 1; **36**: dihydrocaffeic acid *O*-hexoside; **39**: ferulic acid *O*-hexoside isomer 1; **40**: caffeic acid *O*-hexoside isomer 2; **41**: coumaric acid *O*-hexoside isomer 2; **42**: chlorogenic acid; **46**: caffeic acid; **48**: ferulic acid *O*-hexoside isomer 2; **49**: caffeoylquinic acid *O*-hexoside isomer 2; **53**: *p*-coumaric acid; **55**: neochlorogenic acid; **56**: *O*-coumaroylquinic acid; **73**: dicaffeoylquinic acid) and 8 hydroxybenzoic acids (numbered as: **21**: gallic acid; **22**: dihydroxybenzoic acid; **28**: homovanillic acid *O*-hexoside; **30**: vanillic acid; **37**: syringic acid; **58**: syringic acid *O*-hexoside derivative; **60**: syringic acid *O*-hexoside; **72**: sinapic acid *O*-hexoside) were putatively identified. Compound **21** displayed a [M-H]$^-$ ion at *m/z* 169 and a base peak ion at *m/z* 125, corresponding to the loss of CO_2. The product ions at *m/z* 151 [M-H-H_2O]$^-$, *m/z* 141 [M-H-CO]$^-$, and *m/z* 97 [M-H-CO_2-CO]$^-$ suggested the linkage with a carboxylic acid and a

phenolic group. In agreement with literature data, this compound was identified as gallic acid (F. Sheng et al., 2021). Compound **22** showed a $[M-H]^-$ ion at *m/z* 153 and a base peak ion at m/z 125, due to the loss of CO. The tandem mass spectrum exhibited some fragment ions at *m/z* 135 $[M-H-H_2O]^-$, *m/z* 109 $[M-H-CO_2]^-$, and *m/z* 97 $[M-H-2CO]^-$. This fragmentation pattern agreed with the dihydroxybenzoic acid (Hong et al., 2021). Compound **23** displayed a $[M-H]^-$ ion at *m/z* 195 and a base peak ion at *m/z* 151 $[M-H-CO_2]$-. The product ions at *m/z* 177 $[M-H-H_2O]^-$, *m/z* 167 $[M-H-CO]^-$ and *m/z* 133 $[M-H-CO_2$-H2O$]^-$ were formed by the neutral loss fragmentation of the carboxylic acid and phenolic groups. Based on the fragmentation pattern, compound **23** was annotated as hydroxycaffeic acid (Hong et al., 2021). Homovanillic acid *O*-hexoside (**28**) showed a $[M-H]^-$ ion at *m/z* 343 and a base peak ion at *m/z* 297, produced by the neutral loss of water and CO. The fragmentation pattern ion at *m/z* 181 $[M-H-Hex]^-$ proved the linkage of a hexoside group to the phenolic moiety (Anton et al., 2017). Compound **30** gave a $[M-H]^-$ ion at *m/z* 167 and a base peak ion at *m/z* 123 $[M-H-CO_2]^-$. The tandem mass spectrum exhibited some fragment ions at *m/z* 149 $[M-H-H_2O]^-$, *m/z* 139 $[M-H-CO]^-$ and *m/z* 95 $[M-H-CO-CO_2]^-$, formed by the neutral losses of water and a carboxylic group. In agreement with literature data, compound **30** was identified as vanillic acid (Grieman et al., 2015). Two coumaric acid *O*-hexoside (compounds **31** and **41**) were detected, with a $[M-H]^-$ ion at *m/z* 371. They displayed a base peak ion at *m/z* 163 $[M-H-Hex]^-$ and other product ions at *m/z* 353 $[M-H-H_2O]^-$, *m/z* 325 $[M-H-H_2O-CO]^-$ and *m/z* 119 $[M-H-Hex-CO_2]^-$, which suggested the linkage with a carboxylic acid and a hexoside groups. According to this fragmentation pattern, compounds **31** and **41** were identified as coumaric acid *O*-hexoside (Barros et al., 2012). Compounds **32** and **40** showed a $[M-H]^-$ ion at *m/z* 341 and was annotated as caffeic acid *O*-hexoside isomers. The base peak ion at *m/z* 179 $[M-H-Hex]^-$ and the fragment ions at *m/z* 323 $[M-H-H_2O]^-$, *m/z* 297 $[M-H-CO_2]^-$, and *m/z* 135 $[M-H-Hex-CO_2]^-$ displayed the same fragmentation pattern of compounds **31** and **41**, allowing the identification of two *O*-hexoside phenolic acid derivatives. Since the fragment ion at *m/z* 179 matched with the aglycone caffeic acid ion, compounds **32** and **40** were recognized as caffeic acid *O*-hexoside derivatives (Anton et al., 2017). Compounds **35** and **49** gave a $[M-H]^-$ ion at *m/z* 515 and a base peak ion at *m/z* 353 $[M-H-Hex]^-$, due to the loss of a hexoside moiety. The fragment ions at *m/z* 341 $[M-H-QA]^-$, *m/z* 323 $[M-H-QA-H_2O]^-$ and *m/z* 191 $[QA-H]^-$ have been justified as different products for the cleavage of a quinic acid group. Established the similarity of the fragment patterns of these compounds with the caffeic acid *O*-hexoside fragmentation, compounds **35** and **49** was annotated as caffeoylquinic acid *O*-hexoside

isomers (J. Zhang et al., 2018). Compound **36** displayed a $[M-H]^-$ ion at *m/z* 343 and a base peak ion at *m/z* 181 $[M-H-Hex]^-$. The fragment ions of the tandem mass spectrum at *m/z* 137 $[M-H-Hex-CO_2]^-$ differed from the fragments of caffeic acid *O*-hexoside (compounds **32** and **40**) for 2 Da, which corresponded to a single double bond difference. Therefore, compound **36** was identified as dihydrocaffeic acid *O*-hexoside (Velderrain-Rodríguez et al., 2021). Compound **37** showed a $[M-H]^-$ ion at *m/z* 197 and a base peak ion at *m/z* 153 $[M-H-CO_2]^-$. The fragment ions at *m/z* 179 $[M-H-H_2O]^-$, *m/z* 169 $[M-H-CO]^-$ and *m/z* 161 $[M-H-2H_2O]^-$ agreed with the presence of a carboxylic acid and a phenolic group. Therefore, compound **37** was annotated as syringic acid (Shao et al., 2014). Two ferulic acid *O*-hexoside were detected, of which compound **39** was identified as formate adduct with a $[M+HCOO]^-$ at *m/z* 401 while compound **48** displayed a $[M-H]^-$ ion at *m/z* 355. Compound **48** showed a base peak ion at *m/z* 193 $[M-H-Hex]^-$, which matched with the ferulic acid molecular ion for the loss of a hexoside molecule, and a typical fragment ion at *m/z* 149 $[M-H-Hex-CO_2]^-$, which was due to the cleavage of a carboxylic acid group. The fragmentation pattern of ferulic acid *O*-hexoside agreed with literature data (Anton et al., 2017). The tandem mass spectrum of compound **39** was characterized by a base peak ion at *m/z* 355, corresponding to the $[M-H]^-$ ion, and two diagnostic product ions at *m/z* 193 $[M-H-Hex]^-$ and *m/z* 149 $[M-H-Hex-CO_2]^-$, which matched with the fragments of compound **48**. Based on the fragmentation pattern, compound **39** was identified as a ferulic acid *O*-hexoside isomer (Anton et al., 2017; Tavarini et al., 2021). Compounds **42** and **55** displayed a $[M-H]^-$ ion at *m/z* 353 and were annotated as two caffeoylquinic acids. The product ions at *m/z* 191 $[M-H-CA]^-$ and *m/z* 179 $[M-H-QA]^-$ matched with quinic acid and caffeic acid ions, respectively. The identification of each geometric caffeoylquinic acid isomers was supported by comparison with analytical standards. Therefore, compounds **42** and **55** were identified as chlorogenic acid and neochlorogenic acid, respectively (Anton et al., 2017). Compound **46** displayed a $[M-H]^-$ ion at *m/z* 179. Its tandem mass spectrum was characterized by a base peak ion at *m/z* 135 and three product ions at *m/z* 161 $[M-H-H_2O]^-$, *m/z* 143 $[M-H-2H_2O]^-$ and *m/z* 107 $[M-H-CO-CO_2]^-$, which derived from the cleavage of a carboxylic acid and a phenolic group. Therefore, compound **46** was identified as caffeic acid (Sinosaki et al., 2020). Compound **53** gave a $[M-H]^-$ ion at *m/z* 163 and a base peak ion at *m/z* 119 $[M-H-CO_2]^-$. The product ions at *m/z* 145 $[M-H-H_2O]^-$, *m/z* 135 $[M-H-CO]^-$ and *m/z* 101 $[M-H-H_2O-CO_2]^-$ indicated the presence of a hydroxycinnamic acid group and a phenolic moiety. Based on literature data, compound **53** was identified as *p*-coumaric acid (Sinosaki et al., 2020). Compound **56** showed a $[M-H]^-$ ion at *m/z* 337, a base peak ion at *m/z* 191 $[QA-H]^-$ and three product ions

at *m/z* 301 $[M-H-2H_2O]^-$, *m/z* 173 $[QA-H-H_2O]^-$ and *m/z* 163 $[M-H-QA]^-$. Its tandem mass spectrum indicated the linkage with a quinic acid moiety. For this reason, compound **56** was identified as an *O*-coumaroylquinic acid (Y. Li et al., 2015). Based on literature data, the base peak ion value allowed to recognize the connectivity between quinic acid and coumaric acid groups. The base peak ion at *m/z* 191 was diagnostic for the linkage of coumaric acid at the hydroxyl group at position 5' of the quinic acid moiety. Therefore, compound **56** was annotated as a 5-*O*-coumaroylquinic acid (Elsadig Karar & Kuhnert, 2016; Y. Li et al., 2015). Compound **58** displayed a $[M-H]^-$ ion at *m/z* 403 and a base peak ion at *m/z* 241 $[M-H-Hex]^-$, due to the cleavage of the hexoside group. The fragment ions at *m/z* 223 $[M-H-Hex-H_2O]^-$, *m/z* 197 $[M-H-Hex-CO_2]^-$ and *m/z* 179 $[M-H-Hex-H_2O-CO_2]^-$ indicated the presence of a carboxylic acid and a phenolic group in the aglycone component. In agreement with literature data and the fragmentation pattern of syringic acid (**37**), this compound was identified as a syringic acid *O*-hexoside derivative (Spínola et al., 2015). Compound **60** showed a $[M-H]^-$ ion at *m/z* 359 and was annotated as syringic acid *O*-hexoside. Its tandem mass spectrum was characterized by a base peak ion at *m/z* 197 $[M-H-Hex]^-$ and two fragment ions at *m/z* 315 $[M-H-CO_2]^-$ and *m/z* 153 $[M-H-Hex-CO_2]^-$. The fragmentation pattern proved that the glucose molecule related to syringic acid by an ether linkage. Among these ones, the fragments at *m/z* 197 and *m/z* 153 agreed with free syringic acid (**37**) ions (Castro & Llerena, 2020). Compound **72** displayed a $[M-H]^-$ ion at *m/z* 385. The base peak ion at *m/z* 223 $[M-H-Hex]^-$, which was identical to sinapic acid ion, and the patent ions at *m/z* 341 $[M-H-CO_2]^-$ and *m/z* 179 $[M-H-Hex-CO_2]^-$ were formed by the loss of a hexoside molecule and the cleavage of the free carboxylic acid group. Therefore, compound **72** was identified as sinapic acid *O*-hexoside (Bystrom et al., 2008). Compound **73** showed a $[M-H]^-$ ion at *m/z* 515 and was annotated as a dicaffeoylquinic acid. The base peak ion at *m/z* 353 $[M-H-CA]^-$ and the parent ions at *m/z* 335 $[M-H-CA-H_2O]^-$ and *m/z* 179 $[CA-H]^-$ suggested that two molecules of caffeic acid were connected with quinic acid by two ester bonds (Zhang et al., 2018).

Flavanols, a polyphenols class characterized by a 2-phenylchroman scaffold, are largely widespread in plants. They include monomeric compounds, such as (+)-catechin and (-)-epicatechin, and their oligomeric and polymeric derivatives, called procyanidins (Schiano et al., 2022). Procyanidins can be divided in two groups, A-type and B-type, based on the linkage between monomers. The A-type linkage procyanidins show two linkages between the monomeric units, an interflavan carbon-carbon bond and an ether linkage, which links

the monomers by a six-membered ring. Instead, B-type linkage procyanidins are characterized by a single carbon-carbon bond between monomers. Procyanidins fragment pattern is characterized by three distinctive fragmentations, the heterocyclic ring fission (HRF), the retro Diels-Alder fission (RDA), and the quinone methide cleavage (QM) (Rue et al., 2018). The heterocyclic ring fission (HRF) derived from the neutral loss of the phloroglucinol unit (-126 Da) and not involved the cleavage of the interflavanic bond between monomers. The retro Diels-Alder fission (RDA) derived from the neutral loss of hydroxyvinyl benzenediol unit (-152 Da). The quinone methide cleavage (QM) is given by the fragmentation of the interflavanic linkage between two monomers. Therefore, the resulting ions indicate the monomers number in the oligomeric and polymeric compounds (Schiano et al., 2022). Flavanones represent a class of flavan-3-ols characterized by a different fragmentation pattern. These polyphenols are widespread in the plant kingdom as aglycone or linked to a sugar and display a diagnostic fragmentation profile which includes the fragment ions due to the retro Diels-Alder fission (RDA) and the neutral loss of sugar (Fabre et al., 2001). Another diagnostic fragment ion is due to the cross-ring cleavage of the glycosidic group with the neutral loss of $C_4H_8O_4$ (-120 Da). Among the compounds of our chemical characterization, six flavanols were putatively detected (numbered as: **33**: procyanidins B1+B3; **38**: catechin; **43**: epicatechin; **57**: procyanidin B2; **59**: procyanidin C1; **62**: eriodyctiol *O*-hexoside).

Three procyanidins dimer B-type linkage (compounds **33** and **57**) were detected. They displayed a $[M-H]^-$ ion at *m/z* 577 and a base peak ion at *m/z* 425 $[M-H-C_8H_8O_3]^-$, due to the RDA fragmentation. The tandem mass spectrum exhibited some fragment ions at *m/z* 451 $[M-H-C_6H_6O_3]^-$, formed by the HRF fragmentation, and at *m/z* 289 $[M-H-C_{15}H_{12}O_6]^-$ and *m/z* 287 $[M-H-C_{15}H_{14}O_6]^-$, due to the QM cleavage. In agreement with literature data, compounds **33** and **57** were identified as procyanidins dimer B-type linkage. The identity of these compounds was confirmed by the comparison with the analytical external standards. Therefore, compound **33** was represented by a mixture of procyanidins B1 and B3, while compound **57** was recognized as the B2 isomer. Two flavanol monomers (compounds **38** and **43**) were identified and gave a $[M-H]^-$ ion at *m/z* 289. The base peak ion at *m/z* 245 $[M-H-C_2H_4O]^-$ and the parent ions at *m/z* 271 $[M-H-H_2O]^-$ and *m/z* 205 $[M-H-C_4H_4O_2]^-$ were in according to literature data (Rockenbach et al., 2012). Flavanol monomer identity was verified by comparison with external standards. Consequently, compounds **38** and **43** were identified as catechin and epicatechin, respectively. Compound **59** displayed a $[M-H]^-$ ion at

m/z 865 and a base peak ion at *m/z* 695 [M-H-$C_8H_{10}O_4$]$^-$, that was produced by the RDA fission and the loss of a molecule of water. Its tandem mass spectrum was characterized by three product ions at *m/z* 577 [M-H-$C_{15}H_{12}O_6$]$^-$, which derived from the loss of a flavanol monomer, at *m/z* 451 [M-H-$C_{21}H_{18}O_9$]$^-$ and *m/z* 425 [M-H-$C_{23}H_{20}O_9$]$^-$, which was formed by the HRF and the RDA fragmentation of the dimeric procyanidin ion at *m/z* 577. Therefore, compound **59** was identified as procyanidin C1 (Rue et al., 2018). Flavanones represents a class of flavan-3-ols characterized by a different fragmentation pattern. These polyphenols are common in the plant kingdom as aglycone or glycosides and display a diagnostic fragmentation pattern which include the fragment ions due to the retro Diels-Alder fission (RDA) and the loss of sugar (Fabre et al., 2001). Another fragment ion is due to the cross-ring cleavage of the glucidic moiety for the neutral loss of $C_4H_8O_4$ (-120 Da). Eriodyction *O*-hexoside (**62**) displayed a [M-H]$^-$ ion at *m/z* 449 and a base peak ion at m/z 287 [M-Hex]$^-$, due to the loss of the hexoside group. Other fragment ions included the m/z 329 [M-H-$C_4H_8O_4$]$^-$ and the m/z 151 [M-H-Hex-$C_8H_8O_2$]$^-$, that derived from the cross-ring cleavage of the hexoside and the RDA fragmentation of the base peak ion, respectively (De Beer et al., 2012). Compound **69** showed a [M-H]$^-$ ion at m/z 271 and was annotated as naringenin. The base peak ion at m/z 151 [M-H-C8H8]-, that derived from the RDA pattern, and the parent ion at m/z 203 [M-H-C3O2]- allowed to identify the flavanone scaffold (F. Xu & Tian, 2009).

Flavonols represent a group of polyphenols characterized by a 3-hydroxy-3-phenylchromen-4-one moiety. They displayed a flavanone-like fragmentation pattern, with an aglycone ion which often represent the base peak ion for the cleavage of sugars. Two diagnostic fragment ions are *m/z* 301 and *m/z* 285, which represent the quercetin and kaempferol scaffolds, respectively. Another diagnostic product ion of flavonols scaffold is given by the *m/z* 179, which is the product of the retro Diels-Alder fission (RDA). Moreover, the glycosylated flavonols exhibited two important fragment ions due to the loss of the sugar groups and the cross-ring cleavage of the sugar group (Vallverdú-Queralt et al., 2011). The tandem mass spectra allowed to tentatively identify eleven flavonols (numbered as: **47**: quercetin *O*-hexoside-*O*-rutinoside; **61**: quercetin *O*-(pentosylrutinoside); **64**: rutin; **65**: kaempferol *O*-(pentosylrutinoside); **67**: quercetin 3-*O*-glucoside; **68**: kaempferol *O*-rutinoside; **70**: isorhamnetin *O*-rutinoside; **71**: luteolin *O*-hexoside; **74**: quercetin tetrahexoside isomer 1; **75**: quercetin tetrahexoside isomer 2; **76**: quercetin). Compound **47** showed a [M-H]$^-$ ion at *m/z* 771 and a base peak ion at *m/z* 609 [M-H-Hex]$^-$. The parent ions at *m/z* 463 [M-H-Hex-

Rha]$^-$ and *m/z* 301 [M-H-2Hex-Rha]$^-$ confirmed the presence of a quercetin moiety linked to a trisaccharide group represented by an hexoside and a rutinoside. The fragment ions at *m/z* 301 and *m/z* 609 corresponded to quercetin and rutin ions, respectively. Based on these fragments, compound **47** was identified as quercetin *O*-hexoside-*O*-rutinoside (Brito et al., 2014). Compound **61** displayed a [M-H]$^-$ ion at *m/z* 741, a base peak ion at *m/z* 609 [M-H-Pent]$^-$ and a diagnostic fragment at *m/z* 301 [M-H-Pent-Rha-Hex]$^-$, which indicated the loss of a pentoside and a rutinoside groups. Therefore, compound **61** was annotated as quercetin-*O*-(pentosylrutinoside) (Barros et al., 2012). Compound **64** showed a [M-H]$^-$ ion at *m/z* 609 and a base peak ion at *m/z* 301 [M-H-Rha-Hex]$^-$. The fragment ions at *m/z* 463 [M-H-Rha]$^-$ and *m/z* 179 [M-H-Rha-Hex-$C_7H_6O_2$]$^-$ suggested the linkage between a rutinoside group with the aglycone quercetin moiety. Therefore, compound **64** was identified as rutin (Vallverdú-Queralt et al., 2011). Kaempferol-*O*-(pentosylrutinoside) (**65**) gave a [M-H]$^-$ ion at *m/z* 725 and a base peak ion at *m/z* 707 [M-H-H_2O]$^-$, due to the neutral loss of water. The parent ions at *m/z* 593 [M-H-Pent]$^-$ and *m/z* 285 [M-H-Pent-Rha-Hex]$^-$ proved the linkage of a kaempferol scaffold with a trisaccharide moiety, which is formed by a pentoside and a rutinoside (Barros et al., 2012). Compound **67** displayed a [M-H]$^-$ ion at *m/z* 463. Its tandem mass spectrum was characterized by a base peak ion at *m/z* 301 [M-H-Hex]$^-$ and a fragment ion at *m/z* 179 [M-H-Hex-$C_7H_6O_2$]$^-$, which suggested a quercetin-like scaffold linked to an hexoside group. Based on literature data, compound **67** was annotated as quercetin 3-*O*-glucoside (Z. H. Li et al., 2016a). Compound **68** gave a [M-H]$^-$ ion at *m/z* 593 and was annotated as kaempferol *O*-rutinoside. The base peak ion at *m/z* 575 [M-H-H_2O]$^-$ and the fragment ions at *m/z* 285 [M-H-Hex]$^-$ and *m/z* 179 [M-H-Hex-C_7H_6O]$^-$ were referred to the loss of the sugar and the RDA fragmentation and indicated the presence of the rutinoside group and the aglycone kaempferol (Vallverdú-Queralt et al., 2011). Compound **70** displayed a [M-H]$^-$ ion at *m/z* 623 and a base peak ion at *m/z* 315 [M-H-Rha-Hex]$^-$, due to the neutral loss of a rutinoside group. The base peak ion and the parent ion at *m/z* 300 [M-H-Rha-Hex-CH_3]$^-$ allowed to identify isorhamnetin, a methylated derivative of quercetin, as the aglycone scaffold. In agreement with literature data, compound **70** was identified as isorhamnetin *O*-rutinoside (Brito et al., 2014). Compound **71** showed a [M-H]$^-$ ion at *m/z* 447 and was annotated as luteolin *O*-hexoside. The base peak ion at *m/z* 285 [M-H-Hex]$^-$ and the parent ion at *m/z* 327 [M-H-$C_4H_8O_4$]$^-$ proved the presence of an hexoside group while the fragment ion at *m/z* 151 [M-H-Hex-$C_8H_6O_2$]$^-$ derived from the RDA fragmentation and the neutral loss of CO by the luteolin aglycone scaffold (Brito et al., 2014). Two quercetin tetrahexoside isomers (**74** and **75**) were identified and gave a [M-H]$^-$ ion at *m/z*

949. The base peak ion at *m/z* 931 $[M-H-H_2O]^-$ and the fragment ions at m/z 787 [M-H-Hex]-, m/z 625 [M-H-2Hex]- and m/z 463 [M-H-3Hex] was produced by the neutral losses of water and of one, two and three hexose groups to obtain the quercetin aglycone (Degeneve, 2004). Quercetin (**76**) displayed a $[M-H]^-$ ion at *m/z* 301 and a base peak ion at *m/z* 283 $[M-H-H_2O]^-$, due to the neutral loss of water. Its tandem mass spectrum was characterized by two parent ions at *m/z* 179 $[M-H-C_7H_6O_2]^-$ and *m/z* 151 $[M-H-C_8H_6O_3]^-$, derived from the RDA fragmentation and the neutral loss of CO (Vallverdú-Queralt et al., 2011).

In addition to the polyphenols, the analysis allowed to putatively identify other compounds common in foods, such as organic acids, phytohormones, and terpenoids. Organic acids are found in natural matrices and are formed in fermentation processes and by the enzymatic oxidation of sugars. They are characterized by a free carboxylic acid group, which determines their acidic properties, but also other functional groups, in particular the hydroxy moieties, are often present in the compounds. The presence of several hydroxyl groups determines their high polarity. Therefore, these compounds are eluted in chromatographic conditions at low retention times. Their fragmentation pattern included a diagnostic base peak ion for the carboxylic acid cleavage (-48 Da), but other parent ions are represented by the neutral losses of one or more molecules of water (-18 Da). Five organic acids and sugars (numbered as: 24: dihexoside; 25: shikimic acid; 26: quinic acid; 27: citric acid; 29: quinic acid derivative) were putatively identified. Compound **24** displayed a $[M-H]^-$ ion at *m/z* 341 and was annotated as a dihexoside derivative. The base peak ion at *m/z* 179 $[M-H-Hex]^-$, which represented the pseudomolecular ion of a hexoside, and the parent ions at *m/z* 323 $[M-H-H_2O]^-$, *m/z* 161 $[M-H-Hex-H_2O]^-$ and *m/z* 143 $[M-H-Hex-2H_2O]^-$ indicated the presence of two hexosides groups and excluded the linkage with other functional groups (Calvano et al., 2017). Compound **25** showed a $[M-H]^-$ ion at *m/z* 173. The base peak ion at *m/z* 129 $[M-H-CO_2]^-$ and the fragment ion at *m/z* 93 $[M-H-2H_2O-CO_2]^-$ indicated the linkage with a free carboxylic acid group and two hydroxyl groups. Based on literature data, compound **25** was identified as shikimic acid (S. Chen et al., 2014). Compound **26** gave a $[M-H]^-$ ion at *m/z* 191 and was identified as quinic acid. The tandem mass spectrum is characterized by a base peak ion at *m/z* 173 $[M-H-H_2O]^-$ and a parent ion at *m/z* 111 $[M-H-2H_2O-CO_2]^-$, which were due to the cleavage of a carboxylic acid group and the neutral loss of two molecules of water (Masike et al., 2017). Compound **27** displayed a $[M-H]^-$ ion at *m/z* 191 and was annotated as citric acid. The base peak ion at *m/z* 147 $[M-H-CO_2]^-$ and the

fragment ions at *m/z* 173 $[M\text{-}H\text{-}H_2O]^-$ and *m/z* 129 $[M\text{-}H\text{-}H_2O\text{-}CO_2]^-$ can be rationalized as the products of the cleavage of a carboxylic acid and a hydroxyl groups (Masike et al., 2017). Compound **29** showed a $[M\text{-}H]^-$ ion at *m/z* 405. The base peak ion at *m/z* 191 $[QA\text{-}H]^-$ suggested the linkage of a quinic acid moiety. The lack of fragmentation due to the cleavage of a carboxylic acid group indicated that the organic acid scaffold could be functionalized by an ester bond. Therefore, compound **29** was identified as a quinic acid derivative (López-fernández et al., 2020). Phytohormones are a class of plant-based small molecules, showing bioactivity at low concentrations and controlling plants germination, reproduction, growth, and biotic and abiotic response for environmental stress conditions. The most important phytohormone class is represented by apocarotenoids, which derived from carotenoids oxidative cleavage. They are characterized by different chemical structures, that can differ for the number of carbon atoms. For example, abscisic acid (ABA) derivatives and blumenols are two classes of phytohormone characterized by fifteen and thirteen carbon atoms, respectively. ABA represents the most important phytohormone and inhibits the fruit ripening (Fiorilli et al., 2019). ABA is metabolized through oxidative and conjugative reaction to obtain glucosyl ester derivatives. Among this characterization, two ABA catabolism products (numbered as: **34**: dihydrophaseic acid *O*-hexoside; **63**: abscisyl acid *O*-hexoside) were tentatively identified in the investigated tomato matrices. Compound **34** displayed a $[M\text{-}H]^-$ ion at *m/z* 443 and was annotated as dihydrophaseic acid *O*-hexoside. Its tandem mass spectrum was characterized by a base peak ion at *m/z* 425 $[M\text{-}H\text{-}H_2O]^-$, due to the neutral loss of water, and two fragment ions at *m/z* 281 $[M\text{-}H\text{-}Hex]^-$ and *m/z* 237 $[M\text{-}H\text{-}Hex\text{-}CO_2]^-$ (Cebadera et al., 2020). Compound **63** was detected as formate adduct with a $[M+HCOO]^-$ ion at *m/z* 471 and was identified as abscisyl acid *O*-hexoside. The fragmentation pattern showed a base peak ion at *m/z* 425 $[M\text{-}H]^-$ and the parent ions at *m/z* 263 $[M\text{-}H\text{-}Hex]^-$ and *m/z* 219 $[M\text{-}H\text{-}Hex\text{-}CO_2]^-$ (Mcgraphery, 2021). The fragmentation of the two compounds suggested the linkage of the apocarotenoid scaffold with the hexoside group. Therefore, the absence of the neutral loss of CO_2 allowed to verify that the sugar is linked with a glucosyl ester at the aglycon group. Blumenols represent a class of phytohormone produced by the symbiotic interaction between arbuscular mycorrhizal fungi and many types of plants of genus Solanum (Fiorilli et al., 2019). Therefore, these compounds could represent interesting markers to evaluate the ecological conditions of plant growing. One blumenol glycoside (**52**) was identified and detected as formate adduct with a $[M+HCOO]^-$ ion at *m/z* 431. Its tandem mass spectrum agreed with the neutral loss of a hexoside moiety, with a base peak ion at *m/z* 385 $[M\text{-}H]^-$ and a diagnostic fragment ion at

m/z 223 $[M-H-Hex]^-$. Based on literature data, compound **52** was annotated as roseoside (Ak et al., 2021). Two benzyl glucosides (**45** and **51**) were identified. They were detected as formate adduct $[M+HCOO]^-$ in negative ionization mode as they are devoid of ionizable functional groups and are characterized by a base peak ion corresponding to the molecular ion $[M-H]^-$. Another diagnostic fragment ion was due to the loss of sugar moieties. Compound **45** displayed a $[M+HCOO]^-$ ion at *m/z* 447. The base peak ion at *m/z* 401 $[M-H]^-$ and the fragment ion at *m/z* 239 $[M-H-Hex]^-$ agreed with the fragmentation pattern of benzyl-xylopyranosyl-glucopyranoside (Cho et al., 2020). Compound **51** showed a $[M+HCOO]^-$ ion at *m/z* 431. Its tandem mass spectrum was characterized by a base peak ion at *m/z* 385 $[M-H]^-$ and the fragment ion at *m/z* 223 $[M-H-Hex]^-$. Based on these data, compound **51** was annotated as benzyl-deoxyxylopyranosyl-glucopyranoside.

Oxylipins represent a class of oxygenated fatty acids with antimicrobial activities and are involved in the defence of the plants. Generally, these compounds are characterized by a high apolarity and volatility, for which they are not extractable by classic hydroalcoholic extraction. However, the presence of the hexoside moiety in this molecule greatly increases its polarity, reducing the volatile behaviour and allowing its extraction with these solvents. Furthermore, hydroxy jasmonic acid *O*-hexoside is an oxylipin that was already annotated in the genus Solanum (Fiorilli et al., 2019). In our investigation, three isomers of this oxylipin (numbered as: **44**: hydroxy jasmonic acid *O*-hexoside isomer 1; **50**: hydroxy jasmonic acid *O*-hexoside isomer 2; **54**: hydroxy jasmonic acid *O*-hexoside isomer 3) were tentatively identified. Their tandem mass spectra displayed a $[M-H]^-$ ion at *m/z* 387 and characteristic fragment ions at *m/z* 369 $[M-H-H_2O]^-$ and *m/z* 225 $[M-H-Hex]^-$, due to the neutral loss of the hexoside group.

No.	Putatively compound	R_t	Precursor ion	Charge	Characteristic fragment ions
21	Gallic acid*	0.71	169.85	$[M-H]^-$	151.83 $[M-H-H_2O]^-$, 141.90 $[M-H-CO]^-$, 125.81 $[M-H-CO_2]^-$, 97.75 $[M-H-CO_2-CO]^-$
22	Dihydroxybenzoic acid	1.12	152.94	$[M-H]^-$	134.94 $[M-H-H_2O]^-$, 124.94 $[M-H-CO]^-$, 108.97 $[M-H-CO_2]^-$, 96.86 $[M-H-2CO]^-$

23	Hydroxycaffeic acid	2.36	195.28	$[M-H]^-$	177.02 $[M-H-H_2O]^-$, 166.96 $[M-H-CO]^-$, 151.01 $[M-H-CO_2]^-$, 133.08 $[M-H-H_2O-CO_2]^-$
24	Dihexoside	3.09	341.11	$[M-H]^-$	322.94 $[M-H-H_2O]^-$, 179.04 $[M-H-Hex]^-$, 160.95 $[M-H-Hex-H_2O]^-$, 142.98 $[M-H-Hex-2H_2O]^-$
25	Shikimic acid	3.12	172.89	$[M-H]^-$	154.89 $[M-H-H_2O]^-$, 128.91 $[M-H-CO_2]^-$, 110.87 $[M-H-H_2O-CO_2]^-$, 92.78 $[M-H-2H_2O-CO_2]^-$
26	Quinic acid	3.14	191.14	$[M-H]^-$	172.96 $[M-H-H_2O]^-$, 154.84 $[M-H-2H_2O]^-$, 146.76 $[M-H-H_2O-CO]^-$, 110.91 $[M-H-2H_2O-CO_2]^-$
27	Citric acid	3.35	191.01	$[M-H]^-$	172.97 $[M-H-H_2O]^-$, 146.96 $[M-H-CO_2]^-$, 128.96 $[M-H-H_2O-CO_2]^-$, 110.82 $[M-H-2H_2O-CO_2]^-$
28	Homovanillic acid *O*-hexoside	3.65	343.09	$[M-H]^-$	325.02 $[M-H-H_2O]^-$, 297.03 $[M-H-H_2O-CO]^-$, 261.02 $[M-H-3H_2O-CO]^-$, 180.92 $[M-H-Hex]^-$
29	Quinic acid derivative	3.77	405.11	$[M-H]^-$	387.17 $[M-H-H_2O]^-$, 358.90 $[M-H-H_2O-CO]^-$, 190.96 $[QA-H]^-$
30	Vanillic acid*	6.89	166.95	$[M-H]^-$	148.97 $[M-H-H_2O]^-$, 139.06 $[M-H-CO]^-$, 122.81 $[M-H-CO_2]^-$, 94.75 $[M-H-CO-CO_2]^-$
31	Coumaric acid *O*-hexoside isomer 1	12.64	371.11	$[M-H]^-$	352.92 $[M-H-H_2O]^-$, 325.13 $[M-H-H_2O-CO]^-$, 163.03 $[M-H-Hex]^-$, 119.08 $[M-H-Hex-CO_2]^-$
32	Caffeic acid *O*-hexoside isomer 1	12.69	341.25	$[M-H]^-$	323.30 $[M-H-H_2O]^-$, 297.05 $[M-H-CO_2]^-$, 178.93 $[M-H-Hex]^-$, 134.97 $[M-H-Hex-CO_2]^-$
33	Procyanidin B1 + B3*	13.71	577.15	$[M-H]^-$	451.14 $[M-H-C_6H_6O_3]^-$, 425.04 $[M-H-C_8H_8O_3]^-$, 289.21 $[M-H-C_{15}H_{12}O_6]^-$, 286.99 $[M-H-C_{15}H_{14}O_6]^-$
34	Dihydrophaseic acid *O*-hexoside	14.07	443.14	$[M-H]^-$	425.47 $[M-H-H_2O]^-$, 281.31 $[M-H-Hex]^-$, 237.21 $[M-H-Hex-CO_2]^-$, 219.16 $[M-H-Hex-H_2O-CO_2]^-$
35	Caffeoylquinic acid *O*-hexoside isomer 1	14.78	515.18	$[M-H]^-$	353.01 $[M-H-Hex]^-$, 341.17 $[M-H-QA]^-$, 323.16 $[M-H-QA-H_2O]^-$, 191.04 $[QA-H]^-$
36	Dihydrocaffeic acid *O*-hexoside	14.88	343.09	$[M-H]^-$	314.70 $[M-H-CO]^-$, 271.26 $[M-H-CO-CO_2]^-$, 181.06 $[M-H-Hex]^-$,

					137.11 [M-H-Hex-CO_2]$^-$
37	Syringic acid*	14.94	196.99	[M-H]$^-$	179.05 [M-H-H_2O]$^-$, 168.97 [M-H-CO]$^-$, 160.82 [M-H-2H_2O]$^-$, 152.99 [M-H-CO_2]$^-$
38	Catechin*	15.58	289.12	[M-H]$^-$	271.05 [M-H-H_2O]$^-$, 245.02 [M-H-C_2H_4O]$^-$, 205.01 [M-H-$C_4H_4O_2$]$^-$, 150.99 [M-H-$C_7H_6O_3$]$^-$
39	Ferulic acid *O*-hexoside isomer 1	15.63	401.04	[M+HCOO]$^-$	383.17 [M-H+HCOOH-H_2O]$^-$, 355.15 [M-H]$^-$, 193.04 [M-H-Hex]$^-$, 148.96 [M-H-Hex-CO_2]$^-$
40	Caffeic acid *O*-hexoside isomer 2	15.66	341.25	[M-H]$^-$	323.27 [M-H-H_2O]$^-$, 297.18 [M-H-CO_2]$^-$, 179.04 M-H-Hex]$^-$, 135.00 [M-H-Hex-CO_2]$^-$
41	Coumaric acid *O*-hexoside isomer 2	15.81	325.25	[M-H]$^-$	307.03 [M-H-H_2O]$^-$, 289.27 [M-H-2H_2O]$^-$, 162.89 [M-H-Hex]$^-$, 118.97 [M-H-Hex-CO_2]$^-$
42	Chlorogenic acid*	16.84	353.11	[M-H]$^-$	335.22 [M-H-H_2O]$^-$, 191.07 [M-H-CA]$^-$, 179.02 [M-H-QA]$^-$, 173.02 [M-H-CA-H_2O]$^-$
43	Epicatechin*	16.93	289.14	[M-H]$^-$	271.03 [M-H-H_2O]$^-$, 245.03 [M-H-CO_2]$^-$, 205.00 [M-H-C4H4O2]$^-$, 124.95 [M-H-$C_9H_8O_3$]$^-$
44	Hydroxy jasmonic acid *O*-hexoside isomer 1	17.19	387.32	[M-H]$^-$	369.21 [M-H-H_2O]$^-$, 225.13 [M-H-Hex]$^-$, 207.04 [M-H-Hex-H_2O]$^-$, 162.96 [M-H-Hex-H_2O-CO_2]$^-$
45	Benzyl-xylopyranosyl-glucopyranoside	17.80	447.10	[M+HCOO]$^-$	401.19 [M-H]$^-$, 269.09 [M-H-Xyl]$^-$, 239.19 [M-H-Hex]$^-$, 160.96 [Hex-H-H_2O]$^-$
46	Caffeic acid*	18.29	179.05	[M-H]$^-$	160.92 [M-H-H_2O]$^-$, 143.06 [M-H-2H_2O]$^-$, 134.94 [M-H-CO_2]$^-$, 106.68 [M-H-CO-CO_2]$^-$
47	Quercetin *O*-hexoside-*O*-rutinoside	18.33	771.29	[M-H]$^-$	753.27 [M-H-H_2O]$^-$, 609.18 [M-H-Hex]$^-$, 463.19 [M-H-Hex-Rha]$^-$, 301.22 [M-H-2Hex-Rha]$^-$
48	Ferulic acid *O*-hexoside isomer 2	18.62	355.12	[M-H]$^-$	337.19 [M-H-H_2O]$^-$, 193.08 [M-H-Hex]$^-$, 175.03 [M-H-Hex-H_2O]$^-$, 148.94 [M-H-Hex-CO_2]$^-$
49	Caffeoylquinic acid *O*-hexoside isomer 2	18.99	515.19	[M-H]$^-$	353.18 [M-H-Hex]$^-$, 341.13 [M-H-QA]$^-$, 323.11 [M-H-QA-H2O]$^-$, 191.03 [QA-H]$^-$

50	Hydroxy jasmonic acid *O*-hexoside isomer 2	19.09	387.27	$[M-H]^-$	369.28 $[M-H-H_2O]^-$, 225.07 $[M-H-Hex]^-$, 206.99 $[M-H-Hex-H_2O]^-$, 163.06 $[M-H-Hex-H_2O-CO_2]^-$
51	Benzyl-deoxyxylopyranosyl-glucopyranoside	19.20	431.31	$[M+HCOO]^-$	385.28 $[M-H]^-$, 223.15 $[M-H-Hex]^-$, 205.21 $[M-H-Hex-H_2O]^-$, 160.98 $[Hex-H-H_2O]^-$
52	Roseoside	19.24	431.13	$[M+HCOO]^-$	385.27 $[M-H]^-$, 223.08 $[M-H-Hex]^-$, 205.08 $[M-H-Hex-H_2O]^-$, 152.95 $[M-H-Hex-H_2O-C_4H_6O]^-$
53	*p*-Coumaric acid*	19.40	162.66	$[M-H]^-$	145.04 $[M-H-H_2O]^-$, 134.74 $[M-H-CO]^-$, 118.91 $[M-H-CO_2]^-$, 101.03 $[M-H-H_2O-CO_2]^-$
54	Hydroxy jasmonic acid *O*-hexoside isomer 3	19.47	387.23	$[M-H]^-$	369.22 $[M-H-H_2O]^-$, 225.17 $[M-H-Hex]^-$, 207.07 $[M-H-Hex-H_2O]^-$, 163.00 $[M-H-Hex-H_2O-CO_2]^-$
55	Neochlorogenic acid*	19.71	353.10	$[M-H]^-$	335.26 $[M-H-H_2O]^-$, 191.03 $[M-H-CA]^-$, 179.08 $[M-H-QA]^-$, 173.02 $[M-H-CA-H_2O]^-$
56	*O*-Coumaroylquinic acid	21.67	337.25	$[M-H]^-$	301.22 $[M-H-2H_2O]^-$, 191.02 $[QA-H]^-$, 172.98 $[QA-H-H_2O]^-$, 162.96 $[M-H-QA]^-$
57	Procyanidin B2*	23.64	577.21	$[M-H]^-$	451.22 $[M-H-C_6H_6O_3]^-$, 425.13 $[M-H-C_8H_8O_3]^-$, 289.09 $[M-H-C_{15}H_{12}O_6]^-$, 287.06 $[M-H-C_{15}H_{14}O_6]^-$
58	Syringic acid *O*-hexoside derivative	24.17	403.17	$[M-H]^-$	241.07 $[M-H-Hex]^-$, 223.02 $[M-H-Hex-H_2O]^-$, 197.11 $[M-H-Hex-CO_2]^-$, 179.06 $[M-H-Hex-H_2O-CO_2]^-$
59	Procyanidin C1*	24.47	865.01	$[M-H]^-$	695.28 $[M-H-C_8H_{10}O_4]^-$, 577.18 $[M-H-C_{15}H_{12}O_6]^-$, 451.41 $[M-H-C_{21}H_{18}O_9]^-$, 425.24 $[M-H-C_{23}H_{20}O_9]^-$
60	Syringic acid *O*-hexoside	26.42	359.17	$[M-H]^-$	341.23 $[M-H-H_2O]^-$, 315.05 $[M-H-CO_2]^-$, 197.12 $[M-H-Hex]^-$, 152.96 $[M-H-Hex-CO_2]^-$
61	Quercetin-*O*-(pentosylrutinoside)	26.71	741.37	$[M-H]^-$	723.27 $[M-H-H_2O]^-$, 609.24 $[M-H-Pent]^-$, 591.20 $[M-H-Pent-H_2O]^-$, 301.03 $[M-H-Pent-Rha-Hex]^-$
62	Eriodyctiol-*O*-hexoside	27.66	449.46	$[M-H]^-$	431.24 $[M-H-H_2O]^-$, 329.22 $[M-H-C_4H_8O_4]^-$, 287.17 $[M-H-Hex]^-$, 150.72 $[M-H-Hex-C_8H_8O_2]^-$

63	Abscisyl acid *O*-hexoside	28.04	471.20	$[M+HCOO]^-$	425.10 $[M-H]^-$, 263.23 $[M-H-Hex]^-$, 245.41 $[M-H-Hex-H_2O]^-$, 219.15 $[M-H-Hex-CO_2]^-$
64	Rutin*	29.02	609.27	$[M-H]^-$	591.32 $[M-H-H_2O]^-$, 463.27 $[M-H-Rha]^-$, 301.09 $[M-H-Rha-Glu]^-$, 178.97 $[M-H-Rha-Glu-C_7H_6O_2]^-$
65	Kaempferol-*O*-(pentosylrutinoside)	29.31	725.45	$[M-H]^-$	707.15 $[M-H-H_2O]^-$, 593.19 $[M-H-Pent]^-$, 575.24 $[M-H-Pent-H_2O]^-$, 285.10 $[M-H-Pent-Rha-Hex]^-$
66	Phloretin dihexoside	29.56	597.13	$[M-H]^-$	477.17 $[M-H-C_4H_8O_4]^-$, 459.25 $[M-H-C_4H_8O_4-H_2O]^-$,417.17 $[M-H-Hex-H_2O]^-$, 399.22 $[M-H-Hex-2H_2O]^-$
67	Quercetin 3-*O*-glucoside*	30.18	463.16	$[M-H]^-$	445.12 $[M-H-H_2O]^-$, 301.09 $[M-H-Glu]^-$, 273.29 $[M-H-Glu-CO]^-$, 179.02 $[M-H-Glu-C_7H_6O_2]^-$
68	Kaempferol *O*-rutinoside	32.43	593.36	$[M-H]^-$	575.25 $[M-H-H_2O]^-$, 285.07 $[M-H-Hex]^-$, 256.98 $[M-H-Hex-CO]^-$, 179.11 $[M-H-Hex-C_7H_6O]^-$
69	Naringenin*	33.08	271.04	$[M-H]^-$	253.07 $[M-H-H_2O]^-$, 202.99 $[M-H-C_3O_2]^-$, 150.92 $[M-H-C_8H_8O]^-$, 106.92 $[M-H-CO_2-C_8H_8O]^-$
70	Isorhamnetin *O*-rutinoside	33.23	623.11	$[M-H]^-$	357.38 $[M-H-Rha-C_4H_8O_4]^-$, 315.13 $[M-H-Rha-Hex]^-$, 300.24 $[M-H-Rha-Hex-CH_3]^-$, 271.14 $[M-M-H-Rha-Hex-CO_2]^-$
71	Luteolin *O*-hexoside	33.76	447.38	$[M-H]^-$	327.23 $[M-H-C_4H_8O_4]^-$, 285.02 $[M-H-Hex]^-$, 242.96 $[M-H-Hex-C_2H_2O]^-$, 151.11 $[M-H-Hex-C_8H_6O_2]^-$
72	Sinapic acid *O*-hexoside	35.29	385.25	$[M-H]^-$	340.94 $[M-H-CO_2]^-$, 223.01 $[M-H-Hex]^-$, 179.08 $[M-H-Hex-CO_2]^-$, 161.06 $[M-H-Hex-H_2O-CO_2]^-$
73	Dicaffeoylquinic acid	35.72	515.18	$[M-H]^-$	353.08 $[M-H-CA]^-$, 335.00 $[M-H-CA-H_2O]^-$, 316.87 $[M-H-CA-2H_2O]^-$, 179.12 $[CA-H]^-$
74	Quercetin tetrahexoside isomer 1	38.43	949.52	$[M-H]^-$	931.55 $[M-H-H_2O]^-$, 787.51 $[M-H-Hex]^-$, 625.41 $[M-H-2Hex]^-$, 463.58 $[M-H-3Hex]^-$
75	Quercetin tetrahexoside isomer 2	39.59	949.51	$[M-H]^-$	931.54 $[M-H-H_2O]^-$, 787.54 $[M-H-Hex]^-$, 625.49 $[M-H-2Hex]^-$, 607.53 $[M-H-2Hex-H_2O]^-$

76	Quercetin*	44.35	301.03	$[M-H]^-$	283.25 $[M-H-H_2O]^-$, 232.85 $[M-H-C_3O_2]^-$, 179.11 $[M-H-C_7H_6O_2]^-$, 150.88 $[M-H-C_8H_6O_3]^-$

Table 10. Polyphenols putatively identified in green tomato extracts by their MS/MS spectra in agreement with literature by HPLC-MS analysis in negative acquisition mode. * The identification of this molecule was confirmed using commercial standard. Glu, Rha, Xyl, Hex, Pent, HCOOH, CA and QA indicate glucose, rhamnose, xylose, hexose, pentose, formic acid, caffeic acid, and quinic acid moieties, respectively.

3.3.3. Development of glycoalkaloids and polyphenols HPLC methods

3.3.3.1. Development of glycoalkaloids HPLC-HESI-MS/MS method

The method used for SGAs quantitative analysis is accurately described in the previous paragraph **3.2.4. Quantitative SGAs analysis**. The method development was performed by the method proposed by Caprioli et al. (2014), with slight modification. In the method, the use of a percentage of formic acid (0.01%) allows to improve the ionization of SGAs amine group, increasing the sensitivity of the method. In the initial conditions, after 2 min hold at 20% of solvent B, the elution was performed with a linear gradient to 95% of solvent B in 10 minutes, followed by a re-equilibration of the column to the initial conditions for 4 minutes. The real gradient was zoomed in the range of phase B solvent (methanol at 0.01% HCOOH) of 20-95%, which represents the conditions for SGAs elution, allowing to reduce the time of analysis with a satisfying chromatographic separation. Among all the LC-MS methods, multiple reaction monitoring (MRM) method was selected to provide the better conditions for SGAs quantification. Instead, the tandem mass spectrometry (MS/MS) in data dependent acquisition (DDA) mode was selected to provide the best conditions for the study of the fragmentation pattern of the two standards for the method development. MRM acquisition mode is characterized by high sensitivity, thus allowing an accurate simultaneous quantification for several compounds. It allows the detection of a selected fragment that derive from a single selected precursor ion (MS^2 spectra) (Chiriac et al., 2021). In the MRM method, one transition, called quantifier, is used for the quantification of the analyte of interest, while another transition, called qualifier, is used for qualitative purposes to confirm the structural identity of the compound. Instead, tandem mass spectrometry, also known as MS/MS, two or more mass analyzers are coupled together thus enhancing analysis capacity through an additional fragmentation step and enabling the identification and separation of ions with similar *m/z*. After ionization, target analytes are separated by the first mass spectrometer, appointed as MS^1, according to their *m/z*, and ions with a particular *m/z* are selected and made to split into smaller fragment ions. Then, the second mass spectrometer (MS^2) further separates these smaller fragment ions according to their *m/z*, which are then detected. DDA acquisition mode is characterized by a lower sensitivity than MRM method, therefore it's mainly used for qualitative purposes.

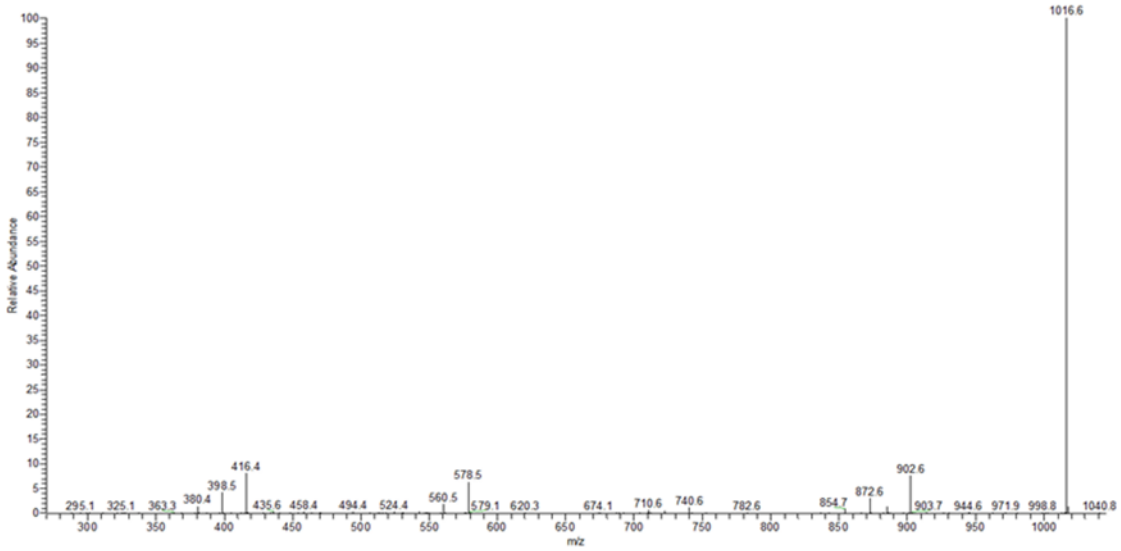


Figure 12: α-TM MS^2 spectrum by using a MS/MS analysis mode with a CID of 35 eV.

Figure 12 displays the MS^2 spectrum of α-TM analytical standard (parent ion: *m/z* 1034.6), obtained with an MS/MS analysis mode. α-TM MS/MS spectrum allows to clarify the fragmentation pattern of the molecule. The following ions represent the most important fragments:

- *m/z* 1016.4 corresponds to the neutral loss of a molecule of water;
- *m/z* 902.6 corresponds to the neutral loss of a terminal xylose unit;
- *m/z* 872.6 represents the neutral loss of the terminal glucose unit;
- *m/z* 854.7 is the fragment ion obtained by the neutral losses of the terminal glucose unit and a molecule of water;
- *m/z* 578.5 is the fragment ion obtained by the neutral losses of both terminal glucose and xylose units;
- *m/z* 560.5 is the fragment ion obtained by the neutral losses of the terminal glucose and xylose units and a molecule of water;
- *m/z* 416.2 represents the neutral loss of the entire tetrasaccharide side chain;
- *m/z* 398.5 corresponds to the losses of the entire tetrasaccharide side chain and a molecule of water.

An important diagnostic fragment in α-TM MS/MS spectrum is represented by the neutral losses of water (-18 Da), due to the presence of many alcoholic groups in the sugar moiety. By considering that the transition 1034.4-1016.4 (corresponding to the loss of a water molecule) provided the base peak fragment ion, it has been chosen as the quantifier transition for SGAs analysis. On the other hand, transition 1034.4 - 416.2 (corresponding to the loss of the entire lycotetraose moiety) has been chosen as a qualifier transition. For all the other steroidal SGAs, whose analytical standards are not available, the MS/MS analysis was performed directly on DT hydroalcoholic extract during the DDA analysis and was useful in obtaining the fragmentation pattern of these compounds of interest. Their fragmentation pattern was found to be very similar to α-TM MS/MS spectrum. For example, the compound hydroxytomatine provides the following fragment ions in the MS^2 spectrum:

- *m*/*z* 1032.4 corresponds to the neutral loss of a molecule of water;
- *m*/*z* 918.6 corresponds to the neutral loss of a terminal xylose unit;
- *m*/*z* 888.6 represents the neutral loss of the terminal glucose unit;
- *m*/*z* 870.7 is the fragment ion obtained by the neutral losses of the terminal glucose unit and a molecule of water;
- *m*/*z* 756.5 is the fragment ion obtained by the neutral losses of both terminal glucose and xylose units;
- *m*/*z* 738.5 is the fragment ion obtained by the neutral losses of the terminal glucose and xylose units and a molecule of water;
- *m*/*z* 432.5 represents the neutral loss of the entire tetrasaccharide side chain;
- *m*/*z* 414.5 corresponds to the losses of the entire tetrasaccharide side chain and a molecule of water.

The following **Figure 13** displays the MS^2 spectrum of hydroxytomatine, obtained with an MS/MS analysis mode.

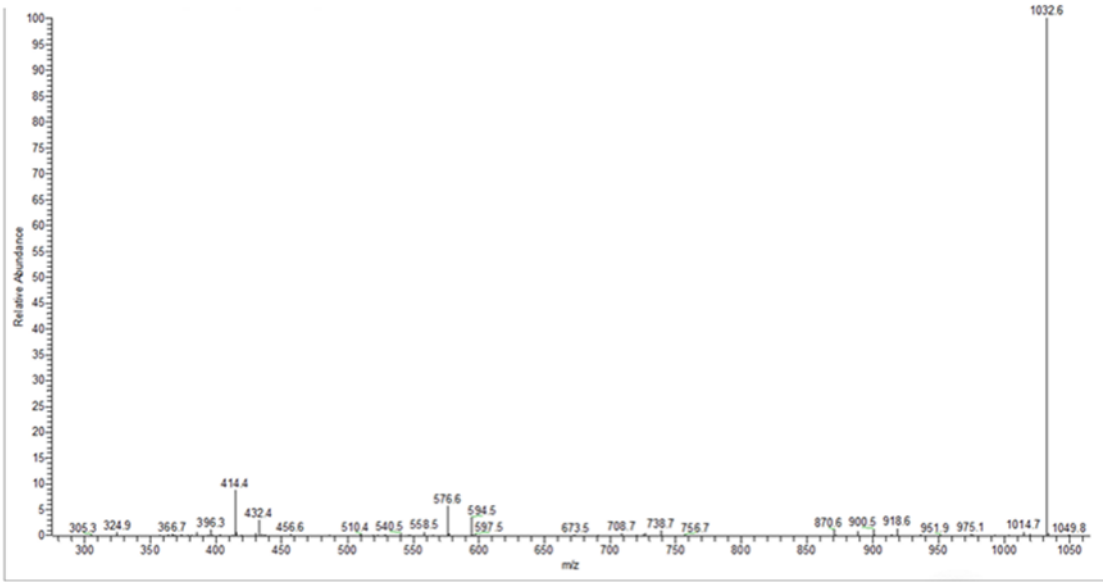


Figure 13: MS^2 spectrum of hydroxytomatine, by using a MS/MS analysis mode with a CID of 35 eV.

Tandem mass spectrometry analysis of hydroxytomatine (*m/z* 1050.6) clearly shows the two most intense fragment ions: *m/z* 1032.6, corresponding to the loss of a water molecule, and *m/z* 414.4, corresponding to the loss of the tetrasaccharide side chain and of a water molecule (**Figure 13**). Therefore, due to the lack of purified analytical standards, all the other tSGAs have been only quantified as α-TM equivalents, by relating the base peak areas of the analytes to the calibration curve of the standard compound. Although the fragment corresponding to the loss of a water molecule is the most intense on the mass spectrum, it's not specific for this class of compounds, thus providing a poorer qualitative value. On the contrary, the loss of the lycotetraose moiety is specific and highly selective, thus allowing both a quantitative analysis and a confirmation of the structural identity of steroidal SGAs found in tomato plant's extracts. Therefore, α-TM *m/z* transition 1034.6-416.4 proved to be sufficiently intense for a suitable quantification of other secondary SGAs. Another reason for the selection of a single MRM transition for the development of the method for secondary SGAs and α-TM quantification is related to necessity to ensure a correct number of points in the compound peaks. A chromatographic peak consists of data points that are connected by a line. For a small number of points, it looks like a distorted triangle and is not enough for a quantitative integration. On the other hand, for a high number of points, the peak has too many features. Therefore, an optimal amount of data points for a

chromatographic peak is between 12-20. During the spectrometric acquisition in the most common approaches of quantitative analysis (e.g., MS/MS, SIM, MRM) the instrument is not able to measure simultaneously two parent ions. Therefore, it has to switch between the different masses of the analysis. The speed of the instrument in the monitoring switch is determined by the dwell time and the cycle time. The dwell time represents the amount of time that the instrument requires to monitor one mass. The cycle time represents the total time that the instrument requires to acquire all the masses. Therefore, by considering both the qualifier and quantifier transitions for all the selected secondary SGAs, there would have been a problem of excess transitions and therefore a distortion of the chromatographic peaks, not providing enough points in the peak. Moreover, the choice to monitor the neutral loss of the lycotetraose moiety rather than the neutral loss of a water molecule is due to this fragment does not always correspond to the base peak ion and therefore to the predominant peak in an MS^2 spectrum. For example, SGAs such as acetoxytomatine and acetoxyhydroxytomatine have as their base peak ion the one corresponding to the neutral loss of the acetoxy group (-60 Da), while much less significant for these compounds is the neutral loss of a water molecule.

Therefore, by considering the different fragmentation tendencies of these two compounds, there would have been an error in the quantification phase, underestimating the quantity of analyte. For this reason, it was preferred to monitor the loss of the tetrasaccharide side chain instead of the neutral loss of a water molecule. For example, the MS^2 spectrum of the compound acetoxytomatine (provided in the **Figure 14**) shows the fragment ion 1032.5 (corresponding to the neutral loss of the acetoxy group) as the predominant, while the fragment ion 1074.6, corresponding to the neutral loss of a water molecule, is clearly much less intense.

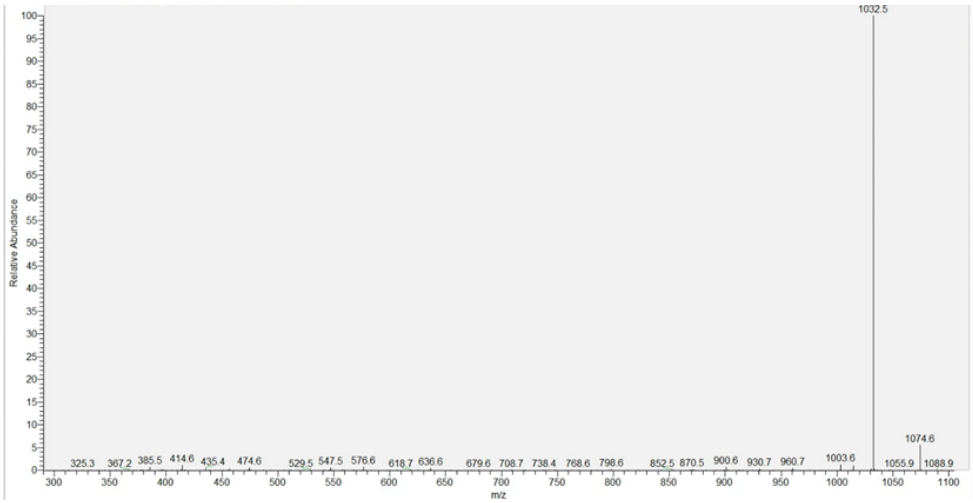


Figure 14: MS^2 spectrum of acetoxytomatine, obtained by a MS/MS analysis mode with a CID of 35 eV.

By considering all these aspects it was possible to develop an adequate MRM method for the analysis of 7 compounds of interest, which were quantified according to their corresponding chosen MRM transitions (**Table 13**). A comprehensive overview of all the peaks, obtained from the MRM method for SGAs is provided in the **Figure 15**. The chemical structures of the 7 SGAs quantified in the study are summarised in the **Figure 16**.

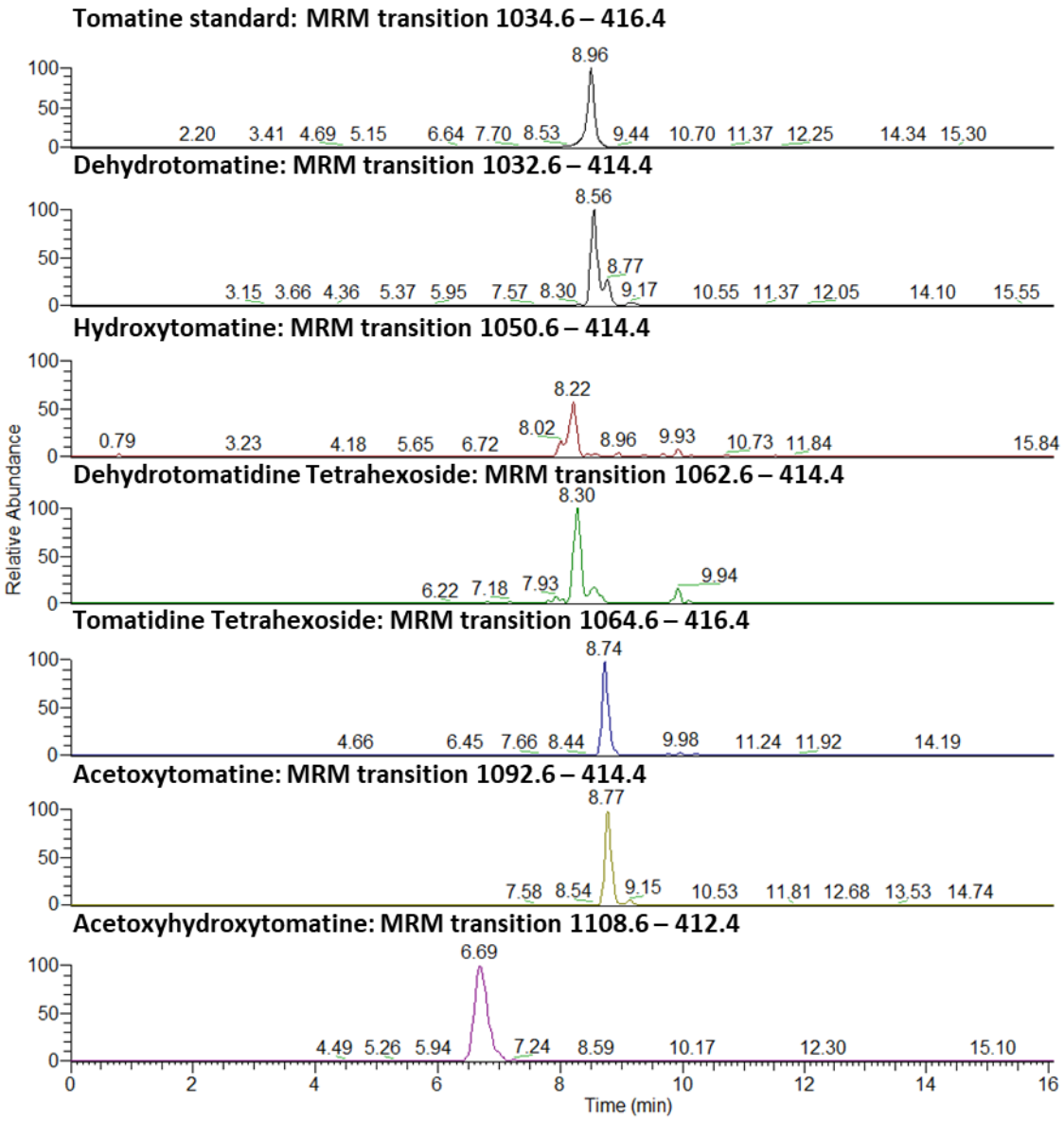


Figure 15: α-TM and the other 6 SGAs peaks obtained by the MRM method with a CID of 35 eV.

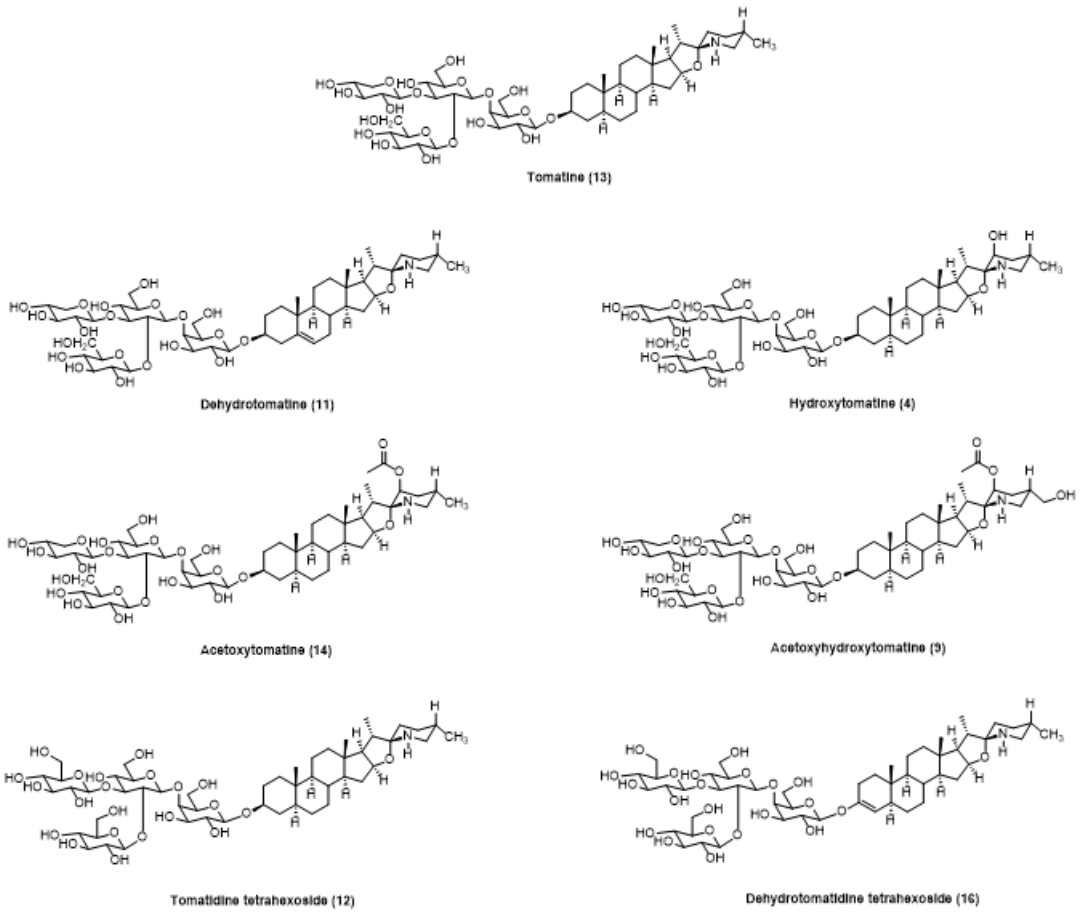


Figure 16: Chemical structure of 7 SGAs quantified during green tomato cultivars selection.

3.3.3.2. Development of polyphenols HPLC-DAD-FLD method

The development of the HPLC-DAD-FLD analysis for the quantitative analysis of polyphenols of unripe tomato extracts has been proposed by Maisto et al. (2022) and is accurately described in the previous paragraph **3.2.6. Quantitative polyphenols analysis**. This method agrees with the chromatographic conditions described in the literature for polyphenols HPLC-DAD analysis. In fact, several studies describe a separation by reversed-phase liquid chromatography (RP-LC) by using a C18 column. Water with organic solvents (methanol, acetonitrile) as a mobile phase, and a slow solvent gradient (duration from 45 to 80 min) are commonly used to provide sharper peaks. Moreover, organic acids, such as formic acid, can be successively used as mobile phase additives to improve the chromatographic separation (Chiriac et al., 2021). Therefore, the method proved to be extremely valid for separating a large number of polyphenolic compounds with a high

resolution, high efficiency, and high selectivity, as shown in **Figure 17,** where peaks clearly appear to be sharp and well separated. Since polyphenolic compounds absorb the UV-vis radiation, they can be analyzed with a Diode Array Detector (DAD), by selecting two specific wavelengths, which are 360 nm and 280 nm. The wavelength of 360 nm has been chosen to monitor flavonols (such as rutin, quercetin and quercetin 3-*O*-xylosil rutinoside). The wavelength of 280 nm proved to be suitable for both hydroxycinnamic acids (such as ferulic, chlorogenic acid and *p*-coumaric acid) and hydroxybenzoic acids (such as gallic acid). For example, the UV-spectrum of rutin standard cleary shows the absorbance peaks at these two wavelengths, as shown in **Figure 18**. The fluorimetric detector (FLD) has been chosen for flavanols (such as catechin, epicatechin, procyanidins B1, B2, B3, C1) quantification, applying an excitation wavelength of 272 nm and an emission wavelength of 312 nm. Fluorimetric detection was selected for the higher sensitivity and selectivity than UV-vis detection. The chemical structures of the 17 polyphenols quantified in the study are summarised in the **Figure 19**.

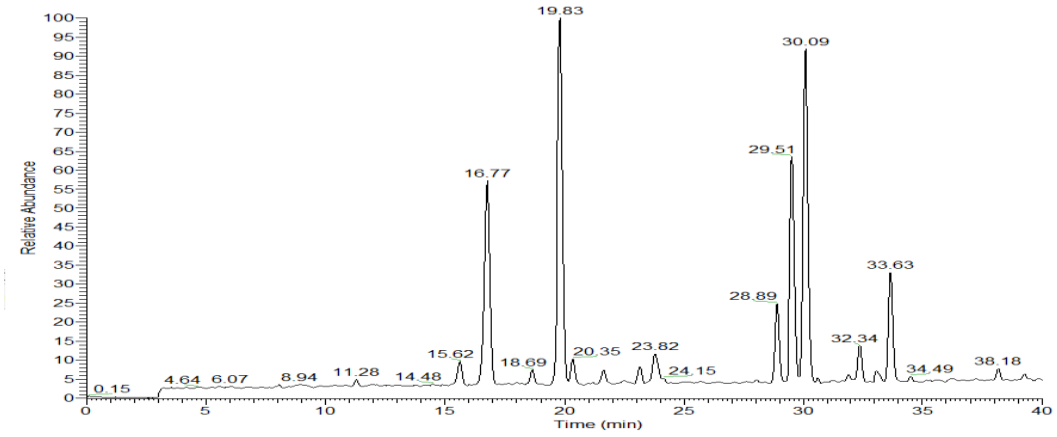


Figure 17: HPLC-DAD analysis of polyphenolic DT extracts at a wavelength of 280 nm.

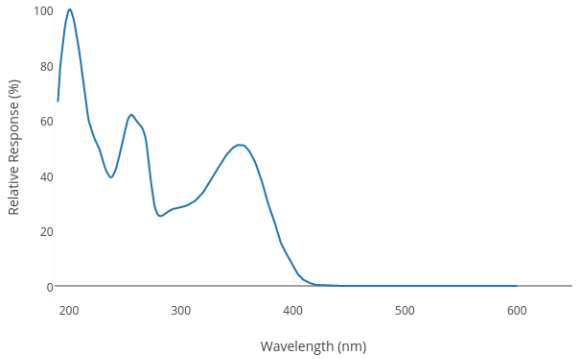


Figure 18: UV spectrum of rutin standard.

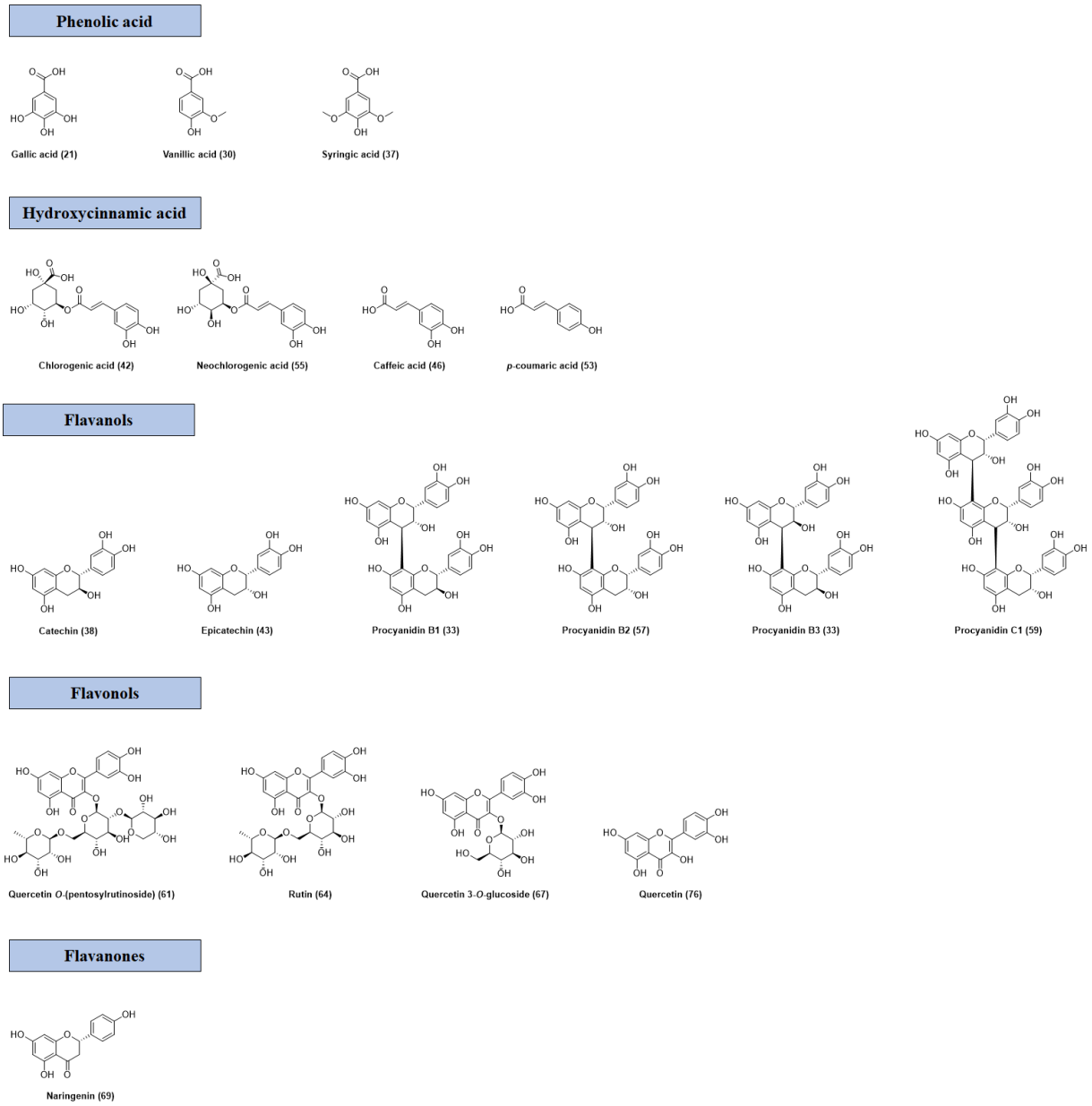


Figure 19: Chemical structure of 17 polyphenols quantified during green tomato cultivars selection.

3.3.4. HPLC method validation

3.3.4.1. Method validation according to ICH guidelines

The validation of polyphenols and SGAs methods was performed according to the ICH validation guideline (ICH.Q2[R2], 2022), which included the evaluation of a set of parameters, such as the linearity range, the limit of detection (LOD), the limit of quantification (LOQ), precision, and accuracy. LODs and LOQs values were determined to evaluate the sensitivity of the method. As a matter of fact, these parameters are needed to evaluate the method capacity for quantification analysis. LODs and LOQs values were calculated for each standard analyte according to signal to noise ratio (S/N). The S/N (S (signal of compound)/N (signal of noise)) represents a measure that compares the level of a signal to the level of background noise. Determination of the signal-to-noise ratio is performed by comparing measured signals from samples with known low concentrations of analyte with those of blank samples (Maisto et al., 2022). LOD represents the minimum concentration at which the analyte can be reliably detected and is defined as the lowest detectable concentration of the analyte that gives a response that the analytical system can distinguish from the background level. According to (S/N) parameter, the LODs were calculated as the standard concentration with a S/N value of 3. LOQ, instead, is defined as the lowest quantifiable concentration of analyte that can be measured with a standard level of confidence, and it is typically calculated as the standard concentration with a S/N value of 10 . As recommended by the ICH validation guideline (ICH.Q2[R2], 2022), besides LODs and LOQs values, the determination of the other two parameters (i.e., precision and accuracy) was required for the validation of the analytical method. Precision and accuracy are two parameters that define the observational error of a measurement process, established by repeated and averaged measurements. The precision of a measurement system is defined as the degree to which repeated or reproducible measurements show the same results under unchanged conditions. In other words, precision represents how close the measurements are to each other and it is a description of random errors, a measure of the statistical variability. Moreover, the concept of precision includes the concepts of repeatability and reproducibility. Repeatability defines the variation between analysis conducted in a short period of time analysis with the aim to keep conditions constant by using the same instrument and operator, while reproducibility defines the variation between analysis conducted in a longer time analysis using the same measurement process among different

instruments and operators. Precision is estimated by calculating the coefficient of variation (CV %), therefore the set of data points from repeated measurements of the same quantity can be said to be *precise* if their standard deviation is relatively small. On the other hand, the accuracy of a measurement system is the degree of closeness of a set of measurements of a quantity to that quantity true value. In other words, accuracy represents the proximity of a given set of measurement results to their true value. Therefore, a given set of data points from repeated measurements of the same quantity can be said to be *accurate* if their average is close to the true value of the quantity being measured. Accuracy is estimated by calculating the % bias which is the difference between the expected value and the true valor being estimated x 100. The terms variability and bias are often used in the statistics field instead of precision and accuracy and these terms indicate respectively the amount of imprecision and the amount of inaccuracy. A measurement device for quantitative analysis should be both precise and accurate, providing measurements all close to and tightly clustered around the true value. According to ICH validation guideline (ICH.Q2[R2], 2022), the evaluation of linearity range is required for the method validation. The linearity of an analytical procedure is its ability (within a given range) to obtain test results which are directly proportional to the concentration (amount) of analyte in the sample. The range of an analytical procedure is defined as the interval between the upper and lower concentration (amounts) of analyte in the sample (including these concentrations) for which it has been demonstrated that the analytical procedure has a suitable level of linearity, accuracy, and precision.

3.3.4.2. Validation of glycoalkaloids method

The procedures described above in the paragraphs **3.1.11. Method validation according to ICH guidelines** were applied to the method reported in the paragraph **3.1.4. Quantitative glycoalkaloids analysis**. α-TM calibration curve has been performed by considering the quantifier MRM transition 1034.4 – 416.2 and a range of eight concentration between 1.5 ppm and 0.001 ppm (**Figure 20**). For the calibration curve, an α-TM stock solution was prepared by dissolving the analytical standard in methanol to achieve a concentration of 1 mg/ml. According to literature, α-TM is soluble in organic solvents such as methanol, but not in aqueous solution with a neutral pH. The calibration curve displayed a favorable linear regression ($R^2 > 0.99$), thus demonstrating the linearity of the standard response in the range of concentrations analyzed. LODs and LOQs values were determined to evaluate the sensitivity of the method. α-TM displayed a LOD value of 0.011 ppm and a LOQ value of

0.033 ppm (**Table 11**), which were above the compound values in the analysed matrices, confirming the efficiency of the method for the quantification in the real samples.

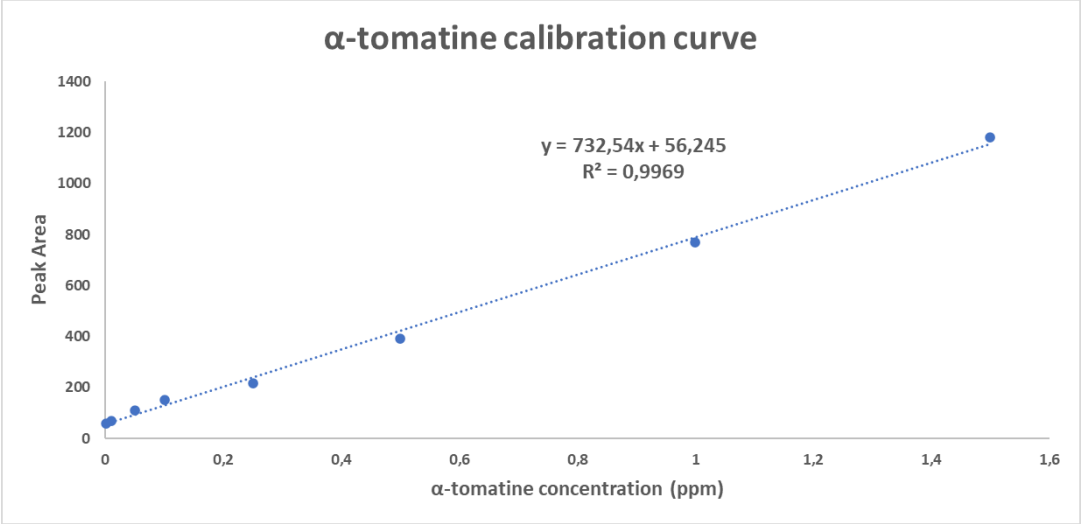


Figure 20: α-TM calibration curve for the quantifier transition 1034.4 – 416.2.

Compound	Linearity range (ppm)	Calibration curve	LOD (ppm)	LOQ (ppm)
α-TM	0.001 – 1.5	y = 2832.9x + 186.79	0.011	0.033
Gallic acid	0.1 – 1000	y = 2E+07x – 28492	6.240	18.908
Chlorogenic acid	0.1 – 1000	y = 3E+07x – 30148	7.102	21.522
Catechin	0.1 – 1000	y = 9E+06x – 11907	5.405	16.377
Epicatechin	0.1 – 1000	y = 1E+07x – 4563.5	4.849	14.695
Procyanidin B1	0.5 – 1000	y = 3E+06x – 3730.6	5.518	16.722
Procyanidin B2	0.5 – 1000	y = 8E+06x – 8832.4	5.200	15.758
Rutin	0.1 – 1000	y = 2E+07x – 1076.9	2.372	7.189
Quercetin	0.1 – 1000	y = 5E+07x – 41742	2.893	8.766

Table 11. Linearity range, calibration curves, limit of detection (LOD) and limit of quantification (LOQ) for SGAs and polyphenols analysis.

Although α-TM and TD can be potentially analyzed via HPLC-DAD (by exploiting their absorbance at a wavelength of 200 nm), it was preferred to use an HPLC-MS/MS approach, given the extremely lower sensitivity associated with the Diode Array Detector and the necessity to make time-consuming clean-up procedures before the analysis.

In agreement with the ICH validation guideline (ICH.Q2[R2], 2022), precision and accuracy were evaluated as well to validate the HPLC-MS/MS method, by considering that a measurement device for quantitative analysis should be both precise and accurate, providing measurements all close to and tightly clustered around the true value. Precision and accuracy were calculated by an intra-day and an inter-day analysis of α-TM standard solutions at 3 different concentrations (**Tables 12** and **13**). The 3 concentrations have been selected to represent the calibration levels (e.g., high, medium, low) included in the linearity range. The selection of these concentrations allowed to establish precision and accuracy of the entire calibration curves. The intra-day analysis was performed by injecting the two standard solutions three times per day. Instead, the inter-day analysis was performed by injecting the three selected standard solutions for 3 consecutive days. In the validation of the HPLC-MS/MS analysis, for the evaluation of intraday and interday precision and accuracy, the RSD value ranged from 0.461 to 3.128 % ppm and from -2.579 to 0.292 %, respectively. These results assessed that the developed method was satisfactory with acceptable precision, accuracy, and reproducibility.

Analyte	**Concentration (ppm)**	**Precision**	
		Intra-day (%, *n=3*)	Inter-day (%, *n=3*)
α-TM	1.5	0.461	2.790
	0.25	3.128	1.069
	0.01	1.470	2.400
Gallic acid	100	2.620	3.172
	50	1.682	1.300
	10	0.896	0.547
Chlorogenic acid	100	0.657	1.491
	50	2.285	2.931
	10	2.952	4.876
Catechin	100	0.611	0.122
	50	1.463	1.867
	10	8.860	7.974
Epicatechin	100	2.350	2.296
	50	7.913	1.800
	10	7.613	7.319

Procyanidin B1	100	1.539	8.147
	50	0.995	1.105
	10	2.202	2.312
Procyanidin B2	100	0.819	2.663
	50	1.328	1.949
	10	1.258	3.536
Rutin	100	1.354	1.378
	50	0.126	2.913
	10	1.922	2.920
Quercetin	100	0.360	4.637
	50	1.375	6.975
	10	2.276	4.260

Table 12. Intra- and inter-day precision for α-TM and polyphenols analysis.

Analyte	**Concentration (ppm)**	**Accuracy**	
		Intra-day (% bias, *n=3*)	Inter-day (% bias, *n=3*)
α-TM	1.5	-2.579	-1.543
	0.25	-2.457	-1.692
	0.01	0.292	-0.026
Gallic acid	100	3.508	3.926
	50	1.272	1.506
	10	0.368	0.394
Chlorogenic acid	100	-2.960	-2.980
	50	-1.483	-1.574
	10	-0.184	-0.196
Catechin	100	1.312	1.284
	50	0.076	-0.080
	10	-0.564	-0.509
Epicatechin	100	0.894	0.882
	50	0.620	1.250
	10	-0.011	0.144
Procyanidin B1	100	-0,507	-1,075
	50	-0,488	-0,486
	10	-0,189	-0,192
Procyanidin B2	100	-0.612	0.814
	50	-0.390	0.007
	10	-0.122	0.008
Rutin	100	0.601	0.643
	50	0.100	0.001
	10	0.034	0.020

	100	-2.765	-2.788
Quercetin	50	-1.561	-1.709
	10	-0.261	-0.265

Table 13. Intra- and inter-day accuracy for α-TM and polyphenols analysis.

3.3.4.3. Validation of polyphenolic method

The procedures described above in the paragraphs **3.1.11. Method validation according to ICH guidelines** were applied to the method reported in the paragraph **3.1.6. Quantitative polyphenols analysis**. Eight polyphenols (catechin, epicatechin, procyanidins B1 and B2, gallic acid, chlorogenic acid, rutin, and quercetin) were selected for HPLC-DAD-FLD method development and validation. Stock solutions of individual compounds, with a concentration of 1 mg/ml in methanol, were diluted in the same solvent to obtain six standard dilutions for the plotting of the calibration curves, with a dilution factor of 2 and 10. As reported by several authors, the phenolic nature of these compounds (in the form of aglycones and glycosides) makes them relatively hydrophilic and thus soluble in polar organic solvents such as methanol, justifying the choice of this solvent to fully solubilize reference standards. Calibration curves of flavonols, which were rutin and quercetin, were performed by monitoring their absorbance at 360 nm. Hydroxycinnamic acids (i.e., chlorogenic acid) and hydroxybenzoic acids (i.e., gallic acid) were monitored at 280 nm, according to their absorption spectrum in the UV-vis region. Instead, catechins (i.e., catechin, epicatechin, procyanidins B1 and B2) were analyzed by fluorimetric detection. Calibration curves were performed by considering 6-point lines in the range 1000 ppm and 0.1 ppm. The linearity of the standard response, in the range of concentrations analyzed, is demonstrated by an $R^2 > 0.99$ for all the phenolic compounds. The validation of the HPLC-DAD method was performed by evaluating the limit of quantification (LOQ) and limit of detection (LOD), following the procedure described above in paragraph **3.2.11. Method validation according to ICH guidelines**. LOD and LOQ values, along with the R^2 value of the six analytical standards, are provided in **Table 11**. These values are higher than those obtained for α-TM and TD, due to the intrinsic greater sensitivity associated with the HPLC-MS/MS method. In particular, LOD values range from 2.893 ppm and 7.102 ppm, while LOQ values range from 7.189 ppm and 21.522 ppm. Polyphenols LODs and LOQs values were above the quantification results of the analysed matrices, confirming the efficiency of

the method for the quantification in the real samples. It's interesting to note that the compounds quantified by fluorimetric detection (i.e., catechins and procyanidins) displayed LOQs and LODs values similar to those reported for other polyphenols quantified by HPLC-DAD analysis. The advantage of using the fluorimeter for their quantification is mainly due to the greater selectivity of fluorimetry, which reduces the signal to noise of the analysis and thus also any enhancing matrix effect in the quantification of the compounds of interest.

As recommended by the ICH validation guideline (ICH.Q2[R2], 2022), precision and accuracy of the analysis method were evaluated as well by an intra-day and an inter-day analysis of the mixture of standards at 3 different concentrations, as described in the previous paragraph **3.2.4.2. Validation of glycoalkaloids method**. Their value, expressed as % CV (coefficient of variation) and % Bias, respectively, are both provided in the previous **Tables 12** and **13.** The intraday precision values (CV %) are in the range of 0.126 % and 8.860 %, while the interday precision values (CV %) vary from 0.122 % to 8.147 %. In addition, intraday accuracy values range from -2.960 % to 3.508, while interday accuracy values vary from -2.980 % to 3.926 %. These results assessed that the developed method was satisfactory with acceptable precision, accuracy, and reproducibility.

3.3.5. Quantitative analysis of green tomato extracts

3.3.5.1. Glycoalkaloids quantitative analysis

Chromatographic analysis of unripe tomato SGAs and polyphenolic composition was carried out for the identification and quantification of 24 different compound content, as reported in Sections 2.4 and 2.6. Quantification of 7 SGAs was performed by HPLC-MS/MS analysis with an MRM scan mode. The quantitative MRM transition and the results expressed as µg α-TM equivalent/g DW, are reported in **Table 14**. Although there are many research studies about the phytochemical profile of the unripe tomato fruits, there is a disagreement between the data regarding the α-TM content. Some authors have reported an amount of the active ingredient ranging between 0.5 – 5 mg α-TM/g DW (Rick et al., 1994). Other literature data displayed a higher α-TM content of over 16 mg/g DW (Kozukue et al., 2004). The great variety of quantitative data could be explained by the different geographical and cultivation conditions of the plant. α-TM content in green tomatoes for human consumption (AT, CT, ST) are in agreement with the data reported in literature, ranging between 0.5 – 5 mg/g DW (Rick et al., 1994). Instead, agri-food waste unripe tomatoes TT, DT, ET and MT are characterized by a higher SGAs content, being 10 to 100-fold higher than the other cultivars. Among these, DT and ET were the most promising cultivars, with an α-TM content of 34.699 ± 1.101 and 34.354 ± 1.093 (mg/g DW), respectively. However, the DT represented the most interesting cultivar due to the high content of secondary SGAs, which could contribute to the pharmacological properties of the fruit. For example, dehydrotomatine and acetoxytomatine content appeared to be exceptionally high, with a value of 1.459 ± 0.086 and 0.948 ± 0.028, respectively (mg α-TM equivalent/g DW). However, these data agreed with previous studies on secondary SGAs content in unripe tomatoes (Kozukue et al., 2004).

Compound	MRM transition	Content (Mean ±SD, µg tomatine equivalent/g DW)						
		AT	TT	DT	ET	MT	CT	ST
α-Tomatine	1034.4 – 416.2	2611.05 ± 425.73^{a}	11054.79 ± 1101.33^{b}	34699.07 ± 1364.88^{c}	34353.73 ± 1094.41^{c}	3214.87 ± 258.73^{a}	282.05 ± 18.76^{d}	734.87 ± 17.45^{d}
Dehydrotomatine	1032.6 – 414.4	28.13 ± 3.54^{a}	600.61 ± 31.50^{b}	1458.83 ± 86.14^{c}	447.95 ± 8.34^{d}	563.42 ± 18.44^{b}	876.30 ± 27.29^{a}	227.46 ± 7.04^{f}
Acetoxytomatine	1092.6 – 414.4	22.38 ± 4.05^{a}	226.19 ± 10.36^{b}	947.95 ± 28.09^{c}	63.12 ± 3.39^{d}	118.16 ± 3.47^{e}	246.53 ± 21.81^{b}	59.86 ± 4.06^{d}
Acetoxyhydroxytomatine	1108.6 – 412.4	3.48 ± 0.57^{a}	7.07 ± 0.75^{b}	26.94 ± 2.39^{c}	n.d.	26.35 ± 0.38^{c}	5.80 ± 0.08^{a,b}	19.80 ± 0.79^{d}
Hydroxytomatine	1050.6 – 414.5	2.93 ± 0.66^{a}	78.62 ± 4.13^{b}	219.25 ± 3.80^{c}	n.d.	40.51 ± 2.06^{d}	11.06 ± 1.40^{e}	18.54 ± 0.45^{f}
Tomatidine tetrahexoside	1064.6 – 416.4	3.87 ± 0.65^{a}	129.97 ± 7.57^{b}	270.40 ± 22.30^{c}	67.86 ± 3.21^{d}	133.38 ± 2.38^{b}	13.11 ± 0.69^{a}	44.57 ± 3.40^{e}
Dehydrotomatidine tetrahexoside	1062.6 – 414.4	n.d.	3.57 ± 1.86^{a}	19.30 ± 1.88^{b}	25.56 ± 1.26^{c}	2.60 ± 1.00^{a}	n.d.	n.d.

Table 14. Quantitative analysis of SGAs profile. Results are expressed as mean ± SD. Statistical significance was calculated by one-way ANOVA followed by Tukey's post-hoc

test. Different letters reveal significant differences ($p < 0.05$) between each tomatoes cultivar. “n.d.” means “not detected”.

3.3.5.2. Polyphenols quantitative analysis

Quantification of 17 polyphenols was performed by HPLC-DAD-FLD analysis, and the results are reported in **Table 15**. The chemical structures of the 17 polyphenols are reported in the **Figure 19**. Similar to SGAs quantification, agri-food waste unripe tomatoes (TT, DT, ET, MT) displayed a greater amount of active ingredients than green tomatoes for food consumption (AT, CT, ST). The presence of three representative polyphenols in a great amount, chlorogenic acid (0.15 to 1.4 mg/g DW), rutin (0.05 to 1 mg/g DW) and quercetin *O*-pentosylrutinoside (0.05 to 0.5 mg/g DW), was observed in all unripe tomato cultivars. Chlorogenic acid represents the most representative polyphenol of unripe tomatoes, accounting for 75% of the total amount. Its content in the seven unripe tomato cultivars was in accordance with literature data, ranging from 0.5 to 1 mg/g DW (Slimestad & Verheul, 2009). Among these, the DT cultivar was the most attractive cultivar, with a content of chlorogenic acid, rutin and quercetin *O*-pentosylrutinoside of 1.412 ± 0.010, 0.996 ± 0.003, and 0.148 ± 0.001, respectively (mg/g DW). However, it is interesting to note that some polyphenols like flavanols and phenolic acid aglycones have a greater concentration in green tomatoes for food consumption than in agri-food waste ones. For example, catechin and *p*-coumaric acid were present only in traces or were not detectable in agri-food waste cultivars while they showed a high amount in cultivars for human consumption. Indeed, AT cultivar displayed a significant quantity of the two active ingredients, equal to 260.50 ± 19.50 and 8.28 ± 0.36, respectively (µg/g DW).

Chemical class	Compound	Content (Mean ± SD, µg/g DW)						
		AT	TT	DT	ET	MT	CT	ST
Phenolic acids	Gallic acid	22.21 ± 0.64^{a}	56.06 ± 2.22^{b}	72.40 ± 4.58^{c}	66.33 ± 2.28^{c}	42.51 ± 1.30^{d}	99.29 ± 0.50^{e}	92.11 ± 2.52^{f}
	Vanillic acid	36.98 ± 2.37^{a}	32.54 ± 3.10^{a,b}	58.42 ± 0.86^{c}	30.13 ± 0.74^{b}	35.88 ± 0.79^{a}	37.31 ± 0.57^{a}	n.d.
	Syringic acid	6.24 ± 0.58^{a}	9.87 ± 0.01^{b}	11.73 ± 0.24^{c}	18.46 ± 0.70^{d}	14.77 ± 0.37^{e}	n.d.	15.56 ± 0.22^{e}
Hydroxycinnamic acids	Chlorogenic acid	149.38 ± 3.68^{a}	862.50 ± 8.87^{b}	1411.59 ± 10.27^{c}	631.68 ± 16.16^{d}	339.74 ± 1.94^{e}	223.39 ± 0.60^{f}	166.15 ± 1.23^{a}
	Neochlorogenic acid	176.70 ± 0.11^{a}	138.30 ± 14.83^{b}	115.52 ± 2.52^{b}	84.93 ± 2.66^{c}	29.97 ± 0.35^{d}	n.d.	n.d.
	Caffeic acid	37.72 ± 1.18^{a}	37.72 ± 1.18^{b}	13.79 ± 0.91^{c}	n.d.	n.d.	17.77 ± 0.17^{b}	27.67 ± 0.01^{d}
	p-Coumaric acid	8.28 ± 0.36^{a}	0.59 ± 0.11^{b}	0.98 ± 0.01^{b}	n.d.	n.d.	0.56 ± 0.04^{b}	3.20 ± 0.03^{c}
Flavanols	Catechin	260.50 ± 19.50^{a}	178.24 ± 2.48^{b}	27.43 ± 0.78^{c}	55.76 ± 5.54^{d}	19.36 ± 0.73^{c}	107.52 ± 2.17^{e}	127.28 ± 1.01^{e}
	Epicatechin	7.99 ± 0.38^{a}	13.41 ± 1.31^{a,b}	n.d.	21.56 ± 1.14^{b}	58.72 ± 8.98^{c}	n.d.	9.58 ± 0.50^{a}
	Procyanidins B1 + B3	6.17 ± 0.01^{a}	5.47 ± 0.01^{b}	7.16 ± 0.01^{a}	4.73 ± 0.01^{b}	7.09 ± 0.01^{a}	19.99 ± 0.72^{c}	21.08 ± 0.75^{c}
	Procyanidin B2	5.25 ± 0.34^{a}	n.d.	5.82 ± 0.01^{a}	5.54 ± 0.01^{a}	5.73 ± 0.01^{a}	n.d.	26.50 ± 0.45^{b}
	Procyanidin C1	15.18 ± 1.62^{a}	n.d.	13.91 ± 0.30^{a}	7.65 ± 0.01^{b}	13.69 ± 0.15^{a}	10.57 ± 0.22^{c}	10.25 ± 0.09^{c}
Flavonols	Quercetin	5.55 ± 0.14^{a}	n.d.	n.d.	n.d.	n.d.	n.d.	n.d.
	Quercetin-3-*O*-glucoside	n.d.	9.12 ± 0.48^{a,b}	17.45 ± 0.52^{c}	10.75 ± 0.82^{b}	8.24 ± 0.99^{a}	n.d.	n.d.
	Quercetin-*O*-(pentosylrutinoside)	41.23 ± 0.49^{a}	103.68 ± 0.66^{b}	148.54 ± 0.62^{c}	244.59 ± 7.00^{d}	94.17 ± 1.00^{e}	53.50 ± 0.17^{f}	57.51 ± 1.05^{f}
	Rutin	47.01 ± 0.79^{a}	366.03 ± 1.53^{b}	995.57 ± 3.46^{c}	390.04 ± 11.87^{d}	264.40 ± 1.06^{e}	67.42 ± 0.15^{f}	90.64 ± 2.21^{g}
Flavanones	Naringenin	n.d.	2.98 ± 0.57^{a}	1.79 ± 0.17^{b}	n.d.	n.d.	n.d.	n.d.

Table 15. Quantitative analysis of polyphenols profile. Results are expressed as mean ± SD. Statistical significance was calculated by one-way ANOVA followed by Tukey's post-hoc test. Different letters reveal significant differences ($p < 0.05$) between each tomatoes cultivar. "n.d." means "not detected".

3.3.5.3. Green tomato extracts metabolomics analysis

The word "metabolomics" was used for the first time by Oliver Fiehn in 2002 (Fiehn, 2002). It is referred to the identification and the quantification of a set of metabolites with low molecular weight (< 1.5 kDa) which constitute the metabolome of the organism in analysis, as aminoacids, lipids, fatty acids, nucleic acids, organic acids, carbohydrates. Two different approaches are used in metabolomics, the target approach and the untargeted approach. The target approach, also called quantitative metabolomics, is mainly focused on a specific number of metabolites which are distinctive of a metabolic pathway, generally thought to an absolute quantification of them. The untargeted approach, also called qualitative

metabolomics, provides a general fingerprint of the metabolome of the organism in analysis. The most common analytical platforms used in metabolomics are the Mass Spectrometry (MS) and the Nuclear Magnetic Resonance (NMR). In this Ph.D. project, both targeted and untargeted approaches are used, applying both MS and NMR platforms. Usually, in metabolomics studies, data analysis is coupled with chemometric methods such as PCA and PLS-DA (Partial Least Square Discriminant Analysis) to understand the patterns in the data and to identify molecular markers. These approaches are supervised statistical methods for classification and discriminant analysis which can be used to describe the relationship among the measured variables. These methods aim to maximize the covariance between variables X (samples readings, which represent the metabolomic data) and corresponding dependent variable Y (classes or groups) of highly multidimensional data. Therefore, these tests are used to clarify metabolomic similarities or differences among the groups, by providing graphical interpretations of data in which similar samples cluster close together and dissimilar samples are distinctly separated. Generally, the samples can be represented by colored ellipses, grouped under a confidence interval of 95%. The PCA plot describes a certain % of data variance, represented by a specific number of Principal component (PC), which are indicated in pairs on the X and the Y axes, respectively. Finally, the heatmap was constructed to illustrate the relative metabolite concentration differences that occur among groups. This approach is well-suited for visualizing large numbers of multidimensional data and can be used to highlight clusters of rows with similar values, as these are displayed with similar colors. Therefore, similar concentrations of a specific metabolite among groups were indicated with the same color, which ranged from blue (for the lowest concentration), to red (for the highest concentration) and the intensity of the color was directly correlated to the amount of that compound found in the group. Heatmap was combined with hierarchical clustering, which is a way of arranging items in a hierarchy based on the distance or similarity between them. It is possible to cluster both rows and columns in the heatmap. The result of a hierarchical clustering calculation is displayed in a heat map as a dendrogram, which is a tree-structure of the hierarchy. Row dendrograms show the distance (or similarity) between rows and which nodes each row belongs to as a result of the clustering calculation. Column dendrograms show the distance (or similarity) between the variables (the selected cell value columns). A preliminary common step in metabolomics analysis is represented by the data pre-treatment, which can include several steps, such as the alignment, the normalization and the scaling of data.

In order to achieve a better evaluation of the quantitative profile of the 7 unripe tomato cultivars, a statistical metabolomic approach was performed to explore the relationship between the quantitative polyphenols and SGAs content and the cultivar of green tomatoes. It includes a biplot of the principal component analysis (PCA) and a heatmap combined with a hierarchical clustering analysis was performed as well. In the PCA score plot of the first three principal components (PCs) (**Figure 18**), the unripe tomato cultivars were clustered based on the content of each compound. As displayed in the picture, the first, the second and the third PCs explained 42.49%, 18.88% and 14.19% of the total variation, respectively. The biplot revealed a broad dispersion of the quantified compounds and explained 61.37% and 56.68% of the variability, respectively for the first and the second biplot. This analysis revealed that the seven tomato cultivars showed several differences in the metabolic composition.

Positive value at PC1 indicated samples with high SGAs (i.e. α-TM, Dehydrotomatine, Dehydrotomatidine tetrahexoside, Hydroxytomatine, Acetoxytomatine, Tomatidine tetrahexoside, Acetoxyhydroxytomatine), glycosylated phenolic acids (i.e., Chlorogenic acid and Neochlorogenic acid) and flavonols (i.e., Rutin Quercetin 3-*O*-glucoside, Quercetin *O*-(xylosylrutinoside),) content. Instead, negative values at PC1 were referred to high flavanols (i.e., Catechin, Procyanidins B1, B2, B3, C1) and polyphenols aglycones (i.e., *p*-Coumaric acid, Quercetin, Caffeic acid) content. An exception to this distribution is represented by the flavonol Epicatechin and the polyphenols aglycones Gallic acid and Syringic acid, which displayed a positive value at PC1. The second and third PCs had a minor capability to describe the system variability. All samples could be divided into two clusters, which included the agri-food waste unripe tomatoes (TT, DT, ET, MT) and the green tomatoes for human consumption (AT, CT, ST). The two groups were characterized by a positive and a negative PC1 value, respectively. The first cluster could be divided in two subclusters according to the different polyphenol content. As shown in **Figure 21** and **Table 15**, ET and MT cultivars showed higher epicatechin and a lower neochlorogenic acid content compared to TT and DT cultivars, thus being the main factor for intra-cluster diversity. In the second cluster, CT and ST cultivars displayed some differences in the polyphenol content compared to AT one. In fact, AT cultivar represented the only one in which quercetin has been detected and displayed a higher content of *p*-coumaric acid than other samples. These differences can be explained by the opposite loadings of some polyphenols (e.g., quercetin, dimeric procyanidins B1, B2, and B3) on the second and third principal component (PC2 and PC3).

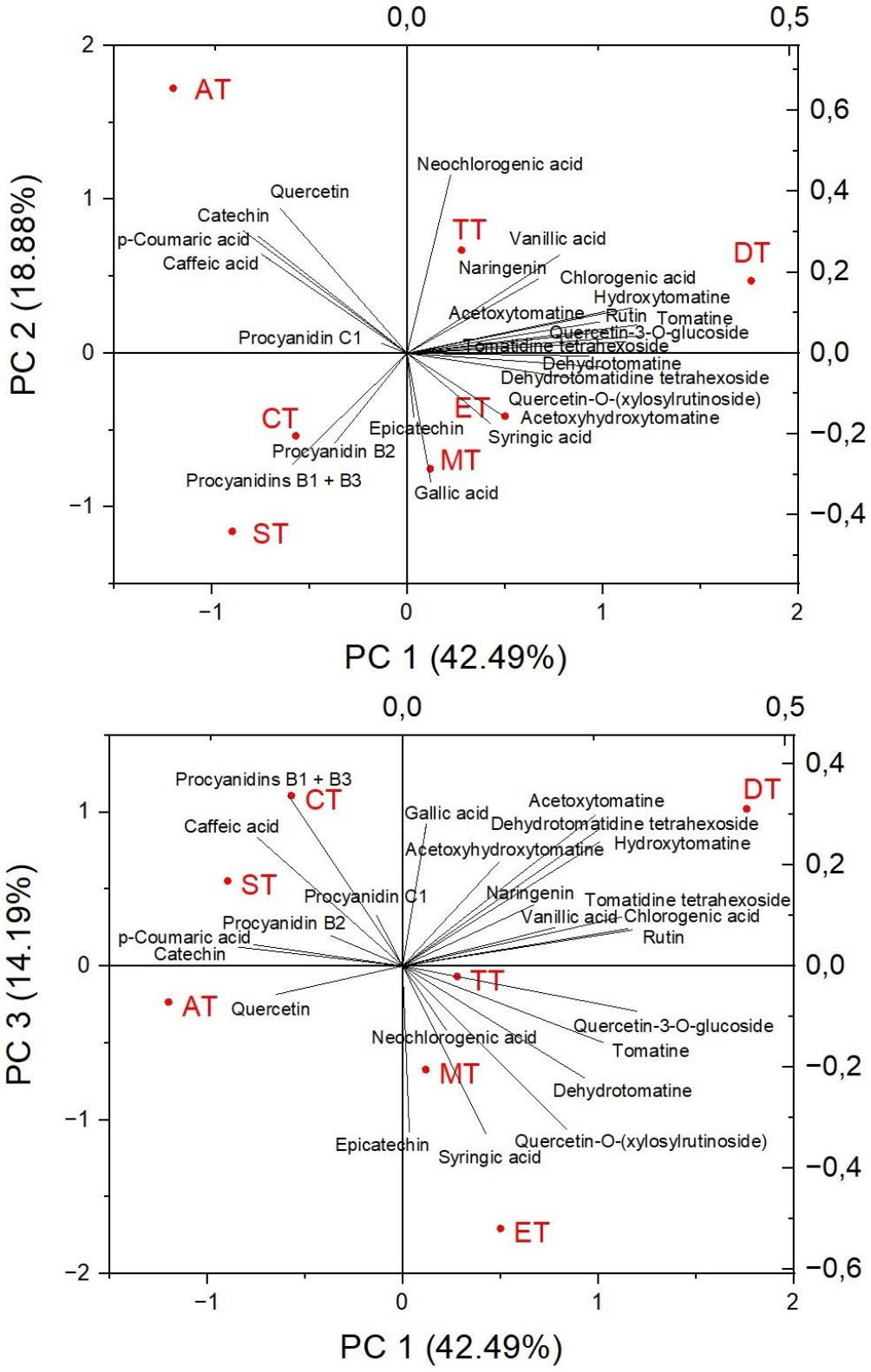


Figure 21. Biplot of the first three principal components in the principal component analysis (PCA) of metabolites in 7 unripe tomato cultivars and 24 quantified compounds.

The heatmap and the hierarchical cluster analysis in **Figure 22** was consistent with the classification shown in the PCA score plot. This analysis allowed to divide the groups since the similarity of the metabolomic profile, with results in agreement with the PCA biplot. Furthermore, the quantified compounds were already clustered and subdivided in two groups. The first cluster included most of SGAs, glycosylated phenolic acids and flavonols, while the second cluster contained phenolic acid aglycones and flavanols. This analysis allowed to confirm the high correlation observed between some compounds. For example, the highest levels of α-TM, chlorogenic acid, rutin and quercetin *O*-(pentosylrutinoside) were quantified in the DT cultivar. Instead, the greatest amounts of *p*-coumaric acid and quercetin were identified in the AT cultivar. The different distribution of these molecules could be explained by the different harvesting conditions or the geographical origins. Indeed, several studies had already demonstrated the impact of plant harvest and growth conditions on the production of active metabolites (Slimestad & Verheul, 2009). However, it will still be necessary to carry out further analyses to evaluate the effect of cultivation and climatic conditions and agronomic effects on active ingredient content.

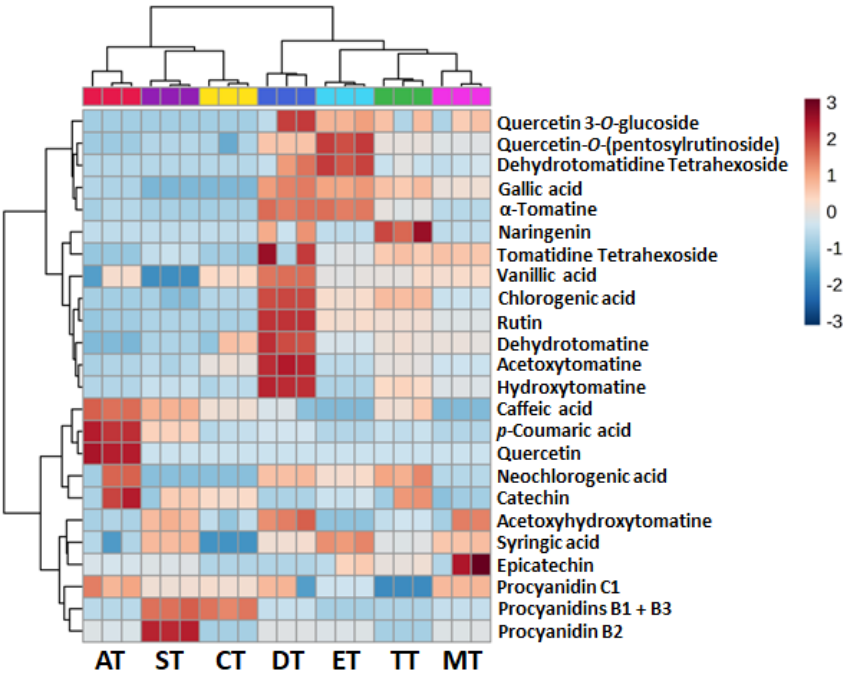


Figure 22. Heat map of hierarchical cluster analysis of quantified polyphenols and SGAs in seven unripe tomato cultivars; the different colours indicate differential abundances of compounds, the columns represent the cultivars, and the rows represent the quantified compound.

3.3.6. Green tomatoes: a rich source of antioxidants

3.3.6.1. Antioxidant properties of green tomatoes

The antioxidant activity of unripe tomato cultivars was evaluated by the total polyphenol content (FOLIN) assay and by three single electron transfer (SET) assays, which included DPPH, ABTS, and FRAP tests. The Folin-Ciocalteau (FC) assay provides a rough estimate of the total amount of polyphenols in the sample, expressed as mg/ml of gallic acid equivalents. The total phenolic content is directly proportional to the absorbance, recorded at a wavelength of 760 nm. FC reagent is probably a complex mixture of hetero polyacid, phosphomolibdenum and phosphotungstenic acids, even if its structure it's not fully elucidated yet (Platzer et al., 2021). Briefly, when the FC reagent is exposed to an antioxidant molecule, the molybdenum ion is reduced (from Mo^{+6} to Mo^{+5} and Mo^{+4}), by a reaction based on a single electron transfer (SET) mechanism (**Figure 23**).

$$Mo^{+6}\,(\text{yellow}) + e^{-1} \longrightarrow Mo^{+5}\,(\text{blue})$$

$$Mo^{+5} + e^{-1} \longrightarrow Mo^{+4}\,(\text{blue})$$

Figure 23. Reaction mechanism between an antioxidant molecule and the Folin-Ciocalteau reagent.

In particular, this reaction is carried out at pH 10, by using an alkaline solution of potassium carbonate. These conditions allow the phenolate ion to be formed, which is then capable of reducing the FC reagent, by transferring its electron. For this reason, the reaction is slow at acid pH and faster at alkaline pH. Since the plant matrices are a complex mixture of polyphenolic and not-polyphenolic compounds, each structure can contribute to the redox reaction and therefore to the final result. Interestingly, among polyphenols, some structure-activity relationships have been highlighted: both the number and positions of OH groups in the B and A-ring contribute to the final value. Generally, OH groups at the *para* or *ortho* position confer a stronger reducing ability than those in the *meta* position, thanks to the stabilization effect of the phenoxy radical, by intramolecular hydrogen bonds. Moreover, by replacing an OH group with a methoxyl group the reducing ability drastically decreases. Among polyphenols, hydroxycinnamic acids are characterized by a stronger reducing

activity than hydroxybenzoic acids, mainly due to the resonance stabilization effect of the phenoxy radical. Unfortunately, the Folin-Ciocalteau method can be affected by a low accuracy due to the presence of interfering substances. Among them, reducing sugars (e.g., glucose and fructose), ascorbic acid, dehydroascorbic acid, aromatic amines, sulfur dioxide (and other enediols and reductones), organic acids, and Fe(II) can react with the FC reagent, thus contributing to the absorbance and leading to an overestimation of the final result. For this reason, there might not be a direct correlation between the total phenolic content (TPC) evaluated with this assay, and the content of single polyphenols. In order to eliminate these interfering substances, different methods may be used, including the partial purification of extracts by SPE cartridges, the calculation of a correct total phenolic content by subtracting the value of reducing activity associated with ascorbic acid, and the use of oxidative agents (e.g., hydrogen peroxide) to remove the interferents before performing the FC assay. After a suitable reaction time between the antioxidant molecules and the FC reagent (at a pH of 10), an intense blue color of the solution can be observed, and the absorbance is measured spectrophotometrically at 760 nm. The total phenolic content is calculated by comparing the absorbance value with the gallic acid calibration curve (**Figure 24**), which is the reference compound used to quantify the total phenolics in the sample.

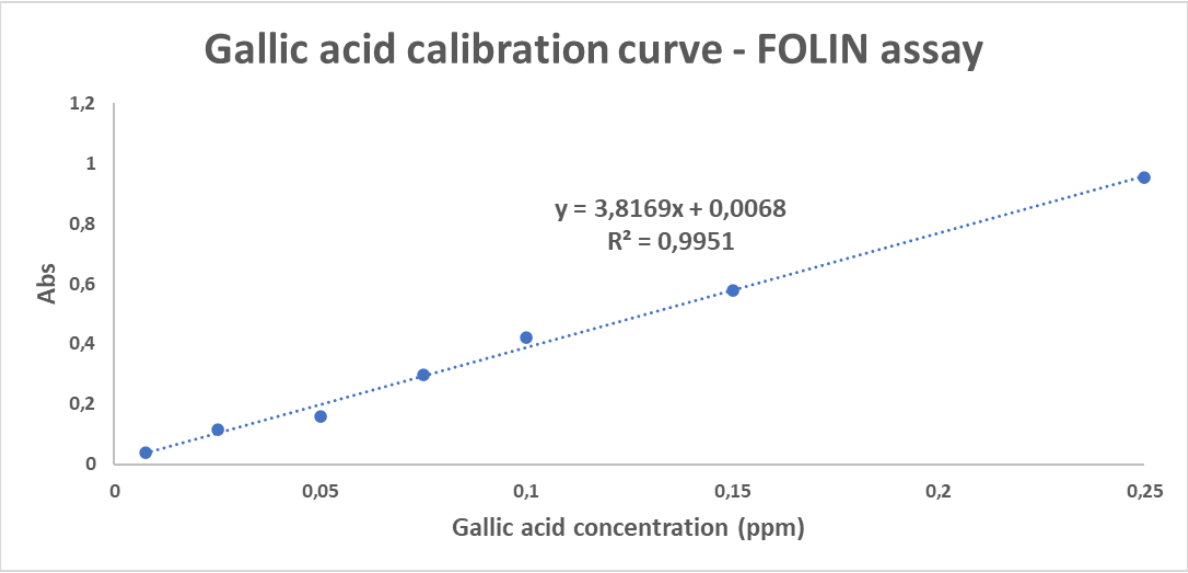


Figure 24. Gallic acid calibration curve for total polyphenols content (FOLIN) quantification in the extracts.

The antiradical activity of tomato plant extracts has been evaluated as well by a DPPH test. The 1,1-diphenyl-2-picrylhydrazil (DPPH) radical is a stable free radical used as a reagent for this assay; the relative stability is due to the delocalization of the spare electron on the nitrogen atom in the whole molecule (**Figure 25**). The overall relative stability makes the DPPH solutions stable for a long time since this compound does not react to form dimers. However, in the presence of light, this radical reacts slightly with the atmospheric O_2. Therefore, DPPH solutions should be kept in the dark to limit this unwanted reaction. Moreover, DPPH reagent is slightly soluble in not-polar organic solvents and completely soluble in polar-organic solvents, such as methanol, that are commonly used to perform this test. The methanolic DPPH solution (associated with an intense purple color, monitored at a wavelength of 517 nm) may react with either hydrogen atom donors (HAD) or other radicals at different reaction sites. The first ones react with the divalent nitrogen atom, to form the corresponding hydrazine (DDPH-H), while the second ones attack the phenyl ring, although the limited space around the nitrogen atom may sterically inhibit the access of bulky radicals in this region. However, when these antioxidant molecules act as hydrogen atom donors towards the DPPH radical, the corresponding reduced compound (DPPH-H) is formed, and the intense violet color of the solution disappears.

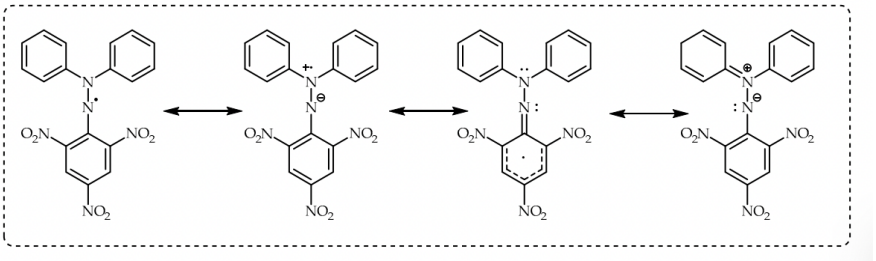


Figure 25. Chemical structure of 1,1-diphenyl-2-picrylhydrazil radical, used for the DPPH assay.

Phenolic compounds may react through two possible mechanisms: in the first one, called Hydrogen Atom Transfer, an H atom is transferred from the phenolic group to the DPPH molecule, thus forming the hydrazine. In the second one, called Single-Electron Transfer, an electron and then a proton are transferred to the reagent. However, several interferents may reduce or completely inhibit the access of phenolic compounds to the DPPH reagent. Among them, complex molecules may block access to the DPPH radical, even at low concentrations. Analogously to the Folin-Ciocalteau method, the DPPH assay cannot be

directly correlated with the polyphenol content in the extract since several not-polyphenolic compounds are responsible for the positivity to the test. Among them, the amino acid tyrosine and cysteine may donate their H atom to the DPPH reagent, thus forming the radical RS• or RO•, which then dimerizes with another molecule (**Figure 26**).

$$Z\bullet + RSH = ZH + RS\bullet \quad (1)$$

$$RS\bullet + RS\bullet = RS - SR \quad (2)$$

Figure 26. H atom transfer reaction between the DPPH radical (Z) and the amino acid cysteine (RSH).

On the other hand, methanol is generally used as a solvent for the test, but it strongly binds H atoms of phenolic compounds and inhibits HAT processes. However, the problem can be solved by adding water to the solution, which disrupts the bonding and thus facilitates the hydrogen atom transfer (Kedare & Singh, 2011). By considering this important aspect, our extracts were prepared by dissolving them in a hydroalcoholic mixture (at 80% of methanol) instead of pure methanol. Another problem is represented by carotenoids, particularly abundant in the green unripe fruits of tomato plants, which can interfere with the 517 nm-absorbance measurement of DPPH. Although these described limitations, the DPPH assay can be considered as an easy, fast and reproducible method for a first screening of the antiradical activity associated with plant extracts and foods. The test allows the antioxidant power to be determined by reacting the sample with a DPPH solution, which is intensely colored purple and provides an absorbance at 517 nm. Therefore, a decrease in this absorbance is observed, due to the scavenging activity of the antioxidant toward the DPPH radical, after a predetermined incubation time. This decrease is proportional to the content of antioxidants present in the sample. The results are expressed as Trolox equivalent micromoles, thus using this compound as a reference standard for the plotting of the calibration curve (**Figure 27**). Trolox (6-hydroxy-2,5,7,8-tetramethylchroman-2-carboxylic acid) is a water-soluble analogue of vitamin E, which exhibits a well-known antioxidant activity, due to the presence of the phenolic group. The results were obtained by comparing the % inhibition value, calculated for the sample test, with the Trolox calibration curve, which reported the % inhibition in the function of the Trolox concentration (μM).

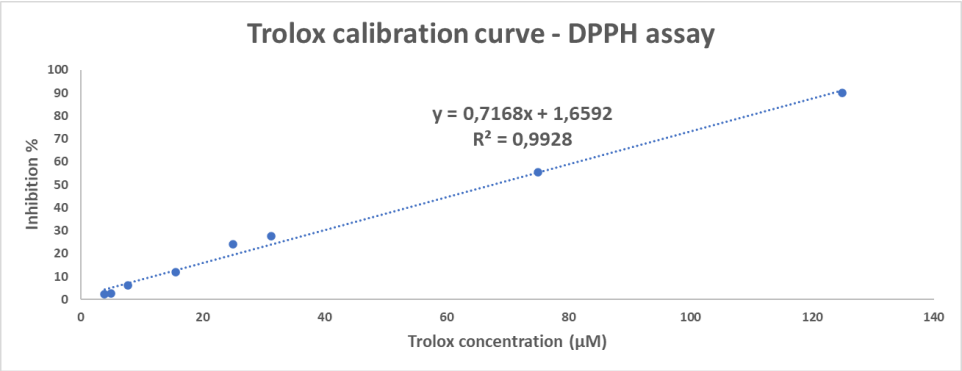


Figure 27. Trolox calibration curve for DPPH assay.

Another assay used for the evaluation of the antioxidant activity is represented by the ABTS (2,2'-azino-bis(3-ethylbenzothiazoline-6-sulfonic acid) assay. This compound is a neutral reactive that reacts with an oxidant agent, as the sodium persulfate $Na_2S_2O_8$ or the potassium persulfate $K_2S_2O_8$, to generate a cationic radical (**Figure 28**). The radical produced by the reaction can react with antioxidants, reducing the value of absorbance of the ABTS solution. The results are expressed as Trolox equivalent micromoles, thus using this compound as a reference standard for the plotting of the calibration curve (**Figure 29**). The results were obtained by comparing the % inhibition value, calculated for the sample test, with the Trolox calibration curve, which reported the % inhibition in the function of the Trolox concentration (µM).

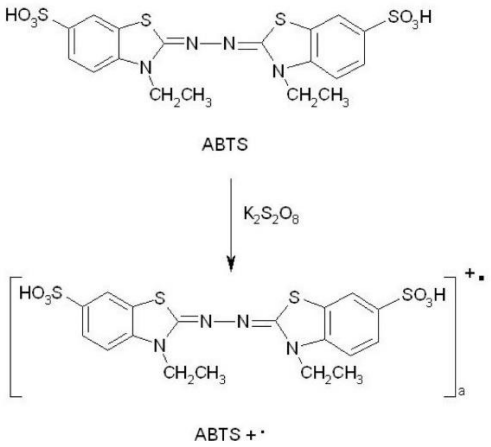


Figure 28. Reaction between the ABTS reagent and potassium persulfate to generate the cationic radical reagent of the ABTS assay.

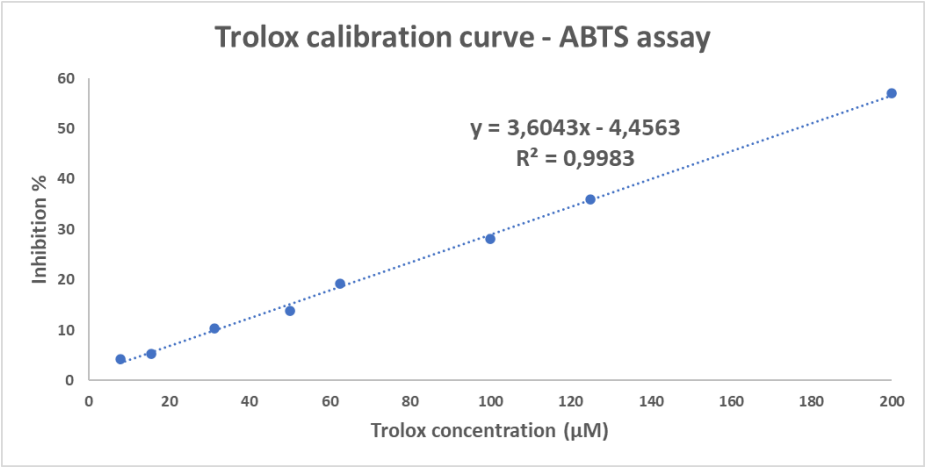


Figure 29. Trolox calibration curve for ABTS assay.

In addition to FOLIN, DPPH, and ABTS assays, the antioxidant activity can be also investigated by performing the FRAP assay. The ferric-reducing antioxidant potency was evaluated by measuring the ferric–to–ferrous reduction in the presence of a Fe(II)-stabilizing ligand, which is the tripyridyltriazine (TPTZ) (Prior et al., 2005), thus leading to the formation of an intensely blue ferrous complex. The reaction was carried out under acidic conditions (pH = 3.6) to ensure an adequate solubility of the iron (II)/iron (III) ion. Moreover, in an acid environment, the mechanism is totally based on a single electron transfer reaction from the antioxidant to the ferric ion (**Figure 30**), and this reduction was spectrophotometrically monitored by measuring the change in absorption at 593 nm.

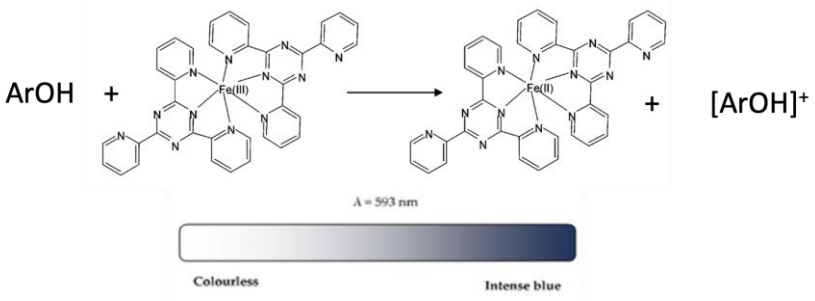


Figure 30. Reaction mechanism for FRAP assay.

Unfortunately, the reaction is not-specific, since any compound with a suitable redox potential (i.e., lower than that of the redox pair Fe^{3+}/Fe^{2+}) may drive the Fe III-TPTZ

reduction. On the other hand, this method is not able to measure all the antioxidants in a complex vegetable matrix, in particular those lipophilic and the thiol antioxidants, such as glutathione. Moreover, some antioxidants (i.e., reductants) are characterized by a slow reaction time with the reagent and therefore they may not be totally oxidized within the recommended time of protocol, with a consequent underestimation of the final result. Therefore, not all polyphenols are able to reduce Fe^{3+} in the time required by the protocol, thus leading to a drastic change in the results, depending on the reaction time. For example, absorbance values (at 593 nm) increase slowly for polyphenols such as caffeic acid, tannic acid, ferulic acid, ascorbic acid, and quercetin, even after several hours of reaction time. Another problem of this assay is the concomitant generation of Fe^{2+}, a well-known prooxidant involved in the production of additional radicals, such as $OH^{\cdot}$ from H_2O_2, which can further react with the antioxidants. Finally, compounds that absorb at the same wavelength of Fe(II)-TPTZ may interfere with the measurement, thus causing an overestimation of the FRAP value. However, this method proved to be fast, easy, inexpensive, and robust, thus justifying its application for the first screening of plant extracts' bioactivity. The reducing activity of antioxidant molecules, which corresponds to an increase in absorbance at 593 nm, can be expressed as micromolar equivalents of Fe^{2+} or in relation to a standard antioxidant, such as Trolox. The results are expressed as Trolox equivalent micromoles, thus using this compound as a reference standard for the plotting of the calibration curve (**Figure 31**). The results were obtained by comparing the % inhibition value, calculated for the sample test, with the Trolox calibration curve, which reported the % inhibition in the function of the Trolox concentration (µM).

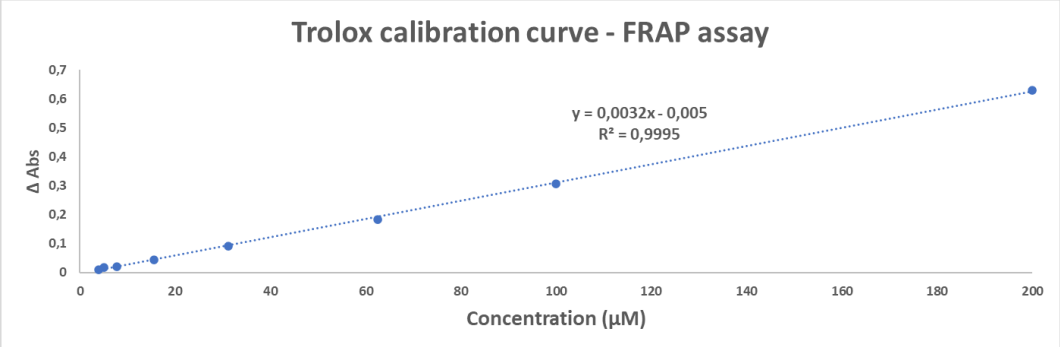


Figure 31. Trolox calibration curve for FRAP assay.

The radical scavenging activity assays showed a similar trend among the unripe tomato cultivars with some differences for the absolute values, as reported in the **Table 16**. Based on these data, agrifood waste cultivars were characterized by greater antioxidant properties, while the green tomatoes for food consumption showed lower radical scavenging activities ($p < 0.05$). Among these, DT displayed the highest SET antioxidant properties than other cultivars. The DPPH, ABTS, and FRAP values of DT were 8.45 ± 0.21, 9.28 ± 0.39 and 14.47 ± 0.48 (µmol TE/g DW), respectively. Interestingly, green tomatoes for human consumption did not show statistically significant differences in most antioxidant assays ($p < 0.05$).

Antioxidant assay	Content (Mean ± SD)						
	AT	TT	DT	ET	MT	CT	ST
Folin-Ciocalteau (mg GAE/g DW)	1.86 ± 0.10^{a}	1.49 ± 0.04^{a}	6.74 ± 0.54^{b}	3.95 ± 0.27^{c}	2.95 ± 0.14^{d}	2.01 ± 0.08^{a}	1.95 ± 0.06^{a}
DPPH (µmol TE/g DW)	2.52 ± 0.03^{a}	2.86 ± 0.08^{a}	8.45 ± 0.21^{b}	7.77 ± 0.29^{c}	7.28 ± 0.05^{d}	3.41 ± 0.12^{e}	3.25 ± 0.08^{e}
ABTS (µmol TE/g DW)	4.29 ± 0.07^{a}	6.16 ± 0.06^{b}	9.28 ± 0.39^{c}	7.22 ± 0.05^{d}	5.87 ± 0.03^{b}	5.31 ± 0.19^{e}	5.05 ± 0.06^{e}
FRAP (µmol TE/g DW)	5.13 ± 0.20^{a}	9.77 ± 0.05^{b}	14.47 ± 0.48^{c}	13.00 ± 0.49^{d}	11.30 ± 0.32^{e}	8.74 ± 0.26^{f}	7.95 ± 0.16^{g}

Table 16. Antioxidant assays of unripe tomato cultivars. Results are expressed as mean ± SD, and $p < 0.05$ was considered statistically significant. Statistical significance was calculated by one-way ANOVA followed by Tukey's post-hoc test. Different letters indicate significant differences. Abbreviations: DPPH: radical 2,2-diphenyl-1-picrylhydrazyl; ABTS: 2,20-azino-bis (3-ethylbenzothiazoline-6-sulfonic acid); FRAP: ferric reducing antioxidant power; TE: Trolox equivalent; GAE: Gallic acid equivalent.

3.3.6.2. Statistical correlation between antioxidant properties and polyphenols content

The correlation analysis is an additional or alternative tool useful for the elaboration of metabolomic data. It is commonly obtained by pairwise correlations between concentrations of the metabolites in the samples (Steuer, 2006). The most common correlation technique is represented by Pearson Correlation Test, which describes the linear correlation between variables. To assess the biological activities of unripe tomato cultivars, this statistical assay was performed to correlate the antioxidant properties with the content of polyphenolic compounds. As shown in the **Figure 32**, the quantified compounds do not contribute equally to the antioxidant activities of tomato cultivars. A not significant statistical correlation (*p*-value > 0.05) was assessed by some polyphenols quantified in traces in the samples. Furthermore, the diagnostic polyphenol of green tomato cultivars for human consumption, as catechin and *p*-coumaric acid, displayed negative correlations with antioxidant assays values (DPPH/(mg catechin/g DW), R^2 = -0.868, *p*-value = 0.0112; FRAP/(mg catechin/g DW), R^2 = -0.864, *p*-value = 0.0122; FRAP/(mg *p*-coumaric acid/g DW), R^2 = -0.773, *p*-value = 0.042). Instead, the compounds quantified in the agri-food waste unripe tomato cultivars were characterized by strongly positive correlations and a good degree of statistical significance (**Figure 32**, **Table 17**). Among these, some compounds, e.g., rutin, chlorogenic acid, and quercetin *O*-pentosylrutinoside, were highly significant (DPPH/(mg quercetin-*O*-pentosylrutinoside/g DW), R^2 = 0.749, *p*-value = 0.050; ABTS/(mg chlorogenic acid/g DW), R^2 = 0.927, *p*-value = 0.003; FRAP/(mg rutin/g DW), R^2 = 0.837, *p*-value = 0.019). An evaluation of the correlation between FOLIN and the other antioxidant assays (DPPH, ABTS, and FRAP) was assessed to confirm that these biological properties were directly related to the polyphenols content. The Pearson correlation test proved the positive and the statistical significance of this correlation (FOLIN/DPPH, R^2 = 0.857, *p*-value = 0.014; FOLIN/ABTS, R^2 = 0.917, *p*-value = 0.004; FOLIN/FRAP, R^2 = 0.819, *p*-value = 0.024). To our knowledge, this is the first report that systematically analysed several unripe tomato cultivars to investigate the correlation between the antioxidant activities and the content of some polyphenols. Nevertheless, it should be considered that other compounds identified in the qualitative analysis could contribute to antioxidant activities. Thus, further analysis will be performed to assess the correlation between the other constituents and the biological properties of the extract.

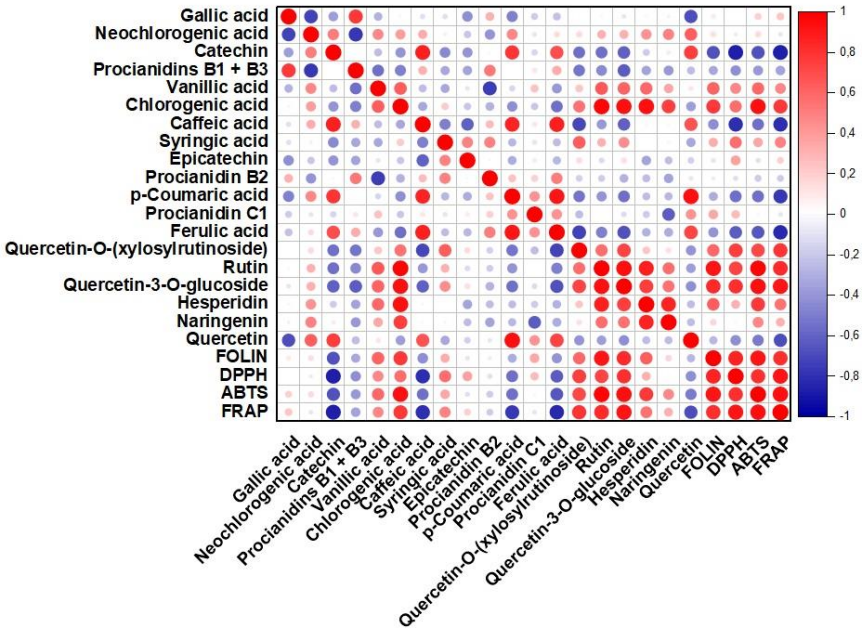


Figure 32. Pearson correlation plot of quantified polyphenols and antioxidant assay values. The different colours indicate a differentially correlation between two factors reported in the two axes, blue indicates a strong negative correlation while red indicates a strong positive correlation.

Factor		FOLIN	DPPH	ABTS	FRAP	Chlorogenic acid	Rutin	Quercetin *O*-(pentosylrutinoside)
FOLIN	Pearson coefficient	1	0.857	0.917	0.819	0.776	0.905	0.596
	p-value	-	0.014	0.004	0.024	0.040	0.005	0.158
DPPH	Pearson coefficient	0.857	1	0.808	0.902	0.579	0.728	0.749
	p-value	0.014	-	0.028	0.002	0.173	0.064	0.050
ABTS	Pearson coefficient	0.917	0.808	1	0.929	0.927	0.968	0.711
	p-value	0.004	0.028	-	0.002	0.003	0.001	0.073
FRAP	Pearson coefficient	0.819	0.902	0.929	1	0.779	0.837	0.791
	p-value	0.024	0.002	0.002	-	0.039	0.019	0.034
Chlorogenic acid	Pearson coefficient	0.776	0.579	0.927	0.779	1	0.965	0.559
	p-value	0.040	0.173	0.003	0.039	-	0.001	0.192
Rutin	Pearson coefficient	0.905	0.728	0.968	0.837	0.965	1	0.573
	p-value	0.005	0.064	0.001	0.019	0.001	-	0.179
Quercetin *O*-(pentosylrutinoside)	Pearson coefficient	0.596	0.749	0.711	0.791	0.559	0.573	1
	p-value	0.158	0.050	0.073	0.034	0.192	0.179	-

Table 17. Pearson correlation analysis between antioxidant assays and the content of the main polyphenols of unripe tomatoes.

3.4. Summary of cultivar selection

Tomato fruits are consumed and appreciated worldwide. During the tomatoes industrial processing, a large amount of unripe tomatoes is considered a waste to be disposed, and it is not utilized during the industrial processes, representing an unevaluated by-product and a significant cost for the agri-food industries. The present work suggests the possibility of utilizing this waste product for the development of new nutraceutical formulations due to their chemical abundance of SGAs and polyphenols with high antioxidant properties. The analyses identified and quantified 76 and 18 compounds of the two abovementioned classes, respectively. Interestingly, the profile of the unripe tomatoes and the green tomato for human consumption shows the difference in the compositions. The multivariate statistical analysis of the quantitative results revealed that the *Datterini* tomatoes cultivar (DT) has a characteristic metabolic profile compared with the other unripe tomato cultivars. The knowledge of the phytochemical content and the antioxidant activities of DT cultivar may encourage its recovery from agri-food waste produced by tomato farmers to be utilised in the pharmaceutical and nutraceutical industries. The high concentration of α-TM in *Datterini* tomatoes cultivar (34.699 ± 1.365 mg of α-TM/g of dried matrix) suggests a possible use of this cultivar as a possible anti-aging matrix for the prevention of sarcopenia. Therefore, it was selected for a subsequent pharmacological study to evaluate its activity in an elderly mouse model.

CHAPTER 4

DATTERINI GREEN TOMATOES EFFICACY STUDY: NUTRACEUTICAL EFFECTS IN SARCOPENIA PREVENTION

4.1. Introduction of the project

The development of a nutraceutical formulation requires the uses of appropriate *in vitro* and *in vivo* studies to demonstrate its ability to prevent or treat a specific disease state. Based on the results obtained in the **chapter 3**, Datterini green tomatoes were selected for this pharmacological in-depth study for the prevention of sarcopenia as anti-aging approach for its high α-TM concentration (34.699 ± 1.365 mg of α-TM/g of dried matrix). Since sarcopenia is a recently studied pathological state, there are no adequate *in vitro* tests that can show a biological activity in the prevention of the disease. Therefore, it was decided to carry out an *in vivo* study on a mouse model and *in vitro* tests able to identify possible metabolic mechanisms responsible for anti-aging activity. The *in vivo* mice study was performed by considering the experimental approach and the results reported by Dyle et al. (2014), in which the anti-sarcopenic properties of pure TD were studied in an aged mice model. These studies were carried out in collaboration with the research group of Prof. Monica Dentice of the University of Naples Federico II and the research group of Prof. Mariano Stornaiuolo of the Department of Pharmacy of the University of Naples Federico II.

In this context, the goals of this part of the thesis are as follows:

1) To demonstrate the safety of the lyophilized of Datterini green tomatoes on the mouse model;
2) To evaluate the efficacy of Datterini green tomatoes and TD for sarcopenia prevention as anti-aging approach;
3) To demonstrate the mechanism of action of Datterini green tomatoes and TD in muscle aging processes.

4.2. Materials and Methods

4.2.1. Animal experiments

5 weeks old C57BL/6J mice were purchased from ENVIGO (Envigo Teklad Rodent Diet, Madison, WI, USA). Animals were handled in agreement with National and European guidelines, and protocols were approved by the Animal Research Committee of the University of Naples ‘‘Federico II’’. Mice were housed in cages containing fresh bedding under controlled conditions (20–24 °C, 50–60% relative humidity, and 14:10 light-dark cycle). Food and water were available *ad libitum* for all animals. All animals received a control diet (CD; Envigo Teklad Rodent Diet, Madison, WI, USA) or lyophilized Green Tomatoes (LGT) diet in an amount of 1g/kg bw/day from week 17 to week 55 (total length of the treatment 37-weeks). The dose of nutraceutical ingested relative to weight was within clinical recommendations. All animal procedures were approved by Institutional Animal Care and Use Committee (IACUC) (protocol n. 354/ 2019-PR).

4.2.2. Reagents

All chemicals, reagents, and standards used were of analytical or LC-MS grade reagents. The water was treated in a Milli-Q water purification system (Millipore, Bedford, MA, USA) before use. Rutin (purity ≥ 94% HPLC), calcium chloride dihydrate $CaCl_2(H_2O)_2$, potassium chloride KCl, potassium dihydrogen phosphate KH_2PO_4, sodium bicarbonate, sodium chloride NaCl, magnesium chloride hexahydrate $MgCl_2(H_2O)_6$, ammonium carbonate $NH_4(CO_3)_2$, hydrochloride acid (HCl), sodium hydroxide NaOH, α-amylase (75 U/ml), pepsin from porcin gastric mucose (2000 U/ml), pancreatin (100 U/ml of trypsin activity), bile salts, protease from Streptomyces griseus, also named Pronase E (3.5 U/mg solid), Viscozyme L, glutamine, penicillin, streptomycin, 3-(4,5-dimethylthiazon-2-yl)-2,5-diphenyltetrazolium bromide (MTT), glucose, Dulbecco’s modifies Eagle medium (DMEM), Mitotracker® Red CMXRos, MitoGreen, Triton X-100, DAPI, Bovin serum albumin (BSA), 2-Deoxy-2-[(7-nitro-2,1,3-benzoxadiazol-4-yl)amino]-D-glucose (2-NBDG), dimethylsulfoxide (DMSO), deuterium oxide (D_2O) were purchased from Sigma-Aldrich (Milan, Italy). α-TM (purity ≥ 95% HPLC) and TD (purity ≥ 95% HPLC) were obtained from Phytolab (Vestenbergsgreuth, Germany).

4.2.3. Chow preparation for LGT

Green “Datterini” tomatoes were purchased by a local farmer (Licata, Sicily, 37°6'29"52 N) in March 2021 and was harvested as an agri-food wastes during mature tomatoes harvesting. Tomatoes were cut, frozen at -80 °C, dried by lyophilization, and stored in 50 ml plastic tubes at -20 °C until use. The nutraceutical supplement LGT were added into the control diet (CD) at a concentration of 1% (*w/w*). Each LGT diet batch was evaluated with a weight uniformity test to assess the average weight. The test was performed by randomly weighted 10 single unit of LGT diet and calculating the average weight. The final number of chow batches where seven and they averaged in the same range of weight.

4.2.4. LGT diet extraction

LGT diet extraction was carried out according to the procedure reported by Schiano et al. (2022), with slight modifications. 20 ml of a solution at 80% aqueous methanol containing 1% of formic acid was added to 2 g of the control diet (CD) chow. The suspension was vortexed for 1 min, sonicated (Branson Fisher Scientific 150E Sonic Dismembrator) for 10 min, and shaken on an orbital shaker (Sko-DXL, Argolab, Carpy, Italy) at 600 rpm for 10 min. After centrifugation for 10 min at 9.000 rpm, the supernatant was transferred into another plastic tube. The pellet was extracted for a second time with 20 ml of the extraction mixture, with the same previously reported procedure. The supernatants were combined, filtered with a 0.22 µm nylon filter (CellTreat, Shirley, MA), and stored at -20 °C until SGAs and polyphenols quantitative analysis. The solution was dried under a gentle stream of nitrogen and dissolved in a methanolic solution containing 0.1 % of formic acid at a concentration of 5 mg/ml. The solution was filtered with a 0.22 µm nylon filter, and stored at -20°C until analysis. A C_{18} solid phase extraction (SPE) was used as clean-up protocol for the qualitative analysis, as described by Piccolo et al. (2023) with slight modifications. 40 ml of the extraction supernatant was dried and reconstituted with 15 ml of water. The SPE tube was conditioned with methanol (10 ml) followed by water (10 ml). Samples were loaded on each cartridge using a vacuum pump, washed with water (10 ml), and eluted using methanol (15 ml). The eluted solution was dried under a gentle stream of nitrogen, reconstituted in in a methanolic solution containing 0.1 % of formic acid at a concentration of 5 mg/ml. The solution was filtered with a 0.22 µm nylon filter, and stored at -20°C until analysis. Extraction was performed on both the LGT diet and the control diet (CD) as control group chow, under the same extraction conditions. CD extract was reconstituted in a

methanolic solution containing 0.1 % of formic acid at a concentration of 10 mg/ml as solution for the preparation of the calibration curves in the matrix.

4.2.5. LGT diet qualitative analysis by HPLC-HESI-MS/MS analysis

An HPLC DIONEX UltiMate 3000 (Thermo Fisher Scientific, San Jose, CA, USA) equipment, coupled with an autosampler, a binary solvent pump, a diode-array detector (DAD), and an LTQ XL mass spectrometer (Thermo Fisher Scientific, San Jose, CA, USA), were used for the analysis. Separation was performed according to Maisto et al., 2023, with slight modifications. The column used for the analysis was a Kinetex® C18 column (75 mm × 2.1 mm, 2.6 µm; Phenomenex, Torrance, CA, USA). The mobile phases were water at 0.1% formic acid (A) and acetonitrile at 0.1% formic acid (B). Elution was performed according to the following conditions: 0–1.5 min hold at 15% solvent B, from 15% (B) to 50% (B) in 14.5 min, to 50% (B) to 95% (B) in 2 min, followed by 2 min of maintenance; for the remaining 3 min, the column was equilibrated to the initial conditions. The injection volume was 5 µL, the column temperature was set at 35 °C, and the flow rate was 0.35 mL/min. For the mass parameters, the source was a heated electrospray interface (HESI) operated in full scanning (FS) and data-dependent acquisition (DDA). Collision-induced fragmentation was made using argon, with a collision energy of 35.0 eV. The source operated in negative ionization mode for the analysis of polyphenols and in positive ionization mode for SGAs analysis. The ion source was set for positive ionization mode using the following parameters: auxiliary gas flow rate: 10; sheath gas flow rate: 30 l/min; source heated temperature: 150 °C; capillary temperature: 320 °C; source current: 100 µA; source voltage: 3.5 kV; tube lens: 80 V; and capillary voltage: 32 V. The ion source was set for negative ionization mode using the following parameters: auxiliary gas flow rate: 10; sheath gas flow rate: 30 l/min; source heated temperature: 150 °C; capillary temperature: 320 °C; source current: 100 µA; source voltage: 3.5 kV; tube lens: 90 V; and capillary voltage: 31 V. The separation conditions and the source parameters are summarized in the **Tables 18** and **19**, respectively.

Time (min)	% B
0	15
1.5	15
14.5	50
16.5	95
18.5	95
21.5	15

Table 18. Summary of the gradient condition of the HPLC-HESI-MS/MS qualitative method used for LGT diet analysis.

Column	Kinetex® C18 column (75 mm x 2.1 mm; 2.6 µm)
Phase A	Water at 0.1% HCOOH
Phase B	Acetonitrile at 0.1% HCOOH
Column Temperature	35 °C
Injection volume	5 µl
Flow rate	0.35 ml/min
Collision Energy	35 eV
Sheath gas flow rate	30 l/min
Auxiliary gas flow rate	10 l/min
Capillary temperature	320 °C
Source heated temperature	150 °C
Source voltage	3.5 kV
Source current	100 µA
Capillary voltage	31 V
Tube lens	90 V

Table 19. Summary of the chromatographic and source parameters of the HPLC-HESI-MS/MS qualitative method used for LGT diet analysis.

4.2.6. α-tomatine quantitative analysis of LGT diet by HPLC-HESI-MS/MS

An HPLC DIONEX UltiMate 3000 (Thermo Fisher Scientific, San Jose, CA, USA) equipment, coupled with an autosampler, a binary solvent pump, and an LTQ XL mass spectrometer (Thermo Fisher Scientific, San Jose, CA, USA), were employed for the analysis. α-TM quantification was performed using the same chromatographic method described in the paragraph **4.2.4. LGT diet qualitative analysis by HPLC-DAD-HESI-MS/MS analysis**. For the mass parameters, the source was a heated electrospray interface (HESI) operated in Multiple Reaction Monitoring (MRM) scanning mode. One MRM transition was used as a quantifier transition and a second MRM transition served as a qualifier transition. The first transition (1034.6 – 1016.3) and the second transition (1034.6 – 416.2) were performed with the same collision energy of 40.0 eV, using argon as a gas for collision-induced fragmentation. The ion source was set for positive ionization mode using the following parameters: auxiliary gas flow rate: 5 l/min; sheath gas flow rate: 35 l/min; source heated temperature: 200 °C; capillary temperature: 320 °C; source current: 100 µA; source voltage: 3.5 kV; tube lens: 205 V; and capillary voltage: 49 V. The MRM analyte parameters were optimized using a methanolic solution with 0.1% of formic acid of α-TM at a concentration of 5 ppm. To prepare the calibration curve, seven 0.5 ml of a CD hydroalcoholic extract (10 mg/ml) were added into seven 2-ml vials, respectively. Seven 0.5 aliquots of different concentrations of α-TM standard solutions were added, respectively, to the seven vials to prepare the calibration standards with a final matrix concentration of 5 mg/ml. α-TM was quantified according to a calibration curve ($R_2 \geq 0.99$) made with 7 different concentrations (10, 5, 2.5, 1.25, 0.62, 0.31, 0.16 ppm) and triplicate injections at each concentration. The separation conditions and the source parameters are summarized in the **Table 20**.

Column	Kinetex® C18 column (75 mm x 2.1 mm; 2.6 µm)
Phase A	Water at 0.1% HCOOH
Phase B	Acetonitrile at 0.1% HCOOH
Column Temperature	35 °C
Injection volume	5 µl
Flow rate	0.35 ml/min
Collision energy transition quantifier	40 eV

Collision energy transition qualifier	40 eV
Sheath gas flow rate	35 l/min
Auxiliary gas flow rate	5 l/min
Capillary temperature	320 °C
Source heated temperature	200 °C
Source voltage	3.5 kV
Source current	100 µA
Capillary voltage	49 V
Tube lens	205 V

Table 20. Summary of the chromatographic and source parameters of the HPLC-HESI-MS/MS α-TM quantitative method for LGT diet analysis.

4.2.7. Rutin quantitative analysis of LGT diet by HPLC-HESI-MS/MS

An HPLC DIONEX UltiMate 3000 (Thermo Fisher Scientific, San Jose, CA, USA) equipment, coupled with an autosampler, a binary solvent pump, and an LTQ XL mass spectrometer (Thermo Fisher Scientific, San Jose, CA, USA), were used for the analysis. Separation was performed using as column a Kinetex® C18 column (75 mm × 2.1 mm, 2.6 µm; Phenomenex, Torrance, CA, USA). The mobile phases were water at 0.1% formic acid (A) and acetonitrile at 0.1% formic acid (B). Elution was performed according to the following conditions: 0–1.5 min hold at 5% solvent B, from 5% (B) to 50% (B) in 6.5 min, to 50% (B) to 95% (B) in 0.5 min, followed by 2 min of maintenance; for the remaining 3 min, the column was equilibrated to the initial conditions. The injection volume was 5 µL, the column temperature was set at 35 °C, and the flow rate was set at 0.35 mL/min. For the mass parameters, the source was a heated electrospray interface (HESI) operated in Multiple Reaction Monitoring (MRM) scanning mode. One MRM transition was used as a quantifier transition and a second MRM transition served as a qualifier transition. For rutin quantification, the first transition (609.5 – 301.0) and the second transition (609.5 – 271.0) were performed with the same collision energy of 40.0 eV, using argon as a gas for collision-induced fragmentation. The ion source was set for negative ionization mode using the following parameters: auxiliary gas flow rate: 10 l/min; sheath gas flow rate: 30 l/min;

source heated temperature: 150 °C; capillary temperature: 320 °C; source current: 100 µA; source voltage: 3.0 kV; tube lens: -122.54 V; and capillary voltage: -50 V. The MRM analyte parameters were optimized using a methanolic solution containing the 0.1% of formic acid of rutin at a concentration of 5 ppm. To prepare the calibration curve, six 0.5 ml of a CD hydroalcoholic extract (10 mg/ml) were added into six 2-ml vials, respectively. Six 0.5 aliquots of different concentrations of rutin standard solutions were added, respectively, to the six vials to prepare the calibration standards with a final matrix concentration of 5 mg/ml. Rutin was quantified according to a calibration curve ($R_2 \geq 0.99$) made with 6 different concentrations (50, 35, 25, 5, 2.5, 0.5 ppm) and triplicate injections at each concentration. The separation conditions and the source parameters are summarized in the **Tables 21** and **22**, respectively.

Time (min)	% B
0	5
1.5	5
8	50
8.5	95
10.5	95
13.5	5

Table 21. Summary of the gradient condition of the HPLC-HESI-MS/MS rutin quantitative method used for LGT diet analysis.

Column	Kinetex® C18 column (75 mm x 2.1 mm; 2.6 µm)
Phase A	Water at 0.1% HCOOH
Phase B	Acetonitrile at 0.1% HCOOH
Column Temperature	35 °C
Injection volume	5 µl
Flow rate	0.35 ml/min
Collision energy transition quantifier	40 eV
Collision energy transition qualifier	40 eV
Sheath gas flow rate	30 l/min
Auxiliary gas flow rate	10 l/min
Capillary temperature	320 °C
Source heated temperature	150 °C
Source voltage	3.0 kV
Source current	100 µA
Capillary voltage	-50 V
Tube lens	-122.54 V

Table 22. Summary of the chromatographic and source parameters of the HPLC-HESI-MS/MS rutin quantitative method used for LGT diet analysis.

4.2.8. Linearity and Sensitivity of α-tomatine and rutin HPLC-HESI-MS/MS analysis

The validation and the development of the HPLC-HESI-MS/MS methods used for the evaluation of α-TM and rutin content in LGT diet in each extraction was performed with the analytical standards of the two compounds. The calibration curves of the two compounds were plotted using the peak area of the standard concentration to evaluate the linearity of the method. The values of the limits of detection (LODs) and limits of quantification (LOQs) were calculated to determine the sensitivity of the method. Evaluation of the signal-to-noise ratios was performed by comparing measured signals from samples with known low concentrations of analyte (0.16 ppm for α-TM and 0.5 ppm for rutin) with those of blank matrix samples. The blank matrix sample was obtained by a methanolic solution of CD extract at a concentration of 5 mg/ml with the 0.1% of formic acid. LODs establishing the minimum concentration at which the analyte can be reliably detected as is defined as the lowest detectable concentration of analyte that the analytical system can reliably distinguish

from the background level (S (signal of compound)/N (signal of noise)) = 3, while LOQ is defined as the lowest quantifiable concentration of analyte that can be measured with a standard level of confidence, and it is typically calculated using (S/N) = 10, according to the ICH validation guideline (ICH.Q2[R2], 2022).

4.2.9. Precision and accuracy of α-tomatine and rutin HPLC-HESI-MS/MS analysis

The calculation of accuracy (estimated as % bias) and precision (calculating as coefficient of variation % CV) was determined for the development and the validation of the analytical methods. Precision and accuracy were calculated by an intraday and an interday analysis of α-TM and rutin calibration standards at three different concentrations (5, 1, 0.1 ppm for α-TM and 50, 5, 0.5 ppm for rutin). Each compound was injected 3 times per day (intraday) and for 3 consecutive days (interday). The procedure was performed in agreement with the ICH validation guideline (ICH.Q2[R2], 2022).

4.2.10. Matrix effect and Recovery of α-tomatine and rutin extraction

The matrix effect was calculated by comparing the slope of the calibration curves of the analytical standard in the presence of the matrix (blank matrix sample spiked with α-TM and rutin post extraction) and the calibration curves of the analytical standards in the absence of the matrix (α-TM and rutin in methanol at 0.1% of formic acid). The significance of the matrix effect comparison was performed using the student t-test, with a significant difference accepted at the 95% of confidence level. An evaluation of the matrix effect (%) was obtained by calculating the ratio of the peak area in the spiked blank matrix samples and in the blank solvent. The matrix was spiked with the analyte in triplicate with 1 µg (low), 5 µg (medium), and 10 µg (high) for α-TM and with 5 µg (low), 20 µg (medium), 40 µg (high) for rutin. The ratio was calculated as follows:

$$\boldsymbol{Matrix\ effect}\ \% = \frac{\textbf{Peak area}_{\boldsymbol{in\ presence\ of\ matrix}}}{\textbf{Peak area}_{\boldsymbol{in\ solvent}}} \cdot \mathbf{100}$$

The recovery was calculated by using the ratio of the peak area in the pre-extraction spiked samples (matrix spiked with known concentration of analytes pre-extraction) to the peak area in the post-extraction spiked samples (matrix spiked with known concentration of analytes post-extraction). The spiked concentrations used for the recovery experiments were the same reported for the matrix effect analysis. The ratio was calculated as follows:

$$\boldsymbol{Recovery}\ \% = \frac{\textbf{Peak area}_{\boldsymbol{pre-extraction\ spiked\ sample}}}{\textbf{Peak area}_{\boldsymbol{post-extraction\ spiked\ sample}}} \cdot \mathbf{100}$$

4.2.11. Simulated gastro-intestinal digestion protocol

LGT was subjected to successive oral, gastric, and intestinal *in vitro* digestion, following a harmonized procedure reported by the COST action INFOGEST network and by Izzo et al. (2020). The protocol was performed by using simulated digestion fluids, namely gastric fluid (SGF), salivary fluid (SSF), and intestinal fluid (SIF), which were prepared using the procedure reported by Izzo et al. 2020. The chemical composition of the solutions is reported in **Table 23**. Briefly, 1 g of the LGT were mixed with 3.5 ml of SSF at the temperature of 37 °C. Next, 25 µL of 0.3 M calcium chloride, 0.5 mL of α-amylase solution (75 U/mL), and 975 µL of water were added and mixed. A solution 1 M hydrochloride acid (HCl) was added to reduce the pH of the solution to 7, and the mixture was incubated at 37 ◦C for 2 min in an orbital shaker bath at 200 rpm. Then, for simulating gastric conditions, 7.5 mL SGF, 5 µL 0.3 M calcium chloride, 1.6 mL pepsin solution (2000 U/mL), and 695 µL of water were added and thoroughly mixed. Next, a solution 1 M HCl was used to modify the pH of the solution to 3, and the mixture was incubated for 120 min at 37 ◦C in an orbital shaker bath at 200 rpm. Afterward, to recreate the intestinal stage, 11 mL SIF, 5 mL pancreatin solution (100 U/mL of trypsin activity), 2.5 mL bile salt solution (65 mg/mL), 1.3 mL of water, and 40 µL of 0.3 M calcium chloride were added. After that, the solution was mixed, and 1 M NaOH was added to modify the pH of the mixture to 7. The solution was incubated at 37 ◦C for 120 min in an orbital shaker bath at 200 rpm. At the end of the intestinal phase, the tube was centrifuged at 9000 rpm for 10 min at 25 °C. The supernatant was collected and freeze-dried. The residue was subjected to a methanolic extraction to remove salts and enzymes added during the simulated gastro-intestinal digestion before the analysis. To the solid residue, a volume of 10 mL of methanol was added. The mixture was vortexed for 1 min and placed in an ultrasonic bath (Branson Fisher Scientific 150 E Sonic

Dismembrator) for 10 min. Samples were then shaken on an orbital shaker (Sko-DXL, Argolab, Carpi, Italy) at 600 rpm for 10 min and centrifuged at 9000 rpm for 10 min at 25 °C. The pellet obtained by centrifugation of the intestinal phase was subjected to the colon digestion simulated process to evaluate the effect of the intestinal bacterial flora on α-TM stability. The pellet was mixed with 5 ml of a 5 mg/ml aqueous solution of Pronase E. Next, a solution 1 M NaOH was used to modify the pH of the solution to 8, and the mixture was incubated for 60 min at 37 °C. At the end of this phase, the tube was centrifuged at 9000 rpm for 10 min at 25 °C. The supernatant of the Pronase E stage was collected and freeze-dried. The pellet was mixed with 150 µl of Viscozyme L and a solution of 1 M HCl was used to modify the pH of the solution to 4 and was incubated for 16 hours at 37 °C. Finally, the tube was centrifuged at 9000 rpm for 10 min at 25 °C. All the supernatants were collected and stored at 4 °C protected from the light. The obtained pellets were re-extracted with 10 mL of methanol at the 1% of formic acid using the same procedure. Finally, the extracts obtained were evaporated to dryness under a light stream of nitrogen, reconstituted in an aqueous solution at 50% of methanol at a concentration of 10 mg/mL, and stored at −20 °C until analysis.

		SSF (pH 7)		**SGF (pH 3)**		**SIF (pH 7)**	
Salt solution	**Stock conc. (mol/L)**	mL of Stock added to prepare 0.4 L (mL)	Final salt concentration in sample (mmol/L)	mL of Stock added to prepare 0.4 L (mL)	Final salt conc. In sample (mmol/L)	mL of Stock added to prepare 0.4 L (mL)	Final salt conc. In sample (mmol/L)
KCl	0.5	15.1	15.1	6.9	6.9	6.8	6.8
KH_2PO_4	0.5	3.7	1.35	0.9	0.9	0.8	0.8
$NaHCO_3$	1	6.8	13.68	12.5	25	42.5	85
NaCl	2	-	-	11.8	47.2	9.6	38.4
$MgCl_2(H_2O)_6$	0.15	0.5	0.15	0.4	0.12	1.1	0.33
$NH_4(CO_3)_2$	0.5	0.06	0.06	0.5	0.5	-	-
$CaCl_2(H_2O)_2$	0.3	-	1.5	-	0.15	-	0.6

Table 23. Chemical composition of the gastro-simulated digestion fluids.

4.2.12. Cell lines and culture conditions

C2C12 cells were purchased from American Type Culture Collection (ATCC, Manassas, VA, USA) and cultured in Dulbecco's modified Eagle Medium (DMEM, Loza,

Walkersville, MD, USA) supplemented with 10% Fetal Bovine Serum (FBS, GIBCO, Milan, Italy), 2 mM glutamine, 50 i.u. penicillin, and 50 mg/mL streptomycin. In the treated condition, a TD solution 300 mM in DMSO was added in culture medium at the indicated concentrations for 48 hours. DMSO was used as vehicle as comparison with TD treatment. TD addition to the culture medium was performed applying a dilution 1:1000, with a final TD maximum concentration of 300 µM and a final DMSO % of 0.1%.

4.2.13. MTT assay

C2C12 cells were plated in 96-well plates at 5.000 cells per well in complete DMEM (20 mM glucose, 2 mM glutamine, 10% FBS; Invitrogen, Carlsbad, CA, USA). Cell viability was measured at same time points (48 hours) by the 3-(4,5-Dimethylthiazol-2-yl)-2,5-diphenyltetrazolium bromide (MTT; Sigma Aldrich, Milan, Italy) assay according to the manufacturer's instructions. Briefly, 20 mL of 5 mg/mL MTT solution in PBS was added to each well and incubated for 4 hours in a cell incubator (37°C, 95% rel. humidity, 5% CO_2; Heracell 150, Thermo Scientific, Waltham, MA, USA). Cell viability dependent absorbance of the dark blue formazan crystals was measured in a spectrophotometer at a wavelength of 570 nm. All the analysis were performed in triplicate.

4.2.14. Measurement of mitochondrial activity

The TD effect in the control of oxidative phosphorylation and mitochondriogenic promoting activity was measured in C2C12 cells using the probes MitoTracker® Red CMXRos and MitoGreen (Thermo Fisher Scientific), respectively. Briefly, each probe was diluted in DMEM to a final 100 nM working solution. C2C12 were washed twice in PBS and were incubated with the probe for 60 min in a cell incubator (37°C, 95% rel. humidity, 5% CO_2; Heracell 150, Thermo Scientific, Waltham, MA, USA). After the incubation, cells were washed three times with DMEM solution and one with PBS solution. Then, the cells were fixed in 3.7% formaldehyde for 30 min. Single cell fluorescence analysis of the two probes was measured by FACS (Mindray BriCyte E6; Mindray, Shenzhen, China). Total Fluorescence of MitoTracker® Red CMXRos (e.g., tetramethylrhodamine methyl ester (TMRM)) was measured using a Perkin Elmer Envision 2105 Multiplate Reader (Perkin Elmer, Waltham, MA, USA). The fluorescence was acquired at an excitation wavelength of

579 nm and an emission wavelength of 599 nm. Cells were then permeabilized in 0.1% Triton X-100 in PBS, and stained with the nuclear dye DAPI. DAPI fluorescence was measured with an excitation wavelength of 351 nm and an emission wavelength of 450 nm. MitoTracker fluorescence was normalized with DAPI fluorescence in order to correlate mitochondrial activity to total number of cells. All the analysis were performed in triplicate.

4.2.15. Measurement of glucose uptake

TD effect in the modification of cells glucose uptake was evaluated with the fluorescent glucose analogue 2-NBDG. C2C12 cells were seeded (5 x 10^3/well) on a 96-well black bottom microtiter plate with (Perkin Elmer, Waltham, MA, USA) in a final volume of 100 µL/well of growth media. When cells achieved 80–90% of confluency, the culture media was carefully removed and replaced with 100 µL of HBSS containing 100 µM, 2-Deoxy-Glucose (2-DG), 0.4 g/L BSA, and 1.27 mM $CaCl_2$ (without any growth factors or FBS) and when indicated a TD solution 300 mM in DMSO for the treatment and the vehicle as control. TD was added to achieve a maximum final concentration of 300 µM and a final DMSO % of 0.1%. Cells were incubated for 1 hour at 37 °C. After the incubation, the cells were supplemented with a solution 64 µM of NBDG. After 45 min of incubation, plates were washed twice in PBS. Uptake of 2-NBDG was determined using Perkin Elmer Envision 2105 Multiplate Reader (Perkin Elmer). The fluorescence was acquired at an excitation wavelength of 471 nm, an emission wavelength of 529 nm, and a monochromator cut off at 360 nm. Cells were then fixed in 3.7% paraformaldehyde for 30 min, permeabilized in 0.1% Triton X-100 in PBS, and stained with a solution 100 µM of nuclear dye DAPI. DAPI fluorescence was measured with an excitation wavelength of 351 nm and an emission wavelength of 450 nm. The ratio between intracellular 2-NBDG fluorescence and DAPI fluorescence was used for the normalization. All the analysis were performed in triplicate.

4.2.16. Real time qRT-PCR of myblast cells

The extraction of messenger RNAs was performed with a Quiagen RNA extraction kit (Qiagen, Hilden, Germany). Complementary DNAs were prepared with SuperScript VILO Master Mix (Life Technologies, Ltd, Carlsbad, CA, USA) as indicated by the manufacturer. The cDNAs were amplified by PCR in a One Step Real-Time PCR Detection System

(Applied Biosystem, Foster City, CA, USA). Specific primers for each gene were designed to work under the same cycling conditions (95 °C for 10 min followed by 40 cycles at 95 °C for 15 s and 60 °C for 1 min), thereby generating products of comparable sizes (about 200 bp for each amplification). Primer combinations were positioned whenever possible to span an exon–exon junction and the RNA digested with DNase to avoid genomic DNA interference. Primer sequences are reported in the **Table 24**. The relative amounts of gene expression were calculated using β-actin as an internal standard (housekeeping gene). The samples were treated with the vehicle and a TD solution 300 mM in DMSO in culture medium at the indicated concentrations for 48 hours. All samples were run in triplicate. The results, expressed as N-fold differences in target gene expression, were determined as follows:

$$\boldsymbol{N_{fold} = 2 - \left(DC_{GTE\,Treated} - DC_{Control}\right)}$$

qPCR analysis was performed using the following primers:

PGC1α: 5'-TGATGTGAATGACTTGGATACAGACA-3'; 5'-GCTCATTGTTGTACTGGTTGGATATG-3'

myoD: 5'- GACCTGCGCTTTTTTGAGGACC-3'; 5'- CAGGCCCACAGCAAGCAGCGAC-3'

myogenin: 5'- TTGCTCAGCTCCCTCAACCAGGA-3'; 5'-TGCAGATTGTGGGCGTCTGTAGG-3'

GPT2: 5'- GCTTTGAATGTGGACGAGCT-3'; 5'- TCGTGCCCCATCTGGTAAAG-3'

4.2.17. Measurement of total protein synthesis

C2C12 cells were plated in 96-well plates at 5.000 cells per well in complete DMEM and maintained in a cell incubator (37°C, 95% rel. humidity, 5% CO_2; Heracell 150, Thermo Scientific, Waltham, MA, USA). On day 2, TD solutions 75 µM in DMSO and/or 100 nM of rapamycin in DMSO were added and 24h later cells were washed three times in DMEM and once in PBS to be then fixed in 3.7 % formaldehyde for 30 minutes. Intracellular fluorescence of GFP was measured using a Perkin Elmer Envision 2105 Multiplate Reader (Perkin Elmer) with the following parameters: λ excitation 488 nm, λ emission 510 nm. Cells were then permeabilized in 0.1 % Triton X-100 in PBS and stained with the nuclear dye DAPI. DAPI fluorescence was measured with λ excitation 351 nm, and emission 450

nm. Intracellular GFP fluorescence was normalized with DAPI fluorescence in order to correlate intracellular GFP fluorescence to total number of cells.

4.2.18. NMR data acquisition and processing

A volume of 600 µl of cell culture supernatants were frozen and freeze-dried. The cell culture supernatans were obtained with TD stock solution 300 mM in DMSO to obtain a final TD concentration of 300 µM and the DMSO vehicle. The solid residues of the samples were dissolved with 540 µl of deuterium oxide D_2O and 60 µl of a solution of 10 µM sodium 3-trimethylsilyl-tetradeuteriopropionate (TSP) in D_2O. The resulting samples were transferred in the 5 mm SampleJet samples tubes. Tubes were closed with polyoxymethylene (POM) balls and were placed on the sample changer while queued for data acquisition. ^{1}H NMR data were obtained using a Bruker Avance Neo spectrometer 700 MHz (Bruker BioSpin Corporation, Billerica, MA, USA) equipped with a 5 mm TCI cryoprobe. A Bruker SampleJet sample changer system was used for sample transfer. Standard one-dimensional (1D) ^{1}H NMR spectra were acquired at 300 K by using a "zgpr" pulse sequence, with 64 transients, a recycle delay of 3 s, an acquisition time of 1.51 s, a 90° flip angle pulse of 11.53 µs, and 33 K data points. The water signal was suppressed using solvent pre-saturation. The spectra were manually phase and baseline corrected and automatically referenced to the internal standard (TSP = 0.0 ppm). Two-dimensional (2D) ^{1}H-^{13}C Heteronuclear Single Quantum Coherence (HSQC) was acquired in the echo–antiecho phase-selective mode with a "hsqcedetgpsisp2.2" pulse sequence, by using the following parameters: 2048 complex data points per increment to a total of 16 increments, 1 K data points in f_2 and 256 increments in f_1 with 7142.857 and 26397.197Hz spectral width for ^{1}H and ^{13}C dimensions, respectively. Two-dimensional (2D) ^{1}H-^{1}H Correlated Spectroscopy (COSY) was performed in quantum-filtered phase-selective mode with a "cosygpprqf" pulse sequence, by applying the following parameters: 2048 complex data points per increment to a total of 8 increments, 1 K data points in f_2 and 256 increments in f_1 with 7142.857 and 26397.197Hz spectral width in both dimensions.

4.2.19. Treadmill exercise running

C57BL/6 wild type mice were randomly assigned to one of four experimental groups of 3 male and 3 female mice per group: the CD treated sedentary control, the LGT treated

sedentary control, the CD treated training, and the LGT treated training group. Mice assigned to exercise were submitted to the increasing speed protocol as previously described by Werneck-De-Castro et al. (2015), testing the maximal speed and set the exercise intensity before the endurance exercise protocol. The endurance exercise protocol consists of treadmill running at 60% of maximal speed until exhaustion. Mouse exhaustion is defined as 10 continuous seconds of no longer attempting to run on the belt. All tests and exercise protocols were carried out with a motor-driven treadmill (TSE Systems, Berlin, Germany). Animals undergoing exercise were euthanized 24 h after the last exercise session to evaluate the effects of TD on exercise response. Sedentary mice were housed in cages without any stimulus to movement. At the experimental endpoint, the blood, gastrocnemius (GC) and tibialis anterior (TA) muscles were collected and stored at −80 °C for molecular and histological.

4.2.20. Real time qRT-PCR of gastrocnemius muscles

RNA preparation and quantitative real time-PCR were performed as previously described by Cicatiello et al. (2022). In brief, messenger RNAs were extracted with Trizol reagent (Life Technologies, Carlsbad, CA, USA) starting from 50 mg GC muscles. Complementary DNAs were prepared with SuperScript VILO Master Mix (Life Technologies, Carlsbad, CA, USA) as indicated by the manufacturer starting from 2000 ng of total RNA (A 260/280 ratio of ~1.8–2.0). The cDNAs were amplified by PCR in a CFX Connect Real-Time PCR Detection System (Bio-Rad, Hercules, CA, USA) with the fluorescent double-stranded DNA-binding dye SYBR Green (BioRad, Hercules, CA, USA). Specific primers for each gene were designed to work under the same cycling conditions (95 °C for 10 min followed by 40 cycles at 95 °C for 15 s and 60 °C for 1 min), thereby generating products of comparable sizes (about 200 bp for each amplicon). Primer combinations were positioned whenever possible to span an exon–exon junction and the RNA digested with DNase to avoid genomic DNA interference. Relative mRNA levels (in which the control sample was arbitrarily set as 1) are reported as results of Real-Time qRT-PCR, in which the expression of cyclophilin-A (e.g., housekeeping gene) served as internal standard. All samples were run in triplicate. The results, expressed as N-fold differences in target gene expression, were determined as follows:

$$N_{fold} = 2 - \left(DC_{GTE\ Treated} - DC_{Control}\right)$$

qPCR analysis was performed using the following primers:

MHCI: 5’-ACAGAGGAAGACAGGAAGAACCTAC-3’; 5’-GGGCTTCACAGGCATCCTTAG-3’

MHCIIA: 5’-TATCCTCAGGCTTCAAGATTTG-3’; 5’-TAAATAGAATCACATGGGGACA-3’

MHCIIB: 5’-CTGAGGAACAATCCAACGTC-3’; 5’-TTGTGTGATTTCTTCTGTCACCT-3’

MHCIIX: 5’-CGCGAGGTTCACACCAAA-3’; 5’-TCCCAAAGTCGTAAGTACAAAATGG-3’

4.2.21. Histology, MHC, and Pax7 immunostaining

Hematoxylin/Eosin (H/E) staining (Sigma-Aldrich, St. Louis, MO, USA) was carried out on 8 μm muscle cryosections according to classical methods (Dubowitz V. Ann. Clin. Res. 1974). Cross-sectional area (CSA) was measured by considering six hundred myofibers per muscle using ImageJ 1.52k Wayne Rasband, NIH (Bethesda, MD, USA) (http://imagej.nih.gov/ij). For MHC and Pax7 immunostaining, sections were fixed with 4% paraformaldehyde or 100% methanol for 15 min, blocked with 3% normal goat serum and 0.3% Triton X-100 in PBS and sequentially incubated with the primary and secondary fluorescent antibodies. Then, nuclei were stained with DAPI and mounted in 80% glycerol. The quantification of myofiber type was conducted by quantifying the total fluorescent signal expressed as integrated density and by counting the number of positive fibers compared to the total fibers in the same field of view (Sawano et al., PLoS ONE, 2016). Images were captured with a fluorescent Leica DMi8 microscope using the Leica Application Suite LAS X Imaging (Leica, Berlin, Germany) for the acquisitions.

4.2.22. GC-MS analysis of myoblast cells

Gastrocnemius tissues of CD and LGT groups (25 mg) and the myoblast cells (1 x 10^6) were rinsed three times in PBS solution and then homogenized in 1 ml of pre-chilled methanol/water 1:1 solution containing 10 nmol of internal standard. Samples were centrifuged at 10.000 g for 10 minutes at 4 °C. The supernatants were collected, transferred into Eppendorf tubes, and dried using the speedvac. The samples were resuspended in 1 ml of acetonitrile and centrifuged at 10.000 g for 10 min at 4 °C. The supernatants were collected, transferred into Eppendorf tubes, and dried using the speedvac. Then, samples

were solubilized in pyridine (500 µl) and derivatized with 25 µl of N,O-Bis(trimethylsilyltrifluoroacetamide) (BSTFA) in 90 min. For each sample, 1 ml of solution was injected with a split ratio 1:10. GC-MS analyses were carried out on a Shimadzu GCMS 2010plus (Kyoto, Japan) with the following parameters. Injection temperature 280 °C, Ramp 0–1.00 min 100 °C, 1.00–35.00 min 100–320 °C, hold for 10 min. Column flow 1.10 mL/min Linear velocity 39 cm/s. Helium gas was used. Ion source Temp. 200 °C, Interface 320 °C, Solvent cut 5.9 min, Scan 35–600 m/z. Detector voltage 0.1 kV. Tentative identification of compounds based on accurate MS measurements and isotopic fine distribution (ISF) was performed by Metaboscape 4.0 and confirmed after comparison with a NIST internal database. The experiment on gastrocnemius tissues of CD and LGT treated group was performed with the muscle tissues provided from 6 male and 6 female mice.

4.2.23. Statistical analysis

The results are represented as the mean ± Standard Deviation (SD) throughout. Differences between samples were assessed by the Student's two-tailed t-test for independent samples. Multiple comparisons and differences were analyzed for statistical significance by the two-way ANOVA test and Bonferroni post-test analysis. All graphs, bars, or lines indicate the mean, and error bars indicate the standard error of the mean (SEM). In all experiments, differences were considered significant when the p-value (p) was less than 0.05. Asterisks indicate significance at * $p < 0.05$, ** $p < 0.01$, and *** $p < 0.001$ throughout.

4.3. Results and discussion

4.3.1. Design of the experimental study

The analysis of the phytochemical profile of green Datterini tomatoes has been extensively described in **Chapter 3**. In particular, the food matrix is a rich SGAs (e.g., mg α-TM/g dry weight: 34.699 ± 1.365) and polyphenols source (e.g., µg Rutin/g dry weight: 0.996 ± 0.003). The matrix is also a rich source of antioxidants (DPPH assay: 8.45 ± 0.21 µmol TE/g dry weight; FRAP assay: 14.47 ± 0.48 µmol TE/g dry weight), which could globally corroborate the *in vivo* pharmacological activity. The first goal for the pharmacological study was the selection of the in-house experimental mouse model. This study was designed based on the *in vivo* protocol reported by Dyle et al. (2014), in which the pure TD was used to evaluate the anti-sarcopenic properties in an aged mice model. This type of study could be performed either using an elderly mouse model or in a young mouse model treated during the aging process. The second experimental model was preferred for the main goal of the experiment by evaluating the preventive effect of the nutraceutical in the aging-related sarcopenia disease. Therefore, mice were purchased at an age of the week 5 and fed with CD until the week 17. After that, the mice were divided into two groups of 45 mice each, a control group and a treated group. The separation was performed maintaining a uniformity between male and female mice number to assess the effect of the nutraceutical according to sexual variability. Mice in the control group were fed with CD while mice in the treated group were fed with LGT diet till the week 55. Mice of the treated group were monitored during the LGT diet treatment assess possible weight loss due to reduced appetite, which could reduce the amount of nutraceutical fed during treatment. At the end of the week 55, the mice were subjected to an *in vivo* efficacy study of muscle performance using the treadmill test, assessing the effect on exercise in the aged mouse model. Afterwards, the mice were sacrificed for organ, muscle and biological (plasma, urine, and faeces) samples for subsequent histochemical and haematochemical analysis. The design of the in-house experimental mouse protocol is summarized in **Figure 33**.

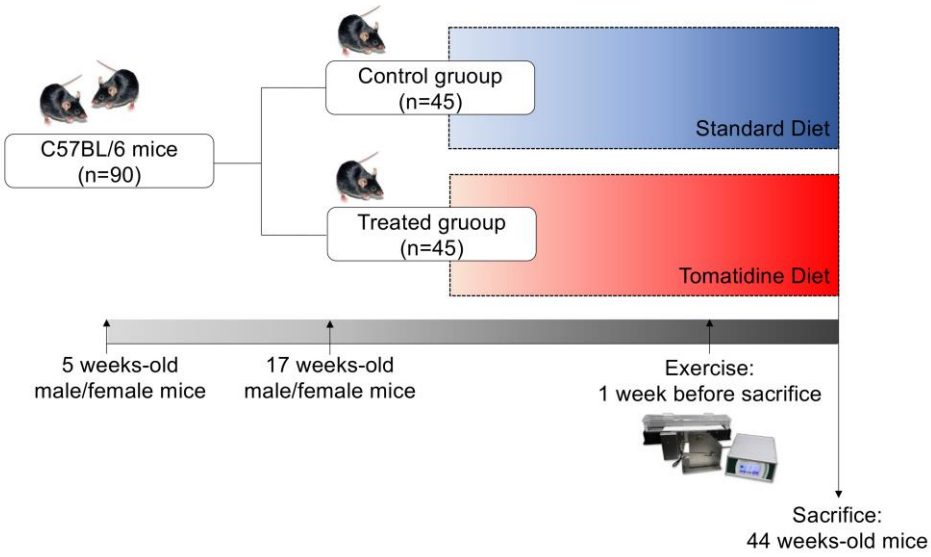


Figure 33. Design of in-house experimental mice protocol.

During the *in vivo* studies, nutraceuticals can be administered similarly to oral drugs, either by gavage using a stomach tube or by adding the product to the diet. Although treatment by gavage is very effective for an acute study, it becomes invasive and debilitating for the mouse for the chronic treatment. Therefore, the nutraceutical was administered by addition to the diet.

Another key step in the design of the *in vivo* study was the setup of the amount of nutraceutical to be administered. In this case, the maximum amount of nutraceutical permitted in a mouse study of 1g/kg bw/day was selected. Since the average consumption of the mice observed for the first 5 weeks is 3g/day, an amount of LGT to be administered of 30 mg/day was selected. Since α-TM amount in Datterini LGT cultivar is 34.699 ± 1.365 mg of α-TM/g of dried matrix, the amount of active ingredient in 30 mg in Datterini LGT is approximately 990 µg of α-TM. Therefore, adding Datterini LGT to the feed allowed to obtain an enriched diet containing 0.033% (*w/w*) of α-TM. The diet obtained is different from the protocol used by Dyle et al. (2014), in which the mice were fed with a TD-enriched diet at 0.05 % (*w/w*). Assuming the same diet consumption by the mice of 3g/day, the daily amount of active ingredient fed by the mice is 1.5 mg. Therefore, the amount of active ingredient used in the in-house experimental protocol is approximately half than the amount used by Dyle et al. (2014). Relating the doses to the mice weight, the in-house experimental protocol was performed with the administration of an amount of 34.7 mg of α-TM/kg of mice, while the protocol proposed by Dtyle et al. (2014) employed an amount of 50 mg of α-

TM/kg of mice. The second difference between the study managed by Dyle et al. (2014) and the in-house experimental protocol is the chemical nature of the active ingredient. Indeed, Dyle directly used TD, which is the active compound in sarcopenia prevention as mTORC1 activator and as AFT4 inhibitor. In contrast, our in-house experimental protocol involved the use of LGT, in which TD is absent but there is a high amount of the glycosidic derivative α-TM. Finally, the third difference between the two studies is the treatment time. As matter of fact, Dyle et al. (2014) performed the study on old-aged mice of 61 weeks for a period of 9 weeks, while our in-house experimental protocol was performed on young-aged mice of 17 weeks for the longer period of 38 weeks. The differences between Dyle et al. (2014) and in-house experimental protocols are summarized in **Table 24**. The decision to use a rich natural source of α-TM assumes that the glycoside undergoes *in vivo* metabolism releasing the aglycone, which can exert its pharmacological activity in the muscles.

Experimental differences	Dyle et al. (2014)	In-house protocol
Administration	Diet	Diet
Active ingredient	Tomatidine	α-tomatine
% Enrichment diet	0.05 %	0.033 %
Daily active ingredient amount	1.5 mg	0.99 mg
Dose/kg mice	50 mg/kg	34.7 mg/kg
Starting treatment age	61 weeks	17 weeks
Finish treatment age	70 weeks	55 weeks
Treatment time	9 weeks	38 weeks

Table 24. Differences between Dyle et al. (2014) and in-house experimental mice protocols.

4.3.2. α-tomatine metabolism

The correlation between the pharmacological properties and the beneficial activity on human health needs the evaluation of α-TM pharmacokinetics, which include the absorption, the distribution, the metabolism, and the excretion. The *in vivo* fate of SGAs as α-solanine and α-chaconine has been extensively studied (Schrenk et al., 2020). Instead, α-TM has only been evaluated for possible toxicological risks and few studies are reported about its pharmacokinetics. For many years, α-TM was evaluated as a compound with low bioavailability and stable at 37 °C, under stomach acidic conditions. Furthermore, it's able to form insoluble complexes with cholesterol that are eliminated through feces (Friedman, 2002). The first study that reported α-TM metabolism in an animal mice model was made by Cichon et al. (2017), which reported the annotation of some metabolites in mouse plasma following the administration of a red tomato enriched diet. In the diet, α-TM has been detected, while the aglycones were absent. Instead, the analysis of mouse plasma samples

allowed to detect tomatoes aglycones as TD, hydroxytomatidine, and didehydrotomatidine, while α-TM was absent. Therefore, Cichon et al. (2017) proposed α-TM biotransformation by removing the tetrasaccharide group for the phase I metabolism. Other two studies about α-TM metabolism have been reported by Dzakovich et al. (2023) and Cooperstone et al. (2017), which studied the active compound biotransformation in skin and liver, respectively. (Dzakovich et al., 2023) annotated 19 α-TM metabolites and recognized some sulphated and glucuronidated compounds obtained by phase II metabolism reactions. Although these studies improved the knowledge about α-TM biotransformation, they didn't quantify TD in animal plasma samples and identify the enzymes necessary for SGAs metabolism. A preliminary study about intestinal microbiota role about α-TM metabolism was given by (Kasimir et al., 2023), who studied pure compound α-TM biotransformation in a pig cecum model. It verified α-TM metabolism in an active cecum suspension by the cleavage of the single sugars and the detection of intermediate cleaved derivatives (e.g., β1-TM, β2-TM, γ-TM, TD). However, α-TM degradation was slow and constant in the time till a 60% of the initial concentration after 24 hours. As reported in literature, phase I and II biotransformation generally improve drug polarity to accelerate urine elimination rate. Therefore, it is reasonable to assume that glucuronidated and sulphated metabolites are involved in the excretion of α-TM. Some paper about other SGAs metabolism reported the presence of sulphated metabolites in human urine. For example, esculeogenin B sulfonate derived from esculeogenin B metabolism after the administration of ripe tomatoes products as juices (Hövelmann et al., 2020).

4.3.3. Preparation of LGT diet

The LGT diet was prepared by wet addition of Datterini tomatoes product to the feed. For this procedure, the CD feed was pulverized and added to the LGT in presence of water. The obtained mixture was mixed and subsequently freeze-dried to obtain the LGT diet. A schematic representation of LGT diet production is shown in **Figure 34**. The preparation of LGT diet required the preparation of several feed batches. Then, each of these was analyzed to evaluate the average weight and subjected to a qualitative and quantitative analysis to evaluate the phytochemical composition and α-TM content. According to the calculations described in paragraph **4.3.1. Design of the experimental study**, the feed needs to contain an α-TM content of 0.033% (*w/w*). During the production of the feed batches, those with an α-TM content 15% higher or lower than the established value were excluded. Seven production batches were thus obtained, with amounts varying between 0.5 kg and 6.0 kg in

the period necessary for the pharmacological treatment between 27/01/2022 and 12/07/2022. All feed batches have an average weight of each chow unit of approximately 3g. To carry out the analysis of the LGT diet, a qualitative-quantitative analysis of the composition of the diet was performed, a validation of the quantitative analysis method and the extraction process, and a subsequent analysis of all the production batches of the diet.

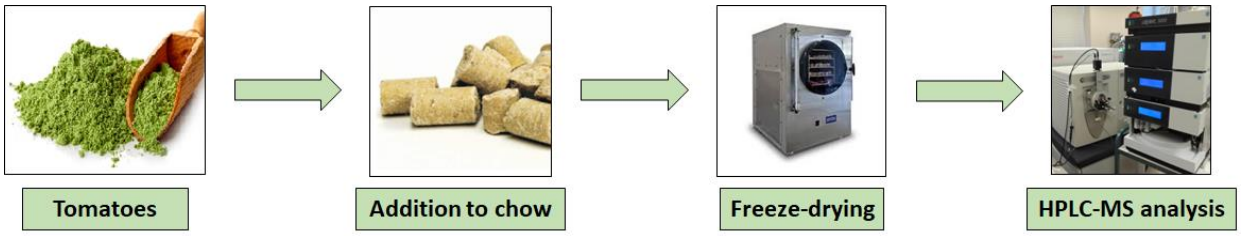


Figure 34. Workflow of LGT diet production.

4.3.4. Qualitative analysis of LGT diet

The analysis of LGT diet extracts allowed to tentatively identify 10 compounds by comparison with literature data and with the results of Datterini green tomatoes chemical characterization reported in the paragraph **3.3.1 Preparation of the matrix and extraction method**. The qualitative screening was preliminary to the quantitative analysis of each production LGT diet batch. The clean-up of the extract was necessary to improve the sensitivity of the analysis and was performed with a purified SPE purification of the hydroalcoholic LDT diet extract. The qualitative analysis of LGT diet agreed with the results of Datterini green tomatoes chemical characterization, both for the compounds elution gradient and the fragmentation pattern. The only exception is represented by the order of elution of α-TM and acetoxytomatine. This variation of gradient elution could be due to the change of the phase B solvent, with the replacement of methanol used for the Datterini green tomatoes characterization (paragraph **3.2.3. Qualitative glycoalkaloids analysis**) with the acetonitrile used for the LGT diet characterization (paragraph **4.2.5. LGT diet qualitative analysis by HPLC-HESI-MS/MS analysis**). The retention time, the local maximum values of UV spectrum, the ionization mode (positive: $[M+H]^+$; negative: $[M-H]^-$) the precursor ion (*m/z*), and the fragment ions with the base peak in bold were listed in **Table 25**. These compounds include 4 polyphenols and 6 SGAs. The molecular identity of

rutin and α-TM was confirmed by comparison with analytical standards. These two compounds were selected for further quantitative investigation in LGT diet analysis.

No	Compound	Rt	UV	Ionization	Precursor ion (*m/z*)	Fragmentation
61	Quercetin *O*-(pentosylrutinoside)	6.86	205, 255	$[M-H]^-$	741.3	723.2 $[M-H-H_2O]^-$, **609.1 [M-H-Pent]$^-$**, 591.2 $[M-H-Pent-H_2O]^-$, 301.1 [M-H-Pent-Rha-Hex]$^-$
64	Rutin*	7.14	205, 255	$[M-H]^-$	609.3	591.4 $[M-H-H_2O]^-$, 463.1 [M-H-Rha]$^-$, **301.0 [M-H-Rha-Glu]$^-$**, 179.1 $[M-H-Rha-Glu-C_7H_6O_2]^-$
65	Kaempferol *O*-(pentosylrutinoside)	7.31	205, 255	$[M-H]^-$	725.2	707.1 $[M-H-H_2O]^-$, **593.2 [M-H-Pent]$^-$**, 575.1 $[M-H-Pent-H_2O]^-$, 284.9 [M-H-Pent-Rha-Hex]$^-$
4	Hydroxytomatine	7.42	-	$[M+H]^+$	1050.6	**1032.5 $[M+H-H_2O]^+$**, 918.6 $[M+H-Pent]^+$, 756.6 $[M+H-Pent-Hex]^+$, 576.4 $[M+H-Pent-2Hex-H_2O]^+$, 414.3 $[M+H-Pent-3Hex-H_2O]^+$
68	Kaempferol *O*-rutinoside	7.50	205, 255	$[M-H]^-$	593.2	575.0 $[M-H-H_2O]^-$, **284.9 [M-H-Hex]$^-$**, 257.1 $[M-H-Hex-CO]^-$, 179.0 $[M-H-Hex-C_7H_6O]^-$
5	Lycoperoside G/F or esculeoside A	7.64	-	$[M+H]^+$	1270.8	**1210.6 [M+H-AcOH]$^+$**, 1048.5 $[M+H-Hex-AcOH]^+$, 754.5 $[M+H-Pent-2Hex-AcOH]^+$, 592.5 $[M+H-Pent-3Hex-AcOH]^+$, 412.3 $[M+H-Pent-4Hex-AcOH-H_2O]^+$
9	Acetoxyhydroxytomatine	7.93	-	$[M+H]^+$	1108.6	**1048.5 [M+H-AcOH]$^+$**, 1030.5 $[M+H-H_2O-AcOH]^+$, 652.6 $[M+H-Pent-2Hex]^+$, 412.4 $[M+H-Pent-3Hex-H_2O-AcOH]^+$
11	Dehydrotomatine	8.29	-	$[M+H]^+$	1032.6	**1014.5 $[M+H-H_2O]^+$**, 900.5 $[M+H-Pent]^+$, 870.5 $[M+H-Hex]^+$, 576.4 $[M+H-Pent-2Hex]^+$, 414.4 $[M+H-Pent-3Hex]^+$
14	Acetoxytomatine	8.42	-	$[M+H]^+$	1092.5	**1032.6 [M+H-AcOH]$^+$**, 900.6 $[M+H-Pent-AcOH]^+$, 738.7 $[M+H-Pent-Hex-AcOH]^+$, 576.5 $[M+H-Pent-2Hex-AcOH]^+$, 414.5 $[M+H-Pent-3Hex-AcOH]^+$
13	α-Tomatine*	8.50	-	$[M+H]^+$	1034.7	**1016.6 $[M+H-H_2O]^+$**, 902.6 $[M+H-Xyl]^+$, 740.6 $[M+H-Xyl-Glu]^+$, 578.5 $[M+H-Xyl-2Glu]^+$, 416.3 $[M+H-Xyl-2Glu-Gal]^+$

Table 25. SGAs and polyphenols putatively identified in LGT diet by their MS/MS spectra in agreement with literature by HPLC-MS analysis in positive and negative acquisition modes. Hex, Pent, Xyl, Glu, Agl, and AcOH indicate hexoside, pentoside, xylose, glucose, aglycone, and acetoxy groups, respectively. * The identification of this molecule was confirmed using commercial standard.

4.3.5. Development of α-tomatine HPLC-HESI-MS/MS method for LGT diet analysis

The method used for SGAs quantitative analysis is accurately described in the previous paragraph **4.2.6 α-tomatine quantitative analysis of LGT diet by HPLC-HESI-MS/MS**.

The method development was performed by modifying the method applied for the phytochemical cultivars screening and reported in the paragraph **3.3.2.1. Development of SGAs HPLC-HESI-MS/MS method**, with slight modification. One great difference between the two methods is the replacing of methanol at 0.01% of formic acid as phase B with acetonitrile at 0.1% of formic acid. This modification was due to acetonitrile provides sharper peaks in the chromatogram than methanol. Moreover, the increment of the percentage of formic acid from the 0.01% to the 0.1% allows to improve the ionization of SGAs amine group, increasing the sensitivity of the method. In addition, the temperature column was increased from 30°C to 35°C to improve peak resolution and reduce column pressure. The solubilization solvent for α-TM standard solutions and the real samples was changed, substituting the neutral methanol with a methanolic solution with 0.1% of formic acid to improve the extract solubility in acidic conditions. Moreover, the use of an acidic pH for the solubilization allow to improve the ionization of the amine group of α-TM and the sensitivity of the method. Based on α-TM MS/MS spectrum reported in the paragraph **3.3.2.1. Development of SGAs HPLC-HESI-MS/MS method**, the same qualifier (1034.6 – 416.2) and quantifier (1034.6 – 1016.3) MRM transitions were applied for α-TM quantification in LGT diet batches. Another difference with the method reported in the paragraph **3.3.2.1. Development of SGAs HPLC-HESI-MS/MS method** is the inversion of the qualifier and quantifier transitions. As matter of fact, the previously reported method required to use the transition 1034.6 – 416.2 as quantifier due to the necessity to quantify the secondary SGAs in α-TM equivalent. Instead, this method is used only for α-TM quantification in LGT diet, allowing to use the base peak ion with *m/z* 1016.3 as fragment ion for the quantifier MRM transition. The peak obtained by α-TM standard analysis at a concentration of 5 ppm was provided in **Figure 34**.

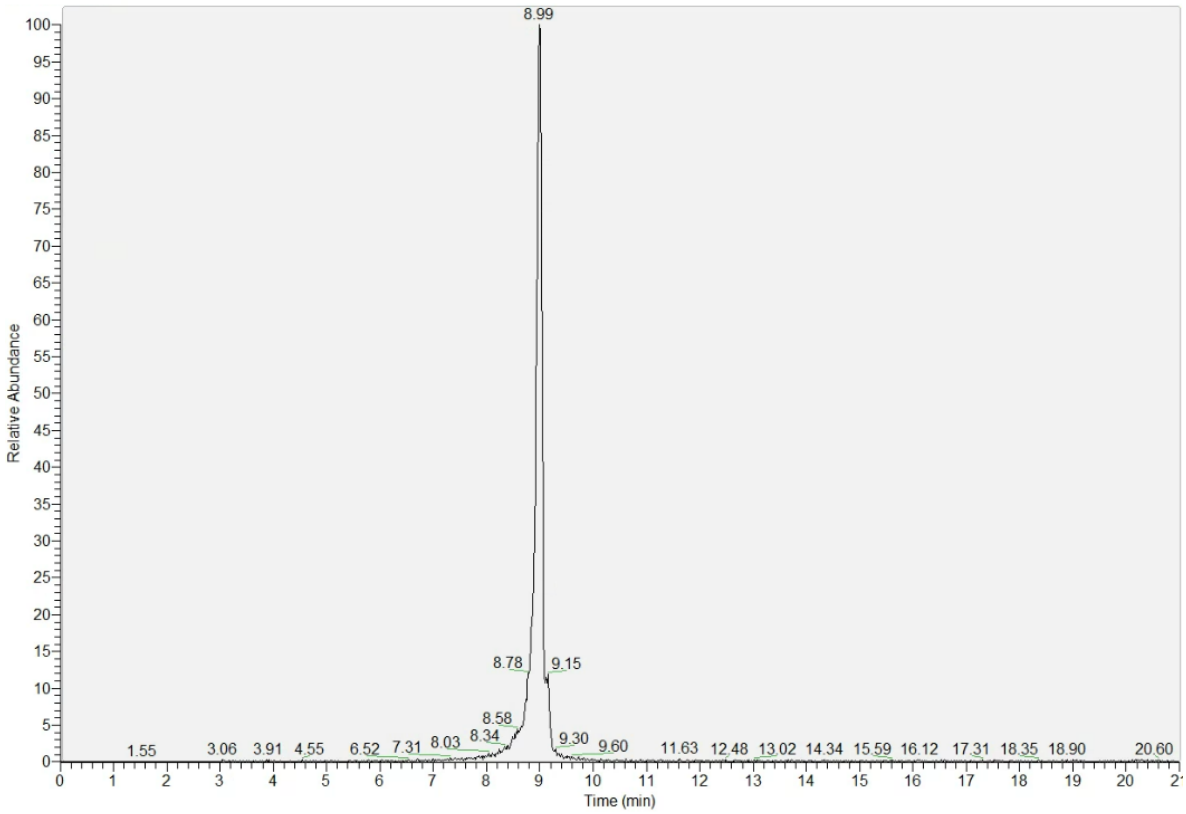


Figure 34. α-TM standard at a concentration of 5 ppm, obtained by the MRM transition 1034.6 – 1016.3 with a CID of 40 eV.

4.3.6. Development of rutin HPLC-HESI-MS/MS method for LGT diet analysis

The method used for rutin quantitative analysis is accurately described in the previous paragraph **4.2.7. Rutin quantitative analysis of LGT diet by HPLC-HESI-MS/MS**. The method development was performed by the method proposed by Maisto et al., 2023, with slight modification. In the method, the selection of acetonitrile as phase B of the HPLC-HESI-MS/MS method provides sharper peaks in the chromatogram than methanol. In the initial condition, after 1.5 min hold at 5% of solvent B, the elution was performed with a linear gradient to 50% of solvent B in 6.5 minutes, followed by an isocratic at 95% for 2 minutes and a re-equilibration of the column to the initial conditions for 3 minutes. The real gradient was zoomed in the range of phase B solvent of 5-50%, which represents the conditions for SGAs elution, allowing to reduce the time of analysis with a satisfying chromatographic separation. In this way, the total time of analysis, including cleaning time and equilibration time, was only 13.5 minutes, thus providing a shorter method, potentially

suitable for a High Throughput Screening analysis (HTS). Among the HPLC methods, the LC-MS analysis in MRM acquisition mode was selected to provide the better conditions for rutin quantification in LGT diet. Rutin quantification in Datterini green tomatoes was previously performed by HPLC-DAD analysis. The estimated rutin amount in LGT diet is about 30 µg. Although the rutin incorporation in the diet and the extraction recovery could be like the 100%, this amount is low and can be lower than the LOQ values provided by classic HPLC-DAD analysis. Therefore, a more sensitive method as the LC-MS analysis in MRM acquisition mode was preferred for rutin quantification in LGT diet.

As the same way of α-TM MRM development method, tandem mass spectrometry (MS/MS) in data dependent acquisition (DDA) was selected to evaluate the fragmentation pattern of rutin standard for the development of the method.

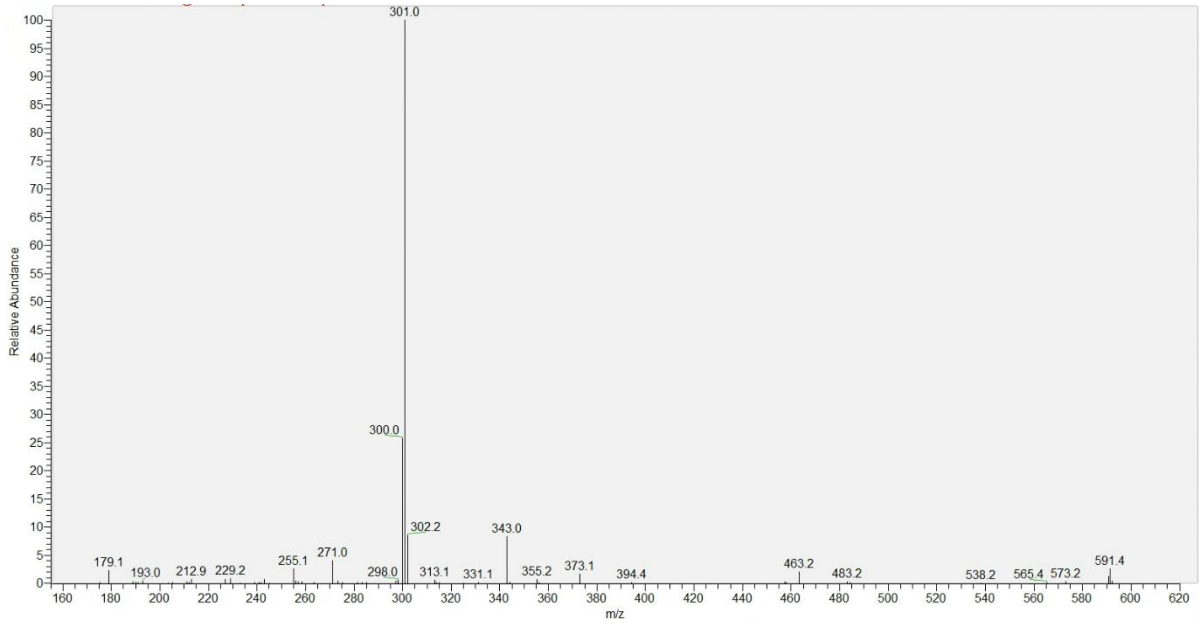


Figure 35. MS^2 spectrum of rutin, by using a MS/MS analysis mode with a CID of 35 eV.

Figure 35 displays the MS^2 spectrum of the analytical standard of rutin (parent ion: *m/z* 609.3), obtained with a MS/MS analysis mode. The MS/MS spectrum of rutin allows to clarify the fragmentation pattern of the molecule. The following ions represent the most important fragments:

- *m/z* 591.4 corresponds to the neutral loss of a molecule of water;
- *m/z* 463.2 corresponds to the neutral loss of a terminal rhamnose unit;
- *m/z* 301.0 corresponds to the cleavage of rutinose moiety through a homolytic fragmentation;

- *m/z* 300.0 corresponds to the cleavage of rutinose moiety through a heterolytic fragmentation;
- *m/z* 271.0 corresponds to the cleavage of rutinose moiety and a molecule of monoxide carbon CO;

An important diagnostic fragment in rutin MS/MS spectrum is represented by the rutinose cleavage through a homolytic fragmentation (-308 Da). By considering that the transition 609.5 – 301.0 provided the base peak fragment ion, it has been chosen as the quantifier transition for rutin analysis. On the other hand, transition 609.5 – 271.0 has been chosen as a qualifier transition. The peak obtained by rutin standard analysis for the MRM quantifier transition 609.5 – 301.0 at a concentration of 10 ppm was provided in **Figure 36**.

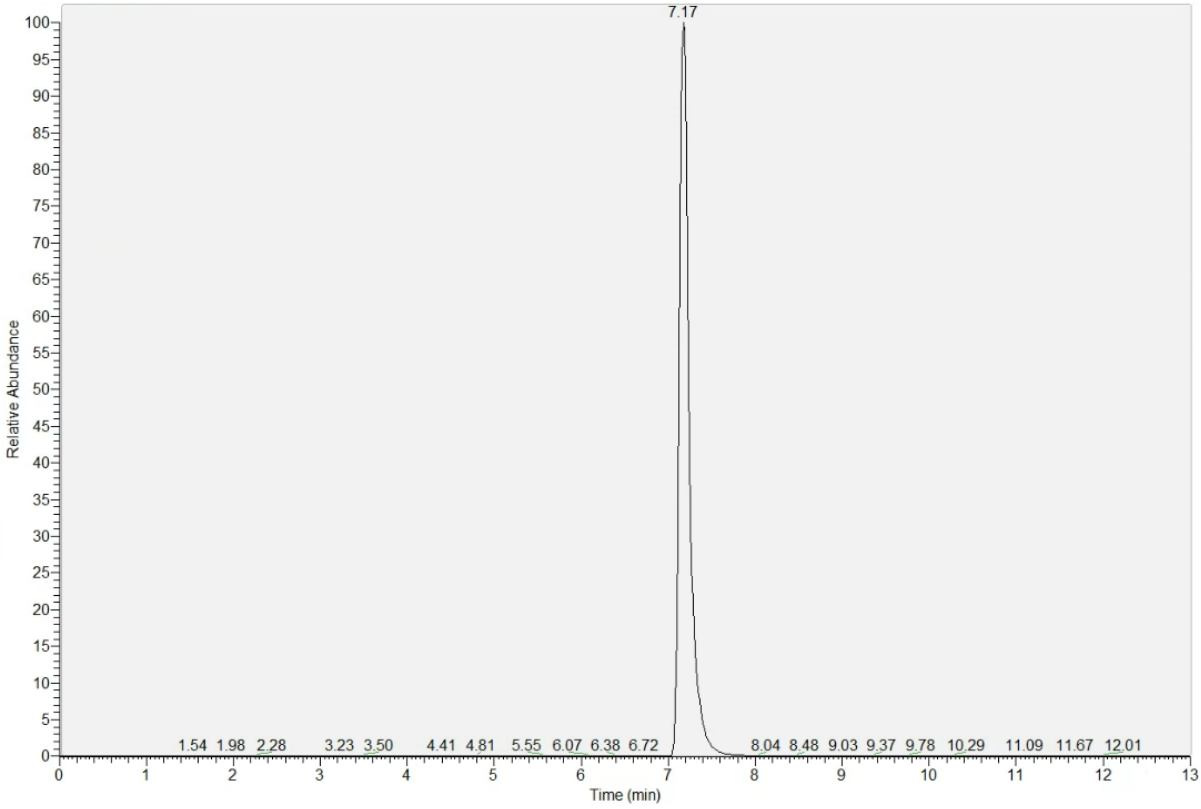


Figure 36. Rutin standard at a concentration of 10 ppm, obtained by the MRM transition 609.5 – 301.0 with a CID of 40 eV.

4.3.7. HPLC-HESI-MS/MS method validation

4.3.7.1. Validation of α-tomatine method

The procedures described above in the paragraphs **3.1.11. Method validation according to ICH guidelines** were applied to the method reported in the paragraph **4.2.6. α-tomatine quantitative analysis of LGT diet by HPLC-HESI-MS/MS**. α-TM calibration curve has been performed by considering both the quantifier MRM transition 1034.4 – 1016.3 and the qualifier 1034.4 – 416.2 in a range of seven concentration between 10 ppm and 0.16 ppm. A preliminary analysis for the evaluation of the matrix effect was performed by comparing the calibration curves of α-TM analytical standard in solvent (methanol with 0.1% of formic acid) and in matrix (hydroalcoholic extract of CD dissolved in methanol with 0.1% of formic acid at concentration of 5 mg/ml). Both the calibration curves displayed a favourable linear regression ($R^2 > 0.99$), thus demonstrating the linearity of the standard response in the range of concentrations analyzed (**Figure 37**). Moreover, both the calibration curves displayed a matrix effect for the use of the hydroalcoholic extract of CD at a concentration of 5 mg/ml. The matrix effect was confirmed by comparing the slope of the calibration curves and using a significance at the 95% confidence level by the student t-test. Therefore, the hydroalcoholic extract of CD dissolved in methanol with 0.1% of formic acid at a concentration of 5 mg/ml was selected as solubilization solvent for the preparation of α-TM calibration curve. LOD and LOQ values were determined to evaluate the sensitivity of the method. α-TM displayed a LOD value of 0.193 ± 0.051 ppb and a LOQ value of 0.642 ± 0.171 ppb (**Table 26**), which were above the compound values in the analysed real samples, confirming the efficiency of the method for the quantification of LGT diet batches.

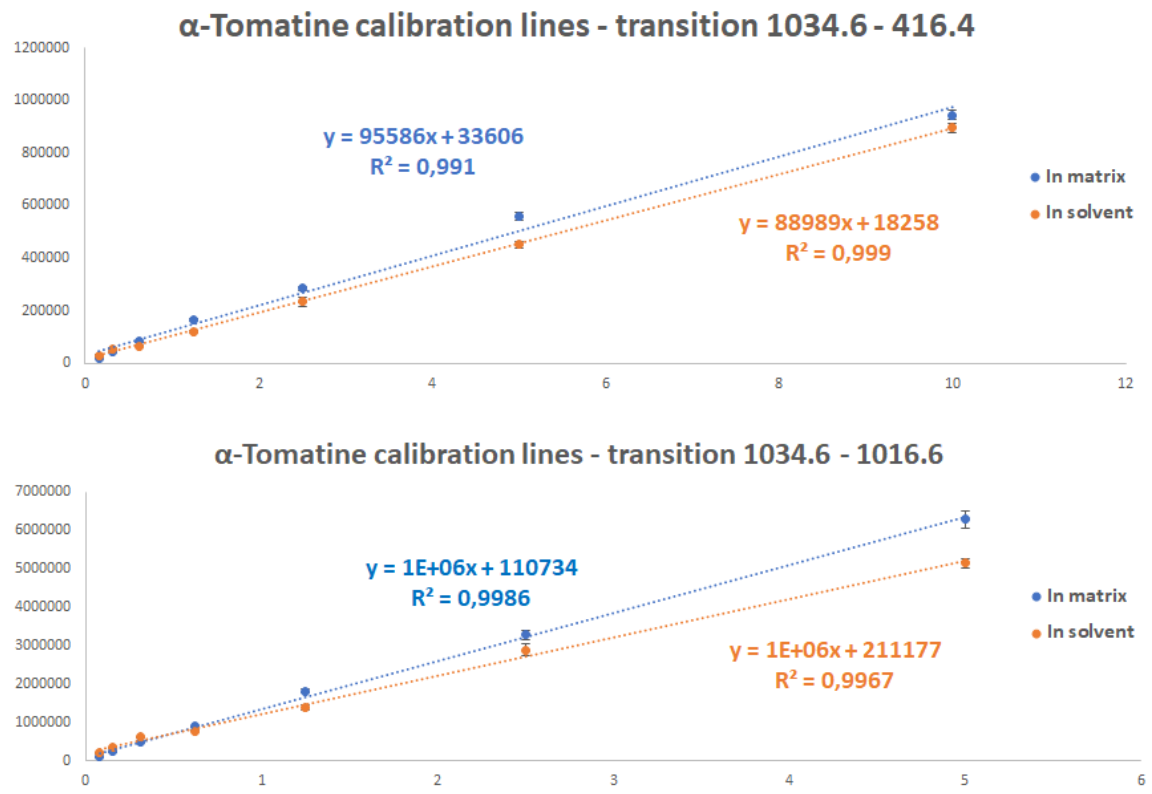


Figure 37. α-TM calibration curves of qualifier MRM transition (1034.6 – 416.4) and quantifier MRM transition (1034.6 – 1016.6) using as solubilization solvent the methanol with 0.1% of formic acid (orange) and the hydroalcoholic extract of CD dissolved in methanol with 0.1% of formic acid at concentration of 5 mg/ml (blue).

Compound	Linearity range (ppm)	Calibration curve	LOD (ppb)	LOQ (ppb)
α-TM	0.16 – 10	y = 1E+06x + 110734	0.193 ± 0.051	0.642 ± 0.171

Table 26. Linearity range, calibration curve, limit of detection (LOD) and limit of quantification (LOQ) for α-TM analysis.

In agreement with the ICH validation guideline (ICH.Q2[R2], 2022), precision and accuracy were evaluated to validate the HPLC-MS/MS method. Precision and accuracy were calculated by an intra-day and an inter-day analysis of α-TM standard solutions at 3 different concentrations (**Table 27**). The 3 concentrations have been selected to represent the calibration levels (e.g., high: 5 ppm; medium: 1 ppm; low: 0.1 ppm) included in the linearity range. The selection of these concentrations allowed to establish precision and accuracy of the entire calibration curves. The intra-day analysis was performed by injecting α-TM

solutions three times per day. Instead, the inter-day analysis was performed by injecting the three selected standard solutions for 3 consecutive days. In the validation of the HPLC-MS/MS analysis, for the evaluation of intraday and interday precision and accuracy, the RSD value ranged from 1.55 to 4.86 % ppm and from -4.86 to 3.62 %, respectively. Therefore, all % CV and % bias values for precision and accuracy evaluation showed values lower than ± 5%. These results assessed that the developed method was satisfactory with acceptable precision, accuracy, and reproducibility for α-TM analysis.

Compound	Concentration (ppm)	Precision (CV %)		Accuracy (% bias)	
		Intraday	Interday	Intraday	Interday
α-TM	5	4.86	4.33	0.83	-4.86
	1	4.38	3.57	-4.33	-3.81
	0.1	1.55	5.28	2.17	3.62

Table 27. Intra-day and inter-day precision and accuracy of α-TM analysis.

4.3.7.2. Validation of rutin method

The procedures described above in the paragraphs **3.1.11. Method validation according to ICH guidelines** were applied to the method reported in the paragraph **4.2.7. Rutin quantitative analysis of LGT diet by HPLC-HESI-MS/MS**. Rutin calibration curve has been performed by considering both the quantifier MRM transition 609.5 – 301.5 and the qualifier 609.5 – 271.5 in a range of seven concentration between 50 ppm and 0.5 ppm. A preliminary analysis for the evaluation of the matrix effect was performed by comparing the calibration curves of rutin analytical standard in solvent (methanol with 0.1% of formic acid) and in matrix (hydroalcoholic extract of CD dissolved in methanol with 0.1% of formic acid at concentration of 5 mg/ml). Both the calibration curves displayed a favourable linear regression ($R^2 > 0.99$), thus demonstrating the linearity of the standard response in the range of concentrations analyzed (**Figure 38**). Moreover, both the calibration curves displayed a matrix effect for the use of the hydroalcoholic extract of CD at a concentration of 5 mg/ml. The matrix effect was confirmed by comparing the slope of the calibration curves and using a significance at the 95% confidence level by the student t-test. Therefore, the hydroalcoholic extract of CD dissolved in methanol with 0.1% of formic acid at a concentration of 5 mg/ml was selected as solubilization solvent for the preparation of rutin calibration curve. LOD and LOQ values were determined to evaluate the sensitivity of the method. Rutin displayed a LOD value of 0.382 ± 0.009 ppb and a LOQ value of 1.272 ±

0.030 ppb (**Table 28**), which were above the compound values in the analysed real samples, confirming the efficiency of the method for the quantification of LGT diet batches.

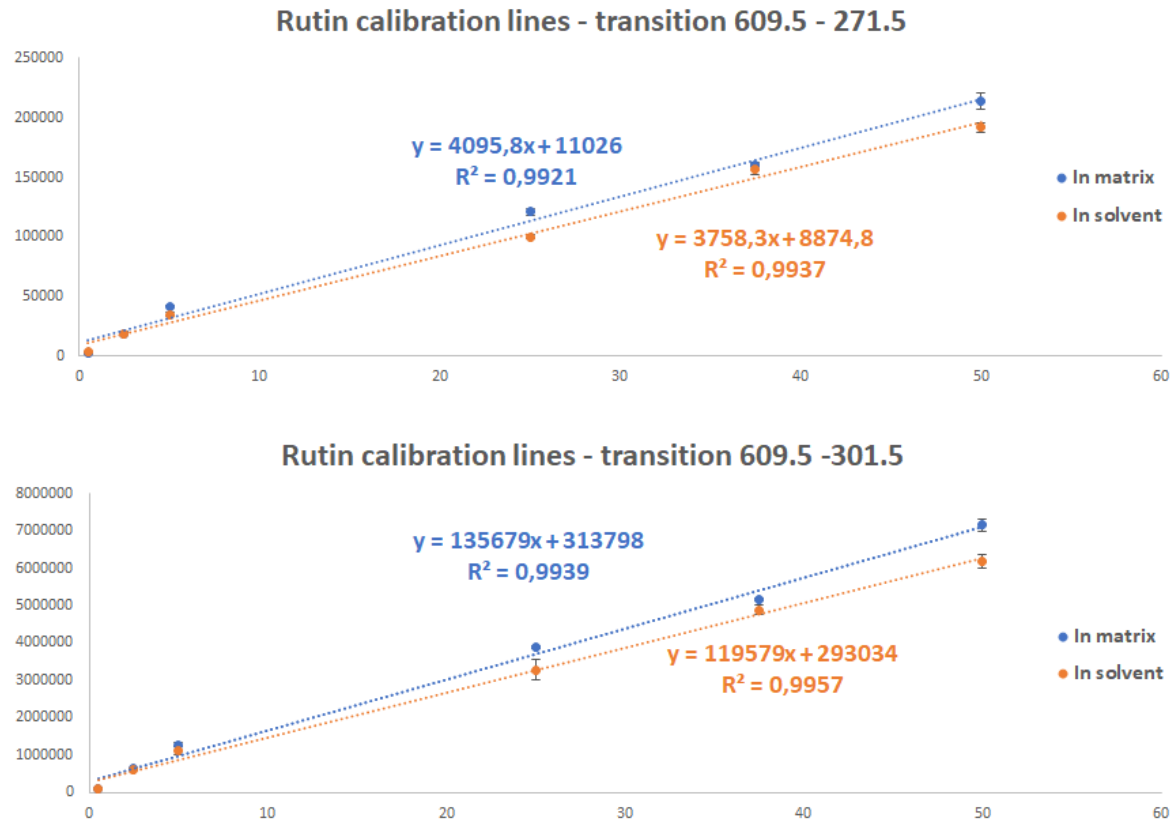


Figure 38. Rutin calibration curves of qualifier MRM transition (609.5 – 271.5) and quantifier MRM transition (609.5 – 301.5) using as solubilization solvent the methanol with 0.1% of formic acid (orange) and the hydroalcoholic extract of CD dissolved in methanol with 0.1% of formic acid at concentration of 5 mg/ml (blue).

Compound	Linearity range (ppm)	Calibration curve	LOD (ppb)	LOQ (ppb)
Rutin	0.5 – 50	y = 135679x + 313798	0.382 ± 0.009	1.272 ± 0.030

Table 28. Linearity range, calibration curve, limit of detection (LOD) and limit of quantification (LOQ) for rutin analysis.

In agreement with the ICH validation guideline (ICH.Q2[R2], 2022), precision and accuracy were evaluated to validate the HPLC-MS/MS method. Precision and accuracy were calculated by an intra-day and an inter-day analysis of rutin standard solutions at 3 different concentrations (**Table 29**). The 3 concentrations have been selected to represent the calibration levels (e.g., high: 50 ppm; medium: 5 ppm; low: 0.5 ppm) included in the linearity range. The selection of these concentrations allowed to establish precision and accuracy of the entire calibration curves. The intra-day analysis was performed by injecting rutin solutions three times per day. Instead, the inter-day analysis was performed by injecting the three selected standard solutions for 3 consecutive days. In the validation of the HPLC-MS/MS analysis, for the evaluation of intraday and interday precision and accuracy, the RSD value ranged from 1.00 to 4.81 % ppm and from -4.89 to 4.98 %, respectively. Therefore, all % CV and % bias values for precision and accuracy evaluation showed values lower than ± 5%. These results assessed that the developed method was satisfactory with acceptable precision, accuracy, and reproducibility for rutin analysis.

Compound	**Concentration (ppm)**	**Precision (CV %)**		**Accuracy (% bias)**	
		Intraday	Interday	Intraday	Interday
Rutin	50	3.35	4.81	0.39	2.42
	5	1.00	1.90	3.57	1.74
	0.5	2.60	4.52	-4.89	4.98

Table 29. Intra-day and inter-day precision and accuracy of rutin analysis.

4.3.8. Validation and extraction of LGT diet

4.3.8.1. Development of LGT diet extraction

The extraction of LGT diet was performed by reducing the diet in powder by grinding and by storing it in the dark, protected from light. The features and the advantages of the extraction procedure were previously described in the paragraph **3.3.1. Preparation of the matrix and extraction method**. The main difference between the procedure previously reported and the extraction of LGT diet was the solid matrix/extraction solvent ratio. The first procedure was performed by extracting 1.5 g of dried green tomatoes powder with a total volume of 15 ml of hydroalcoholic solvent at 80% of methanol and 1% of formic acid. Instead, the actually applied procedure was performed by extraction 2 g of dried LGT diet powder with a total volume of 40 ml of hydroalcoholic solvent at 80% of methanol and 1% of formic acid. For the second procedure, a larger volume of extracting solvent was preferred due to the larger particle size of the LGT diet powder. This reduces the extraction surface area and solid-liquid contact, requiring a larger extractant volume than normally is used in food matrices extraction.

4.3.8.2. Validation of α-tomatine extraction

Recovery experiments of α-TM extraction has been performed following the procedure described in paragraph **4.2.10. Matrix effect and Recovery of α-tomatine and rutin extraction**. The recovery is the closeness of agreement between the true value of the analyte concentration and the experimental results and represents the efficiency of the extraction method for that analyte. Therefore, recovery describes the amount actually recovered by the matrix and is expressed as the percentage (%) yield of the extraction method. According to FDA, a good recovery for the working analytes concentrations for this assay should be between 80-110% (Fda, 2011). For the experiment, the matrix was spiked in triplicate either before (pre-extraction spiked) or after (post-extraction spiked) extraction with the solution of the analyte, using three different concentrations according to the values obtained from the quantification. α-TM standard concentrations (e.g., high: 10 µg; medium: 5 µg; low: 1 µg) have been selected in a way that even the lowest concentrations could have provided a statistically significant impact on the quantification of each compound for the evaluation of SGAs recovery. The recovery has been therefore investigated by calculating the ratio of the

peak area in the pre-extraction spiked samples to the peak area in the post-extraction spiked samples. The ratio was calculated as follows:

$$\textbf{Recovery (\%)} = \left[\left(\frac{\boldsymbol{Peak\ area_{pre-extraction\ spiked\ sample}}}{\boldsymbol{Peak\ area_{post-extraction\ spiked\ sample}}}\right) \boldsymbol{x\ 100}\right]$$

As shown in **Table 30**, the recovery values are close to 100% at three concentration levels, confirming the effectiveness of the procedure proposed for SGAs extraction. Recovery results obtained in our experiments were compared to literature data to evaluate the efficacy of the procedures for SGAs extraction. For example, Taveira et al. (2012) proposed a procedure for the extraction of SGAs from dried leaves of *Solanum lycopersicum* L. According to this procedure, the recovery (%) of α-TM was found between 92 and 93%, while recovery (%) of TD was found between 95 and 98%. Although these values are close (or slightly lower) to those provided by our extraction procedure, it is also true that the method proposed by Taveira et al. (2012) for SGAs extraction is more time-consuming and more expensive, since it does not allow SGAs and polyphenols to be extracted simultaneously. In fact, another separated extraction procedure (performed by using a mixture of methanol:water (1:1)) is required for the extraction of phenolic compounds. Moreover, our procedure was compared with the method proposed by Martínez Bueno et al. (2018) for the extraction of dried tomato powder. This author reported recovery % values for α-TM of 55% and for TD of 60% using pure methanol as extraction solvent. The lower recovery values could be due to the use of pure methanol as extraction solvent on dried samples, without the use of water or acidic organic modificators.

α-TM		
Spiked (µg)	**Recovery (%)**	**Matrix effect (%)**
1	96.7 ± 4.1	19.3 ± 4.7
5	102.1 ± 1.9	9.8 ± 9.4
10	100.8 ± 6.4	20.5 ± 7.1

Table 30. Recovery % and matrix effect % of α-TM extraction.

After SGAs quantification in LGT diet hydroalcoholic extracts, the matrix effect has been investigated to evaluate the correctness and reliability of the quantification data provided by the HPLC-HESI-MS/MS method. The aim of this assay was to assess the influence of all the other sample components on SGA response in quantitative analysis. The matrix effect is caused by the co-elution of target analytes with other compounds present in complex

matrices, which are responsible for the peak tailing and the failure in providing an accurate quantification by alteration of the ionization efficiency (Hooshmand & Fomsgaard, 2021). The alteration of compounds ionization can be observed as a phenomenon of ion suppression or ion enhancement. Ion suppression is a loss in target analytes responses which leads to underestimation of the target analytes amount. Ion enhancement is an increment of target analytes responses, resulting in an overestimation of target analytes amounts. The matrix effect of ion suppression is extremely common in mass spectrometry analysis and its evaluation represents the main goal in matrix effect experiments. Since the matrix may considerably affect the quality of analysis, to provide an accurate estimation of SGAs content in the matrix, the matrix effect had to be estimated. For the investigation of the matrix effect, α-TM analytical standard solutions at three different concentrations have been considered and the matrices chosen were the same used for the recovery experiment. The procedure for the evaluation of the matrix effect is accurately described in the paragraph **4.2.10. Matrix effect and Recovery of α-tomatine and rutin extraction**. The matrix effect was calculated with this ratio:

$$\textbf{Matrix effect (\%)} = \left[\left(\frac{\boldsymbol{Peak\ area_{post\ extraction\ spiked\ sample} - Peak\ area_{not\ spiked\ sample}}}{\boldsymbol{Peak\ area_{blank}}}\right) - \mathbf{1}\right] \boldsymbol{x}\ \mathbf{100}$$

Matrix effect in the analysis of α-TM ranged from 9.8 ± 9.4 and 20.5 ± 7.1 (**Table 30**). These positive values can be explained by considering a phenomenon of ion enhancing. The matrix effect was previously confirmed by the significant matrix effect obtained by the comparison of the slopes of α-TM calibration curves in solvent and the hydroalcoholic extract of CD dissolved in methanol with 0.1% of formic acid at a concentration of 5 mg/ml (**Figure 37**). Therefore, in order to avoid the problem of the matrix effect that could overestimate the result of α-TM quantification, it was decided to carry out the quantization with α-TM calibration curve in the hydroalcoholic extract of CD dissolved in methanol with 0.1% of formic acid at a concentration of 5 mg/ml. Therefore, these results allowed an accurate quantitative analysis of the metabolites of interest in the real samples.

4.3.8.3. Validation of rutin extraction

Recovery experiments of rutin extraction has been performed following the procedure described in paragraph **4.2.10. Matrix effect and Recovery of α-tomatine and rutin**

extraction. For the experiment, the matrix was spiked in triplicate either before (pre-extraction spiked) or after (post-extraction spiked) extraction with the solution of the analyte, using three different concentrations according to the values obtained from the quantification. Rutin standard concentrations (e.g., high: 40 µg; medium: 20 µg; low: 5 µg) have been selected in a way that even the lowest concentrations could have provided a statistically significant impact on the quantification of each compound for the evaluation of rutin recovery. The recovery has been therefore investigated by using the same equation described in the paragraph **4.3.8.2 Validation of α-tomatine extraction**. As shown in **Table 31**, the recovery values are close to 100% at three concentration levels, confirming the effectiveness of the procedure proposed for rutin extraction. Recovery results obtained in our experiments were compared to literature data to evaluate the efficacy of the procedures for SGAs extraction. For example, Vallverdú-Queralt et al. (2012) found a rutin recovery of 93.44 ± 4.72 %. According to several procedures described in the literature, methanol as a pure organic solvent is sufficient to provide excellent rutin recovery values. However, for our extractions, it was preferred to use a hydroalcoholic mixture at 80% methanol and 1% formic acid, since this solvent is more suitable for extracting a huge number of heterogeneous polyphenolic compounds and for ensuring an excellent SGAs recovery from different anatomical parts of the plant.

Rutin		
Spiked (µg)	**Recovery (%)**	**Matrix effect (%)**
5	98.7 ± 2.3	13.1 ± 5.9
20	100.0 ± 5.7	47.4 ± 1.8
40	103.1 ± 1.4	22.5 ± 3.6

Table 31. Recovery % and matrix effect % of rutin extraction.

After the quantification of rutin in LGT diet hydroalcoholic extracts, the matrix effect has been investigated to evaluate the correctness and reliability of the quantification data provided by the HPLC-HESI-MS/MS method. For the investigation of the matrix effect, solutions of rutin analytical standard at three different concentrations have been considered and the matrices chosen were the same used for the recovery experiment. The procedure for the evaluation of the matrix effect is accurately described in the paragraph **4.2.10. Matrix effect and Recovery of α-tomatine and rutin extraction**. The matrix effect has been therefore investigated by using the same equation described in the paragraph **4.3.8.2 Validation of α-tomatine extraction**. Matrix effect in the analysis of rutin ranged from 13.1 ± 5.9 and 47.4 ± 1.8 (**Table 31**). These positive values can be explained by considering a

phenomenon of ion enhancing. The matrix effect was previously confirmed by the significant matrix effect obtained by the comparison of the slopes of rutin calibration curves in solvent and the hydroalcoholic extract of CD dissolved in methanol with 0.1% of formic acid at a concentration of 5 mg/ml (**Figure 38**). Therefore, in order to avoid the problem of the matrix effect that could overestimate the result of rutin quantification, it was decided to carry out the quantization with rutin calibration curve in the hydroalcoholic extract of CD dissolved in methanol with 0.1% of formic acid at a concentration of 5 mg/ml. Therefore, these results allowed an accurate quantitative analysis of the metabolites of interest in the real samples.

4.3.8.4. Quality control of LGT diet

After validating the extraction and analysis method of α-TM and rutin for the LGT diet, quantification was performed on the actual samples of the LGT diet for the mouse trial. The quantitative analysis of rutin was only performed on the first batch of the LGT diet to verify the content and % incorporation during diet production (**Table 32**). The quantification results showed that α-TM is stable during the wet incorporation process of LGT in the diet, with values close to 100%. In contrast, rutin has a much lower incorporation %, around the 10%, which could be due to chemical, thermal, or light instability during wet incorporation process.

Compound	Content	% incorporation
α-TM	1.02 ± 0.09 mg/LGT unit	103 ± 8
Rutin	2.92 ± 0.59 µg/LGT unit	10 ± 2

Table 32. Content and % of incorporation of α-TM and rutin in LGT diet.

In contrast, α-TM analysis was performed for each batch of the LGT diet. Seven production batches were thus obtained, with amounts varying between 0.5 kg and 6.0 kg in the period necessary for the pharmacological treatment between 27/01/2022 and 12/07/2022. During the production of the feed batches, those with an α-TM content 15% higher or lower than the established value were excluded. A constant α-TM amount (mg α-TM/LGT unit) was quantified in a range of 0.94 ± 0.06 and 1.07 ± 0.16. The results of α-TM quantification are summarised in **Table 33**. The results of the quantification demonstrated that the mice were

fed with a constant α-TM amount for the entire preclinical study using a LGT diet with the 0.033% (*w/w*) of α-TM.

LGT diet date production	Amount (kg)	α-TM content (mg α-TM/LGT unit)	% α-TM incorporation
27/01/2022	2.1	1.02 ± 0.09	103 ± 8
03/03/2022	1.0	1.07 ± 0.16	109 ± 16
05/03/2022	1.0	1.05 ± 0.16	113 ± 14
30/03/2022	0.5	0.97 ± 0.09	99 ± 9
12/04/2022	3.0	0.97 ± 0.06	98 ± 6
12/05/2022	5.0	0.94 ± 0.06	95 ± 5
12/07/2022	6.0	0.98 ± 0.03	99 ± 3

Table 33. Date of production, amount (kg), content and % of incorporation of α-TM in LGT diet batches.

4.3.9. LGT gastro-intestinal digestion

The pharmacokinetics of α-TM are poorly understood and there are no adequate studies on its metabolism during the gastro-intestinal tract. As matter of fact, the studies reported in the literature and summarised in paragraph **4.3.2. α-tomatine metabolism** represent the first attempts to elucidate the pharmacokinetics of this molecule. Therefore, a LGT gastro-simulated digestion experiment was performed to assess the conversion effect in the gastro-intestinal tract of α-TM to TD. Digestion was performed using the harmonised procedure reported by the COST action INFOGEST, with the procedure previously described in paragraph **4.2.11. Simulated gastro-intestinal digestion protocol**. The analysis was performed using the DDA analysis in positive acqusition mode previously reported in the paragraph **4.2.5. LGT diet qualitative analysis by HPLC-HESI-MS/MS analysis**. α-TM (*m/z* 1034.6) and TD (*m/z* 416.6) ions were extracted from full MS to verify α-TM conversion to TD. The analysis was performed on the supernatant of gastro-intestinal digestion and the Viscozyme and Pronase phases of intestinal fermentation, which mimic the action of the bacterial flora. In all samples, TD ion with *m/z* 416.6 was not detected, demonstrating that α-TM is stable to the effects of digestion assessed during the INFOGEST protocol. However, it must be emphasised that the INFOGEST protocol can only explain pH-dependent digestion processes and the action of the bacterial flora mediated by the enzymes Viscozyme and Pronase, which do not contain all the contained enzymes present in the gut microbiome. An example of α-TM and TD extracted ions in Viscozyme digestion phase is shown in **Figure 39**.

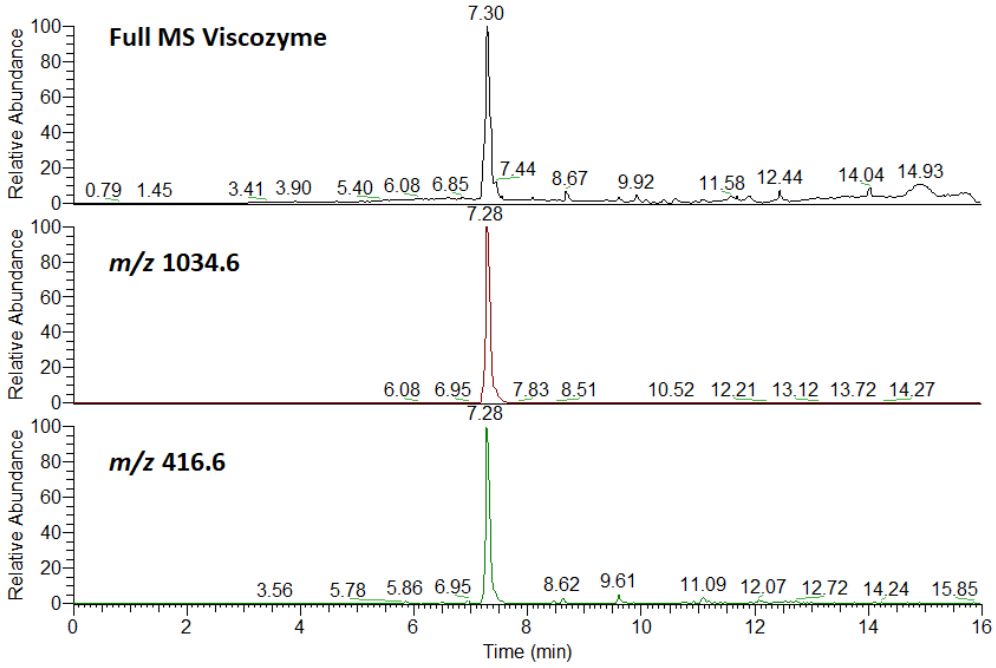


Figure 39. Full MS and extracted ions of α-TM with *m/z* 1034.6 and TD with *m/z* 416.6 in Viscozyme intestinal phase of LGT gastro-simulated digestion.

It is interesting to note that in the extracted ion of TD (*m/z* 416.6), the extracted peak has the same retention time as α-TM (*m/z* 1034.6), which derives from α-TM in-source fragmentation (MS^1), which was clearly shown in **Figure 40**.

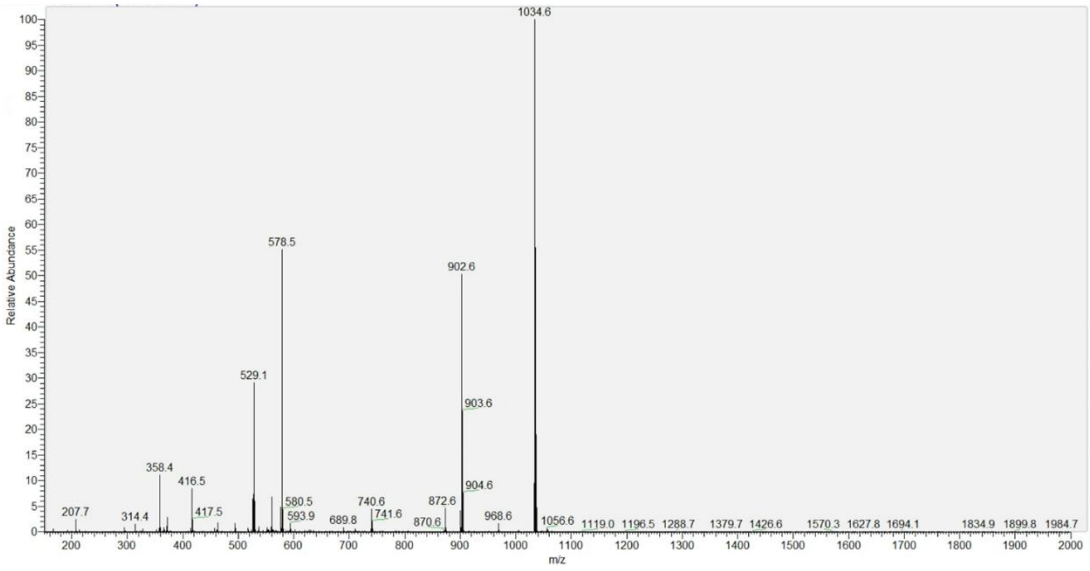


Figure 40. MS^1 spectrum of α-TM with DDA in positive acquisition mode.

4.3.10. Green tomatoes: a valuable healthy matrix for muscle cells

4.3.10.1. Tomatidine activity on muscle cells metabolism

To evaluate the anti-sarcopenic TD mechanism of action, a study of the effects on the myoblast cells line C2C12 was performed. As first step, the cytotoxicity of TD standard on the cells was evaluated with the MTT assay. Cells were treated with increased concentration of the standard (1 - 300 µM) for 48 hours, evaluating the cell viability. TD standard solution in DMSO was added to achieve a maximum final concentration of 600 µM, 300 µM, and 150 µM, with a final DMSO % of 0.1%. Therefore, the higher TD not-toxic concentration of 300 µM was selected for further cell assays. The cell viability was compared to the vehicle, represented by the same added volume of DMSO.

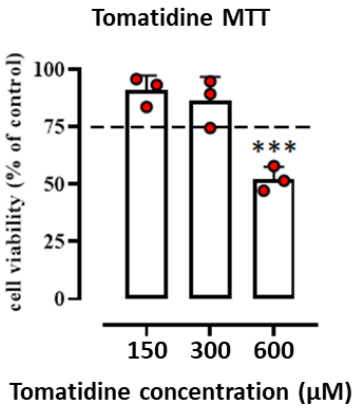


Figure 41. TD Cytotoxicity on myoblast cells line C2C12 after 48h, evaluated by the MTT assay. Data were shown as mean ± SEM of at least three independent experiments (*** $p <$ 0.001 *vs* CTR).

After the selection of the concentration of the maximum TD standard stock solution in DMSO (300 mM), the effects on total protein synthesis in myoblast cells line C2C12 was evaluated. TD standard displayed a significant increment of total protein synthesis after 24 hours of treatment with 75 µM TD in DMSO (**Figure 38**,**** $p <$ 0.0001 *vs* CTR). The

total protein synthesis was evaluated in the presence of a solution 100 nM of rapamycin, a well-known inhibitor of protein synthesis, which displayed a significant reduction of total protein synthesis (**Figure 42**,**** $p < 0.0001$ *vs* CTR). Therefore, the capacity of TD to revert the rapamycin activity indicates the role of TD in the regulation of total protein synthesis.

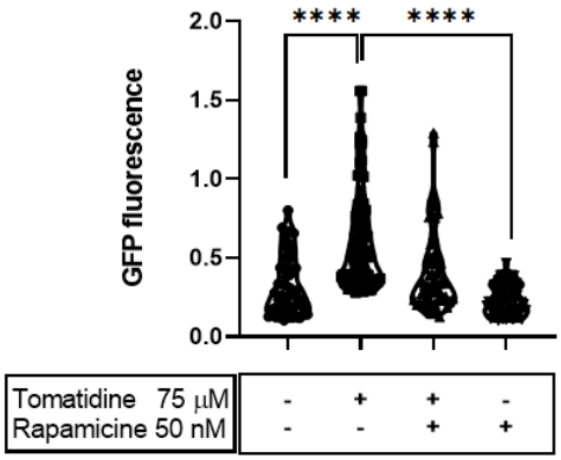


Figure 42. TDs effect on total protein synthesis on myoblast cells line C2C12 after 4h, evaluated by the MTT assay. Data were shown as mean ± SEM of at least three independent experiments (**** $p < 0.0001$ *vs* CTR).

To evaluate TD capacity to promote metabolic performance, the mitochondriogenesis was evaluated by considering the mitochondrial function after treatment with TD stock solution 300 mM in DMSO to obtain a final TD concentration of 300 µM and the DMSO vehicle. The evaluation of mitochondrial functions was performed by using the two cationic probes MitoTracker Green and MitoTracker Red CMXROS (tetramethylrhodamine methyl ester (TMRM)), which measure the mitochondrial mass and the membrane potential after being sequestered in the mitochondrial matrix space (Gibellini et al., 2015). The MitoTracker Green dye uptake was significantly improved in myoblast cells line C2C12 after the treatment, indicating an improvement of mitochondrial mass (**Figure 43**, *** $p < 0.001$ *vs* vehicle). Therefore, the treatment with the probe TMRM was employed to evaluate the changes of mitochondrial membrane potential. As demonstrated by the MitoTracker Green results, the MitoTracker Red CMXROS assay displayed a significant increment of mitochondrial potential after the incubation of myoblast cells line C2C12 with different final TD concentrations in the cell medium (75 µM, 150 µM, 300 µM) (**Figure 39**, * $p < 0.05$ *vs*

vehicle; ** $p < 0.01$ *vs* vehicle; *** $p < 0.001$ *vs* vehicle). Therefore, TD increases the dimension and the function of mitochondria, which could represent a strong indication of a promotion of metabolic performance.

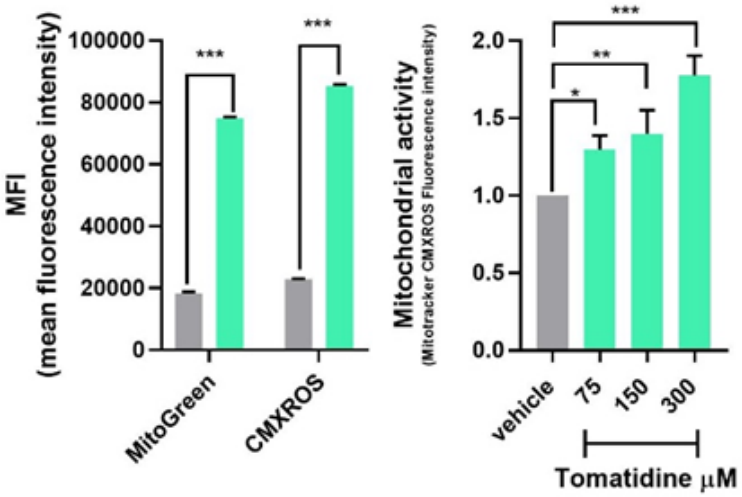


Figure 43. Quantification of mean fluorescence intensity (MFI) of MitoTracker Green at a final TD concentration of 300 µM and MitoTracker Red CMXROS at different final TD concentrations of 75 µM, 150 µM, and 300 µM in myoblast cells line C2C12 after 1 hour of treatment. Data were compared with the vehicle. Data were shown as mean ± SEM of at least three independent experiments (* $p < 0.05$ *vs* vehicle; ** $p < 0.01$ *vs* vehicle; *** $p < 0.001$ *vs* vehicle).

Skeletal muscle cells use glucose from the blood as an energy source for the exercise. Therefore, a compound acting in the glucose uptake could promote metabolic performance and could be effective in the prevention of muscle aging-related diseases. The evaluation of the glucose uptake was performed with the treatment of TD stock solution 300 mM in DMSO to obtain a final TD concentration of 300 µM and the DMSO vehicle. The evaluation of glucose uptake was performed by using the 2-Deoxy-2-[(7-nitro-2,1,3-benzoxadiazol-4-yl)amino]-D-glucose (2-NBDG), a fluorescent derivative of glucose which can be internalized in the cells instead of glucose. 2-NBDG structure is reported in the **Figure 44**.

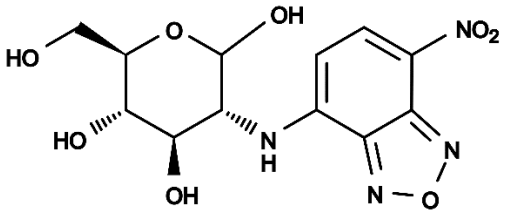


Figure 44. Structure of 2-Deoxy-2-[(7-nitro-2,1,3-benzoxadiazol-4-yl)amino]-D-glucose (2-NBDG).

The glucose uptake was significantly improved in myoblast cells line C2C12 after the treatment (**Figure 45**, *** $p < 0.001$ *vs* vehicle). Therefore, TD increases cells metabolic requirements and promote the metabolic performance.

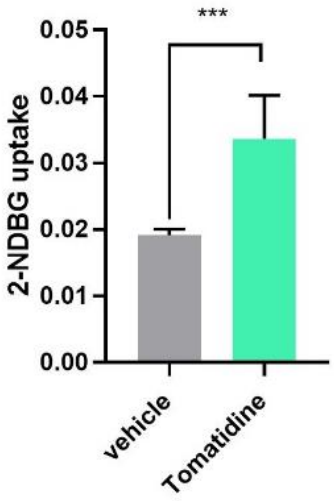


Figure 45. Quantification of 2-NDBG uptake for the measurement of glucose uptake in myoblast cells line C2C12 after 1 hour of treatment. The analysis was performed with the vehicle and with DMSO TD solution a final concentration of 300 µM. Data were shown as mean ± SEM of at least three independent experiments (*** $p < 0.001$ *vs* vehicle).

To elucidate the mechanism of action which leads to TD healthy effects on metabolic performance promotion, a qPCR of myoblast cells line C2C12 was performed after 48 hours of treatment with TD stock solution 300 mM in DMSO to obtain a final TD concentration of 300 µM and the DMSO vehicle. This assay was performed to evaluate the mRNA expression of PGC1-α, myoD, and myogenin (**Figure 46**). TD standard displayed a significant improvement of mRNA expression of PGC1-α (*** $p < 0.001$ *vs* vehicle) and myoD (** $p < 0.01$ *vs* vehicle). The factor peroxisome proliferator activated receptor gamma coactivator 1-α (PGC1-α) is a master regulator of mitochondrial biogenesis, which stimulates the mitochondrial biogenesis and function and negatively regulate senescence. Instead, myoblast determination protein (myoD) is a factor which regulates the muscle differentiation and growth. However, TD is not active on the mRNA expression of all the factors involved in metabolic performance promotion. For example, TD didn't show a significant variation of myogenin mRNA expression compared to the vehicle (**Figure 46**).

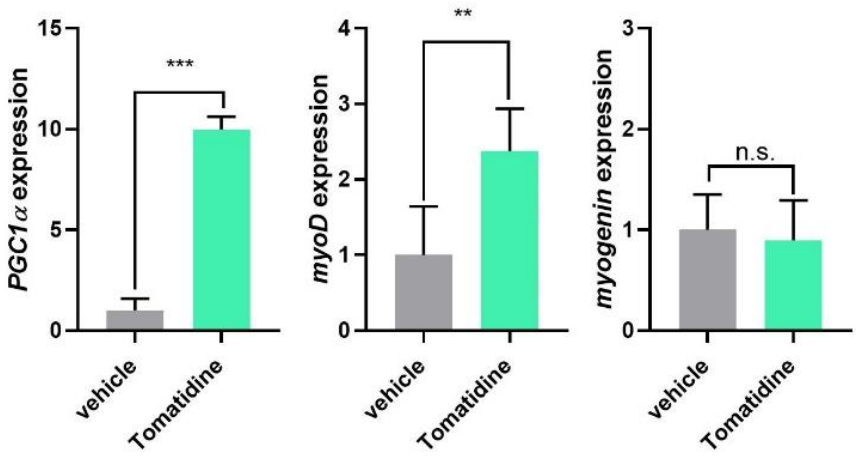


Figure 46. mRNA expression of PGC1-α, myoD, and myogenin evaluated with qPCR on myoblast cells line C2C12 after 48 hours of treatment with a final TD concentration of 300 µM. Data were shown as mean ± SEM of at least three independent experiments (** $p < 0.01$ *vs* vehicle; *** $p < 0.001$ *vs* vehicle).

4.3.10.2. Tomatidine modifies aminoacidic composition of muscle cells

The promotion of metabolic performance is linked to a modification of aminoacidic cells profile. Aminoacids analysis represents a clear indication of a nutraceuticals product to promote the protein synthesis. Usually, aminoacids analysis is performed using metabolomics NMR analysis or mass spectrometry associated with the hydrophilic interaction liquid chromatography (HILIC). However, for its great simplicity, metabolomics NMR analysis was selected for the further evaluation of aminoacidic composition in muscle cells. NMR is less sensitive compared to mass spectrometry and the lack of chromatographic separation reduce the number of detected analytes. However, metabolomics NMR displayed many advantages compared to other metabolomics techniques (Nagana Gowda & Raftery, 2021):

1) NMR is high quantitative and reproducible;
2) The quantification of each analyte doesn't require the use of an analytical standard, which can be provided by the use of a single internal reference;
3) NMR allows to identify possible unknown metabolites in a biological mixture;
4) NMR is a not destructive technique;
5) NMR doesn't require the use of preprocessing or cleaning-up techniques, without any treatment of the sample.

For the evaluation of TD effects on aminoacidic profile, myoblast cells line C2C12 were treated with TD stock solution 300 mM in DMSO to obtain a final TD concentration of 300 µM and the DMSO vehicle. Both the samples were compared with not treated myoblast cell line C2C12 to evaluate the effect of DMSO treatment of cells aminoacidic profile. The supernatants were freeze-dried to remove the water and re-dissolved in deuterium oxide D_2O, adding a volume of a solution of sodium 3-trimethylsilyl-tetradeuteriopropionate (TSP) dissolved in D_2O as reference standard. Although metabolomics NMR doesn't require sample pre-treatment as the freeze-drying, the lyophilization of the samples was performed to remove the not deuterated water from cells supernatants. As matter of fact, monodimensional ^1H NMR experiment can be performed with water signal suppression using solvent pre-saturation. However, bidimensional experiments (e.g., COSY, HSQC) for the assignment of aminoacids identity in the cell mixture can't be run with water signal suppression. Therefore, the elimination of supernatants water represents the most effective

way for the absolute identification of the aminoacids without the comparison with corresponding analytical standards. In addition, the reference standard TSP was selected as internal standard for the spectra calibration (TSP = 0.0 ppm). The sodium 3-trimethylsilyl-tetradeuteriopropionate (TSP) was selected as internal standard for the metabolomics NMR experiments for the great solubility in D_2O. The myoblast cells line C2C12 supernatants allows to evaluate the chemical profile of the extracellular compartment, displaying results which are complementary to those previously reported for the intracellular compartment in the paragraph **4.3.10.1 Tomatidine activity on muscle cells metabolism**. The analysis of monodimensional ^{1}H NMR and bidimensional COSY and HSQC allowed to confirm the identity of 15 compounds, which include 1 organic acid (e.g., lactic acid), 2 sugars (e.g., α-glucose, β-glucose), and 13 aminoacids (e.g., alanine Ala, tyrosine Tyr, glutamate Glu, glutamine Gln, histidine His, phenylalanine Phe, threonine Thr, lysine Lys, arginine Arg, valine Val, leucine Leu, isoleucine Ile). An overview of the comparison between the myoblast cells line C2C12 supernatants after TD and vehicle treatment and a bidimensional assignment of alanine by HSQC NMR experiment is provided in the **Figures 47** and **48**, respectively. In addition, the results of the NMR identification, including the ^{1}H and the ^{13}C assignment and the ^{1}H multiplicity, were reported in the **Table 35**.

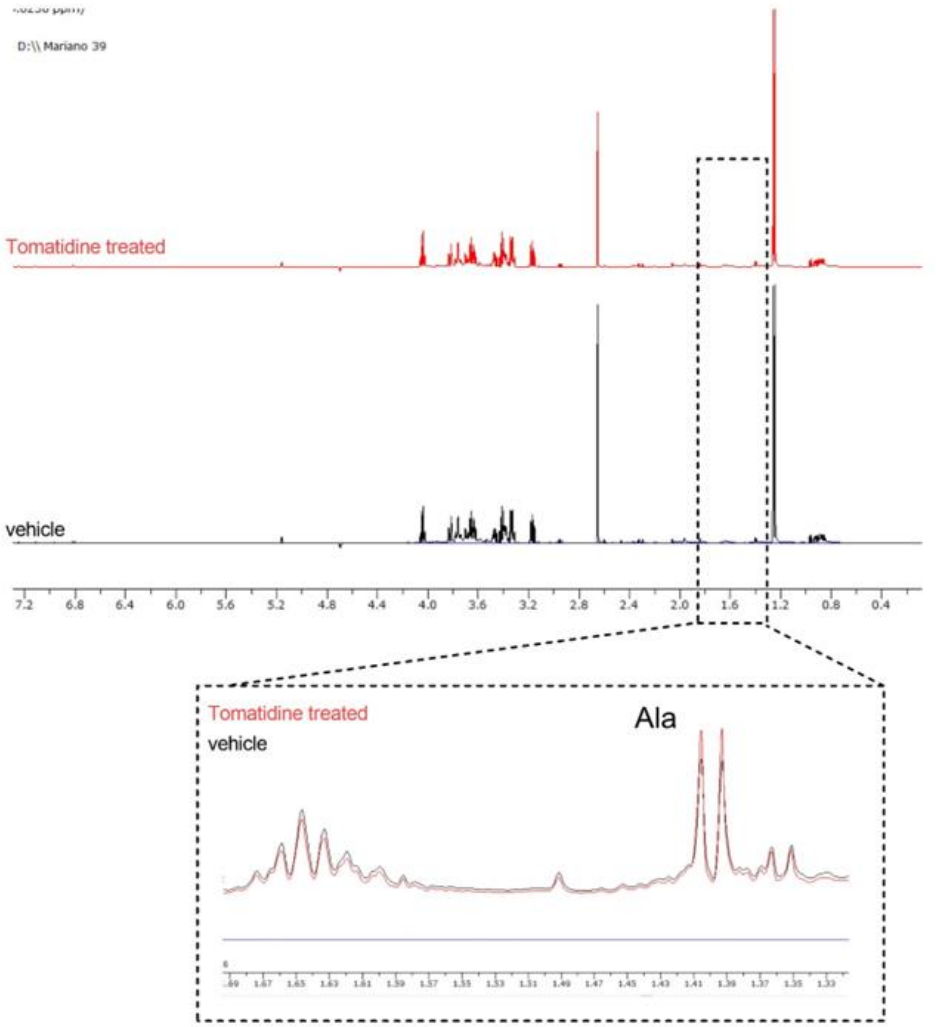


Figure 47. ^{1}H NMR comparison between myoblast cells line C2C12 supernatants after TD and vehicle treatment, with an overview of the alanine signal of the CH_3 in position 3.

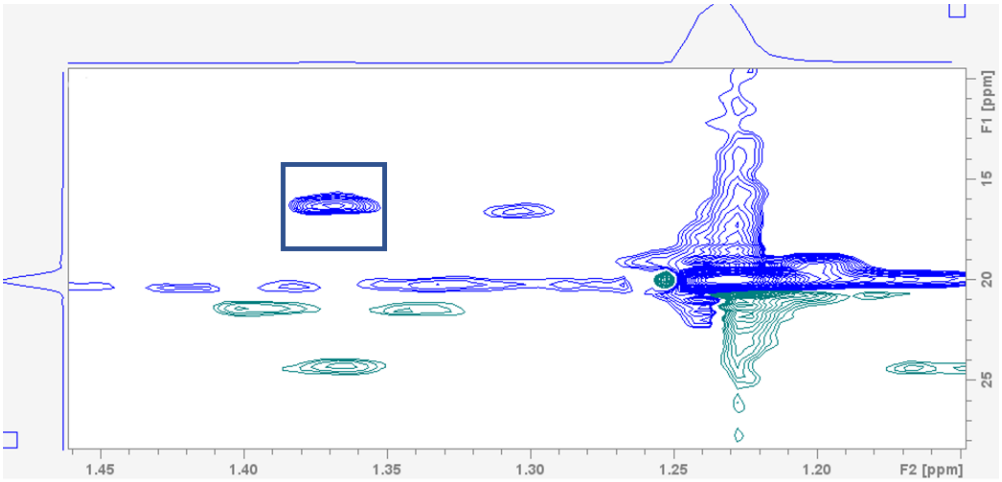


Figure 48. Bidimensional HSQC NMR experiment of the alanine signal of the CH_3 in position 3 in the myoblast cells line C2C12 supernatants after TD treatment.

Compound	Assignment	Position	^{1}H (ppm)	Multiplicity	^{13}C (ppm)
Lactic acid	CH_3	3	1.23	d	20
	CH	2	4.12	q	68
β-Glucose	CH	1	4.55	d	96
α-Glucose	CH	1	5.14	d	92
Alanine	CH_3	3	1.37	d	16
Tyrosine	CH	2,6	6.78	d	116
	CH	3,5	7.08	d	131
Glutamate	CH_2	4	2.32	t	31
Glutamine	CH_2	4	2.53	t	29
Histidine	CH	2	7.03	s	131
Phenylalanine	CH	2,6	7.41	d	128
	CH	3,5	7.36	t	129
	CH	4	7.31	t	130
Threonine	CH	3	4.17	m	67
Lysine	CH_2	6	3.02	t	41
Arginine	CH_2	5	3.24	t	74
Ile-Val-Leu	CH_3 - CH_2 – CH	-	0.92 – 1.53	m	8 - 30

Table 35. NMR assignment of 15 compounds identified in myoblast cells line C2C12 supernatants.

The identification of aminoacids NMR identity was not performed by the evaluation of the chemical shift of the Hα, due to the high overlapping of the aminoacidic signals in ^{1}H monodimensional and COSY and HSQC bidimensional experiments. An example is provided by an overview of the region of 3.4 – 4.0 ppm of the ^{1}H monodimensional and COSY and HSQC bidimensional NMR experiments provided the **Figures 49**, **50**, and **51**, respectively. ^{1}H monodimensional and COSY and HSQC bidimensional experiments of the other identified compounds are provided in **Supplementary Material**, **Figures S15 – S25**. In addition, the identification and the relative percentage of fold-change variation of 8 aminoacids have been prevented by some detection and overlapping problems. Tryptophan Trp and proline Pro were not detected in the samples, probably due to the low limit of detection of NMR metabolomics approach. Aspartic acid Asp, asparagine Asn, and methionine Met displayed signals in overlapping with sugar NMR peaks (range: 3.8 – 3.9 ppm). Cysteine Cys and Serine Ser signals overlapped each other, avoiding the relative quantification of these two aminoacids. Finally, glycine Gly is the simplest aminoacids and has not other protons monitoring by ^{1}H NMR experiments over the Hα. Therefore, its signal is not distinguishable from the Hα NMR signal of the other aminoacids.

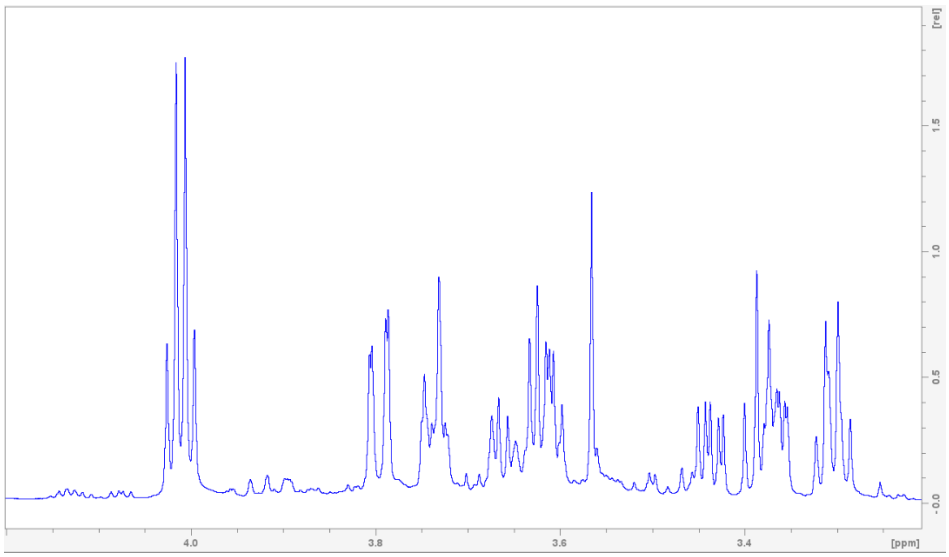


Figure 49. Overview of the region of 3.4 – 4.0 ppm in the ^{1}H monodimensional NMR experiment in the myoblast cells line C2C12 supernatants after TD treatment.

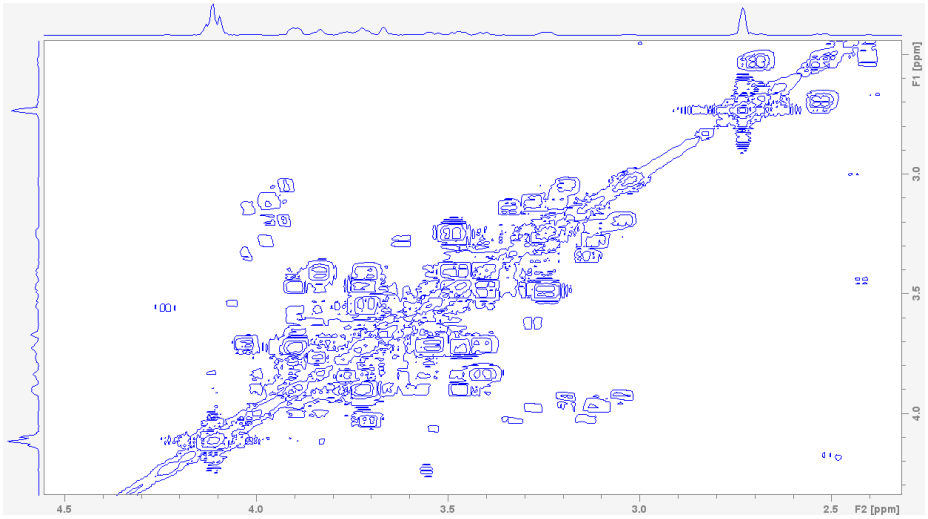


Figure 50. Overview of the region of 3.4 – 4.0 ppm in the bidimensional COSY NMR experiment in the myoblast cells line C2C12 supernatants after TD treatment.

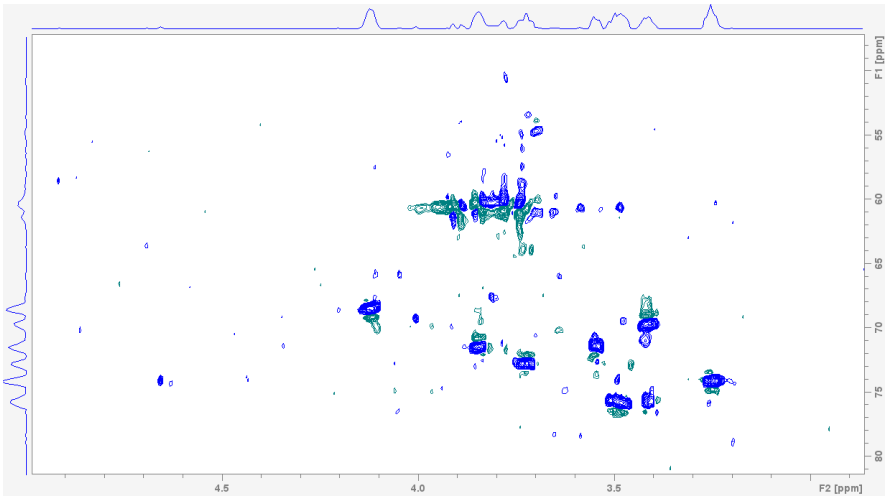


Figure 51. Overview of the region of 3.4 – 4.0 ppm in the bidimensional HSQC NMR experiment in the myoblast cells line C2C12 supernatants after TD treatment.

After the assignment of NMR compound identity, different comparisons were performed (1: TD *vs* vehicle; 2: vehicle *vs* not treated; 3: TD *vs* not treated) and the results were reported in the **Table 36**. As shown by the comparison of vehicle *vs* not treated, DMSO treatment didn't modify the aminoacidic composition of myoblast cells line C2C12 supernatants. Therefore, the comparison of TD *vs* vehicle was displayed to evaluate the % of variation for the treatment with the bioactive compound. A quali-quantitative analysis was performed to evaluate the fold change for TD treatment (comparison TD *vs* vehicle). TD didn't drastically modify the aminoacidic myoblast cells line C2C12 supernatants composition. However, monodimensional ^{1}H NMR experiment analysis confirmed an alanine and lactic acid increment in the conditioned medium of 46.24 ± 12.96 ($p \leq 0.001$) and 11.34 ± 4.64 ($p < 0.01$), respectively.

Compound	Tomatidine *vs* vehicle		Vehicle *vs* not treated		Tomatidine *vs* not treated	
	% variation	*p*-value	% variation	*p*-value	% variation	*p*-value
Lactic acid	11.34 ± 4.64	0.0052	0.73 ± 6.73	0.4579	6.71 ± 6.82	0.3191
Ile-Val-Leu	4.83 ± 8.58	0.1586	6.57 ± 9.67	0.2019	2.56 ± 5.33	0.3316
Ala	46.24 ± 12.96	0.0010	5.27 ± 11.59	0.3951	39.85 ± 26.00	0.0068
β-glucose	1.20 ± 1.29	0.3936	1.31 ± 6.96	0.4835	-1.88 ± 8.90	0.3630
α-glucose	0.80 ± 2.75	0.3904	6.61 ± 9.38	0.3475	1.63 ± 11.54	0.4476
Tyr	6.48 ± 3.73	0.0665	5.11 ± 10.22	0.4130	7.26 ± 8.56	0.0627
Arg	-1.71 ± 0.89	0.2724	6.16 ± 10.04	0.3803	-3.17 ± 6.66	0.2799
Lys	5.58 ± 7.23	0.1869	5.78 ± 7.95	0.2770	11.05 ± 0.91	0.4353
Thr	-3.74 ± 3.92	0.1430	-2.63 ± 7.21	0.2620	-17.96 ± 16.90	0.0643
Glu	7.97 ± 18.86	0.4598	8.64 ± 12.18	0.4163	-3.22 ± 12.41	0.4584
Gln	-5.06 ± 4.41	0.4253	11.63 ± 12.09	0.4142	4.44 ± 19.43	0.2577
Phe	9.85 ± 9.21	0.4510	6.13 ± 4.32	0.4705	10.96 ± 4.51	0.4273
His	2.74 ± 7.70	0.3347	14.21 ± 2.58	0.2077	14.44 ± 11.63	0.0398

Table 36. Comparison of the fold change of myoblast cells line C2C12 supernatants after treatment with TD, the vehicle and without treatments. Data were shown as mean ± SD of at least three independent experiments.

4.3.10.3. Green tomatoes represent a safe product in chronic treatments

The evaluation of anti-sarcopenic properties of LGT was performed with an *in vivo* study on a mouse model. The *in vivo* mice study was executed applying a similar experimental protocol reported by Dyle et al. (2014), in which the anti-sarcopenic properties of pure TD standard was studied in an aged mice model. The C57BL/6J mice (90 mice: 50 female mice and 40 male mice) were fed with the LGT diet for 37 weeks (from week 17 to week 55) or with CD diet. At the end of the *in vivo* treatment, a haematological, toxicological and necropsy study was performed to evaluate the system effects of LGT chronic treatment. The haematological analysis included many plasmatic parameters which describe the mice health. They included the following parameters: the lactate dehydrogenase (LDH) activity (U/l), the creatinine phosphokinase (CPK) activity (U/l), the prothrombin time (PT) (s), the total protein (g/dl), the albumin (g/dl), the aspartate aminotransferase (AST) (U/l), the cholinesterase activity (µmol/min/l), the urea level (mg/dl), the nitrogen content (mg/dl), the creatinine content (mg/dl), the haematocrit test (HCT), the platelet count (PLT) (x 10^3/µl), the white blood count (WBC) (x 10^3/µl), the neutrophile (NE) count (x 10^3/µl), the lymphocyte (LY) count (x 10^3/µl), the monocyte (MO) count (x 10^3/µl), the eosinophil (EO) count (x 10^3/µl), the basophil (BA) count (x 10^3/µl), the red blood cells (RBC) count (x 10^6/µl), the reticulocyte (RET) count (x 10^9/µl), the haemoglobin (HB) amount (g/dl), the

sodium content (mM), the potassium content (mM), the calcium content (mg/dl), the phosphorus content (mg/dl), the metahaemoglobin content (% of total Hb), the glucose content (mg/dl), the total cholesterol content (mg/dl), the HDL content (mg/dl), the LDL content (mg/dl), the triglycerides content (mg/dl), the thyroid-stimulating hormone (TSH) content (ng/ml), the triiodothyronine (T3) content (ng/ml), and the thyroxine (T4) content (ng/ml). In addition, many sexual parameters were assessed, as the cauda epididymis sperm concentration (x 10^6/ml), the sperm motility (%), and the number of normal and abnormal spermatozoa (%). Therefore, the necropsy parameters were evaluated for the assessment of organs weight (g), including the liver, the thyroid, the kidneys, the heart, the thymus, the spleen, the pituitary gland, the adrenal glands, the seminal vescicles, the testis, the prostate, the epididemides, the uterus, and the ovary. Furthermore, many toxicological and behavioural aspects (e.g., menstrual cycle disorders, pilo-erection, lacrimation, excretion, secretion, mortality, morbidity, behavioural changes, skin alterations, eyes alterations, mucous membrane damages and alterations, variation of pupil size, unusual respiration, postures alterations, response to handling, clonic and tonic movements, excessing grooming, repetitive circling, self-mutilation, and walking backwards) were investigated during the treatment to assess the safety of LGT. None of the above-mentioned disorders were observed in the mice during the chronic treatment. The results of these analysis corroborate the safety of the product, although SGAs are well-known compounds with possible toxicological effects, as previously described in the paragraph **2.4.7. α-tomatine and green tomato extract toxicological aspects**. In addition, the study was performed at the maximum dosage admitted by the European Food Safety Agency (EFSA) of 1 g of product/kg of mice, highlighting the safety and the tolerance of the product at any dosage of administration. Furthermore, both the diets LGT and CD were well tolerated, without significant variations in appetite and average daily chow consumption of approximately 3 grams of feed per day. In addition, animals treated with LGT diet displayed a similar biochemical profile compared to the animals feed with CD diet. The results of haematological analysis results are summarized in the **Tables 37** and **38** for male and female mice, respectively. The statistical significance of the analysis was calculated with the Wilcoxon-Mann-Whitney, which represent the not-parametric analogue of t-student test for the comparison of the medium of two groups.

Parameter	Male Control	Male Treated	*p*-value from U Mann-Whitney test
Start Weight (g)	29.4 ± 0.2	29.9 ± 0.2	0.102
Final Weight (g)	30.8 ± 0.3	30.9 ± 0.3	0.989
LDH (U/l)	531 ± 19	597 ± 17	0.023
CPK (U/l)	366 ± 20	306 ± 13	0.009
PT (s)	8.70 ± 0.02	8.71 ± 0.01	0.602
Total Protein (g/dl)	5.21 ± 0.08	3.56 ± 0.08	< 0.001
Albumin (g/dl)	2.24 ± 0.04	1.83 ± 0.04	< 0.001
AST (U/l)	116 ± 3	116 ± 3	0.602
Cholinesterase (umol/min/l)	3527.04 ± 171.19	4143.96 ± 175.00	0.028
Liver weight (g)	1.306 ± 0.008	1.298 ± 0.010	0.678
Urea (mg/dl)	11.06 ± 0.42	14.28 ± 0.42	< 0.001
Nitrogen (mg/dl)	5.19 ± 0.19	6.70 ± 0.20	< 0.001
Creatinine (mg/dl)	0.28 ± 0.01	0.23 ± 0.02	0.028
HCT (%)	41.8 ± 0.1	40.0 ± 0.1	< 0.001
PLT (x 10^3/µl)	582.0 ± 3.8	582.3 ± 4.0	0.883
WBC (x 10^3/µl)	7.20 ± 0.06	7.31 ± 0.07	0.231
NE (x 10^3/µl)	1.59 ± 0.02	1.92 ± 0.03	< 0.001
LY (x 10^3/µl)	4.41 ± 0.12	4.90 ± 0.12	0.006
MO (x 10^3/µl)	0.27 ± 0.01	0.27 ± 0.01	0.529
EO (x 10^3/µl)	0.06 ± 0.01	0.08 ± 0.01	0.033
BA (x 10^3/µl)	0.07 ± 0.01	0.06 ± 0.01	0.076
RBC (x 10^6/µl)	8.03 ± 0.02	8.03 ± 0.02	0.968
RET (x 10^9/µl)	288.8 ± 5.53	281.4 ± 5.15	0.301
HB (g/dl)	9.72 ± 0.05	9.79 ± 0.05	0.512
Sodium (mM)	158.71 ± 1.58	158.98 ± 1.83	1.000
Potassium (mM)	3.35 ± 0.08	3.59 ± 0.12	0.142
Calcium (mg/dl)	5.66 ± 0.14	6.58 ± 0.17	< 0.001
Phosphorus (mg/dl)	6.99 ± 0.13	7.45 ± 0.11	0.006
Metahaemoglobin (% of total Hb)	0.25 ± 0.03	0.24 ± 0.02	0.698
Glucose (mg/dl)	282.34 ± 5.18	287.41 ± 5.43	0.242
Total Cholesterol (mg/dl)	92.54 ± 1.05	93.40 ± 1.10	0.547
HDL (mg/dl)	72.64 ± 1.01	67.10 ± 1.49	0.003
LDL (mg/dl)	8.20 ± 0.20	6.93 ± 0.27	0.002
Triglycerides (mg/dl)	92.17 ± 3.73	93.43 ± 3.48	0.583
TSH (ng/ml)	0.62 ± 0.02	0.64 ± 0.02	0.659
T3 (ng/ml)	0.83 ± 0.10	0.83 ± 0.09	0.779
T4 (ng/ml)	38.1 ± 0.1	38.3 ± 0.1	0.341
Thyroid weight (g)	0.0029 ± 0.0001	0.0028 ± 0.0001	0.620
Pituitary weight (g)	0.0024 ± 0.0002	0.0027 ± 0.0003	0.678
Cauda Epididymis sperm concentration (x 10^6/ml)	5.1 ± 0.2	4.3 ± 0.2	0.026
Sperm motility (%)	56.2 ± 0.2	58.3 ± 0.3	< 0.001
Normal spermatozoa (%)	75.0 ± 0.2	73.9 ± 0.2	0.003
Abnormal spermatozoa (%)	23.0 ± 0.3	21.7 ± 0.2	0.001
Seminal vescicles weight (g)	0.282 ± 0.007	0.281 ± 0.007	0.925
Testis weight (g)	0.050 ± 0.001	0.049 ± 0.001	0.820
Prostate weight (g)	0.046 ± 0.001	0.047 ± 0.001	0.678
Epididemides weight (g)	0.0031 ± 0.0001	0.0029 ± 0.0001	0.221
Kidneys weight (g)	0.306 ± 0.010	0.337 ± 0.012	0.040
Heart weight (g)	0.123 ± 0.004	0.124 ± 0.005	0.758
Thymus weight (g)	0.068 ± 0.001	0.071 ± 0.001	0.289
Spleen weight (g)	0.080 ± 0.001	0.080 ± 0.001	0.968
Adrenal glands weight (g)	0.0020 ± 0.0001	0.0019 ± 0.0001	0.445
Age at arrival	5.000 ± 0.000	5.000 ± 0.000	1.000
Age at start treatment	17.000 ± 0.000	17.000 ± 0.000	1.000
Weight at start treatment (g)	29.35 ± 0.250	29.94 ± 0.19	0.091
Age at sacrifice	55.00 ± 0.00	55.00 ± 0.00	1.000
Weight at sacrifice (g)	30.84 ± 0.34	30.90 ± 0.34	0.701

Table 37. Comparison of haematological results in male mice fed with LGT and CD diet. Data were shown as mean ± SD of at least three independent experiments. Data were analyzed with the Wilcoxon-Mann-Whitney test.

Parameter	Female Control	Female Treated	*p*-value from U Mann-Whitney test
Start Weight (g)	29.2 ± 0.3	29.5 ± 0.3	0.540
Final Weight (g)	30.2 ± 0.2	30.4 ± 0.2	0.741
LDH (U/l)	565 ± 12	675 ± 17	< 0.001
CPK (U/l)	411 ± 12	327 ± 17	< 0.001
PT (s)	8.68 ± 0.02	8.77 ± 0.02	0.003
Total Protein (g/dl)	5.17 ± 0.06	3.55 ± 0.07	< 0.001
Albumin (g/dl)	2.47 ± 0.04	1.89 ± 0.03	< 0.001
AST (U/l)	117 ± 4	110 ± 3	0.054
Cholinesterase (umol/min/l)	3935.64 ± 192.54	3809.73 ± 135.69	0.516
Liver weight (g)	1.107 ± 0.010	1.090 ± 0.012	0.225
Urea (mg/dl)	11.98 ± 0.29	20.11 ± 0.26	< 0.001
Nitrogen (mg/dl)	5.50 ± 0.08	9.60 ± 0.07	< 0.001
Creatinine (mg/dl)	0.15 ± 0.01	0.16 ± 0.01	0.326
HCT (%)	41.0 ± 0.1	40.0 ± 0.1	< 0.001
PLT (x 10^3/µl)	580.4 ± 3.0	572.0 ± 4.3	0.090
WBC (x 10^3/µl)	6.95 ± 0.04	7.07 ± 0.06	0.277
NE (x 10^3/µl)	1.68 ± 0.02	1.80 ± 0.02	< 0.001
LY (x 10^3/µl)	4.22 ± 0.10	4.42 ± 0.12	0.092
MO (x 10^3/µl)	0.28 ± 0.01	0.25 ± 0.01	< 0.001
EO (x 10^3/µl)	0.07 ± 0.01	0.08 ± 0.01	0.144
BA (x 10^3/µl)	0.07 ± 0.01	0.07 ± 0.01	0.845
RBC (x 10^6/µl)	8.00 ± 0.02	8.11 ± 0.03	0.002
RET (x 10^9/µl)	274.2 ± 3.77	285.8 ± 4.24	0.107
HB (g/dl)	9.51 ± 0.03	9.57 ± 0.05	0.079
Sodium (mM)	158.28 ± 1.25	157.70 ± 1.60	0.467
Potassium (mM)	3.43 ± 0.09	3.50 ± 0.10	0.648
Calcium (mg/dl)	6.07 ± 0.16	5.73 ± 0.18	0.211
Phosphorus (mg/dl)	7.08 ± 0.13	7.72 ± 0.14	0.004
Metahaemoglobin (% of total Hb)	0.24 ± 0.02	0.21 ± 0.02	0.217
Glucose (mg/dl)	333.01 ± 6.23	300.97 ± 6.44	0.001
Total Cholesterol (mg/dl)	81.98 ± 1.13	82.92 ± 1.29	0.969
HDL (mg/dl)	69.14 ± 0.79	68.82 ± 1.11	0.749
LDL (mg/dl)	6.57 ± 0.20	6.98 ± 0.27	0.211
Triglycerides (mg/dl)	84.07 ± 3.11	87.74 ± 3.62	0.290
TSH (ng/ml)	0.63 ± 0.02	0.58 ± 0.02	0.156
T3 (ng/ml)	0.85 ± 0.07	0.83 ± 0.10	0.580
T4 (ng/ml)	37.2 ± 0.1	38.0 ± 0.1	0.014
Thyroid weight (g)	0.0021 ± 0.0001	0.0020 ± 0.0001	0.258
Pituitary weight (g)	0.0027 ± 0.0002	0.0026 ± 0.0002	0.591
Uterus weight (g)	0.333 ± 0.007	0.338 ± 0.006	0.580
Ovary weight (g)	0.080 ± 0.003	0.080 ± 0.004	0.585
Kidneys weight (g)	0.284 ± 0.008	0.252 ± 0.009	0.021
Heart weight (g)	0.119 ± 0.004	0.118 ± 0.004	0.884
Thymus weight (g)	0.072 ± 0.001	0.071 ± 0.001	0.573
Spleen weight (g)	0.078 ± 0.001	0.080 ± 0.001	0.316
Adrenal glands weight (g)	0.0019 ± 0.0001	0.0020 ± 0.0001	0.429
Age at arrival	5.000 ± 0.000	5.000 ± 0.000	1.000
Age at start treatment	17.000 ± 0.000	17.000 ± 0.000	1.000
Weight at start treatment (g)	29.190 ± 0.340	29.52 ± 0.26	0.652
Age at sacrifice	55.00 ± 0.00	55.00 ± 0.00	1.000
Weight at sacrifice (g)	30.23 ± 0.21	30.36 ± 0.20	0.726

Table 38. Comparison of haematological results in female mice fed with LGT and CD diet. Data were shown as mean ± SD of at least three independent experiments. Data were analyzed with the Wilcoxon-Mann-Whitney test.

4.3.10.4. Green tomatoes improve the muscle performance

The evaluation of LGT properties in the improvement of muscle performance was performed with the treadmill test, a measurement system of mice fatigue during an exercise endurance. This test is generally executed in a short fatigue time, in which some parameters (e.g., the resistance time (minutes), the number of interruptions (LB), the running speed (m/s), the distance performed (m), and the muscle power (W)) were evaluated as indicators of muscle strength and resistance. In this study, a treadmill test was conducted using four experimental groups of 3 male and 3 female mice per group: the CD sedentary control, the LGT treated sedentary control, the CD training group, and the LGT treated training group (**Table 39**). The CD and LGT treated sedentary controls didn't perform the treadmill test and were directly sacrificed for further chemical and histological analysis. Instead, the comparison of muscle performance for the LGT treatment was performed by considering the CD and LGT treated training groups. The treadmill test was performed with a first period of four days training of the mice, which was preliminary for the adaptation to the fatigue endurance.

RESTING		**EXERCISE**	
CD diet	LGT diet	CD diet	LGT diet
3 female mice (CTR resting)	3 female mice (LGT resting)	3 female mice (CTR exercise)	3 female mice (LGT exercise)
3 male mice (CTR resting)	3 male mice (LGT resting)	3 male mice (CTR exercise)	3 male mice (LGT exercise)

Table 39. Experimental design of mice groups in the treadmill test.

The treadmill test displayed a significant improvement of the muscle performance, as shown by the longer running time, the distance, and the lower number of interruptions per minute of the LGT treated training group and the CD training group. Interestingly, the LGT treatment doesn't significantly modify the running speed and the power, demonstrating a more significant improvement of exercise endurance rather than an increased energy utilisation during the treadmill. This data provided that LGT treatment significantly increased the aging-related reduced muscle performance, probably altering muscle fiber type distribution. In addition, there was no significant differences in LGT action between male and female mice, providing that the nutraceutical activity is not sexual dependent (**Figure 52**). To confirm the LGT effects on muscle fiber type distribution, an evaluation of muscle morphology and biomarkers was performed to assess the satellite cell content and the

skeletal muscle fibers composition and size. The analysis was performed on the gastrocnemius tissue, which represents one of the most sensitive muscles to the muscle atrophy processes. The histological analysis of muscle fibers composition displayed a significant increment of the number of fiber of small diameters, which indicated a rejuvenation of the muscle tissue (**Figures 53**, **Table 40**).

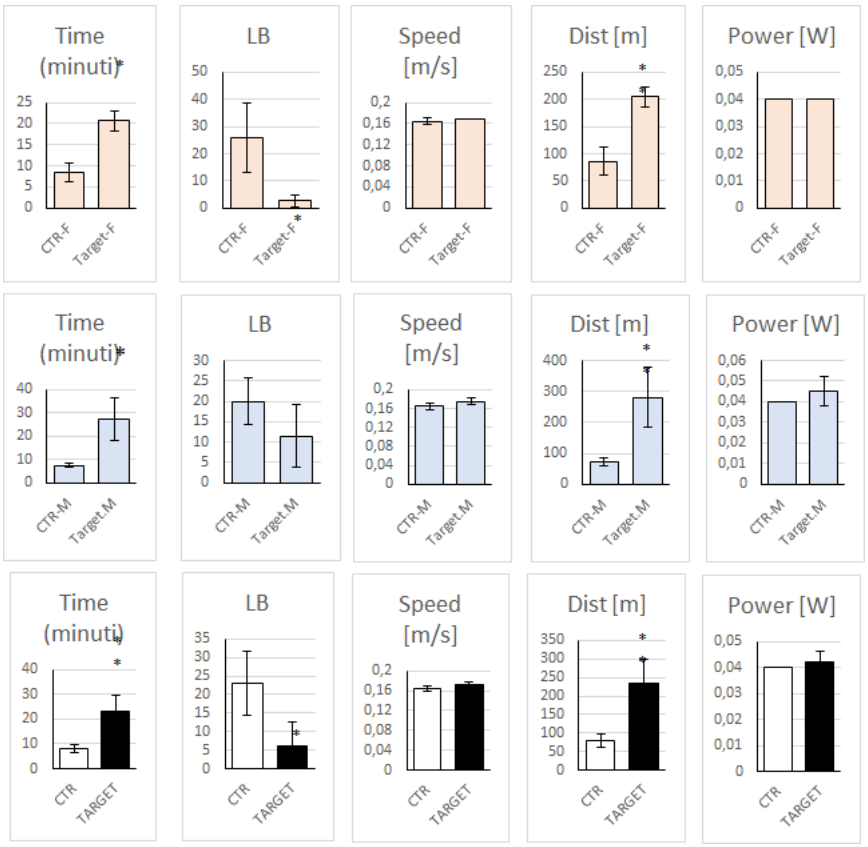


Figure 52. Results of treadmill test on CD training group and LGT training group (* $p < 0.05$ *vs* CTR; ** $p < 0.01$ *vs* CTR).

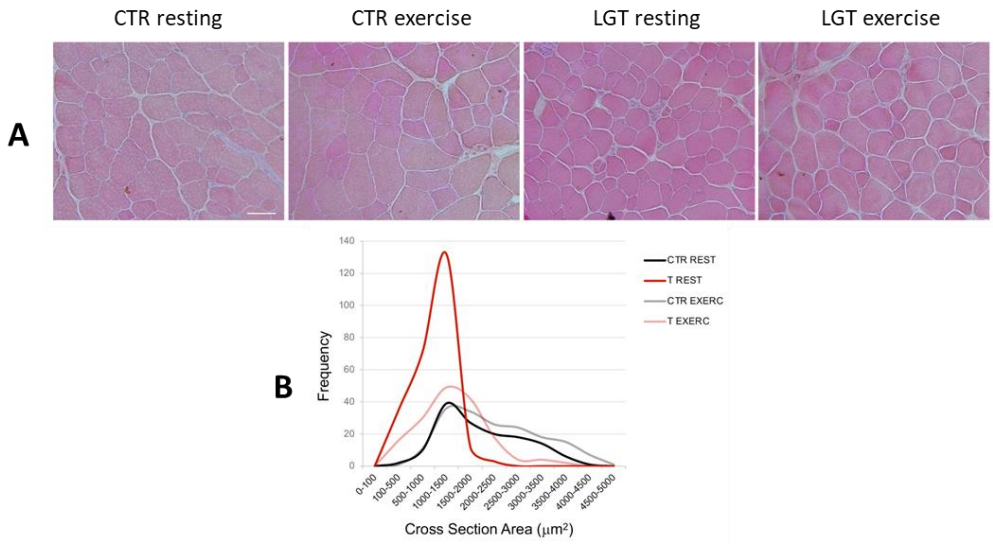


Figure 53. (**A**) Histological analysis of gastrocnemius tissues of CD sedentary control, LGT treated sedentary control, CD training group, and LGT treated training group. (**B**) Frequency measurement of fibers with different cross section area (μm^2) in CD sedentary control, LGT treated sedentary control, CD training group, and LGT treated training group.

Area (μm^2)	CTR resting	LGT resting	CTR exercise	LGT exercise
0 – 100	0	0	0	0
100 – 500	2	35	1	16
500 - 1000	10	71	11	30
1000 – 1500	39	132	36	49
1500 – 2000	27	12	34	42
2000 – 2500	20	3	26	18
2500 – 3000	18	0	24	4
3000 – 3500	14	0	18	4
3500 – 4000	6	0	15	2
4000 – 4500	1	0	7	0
4500 - 5000	0	0	1	0

Table 40. Values of frequency measurement of fibers with different cross section area (μm^2) in CD sedentary control, LGT treated sedentary control, CD training group, and LGT treated training group.

An immunostaining analysis was performed to investigate the differences between the fiber type specific compositions of the control and treated groups gastrocnemius tissues. The human muscle fibers are usually classified based on the myosin heavy chain (MHC)

isoforms, which are characterized by a different contractile speed (Plotkin et al., 2021). They are divided into several types:

1) Type I, which are fibers with a slower speed but a relatively high fatigue resistance;
2) Type IIA, which are fibers with a fast oxidative glycolytic activity, a medium speed and a medium fatigue resistance;
3) Type IIX, which are fibers with a fast oxidative glycolytic activity, a high speed and a low fatigue resistance.

The LGT treatment displayed a significant improvement of the number of fibers MHCI and MHCIIA and a reduction of the number of fibers MHCIIB, which are strictly correlated with an increment of muscle performance and fatigue endurance (**Figures 54** and **55**). These data agreed with the results provided by the treadmill test and previously described in the **Figure 52**. To confirm the effect of remodelling of muscle fibers composition, a qPCR of gastrocnemius tissues of the controls and treated groups were performed. This assay was performed to evaluate the mRNA expression of MHCI, MHCIIA, MHCIIX, MHCIIB, and neoMHC (**Figure 56**). The LGT treatment displayed a significant improvement of mRNA expression of MHCI and MHCIIA, confirming the results obtained by the immunostaining analysis.

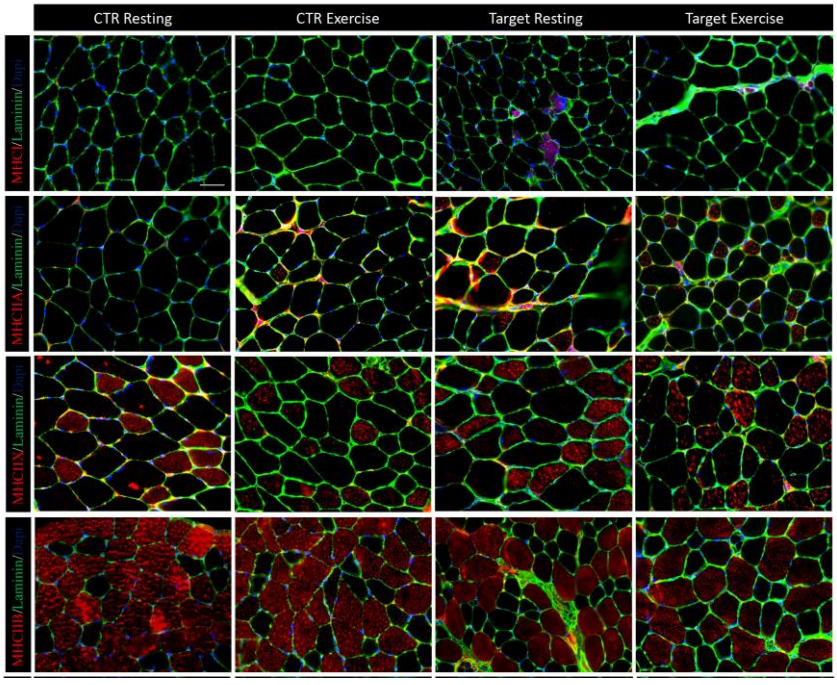


Figure 54. Immunostaining analysis of gastrocnemius tissues of CD sedentary control, LGT treated sedentary control, CD training group, and LGT treated training group.

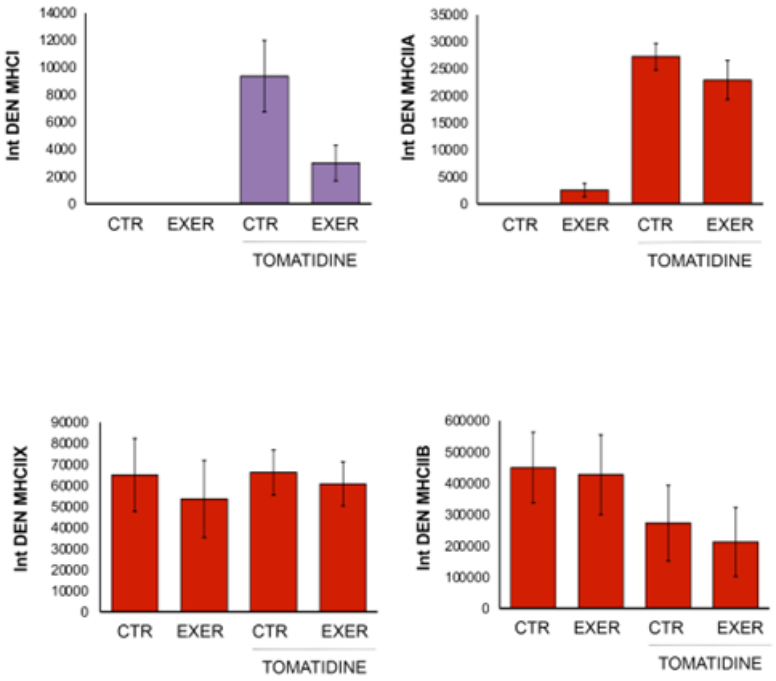


Figure 55. Values of immunostaining analysis of gastrocnemius tissues for the MHC fibers (e.g., MHCI, MHCIIA, MHCIIX, MHCIIB) in CD sedentary control, LGT treated sedentary control, CD training group, and LGT treated training group.

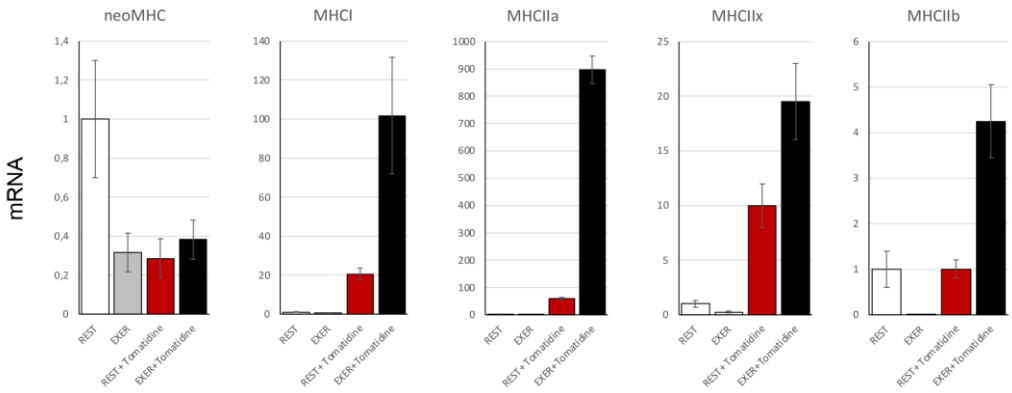


Figure 56. mRNA expression of MHCI, MHCIIA, MHCIIX, MHCIIB, and neoMHC evaluated with qPCR on gastrocnemius tissues comparing CD sedentary control, LGT treated sedentary control, CD training group, and LGT treated training group.

To elucidate the biological mechanisms involved in the muscle fibers remodelling, an evaluation of the satellite cells expression was performed. The skeletal satellite stem cells represent the precursors of muscle fibers by a differentiation mechanism which is mediated by the expression of several factors. They include the transcription factor Paired box protein

(e.g., Pax7) and the myoblast determination protein (e.g., myoD). In the differentiation of satellite stem cells, the two factors are expressed. Pax7 drives the transcription by switching the satellite stem cells from a quiescent state into an activated state. After this, myoD drives the differentiation process in the myoblast cells state (Zammit et al., 2006). In the paragraph **4.3.10.1. Tomatidine activity on muscle cells metabolism**, the study of TD effects on myoblast cells already demonstrated its capacity to improve the mRNA expression of the factor myoD. Therefore, an immunostaining analysis was performed to investigate the expression of the factor Pax7, providing an information about the capacity of LGT diet to promote the satellite stem cells differentiation into young myoblast. After the differentiation, young myoblasts display a MHC profile characterized by an high number of fibers with low oxidative glycolytic activity and an high fatigue resistance. Therefore, this effect could clarify the information about the distinctive muscle fibers compositions observed in the immunostaining analysis of gastrocnemius tissues in the comparison between CD and LGT treated groups. The LGT treatment displayed a significant improvement of the expression of factor Pax7 compared to the CD group. In addition, the comparison between the LGT treated sedentary control and the LGT treated training group, which differ for the performance of the exercise in the treadmill tests, displayed a different expression of the factor Pax7, with a greater value in the training group compared to the control group (**Figure 57**).

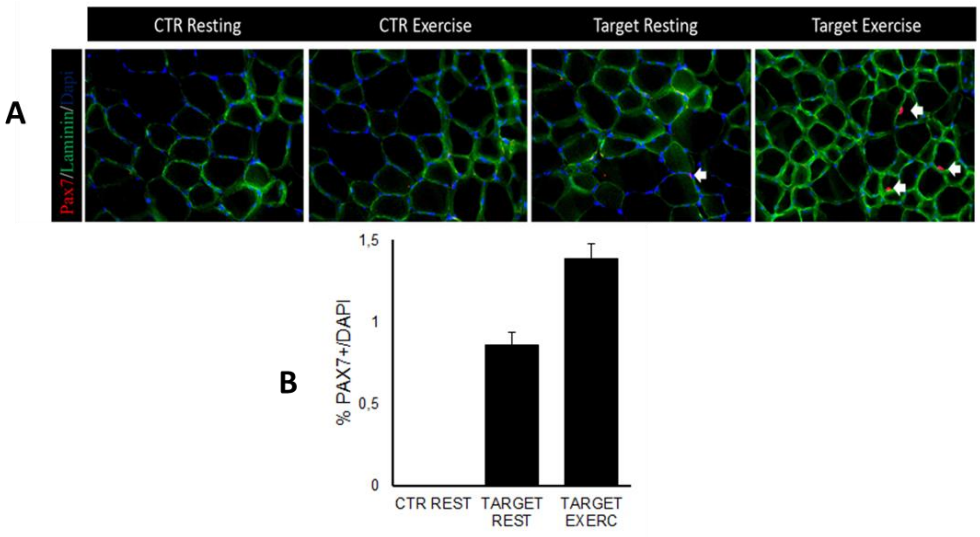


Figure 57. Pax7 Immunostaining analysis for the evaluation of satellite cells content in CD sedentary control, LGT treated sedentary control, CD training group, and LGT treated training group.

Muscle energy production is based on fatty acid and aminoacids metabolism. Therefore, to corroborate the experimental histological results, a GC-MS metabolomic analysis was performed on the muscle tissues of CD and LGT treated groups. GC-MS analysis was preferred to other mass spectrometry approaches for the possibility to obtain robust and reproducible results for different chemical compounds, which include both polar (e.g., aminoacids, sugars) both apolar (e.g., fatty acids) molecules. However, a critical step of GC-MS analysis is represented by the derivatization step, which allow to improve the apolarity and the volatility of polar molecules. In our protocol, the trimethylsililation was selected for the derivatization of the samples. The analysis of muscle gastrocnemius extracts allowed to putatively identify 10 compounds, which include 4 polar compounds (e.g., alanine, glucose, phenylalanine, glycerol-phosphate) and 6 apolar compounds (e.g., palmitic acid, palmitoleic acid, stearic acid, oleic acid, docosaesaenoic acid, cholesterol) (**Table 41**).

Metabolites	m/z	R_t
Alanine, TMS	147; 117; 103; 73	6.2
Glucose, TMS	317; 217; 201; 129; 117; 75	6.3
Phenylalanine, TMS	266; 218; 192	9.2
Glycerol-phosphate, TMS	445; 357; 299; 147	9.8
Palmitoleic acid, methyl ester (C16:1)	268; 236; 194; 152; 138; 123; 110; 96; 74; 69; 55	17.6
Palmitic acid, methyl ester (C16:0)	270; 239; 227; 143; 129;87; 74; 55; 43	18.9
Oleic acid, methyl ester (C18:1)	296; 264; 222; 180; 123; 111; 97; 87; 83; 74; 69; 55; 41	20.6
Stearic acid, methyl ester (C18:0)	298; 255; 199; 143; 129; 87; 74; 55; 43	20.8
Docosaesanoic acid, methyl ester (DHA)	236; 197; 167; 117; 91; 73	22.5
Cholesterol, methyl ester	458; 368; 353; 329; 145; 129; 73	31.7

Table 41. Metabolites putatively identified in muscle gastrocnemius tissues of CD and LGT treated groups, according to their MS/MS spectra and the comparison with NIST database by GC-MS analysis.

After the qualitative GC-MS analysis of gastrocnemius tissues of CD and LGT treated groups, a quali-quantitative metabolomics analysis was performed to evaluate the significant differences due to the LGT treatment. The metabolite profiles of CD and LGT treated groups were very similar, suggesting that the LGT treatment didn't determine a strong metabolomics variation of the muscle tissues. Some variations were related to specific primary metabolites which are involved in the cell energy metabolism. The main metabolomics differences (**Figures 58** and **59**) are summarized as follows:

1) The LGT treatment decreased the levels of Phe (0.37 ± 0.25 fold-reduction, *** $p < 0.001$ *vs* CTR), an aminoacid which is not involved in ketogenic and glycogenic

processes and doesn't represent an energy source for muscle cells. However, its decreased value could indicate a LGT promotion of protein synthesis in the muscle compared to the CD group.

2) The LGT treatment increased the levels of Ala (1.12 ± 0.4 fold-reduction, * $p < 0.05$ *vs* CTR), an aminoacid produced in muscle cells by the conversion of pyruvate in a reaction catalyzed by the enzyme glutamic-pyruvic aminotransferase GPT2. This enzyme is localized in the muscle cells mitochondria and its transcription is induced as response to the muscle fatigue for the stimulation of muscle metabolism. After its biosynthesis, Ala is generally secreted by the muscle cells and is transported with the plasmatic system to the liver, where represents the substrate of Cahill cycle. In this metabolic system, Ala is converted to pyruvate in the liver, which represents a substrate for the gluconeogenesis and the energy production. A summary of the Cahill cycle is reported in the **Figure 60**. Therefore, the increment of Ala value indicated a LGT promotion of mitochondrial activity and an improvement of protein synthesis in the muscle compared to the CD group. These results agreed with the promotion of mitochondrial activity observed in the vitro study on myoblast cells for the treatment with TD, as previously described in the paragraph **4.3.10.1 Tomatidine activity on muscle cells metabolism** (**Figure 39**).
3) The LGT treatment decreased the level of glucose Glu (0.88 ± 0.14 fold-reduction, * $p < 0.05$ *vs* CTR), which represents the main energetic source of the muscles. Therefore, the reduction of Glu value indicated a LGT promotion of muscle metabolism for the energy production compared to the CD group.
4) The LGT treatment decreased the level of palmitoleic acid (0.86 ± 0.12 fold-reduction, * $p < 0.05$ *vs* CTR), oleic acid (0.81 ± 0.09 fold-reduction, * $p < 0.05$ *vs* CTR), and docosaesaenoic acid (0.73 ± 0.14 fold-reduction, * $p < 0.05$ *vs* CTR). In addition, the LGT treatment increased the level of glycerol-phosphate (1.24 ± 0.08 fold-reduction, * $p < 0.05$ *vs* CTR).

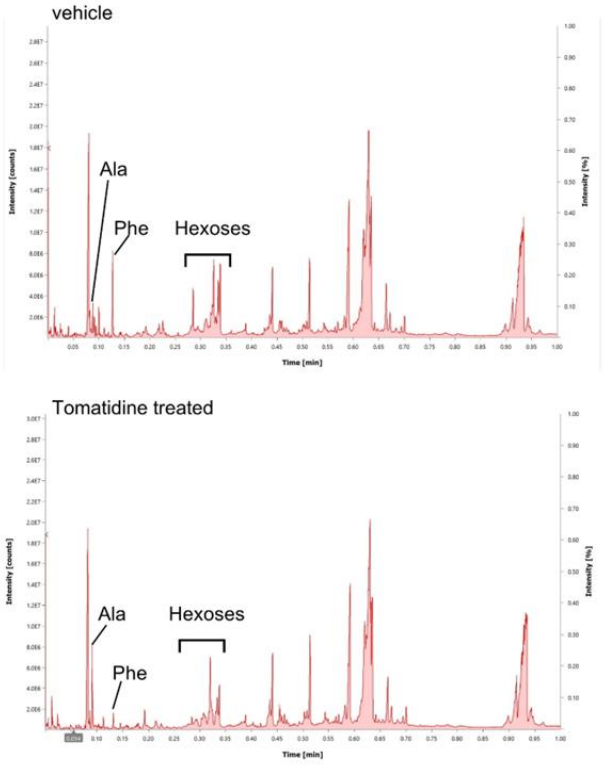


Figure 58. GC-MS profile of the extracts obtained by the muscle gastrocnemius tissues of CD and LGT treated groups.

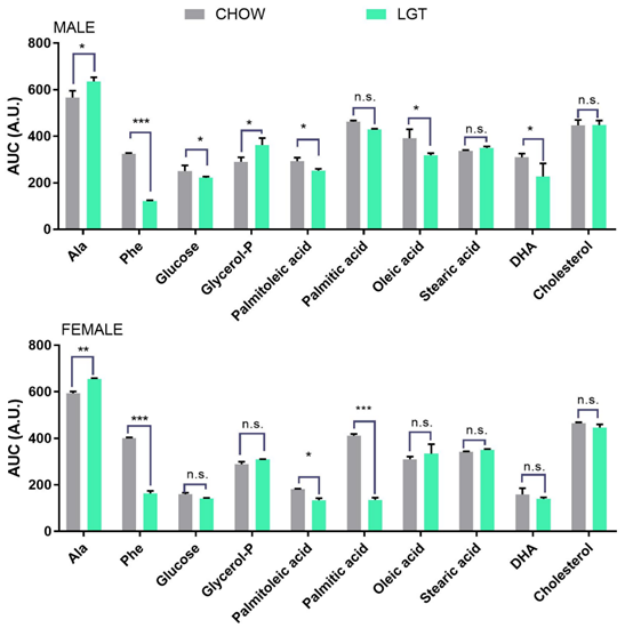


Figure 59. Quantification of selected metabolites by GC-MS analysis in muscle gastrocnemius tissues of CD and LGT treated groups in male and female mice (* $p < 0.05$ *vs* CTR; ** $p < 0.01$ *vs* CTR; *** $p < 0.001$ *vs* CTR)

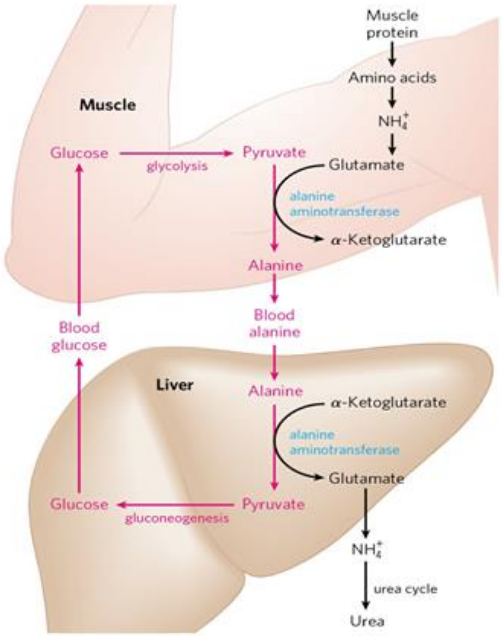


Figure 60. Summary of the biochemical reactions of Cahill cycle.

The metabolomic analysis of gastrocnemius tissues extracts clearly suggested a potential activity of LGT treatment to improve the muscle cells metabolism, enhancing the protein synthesis and the glucose consumption for energy production. To confirm the results of the analysis of the tissues obtained by the mice study and to evaluate the TD efficacy in the control of muscle metabolism, another metabolomics evaluation was performed on the myoblast cells C2C12 using the TD standard with the same GC-MS protocols previously described. The metabolite profile of the C2C12 and the gastrocnemius tissues extracts were very similar, confirming the prominent role of SGAs in the control of muscle metabolism. As previously described for the gastrocnemius tissues metabolomics variation for the LGT treatment, the TD addition determined a decrease of the levels of Phe (0.24 ± 0.02 fold-reduction, *** $p < 0.001$ *vs* CTR), Glu (0.22 ± 0.03 fold-reduction, * $p < 0.05$ *vs* CTR), and palmitoleic acid (0.42 ± 0.02 fold-reduction, *** $p < 0.001$ *vs* CTR), and an increase of the levels of Ala (1.77 ± 0.08 fold-reduction, *** $p < 0.001$ *vs* CTR), and glycerol-phosphate (0.72 ± 0.14 fold-reduction, * $p < 0.05$ *vs* CTR) (**Figure 61**).

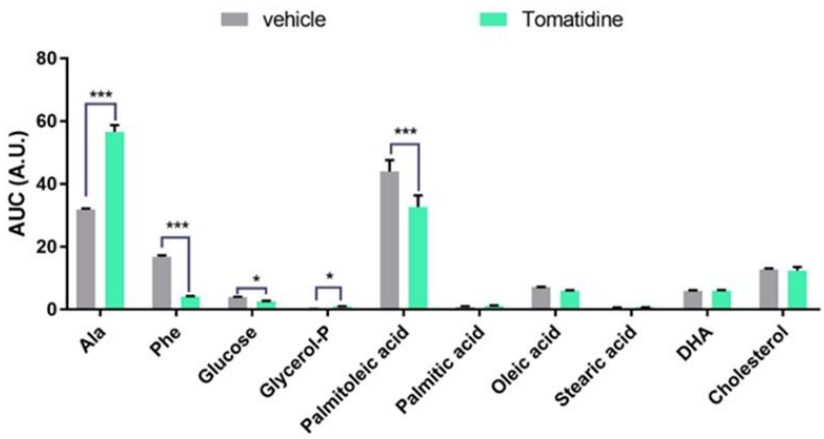


Figure 61. Quantification of selected metabolites by GC-MS analysis in myoblast cells C2C12 treated with vehicle or with DMSO TD solution a final concentration of 300 µM (* $p < 0.05$ *vs* vehicle; ** $p < 0.01$ *vs* vehicle; *** $p < 0.001$ *vs* vehicle).

The prominent role of Ala in the muscle metabolism was clearly confirmed by many experimental results obtained in myoblast cells C2C12 and in the gastrocnemius tissues. As matter of fact, the increment of muscle cells metabolism determines an increment of Ala production in the myoblast cells C2C12 model, which improved both in the intracellular compartment, as shown by the GC-MS metabolomics analysis, both in the extracellular compartment, as shown by the NMR metabolomics analysis. To evaluate the mechanism which determines the increment of Ala production, an mRNA expression study of the enzyme GPT2 was performed. As shown in the **Figure 62**, TD treatment displayed a significant increment of mRNA expression of GPT2 (*** $p < 0.001$ *vs* vehicle), determining a greater conversion of pyruvate to Ala in the mitochondrial compartment.

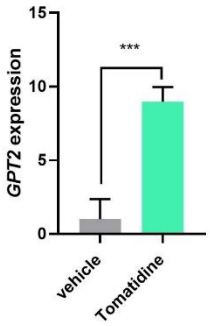


Figure 62. mRNA expression of GPT2 evaluated with qPCR on myoblast cells line C2C12 after treatment with a final TD concentration of 300 µM. Data were shown as mean ± SEM of at least three independent experiments (** $p < 0.01$ *vs* vehicle; *** $p < 0.001$ *vs* vehicle).

4.4. Summary of green tomatoes efficacy study

The *in vitro* and *in vivo* studies descibed in this chapter represent clear evidence of the efficacy of rich source of α-TM as Datterini tomatoes cultivar, and more generally of green tomatoes, in sarcopenia prevention. These pharmacological properties, associated with an in-depth study of the qualitative-quantitative chemical profile of the food matrix, represent the starting point for the development of an innovative nutraceutical formulation with the ability to prevent muscle atrophy. The *in vivo* assay was performed using a controlled in-house protocol which included several steps. In particular, a chemical study was carried out on the production of animal feed, in order to guarantee a constant intake of the active ingredient in the chronic study, with a α-TM content in a maximum range of variability of 15%. Furthermore, several studies were performed to assess muscle performance and chemical and histological studies to evaluate the muscle fibers composition and the metabolome of gastrocnemius muscle cells. These studies have highlighted a remodeling of the composition of muscle fibres, with an increase in the number of young fibers with greater resistance to fatigue endurance. Furthermore, the chronic study represented evidence of the safety of the product, clarifying all possible doubts related to safety and toxicity risks due to α-TM presence in the matrix. In fact, despite the *in vivo* assay was performed through chronic administration at the maximum dosage established by EFSA for a food supplement (1 g of supplement/kg of mouse), no toxicity effects were found during the study and at the necropsy examination. The molecular mechanisms observed in the *in vivo* study were elucidated by *in vitro* studies on myoblast cells using the TD standard. These studies confirmed the ability of TD to stimulate the energy metabolism of muscle cells, increasing protein synthesis, in particular modifying Ala metabolism and biosynthesis, mitochondrial function and cellular energy metabolism. All these data represent clear evidence of the potential of green tomatoes, in particular cultivars with a high α-TM content such as the Datterini green tomatoes, for the development of a nutraceutical product for the prevention of sarcopenia. Therefore, the subsequent studies of this project, but not included in this Ph.D. thesis, will include an in-depth study of the pharmacokinetic profile of α-TM, to evaluate the *in vivo* conversion to TD, and a clinical study to verify the efficacy of green tomatoes in sarcopenia prevention in the humans.

CHAPTER 5

CHEMICAL AND MICROBIOLOGICAL APPROACHES TO IMPROVE GREEN TOMATOES NUTRACEUTICAL PROPERTIES

TD exhibits several interesting pharmacological activities, including a novel anti-aging activity that may be effective in sarcopenia and aging prevention, as previously described in the paragraph **2.4.4. SGAs anti-aging activity**. However, this aglycone is only found in traces in green tomatoes, in which it is massively converted to α-TM. Although conversion of α-TM to TD may occur *in vivo*, this metabolism of this molecule is currently not clarified and would be subject to the individual metabolism of the individual, changing the amount of active ingredient that is produced in the organism. Therefore, an innovative approach for the formulation of a TD-enriched nutraceutical product and to improve the SGAs production in tomato plant could be to use chemical and microbiological methods to modify the metabolome of the fruits and to obtain a TD-enriched green tomato. For this project, two distinct food-grade approaches accepted by the food industry were applied in the development of a nutraceutical product. A first microbiological approach was tried by treating the plant with a biological control agent (BCA) that can improve the microbiological quality of the plant's soil and thus positively modify its metabolome. These studies were carried out in collaboration with the research group of Prof. Sheridan Woo of the University of Naples Federico II. The method was performed on the Piennolo tomato plant, a typical variety from Campania region in Southern Italy. The second approach is a food-grade chemical treatment of the tomato to modify its metabolomics through chemical hydrolysis reactions.

In this context, the goals of the part of the thesis are as follows:

1) To determine whether the microbiological approach with *Trichoderma* spp. is able to improve the nutraceutical properties of the green tomato.
2) To clarify the SGAs and polyphenols composition of different anatomical parts of *Solanum lycopersicum* L.
3) To determine whether the microbiological approach with *Trichoderma* spp. is able to modify the metabolome of the anatomical parts of *Solanum lycopersicum* L.
4) To determine whether the chemical approach is able to modify the nutraceutical properties of the green tomato.

5.1. Metabolome of *Solanum lycopersicum* L. plant

The protective role of SGAs as phytoanticipins for the defence of tomato plants is rather well known, as discussed above in the paragraph **2.4.2. Chemotherapic activity**. However, the concentration of these compounds is rather variable and may depend on various factors, such as the time of harvest, the degree of ripeness of the fruit and the anatomical part of the *Solanum lycopersicum* L. plant. As matter of fact, although several studies have reported the qualitative and quantitative characterisation of different botanical parts of tomato plant, there is no unambiguous agreement on the composition of these about the SGAs and polyphenolic composition. For example, α-TM concentration in tomato anatomical parts significantly vary, and literature reports a strong disagreement about the part which contains the highest α-TM concentration. The fruits were identified as the part with the highest SGAs concentration from some authors (Kozukue et al., 2004), while others reported higher concentrations in leaves and stems (Friedman, 2002). Changing in phytochemical profile can be achieved with an optimization of cultivar selection, agronomic practices, environmental factors (e.g., temperature, light, presence of contaminants, CO_2 concentration, and air quality), and by modifying the ripeness stage during the harvesting (Dorais et al., 2008). For example, it's demonstrated that α-TM quantification is influenced by different parameters, including tomato cultivar (Pardini et al., 2021), cultivation methods (e.g., conventional, or organic), and the presence of organic compounds for plant health in the soil (Koh et al., 2013). **Table 42** summarized α-TM quantification in unripe green tomatoes and some anatomical parts of *Solanum lycopersicum* L. plants, as reported in literature by some authors.

Sample	α-TM content	Reference
Lyophilized green tomatoes	0.734 ± 0.028 – 0.175 ± 0.011 mg/g DW	Pardini et al., 2021
Lyophilized green tomatoes	1.993 ± 0.033 – 0.181 ± 0.012 mg/g DW	Tamasi et al., 2021
Fresh green tomatoes	1.894 ± 0.008 – 0.278 ± 0.004 mg/g FW	Trung Huy Ngo et al., 2022
Hot air dried sample	2.430 ± 0.467 – 0.170 ± 0.002 mg/g DW	Silva-Beltran et al., 2015
Fresh sample	0.087 ± 0.027 – 0.036 ± 0.014 mg/g FW	Choi et al., 2013
Fresh sample	0.089 ± 0.004 – 0.010 ± 0.001 mg/g FW	Kozukue & Friedman, 2003
Lyophilized leaves	9.620 ± 0.201 – 6.030 ± 0.303 mg/g DW	Taveira et al., 2012
Lyophilized leaves	0.640 ± 0.002 – 0.402 ± 0.001 mg/g DW	Taveira et al., 2014
Air dried red tomatoes	0.112 – 0.005 mg/g DW	Koh et al., 2013
Lyophilized green tomatoes	2.240 ± 0.010 – 1.130 ± 0.035 mg/g DW	Friedman et al., 1994
Lyophilized samples	7.435 ± 0.015 – 0.003 ± 0.001 mg/g DW	Friedman & Levin, 1995

Fresh samples	4.985 ± 0.115 – 0.144 ± 0.005 mg/g FW	Friedman & Levin, 1998
Fresh samples	3.610 ± 0.255 – 0.138 ± 0.010 mg/g FW	S.-H. Choi et al., 2010
Fresh samples	0.308 – 0.003 mg/kg FW	Caprioli et al., 2013
Fresh samples	0.041 – 0.008 mg/g FW	Leonardi et al., 2000
Fresh samples	0.065 – 0.006 mg/g FW	Bushway et al., 1994
Hot air dried sample	31.000 – 0.001 mg/g DW	Rick et al., 1994

Table 42. α-TM amount reported in different anatomical parts of *Solanum lycopersicum* L.

5.1.1. Metabolomics profile of green tomato fruits

Several relevant changes can be observed during the ripening process. The fruits become softer, the tomato skin properties change, the green color is turning red due to chlorophyll degradation and lycopene synthesis, the ethylene production increases in the respiration rate, and a new synthesis of sugars, acids and aroma compounds takes place (Anton et al., 2017). Green fruits remain able to perform photosynthesis, thanks to the presence of chlorophyll in the immature fruits, which are responsible for 20% of the overall photosynthesis of the plant (Quinet et al., 2019). The proximate composition of freeze-dried green and red tomatoes can be considered similar in terms of solid content %, fat %, ash %, insoluble and soluble fiber %, as reported in the following table (**Table 43**), while on the other hand, the acidity decreases during the ripening process (Anton et al., 2017).

tomato component	green tomatoes	red tomatoes
tomatine, mg/kg of fresh wt	48	0.4
tomatine, mg/kg of dry wt	743	0.7
solid content, %	6.4	5.8
N, %	2.49	2.11
fat, %	3.24	3.20
ash, %	10.31	10.02
insoluble fiber, %	19.76	17.03
soluble fiber, %	4.26	4.91

Table 43. Composition comparison between freeze-dried green and red tomatoes (picture from Friedman (2002a)).

The content of hydrophilic antioxidants and ascorbic acid remains practically unchanged between greed unripe and red ripe tomatoes, but the total antioxidant activity is higher in the red fruit, due to the increase of lipophilic antioxidants, especially lycopene (Anton et al.,

2017). However, literature data don't agree about the relationship between the vitamin C content and degree of ripeness. According to Chaudhary et al. (2018), tomatoes display a vitamin C content of about 25 mg per 100 grams of fresh fruit, and this content increases as the fruit ripens, but slightly decreases in the ripe red tomatoes stage, reaching a content about 10-20 mg per 100 grams of fresh fruit. Other considerations can be provided regarding the amino acid composition, comparing green and red dehydrated tomatoes, where free amino acids contribute significantly to the total amino acid profile. In particular, the free amino acids of tomato fruits generally vary between 2.0 and 2.5% and the most important are Glu, Asp, and γ-aminobutirric acid (GABA), which perform important functions both in the plant as the control of cytosolic pH and in the human organism as neurotransmitter (Quinet et al., 2019). GABA is present in high concentrations in the unripe green tomato, but its content progressively decreases during the ripening process. Thr is also present in high quantities in the immature fruit, but decreases during the ripening process, due to its metabolization to pyruvate (Quinet et al., 2019), which is the precursor of carotenoids. Moreover, most of the other free amino acids increase during the ripening process, but the protein content decreases, due to the increment in exopeptidase and not-specific protease activity in the plant. The increase in the amino acid content from the green fruit to the red fruit is particularly important for the Glu, whose concentration can reach 10 mmol/kg in the mature fruit. This increase is partly due to stimulation of glutamate dehydrogenase and α-ketoglutarate-dependent–γ-aminobutyrate transaminase (Quinet et al., 2019). On the other hand, glutamate accumulation in the ripening fruit is due to the downregulation of chlorophyll synthesis, considering that glutamate is a direct precursor of chlorophyll. Aromatic amino acids also increase during the ripening of the fruit, considering that they represent the main precursors of flavor volatiles (Quinet et al., 2019). A global overview of metabolic changes occurring during the ripening process is represented in the following picture (**Figure 63**), while the **Table 44** shows the nutritional composition of green unripe tomatoes and red ripe tomatoes, according to the U.S. Department of Agriculture. The values are expressed as an average composition and can change according to the variety, season, maturity, growing conditions, among other factors.

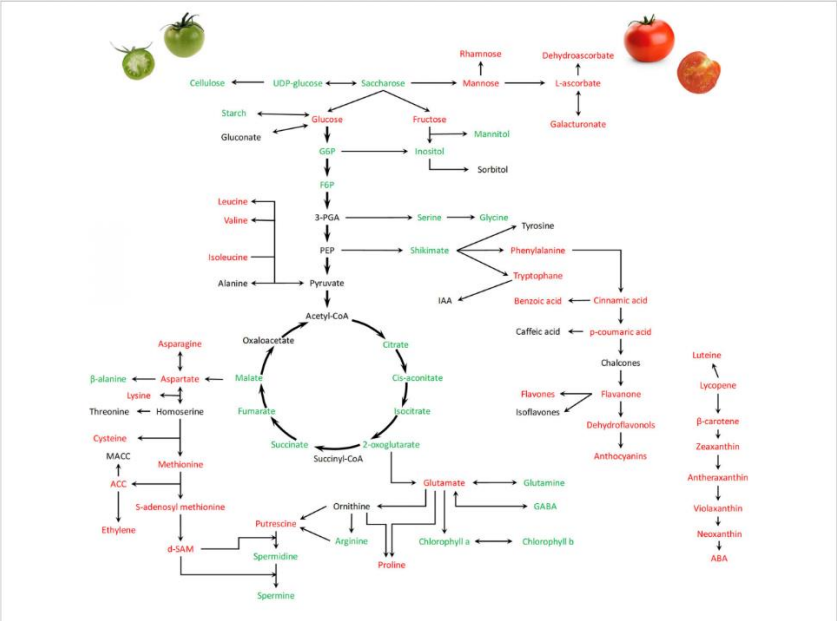


Figure 63. Representation of the main metabolic changes that occur during the transition from green immature fruit to red ripe fruit. Name of metabolites in red, green, and black indicate increase, decrease and no change, respectively (picture from Quinet et al. (2019)).

	Value per 100 g	
Nutrient	**Tomatoes, red, raw**	**Tomatoes, green, raw**
Water (g)	94.5	93
Protein (g)	0.9	1.2
Total lipids (g)	0.2	0.2
Carbohydrate (g)	3.8	5.1
Dietary Fibre	1.2	1.1
Sugars	2.6	4
Minerals (mg):		
Iron (Fe)	0.3	0.51
Calcium (Ca)	10	13
Zinc (Zn)	0.17	0.07
Sodium (Na)	5	13
Magnesium (Mg)	11	10
Potassium (K)	237	204
Phosphorus (P)	24	28
Copper (Cu)	0.06	0.09
Hydrophilic Vitamins (mg):		
Vitamin B1 (Thiamin)	0.04	0.06
Vitamin B2 (Riboflavin)	0.02	0.04
Vitamin B3 (Niacin)	0.59	0.5
Vitamin B5 (Pantothenic acid)	0.09	0.5
Vitamin B6 (Pyridoxine)	0.08	0.081
Vitamin B9 (Folate) (µg)	15	9
Vitamin C (ascorbic acid)	14	23.4
Choline	6.7	8.6

Table 44. Nutritional composition of green unripe tomatoes and red ripe tomatoes, according to the U.S. Department of Agriculture 2019,2020 (picture from Faria-Silva et al. (2022)).

The ripening process is characterized by some modification in the content of some secondary metabolites, which include carotenoids, chlorophylls, and SGAs (Friedman,

2002). SGAs are present in all parts of the tomato plant, especially in the fruit and the leaves. These compounds are essentially found in the skin of immature green tomatoes, but also flowers and leaves (Bailly, 2021), as reported in the following figure (**Figure 64**). While immature green tomatoes contain up to 500 mg α-TM /kg of fresh fruit, red tomatoes have a maximum content of 5 mg of α-TM/kg of fresh fruit, due to the extensive enzymatic degradation that this compound undergoes during the ripening process into the inactive compound of esculeoside A (Bailly, 2021). In fact, a close correlation can be found between the size, stage of maturity, and SGAs content of tomato fruits (Friedman, 2013).

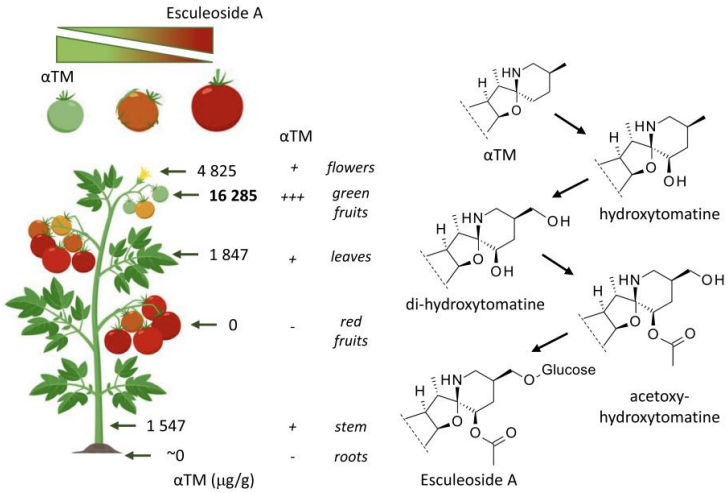


Figure 64. α-TM content in different parts of *Solanum lycopersicum* L. with the description of the enzymatic degradation process, which leads the α-TM conversion to Esculoside A (picture from Bailly (2021a))

A first improved HPLC-PAD analytical method proposed by Friedmann et al. (2002) for the analysis of α-TM and dehydrotomatine made it possible to analyze the content of these SGAs in different anatomical parts of the tomato plant (**Table 45**) (Friedman, 2002). The results of this liquid chromatography analysis have demonstrated that small immature green fruits have a content of about 465 mg of α-TM/kg of fresh fruit and a content of 54 mg of dehydrotomatine/kg of fresh fruit. This amount seems to be higher than that shown by the large immature green fruit (14 mg of dehydrotomatine/kg of dried fruit and 144 mg of α-TM/kg of dried fruit). (Friedman, 2002) has reported a higher α-TM concentration in stems and leaves, but there is no agreement among different authors in the literature. For example, (Kozukue et al., 2004) have identified the fruit as the botanical part with the highest concentration of SGAs.

plant part	mg/kg of fresh wt		% dehydrotomatine
	dehydrotomatine	α-tomatine	
large immature green fruit	14	144	8.8
roots	33	118	23
small immature green fruit	54	465	10
calyxes	62	795	7.3
leaves	71	975	6.9
small stems	138	896	13
large stems	142	465	25
flowers	190	1100	15
senescent leaves	330	4900	6.1

Table 45: α-TM and dehydrotomatine content in different anatomical parts of *Solanum lycopersicum* L. (picture from Friedman (2002a)).

Regarding the polyphenol content of green immature fruits, several trends can be found during the ripening process of tomatoes. Anton et al. (2017a) reported the evaluation of polyphenols content in methanolic tomato extracts obtained at different stages of ripeness. It observed that the green tomatoes contained the highest amount of chlorogenic acid, which continuously decreases during the ripening process (Anton et al., 2017). The same trend is followed by ferulic acid hexoside, rutin pentoside, and neochlorogenic acid, which exhibit a statistical difference between unripe green fruits and both half-ripe and red-ripe fruits. Instead, other flavonols such as rutin, quercetin dihexoside, rutin pentoxide, kaempferol rutinoside pentoxide, and kaempferol rutinoside reach the maximum amount in the green fruits, but their concentration seems to not change significantly during ripening, with a slight decrease (Anton et al., 2017). Only one flavone, apigenin acetylhexoside continuously increases during the ripening till it reaches the highest value in the red fruit. Other flavanones, such as naringenin and its glucoside, have the tendency to accumulate up to the half-ripe stage and then slightly decrease in the red-ripe tomatoes.

5.1.2. Metabolomics profile of green tomato leaves

Several studies have investigated the content of SGAs and other important plant metabolites in tomato leaves, demonstrating that they contain the highest amount of α-TM and dehydrotomatine, compared to all the other anatomical parts of the plant. A first HPLC-PAD analysis carried out by (Friedman, 2002) has demonstrated that leaves contain 71 mg of dehydrotomatine/kg of dried leaves and 975 mg of α-TM/kg of dried leaves, while there are

only 33 mg of dehydrotomatine/kg of dried leaves and 118 mg of α-TM/g of dried fruit in the green unripe fruit (Friedman, 2002). For this reason, extracts from tomato plant leaves, rich in SGAs, have been used to perform several *in vitro* experiments. Silva-Beltrán et al. (2015a) have investigated the SGAs composition in different anatomical parts of the tomato plant by performing an HPLC-DAD analysis on alcoholic extracts and by recording the absorbance at 200 nm, and have found that the leaves of two varieties of tomato evaluated in this study (Pitenza and Floradade) showed the highest content of α-TM and TD, with values of 4.940 and 0.820, and 2.430 and 0.225 mg/g of dried extract by Pitenza and Floradade respectively, as shown in the following table (**Table 46**).

Plant fractions	Tomatine[a]	Tomatidine[b]
Pitenza		
Steam	0.243 ± 0.07[a]	n.d
Leaves	4.940 ± 0.31[c]	0.820 ± 0.07[b]
Root	n.d	n.d
Whole plant	1.460 ± 0.5[b]	0.240 ± 0.084[a]
Floradade		
Steam	0.238 ± 0.01[a]	n.d
Leaves	2.430 ± 0.467[c]	0.225 ± 0.07[b]
Root	n.d	n.d
Whole plant	0.660 ± 0.007[b]	0.170 ± 0.002[a]

Table 46: α-TM and TD composition of tomato plant extracts (mg of active compound/g of dried extract). All values are expressed as mean ± SD (n = 3). Means with different letters within a column are significantly different ($p < 0.05$) and n.d means "not detected" (picture from Silva-Beltrán et al. (2015a)).

It's widely known that high temperatures and light exposure stimulate the production of phenolic acids and other flavonoids. Moreover, the heat stress in the tomato plant increases the activity of phenylalanine ammonia-lyase and the biosynthesis of phenolics, while their oxidation is inhibited. For this reason, the tomato plant leaves, which are directly exposed to light and UV radiation, exhibit the greatest amount of phenolic compounds (Silva-Beltrán et al., 2015). Some polyphenols as gallic acid, chlorogenic acid, caffeic acid, ferulic acid, and rutin can be considered the main components of the tomato plant and the highest amount have been found in the leaves. In particular, the most abundant compound is represented by rutin (Silva-Beltrán et al., 2015).

Interestingly, the concentration of flavonoids in leaves is significantly affected by the variety of the tomato plant, probably due to the genetic differences, the environmental stress

conditions, and the agricultural practices (Periago et al., 2002; Silva-Beltrán et al., 2015). Leaves extract provides the highest antioxidant capacity, compared to the other anatomical parts of the plant (**Figure 66**) and the highest total fenolic and flavonoids content, as shown the **Figure 65** in the next paragraph **5.1.3. Metabolomics profile of green tomato roots and stems**. The leaves are, together with the stem, also an important source of carotenoids and chlorophyll for the plant, considering that the chlorophyll content is directly dependent on the incidence of light, as reported by Lumpkin et al. Therefore, the areas of the plant most exposed to sunlight are characterized by a higher content of pigments, such as carotenoids and chlorophyll (Silva-Beltrán et al., 2015) (**Table 47**).

Table 2: Total chlorophyll, total carotenoids, and chlorophyll a and chlorophyll b contents in tomato plant extracts.

Sample	Chlorophyll a	Chlorophyll b	Total Chlorophyll	Total Carotenoids
		mg/ge		
Pitenza				
Steam	5.542 ± 0.005^{d}	4.113 ± 0.082^{d}	11.028 ± 0.038^{d}	0.409 ± 0.130^{c}
Leaves	4.469 ± 0.002^{c}	1.512 ± 0.004^{b}	5.361 ± 0.010^{c}	1.221 ± 0.025^{d}
Root	1.367 ± 0.003^{a}	0.024 ± 0.001^{a}	1.679 ± 0.008^{a}	0.360 ± 0.007^{a}
Whole plant	2.896 ± 0.002^{b}	1.745 ± 0.002^{c}	4.626 ± 0.009^{b}	$0.211 \pm .002^{b}$
Floradade				
Steam	3.496 ± 0.036^{c}	1.526 ± 0.031^{b}	5.125 ± 0.044^{b}	1.772 ± 0.030^{b}
Leaves	5.362 ± 0.017^{d}	3.846 ± 0.002^{d}	8.348 ± 0.101^{c}	5.354 ± 0.025^{d}
Root	0.120 ± 0.004^{a}	0.381 ± 0.011^{a}	0.460 ± 0.003^{a}	0.493 ± 0.001^{a}
Whole plant	2.243 ± 0.006^{b}	2.495 ± 0.507^{c}	4.491 ± 0.902^{b}	2.845 ± 0.219^{c}

All values are mean ± standard deviation ($n = 3$). Means with different letters within a column are significantly different ($P < 0.05$).

Table 47: Total chlorophyll, total carotenoids, chlorophyll a and chlorophyll b contents, comparing different anatomical parts of two varieties of *Solanum lycopersicum* L. (picture from Silva-Beltrán et al. (2015a)).

5.1.3. Metabolomics profile of green tomato roots and stems

SGAs are metabolites ubiquitously present in the tomato plant, thus they have also been detected in the roots and stem of *Solanum lycopersicum* L. Friedmann has investigated the dehydrotomatine and α-TM content in each part of the tomato plant by performing an HPLC-PAD analysis and has found 33 mg of dehydrotomatine/kg of dried root and 118 mg of α-TM/kg of dried root (Friedman, 2002), but these observed values are much lower than those shown by the leaves, the green fruit and the stem of the plant. On the other hand, the stem of the tomato plant showed higher levels of α-TM and dehydrotomatine than those of immature green fruits and roots: up to 138 mg of dehydrotomatine/kg of dried small stems and 896 mg of α-TM/kg of dried small stems (Friedman, 2002). Instead, 142 mg of dehydrotomatine/kg of dried large stems and 645 mg of α-TM/kg of dried large stems were

detected. However, data can be very heterogeneous between different plant varieties. For example, analyzing the content of α-TM and dehydrotomatine in the roots of two plant varieties (mini tomatoes and sweet tomatoes), conflicting data emerged. The roots of the mini-tomato had only traces of these two SGAs, whereas the roots of sweet tomatoes contain a significant amount of both compounds, with 77 µg of dehydrotomatine/g of dried root and 178 µg of α-TM/g of dried root (**Tables 48** and **49**). These data can be rationalized by considering that a specific absolute amount, as well as different ratios of the two compounds, may be needed for a synergistically optimal defense of the different tomato plant parts against several phytopathogens (bacteria, fungi, nematodes, and viruses).

glycoalkaloid	µg/g of fresh weight[a]
dehydrotomatine (A)	77 ± 7
α-tomatine (B)	178 ± 21
unknown (C)[b]	76 ± 1[b]
total (A + B)	255
ratio (B/A)	2.3
dehydrotomatine (%) [(A/A + B) × 100]	30.2

[a] Average ± SD; $n = 3$. [b] Expressed as α-tomatine.

Table 48: SGAs content in the roots of Sweet-tomato plant (picture from Kozukue et al. (2004)).

tomato part	dehydrotomatine (A) (µg/g of fresh weight)[a]	α-tomatine (B) (µg/g of fresh weight)	sum (A + B)	ratio (B/A)	% dehydrotomatine [(A/A + B) × 100]
fruit (green)	1498 ± 49	16 285 ± 112	17 783	10.9	8.4
flowers	1023 ± 3	4825 ± 191	5848	4.7	17.5
calyxes	370 ± 17	2870 ± 129	3240	7.8	11.4
leaves	304 ± 15	1847 ± 112	2151	6.1	14.1
stems	331 ± 4	1547 ± 32	1878	4.7	17.6
roots	trace	trace	trace		
fruit (red)	ND[b]	ND[b]	ND[b]		

[a] Average ± SD; $n = 3$. [b] ND = not detected.

Table 49: Dehydrotomatine and α-TM content in different parts of the Mini-tomato plant (picture from Kozukue et al. (2004)).

On the other hand, the stem is particularly rich in both chlorophyll a and chlorophyll b, while the roots exhibit the lowest content of this pigment (Silva-Beltrán et al., 2015). In addition, several volatile compounds and carotenoids were not detected in the roots (Kim et al., 2014). These data can be explained by considering that volatile compounds and pigments have evolved to attract pollinators and thus increase fertilization rates, while the

ability to synthesize toxic metabolites as SGAs, with a well-known antimicrobial activity, has evolved to ward off microorganisms and herbivores or to suppress the growth of other plants. For these reasons, edible parts such as fruits are rich in pigments and nutrients (sugars, vitamins, amino acids) to attract pollinators and successively animals who eat the fruit and thereby help seed dispersal (Kim et al., 2014), while the inedible parts, including roots, stem and leaves, don't show relevant levels of volatile compounds, carotenoids, and nutrients, but they are a good source of SGAs.

Furthermore, different extracts obtained from each anatomical part of *Solanum lycopersicum* L. have demonstrated that roots displayed the lowest phenolic and flavonoid content (**Figure 65**), followed by the stem, and also the lowest antioxidant activity, as revealed by the DPPH, ABTS, and ORAC assays (**Figure 66**). In fact, some important phenolic compounds (including chlorogenic acid, vanillic acid, and caffeic acid) were not detected at all in the roots (Kim et al., 2014).

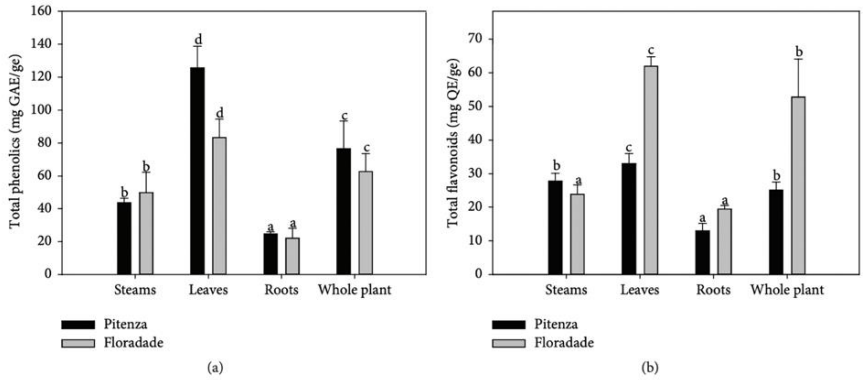


Figure 65: Total phenolic content (a) and total flavonoids (b) in extracts of different parts of the tomato plant, considering two varieties (Pitenza and Floradade). The data are expressed as a mean of at least three determinations ± SD and different letters in each bar reveal a statistical difference, with $p \leq 0.05$ (picture from Silva-Beltrán et al. (2015a)).

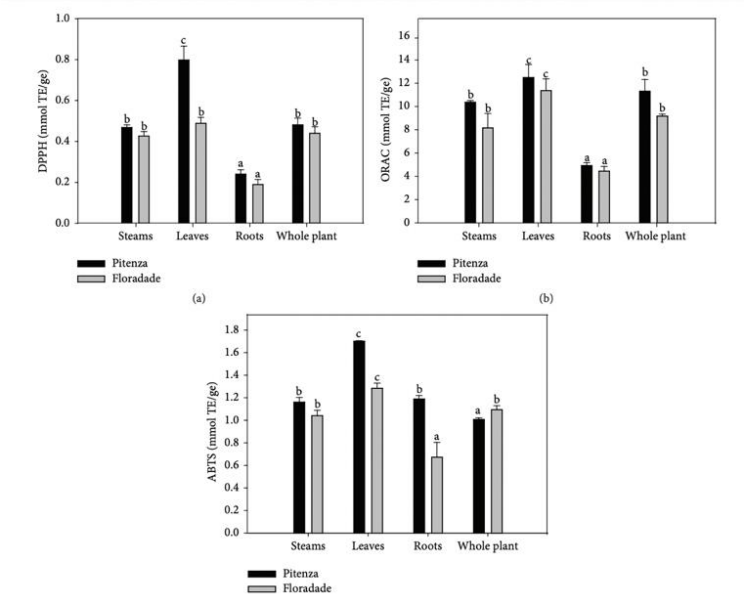


Figure 66: DPPH, ORAC and ABTS assays performed on different extracts of two varieties of tomato plant (Pitenza and Floradade). Data are expressed as means of at least three determinations and different letters in each bar reveal a statistical difference, with $p \leq 0.05$ (picture from Silva-Beltrán et al. (2015a)).

5.2. Vesuvian Piennolo tomatoes

The tomato has been a symbolic crop for Mediterranean and Italian agriculture for many years, particularly in the Campania region (South Italy). Among tomato varieties, the tomato "Piennolo" received the "Protected Designation of Origin" in 2009. The variety is present in the "Register of the Protected Designations of Origin and Protected Geographical Indications" Reg. CE n. 1238/2009 and this designation refers to tomatoes of ecotypes belonging to *Licopercon esculentum Miller* species, traditionally grown in specific areas near Mount Vesuvio (Manzo et al., 2018). This particular name is due to the ancient practice of ripening the tomatoes around a circled twine to form a large buch (with an overall weight of 1-1.5 kg), called "piennolo", which is stored hanging in dry, ventilated rooms (**Figure 67**). According to the PDO regulation, these protected fruits must show some specific requirements and characteristics, such as color, taste, consistency, and an optimal residual that must be a minimum of 6.5° Brix(Manzo et al., 2018). Particularly, Brix is the unit of measurement of the total soluble solids (TSS) content in tomatoes or their by-products: TSSs in tomatoes mainly interest sugars (such as fructose). The characteristics of these tomatoes include: an oval shape with a pointed apex, a thick peel, a weight not exceeding 25 g, a pulp with high consistency, an intense red color, and a livery, intense and sweet-sour taste. Piennolo tomatoes may also exist in different varieties, which include "Piennolo di Pollena", "Principe Borghese", "Centoscocche", "Piennolo Rosso Vesuviano", and "Piennolo Vesuviano".



Figure 67: Ripening practice of Vesuvian Piennolo tomatoes (PDO).

"Piennolo" tomato doesn't need post-harvest ripening or cold temperature storage and belongs to the so-called "long storage" (LS) tomatoes, diffused many centuries ago in several regions of the Mediterranean area from the Eastern Iberian Peninsula to the Balearic Island and to Southern Italy (Campania and Sicily) (Fratianni et al., 2020). Other important peculiarities of the Vesuvian Piennolo tomato are the high consistency of peel, the attachment strength to the peduncle and the high concentration of sugar, acids, and soluble antioxidants. These are closely linked to the soil, the climatic factors, and the volcanic origin of the geographic area in which this tomato is grown. All these properties make it a long-life product whose organoleptic properties don't change over time. An interesting study was conducted by Fratianni et al. 2020, who studied five different landraces of "Piennolo" tomatoes and investigated different aspects. Fiirstly, these Piennolo tomatoes have been analyzed for the °Brix value, the pH, the titrable acidity, and the total reducing sugars (%), and from all data emerged a high °Brix ranging between 6.4 and 7.6, a low pH (in the range 4.27- 4.36) and a sweet taste due to the reducing sugars as fructose. All these mentioned characteristics justify the high shelf-life of the tomato "Piennolo", which can be potentially kept and stored as a fresh product for many months at room temperature (**Table 50**). The low pH of these tomatoes can be justified by the presence of various organic acids, including citric acid, malic acid, oxalic acid, succinic acid, and glutamic acid, the content of which can vary during conservation after 6 months. Among these acids, glutamic acid has been associated with the umami flavor and taste of tomatoes. The whole Piennolo tomato has a high nutritional potential, including the seeds, which contain 27% of lipids, such as oleic and linoleic acid, and the skin, which contains 11% of protein (Manzo et al., 2018).

Landraces	°Brix	pH	Titratable Acidity (% Citric Acid)	Total Reducing Sugars (%)
Centoscocche	6.9 (±0.1)	4.23 (±0.13)	0.56 (±0.01)	4.22 (±0.2)
Principe Borghese	6.4 (±0.12)	4.36 (±0.14)	0.58 (0.01)	4.12 (±0.12)
Piennolo di Pollena	7.6 (±0.38)	4.29 (±0.20)	0.58 (0.02)	4.37 (±0.21)
Piennolo Rosso Vesuviano	6.9 (±0.10)	4.27 (±0.20)	0.55 (±0.04)	4.72 (±0.34)
Piennolo Vesuviano	7.1 (±0.12)	4.28 (±0.15)	0.60 (±0.03)	5.19 (±0.15)

Table 50: °Brexit, pH, titrable acidity (as % of citric acid) and total reducing sugars (%) of five ladrances of Piennolo tomato. Data are expressed as mean ± SD of three determinations (picture from Fratianni et al. (2020)).

Undoubtedly, these five tomato varieties are also a rich source of polyphenols, with a total content found between 230 and 320 µg/g of fresh product. This high content may be due to environmental pressure, which exerts a natural selection and can trigger phenol and carotenoid biosynthesis and accumulation in the fruit. Considering the single polyphenols, an UPLC-DAD analysis allowed to identify hyperoside (quercetin 3-*O*-β-D-galactoside), gallic acid and chlorogenic acid as the most abundant phenolic compounds presents in the fruit. The ferulic acid content also proved to be high, while that of rutin proved to be highly variable between the various cultivars (ranging from 6 µg to 36 µg/g of fresh product). Very low amounts of catechin were found in all varieties (about 4 µg of catechin/g of fresh fruit), while other polyphenols, such as quercetin, epicatechin, apigenin, and *p*-coumaric acid were not detected (Fratianni et al., 2020). The identification of ferulic acid but not of *p*-coumaric acid is probably due to the specific metabolic pathway, with the conversion of *p*-coumaric acid to ferulic acid. However, the antioxidant content of tomatoes depends on several factors, including the genotype, the cultivar, the fruit maturity, the agronomic and environmental conditions (Manzo et al., 2018). The following table summarizes the data obtained from the UPLC analysis (**Table 51**).

Variety	CHL µg g^{-1}	FER µg/g^{-1}	GAL µg g^{-1}	CAT µg g^{-1}	HYP µg g^{-1}	RUT µg g^{-1}
PDC	98.65 (±6.12)	15.25 (±3.38)	45.22 (±5.00)	1.82 (±0.71)	210.01 (±8.88)	6.41 (±1.23)
PDB	125.78 (±5.01)	9.13 (±0.39)	49.97 (±5.21)	2.66 (±0.86)	188.84 (±3.53)	33.51 (±3.63)
PDP	128.19 (±11.97)	25.14 (±5.22)	56.82 (±4.27)	4.42 (±0.49)	154.57 (±4.39)	15.28 (±1.55)
PRS	146.27 (±9.53)	18.12 (±3.35)	61.35 (±4.51)	4.37 (±0.46)	207.48 (±5.16)	0.00 (±0.00)
PDV	154.83 (±5.30)	11.86 (±3.62)	45.14 (±3.50)	2.83 (±0.63)	203.95 (±3.65)	19.51 (±1.53)

Table 51: Chlorogenic acid (CHL), ferulic acid (FER), gallic acid (GAL), catechin (CAT), hyperoside (HYP) and rutin (RUT) content in 5 varieties of Piennolo tomato. Varieties include: PDC = "Piennolo Centoscocche"; PDB = "Piennolo Principe Borghese"; PDP = "Piennolo di Pollena"; PRS = "Piennolo Rosso Vesuviano"; PDV = "Piennolo Vesuviano". Data are expressed as mean ± SD of three determinations. (picture from Fratianni et al. (2020).

The main feature of red Piennolo tomato, which differentiates it from all other industrial tomatoes, is certainly the high content of carotenoids and in particular of lycopene. The lycopene content ranges from 158.71 µg to 218.89 µg/g of fresh product, while the β-

carotene content is in the range 1.07 to 1.93 μg/g of fresh product (Fratianni et al., 2020). These results demonstrated that the Piennolo tomato is not the major source for the dietary intake of β-carotene (which constitutes only 7-10% of the total carotenoid in this fruit). The high lycopene content found in the Piennolo tomato is of great importance from a nutritional point of view, considering that it represents the carotenoid with the highest antioxidant capacity and singlet oxygen-quenching ability. In addition, its bioavailability increases with the assumption of fat, considering that it is a fat-soluble compound. Lycopene, which is 80-90% of the total carotenoid content in the fruit (Manzo et al., 2018), can reduce the risk of many types of cancer, and counteract the serum lipid peroxidation and LDL oxidation, which directly contributes to the onset of atherosclerosis and coronary heart diseases (Fratianni et al., 2020). Interestingly, the antioxidant activity revealed for the different varieties of the Piennolo tomato (ranging from 17.39 to 23.91%) seems to be closely correlated to the amount of total polyphenols, while it is little or not correlated to the presence of ascorbic acid and β-carotene (Fratianni et al., 2020).

Together with polyphenols, ascorbic acid represents one of the most important water-soluble antioxidants present in fruits and vegetables. The five studied varieties of Piennolo tomatoes exhibit a Vitamin C content between 197 and 275 μg/g of fresh fruit (Fratianni et al., 2020). However, the ascorbic acid content slightly decreases during the ripening process or even increases during the last stage of ripening, but with no significant changes, in agreement with the general trend in green unripe tomatoes, as reported in the previous paragraph **5.1.1. Metabolomics profile of green tomato fruits**.

5.3. Biological roles and benefits of *Trichoderma* spp. in agriculture

5.3.1 Taxonomic and biological features of *Trichoderma* spp.

Trichoderma spp. is a genus of opportunistic, avirulent, and plant symbiont fungus which belongs to the family of Hypocreaceae (Woo et al., 2023). This ascomycete fungus is typically found in a large variety of ecosystems, particularly in forest and agricultural soils. *Trichoderma* spp. colonize the rhizosphere, which is the soil area surrounding plant roots, rich in nutrients derived from the pH released by the roots (Zin & Badaluddin, 2020). Morphologically, all the species and strains of *Trichoderma* spp. are characterized by a bright green conidial and repeated branch. Overall, more than 400 species can be identified, based on molecular methods for species classification and identification (Woo et al., 2023), although Waghunde et al. (2016) have found more than 10.000 species, through a classification method based on morphological characteristics (Zin & Badaluddin, 2020). However, those that are of greatest interest in agriculture are: *T. atroviride*, *T. gamsii*, *T. viride*, *T. asperellum*, *T. asperelloides*, *T. harzianum*, *T. afroharzianum*, *T. guizhouense* and *T. virens*, some of which are represented in the following **Figure 68**.

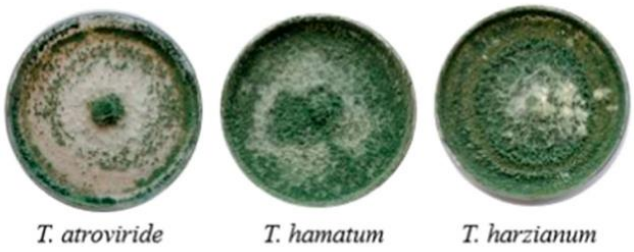


Figure 68: Isolated strains of *T. atroviride*, *T.hamatum* and *T.harzianum*.

During its evolutionary history, *Trichoderma* spp. have undergone several crucial shifts that led to a genetic reshaping and to a great species diversification (Woo et al., 2023). In a first stage, it was a mycoparasite of the wood-decomposing Basidiomycota. In a second stage, it became a saprophyte by growing on plants killed during the Cretaceous-Paleogene extinction event (66 million years ago) and by acquiring some genes encoding for carbohydrates hydrolytic enzymes. Subsequently, in a third stage, *Trichoderma* spp. developed parasitism towards taxonomically close fungi ascomycetes, oomycetes,

basidiomycetes, and towards nematodes. This passage from saprotrophism to parasitism is precisely what has led to the most significant diversification of species. Finally, in the fourth stage, *Trichoderma* spp. have developed a mutualistic relationship with living plants, by colonizing the rhizosphere and internal plants (endophytism) and thus using mechanisms to overcome plant defenses and not be recognized as a foe (Woo et al., 2023). The inoculation of the roots with this opportunistic fungus in agriculture has proved to be extremely useful, thanks to the numerous biological roles that *Trichoderma* spp. can assume, as a biological control agent (BCA), plant growth promoter agent, natural decomposition agent and biological agent of bioremediation (Zin & Badaluddin, 2020).

All these benefits on the host plant led to an increase in production yield and suggest a possible use of this fungus instead of toxic fertilizers and pesticides, with a view to more sustainable agriculture. At the basis of this intricate plant-microorganism association, there is the production of a large number of secondary metabolites, volatile organic compounds, reactive oxygen species (ROS), and cell-wall degrading enzymes (Woo et al., 2023). Particularly, *Trichoderma* spp. may produce more than 120 secondary metabolites, most of which include terpenes, pyrones, polyketides, and not-ribosomal peptides, characterized by a well-known antibiotic activity, and capability to inhibit the growth and multiplication of fungi, oomycetes, and bacteria (Woo et al., 2023). Among them, auxins, gibberellins, abscisic acid, salicylic acid, and cytokines are involved in hyphal growth, root colonization, activation of plant antioxidant defenses, and promotion of plant performance under abiotic stresses (Woo et al., 2023). On the other hand, *Trichoderma* spp. produce several wall-degrading enzymes, as cellulases, proteases, xylanases glucanases, and chitinases (exochitinase and endochitinase). Secondary metabolites that can permeabilize cell membranes might work synergistically with hydrolytic enzymes to promote cell disruption (Woo et al., 2023; Zin & Badaluddin, 2020). Firstly, biocontrol can be defined as the use of living organisms to suppress the pest population by inoculating *Trichoderma* spp. during seeding. Biocontrol mechanisms involve the identification and attack of plant pathogenic fungi, the disruption of nematode eggs and second-stage juveniles, and the induction of resistance mechanisms in plants towards various diseases, by a root architecture alteration (Zin & Badaluddin, 2020). Specifically, five different mechanisms of direct biocontrol (or antagonism) can be found (Woo et al., 2023) and are summarized by the **Figure 69**:

1. Parasitism, since *Trichoderma* spp. are natural predators of other living fungi from which it obtains nutrients;

2. Antibiosis, by the production of secondary metabolites that inhibit competitors proliferation;
3. Production of hydrolytic enzymes and secondary metabolites with antinematode and insecticide activity;
4. The competition for ecological niches and resources;
5. The production of volatile organic compounds that attract parasitoids and predators of other insect pests.

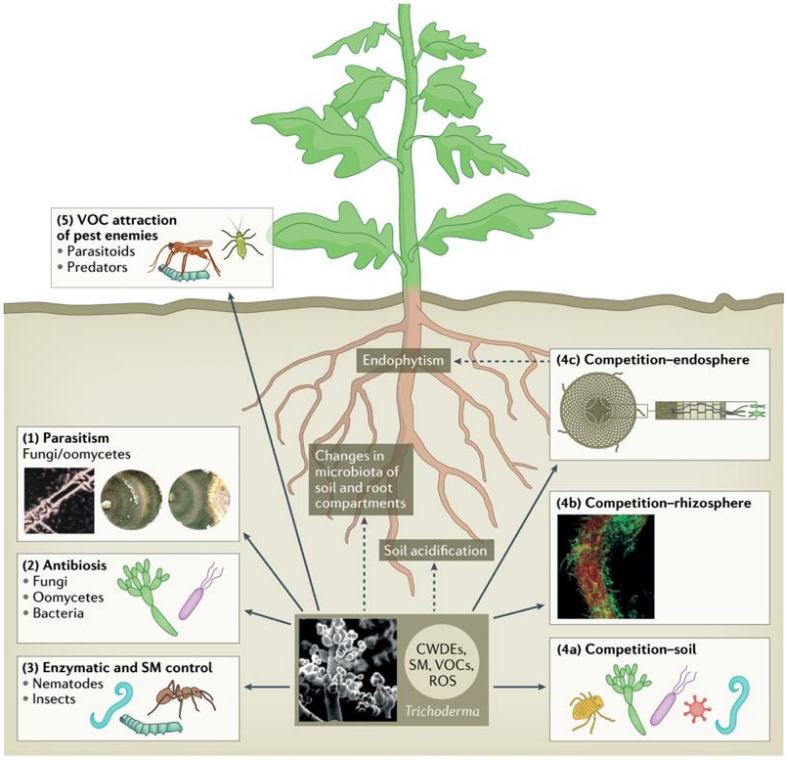


Figure 69: Direct biocontrol mechanisms of *Trichoderma* spp.: parasitism, antibiosis, enzymatic and secondary metabolites control, competition for niches and nutrients, attraction of pest enemies by volatile organic compounds. CWDEs means cell wall degrading enzymes; SM means secondary metabolites, VOCs means volatile organic compounds and ROS means reactive oxygen species (picture from Woo et al. 2023).

For example, by producing specific antimicrobial peptides, called peptaibols, *Trichoderma* spp. may inhibit β-(1,3) glucan synthase activity in pathogenic microorganisms, which is the key enzyme involved in the synthesis of β-(1,3) glucan, the main component of the cell wall. In this way, the incorporation of uridine diphosphate glucose (UDP-Glc) is inhibited, and the synthesis of this polysaccharide is drastically decreased (Lorito et al., 1996). In addition,

many proteases released by *Trichoderma* spp. inhibit several enzymes produced by pathogens to attack and penetrate the plant (Woo et al., 2023). Furthermore, many secondary metabolites secreted by some species of *Trichoderma* spp. can downregulate the expression of pathogenic genes of target microorganisms. An example is given by the polyketides released by *T. arundinaceum*, which negatively modulate the expression of phytotoxic sesquiterpenes of *Botrytis cinerea* (Woo et al., 2023). Other compounds, such as koninginis, have been shown to inhibit the growth of several phytopathogens, such as *Fusarium flocciferum* and *Fusarium oxysporium* (Zin & Badaluddin, 2020). Among these pathogens, *Fusarium oxysporium* is responsible for the wilt of tomato plants, and therefore the inoculation with *T. asperellum* can prevent this plant disease. Interestingly, *Trichoderma* spp. also release siderophores, which greatly help this fungus to compete in the rhizosphere with other microorganisms and solubilize phosphates, which are then absorbed by plants as nutrients, by improving their growth (Woo et al., 2023).

On the other hand, indirect mechanisms involve the colonization of root surfaces and penetration to the root surface, with the subsequent biostimulation of the plant host. In fact, genomic and metabolic modifications, induced by this endophytic fungus, lead to the accumulation of jasmonic acid and enhance the host plant defenses (Zin & Badaluddin, 2020). Specifically, *Trichoderma* spp. may act as an indirect biological control agent, biostimulant, and priming inducer by complex molecular interactions with the plant host (Woo et al., 2023). In fact, some microorganism-associated molecular patterns (MAMPs), along with other damage-associated molecular patterns (DAMPs) are recognized by pattern-recognition receptors (PRRs) on the plant cell membrane. MAMPs are structural components of the fungus cell wall (e.g., chitin, β-glutans, and sterols), while DAMPs are cell wall oligomers released by the enzymatic activity of *Trichoderma* spp. on plant tissues and phytopathogens (Woo et al., 2023). In addition, some small RNA (sRNA) produced by the fungus can induce the expression of nucleotide-binding site leucine-leucine-rich repeat (NLR) receptors in the cytoplasm of plant cells. Overall, these interactions lead to a reprogramming of genes involved in plant defense and development, and to the activation of antioxidant systems and phytohormone signaling (Woo et al., 2023), for example by inducing jasmonic acid biosynthesis and jasmonic acid-responsive genes in the root cells, thus generating a signal that spreads systemically. In particular, jasmonic acid (JA), along with ethylene, is an important phytohormone involved in the plant development and defence. JA mediates the induced systemic resistance against necrotrophic pathogens and herbivorous insects through an up-regulation of specific genes involved in the plant

protection (Salas-Marina et al., 2011). The major role of JA is the enhancement of secondary metabolite production, as SGAs and polyphenols. In fact, (Montero-Vargas et al., 2018) reported that the exogenous application of JA induces α-TM accumulation in wild-type plants and restores α-TM levels in spr2 plants (i.e., mutant plants with a low rate of α-TM expression). On the other hand, it has been found that JA has an important role in the induction of polyphenol biosynthesis. In fact, when abiotic stresses (UV radiation and wounds) are applied simultaneously, an enhanced effect on the accumulation of phenolics is observed due to higher levels of signaling molecules, including ROS, ethylene, and jasmonic acid (Surjadinata et al., 2021).

All this results in an increase in the plant's immune defenses against various microorganisms (fungi, bacteria, viruses, insects, nematodes) and in a release of volatile organic compounds that attract parasites and predators of insect pests. Furthermore, plant tolerance to abiotic stresses (drought, salinity, and extreme temperatures) is enhanced, plant growth is promoted and a priming state (i.e., long-lasting indirect biocontrol and biostimulation effects by a "transcriptional memory", throughout the life of the plant) is induced (Woo et al., 2023). Interestingly, these acquired defense and growth traits can be passed on to offspring by transmission of genetic and epigenetic marks in seeds (Woo et al., 2023). The final effect is the improvement of the overall yield quality and the enhancement of the nutritional value of fruits. The following **Figure 70** summarizes these described mechanisms of *Trichoderma* spp. as indirect biocontrol agent.

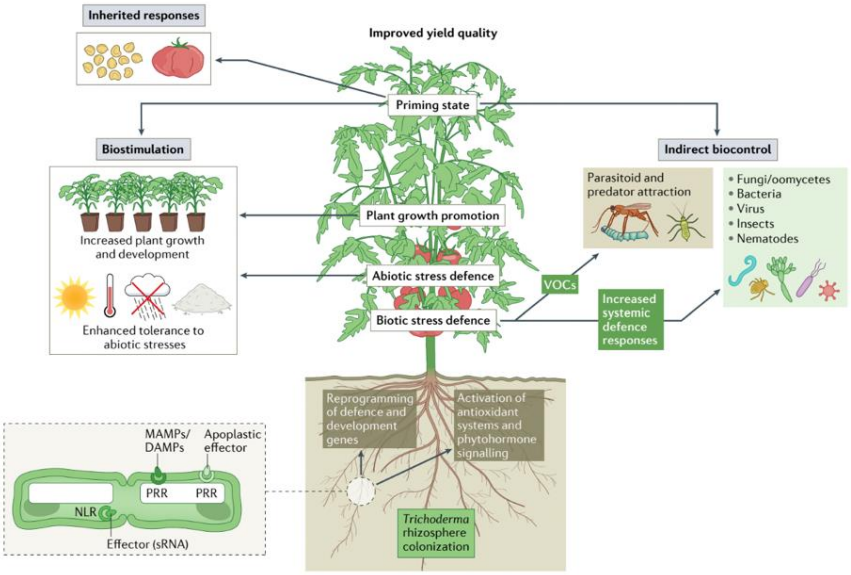


Figure 70: use of Trichoderma spp. in the indirect biocontrol, biostimulation, and priming, that lead to a final improvement in yield quality (picture from Woo et al. 2023).

Another important role of *Trichoderma* spp. is the direct plant growth-promoting fungi (PGPF), which is performed through the generation of favorable environmental conditions and the release or control of plant hormones. These hormones are responsible for improving root development and include auxins (e.g., indoleacetic acid), harzianic acid, and harzionalide. This increase in the surface area of the roots allows to explore a bigger region of soil (Zin & Badaluddin, 2020). For example, the inoculation of tomato plants with *T. harzianum* (strain SQR-T037), which releases harzianolide as a secondary metabolite, resulted in better roots development, for the enhancement of root length and tips, and in the promotion of tomato seedling growth (Cai et al., 2013). In addition, another released compound is harzianic acid, which positively regulates plant growth, due to its Fe^{3+} binding activity, thus enhancing the transport of this element from roots to shoots.

As a natural decomposition agent, *Trichoderma* spp. may promote the degradation of dead organic matter, due to its production of hydrolytic enzymes that reduce the time of the decomposition process, by degrading lignin and cellulose of the cell wall. In this way, organic matter is transformed into nutrients, used by the plant to undergo photosynthesis process and to grow, in a virtuous cycle (Zin & Badaluddin, 2020). For example, *T. virens* produce some hydrolytic enzymes such as xylanases and cellulases which enhance the degradation of cellulose and hemicellulose. Instead, *T. harzianum* can synthetize three different types of cellulases (exoglucanase, endoglucanase and β-glucosidase). Finally, as a biological agent of bioremediation, *Trichoderma* spp. may metabolize different types of pesticides and herbicides, responsible for harmful effects on the environment and human health. *Trichoderma* spp. may metabolize dichlorvos (DDVP), an organophosphate compound able to inhibit the acetylcholinesterase enzyme. The enzymatic activity of this fungus can also detoxify from several synthetic polycyclic aromatic hydrocarbons (PAHs), commonly used in pesticides (Zin & Badaluddin, 2020).

5.3.2. Current and potential uses of *Trichoderma* spp. in eco-sustainable agriculture

By considering all these provided biological roles of *Trichoderma* spp. it is easy to understand the potential use of this microorganism in agriculture (Woo et al., 2023; Zin & Badaluddin, 2020). This opportunistic ascomycete fungus can display many advantages:

1. Reduction of the use of pesticides, insecticides, and herbicides;
2. Protection of plant crops from pathogen microorganisms;

3. Increment of plant defense against abiotic stresses;
4. Enhancement of plant defense priming and plant growth;
5. Increment of nutritional value;
6. Improvement of soil nutrient availability and fertilization.[101]

Currently, available agricultural products containing *Trichoderma* spp. include microbial biopesticides, biostimulants, biofertilizers, soil amendments, and agriculture probiotics, which may be all used to enhance the yield and nutritional value of several crops, including *Solanum lycopersicum* L. (Woo et al., 2023). Among all the possible eco-sustainable applications of this fungus, the seed coating, the root level inoculation, the use of time-release formulations, and the combination with other organic compounds seem to be the most promising (Woo et al., 2023). However, the regulatory framework for the use of *Trichoderma* spp. in agriculture remains rather complex, different from nation to nation, and still open. In fact, *Trichoderma* spp. can be registered in Europe as a plant protection product (PPP) and therefore used as a biocontrol agent substance, only after passing a rigorous evaluation process for efficacy and safety to confirm its claim as PPP. In addition, once this fungus has been registered as PPP, it cannot be registered or commercially distributed in Europe with another claim, for example as a biostimulant (Woo et al., 2023).
Another important aspect concerns the potential danger of some species of *Trichoderma* spp. to human health, which makes them harmful. Therefore, the use of these microorganisms in agriculture must be absolutely avoided (Zin & Badaluddin, 2020). For example, *T. brevicompactum* is the producer of a mycotoxin (trichodermin) which contaminates food, thus leading to gastroenteritis and vomiting (Yang et al. 2017). Apart from these considerations, the use of many plant-beneficial species of *Trichoderma* spp. in new potential agricultural products and formulations, represents the future of environmentally sustainable agriculture (Woo et al., 2023; Zin & Badaluddin, 2020).

5.4. Chemical hydrolysis of α-tomatine

It has been widely discussed that TD exhibits a wide range of pharmacological activities, some of which are different from or complementary to α-TM. Unfortunately, unripe green fruits of *Solanum lycopersicum* L. display very low amounts of this metabolite, and its total content in the whole plant is significantly lower than that of α-TM and dehydrotomatine (Silva-Beltrán et al., 2015). Therefore, the possibility of carrying out a chemical treatment, directly on the vegetable matrix of the green tomatoes, could lead to a matrix rich in TD and consequently to a potential nutraceutical product with new therapeutic applications. The conversion of α-TM into its aglycone TD and its derivatives with one, two, or three sugar groups (δ-TM, γ-TM and β1-TM, and β2-TM, respectively) has been widely investigated in several studies for analytical purposes (Friedman, 2002; Friedman & Levin, 1995). In fact, the final goal was the volatilization of these compounds that could be analyzed by GC-MS for a qualitative and quantitative analysis. Only with the development of appropriate HPLC methods, it was possible to directly analyze α-TM, without the need to hydrolyze it to TD or subject it to other modification (Friedman, 2002). Rick et al. (1994) described a procedure to completely hydrolyze α-TM into its aglycone TD and its free sugar units, by using drastic conditions (HCl 3M at 80°C) in a water bath for 3h. The aim was to demonstrate an abnormally large amount of α-TM in ripe fruits of Andrean *Lycopersicum esculentum*, a particular variant of tomato that deviates from the typical form of the entire species. Therefore, the TD identification in tomato extracts was confirmed from chromatographic elution and mass spectra that matched with TD standard. Finally, the quantitative analysis was carried out by comparing the integrated peak area from the total ion chromatogram from the area of a known amount of cholestane, which was used as internal standard, as shown in the following picture (**Figure 71**).

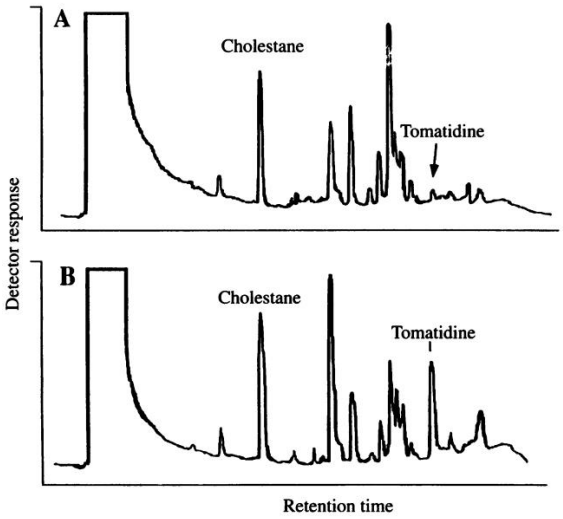


Figure 71: Gas chromatograms obtained from a sample of normal sweet tomato (A) with low amounts of α-TM and from the bitter variant (B) with a high α-TM content (picture from Rick et al., 1994).

Interestingly, by using milder acidic conditions it is possible to obtain from α-TM a mixture of partial hydrolysis products, that can be adequately separated on a preparative scale, to then analyze the different fractions by a GC-MS method (Friedman, 2002). Therefore, the elucidation of the chemical structure of these hydrolysis products and their quantification were performed by (Friedman et al., 1998), by hydrolyzing the pure compound α-TM. The products obtained by removing 1, 2, or 3 sugar units from the starting tetrasaccharide said chain lycotetraose are: β1-TM and β2-TM, obtained by removing the terminal xylose or glucose unit, respectively; γ-TM, obtained by removing both glucose and xylose terminal units; δ-TM, obtained by removing the two glucose units and the xylose unit; TD, which is the aglycone without the entire sugar moiety. The following **Figure 72** shows a summary of the chemical hydrolysis reactions of α-TM.

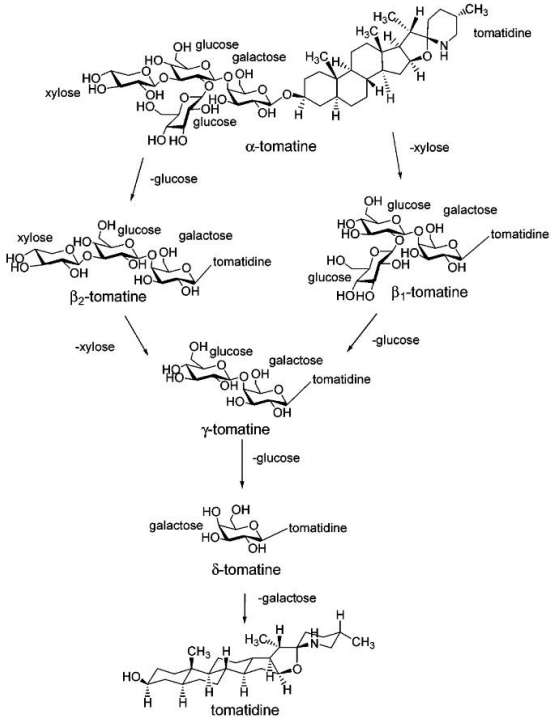


Figure 72: Hydrolytic pathway of α-TM which progressively leads to β1-TM, β2-TM, γ-TM, δ-TM, and TD (picture from Friedman (2013)).

The experiment developed by Friedman et al. (1998) has highlighted some important aspects regarding the stability of α-TM under acidic conditions. Firstly, acid hydrolysis in mild conditions with 1N HCl seems to be better than those with H_2SO4. For example, Keukens et al. (1995) described an acid hydrolysis of α-TM by using 5% H_2SO4 at 60°C for 16 min, but the method presents some problems, related to the subsequent work-up stage. The main problem is the need to precipitate sulfate (thus removing sulfuric acid from the solution) by using $BaCO_3$, prior to derivatization for the GC analysis. Unfortunately, some carbohydrates can be absorbed during this precipitation step and sulfated byproducts can be formed. For this reason, acid hydrolysis with HCl represents the best condition, both because it adequately solubilizes SGAs, and it avoids these problems associated with the work-up phase. In fact, as reported by Nepal & Stine (2019a), the solubility of α-TM in water solutions decreases with pH, being reported as 6 mM at pH 5, 1 mM at 7, and 0.030 mM at pH 8. In addition, the degree of hydrolysis is directly proportional to the reaction time and the temperature: after 3 h at 37°C none of the described hydrolysis products are formed from α-TM, while a mixture of three different SGAs can be obtained after only 20 minutes at 100°C. These data support the hypothesis that α-TM is probably not hydrolyzed by similar acid conditions in the stomach of insects and animals, including humans. In addition,

complete chemical hydrolysis into aglycone TD and individual sugars is obtained after 70 minutes at the same temperature of 100°C (Friedman, 2002).

In conclusion, the acid α-TM hydrolysis procedures were useful either for analytical purposes or to obtain a TD-enriched extract for biological assays (Friedman et al., 1998; Keukens et al., 1995). On the other hand, there are no examples throughout literature of acid hydrolysis by "food-grade" conditions and performed directly on the fresh food matrix. Therefore, this chemical approach, coupled with the development of an appropriate HPLC-MS/MS method, could be used to provide a new product with innovative nutraceutical potential.

5.5. Materials and Methods

5.5.1. Reagents

All the reagents, chemicals and standards used were analytical or LC-MS grade. α-TM (purity ≥ 95% HPLC) and TD (purity ≥ 95% HPLC) were purchased from Phytolab (Vestenbergsgreuth, Germany). Quercetin (purity ≥ 95% HPLC), rutin hydrate (purity ≥ 94% HPLC), *p*-coumaric acid (purity ≥ 98% HPLC), gallic acid (purity ≥ 98% HPLC), ferulic acid (purity ≥ 99% HPLC), chlorogenic acid (purity ≥ 95% HPLC), 2,2-dyphenyl-1-picrylhydrazyl (purity ≥ 99% HPLC), Folin-Ciocalteau's reagent and 2,4,6- tripyridy-*s*-triazine (purity ≥ 99% HPLC), were all obtained from Sigma-Aldrich (Milan, Italy).

5.5.2. Cultivar selection and preparation of the matrix

All vegetal matrices were selected from two farmlands in Campania (Southern Italy), which were "*Vesuvio*" company from San Sebastiano al Vesuvio, Italy (40°50'23.6"N 14°22'58.6"E, 40.839880, 14.382944) and a private agricultural land in Ercolano, Italy (40°49'35.0"N 14°22'02.8"E, 40.826374, 14.367433). They both provided discarded green tomatoes from 80 plants, belonging to the landrace "Principe Borghese" and to two different ecotypes. These green unripe tomatoes were the waste product derived from the harvesting in June and July 2022, indicated as the "**1st harvesting**" and "**2nd harvesting**" respectively. All plants were not treated with *Trichoderma* spp. The microbiological treatment was performed by the research group of Professor Sheridan Woo of the University of Naples Federico II. An accurate description of the sampling is provided in the following **Figure 52**. The green tomatoes used for α-TM stability tests described at the paragraph **5.6.7. Development of a tomatidine-enriched food matrix: α-tomatine hydrolysis assay** were obtained by the company "La Torrente" (Sant'Antonio Abate, Napoli, Italy; 40° 43' 28,92'' N, 14° 32' 50,64'' E, 40.7228, 14.5429).

Name of sample	Source plants	Botanical part	n° of plants for sampling	Harvest period	*Trichoderma* treatment
S. Sebastiano 1st harvesting	Piennolo tomato plants (landrace «Principe Borghese», ecotype «Acampora») of «Vesuvio» company in S. Sebastiano al Vesuvio	Green unripe tomatoes, waste	80	June-July 2022	Not treated
S. Sebastiano 2nd harvesting	Piennolo tomato plants (landrace «Principe Borghese», ecotype «Acampora») of «Vesuvio» company in S. Sebastiano al Vesuvio	Green unripe tomatoes, waste		July-August 2022	Not treated
Ercolano 1st harvesting	Piennolo tomato plants (landrace «Principe Borghese», ecotype «Zizza di vacca») of a private agricoltural land in Ercolano	Green unripe tomatoes, waste	80	June-July 2022	Not treated
Ercolano 2nd harvesting	Piennolo tomato plants (landrace «Principe Borghese», ecotype «Zizza di vacca») of a private agricoltural land in Ercolano	Green unripe tomatoes, waste		July-August 2022	Not treated

Table 52: Sample collection of green discarded companies Piennolo tomatoes from San Sebastiano al Vesuvio and from the private agricultural land in Ercolano (Campania region, Southern Italy).

San Sebastiano al Vesuvio company supplied 80 Piennolo tomato plants of "Principe Borghese" landrace and "Acamporra" ecotype (indicated with the letter "**A**"), for metabolomics studies. Four groups of 16-17 plants each were used for the sampling of unripe green fruits (indicated with the final letter **FG**). In the first group of 16 plants, green unripe tomatoes, not treated with *Trichoderma* spp. and deriving from the growth of the early fruit trusses, were harvested in June-July 2022 and were indicated as the "**1st harvesting**". Moreover, a 2nd harvesting in July-August 2022, obtained from the later upper fruit trusses, was carried out on this group of plants, and was indicated as the "**2nd harvesting**".

Another second group of 17 plants not treated with *Trichoderma* spp. was used for the harvest of only the upper trusses, directly in July-August 2022, and was indicated with "**S**", which means "2nd harvesting only".

A third group of 17 plants, treated with the biological agent *Trichoderma* spp., provided its green unripe tomatoes. The earlier lower trusses were harvested in June-July 2022 (1st harvesting samples) and the later upper trusses in July-August 2022 (2nd harvesting samples). The treatment was carried out directly on the plant's root collars and was indicated with the acronym "**T**" after the letter "A".

Another fourth final group of 16 plants treated with *Trichoderma* spp. was used for the harvesting of only the upper trusses, directly in July-August 2022. These samples were indicated with "**ST**", which means "2nd harvesting only - treated with *Trichoderma* spp.". An accurate description of the sampling, performed on these 4 groups of Piennolo tomato plants (16-17 plants for each group), and of sample nomenclature is provided in the following **Table 53**.

Name of sample	Source plants	n° of plants	Botanical part	Harvest period	*Trichoderma* treatment
A-FG 1st harvesting	Piennolo tomato plants (landrace «Principe Borghese», ecotype «Acampora») of «Vesuvio» company in S. Sebastiano al Vesuvio	16	Green unripe tomatoes	June-July 2022 (earlier fruit trusses)	Not treated
A-FG 2nd harvesting	Piennolo tomato plants (landrace «Principe Borghese», ecotype «Acampora») of «Vesuvio» company in S. Sebastiano al Vesuvio		Green unripe tomatoes	July-August 2022 (later fruit trusses) after the harvest of June-July (early fruit trusses)	Not treated
AS-FG	Piennolo tomato plants (landrace «Principe Borghese», ecotype «Acampora») of «Vesuvio» company in S. Sebastiano al Vesuvio	17	Green unripe tomatoes	July-August 2022 (only the later fruit trusses)	Not treated
AT-FG 1st harvesting	Piennolo tomato plants (landrace «Principe Borghese», ecotype «Acampora») of «Vesuvio» company in S. Sebastiano al Vesuvio	17	Green unripe tomatoes	June-July 2022 (earlier fruit trusses)	Treated
AT-FG 2nd harvesting	Piennolo tomato plants (landrace «Principe Borghese», ecotype «Acampora») of «Vesuvio» company in S. Sebastiano al Vesuvio		Green unripe tomatoes	July-August 2022 (later fruit trusses) after the harvest of June-July (early fruit trusses)	Treated
AST-FG	Piennolo tomato plants (landrace «Principe Borghese», ecotype «Acampora») of «Vesuvio» company in S. Sebastiano al Vesuvio	16	Green unripe tomatoes	July-August 2022 (only the later fruit trusses)	Treated

Table 53: Name of the samples belonging to four different groups of Piennolo tomato plants (16-17 plants for each group).

Other 4 groups, each made up of the remaining 3-4 Piennolo tomato plants of the ecotype "Acampora" (**A**) in San Sebastiano al Vesuvio, were considered as small pools of plants (indicated with the acronym "**RX**"), to carry out a comparative study between different anatomical parts. In the adopted nomenclature, acronym "**FG**" was used to indicate the fruits of green unripe tomatoes; acronym "**LG**" was used for the tomato plant's leaves, while the acronym "**RG**" was used for roots, and "**SG**" for branches and stem. The first group was made up of plants not treated with *Trichoderma* spp., whose harvesting of botanical parts was carried out in two consecutive periods: June-July for the **1st harvesting** samples and

July-August for the **2nd harvesting** samples. The second group was made up of plants not treated with *Trichoderma* spp., whose harvesting of botanical parts was carried out directly in July-August (only 2nd harvesting samples (**S**)). The third group was that of plants treated with *Trichoderma spp.*, whose harvesting of botanical parts was carried out first in June-July (1st harvesting samples, treated) and then in July-August (2nd harvesting samples, treated). The letter "**T**" indicated the presence of the treatment with *Trichoderma* spp., whose frequency and concentration on the root collar of these plants are those described in the **Table 52.** Finally, the fourth group was made up of plants treated with *Trichoderma* spp., whose harvesting was carried out directly in July-August 2022 (only 2nd harvesting samples (**S**), treated). An accurate description of the sampling, carried out on these 4 small groups of Piennolo tomato plants (3-4 plants for each group), and of sample nomenclature is provided in the following **Table 54**. All collected samples were washed, cut, frozen at -80°C, lyophilized, reduced to powder, and finally stored at room temperature in plastic tubes, protected from the light.

Name of sample	n° of plants	Botanical part	Harvest period	*Trichoderma* treatment
A-RX-FG 1st harvesting	4	Green unripe tomatoes	June-July 2022 (earlier fruit trusses)	Not treated
A-RX-FG 2nd harvesting		Green unripe tomatoes	July-August 2022 (later fruit trusses) after the harvest of June-July (early fruit trusses)	Not treated
A-RX-LG 1st harvesting		Leaves	June-July 2022	Not treated
A-RX-LG 2nd harvesting		Leaves	July-August 2022 after the fruit harvest of June-July	Not treated
A-RX-SG 1st harvesting		Stem and branches	June-July 2022	Not treated
A-RX-SG 2nd harvesting		Stem and branches	July-August 2022 after the fruit harvest of June-July	Not treated
A-RX-RG 1st harvesting		Roots	June-July 2022	Not treated
A-RX-RG 2nd harvesting		Roots	July-August 2022 after the fruit harvest of June-July	Not treated
AS-RX-FG	3	Green unripe tomatoes	July-August 2022 (earlier fruit trusses)	Not treated
AS-RX-LG		Leaves	July-August 2022	Not treated
AS-RX-SG		Stem and branches	July-August 2022	Not treated
AS-RX-RG		Roots	July-August 2022	Not treated
AT-RX-FG 1st harvesting	3	Green unripe tomatoes	June-July 2022 (earlier fruit trusses)	Treated
AT-RX-FG 2nd harvesting		Green unripe tomatoes	July-August 2022 (later fruit trusses) after the harvest of June-July (early fruit trusses)	Treated
AT-RX-LG 1st harvesting		Leaves	June-July 2022	Treated
AT-RX-LG 2nd harvesting		Leaves	July-August 2022 after the fruit harvest of June-July	Treated
AT-RX-SG 1st harvesting		Stem and branches	June-July 2022	Treated
AT-RX-SG 2nd harvesting		Stem and branches	July-August 2022 after the fruit harvest of June-July	Treated
AT-RX-RG 1st harvesting		Roots	June-July 2022	Treated
AT-RX-RG 2nd harvesting		Roots	July-August 2022 after the fruit harvest of June-July	Treated
AST-RX-FG	4	Green unripe tomatoes	July-August 2022 (only the later fruit trusses)	Treated
AST-RX-LG		Leaves	July-August 2022	Treated
AST-RX-SG		Stem and branches	July-August 2022	Treated
AST-RX-RG		Roots	July-August 2022	Treated

Table 54: Name of the samples belonging to four different groups of Piennolo tomato plants (3-4 plants for each group, representing a pool).

5.5.3. Samples extraction

Extraction procedure was performed in triplicate according to the procedure described by Maisto et al. (2023), with slight modifications. 500 mg of sample were homogenized with 10 ml of hydroalcoholic solvent at 80% of methanol and 1% of formic acid, sonicated for 10 minutes in an ultrasonic bath (Branson Fisher Scientific 150 E Sonic Dismembrator), and shaken on an orbital shaker (Sko-DXL, Argolab, Carpi, Italy) at 600 rpm for 10 minutes at room temperature. Then, the samples were centrifuged at 9000 rpm for 10 minutes at room temperature. The supernatant was separated from the pellet and transferred to another plastic tube, previously weighed. Another 10 ml of hydroalcoholic solvent was added to the pellet, repeating for a second time the same procedure till the separation of the supernatant. The supernatants of the second cycle of extraction were added to the first ones. The hydroalcoholic extracts were dried with a rotary evaporator (Ika, Staufen, Germany) at a temperature of 37°C to remove methanol, and then frozen and lyophilized to remove water. All the dry extracts obtained were stored at ambient temperature and in the dark, protected from the light.

5.5.4. Recovery experiments

5.5.4.1. α-tomatine recovery experiments

Samples chosen for the recovery experiments were the lyophilized matrices obtained from different anatomical parts of the tomato plant including: "*Ercolano* tomatoes 2nd harvesting" for the fruits, "A-RX-LG 2nd harvesting" for the leaves, "AT-RX-SG 1st harvesting" for the branches and stem, "AST-RX-RG" for the roots. The recovery was investigated by calculating the ratio of the peak area in the pre-extraction spiked samples to the peak area in the post-extraction spiked samples. A hydroalcoholic extraction was performed with a solid: solvent ratio of 25: 1 (mg/ml), by using a related mixture of solvents. The extraction procedure is described above in the previous paragraph **5.5.3. Sample extraction**. Pre-extraction spiked samples were prepared in triplicate by extracting them with pre-spiked solvent mixtures containing three different concentrations of analyte: 50 µg (low), 100 µg (medium), and 200 µg (high), according to the values obtained from the α-TM quantification. Then, the obtained supernatant was diluted with a proportion of 1:2 by using a hydroalcoholic solvent at 80% of methanol and 1% of formic acid. Instead, the post-

extraction spiked samples were prepared in triplicate by extracting 20 mg of the matrix with 800 µl of hydroalcoholic solvent at 1% of formic acid, i.e., with a solid: solvent ratio of 25: 1 (mg/ml). Subsequently, the supernatant was diluted with a proportion of 1:2 by using the α-TM solution, at three different concentrations (50 µg for the low, 100 µg for the medium, and 200 µg for the high), as reported above in **Table 55** in the next paragraph **5.5.4.3. Polyphenols recovery experiments**. The recovery was calculated as follows:

$$\textbf{\textit{Recovery \%}} = \left(\frac{\textbf{\textit{Peak area}}_{\textbf{\textit{pre-extraction spiked sample}}}}{\textbf{\textit{Peak area}}_{\textbf{\textit{post-extraction spiked sample}}}}\right) \textbf{\textit{x}}\ \mathbf{100}$$

5.5.4.2. Tomatidine recovery experiments

The TD recovery was investigated in the roots of tomato plants using "A-RX-RG 2nd harvesting" as the matrix. Pre-extraction spiked samples were prepared by using 25 mg of the matrix, which was spiked in triplicate before extraction with 1 ml of three different concentrations of analyte: 1 µg (low), 10 µg (medium), and 20 µg (high). Then, the obtained supernatant was diluted with a proportion of 1:2 using a hydroalcoholic solvent at 80% of methanol and 1% of formic acid. Instead, the post-extraction spiked samples were prepared by extracting 25 mg of matrix with 1 ml of hydroalcoholic solvent at 80% methanol and 1 % of formic acid. Subsequently, the obtained supernatant was diluted in triplicate with a proportion of 1:2, by using the TD solution at three different concentrations (1 µg for the low, 10 µg for the medium, and 20 µg for the high), as reported above in **Table 55** in the next paragraph **5.5.4.3. Polyphenols recovery experiments**. The recovery was calculated using the same ratio described in the previous paragraph **5.5.4.1. α-tomatine recovery experiments**.

5.5.4.3. Polyphenols recovery experiments

The procedure used for the recovery of polyphenols rutin and chlorogenic acid is analogous to that described in the paragraph **5.5.4.1. α-tomatine recovery experiments**. Matrices chosen for the experiments were: "*Ercolano* tomatoes 1st harvesting" for the fruits (FG), "AS-RX-LG" for the leaves (LG), "A-RX-SG 1st harvesting" for stem and branches (SG), and "AS-RX-RG" for the roots (RG). A hydroalcoholic extraction method was performed on each sample with a solid: solvent ratio of 25: 1 (mg/ml), using a related mixture of solvents.

The matrix was spiked in triplicate either before (pre-extraction spiked) or after (post-extraction spiked) extraction with a mixture of the 2 analytes, by using three different concentrations for each compound, according to the values obtained from the quantification in triplicate. The recovery was calculated using the ratio reported in the previous paragraph **5.5.4.1. α-tomatine recovery experiment**. Concentrations of analytes (rutin, chlorogenic acid, TD, and α-TM) used to perform the experiments on each anatomical part are described in the following **Table 55**:

	Rutin (µg)			Chlorogenic acid (µg)			α-tomatine (µg)			Tomatidine (µg)		
Spiked	Low	Medium	High	Low	Medium	High	Low	Medium	High	Low	Medium	High
FG	100	200	400	100	200	400	50	100	200	-	-	-
RG	5	10	20	5	10	20	50	100	200	1	10	20
LG	50	100	200	10	20	40	50	100	200	-	-	-
SG	10	20	40	10	20	40	50	100	200	-	-	-

Table 55: Standards concentrations used in recovery and matrix effect experiments for each class of matrices.

5.5.5. Matrix effect experiments

5.5.5.1. α-tomatine matrix effect experiments

The matrix effect on the HPLC-MS/MS analysis of α-TM was investigated in each anatomical part of the tomato plant, by selecting the same matrices used in the recovery experiment (paragraphs **5.5.4.1. α-tomatine recovery experiments**). The experiment for the evaluation of the matrix effect was performed in triplicate as follows: 1 mg of dried extract was solubilized in 1 ml of the related mixture of solvents, to obtain a solution of 1 mg/ml. The mixture of solvents used was either a solution of the standard at three different concentrations (post-extraction spiked samples) or a hydroalcoholic solvent at 80% of methanol and 1% of formic acid (not-extraction spiked samples). The concentrations of analyte used were: 50 µg (low), 100 µg (medium), and 200 µg (high) as shown in **Table 55** in the paragraph **5.5.4.3. Polyphenols recovery experiments**). The α-TM solution (at three different concentrations) was used as the blank sample. The matrix effect was calculated using the ratio:

$$\textbf{Matrix effect (\%)} = \left[\left(\frac{Peak\ area_{post\ extraction\ spiked\ sample} - Peak\ area_{not\ spiked\ sample}}{Peak\ area_{blank}}\right) - 1\right] x\ 100$$

5.5.5.2. Tomatidine matrix effect experiments

The matrix effect on the HPLC-MS analysis of TD was investigated in each anatomical part of the tomato plant, by selecting the same matrices used in the recovery experiment (paragraph **5.5.4.2. Tomatidine recovery experiments**). The experiment for the evaluation of the matrix effect was performed in triplicate as follows: 5 mg of dried extract was solubilized in 1 ml of the related mixture of solvents, to obtain a solution of 5 mg/ml. The mixture used was either a solution of the standard at three different concentrations (post-extraction spiked samples) or a hydroalcoholic solvent at 80% of methanol and 1% of formic acid (not-spiked samples). The concentrations of analyte used were 1 µg (low), 10 µg (medium), and 20 µg (high), as shown in **Table 55** in the paragraph **5.5.4.3. Polyphenols recovery experiments**. The TD solution at three different concentrations was used as the blank sample. The matrix effect was calculated with the ratio described in the previous paragraph **5.5.5.1. α-tomatine matrix effect experiments**.

5.5.5.3. Chlorogenic acid and rutin matrix effect experiments

The matrix effect on the HPLC-DAD analysis of rutin and chlorogenic acid was investigated in each anatomical part of the tomato plant, by selecting the same matrices used for the recovery experiment (paragraph **5.5.4.3. Polyphenols recovery experiments**). The experiment for the evaluation of the matrix effect was performed in triplicate as follows: for the fruits, the roots, the branches, and the stem, 40 mg of dried extract was solubilized in 1 ml of the related mixture of solvents to obtain a solution 40 mg/ml. The mixture used for the solubilization was either a solution of rutin and chlorogenic acid at three different concentrations (post-extraction spiked samples) or a hydroalcoholic solvent at 80% of methanol and 1% of formic acid (not-spiked samples). The three different concentrations used to perform the experiment are the same reported in **Table 55** in the paragraph **5.5.4.3. Polyphenols recovery experiments**.

5.5.6. HPLC-HESI-MS/MS method validation

5.5.6.1. Linearity and sensitivity of the HPLC-HESI-MS/MS method

Method validation was performed according to the ICH validation guideline (ICH.Q2[R2], 2022), which included the evaluation of a set of parameters, such as linearity range, the limit of detection (LOD), the limit of quantification (LOQ), precision and accuracy. α-TM and TD stock solutions were prepared by dissolving the individual standards in a hydroalcoholic solvent at 80% of methanol and 0.1% of formic acid, to obtain a concentration of 1 mg/ml. The calibration curves ($R^2 \geq 0.99$) were obtained by diluting the individual stock solutions in the same solvent, with a dilution factor of 2. The standard dilutions were analyzed in triplicate injections at each concentration level. The calibration curves were constructed by plotting the peak area against the standard concentration to evaluate the linearity of the standard response. 11-point calibration curves (from 10 to 0.010 ppm) were used for α-TM, while 9-point calibration curves (from 20 to 0.078 ppm) were used for TD. Limits of detection (LODs) and limits of quantification (LOQs) were determined to evaluate the sensitivity of the method. Determination of the signal-to-noise ratio was performed by comparing measured signals from samples with known low concentrations of analyte with those of blank samples Maisto et al., 2023. LOD represents the minimum concentration at which the analyte can be reliably detected and is defined as the lowest detectable concentration of analyte that gives a response that the analytical system can distinguish from the background level (S (signal of compound)/N (signal of noise)) = 3. Instead, LOQ is defined as the lowest quantifiable concentration of analyte that can be measured with a standard level of confidence, and it is typically calculated using (S/N) = 10 (Maisto et al., 2023).

5.5.6.2. Precision and accuracy of the HPLC-HESI-MS/MS method

As recommended by the ICH validation guideline (ICH.Q2[R2], 2022), the determination of accuracy (estimated by calculating the % bias) and precision (estimated by calculating the coefficient of variation CV %) was performed to validate the analytical method. Precision and accuracy were calculated by an intra-day and an inter-day analysis of individual

standard solutions of α-TM and TD at 3 different concentration levels. The intra-day analysis was performed by injecting the standard solutions 3 times per day. Instead, the inter-day analysis was performed by injecting the individual standard solutions for 3 consecutive days.

5.5.7. HPLC-DAD method validation

5.5.7.1. Linearity and sensitivity of the HPLC-DAD method

Stock solutions of individual standards were prepared by dissolving them in methanol to obtain a concentration of 1 mg/mL. Individual stock solutions were diluted to prepare a standard mixture solution of each standard at a concentration of 100 ppm in methanol. The calibration curves ($R^2 \geq 0.99$) were obtained by diluting the six standards mixture in methanol with a dilution factor of 2 and 10. The polyphenolic compounds used to prepare the standard solutions were: rutin, chlorogenic acid, *p*-coumaric acid, ferulic acid, gallic acid, and quercetin. The standard dilutions were analyzed in triplicate injections at each concentration. The calibration curves were constructed by plotting the peak area against the standard concentration to evaluate the linearity of the standard response. 6-point calibration curves (from 0.1 mg/ml to 0.0005 mg/ml) were used for each compound. Limits of detection (LODs) and limits of quantification (LOQs) were determined to evaluate the sensitivity of the method. Determination of the signal-to-noise ratio was performed by comparing measured signals from samples with known low concentrations of analyte with those of blank samples (Maisto et al., 2023).

5.5.7.2. Precision and accuracy of the HPLC-DAD method

Precision and accuracy were calculated by an intra-day and an inter-day analysis of polyphenols standard mixture at 3 different concentrations. The intra-day analysis was performed by injecting the polyphenols standard mixture 3 times per day. Instead, the inter-day analysis was performed by injecting the polyphenols standard mixture for 3 consecutive days.

5.5.8. Qualitative glycoalkaloids analysis

A HPLC DIONEX UltiMate 3000 (Thermo Fisher Scientific, Waltam, MA, USA) equipment, coupled with an autosampler, a binary solvent pump, and a LTQ XL mass spectrometer (Thermo Fisher Scientific, Waltam, MA, USA), was used for the analysis. The chromatographic analysis was performed according to the method proposed by (Caprioli et al., 2014), with slight modifications. Elution was performed on a Kinetex® C18 column (75 mm × 2.1 mm, 2.6 µm; Phenomenex, Torrance, CA, USA). The mobile phases were water at 0.1% formic acid (A) and acetonitrile at 0.1% formic acid (B). The elution gradient was performed according to the following conditions: 0 – 1.5 min isocratic at 15% solvent B, from 15% (B) to 40% (B) at min 1.6, linear gradient from 40% (B) to 60% (B) at min 6, from 60% (B) to 95% (B) at min 6.10, from min 6.10 to min 8 hold at 95% (B); from 95% (B) to 15% (B) at min 8.10; from min 8.10 to min 11 hold at 15% (B); for the remaining 1 min, the column was equilibrated to the initial conditions at 15% (B) (**Table 56**). The separation conditions were as follows: column temperature was set at 40°C, inject volume was 10 µl, and the flow rate was set at 0.35 ml/min. The source was a heated electrospray interface (HESI), operated in positive ionization with multiple scanning modes. Full scan (FS) and data-dependent acquisition (DDA) were used for the qualitative analysis. Collision-induced fragmentation was made using argon, with a collision energy of 35 eV. α-TM identification was based on external standard addition to the samples. The ion source was set using the following parameters: sheath gas flow rate: 30 ml/min; auxiliary gas flow rate: 10 ml/min; capillary temperature: 320 °C; source heated temperature: 150 °C; source voltage: 3.5 kV; source current: 100 µA; capillary voltage: 32 V; tube lens: 80 V (**Table 57**).

Time (min)	% B
0	15.0
1.5	15.0
1.6	40.0
6.0	60.0
6.1	95.0
8.0	95.0
8.1	15.0
11.0	15.0

Table 56: HPLC-MS/MS method elution for SGAs analysis.

Column	Kinetex® C18 column (75 mm x 2.1 mm; 2.6 µm)
Phase A	Water at 0.1% HCOOH
Phase B	Acetonitrile at 0.1% HCOOH
Column Temperature	40 °C
Injection volume	10 µl
Flow rate	0.35 ml/min
Collision energy	35 eV
Auxiliary gas flow rate	10 l/min
Sheath gas flow rate	30 l/min
Source heated temperature	150 °C
Capillary temperature	320 °C
Source current	100 µA
Source voltage	3.5 kV
Tube lens	80 V
Capillary voltage	32 V

Table 57. Summary of the chromatographic and source parameters of the HPLC-HESI-MS/MS qualitative SGAs method.

5.5.9. Qualitative polyphenols analysis

An HPLC DIONEX UltiMate 3000 (Thermo Fisher Scientific, Walton, MA, USA) equipment, coupled with an autosampler, a binary solvent pump, and an LTQ XL mass spectrometer (Thermo Fisher Scientific, Walton, MA, USA), was used for the analysis. The chromatographic analysis was performed according to the method proposed by Maisto et al. (2021), with slight modifications. Elution was performed on a Kinetex® C18 column (250 mm × 4.6 mm, 5 µm; Phenomenex, Torrance, CA, USA). The mobile phases were: water with 2% formic acid (A) and 0.5% formic acid in acetonitrile and water 50:50, *v/v*. The elution gradient was performed according to the following conditions: 0-2 min, isocratic on 10% phase B; 2-52 min, linear gradient from 10 to 55% B; 52-62 min, linear gradient from 55 to 95% B; 62-70 min, isocratic on 10% B for column recondition. The separation parameters were as follows: column temperature was set at 30 °C, injected volume was 10 µl, and the flow rate was set at 1 ml/min. The source was a heated electrospray interface (HESI), operated in negative ionization with full scanning (FS) and data-dependent

acquisition (DDA) mode. Collision-induced fragmentation was made using argon gas, with a collision energy of 35.0 eV. The ion source was set using the following parameters: sheath gas flow rate: 30 ml/min; auxiliary gas flow rate: 10 ml/min; capillary temperature: 320 °C; source heated temperature: 150 °C; source voltage: 3 kV; source current: 3.20 µA; capillary voltage: -20 V; tube lens: -106.40 V. The separation conditions and the source parameters are summarized in the **Tables 58** and **59**, respectively. The separation was performed adopting the same chromatographic conditions described in paragraph **3.2.5. Qualitative polyphenols analysis**.

Time (min)	% B
0	10
2	10
52	55
62	95
62.1	10
70	10

Table 58. Summary of the gradient condition of the HPLC-HESI-MS/MS qualitative polyphenols method.

Column	Kinetex® C18 column (250 mm x 4.6 mm; 5.0 µm)
Phase A	Water at 2% HCOOH
Phase B	Water/Acetonitrile (50:50 *v/v*) at 0.5% HCOOH
Column Temperature	30 °C
Injection volume	10 µl
Flow rate	1.00 ml/min
Collision Energy	35 eV
Sheath gas flow rate	30 l/min
Auxiliary gas flow rate	10 l/min
Capillary temperature	320 °C
Source heated temperature	150 °C
Source voltage	3.0 kV

Source current	3.20 µA
Capillary voltage	-20 V
Tube lens	-106.4 V

Table 59. Summary of the chromatographic and source parameters of the HPLC-HESI-MS/MS qualitative polyphenols method.

5.5.10. Quantitative glycoalkaloids analysis

A HPLC DIONEX UltiMate 3000 (Thermo Fisher Scientific, Waltam, MA, USA) equipment, coupled with an autosampler, a binary solvent pump, and a LTQ XL mass spectrometer (Thermo Fisher Scientific, Waltam, MA, USA), was used for the analysis. The separation was performed adopting the same chromatographic conditions described in paragraph **5.5.8. Qualitative glycoalkaloids analysis**, as described in the **Tables 56** and **57**. The ion source was set using the following parameters: sheath gas flow rate: 35 ml/min; auxiliary gas flow rate: 5 ml/min; capillary temperature: 320 °C; source heated temperature: 200 °C; source voltage: 3.5 kV; source current: 100 µA; capillary voltage: 49 V; tube lens: 205 V (**Table 60**).

Column	Kinetex® C18 column (75 mm x 2.1 mm; 2.6 µm)
Phase A	Water at 0.1% HCOOH
Phase B	Acetonitrile at 0.1% HCOOH
Column Temperature	40 °C
Injection volume	10 µl
Flow rate	0.35 ml/min
Collision energy	35 eV
Auxiliary gas flow rate	5 l/min
Sheath gas flow rate	35 l/min
Source heated temperature	200 °C
Capillary temperature	320 °C
Source current	100 µA
Source voltage	3.5 kV
Tube lens	205 V
Capillary voltage	49 V

Table 60. Summary of the chromatographic and source parameters of the HPLC-HESI-MS/MS quantitative SGAs method.

The source was a heated electrospray interface (HESI) operated in positive ionization with a multiple reaction monitoring (MRM) scanning mode. For α-TM, one MRM transition was used as a quantifier transition and a second MRM transition served as a qualifier transition. The first transition (1034.4 – 1016.4) and the second transition (1034.4 – 416.2) were performed with a collision energy of 35 eV. For the other SGAs, MRM transitions (monitored with a collision energy of 35 eV) were: 1092.6 - 414.4 for acetoxytomatine; 1032.6 - 416.8 for dehydrotomatine; 1050.6 – 414.5 for hydroxytomatine; 1062.6 - 414.4 for dehydrotomatidine tetrahexoside; 1064.4 - 416.4 for tomatidine tetrahexoside; 1108.6 - 412.4 for acetoxy-hydroxytomatidine.

For TD, the first MRM transition (416.3 - 398.2) and the second transition (416.3 - 255.3) were performed with a collision energy of 35 eV. For the other aglycones, MRM transitions (monitored with a collision energy of 35 eV) were: 414.6 – 396.4 and 414.4 – 252.2 for dehydrotomatidine; 432.4 – 414.3 for hydroxytomatidine ; 430.5 – 412.5 for dehydrohydroxytomatidine.

Argon was used as gas for collision-induced fragmentation. The MRM analyte parameters were optimized using a methanolic solution of α-TM at the concentration of 1 ppm, which is the only commercial analytical standard available. α-TM and TD were quantified according to a calibration curve ($R^2 \geq 0.99$) made with eleven and nine different concentration levels, respectively, and triplicate injections at each concentration. Secondary SGAs quantification was based on α-TM calibration curve; aglycones quantification was based on TD calibration curve.

The samples for HPLC-MS/MS analysis were prepared by suspending the dry extract in a hydroalcoholic solvent at 80% of methanol and sonicating it for 10 minutes. Concentrations used for HPLC-MS analysis were: 10 mg/ml, 5 mg/ml, 1 mg/ml, 0.1 mg/ml.

5.5.11. Quantitative polyphenols analysis

Quantitative polyphenols analysis was performed in triplicate on each sample using a HPLC Jasco Extrema LC-4000 system (Jasco Inc., Easton, MD, USA), coupled with an autosampler, a binary solvent pump and a diode array detector (DAD). Elution was performed on a Kinetex® C18 column (250 mm × 4.6 mm, 5 μm; Phenomenex, Torrance, CA, USA). Chromatographic conditions are previously described in the paragraph **5.5.9. Qualitative polyphenols analysis**. Phenolic acids were monitored at 280 nm, while flavonols were monitored at 360 nm. Peak identifications were based on standard addition to

the samples and were quantified according to a calibration curve ($R^2 \geq 0.99$) generated with six different concentration levels and triplicate injections at each point. Quantification of quercetin-*O*-xylosilrutinoside was based on the rutin calibration curve. The samples for HPLC-DAD analysis were prepared by suspending the dry extract in a hydroalcoholic solvent at 80% of methanol and sonicating it for 10 minutes. The concentrations used for HPLC-DAD analysis were 40 mg/ml and 15 mg/ml.

5.5.12. Total phenolic content (TPC)

The Folin-Ciocalteau assay was performed to determine the total phenolic content (TPC), according to the method proposed by Maisto et al. (2022) with slight modifications. Briefly, 0.5 ml of distilled water and 125 µl of Folin-Ciocalteau's reagent were added to 125 µl of the sample solution at a suitable concentration. After 6 minutes, another 1.25 ml of an aqueous solution of Na_2CO_3 7.5% (w/w) and 1 ml of water were added to the sample, which was then kept in the dark for 90 minutes. After this incubation, the absorbance was measured at 760 nm with a V-730 UV-visible/ NIR spectrophotometer operated by Spectra Manager™ Suite (Jasco Inc., Easton, MD, USA). The blank sample, used as control, was prepared by mixing 0.625 ml of distilled water and 125 µl of Folin-Ciocalteau's reagent and then the absorbance of the blank was subtracted from the absorbance of the samples. A stock solution of gallic acid was prepared by dissolving 1 mg of the reference standard in 1 ml of methanol, to obtain a concentration of 1 mg/ml. The stock solution was then diluted in the same solvent with a dilution factor of 10, to obtain a diluted solution with a concentration of 0.10 mg/ml. A calibration curve was obtained by using five concentrations of gallic acid, in a range from 0.1 to 0.005 mg/ml, obtained with a dilution factor of 2 and 10, and three replicates were performed at each concentration. Linearity range, limit of detection (LOD) and limit of quantification (LOQ) were evaluated. The hydroalcoholic extracts were analyzed in triplicate and the total phenolic content was calculated as mg gallic acid equivalents (GAE)/g dry weight (DW). Samples were prepared by dissolving dry extracts in a hydroalcoholic solution at 80% of methanol, at a suitable concentration for each class of matrices, as described in the following **Table 61**.

Matrices	Concentration (mg/ml)
FG	10
RG	10
LG	5
SG	10

Table 61: Concentrations (mg/ml) used in the Folin-Ciocalteau and the DPPH assays, for each class of matrices.

5.5.13. DPPH assay

The DPPH (radical 2,2-diphenyl-1-picrylhydrazyl) assay was performed to evaluate the antioxidant activity of hydroalcoholic extracts following this procedure: 200 µl of hydroalcoholic extracts were added to 1 ml of a methanolic solution of DPPH 0.05 mM, to obtain a slight discoloration of the solution. After mixing, the solutions were kept in the dark for 10 minutes. After this time, the absorbance was measured at 517 nm using a V-730 UV-visible/NIR spectrophotometer operated by Spectra Manager™ Suite (Jasco Inc., Easton, MD, USA). In this experiment, the blank was the hydroalcoholic solvent used to solubilize the samples, to which a methanolic solution of DPPH radical (0.05 mM) was added and then the absorbance of the blank was subtracted from the absorbance of the samples. The inhibition was calculated with this equation:

$$\textbf{\% inhibition} = \left[\left(\frac{1-A_f}{A_c}\right) x\ 100\right]$$

where A_f is the absorbance after 10 minutes and A_c is the absorbance of the blank after 10 minutes. 6-hydroxy-2,5,7,8-tetramethylchroman-2-carboxylic acid (Trolox) was used as the antioxidant standard to perform the calibration curve. A stock solution of Trolox was prepared by dissolving 1 mg of the reference standard in 1 ml of methanol, to obtain a concentration of 1 mg/ml. The stock solution was then diluted in the same solvent, to obtain a final diluted solution with a concentration of 250 µM (corresponding to 62.5 ppm). Furthermore, the calibration curve was obtained by using ten concentrations, with a concentration range of 7.8 – 250 µM and with two dilution factors of 2 and 5 and three replicates at each concentration. Range of linearity, limit of detection (LOD) and limit of quantification (LOQ) were evaluated. The analysis was performed in triplicate on each

sample and the results were expressed in µM Trolox equivalent (TE) /g DW. Dry extracts for the assay were prepared by dissolving them in a hydroalcoholic solvent at 80% of methanol, at a suitable concentration for each class of matrices (**Table 61**).

5.5.14. FRAP assay

FRAP assay (an acronym for Ferric Ion Reducing Antioxidant Power) was performed in triplicate according to the method proposed by Schiano et al. (2022). Briefly, a working FRAP solution was prepared by mixing 10 ml of 0.3 M pH 3,6 acetate buffer with 1 ml of 20 mM ferric chloride solution and 1 ml of 10 mM TPTZ (2,4,6-tris(2-pyridyl)-s-triazine) solution. 10 mM TPTZ solution was prepared by dissolving the appropriate amount of 2,4,6-tris(2-pyridyl)-s-triazine in 40 mM hydrochloric acid. The obtained mixture was pre-warmed at 37°C. Then 2,850 ml of this FRAP solution was added to 150 µl of sample solution, at a suitable concentration. After mixing and incubating at 37°C for 4 min, an increase in the absorbance was measured at 593 nm with a V-730 UV-visible/NIR spectrophotometer operated by Spectra Manager™ Suite (Jasco Inc., Easton, MD, USA). The absorbance of the FRAP working solution, used as blank, was subtracted from the absorbance of the samples. Trolox (6-hydroxy-2,5,7,8-tetramethylchroman-2-carboxylic acid) was used as an antioxidant standard, to perform the Trolox calibration curve. A stock solution of Trolox was prepared by dissolving 1 mg of the reference standard in 1 ml of methanol, to obtain a concentration of 1 mg/ml. The stock solution was then diluted in the same solvent, to obtain a final diluted solution with a concentration of 600 µM (corresponding to 0.150 ppm). Furthermore, the calibration curve was obtained by using ten concentrations, with a concentration range of 5 - 600 µM and with two dilution factors of 2 and 5 and three replicates at each concentration. Range of linearity, limit of detection (LOD) and limit of quantification (LOQ) were evaluated. The analysis was performed in triplicate on each sample and the results were expressed in µM Trolox equivalent (TE) /g DW. Dry extracts for the assay were prepared by dissolving them in a hydroalcoholic solvent at 80% of methanol, at a suitable concentration for each class of matrices (**Table 62**).

Matrices	Concentration (mg/ml)
FG	5
RG	5
LG	1
SG	2.5 – 5

Table 62: Concentrations (mg/ml) used in the FRAP assay, for each class of matrices.

5.5.15. α-tomatine acid hydrolysis

Acid hydrolysis experiments of α-TM were performed on the reference standard, by using 1N HCl at different temperatures (20, 40, 60, 80 and 100 ° C), in agreement with the method described by Friedman et al. (1998). For each temperature the procedure was performed as follows: 0.85 mg of α-TM was dissolved in 17 ml of 1N HCl, to obtain a concentration of 50 ppm. The solution was then aliquoted into two reaction flasks of 8 mL each, to perform the experiment in duplicate. Solutions were heated to the corresponding temperature, by using an oil bath and a condenser. 1 ml of solution from both flasks was aspirated and transferred in a plastic tube at different time points: 0 min, 15 min, 30 min, 45 min, 60 min and 120 min and neutralized with 2N NaOH, up to a pH of 7. The experiment at 20°C was performed at room temperature, without the need for an oil bath. The solutions were all frozen at -80°C and lyophilized. The obtained solid residue was then dissolved in 1 ml of methanol at 0.05% of formic acid, sonicated for 10 minutes, and then centrifuged at 9000 rpm, 20 °C, for 10 min. The supernatant was aspirated and transferred in a vial for the HPLC-MS/MS analysis.
The HPLC-MS/MS analysis, in Full scan (FS) and data-dependent acquisition (DDA) mode, was performed according to the method described in the previous paragraph **5.5.8. Qualitative glycoalkaloids analysis**. For each sample, α-TM quantification was carried out based on the analyte peak area, normalized to the peak area at time 0 min. The α-TM ion peak (*m*/*z* 1034) has been obtained by an extrapolation process from the Total Ion Current (TIC).

5.5.16. α-tomatine hydrolysis in green tomatoes matrix

The acid hydrolysis experiment of α-TM in green unripe tomatoes was performed by using 1N HCl at 100 ° C. The procedure was performed in duplicate as follows: seven reaction

flasks, each containing 3.20 g of fresh unripe tomatoes (properly ground) and 4 mL of 1N HCl were heated in an oil bath at 100 °C for 0, 15, 30, 45, 60, 120 and 240 min, respectively. Other 3 reaction flasks, each containing 3.20 g of the fresh matrix and 4 mL of water were heated at 100 °C for 0, 60 and 240 minutes, respectively, and were used as control. The solutions, cooled at room temperature, were neutralized with 1N NaOH up to a pH of 7, frozen at -80 °C and lyophilized. The lyophilized matrix was then extracted according to this procedure: 0.1550 g of sample were homogenized with 5 ml of methanol at 1% of formic acid, sonicated for 10 minutes in an ultrasonic bath (Branson Fisher Scientific 150 E Sonic Dismembrator), and shaken on an orbital shaker (Sko-DXL, Argolab, Carpi, Italy) at 600 rpm for 10 minutes at room temperature. Then, the samples were centrifuged at 9000 rpm for 10 minutes at room temperature. The supernatant was separated from the pellet and transferred to another plastic tube, previously weighed. Another 5 ml of extracting solvent was added to the pellet, repeating for a second time the same procedure till the separation of the supernatant. The supernatants of the second cycle of extraction were added to the first ones. The alcoholic extracts were dried with a rotary evaporator (Ika, Staufen, Germany) at a temperature of 37°C to remove methanol. After adding 4 mL of water, samples were frozen and then lyophilized to remove water. All the dry extracts obtained were stored at room temperature and protected from the light. Dry extracts were then solubilized in 1 ml of methanol at 0.05% formic acid for the LC-MS analysis. The HPLC-MS/MS analysis, in Full scan (FS) and data-dependent acquisition (DDA) mode, was performed according to the method described in the previous paragraph **5.5.8. Qualitative glycoalkaloids analysis**. For each sample, α-TM quantification was carried out based on the analyte peak area, normalized to the peak area at time 0 min. The α-TM ion peak (*m*/*z* 1034) has been obtained by an extrapolation process from the Total Ion Current (TIC).

5.5.17. Statistical analysis

All quantitative analyzes were carried out in triplicate using SPSS 27.0 software (IBM corporation, NY, USA). Statistical significance was calculated by one-way ANOVA followed by Turkey's post-hoc test, using a 95% confidence level. Partial least squares discriminant analyses (PLS-DA) with 95% confidence intervals, cross-validation tests, VIP-score tests, and Hierarchical clustering heatmaps based on the "ward" method, were all conducted using MetaboAnalyst^{TM} online software. Variables were normalized using an auto-scaling of data.

5.6. Results and discussion

5.6.1. Samples collection

The collection of the samples (i.e., the different botanical parts of Piennolo tomato plants) has been performed with the approach described in the previous paragraph **5.5.2. Cultivar selection and matrix preparation**. Initially, the goal was to investigate the polyphenolic and SGAs content in unripe discarded tomatoes deriving from agricultural production, in order to evaluate a new matrix with a high nutraceutical potential. Green Piennolo tomatoes of two different ecotypes, deriving from the company located in "San Sebastiano al Vesuvio" and from the private agricultural land in "Ercolano", have been successfully chosen as the waste vegetable matrix on which to carry out the analysis of these metabolites. This choice has been made by considering the great nutritional value of Piennolo tomatoes (Fratianni et al., 2020; Manzo et al., 2018), along with the characteristic presence of SGAs, typical of the only green unripe fruits. In addition, two successive harvesting periods of these green discarded tomatoes have been considered, which were June 2022 and July 2022. In this case, the aim was to evaluate the effect of this parameter on the plant metabolic profile, by considering that the polyphenolic and SGAs content is time-dependent, and therefore closely related to the ripening stage and the harvest period (Anton et al., 2017; Ngo et al., 2022).

Subsequently, 80 Piennolo tomato plants of the "San Sebastiano al Vesuvio" company ("Principe Borghese" landrace, "Acamporra" ecotype), divided into 4 groups, have been used to investigate the effect of other factors on the metabolomic profile of the plant. Four groups of 16-17 plants each were used to investigate the effect of different factors on the metabolic profile and nutraceutical potential of green unripe tomatoes. The presence or the absence of a treatment with *Trichoderma* spp. and the harvest period have been also considered as factors of study. In fact, as widely discussed in the previous paragraph **5.3. Biological roles and benefits of *Trichoderma* spp. in agriculture**, *Trichoderma* spp. as a biological control agent (BCA) may also improve the plant growth and the crop yield and regulate the expression of many secondary metabolites. These effects can be explained by considering that *Trichoderma* spp. may induce a change in the expression of several genes involved in plant defence and development. Therefore, it results that both the content of polyphenols, which play a key role against phytopathogens (Lyu et al., 2019) and abiotic stresses (Šamec et al., 2021), and SGAs, with a well-known antimicrobial activity

(Friedman, 2002), could be increased in the plant to support its defences and growth. To evaluate the benefits of *Trichoderma* spp. on the metabolic profile of the plant and to identify that with the most interesting content of bioactive compounds, samples have been divided into two groups: treated plants and untreated plants. Furthermore, an attempt was made to understand whether TD could be increased with this biological treatment. The other factor that has been considered, as previously mentioned, is the harvesting time. Tomato plants are characterized by the growth of fruit trusses, which develop progressively from the bottom to the up of the plant. By considering these botanical features, the harvest of the early lower fruit trusses was carried out in June-July 2022, while the harvest of the later upper fruit trusses was carried out successively, in July-August 2022. The goal was to understand if the harvest of the first fruit trusses could further influence the metabolic profile of the later fruit trusses, for example by modifying the polyphenolic and SGAs content. Furthermore, another group of plants, whose harvesting was carried out directly in July-August (only 2nd harvesting samples) was considered. The aim was to evaluate if the content of the secondary metabolites of interest could improve waiting directly in July-August for the final harvest.

In a second moment, the study of this project was also focused on a comparison of different botanical parts (harvested at different times, and deriving from treated or untreated plants), to evaluate which of these groups responded better to these factors and which anatomical parts displayed the better SGAs and polyphenolic profile. Great attention has been given to the unripe green tomato, which represents the only anatomical part of *Solanum lycopersicum* L. with a recognized nutritional claim (according to the BELFRIT list). Therefore, 4 other groups, each representing a small pool of 3-4 plants, were considered to investigate the effect of these factors, i.e., the harvest period and presence or absence of biological treatment with *Trichoderma* spp., on the metabolic profile of the different botanical parts.

5.6.2. Development of glycoalkaloids and polyphenols HPLC methods

5.6.2.1. Development of glycoalkaloids HPLC-HESI-MS/MS method

The method used for SGAs quantitative analysis is accurately described in the previous paragraph **5.5.10. Quantitative glycoalkaloids analysis**. The method development was

performed by modifying the method applied for α-TM quantification in LGT diet reported in the paragraph **4.3.5. Development of α-tomatine HPLC-HESI-MS/MS method for LGT diet analysis**, with slight modification. One difference is the increasing of column temperature from 35 °C to 40 °C, which improve peak resolution and reduce column pressure. In addition, the gradient was narrowed precisely in the phase B range of SGAs elution (from 40% of B at min 1.6 to 60% of B at min 6). In this way, the total time of analysis, including cleaning time and equilibration time, was only 12 minutes, thus providing a shorter method, potentially suitable for a High Throughput Screening analysis (HTS) and for the great number of samples considered in this project. On the other hand, chromatographic phases, column, flow rate and injection volume were not changed. Among all the LC-MS methods, multiple reaction monitoring (MRM) method was selected to provide the better conditions for SGAs quantification. For the analysis, the same MRM transitions reported in the paragraph **3.3.3.1. Development of glycoalkaloids HPLC-HESI-MS/MS method** were applied.

Instead, for TD analogues aglycone compounds the quantification was performed by using 8 MRM transitions in total, including both the qualifier and the quantifier of 4 selected compounds. Therefore, it was possible to monitor both of them, thus acquiring a sufficient number of points in the peak. Similarly, the construction of the MRM method for TD analysis was possible by studying the fragmentation pattern of TD analyrical standard, obtained through an HPLC-MS/MS analysis. TD MS^2 spectrum of this compound is provided in the **Figure 73**. TD fragmentation pattern can be described as follows:

- *m*/*z* 398.2 corresponds to the neutral loss of a molecule of water;
- *m*/*z* 273.2 and 255.2 are due to the fragmentation of the ring attached to the spirosolane system (i.e., the ring containing nitrogen as heteroatom) that produces the hydrocarbon ions.

The transition 416.3-398.2, corresponding to the loss of a water molecule, has been successively selected as the MRM quantifier transition, by considering the higher intensity of the fragment peak on the mass spectrum, which is dominated by the water-loss ion. On the other hand, the transition 416.3-255.3 has been selected as the MRM qualifier transition (**Figure 73**).

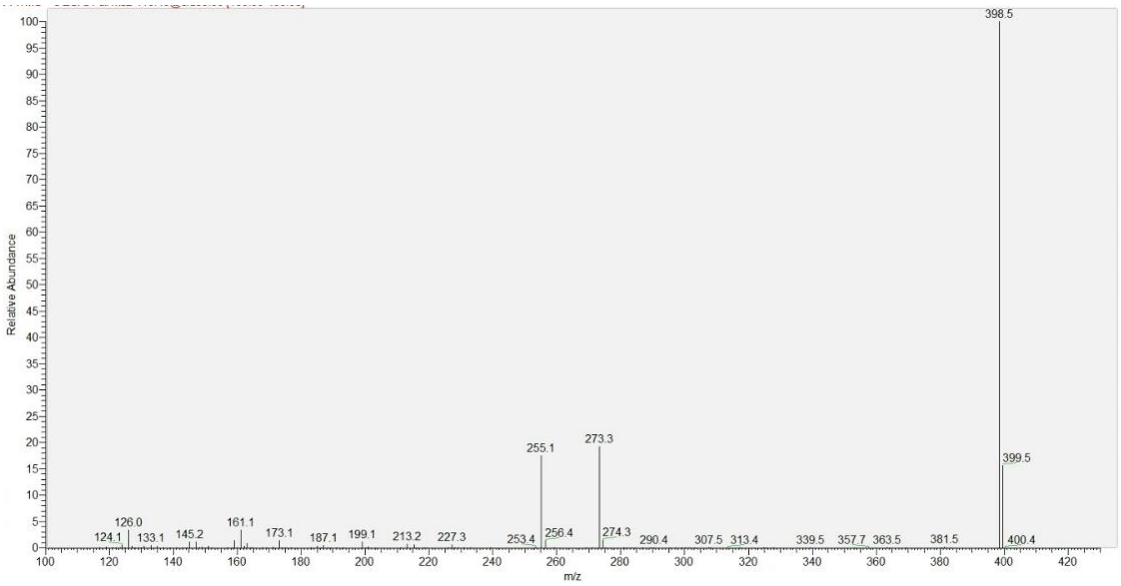


Figure 73: TD MS^2 spectrum, by using a MS/MS analysis mode.

Subsequently, the tandem mass spectrometry analysis was repeated for hydroalcoholic extracts of tomato plants, to investigate the fragmentation pattern of other alkaloid aglycone compounds structurally correlated to the alkaloid TD. The MS/MS analysis revealed that these metabolites displayed a similar fragmentation pattern, as shown in **Figure 74** for the compound dehydrotomatidine.

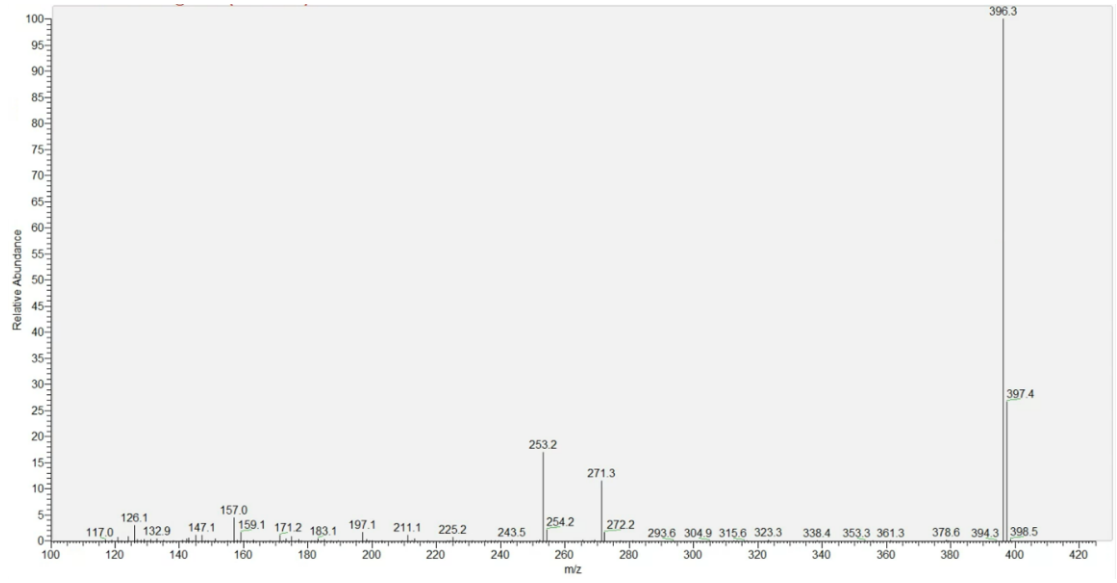


Figure 74: MS^2 spectrum of dehydrotomatidine, obtained by a MS/MS analysis mode.

Most relevant fragments obtained from the parent compound dehydrotomatidine can be described as follows:

- *m*/*z* 396.2 corresponds to the neutral loss of a molecule of water;
- *m*/*z* 271.2 and 253.2 are due to fragmentation of the ring attached to the spirosolane system (i.e., the ring containing nitrogen as heteroatom) that produce the hydrocarbon ions.

Therefore, TD calibration curve obtained by monitoring the MRM transition 416.3-398.2 was found to be suitable for the quantification of all the other correlated aglycones. In fact, the fragment obtained from the loss of a water molecule appears to be particularly intense on the mass spectrum and therefore suitable for quantifying these compounds, which are present in very low amounts in the tomato plant extracts. By considering all these aspects it was possible to develop an adequate MRM method for the analysis of 12 compounds of interest, which were quantified according to their corresponding chosen MRM transitions (**Table 63**). A comprehensive overview of all the peaks, obtained from the MRM method, both for SGAs and aglycone alkaloids, is provided in the **Figure 75** and **Figure 76**. The chemical structures of the 7 SGAs quantified in the study are summarised in the **Figure 16.** Instead, the chemical structures of the 4 alkaloids quantified in the study (e.g., TD, dehydrotomatidine, hydroxytomatidine, and dehydrohydroxytomatidine) are summarized in the **Figure 77**.

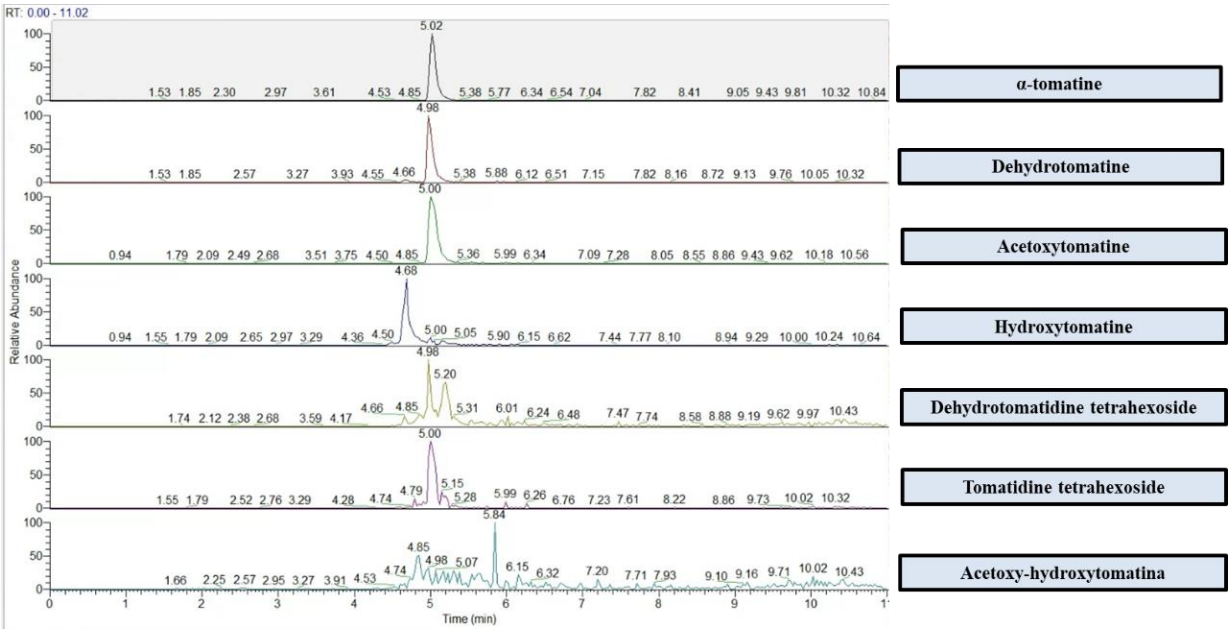


Figure 75: α-TM and other SGAs chromatographic peaks, obtained by the MRM method.

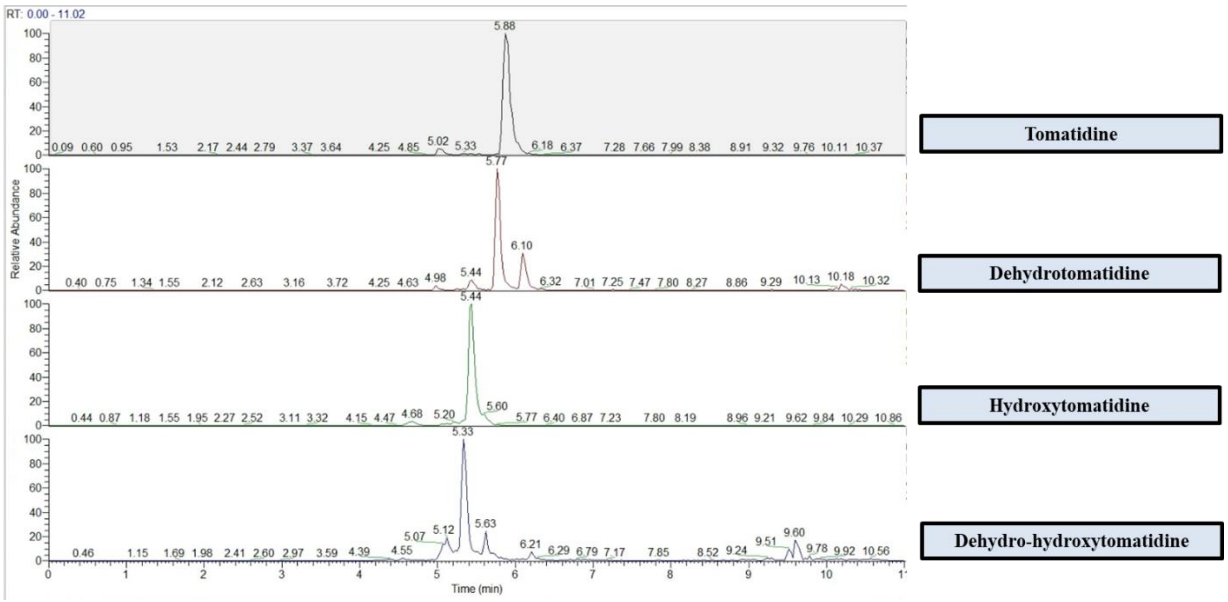


Figure 76: TD and correlated alkaloid aglycones chromatographic peaks, obtained by the MRM method.

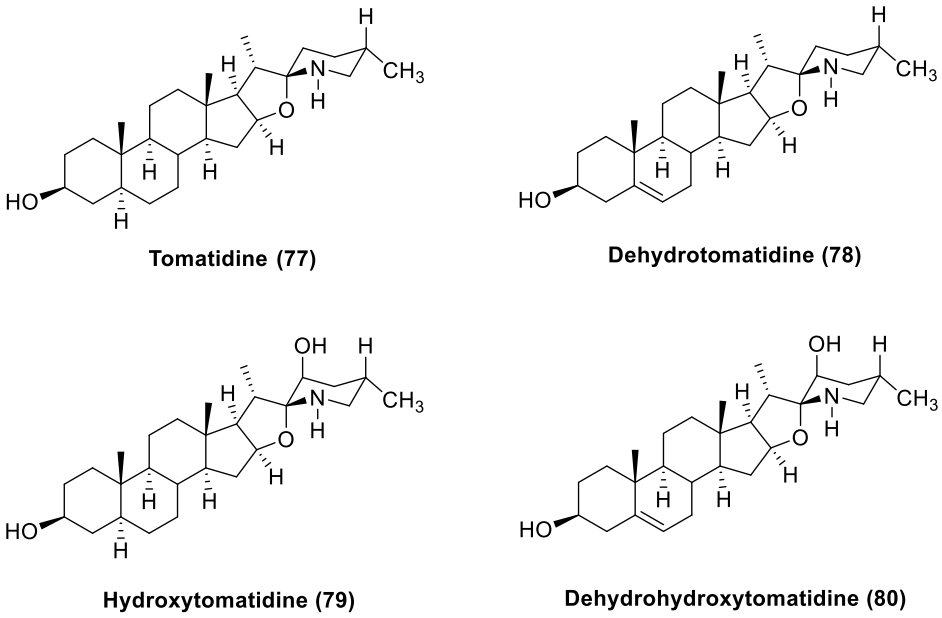


Figure 77: Chemical structure of 4 alkaloids quantified in the comparison of botanical part of *Solanum lycopersicum* L. plant.

No.	Compound	Quantification standard	MRM transition
13	α-TM	α-TM	Quantifier: 1034.6 – 1016.3 Qualifier: 1034.6 – 416.2
11	Dehydrotomatine	α-TM equivalent	1032.6 – 414.8
14	Acetoxytomatine	α-TM equivalent	1092.6 – 414.4
4	Hydroxytomatine	α-TM equivalent	1050.6 – 414.5
16	Dehydrotomatidine tetrahexoside	α-TM equivalent	1062.6 – 414.4
12	Tomatidine tetrahexoside	α-TM equivalent	1064.4 – 416.4
9	Acetoxyhydroxytomatine	α-TM equivalent	1108.6 – 412.4
77	Tomatidine	TD	Quantifier: 416.3 – 398.2 Qualifier: 416.3 – 255.3
78	Dehydrotomatidine	TD equivalent	Quantifier: 414.6 – 396.4 Qualifier: 414.6 – 253.2
79	Hydroxytomatidine	TD equivalent	Quantifier: 432.4 – 414.4 Qualifier: 432.4 – 254.2
80	Dehydrohydroxytomatine	TD equivalent	Quantifier: 430.5 – 412.5 Qualifier: 430.5 – 252.2

Table 63: Selection of the MRM transitions for the quantitative analysis of tSGAs.

5.6.2.2. Development of polyphenols HPLC-DAD method

The method used for the quantitative analysis of polyphenols is accurately described in the previous paragraph **5.5.11. Quantitative polyphenols analysis**. The HPLD-DAD-FLD method for polyphenols quantification of the samples was accurately described in the previous paragraphs **3.3.3.2. Development of polyphenols HPLC-DAD-FLD method.** The method proved to be extremely valid for separating a large number of polyphenolic compounds in all the botanical parts of *Solanum lycopersicum* L. with a high resolution, high efficiency, and high selectivity, as shown in **Figure 78,** where peaks clearly appear to be sharp and well separated.

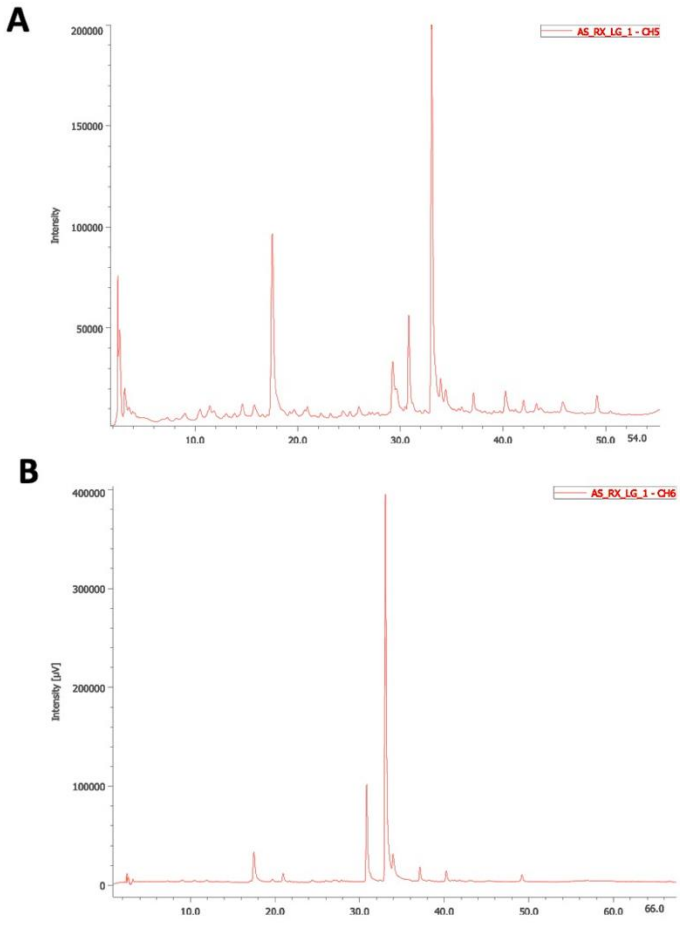


Figure 78: Leaves extract (LG) chromatogram, at 280 nm (**A**) and 360 nm (**B**).

5.6.3. Method validation

5.6.3.1. Validation of glycoalkaloids method

The procedures described above (paragraph **3.2.11. Method validation according to ICH guidelines**) were applied to the method reported in the paragraph **5.5.10. Quantitative glycoalkaloids analysis**. Calibration curves of α-TM and TD, which were the only two available analytical standards, have been performed by considering two different ranges: 10 – 0.010 ppm (11-point lines) for α-TM, and 20 – 0.010 ppm (9-point lines) for TD (**Figure 79**).

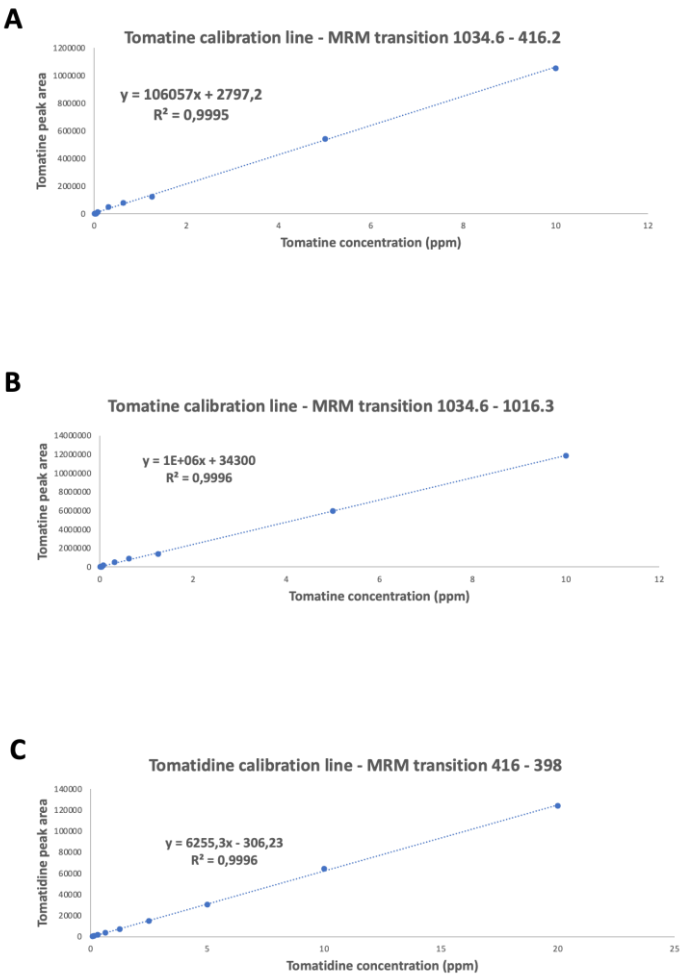


Figure 79: Calibration curves of α-TM (**A**: MRM transitions *m*/*z* 1034.6 – 416.2; **B**: *m*/*z* 1034.6 – 1016.3) and TD (**C**: MRM transition *m*/*z* 416 – 398).

For the calibration curves two different stock solutions of the reference standards were prepared by dissolving them in a hydroalcoholic solvent at 80% of methanol and 0.1% formic acid, to achieve a concentration of 1 mg/ml. As a matter of fact, according to the literature, α-TM and TD are both soluble in organic solvents such as methanol, but not in aqueous solutions with a neutral pH. On the other hand, water solubility increases by decreasing the pH. For this reason, the hydroalcoholic solution was acidified with 0.1% formic acid. All calibration curves displayed an $R^2 > 0.99$, thus demonstrating the linearity of the standard response in the range of concentrations analyzed. LODs and LOQs values were determined to evaluate the sensitivity of the method for both compounds. By considering two different calibration curves of α-TM, LOD values were: 0.19 ± 0.02 (*m*/*z* 1034 – 1016) and 0.62 ± 0.04 (*m*/*z* 1034 - 416). On the other hand, LOQ values were 0.64 ± 0.06 ppb (*m*/*z* 1034 – 1016) and 2.06 ± 0.12 ppb (*m*/*z* 1034- 416). For TD, LOD and LOQ

values, obtained by monitoring the MRM transition *m*/*z* 416 – 398, were 13.80 ± 0.81 ppb and 45.99 ± 2.71 ppb, respectively. These two parameters have been described in the paragraph **3.2.11. Method validation according to ICH guidelines** and have also been reported in the following **Table 64**.

Compound	Calibration curve	R^2	LOD (ppb)	LOQ (ppb)	Detector
α-TM (MRM transition 1034.6 – 1016.3)	y = 1E + 06x +34300	0.9996	0.19 ± 0.02	0.64 ± 0.06	MS
α-TM (MRM transition 1034.6 – 416.2)	y = 106057x + 2797.2	0.9995	0.62 ± 0.04	2.06 ± 0.12	MS
TD (MRM transition 416.3 – 398.2)	y = 6255.3x – 306.23	0.9996	13.80 ± 0.81	45.99 ± 2.71	MS
Rutin	y = 6E + 07x +5529.3	0.9988	30.87 ± 2.56	93.53 ± 7.74	DAD
Chlorogenic acid	y = 1E + 07x +4617.8	1.000	65.42 ± 11.66	198.23 ± 35.33	DAD
Quercetin	y = 5E + 07x – 84803	0.9912	111.4 ± 24.53	336.77 ± 74.35	DAD
Gallic acid	y = 3E + 07x +10044	0.9980	184.88 ± 6.89	560.23 ± 20.89	DAD
p-coumaric acid	y = 9E + 07x +18643	0.9991	14.81 ± 5.34	44.88 ± 1.62	DAD
Ferulic acid	y = 4E + 07x +32115	0.9938	160.88 ± 21.76	487.52 ± 65.95	DAD

Table 64: Calibration curves, R^2, LOD and LOQ values for α-TM, TD and the polyphenols analyzed.

In agreement with the ICH validation guideline (ICH.Q2[R2], 2022), precision and accuracy were evaluated as well to validate the HPLC-MS/MS method, by considering that a measurement device for quantitative analysis should be both precise and accurate, providing measurements all close to and tightly clustered around the true value. Precision and accuracy were calculated by an intra-day and an inter-day analysis of α-TM and TD standard solutions at 3 different concentrations (**Tables 65** and **66**). The 3 concentrations have been selected to represent the calibration levels (e.g., high, medium, low) included in the linearity range. The selection of these concentrations allowed to establish precision and accuracy of the entire calibration curves. The intra-day analysis was performed by injecting the two standard solutions three times per day. Instead, the inter-day analysis was performed by injecting the three selected standard solutions for 3 consecutive days.

Analyte	Concentration (ppm)	Precision	
		Intra-day (%, *n=3*)	Inter-day (%, *n=3*)
α-TM	2.5	0.38	2.65
	0.156	1.49	1.86
	0.02	5.50	3.19

	2.5	1.43	2.89
TD	0.156	0.83	3.76
	0.02	1.26	1.59
	100	2.88	6.34
Rutin	10	1.17	2.96
	1	1.51	6.45
	100	4.22	2.83
Chlorogenic acid	10	0.73	4.67
	1	9.24	9.47
	100	3.88	8.32
Quercetin	10	1.08	4.09
	1	9.58	8.00
	100	2.14	9.20
Gallic acid	10	2.75	3.80
	1	7.46	6.96
	100	9.21	8.24
p-coumaric acid	10	9.05	9.64
	1	1.03	9.01
	100	2.28	9.56
Ferulic acid	10	5.86	9.33
	1	4.40	10.00

Table 65. Intra- and inter-day precision for α-TM, TD, and polyphenols analysis.

Analyte	**Concentration (ppm)**	**Accuracy**	
		Intra-day (% bias, *n=3*)	Inter-day (% bias, *n=3*)
	2.5	0.90	-5.25
α-TM	0.156	4.03	4.44
	0.02	-4.47	-4.52
	2.5	-2.50	-7.39
TD	0.156	3.51	3.48
	0.02	-2.08	-2.18
	100	6.54	1.08
Rutin	10	0.56	-0.08
	1	0.17	-0.02
	100	7.66	8.05
Chlorogenic acid	10	1.83	1.20
	1	0.56	0.04
	100	-2.42	-1.62
Quercetin	10	-0.19	-0.21
	1	0.12	0.12
	100	0.75	1.94
Gallic acid	10	-0.07	-0.01
	1	-0.06	-0.05

	100	1.01	0.99
p-coumaric acid	10	0.03	0.04
	1	0.07	0.09
	100	-0.88	-0.03
Ferulic acid	10	-0.19	-0.14
	1	-0.09	-0.06

Table 66. Intra- and inter-day accuracy for α-TM, TD, and polyphenols analysis.

According to the regulatory guidelines, the sample carry-over effect was calculated to validate our MS/MS analysis. "Carry over" can be defined, in the context of chromatographic analysis, as the influence of one sample on the next and can therefore also be defined as "interaction between samples". If it is observed an elevated, downward drifting baseline in a blank sample analyzed after a high concentration sample, this suggests that the analyte from the previous injection was still eluting off the column when the blank injection was carried out. This is common for analytes with very short run time, thus demonstrating that the analyte peak has had insufficient time to fully elute from the column. In addition, carry-over effect is very frequent for analytes characterized by not-specific adsorption to parts of the analytical system (Maes et al., 2014). These phenomena introduce bias in both identification and quantification assays. The raised baseline in the subsequent samples may affect the analyte if present at low concentrations, generating problems in the differentiation of the peak from the background noise. The problem can be overcome by choosing more suitable columns, by carefully selecting the mobile phase pH, and by adjusting the chromatographic run time (Broughton, n.d.). Sample carry-over can be measured by using this formula:

$$\mathbf{k} = \left[\frac{(b_1 - b_2)}{a_2 - b_2}\right] \boldsymbol{x}\ \mathbf{100}$$

where "a_1" and "a_2" are two identical specimens with a high concentration of analyte and "b_1" and "b_2" are two identical specimens with a low concentration of analyte (Broughton, n.d.). However, regulatory guidelines require not only the evaluation of parameters such as precision, accuracy, linearity, sensitivity, stability and selectivity, but also the evaluation of the carryover effect (Maes et al., 2014). Values obtained in our carry over analysis were 0.000120971 for α-TM and 3.11742 x 10^{-5} for TD, thus demonstrating that our analysis

(characterized by a short run time) allows us to fully eluate the analyte from the column, without causing significant interactions with the blank sample.

5.6.3.2. Validation of polyphenols method

The method validation parameters, including precision, accuracy, limit of detection (LOD), limit of quantification (LOQ), and linearity range, previously described in the paragraph **3.2.11. Method validation according to ICH guidelines**, were also evaluated for the HPLC-DAD analysis of selected polyphenols. Among them, six calibration curves were performed for the phenolic compounds rutin, chlorogenic acid, gallic acid, *p*-coumaric acid, ferulic acid, and quercetin, which were the available analytical standards. Stock solutions of individual compounds, with a concentration of 1 mg/ml in methanol, were diluted in the same solvent to prepare a mixture of standards with a concentration of 100 ppm for each compound. The calibration curves (**Figure 80**) were obtained by diluting the six standards mixture in methanol, with a dilution factor of 2 and 10. As reported by several authors, the phenolic nature of these compounds (in the form of aglycones and glycosides) makes them relatively hydrophilic and thus soluble in polar organic solvents such as methanol, justifying the choice of this solvent to fully solubilize reference standards. Calibration curves of flavonols, which were rutin and quercetin, were performed by monitoring their absorbance at 360 nm, while both hydroxycinnamic acids (ferulic acid, chlorogenic acid, and *p*-coumaric acid) and hydroxybenzoic acids (i.e., gallic acid) were monitored at 280 nm, according to their absorption spectrum in the UV-vis region. Calibration curves were performed by considering 6-point lines in the range 0.0005- 0.1 mg/ml. The linearity of the standard response, in the range of concentrations analyzed, is demonstrated by an $R^2 > 0.99$ for all the phenolic compounds.

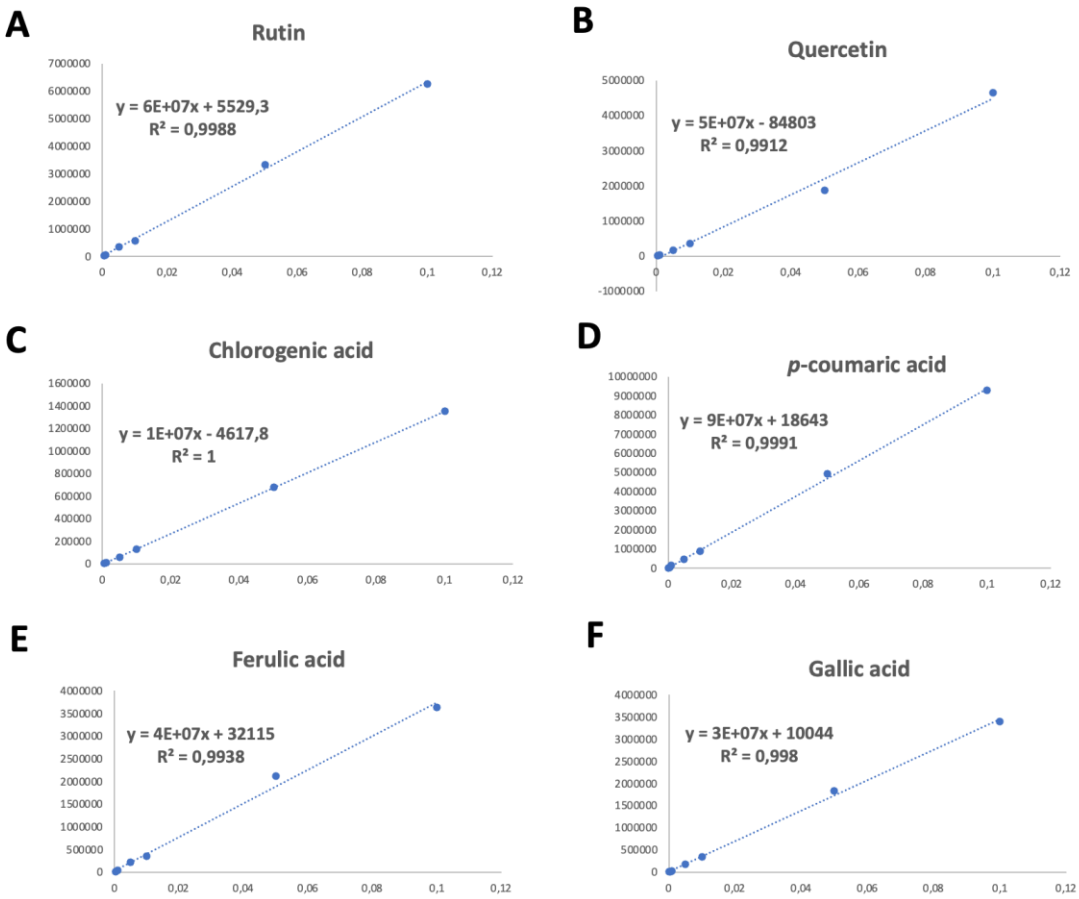


Figure 80: Calibration curves of six selected polyphenols, obtained by a HPLC-DAD analysis. Rutin and quercetin were monitored at 360 nm; chlorogenic acid, *p*-coumaric acid, ferulic acid and gallic acid were monitored at 280 nm.

The validation of the HPLC-DAD method was performed by evaluating the limit of quantification (LOQ) and limit of detection (LOD), following the procedure described above in paragraph **3.2.11. Method validation according to ICH guidelines**. LOD and LOQ values, along with the R^2 value of the six analytical standards, are provided in **Table 64**. In particular, LOD values range from 30.87 ± 2.56 ppb to 160.00 ± 21.76 ppb, while LOQ values range from 44.88 ± 1.62 ppb to 560.23 ± 20.89 ppb. As recommended by the ICH validation guideline (ICH.Q2[R2], 2022), precision and accuracy of the analysis method were evaluated as well by an intra-day and an inter-day analysis of the mixture of standards at 3 different concentrations, as described in the previous paragraph **3.3.4.2. Validation of glycoalkaloids method**. Their value, expressed as % CV (coefficient of variation) and % Bias, respectively, are both provided in the **Tables 65** and **66**. The intraday precision values (% CV) are in the range 0.73 - 11.58, while the interday precision values (% CV) vary from

1.59 to 20.07%. On the other hand, intraday accuracy values range from -2.42 to 17.56 % and interday accuracy values from -1.62 to 18.08.

5.6.4. Validation of the extraction procedure

5.6.4.1. Preparation of the matrix and extraction method

The extraction procedure was accurately described in the previous paragraphs **3.3.1. Preparation of the matrix and extraction method** and **5.5.2. Cultivar selection and matrix preparation.** An interesting parameter is represented by the extraction yield, which is variable from matrix to matrix. Overall, the unripe green tomatoes provided the highest extraction yields, while the roots provided the lowest, as shown in **Table 67**. As a matter of fact, the low extraction yield provided by roots is due to the low amount of medium-high and high polarity metabolites, commonly soluble in a hydroalcoholic solvent, such as polyphenols and SGAs, among others. As demonstrated in several studies, roots display the lowest SGAs content and the lowest total phenolic content (Friedman, 2002; Silva-Beltrán et al., 2015). On the other hand, roots are particularly rich in other secondary metabolites, such as terpenes (Tholl, 2006), which are not-polar hydrocarbon compounds (Jiang et al., 2016), whose extraction in a methanol:water 80:20 mixture is not optimal. On the contrary, all the other botanical parts provided higher extraction yields. Among them, green unripe fruits exhibited the greatest value since they represent a great reservoir of not only medium-high and high polarity compounds, including polyphenols (Silva-Beltrán et al., 2015) and SGAs (Friedman, 2002), but also several other components with a high nutritional value, such as sugars, fibers, minerals, and free amino acids (Blum et al., 2005).

Matrices	Extraction yield (g)
FG	0.1663 – 0.2818
SG	0.1480 – 0.1789
LG	0.0998 – 0.1399
RG	0.0830 – 0.1303

Table 67: Extraction yield (g) of different matrices; FG means fruits, SG means stem and branches, LG means leaves and RG means roots.

5.6.4.2. Recovery and matrix effect of glycoalkaloids method

Recovery experiments of α-TM and TD have been performed following the procedure described in paragraphs **5.5.4.1. α-tomatine recovery experiments** and **5.5.4.2. Tomatidine recovery experiments**. The recovery is the closeness of agreement between the true value of the analyte concentration and the experimental results and represents the efficiency of the extraction method for that analyte. Therefore, recovery describes the amount actually recovered by the matrix and is expressed as the percentage (%) yield of the extraction method. According to FDA, a good recovery for the working analytes concentrations for this assay should be between 80-110% (Fda, 2011). About α-TM, the experiment was performed for each class of matrices which were fruits (FG), leaves (LG), stem and branches (SG), and roots (RG), in order to evaluate the recovery of α-TM on different botanical parts. On the other hand, significant amounts of TD were found only in the roots of the plant and not in the other parts, where values under the limit of quantification were found. Therefore, the recovery of TD was evaluated only in tomato plants roots. For the experiments, the matrix was spiked in triplicate either before (pre-extraction spiked) or after (post-extraction spiked) extraction with the solution of the analyte, using three different concentrations according to the values obtained from the quantification. The standard concentrations used for each anatomical part are resumed in **Tables 68**, **69**, **70**, and **71**. They have been selected in a way that even the lowest concentrations could have provided a statistically significant impact on the quantification of each compound for the evaluation of SGAs recovery. The recovery has been therefore investigated by calculating the ratio of the peak area in the pre-extraction spiked samples to the peak area in the post-extraction spiked samples. The ratio was calculated as follows:

$$\textbf{Recovery (\%)} = \left[\left(\frac{\boldsymbol{Peak\ area_{pre-extraction\ spiked\ sample}}}{\boldsymbol{Peak\ area_{post-extraction\ spiked\ sample}}}\right)\boldsymbol{x}\ \mathbf{100}\right]$$

As shown in these tables (**Tables 68**, **69**, **70**, and **71**), the recovery values for both compounds have ranged between 80-110%, for almost all the working analytes concentrations tested, in accordance with FDA guidelines for a good recovery assay (Fda, 2011). After the quantification of SGAs and steroidal alkaloids in the hydroalcoholic extracts, the matrix effect has been investigated to evaluate the correctness and reliability of the quantification data provided by the HPLC-HESI-MS/MS method. Since the matrix may considerably affect the quality of analysis, to provide an accurate estimation of SGAs

content in the matrix, obtained from different botanical parts of Piennolo tomato plants, the matrix effect had to be estimated. For the investigation of the matrix effect, solutions of α-TM and TD analytical standards, at three different concentrations, have been considered and the matrices chosen were the same used for the recovery experiment. The procedure for the evaluation of the matrix effect is accurately described in paragraphs **5.5.5.1. α-tomatine matrix effect experiments** and **5.5.5.2. Tomatidine matrix effect experiments**. The matrix effect was calculated with this ratio:

$$\textbf{Matrix effect (\%)} = \left[\left(\frac{Peak\ area_{post\ extraction\ spiked\ sample} - Peak\ area_{not\ spiked\ sample}}{Peak\ area_{blank}}\right) - 1\right] x\ 100$$

Matrix effect in α-TM analysis ranged from -1.74 ± 1.08 and -8.64 ± 2.20, while matrix effect in TD analysis ranged from -5.64 ± 2.11 and -18.93 ± 2.67 (**Tables 68**, **69**, **70**, and **71**). These negative values can be explained by considering that ion suppression is a far more common phenomenon. On the other hand, the low values provided a good validation of the method's robustness. Therefore, these results allowed an accurate quantitative analysis of the metabolites of interest in the real samples. Matrix effect results obtained in our experiments were compared to literature data to evaluate the efficacy of the procedures for SGAs extraction. These results allowed an accurate quantitative analysis of the metabolites of interest in the samples and are better than those provided by other authors in the literature.

Compound	Spiked (µg)	Recovery (%)	Matrix effect (%)
Rutin	100	86.45 ± 5.52	0.96 ± 0.10
	200	91.26 ± 4.56	1.05 ± 0.13
	400	88.04 ± 8.11	0.82 ± 0.03
Chlorogenic acid	100	100.21 ± 9.37	0.89 ± 0.04
	200	101.52 ± 7.02	0.93 ± 0.07
	400	73.52 ± 4.68	0.85 ± 0.02
α-tomatine	50	97.91 ± 8.50	-4.51 ± 0.48
	100	101.98 ± 1.25	-4.34 ± 1.61
	200	101.91 ± 4.51	-1.74 ± 1.08

Table 68: Spiked (µg) and Recovery % of rutin, chlorogenic acid, and α-TM in green unripe fruits (FG) of Piennolo tomato plants. Values represent the average ± standard deviation of three replicates.

Compound	Spiked (µg)	Recovery (%)	Matrix effect (%)
Rutin	50	103.38 ± 3.80	-22.86 ± 2.13
	100	100.56 ± 0.65	-20.82 ± 0.51
	200	104.00 ± 1.88	-6.73 ± 4.31
Chlorogenic acid	10	102.96 ± 6.02	-14.36 ± 5.11
	20	104.94 ± 7.86	-7.05 ± 3.09
	40	106.10 ± 9.58	-7.73 ± 0.58
α-tomatine	50	95.74 ± 0.41	-6.49 ± 5.70
	100	94.90 ± 8.71	-7.66 ± 0.94
	200	95.54 ± 4.46	-4.90 ± 1.19

Table 69: Spiked (µg) and Recovery % of rutin, chlorogenic acid, and α-TM in leaves (LG) of Piennolo tomato plants. Values represent the average ± standard deviation of three replicates.

Compound	Spiked (µg)	Recovery (%)	Matrix effect (%)
Rutin	10	92.02 ± 11.17	-14.62 ± 6.27
	20	98.87 ± 5.29	-13.98 ± 3.99
	40	99.70 ± 3.14	-15.17 ± 2.33
Chlorogenic acid	10	92.68 ± 3.20	-13.57 ± 2.13
	20	97.56 ± 6.04	-14.67 ± 2.46
	40	95.92 ± 3.80	-11.35 ± 1.03
α-tomatine	50	102.63 ± 2.75	-8.64 ± 2.20
	100	93.93 ± 3.77	-8.17 ± 0.77
	200	96.28 ± 5.90	-4.70 ± 1.77

Table 70: Spiked (µg) and Recovery % of rutin, chlorogenic acid, and α-TM in stem and branches (SG) of Piennolo tomato plants. Values represent the average ± standard deviation of three replicates.

Compound	Spiked (µg)	Recovery (%)	Matrix effect (%)
Rutin	5	100.63 ± 4.46	38.38 ± 3.16
	10	99.94 ± 2.21	12.50 ± 9.79
	20	100.61 ± 2.49	15.16 ± 0.76
Chlorogenic acid	5	100.94 ± 0.81	17.26 ± 5.18
	10	101.40 ± 3.23	1.16 ± 3.98
	20	100.06 ± 1.61	-8.94 ± 0.40
α-tomatine	50	97.53 ± 6.37	-7.67 ± 1.70
	100	96.33 ± 1.62	-6.04 ± 2.31
	200	100.19 ± 1.36	-5.63 ± 5.17
Tomatidine	1	96.08 ± 9.54	-18.93 ± 2.67
	10	110.60 ± 10.79	-8.53 ± 4.50
	20	113.33 ± 10.47	-5.64 ± 2.11

Table 71: Spiked (µg) and Recovery % of rutin, chlorogenic acid, α-TM and TD in roots (RG) of Piennolo tomato plants. Values represent the average ± standard deviation of three replicates.

5.6.4.3. Recovery and matrix effect of polyphenols method

Recovery experiments of polyphenols were performed by selecting the two most abundant compounds of this class, found in each anatomical part of tomato plants, which were rutin, among flavonoids, and chlorogenic acid, among not-flavonoids. Since polyphenols represent a very large and heterogeneous class of metabolites, our interest was focused only on the two most abundant and representative compounds found in our plant matrices, in agreement with the HPLC-DAD analysis conducted on the extracts. The procedure, provided in the previous paragraph **5.5.4.3. Polyphenols recovery experiments** was performed by spiking in triplicate a mixture solution of the two analytes, either before (pre-extraction spiked) or after (post-extraction spiked) extraction, using three different concentrations according to the values obtained from the quantification. The standard concentrations used for each anatomical part are resumed in **Tables 68**, **69**, **70**, and **71**. They have been selected in such a way that even the lowest concentrations could have provided a statistically significant impact on the quantification of each compound for the evaluation of SGAs recovery. The ratio for the evaluation of the recovery is provided in the previous paragraph **5.5.4.1. α-tomatine recovery extraction**. The recovery values obtained for each anatomical part ranged between 80 and 110%, thus suggesting an excellent recovery from the matrix, in full agreement with the FDA guidelines (**Tables 68**, **69**, **70**, and **71**). The accurate choice of the hydroalcoholic solvent acidified at 1%, the use of a favorable solid-to-solvent ratio, and the suitable setting of the centrifuge and orbital shaker's parameters have led to the excellent recovery of rutin and chlorogenic acid from all the plant matrices. These results fully agree with those provided in rutin recovery experiment reported in the paragraph **4.3.8.3. Validation of rutin extraction**.

As previously described, the HPLC-MS/MS analysis is often subject to ion enhancement or suppression phenomena (depending on the type of matrix) which may invalidate the quantitative analysis, resulting in an overestimation or underestimation, compared to the true value. Differently, matrix effect in the HPLC-DAD analysis is mainly due to other phenomena. In this case, co-eluting substances from the sample matrix may represent the main interferents in the analytical method, thus compromising its performance. According to Lambert-Beer's law, if there are no interactions between the components, the individual absorbances are additive. For this reason, a strong signal enhancement can be observed when the analyte and the co-eluting compound have the same retention time. On the other hand, signal suppression may be noticed mainly as a result of impre(Rejczaaak & Tuzimski,

2017; Ribas-Agustí et al., 2012)ak & Tuzimski, 2017; Ribas-Agustí et al., 2012). Matrix effect values in the HPLC-DAD analysis of rutin and chlorogenic acid, for each botanical part of tomato plants, are accurately described in **Tables 68**, **69**, **70**, and **71** and were calculated using the ratio provided in the previous paragraph **5.5.5.1. α-tomatine matrix effect experiments**. These values clearly show that hydroalcoholic extracts of green unripe fruits (FG) provide the best performance, since their matrix effect is close to 0 (values ranged from 0.82 ± 0.03 and 1.05 ± 0.13). On the other hand, leaves extracts (LG) and stem extracts (SG) exhibit negative and higher matrix effect values, which range from -6.73 ± 4.31 and -22.86 ± 2.13. Moreover, high and positive matrix effect values were found in the analysis of roots extracts (RG), whose values achieve a maximum of 38.38 ± 3.16 %. The heterogeneity of these results is largely due to the different features of the starting matrices, which can be characterized by different interfering substances. Very few authors throughout the literature investigated the matrix effect on the HPLC-DAD analysis of polyphenols and how this effect may affect different botanical parts of tomato plants. Overall, our HPLC-DAD analysis provided acceptable values of the matrix effect in the most of selected samples and allowed us to achieve a good selectivity and resolution.

5.6.5. Metabolomics analysis of Piennolo tomato plants

5.6.5.1. Qualitative profile of Piennolo tomato plants

The qualitative analysis of Piennolo green tomato extracts by HPLC-HESI-MS/MS allowed to putatively identify 11 compounds by comparison with literature data and with the characterization previously described in the paragraph **3.3.2.1. Glycoalkaloids profile of green tomatoes**. The retention time, the quasi-molecular ion, the molecular formula, and the fragment ions were listed in the **Table 72**. The table include the most characteristic glycosylated alkaloids (**4**: hydroxytomatine; **9**: acetoxyhydroxytomatine; **11**: dehydrotomatine; **12**: tomatidine tetrahexoside; **13**: α-TM; **14**: acetoxytomatine; **16**: dehydrotomatidine tetrahexoside) and aglycone alkaloids (**77**: TD; **78**: dehydrotomatidine; **79**: hydroxytomatidine; **80**: dehydrohydroxytomatidine) of the unripe tomatoes. The fragmentation of these 11 compounds agreed with the fragmentation previously reported in the paragraph **3.3.2.1. Glycoalkaloids profile of green tomatoes**. Interestingly, the fragmentation pattern of the compound dehydro-hydroxytomatidine (**80**) has not been reported in the literature. For this putative new TD analogue, fragmentation pattern elucidation was obtained in analogy to TD (**77**) tandem mass spectrum.

No.	Compound	R_t	Precursor ion $[M+H]^+$	Characteristic fragment ions	Ref.
4	Hydroxytomatine	4.68	1050.60	1032.57 $[M+H-H_2O]^+$, 918.71 $[M+H-Pent]^+$, 756.60 $[M+H-Pent-Hex]^+$, 576.48 $[M+H-Pent-2Hex-H2O]^+$, 414.50 $[M+H-Pent-3Hex-H_2O]^+$	(Dzakovich et al., 2020)
11	Dehydrotomatine	4.98	1032.62	1014.55 $[M+H-H_2O]^+$, 900.64 $[M+H-Pent]^+$, 870.56 $[M+H-Hex]^+$, 576.54 $[M+H-Pent-2Hex]^+$, 414.38 $[M+H-Pent-3Hex]^+$	(Itkin et al., 2011)
16	Dehydrotomatidine tetrahexoside	4.98	1062.62	1044.54 $[M+H-H_2O]^+$, 900.56 $[M+H-Hex]^+$, 738.66 $[M+H-2Hex]^+$, 576.56 $[M+H-3Hex]^+$, 414.41 $[M+H-4Hex]^+$	(Itkin et al., 2011)
14	Acetoxytomatine	5.00	1092.63	1032.58 $[M+H-AcOH]^+$, 900.64 $[M+H-Pent-AcOH]^+$, 738.67 $[M+H-Pent-Hex-AcOH]^+$, 576.63 $[M+H-Pent-2Hex-AcOH]^+$, 414.53 $[M+H-Pent-3Hex-AcOH]^+$	(Itkin et al., 2011)

12	Tomatidine tetrahexoside	5.00	1064.70	1046.63 $[M+H-H_2O]^+$, 902.66 $[M+H-Hex]^+$, 740.65 $[M+H-2Hex]^+$, 578.41 $[M+H-3Hex]^+$, 416.37 $[M+H-4Hex]^+$	(Itkin et al., 2011)
13	α-TM	5.02	1034.46	1016.61 $[M+H-H_2O]^+$, 902.51 $[M+H-Xyl]^+$, 740.58 $[M+H-Xyl-Glu]^+$, 578.66 $[M+H-Xyl-2Glu]^+$, 416.46 $[M+H-Xyl-2Glu-Gal]^+$	(Caprioli et al., 2014)
80	Dehydro-hydroxytomatidine	5.33 (isomer 1); 5.63 (isomer 2)	430.50	412.4 $[M+H-H_2O]^+$, 273.2 $[M+H-C_8H_{15}NO_2]^+$, 255.1$[M+H-C_8H_{17}NO_3]^+$, 161.1 $[M+H-C_{15}H_{27}NO_3]^+$	(Heinig & Aharoni, 2014)
79	Hydroxytomatidine	5.44	432.40	414.30 $[M+H-H_2O]^+$, 273.22 $[M+H-C_8H_{17}NO_2]^+$, 255.22 $[M+H-C_8H_{19}NO_3]^+$, 126.10 $[M+H-C_{19}H_{30}O_3]^+$	(Heinig & Aharoni, 2014)
78	Dehydrotomatidine	5.77 (isomer 1); 6.08 (isomer 2)	414.60	396.33$[M+H-H_2O]^+$, 271.21$[M+H-C_8H_{17}NO]^+$, 253.19 $[M+H-C_8H_{19}NO_2]^+$, 161.13 $[M+H-C_{15}H_{27}NO_2]^+$, 126.13 $[M+H-C_{19}H_{28}O_2]^+$	(Heinig & Aharoni, 2014)
9	Acetoxy-hydroxytomatine	5.84	1108.54	1048.57 $[M+H-AcOH]^+$, 1030.62 $[M+H-H_2O-AcOH]^+$, 1001.65 $[M+H-H_2O-AcOH-CH_3N]^+$, 652.64 $[M+H-Pent-2Hex]^+$, 412.43 $[M+H-Pent-3Hex-H_2O-AcOH]^+$	(Itkin et al., 2011)
77	Tomatidine	5.88	416.50	398.34 $[M+H-H_2O]^+$, 273.22 $[M+H-C_8H_{17}NO]^+$, 255.21 $[M+H-C_8H_{19}NO_2]^+$, 161.13 $[M+H-C_{15}H_{29}NO_2]^+$, 126.12 $[M+H-C_{19}H_{30}O_2]^+$	(Caprioli et al., 2015)

Table 72: Qualitative SGAs and alkaloids analysis of Piennolo green tomato extracts.

5.6.5.2. Quantitative profile of Piennolo tomato plants

After the validation of the extraction procedure, the hydroalcoholic extracts were used for a qualitative analysis via HPLC-MS/MS and HPLC-DAD, to evaluate the SGAs and polyphenolic content, respectively. Plant matrices used in this project were extracted following the procedure described in paragraph **5.5.3. Samples extraction**. Then, the extracting method was validated by calculating the recovery rate of different compounds of interest, as described in the paragraph **5.6.4. Validation of the extraction procedure**. Once the extraction procedure and its validation were carried out, samples were analyzed

following the protocol provided in the paragraphs **5.5.10. Quantitative glycoalkaloids analysis** and **5.5.11. Quantitative polyphenols analysis**. Overall, 18 different secondary metabolites of two main chemical classes were quantified in the analyzed matrices. Specifically, among SGAs seven metabolites were detected (i.e., α-TM, dehydrotomatine, acetoxytomatine, tomatidine tetrahexoside, dehydrotomatidine tetrahexoside, hydroxytomatine, and acetoxy-hydroxytomatine). Moreover, other four compounds belonging to this class and structurally correlated to the steroidal aglycone TD were analyzed (i.e., TD, dehydrotomatidine, hydroxytomatidine, and dehydro-hydroxytomatidine). For polyphenols quantification, seven selected metabolites representative of tomato plants were quantified (i.e., rutin, chlorogenic acid, ferulic acid, gallic acid, *p*-coumaric acid, quercetin, and quercetin-*O*-xylosil-rutinoside). The content of these metabolites was investigated in different matrices, in order to evaluate the effect of the biological treatment with *Trichoderma* spp. and the harvesting period, by comparing different cultivars and then different anatomical parts of a selected cultivar, as described in the paragraph **5.6.1. Samples collection**. An accurate description of the sampling is provided in the paragraph **5.5.2. Cultivar selection and matrix preparation**.

All data obtained for SGAs by HPLC-MS/MS analysis and polyphenols by HPLC-DAD analysis were collected in tables, where the amount of these metabolites was described for each group. A single group represented one of the 34 matrices considered for this project, which was extracted in triplicate. The results of the quantification, obtained by analyzing each triplicate, were expressed as mean ± SD (µg/g dried matrix or mg/g dried matrix) and reported in tables. A statistical significance was calculated by one-way ANOVA, followed by Tukey's post-hoc test. In this test, different letters within each bar revealed significant differences among groups. Subsequently, statistical metabolic differences among groups of samples, due to the biological treatment with *Trichoderma* spp. and/or different harvesting times, were evaluated by performing a Partial Least Square Discriminant Analysis (PLS-DA), accompanied by the cross-validation test and VIP (Variable Important for Projection) scores test. In addition, a heatmap combined with a hierarchical clustering was performed as well.

5.6.5.2.1. Comparison between green tomato cultivars

As a first step of this project, two different cultivars of green discarded Piennolo tomatoes, belonging to two different ecotypes, were used to evaluate their SGAs and polyphenol content, as described in Chapter **5.6.1. Samples collection**. Therefore, "*San Sebastiano*"

green tomato extracts and "*Ercolano*" green tomato extracts, both in the 1st and 2nd harvesting (June and July 2022, respectively) were analyzed for SGAs and polyphenols analysis. Data obtained from the quantification in triplicate were used to perform a PLS-DA 2D analysis (**Figure 81A** and **81B**), a cross-validation test (**Figure 81C**), a VIP score test (**Figure 81D**) and a Heatmap with hierarchical clustering (**Figure 81E**). **Figure 81A**, which describes 63% of the data variance, is based on a comparison between Component 1 (43.2% of the variance) and Component 2 (19.8% of the variance). In particular, Component 1 clearly divides the groups based on the corresponding cultivar, thus providing a difference between the *Ercolano* cultivar and the *San Sebastiano* cultivar, since these two groups are spatially far. Specifically, *San Sebastiano* cultivars are described by a negative Component 1 while *Ercolano* cultivars are described by a positive Component 1. Moreover, Component 2 allows the groups to be divided according to their harvesting period. Therefore, both *Ercolano* and *San Sebastiano* discarded green tomatoes harvested in June-July 2022 (1st harvesting) display some differences in the metabolic profile from those obtained in July-August 2022 (2nd harvesting). As a matter of fact, cultivars obtained during the 1st harvesting are described by a negative Component 2, while those obtained during the 2nd harvesting are described by a positive Component 2. On the other hand, Component 3 (9.6% of the variance) does not provide a clear distribution of groups and does not allow dividing cultivars according to their harvesting period. Therefore, for both cultivars, a clear overlap between 1st harvesting and 2nd harvesting samples is shown. Therefore, Component 3 exhibits a poorer ability to describe the data variance, and according to the Cross-validation test it can be discarded. This test (**Figure 81C**) clearly shows that Component 1 and Component 2 are sufficient to describe the data variance, by considering the Q^2 value. Differences in group distribution can be rationalized and explained by a small number of metabolites, as described in the VIP-score test (**Figure 81D**). Overall, three compounds belonging to the SGAs class (i.e., acetoxytomatine, dehydrotomatine, and acetoxy-hydroxytomatine) and two compounds belonging to the polyphenols class (i.e., rutin and quercetin-*O*-xylosil-rutinoside) are responsible for data variance. These data fully agree with those provided by **Table 73** for each compound. Acetoxytomatine and dehydrotomatine values provided by the *San Sebastiano* cultivar are two and three times higher, respectively, compared to the *Ercolano* cultivar. Therefore, these values were found to be statistically different, according to the one-way ANOVA test. Moreover, approximately 20 µg of acetoxy-hydroxytomatine/g of dried matrix has been found in discarded green tomatoes from *San Sebastiano*, while those from *Ercolano* exhibit values under the LOQ. On the

contrary, **Table 74** does not clearly show a statistical difference between these two cultivars in terms of rutin and quercetin-*O*-xylosil-rutinoside content. *Ercolano* 2nd harvesting cultivar is statistically different from all the others in terms of quercetin-*O*-xylosil-rutinoside content. On the other hand, *San Sebastiano* 1st harvesting cultivar differs from the others in terms of rutin content. Interestingly, the VIP-score graphic does not show α-TM among the main metabolites responsible for the data variance (VIP score = 0.6). However, this compound is characterized by statistically different values between the two cultivars and in particular two times higher in the *San Sebastiano* cultivar.

Sample	α-TM	Dehydrotomatine	Acetoxytomatine	Tomatidine tetrahexoside	Acetoxyhydroxy tomatine
	mg α-TM/g DW ± SD	µg α-TM eq/g DW ± SD			
San Sebastiano discarded green tomatoes, 1st harvesting	4.41 ± 0.21[a]	308.19 ± 43.74[a]	253.28 ± 16.98[a]	49.84 ± 3.70[a]	21.75 ± 2.00[a]
San Sebastiano discarded green tomatoes, 2nd harvesting	4.31 ± 0.32[a]	299.11 ± 31.57[a]	225.53 ± 34.28[a]	60.70 ± 5.37[b]	22.74 ± 3.40[a]
Ercolano discarded green tomatoes, 1st harvesting	2.12 ± 0.26[b]	132.62 ± 7.29[b]	110.63 ± 12.69[b]	11.54 ± 1.60[c]	< LOQ
Ercolano discarded green tomatoes, 2nd harvesting	2.64 ± 0.32[b]	167.18 ± 14.08[b]	63.52 ± 4.64[c]	19.95 ± 3.00[d]	< LOQ

Table 73: content of five selected SGAs in *Ercolano* and *San Sebastiano* cultivars (both in 1st and 2nd harvesting), indicated as mg/g dried matrix and µg/g dried matrix. Results are expressed as mean ± SD. Statistical significance was calculated by one-way ANOVA followed by Tukey's post-hoc test. Different letters in each bar reveal significant differences.

Sample	Gallic acid	Quercetin	Chlorogenic acid	Quercetin 3-*O*-xylosylrutinoside	Rutin	*p*-coumaric acid	Ferulic acid
	µg/g DW± SD						
San Sebastiano discarded green tomatoes, 1st harvesting	66.53 ± 6.82[a]	17.58 ± 0.83[a]	550.52 ± 8.95[a]	221.69 ± 3.83[a]	384.12 ± 8.56[a]	10.39 ± 0.42[a]	7.43 ± 0.34[a]
San Sebastiano discarded green tomatoes, 2nd harvesting	28.08 ± 5.34[b]	14.27 ± 0.59[b]	492.66 ± 26.41[a]	247.04 ± 17.58[a]	863.36 ± 67.57[b]	11.67 ± 0.76[a]	9.32 ± 1.97[a]
Ercolano discarded green tomatoes, 1st harvesting	47.73 ± 2.33[c]	22.13 ± 0.94[c]	601.71 ± 90.15[a]	260.22 ± 16.97[a]	771.92 ± 0.35[b]	8.90 ± 0.35[b]	19.01 ± 0.69[b]
Ercolano discarded green tomatoes, 2nd harvesting	42.96 ± 9.73[b,c]	17.48 ± 1.11[a]	793.54 ± 61.19[b]	308.59 ± 31.37[b]	962.30 ± 59.50[b]	11.91 ± 0.90[a]	9.41 ± 1.71[a]

Table 74: content of seven selected polyphenols in *Ercolano* and *San Sebastiano* cultivars (both in 1st and 2nd harvesting), indicated as µg/g dried matrix. Results are expressed as mean ± SD. Statistical significance was calculated by one-way ANOVA followed by Tukey's post-hoc test. Different letters in each bar reveal significant differences.

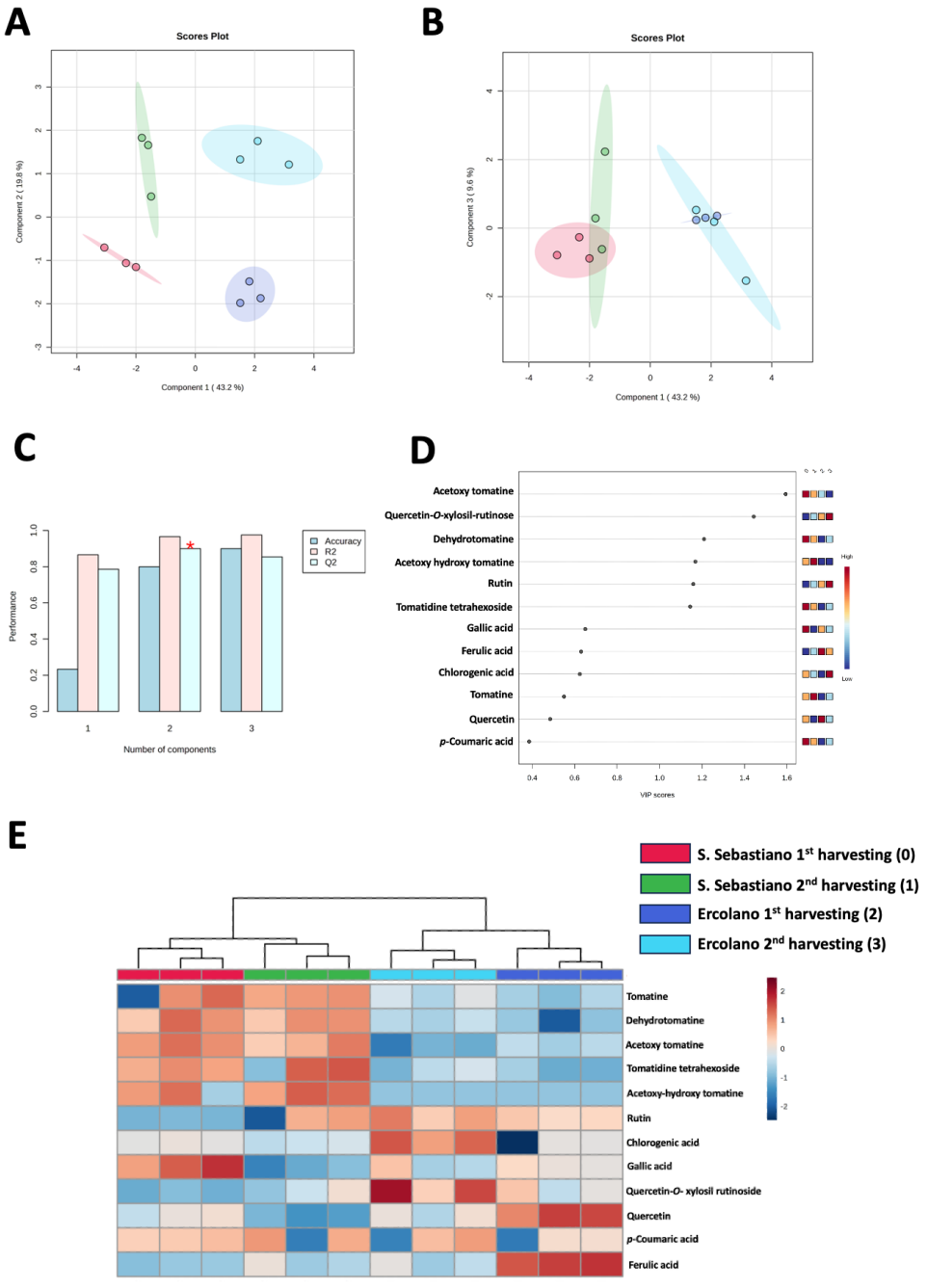


Figure 81: Multivariate analysis. (**A**) and (**B**) Partial least square discriminant analysis (PLS-DA) scores plot, corresponding to a model aimed at the discrimination between cultivars. The colored ellipses denote 95% confidence intervals for each tomato cultivar. (**C**) Cross-validation test, used to assess the correct number of Components to consider, according to the Q^2 value. (**D**) Variable importance on projection (VIP) scores from the PLS-DA model, indicating the most discriminating metabolites between cultivars in descending order of importance and with relative levels of metabolites for each cultivar. (**E**) Heatmap with Hierarchical clustering, illustrating the relative metabolite concentration

among cultivars. The corresponding relative metabolite concentration is expressed as a color of different intensity from blue (lowest amount) to red (highest amount).

Furthermore, the results obtained from the PLS-DA analysis and the VIP-score test substantially agree with those represented in the Heatmap and in the Hierarchical clustering. As a matter of fact, the statistical difference between *San Sebastiano* and *Ercolano* discarded green tomatoes is confirmed by the dendrogram, where the difference between these two cultivars is expressed as a different distance of the columns from a node, by a clustering calculation. Interestingly, the heatmap is able not only to describe the differences between the groups but also the amount of that analyte in each group, through a color map at different intensities. As confirmed by the VIP-score test (**Figure 81D**) and **Table 73**, the *San Sebastiano* cultivar displays an overall higher SGAs content, even if the *Ercolano* cultivar is characterized by a higher polyphenol content. The heatmap also provides a precise distinction between different harvesting times within a given cultivar. For example, the chlorogenic acid (**14**) content is substantially greater in the 2nd harvest of the *Ercolano* cultivar rather than in the 1st, as also confirmed by **Table 74**, where the values are statistically different based on the harvesting, and they are 793.54 ± 61.19 µg of chlorogenic acid/g of dried matrix in the 2nd harvest and 601.71 ± 90.15 µg of chlorogenic acid/g of dried matrix in the 1st harvest. On the other hand, quercetin (**13**) and ferulic acid (**15**) content is higher in the 1st harvesting of *Ercolano* cultivar rather than in the 2nd, as confirmed by the one-way-ANOVA test in the **Table 74**.

Overall, the San Sebastiano cultivar was found to be a better starting plant material for further metabolomic studies and investigations for the higher SGAs content, which are the main metabolites of interest for our nutraceutical purposes. For this reason, the green Piennolo tomatoes of *San Sebastiano* (belonging to the landrace “Principe Borghese” and to the ecotype “Acampora”) were used to investigate the effect of several biological parameters on the metabolic profile of the plant.

5.6.5.2.2. Evaluation of harvesting period

Unripe green tomatoes of *San Sebastiano* cultivar have been used in this project to investigate the effect of the harvesting period on the metabolic profile of the fruit. Specifically, our aim was to find a correlation between this parameter and a change in the SGAs and polyphenol content, thus providing the best period for the fruit harvest, according to our nutraceutical purposes. Therefore, samples were collected and divided into four groups, according to their harvesting period and the presence/absence of the biological

treatment with *Trichoderma* spp. The first group was made up of plants not treated with *Trichoderma* spp., whose harvesting of unripe tomatoes was carried out two times in two consecutive periods: June-July for the **1st harvesting** samples (A-FG 1st harvesting) and July-August for the **2nd harvesting** samples (A-FG 2nd harvesting). The second group was made up of plants not treated with *Trichoderma* spp., whose harvest of fruits was carried out only once, i.e., directly in July-August (AS-FG). An accurate description of the sample collection and nomenclature is provided in Chapter **2.1. Cultivar selection and preparation of the matrix**. The purpose was to understand if the 1st harvest of green tomatoes from the early fruit trusses could cause some stress and therefore some relevant metabolic changes in the tomatoes of the 2nd harvest (i.e., A-FG 2nd harvesting). Furthermore, another purpose was to understand if the A-FG 2nd harvesting samples differed from the AS-FG ones, thus investigating again the effect of harvesting fruits from the early fruit trusses or not. Finally, we tried to understand which of these collection methods was best and thus provided the best metabolic profile. Therefore, tomato extracts were analyzed in triplicate for their SGAs and polyphenol content, and data obtained from the quantification were used to perform a chemometric analysis, including the PLS-DA 2D analysis (**Figure 82A, 82B** and **82C**), the cross-validation test (**Figure 82D**), the VIP score test (**Figure 82E**) and the Heatmap with hierarchical clustering (**Figure 82F**).

The PLS-DA 2D analysis (**Figure 82A**), which describes 72.3 % of the data variance, is based on a comparison between Component 1 (47.7% of the variance) and Component 2 (24.6% of the variance). According to Component 1, a clear division of groups can be obtained based on their harvesting period, since A-FG 1st harvesting sample is described by a negative Component 1, while AS-FG and A-FG 2nd harvesting samples are both described by a positive Component 1. In addition, Component 2 allows to further differentiate the A-FG 2nd harvesting sample from the AS-FG sample, since they do not overlap in the graphic. On the contrary, according to Component 3 (12.5% of the variance) and Component 4 (5.2% of the variance), there is no difference between these two samples, and therefore a clear overlap is shown (**Figure 82B** and **82C**). However, the cross-validation test (**Figure 82D**) suggests considering all four Components for the PLS-DA analysis, according to the Q^2 value. Therefore, the A-FG 2nd harvesting sample and the AS-FG sample can be considered overall similar, while a clear difference is provided between the 1st harvesting group and both the 2nd harvesting groups. By exploring the metabolites responsible for this variance, the VIP-score test (**Figure 82E**) provides both SGAs and polyphenols, including rutin, the

most abundant phenolic compound in all green tomato samples, hydroxytomatidine, tomatidine tetrahexoside, α-TM, dehydrotomatine, gallic acid, and chlorogenic acid. Moreover, the VIP score test allows us to describe an overall higher SGAs content in the A-FG 2nd harvesting sample and a higher polyphenolic content in the AS-FG sample, thus highlighting further interesting differences in the secondary metabolites profile of these two groups. Data obtained from the PLS-DA 2D analysis and from the VIP score test are substantially confirmed by the Heatmap and the Hierarchical clustering (**Figure 82F**), where a poorer metabolic profile of the 1st harvesting sample is shown, as demonstrated by the blue color for almost all the compounds, except for quercetin. As a matter of fact, a difference among groups according to their harvesting period is confirmed by the dendrogram, where the difference between these two main groups is expressed as a different distance of the columns from a node, by using a clustering calculation. An interesting trend concerns glycosylated metabolites, such as rutin, which are present in very low amounts during the first harvest (A-FG 1st harvesting) and at much higher levels in samples deriving from the 2nd harvest (AS-FG and A-FG 2nd harvesting). On the contrary, aglycone metabolites such as quercetin, a biosynthetic precursor of rutin, are present at very high levels in the A-FG 1st harvesting sample, but its content decreases during the 2nd harvesting, as also confirmed by the Heatmap and by the **Table 75**. In particular, the rutin content in the A-FG 1st harvesting group is equal to 252.04 ± 17.71 µg/g of dried matrix, while that found in the AS-FG and A-FG 2nd harvesting groups is equal to 576.69 ± 88.23 µg/g and 681.44 ± 12.82 µg/g, respectively, i.e., more than twice higher and statistically different, according to the one-way ANOVA test.

These data clearly suggest that the biosynthesis of rutin achieves its maximum content only during the 2nd harvest and that, at the same time, the precursor quercetin relatively accumulates during the 1st harvest and is converted in rutin during the 2nd harvest. This same trend is also repeated in the class of SGAs for the compound α-TM, which represents one of the main metabolites that explain the data variance (VIP score = 1.2). As a matter of fact, this compound is present in very high quantities in the A-FG 2nd harvesting and AS-FG groups, while it was found at very low levels in the A-FG 1st harvesting group. As described by **Table 76**, α-TM content is five times higher in the samples derived from the 2nd harvesting, compared to the 1st harvesting.

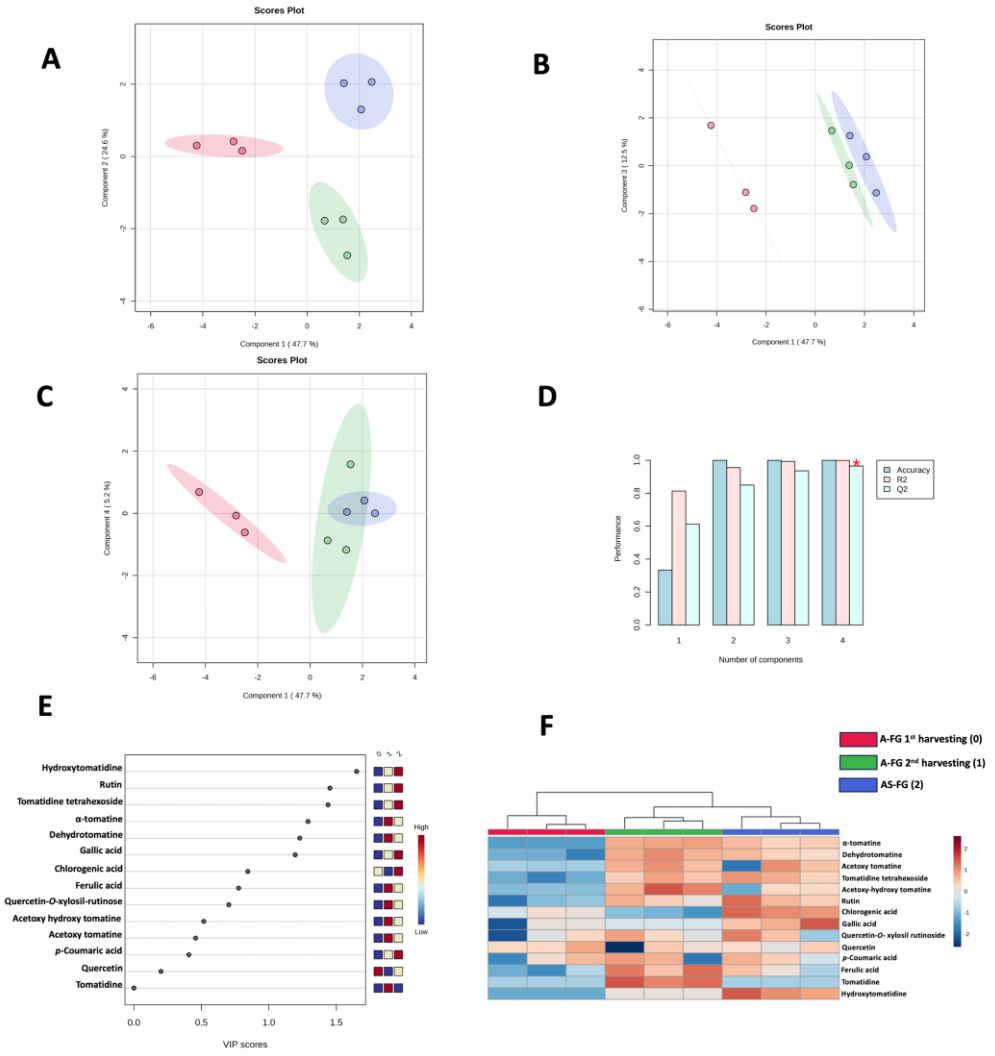


Figure 82: Multivariate analysis. (**A**), (**B**) and (**C**) Partial least square discriminant analysis (PLS-DA) scores plot, corresponding to a model aimed at the discrimination between untreated green tomatoes (FG). The colored ellipses denote 95% confidence intervals for each group. (**D**) Cross-validation test, used to assess the correct number of Components to consider, according to the Q^2 value. (**E**) Variable importance on projection (**VIP**) scores from the PLS-DA model, indicating the most discriminating metabolites between samples in descending order of importance and with relative levels of metabolites for each cultivar. (**F**) Heatmap with Hierarchical clustering, illustrating the relative metabolite concentration among groups. The corresponding relative metabolite concentration is expressed as a color of different intensity from blue (lowest amount) to red (highest amount).

Sample	Gallic acid	Quercetin	Chlorogenic acid	Quercetin 3-*O*-xylosylrutinoside	Rutin	*p*-coumaric acid	Ferulic acid
			µg/g DW± SD				
A-FG 1st harvesting	55.22 ± 2.44[a]	12.30 ± 1.10[a]	298.4 ± 30.0[a]	178.40 ± 13.94[a]	252.04 ± 17.71[a]	9.0 ± 1.1[a]	7.8 ± 1.1[a]
AT-FG 1st harvesting	54.22 ± 8.92[a,b]	15.49 ± 0.71[b]	307.7 ± 9.2[b]	195.36 ± 5.25[a]	267.49 ± 9.80[a]	9.6 ± 0.3[a]	6.8 ± 0.5[a]
A-FG 2nd harvesting	48.50 ± 0.40[a]	11.90 ± 0.70[a]	123.0 ± 40.9[c]	196.15 ± 34.92[a]	576.69 ± 88.23[b]	10.3 ± 0.5[a]	12.7 ± 1.0[a]
AT-FG 2nd harvesting	65.81 ± 4.42[b,c]	n.d.	357.9 ± 11.4[a]	259.26 ± 13.44[a]	804.50 ± 45.05[c]	13.2 ± 0.4[b]	5.7 ± 0.2[a]
AS-FG	76.20 ± 12.20[c]	11.40 ± 0.80[a]	485.0 ± 32.0[d]	194.16 ± 69.84[a]	681.14 ± 120.82[b,c]	8.4 ± 1.9[a]	10.3 ± 1.4[b]
AST-FG	67.49 ± 4.02[b,c]	12.04 ± 1.45[a]	293.4 ± 11.9[a]	244.41 ± 20.19[a]	793.17 ± 59.60[c]	10.24 ± 1.73[a]	12.9 ± 0.2[c]

Table 75: content of five selected SGAs in untreated green fruits (FG), indicated as µg/g dried matrix. Results are expressed as mean ± SD. Statistical significance was calculated by one-way ANOVA followed by Tukey's post-hoc test. Different letters in each bar reveal significant differences. "n.d." means "not detected".

Sample	α-TM	Dehydrotomatine	Acetoxytomatine	Tomatidine tetrahexoside	Acetoxyhydroxy tomatine
	mg α-TM/g DW ± SD		µg α-TM eq/g DW ± SD		
A-FG 1st harvesting	1.62 ± 0.01[a]	126.50 ± 2.77[a]	145.03 ± 6.10[a]	17.64 ± 0.23[a]	6.27 ± 0.84[a]
AT-FG 1st harvesting	2.26 ± 0.02[b]	89.45 ± 2.24[a]	72.95 ± 7.35[b]	11.42 ± 1.02[a]	< LOQ
A-FG 2nd harvesting	5.24 ± 0.12[c]	508.34 ± 37.75[b]	296.88 ± 22.94[c]	69.63 ± 7.07[b]	36.14 ± 6.02[b]
AT-FG 2nd harvesting	7.90 ± 0.63[d]	572.02 ± 32.46[c]	398.70 ± 52.22[d]	107.87 ± 8.61[c]	41.97 ± 6.29[b]
AS-FG	4.62 ± 0.21[c]	422.72 ± 39.50[d]	309.43 ± 32.98[c]	72.79 ± 9.66[b]	25.40 ± 2.77[c]
AST-FG	5.54 ± 0.10[c]	150.62 ± 8.14[a]	118.57 ± 5.07[a,b]	26.02 ± 0.40[a]	3.43 ± 0.90[a]

Table 76: content of five selected SGAs in untreated green fruits (FG), indicated as µg/g dried matrix. Results are expressed as mean ± SD. Statistical significance was calculated by one-way ANOVA followed by Tukey's post-hoc test. Different letters in each bar reveal significant differences.

Other considerations can be provided for green unripe tomatoes treated with the biological control agent (BCA) *Trichoderma* spp. As previously described for the untreated samples, the treated ones were also divided into two further groups based on the harvest period. The first group was made up of plants treated with *Trichoderma* spp., whose harvesting of unripe tomatoes was carried out two times and in two consecutive periods: June-July for the **1st harvesting** samples (AT-FG 1st harvesting) and July-August for the **2nd harvesting** samples (AT-FG 2nd harvesting). The second group was made up of plants treated with *Trichoderma spp.*, whose harvesting of the later fruit trusses was carried out only once, directly in July-August (AST-FG) as described in the previous chapter **2.1. Cultivar selection and preparation of the matrix**.

Therefore, tomato extracts were analyzed in triplicate for their SGAs and polyphenol content, and data obtained from the quantification were used to perform a chemometric analysis, including the PLS-DA 2D analysis (**Figure 83A,** and **83B**), the cross-validation

test (**Figure 83C**), the VIP score test (**Figure 83D**) and the Heatmap with hierarchical clustering (**Figure 83E**). As shown by the PLS-DA analysis in **Figure 83A**, which describes 71.3% of the data variance, Component 1 (40.6% of the variance) clearly allows treated matrices to be divided according to their harvesting period, since AT-FG 1st harvesting sample is described by a negative Component 1 and AST-FG and AT-FG 2nd harvesting samples are both described by a positive Component 1. In addition, Component 3 (11.1% of the data variance) do not provide a clear distinction between the AST-FG sample and the AT-FG 2nd harvesting sample, since these two groups are overlap in the graphic. On the other hand, according to Component 2 (30.7%) these two groups cannot be considered similar and so they are spatially divided. By considering the contribution of three components, as suggested by the cross-validation test based on the Q^2 value (**Figure 83C**), a clear difference can be confirmed only between the treated matrices deriving from the 1st harvest and those derived from the second. More interesting considerations can be provided by observing the VIP-score test (**Figure 83D**). Among the secondary metabolites responsible for the data variance, a group of great interest is represented by the aglycone compounds quercetin, hydroxytomatidine and TD, which are the biosynthetic precursors of rutin, hydroxytomatine, and α-TM, respectively. As matter of fact, they are greatly higher in treated green tomatoes deriving from the first harvesting (AT-FG 1st harvesting sample), but their content drastically decreases in matrices deriving from the 2nd harvesting (AST-FG and A-FG 2nd harvesting). On the other hand, glycosidic compounds such as rutin and α-TM are very low during the 1st harvesting, while they are enhanced during the second. These data are substantially confirmed by observing **Tables 75** and **76**, where rutin and α-TM content is more than two times higher in the 2nd harvesting samples compared to the 1st, and statistically different according to the one-way ANOVA test. This phenomenon confirms the trend observed for the untreated green tomatoes, thus strongly suggesting that the biosynthesis of several compounds of interest, both polyphenols and SGAs, is time-dependent. The concept of time-dependent is not related to the time maturation of the fruit, since the α-TM content in the tomato is not linear, but achieves its maximum in the immature fruit and drastically decreases with the ripening process (Friedman, 2002). Instead, this concept is closely related to the time of plant maturation, where "1st harvesting samples" represent matrices sampled in June, and "2nd harvesting samples" are the matrices collected in July. This difference is also confirmed in the Heatmap graph with Hierarchical clustering (**Figure 83E**). As a matter of fact, a difference among groups belonging to different harvesting periods is expressed by the dendrogram as a different distance of the

columns from the first node, according to the clustering calculation. A predominant blue color (indicating an overall low amount) is provided for almost all the metabolites belonging to the 1st harvesting samples, except for some specific aglycon compounds, as reported just above. On the contrary, a predominant red color (indicating a relatively great amount) is provided by the 2nd harvesting samples, in particular for the AT-FG 2nd harvesting sample. As reported in the VIP score test, the aglycone compounds quercetin, hydroxytomatidine, and TD drastically decrease during the 2nd harvesting, replaced by the corresponding glycosides. Interestingly, the hierarchical clustering can highlight a difference between groups belonging to the 2nd harvesting, and according to the different pattern of color on the heatmap, the AT-FG 2nd harvesting sample seems to provide an overall better response to the treatment than the AST-FG sample, since its SGAs content is higher.

In conclusion, all data collected from the multivariate analysis allowed us to provide some important considerations regarding both treated and untreated green fruits (FG), based on their harvesting period. Overall, the analysis can be summarized as follows:

1) A substantial difference between the fruits obtained in the 1st harvest (poor in almost all metabolites) and those obtained from the 2nd harvest (rich in almost all metabolites);

2) A relative accumulation of a few specific aglycone metabolites during the 1st harvest, which serve as precursors for the development of the corresponding glycosylated compounds during the 2nd harvest. This demonstrated that the development of the glycosylated compounds of interest is time-dependent, i.e., related to the period of harvest (June or July).

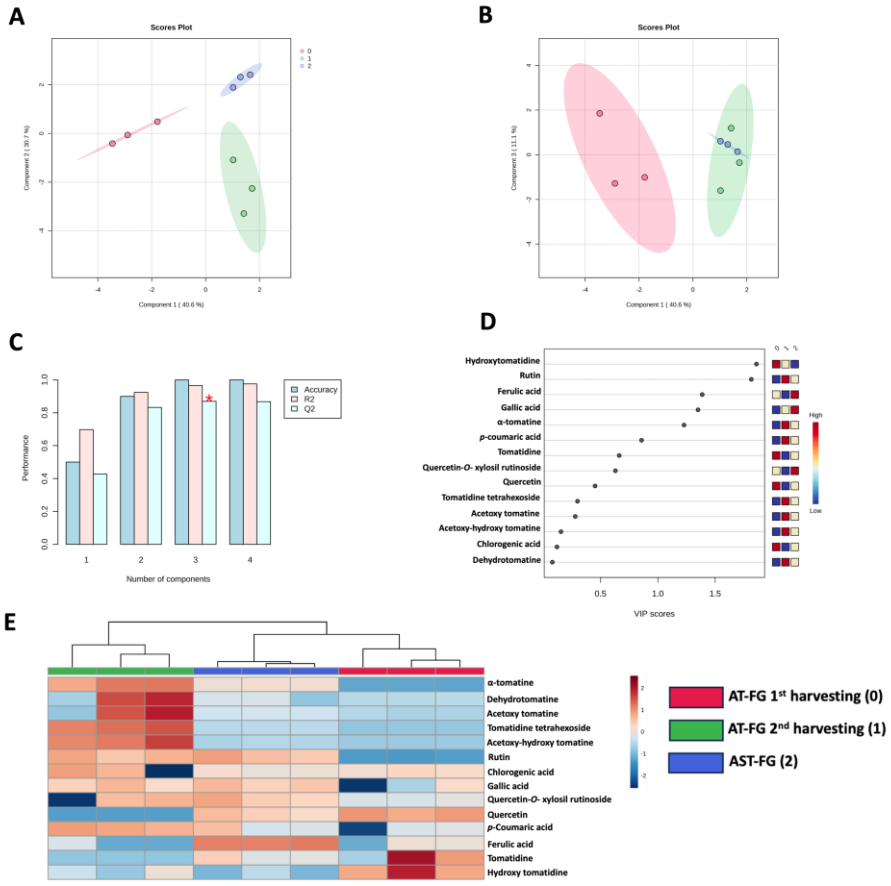


Figure 83: Multivariate analysis. (**A**) and (**B**) Partial least square discriminant analysis (PLS-DA) scores plot, corresponding to a model aimed at the discrimination between treated green tomatoes (FG). The colored ellipses denote 95% confidence intervals for each tomato group. (**C**) Cross-validation test, used to assess the correct number of Components to consider, according to the Q^2 value. (**D**) Variable importance on projection (VIP) scores from the PLS-DA model, indicating the most discriminating metabolites between samples in descending order of importance and with relative levels of metabolites for each cultivar. (**E**) Heatmap with Hierarchical clustering, illustrating the relative metabolite concentration among groups. The corresponding relative metabolite concentration is expressed as a color of different intensity from blue (lowest amount) to red (highest amount).

5.6.5.2.3. Evaluation of *Trichoderma* spp. treatment on green tomato fruits

The effect due to the biological treatment with *Trichoderma* spp. was investigated in all anatomical parts of the tomato plants. Specifically, this effect was evaluated on green immature fruits, which are certainly the most interesting matrix for the development of a potential nutraceutical product. In order to investigate the effect of this parameter, six different groups of green unripe tomatoes have been considered:

1) The first group derived from plants **not treated with *Trichoderma* spp**., whose harvest of the first fruit trusses was carried out only in June (i.e., A-FG 1st harvesting sample);

2) The second group derived from plants **not treated with *Trichoderma* spp.**, whose harvest of the later fruit trusses was carried out in July, after a first previous harvest in June (i.e., A-FG 2nd harvesting).

3) The third group derived from plants **not treated with *Trichoderma* spp.**, whose harvest of the later fruit trusses was carried out once, and only in July (i.e., AS-FG)

4) The fourth group derived from plants **treated with *Trichoderma* spp.**, whose harvest of the first fruit trusses was carried out only in June (i.e., AT-FG 1st harvesting)

5) The fifth group derived from plants **treated with *Trichoderma* spp**., whose harvest of the later fruit trusses was carried out in July, after a first previous harvest in June (i.e., AT-FG 2nd harvesting).

6) The sixth group derived from plants **treated with *Trichoderma* spp.**, whose harvest of the later fruit trusses was carried out once, and only in July (i.e., AST-FG)

These groups differ not only in the presence/absence of the biological treatment with *Trichoderma* spp. but also in the different fruit harvesting periods, thus including both these two parameters in our multivariate analysis. Therefore, a PLS-DA 2D analysis (**Figure 84A**, **84B**, **84C**), a cross-validation test (**Figure 84D**), a VIP-score test (**Figure 84E**) and a heatmap with hierarchical clustering (**Figure 84F**) have been performed, based on the quantitative analysis data.

The PLS-DA in **Figure 84A** describes 56.5% of the data variance and may highlight some interesting differences by comparing the treated matrices with the untreated ones. As a matter of fact, green unripe tomatoes deriving from the first harvesting and not treated (A-FG 1st harvesting sample) slightly differ from those treated (AT-FG 1st harvesting sample), since these two groups do not overlap in the graphic. This difference can be rationalized only by Component 2, which is responsible for 28.7% of the data variance. Interestingly,

among the samples belonging to the 2nd harvest, a clearer difference can be observed between the treated and untreated groups, since they are not close together, but are spaced apart in the graphic. Specifically, the A-FG 2nd harvesting sample and its corresponding treated (i.e., AT-FG 2nd harvesting) are dissimilar mainly according to Component 1 (27.8% of the data variance), and partially Component 3 (8.1% of the data variance), while the AS-FG sample and its corresponding treated (i.e., AST-FG) are dissimilar mainly according to Component 2, 3 and 4 (7.8% of the data variance). The cross-validation test (**Figure 84D**) suggests considering all four Components to correctly evaluate the data variance, according to the Q^2 value. The VIP score test in **Figure 84E** provides several metabolites (both polyphenols and SGAs) responsible for this strong variance between the treated and untreated groups. Interestingly, there is a slight increase in almost all the metabolites found in the treated fruits of the first harvesting (i.e., in AT-FG 1st harvesting sample, compared to A-FG 1st harvesting sample). In particular, the aglycone compounds TD (VIP score = 0.8), quercetin (VIP score = 0.6) and hydroxytomatidine (VIP score = 1.3) are greatly enhanced by the treatment with *Trichoderma* spp. As shown by the comparison between samples A-FG 1st harvesting and AT-FG 1st harvesting (**Table 77)**, TD and hydroxytomatidine are practically not detectable in the untreated sample belonging to the 1st harvesting, while AT-FG 1st harvesting displayed values of 229.27 ± 60.37 μg TD/g of dried matrix and 71.97 ± 15.35 μg of hydroxytomatidine/g dried matrix. On the other hand, quercetin content is 12.30 ± 1.10 μg/g of dried matrix in the untreated matrix and 15.49 ± 0.71 μg/g of dried matrix in the treated one, with a statistical difference calculated by the one-way ONOVA test.

The effect of *Trichoderma* spp. treatment is greatly more visible in green unripe tomatoes during the 2nd harvesting. As a matter of fact, the VIP score test confirms that the glycosidic compounds rutin (VIP score = 1.6) and α-TM (VIP score =1.4) are increased by the biological treatment, as confirmed by the comparison between the samples A-FG 2nd harvesting and AT-FG 2nd harvesting, and by the comparison between the samples AS-FG and AST-FG. These data suggest that this microorganism could potentiate the biosynthetic pathway of rutin and α-TM, by stimulating the formation of the biosynthetic precursors (i.e., the corresponding aglycone compounds), during the period of the 1st harvesting, and consequently the synthesis of the glycosidic derivatives during the 2nd harvesting.

The Heatmap with Hierarchical clustering (**Figure 84F**) confirms the differences between treated and untreated groups described in the PLS-DA graphic and also provides further interesting details regarding the distribution of metabolites in the presence or absence of treatment. Overall, during the 1st harvest, the effect of this treatment (which has been

rationalized by Component 1 in the PLS-DA) seems to be limited to a few metabolites (specifically, quercetin, TD, and hydrohytomatidine) which considerably increase, as evident from the red color on the map. However, the *Trichoderma* spp. effect seems to be very limited, since almost all the other metabolites remain at low levels or slightly increase through the treatment, as shown by the predominant blue color in all these regions of the Heatmap. In addition, the Hierarchical clustering does not provide a clear difference between these two groups. On the other hand, almost all the metabolites, both polyphenols and SGAs, are greatly enhanced by the *Trichoderm*a spp. treatment during the 2nd harvesting, thus confirming that the effect of this biological agent is time-dependent, i.e., related to the harvest period and to the plant maturation. Among them, some important glycosides, such as rutin, α-TM, acetoxy-hydroxytomatine, dehydrotomatine and other secondary SGAs, are enhanced by the action of this microorganism, as it's clear by comparing the AT-FG 2nd harvesting sample with its corresponding untreated A-FG 2nd harvesting sample. Moreover, aglycone compounds such as quercetin and TD are drastically lower during the 2nd harvesting, especially in the treated samples. According to the clustering method of the Heatmap, the A-FG 2nd harvesting sample and its corresponding treated AT-FG 2nd harvesting are statistically different, since they are clearly distant in the graphic. This means, in other words, that the biological treatment is highly efficient during the 2nd harvesting and may enhance the SGAs and polyphenols content (especially for glycosides), by reducing at the same time the content of the aglyconic precursors (i.e., quercetin and TD).

On the contrary, the AS-FG sample and the corresponding treated AST-FG do not demonstrate a clear difference, as provided by the dendrogram. Therefore, the *Trichoderma* spp. treatment effect seems to be related not only to the harvest period but also to the method of harvesting. In fact, green unripe tomatoes from the later trusses could respond better when these fruits are harvested two times in two consecutive periods, by improving the accumulation of several metabolites of interest. However, this aspect should be elucidated and investigated in the future, to better demonstrate this correlation.

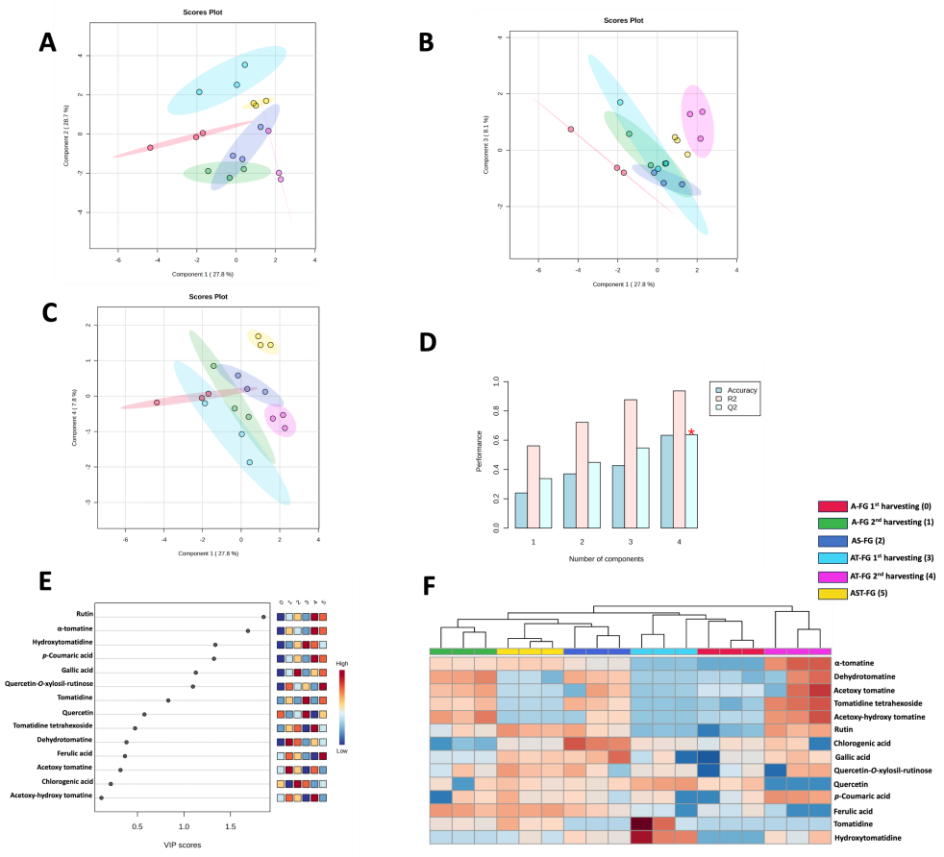


Figure 84: Multivariate analysis. (**A**), (**B**) and (**C**) Partial least square discriminant analysis (PLS-DA) scores plot, corresponding to a model aimed at the discrimination between treated and untreated green tomatoes (FG). The colored ellipses denote 95% confidence intervals for each tomato group. (**D**) Cross-validation test, used to assess the correct number of Components to consider, according to the Q^2 value. (**E**) Variable importance on projection (VIP) scores from the PLS-DA model, indicating the most discriminating metabolites between samples, in descending order of importance and with relative levels of metabolites for each cultivar. (**F**) Heatmap with Hierarchical clustering, illustrating the relative metabolite concentration among groups. The corresponding relative metabolite concentration is expressed as a color of different intensity from blue (lowest amount) to red (highest amount).

Sample	TD	Hydroxytomatidine
	µg α-TM/g DW ± SD	
A-FG 1st harvesting	n.d.	n.d.
AT-FG 1st harvesting	224.40 ± 50.31[a]	69.99 ± 12.35[a]
A-FG 2nd harvesting	54.98 ± 4.80[b,c]	15.62 ± 0.05[b]
AT-FG 2nd harvesting	n.d.	35.78 ± 6.34[b]
AS-FG	n.d.	33.85 ± 3.91[b]
AST-FG	92.90 ± 17.07[b]	26.86 ± 5.77[b]

Table 77: Content of four selected steroidal alkaloids in treated and untreated green fruits (FG), indicated as μg/g dried matrix. Results are expressed as mean ± SD. Statistical significance was calculated by one-way ANOVA followed by Tukey's post-hoc test. Different letters in each bar reveal significant differences. "n.d." means "not detected".

All data, provided by the quantitative and statistical analysis, allow highlighting some important considerations regarding the *Trichoderma* spp. treatment effect. As widely demonstrated in the literature, several metabolites released by *Trichoderma* spp. can be recognized by pattern-recognition receptors (PRRs), expressed on the plant cell membrane. This interaction leads to a specific regulation of several genes, involved in the plant defence and growth. In particular, *Trichoderma* spp. may increase the production in tomato plants of JA, which is a key phytohormone involved in SGAs and polyphenols synthesis as response against biotic and abiotic stresses. As a matter of fact, it has been found that abiotic stresses (such as UV radiations and wounds) may enhance the accumulation of phenolics due to higher levels of signaling molecules such as JA (Surjadinata et al., 2021). In agreement with the literature, our data clearly show that this fungus is able to increase the production of secondary metabolites involved in the plant defense against pathogens. In particular, this effect seems to be strongly correlated to the harvest period. After the fungus inoculation along the root collar in May, a first increment in the production of aglycone alkaloids, such as TD and hydroxytomatidine, and polyphenols, such as quercetin, is visible during the 1st harvest in June. However, the effect of the biological treatment on the metabolic profile of the plant remains still limited to a few metabolites, thus suggesting that it's strongly time-dependent. Successively, during the 2nd harvesting in July, the *Trichoderma* spp. could induce the conversion of these aglycones into their corresponding glycoside derivatives, such as rutin, α-TM, dehydrotomatine, and acetoxytomatine, among others. Therefore, the fruit achieves its greatest SGAs and polyphenols content under the treatment with *Trichoderma* spp. and after an appropriate time, i.e., during the 2nd harvesting.

Our data substantially agree with those provided by Soytong et al. (2014), who studied the effect of three microbial elicitors on the SGAs profile of the tomato plant. Among them, trichotoxin A50, produced by *Trichoderma harzianum*, was used to elicit α-TM in a tomato seedling variety, inoculated with the phytopathogen *Fusarium oxysporum*. Tomato treated with trichotoxin A50 at 15 days expressed α-TM at levels of 205.04 μg/g, which was significantly higher than those resulting from chemical fungicides (such as prochloraz) and

from the inoculated control (131.56 µg/g and 77.46 µg/g). Moreover, Lanzuise et al. (2022) demonstrated the efficacy of new biological formulations based on the combination of small microbial consortia (containing two *Trichoderm*a spp.), with a medium–long chain fatty acids mixture. An untargeted LS-MS analysis confirmed the increasing production of α-TM in treated plants, compared to the controls, thus enhancing the defenses of the tomato plant.

In conclusion, the treatment with *Trichoderma* spp. conducted for our study has greatly enhanced the secondary metabolite content during the 2nd harvest, thus providing an interesting plant matrix rich in several compounds of interest for our nutraceutical purposes (**Figure 85**).

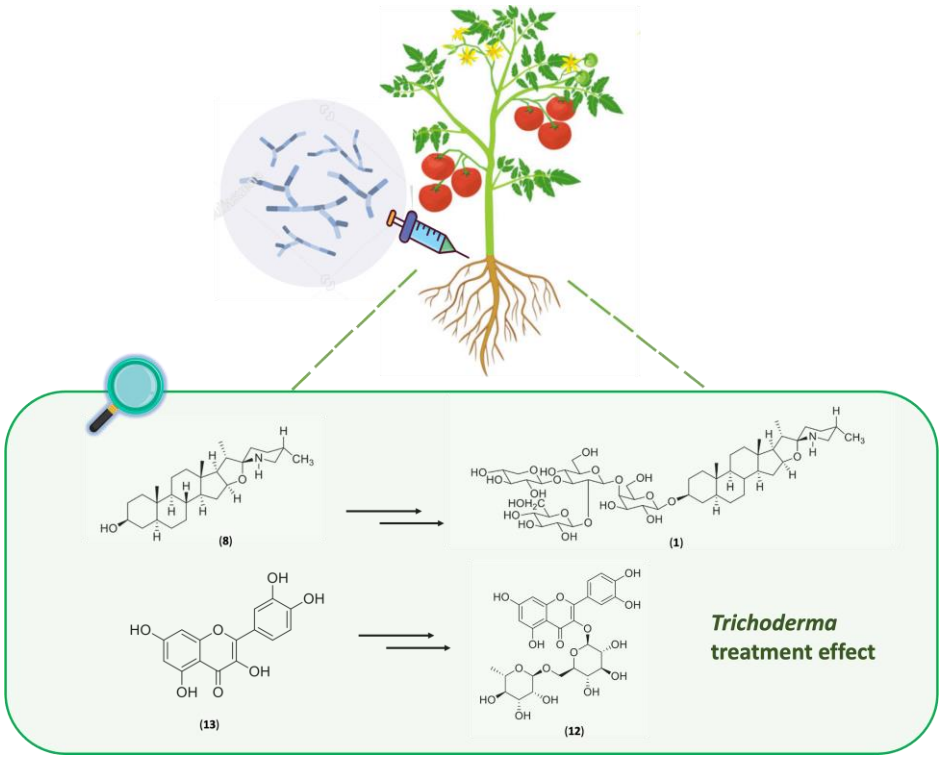


Figure 85: Stimulation of SGAs and polyphenols metabolic pathways by *Trichoderma* spp.

5.6.5.2.4. Evaluation of *Trichoderma* spp. treatment on roots

Trichoderma spp. treatment effect was also evaluated on the roots of the tomato plant, which were the site of *Trichoderma* spp. inoculation. Therefore, the starting hypothesis was to find a direct impact of the biological treatment on the metabolic profile of roots. Therefore, samples were divided into six groups, according to the harvest period and presence or absence of *Trichoderma* spp. treatment, by following the same scheme proposed in the previous paragraph (**3.5.1. Evaluation of Trichoderma spp. treatment effect on green fruits (FG)**) and according to the sampling method described in the chapter **2.2. Cultivar selection and preparation of the matrix**. The chemometric analysis was performed by the assessment of the PLS-DA 2D analysis (**Figure 86A**, **86B**, **86C**), a cross-validation test (**Figure 86D**), a VIP-score test (**Figure 86E**) and a heatmap with hierarchical clustering (**Figure 86F**), based on the quantitative analysis data.

The PLS-DA in **Figure 86A**, which describes 58.2% of the data variance, can provide a statistical difference between the A-RX-RG 1st harvesting sample and the AT-RX-RG 1st harvesting sample, i.e., between the untreated and the treated matrix deriving from the 1st harvest of tomatoes in June. As a matter of fact, this difference can be provided mainly by Component 2 (14.5% of the data variance), since these two groups are described by a negative and a positive Component 2, respectively. This difference can be described also by Component 3 (10.1%), but not by Component 4 (11.5% of variance) and Component 1, which is responsible alone for 43.7% of the data variance. On the other hand, a more remarkable difference can be observed between the A-RX-RG 2nd harvesting sample and the AT-RX-RG 2nd harvesting sample, i.e., between the untreated and the treated matrix, deriving from the 2nd fruit harvesting in July. Specifically, these roots (both treated and untreated) were harvested together with the later fruit trusses, in July, after a first previous fruit harvest in June. As is evident from the graphic, these two groups are clearly spaced apart and their difference is described by all four Components. Another great difference can be observed between the untreated AS-RX-RG sample and its corresponding treated one (i.e., AST-RX-RG). These two matrices were harvested together with the later fruit trusses only once (in July), without repeating the fruit harvest in two consecutive periods. These samples, deriving from the 2nd harvesting, are dissimilar only according to Component 1 and Component 2. The cross-validation test (**Figure 86D**) suggests considering all four components for a correct predictivity of the model, according to the Q^2 value. Therefore, the PLS-DA analysis clearly confirms the efficacy of the *Trichoderma* spp. treatment (in terms

of distance between groups), but this effect seems to be greater for samples deriving from the 2nd harvesting, thus suggesting a time-dependent. The VIP score test (**Figure 86E**) sorts the main metabolites responsible for this variance, based on an assigned VIP score. Among these, SGAs are certainly more relevant, by considering that the roots are very poor in polyphenols. *Trichoderma* spp. treatment can enhance almost all the metabolites in the roots deriving from the 1st harvesting, but the absolute amount of these metabolites is still low, as shown by the predominant blue color. On the contrary, a drastic increase in almost all the metabolites is provided by matrices deriving from the 2nd harvesting, in particular for AT-RX-RG 2nd harvesting, compared to its corresponding untreated. Among them, α-TM (VIP score = 2.0), hydroxytomatidine (VIP score = 1.7), dehydrotomatidine (VIP score = 1.5) and TD (VIP score 1.5) are drastically increased by the *Trichoderma* spp. treatment, as demonstrated by the **Table 78**, with a TD content of 1594.27 ± 40.07 µg/g of dry matrix is provided for the untreated sample and 2192.48 ± 8.48 µg/g of dry matrix for the corresponding treated, thus confirming a significant increase by a one way ANOVA test. Moreover, an increase of approximately 100 and 200 µg is observed for the content of dehydrotomatidine (isomer 2) and hydroxytomatidine, respectively. Among SGAs, the more relevant increase is those provided by α-TM (from 2.34 ± 0.13 mg/g of dry matrix to 3.42 ± 0.10 mg/g of dry matrix) and acetoxytomatine (from 320.69 ± 53.11 µg/g of dry matrix to 432,41 ± 24,59 µg/g of dry matrix), as described by the **Table 79**. Interstingly, acetoxy-hydroxytomatine (VIP score = 1.0), which is the product of the α-TM catabolism, is significantly decreased by the treatment, as confirmed both by the VIP-score (**Figure 86E**) and by **Table 79** (from 9.14 ± 3.63 µg/g of dry matrix to 2.06 ± 0.39 µg/g of dry matrix). These data strongly suggest that the biological treatment may promote the SGAs biosynthetic pathway, on one hand, and inhibit the α-TM catabolism, on the other, thus greatly enriching this anatomical part of several interesting metabolites. Interestingly, a more remarkable difference is provided between the AS-RX-RG sample and its corresponding treated AST-RX-RG, deriving from the 2nd harvesting. As a matter of fact, a clear increase in almost all the SGA, both glycosides and aglycones, and a drastic decrease in several catabolism products, such as acetoxytomatine and acetoxyhydroxytomatine, is shown in the VIP-score graphic and confirmed by **Table 78** and **79**, by a one way ANOVA test. In addition, rutin and chlorogenic acid, i.e., the most abundant polyphenols in the whole tomato plant, are increased as well by the *Trichoderma* spp. treatment in the samples obtain during the fruit 2nd harvesting.

The statistical difference between treated and untreated roots deriving from the first harvesting (i.e., between A-RX-RG 1st harvesting sample and AT-RX-RG 1st harvesting sample) is confirmed by the Hierarchical clustering in the Heatmap graphic (**Figure 86F**). As a matter of fact, these two groups are distant in the dendrogram and belong to two different nodes. However, the *Trichoderma* spp. treatment effect seems to be still limited, as provided by the low color intensity in this region of the heatmap. The greatest difference can be seen between treated and untreated samples deriving from the 2nd harvesting, in particular between AS-RX-RG (characterized by a predominant blue color for almost all the detected metabolites) and AST-RX-RG (characterized by a predominant red color for almost all the detected metabolites). The main difference concerns the drastic increase of aglycone alkaloids by the treatment. As a matter of fact, treated roots of tomato plants, deriving from the 2nd harvesting (i.e., AST-RX-RG sample), are characterized by approximately 14 mg of TD/g of dry matrix, while the corresponding untreated sample provides only 1.8 mg of TD/g of dry matrix, thus confirming that this matrix is an excellent source of TD and could be consider in future for the development of new nutraceutical products (**Table 78**). In addition, acetoxytomatine and acetoxy-hydroxytomatine dramatically decrease in the treated group, as a result of a strong inhibition of SGAs catabolism. This trend is confirmed for the couple A-RX-RG 2nd harvesting and its treated AT-RX-RG 2nd harvesting, even if is less relevant, as also demonstrated by the dendrogram.

The collection of all these data, derived from the quantitative and statistical analysis, allows us to provide some final considerations regarding the impact of this biological treatment:

- *Trichoderma* spp. may exhibit the greatest effect on the roots, i.e. on the site where the inoculation was carried out directly;
- *Trichoderma* spp. significantly increases the SGAs biosynthetic pathway in the root cells, thus leading to a strong increment of both aglycones and glycosidic alkaloids;
- The catabolism pathway of α-TM is strongly inhibited by this microorganism, as shown by the poor acetoxytomatine and acetoxy-hydroxytomatine content after the treatment;
- The effect of this biological treatment is observable during the 1st harvesting (in June) but is drastic during the 2nd harvesting (July), thus confirming that the *Trichoderma* spp. effect is strongly time-dependent;
- 2nd harvesting samples seem to be different from each other and provide a different response to the *Trichoderma* spp. treatment. Specifically, in one case (AST-RX-RG sample), roots were harvested together with the later fruit trusses only once, in July, without repeating the harvest in two consecutive periods. In the other case, roots were harvested together with

the later fruit trusses, in July, after the 1st previous fruit harvest in June (AT-RX-RG 2nd harvesting sample). The treated AST-RX-RG matrix provides the best response to the action of *Trichoderma* spp., thus demonstrating again that the effect of this biological treatment is correlated to fruit harvest method.

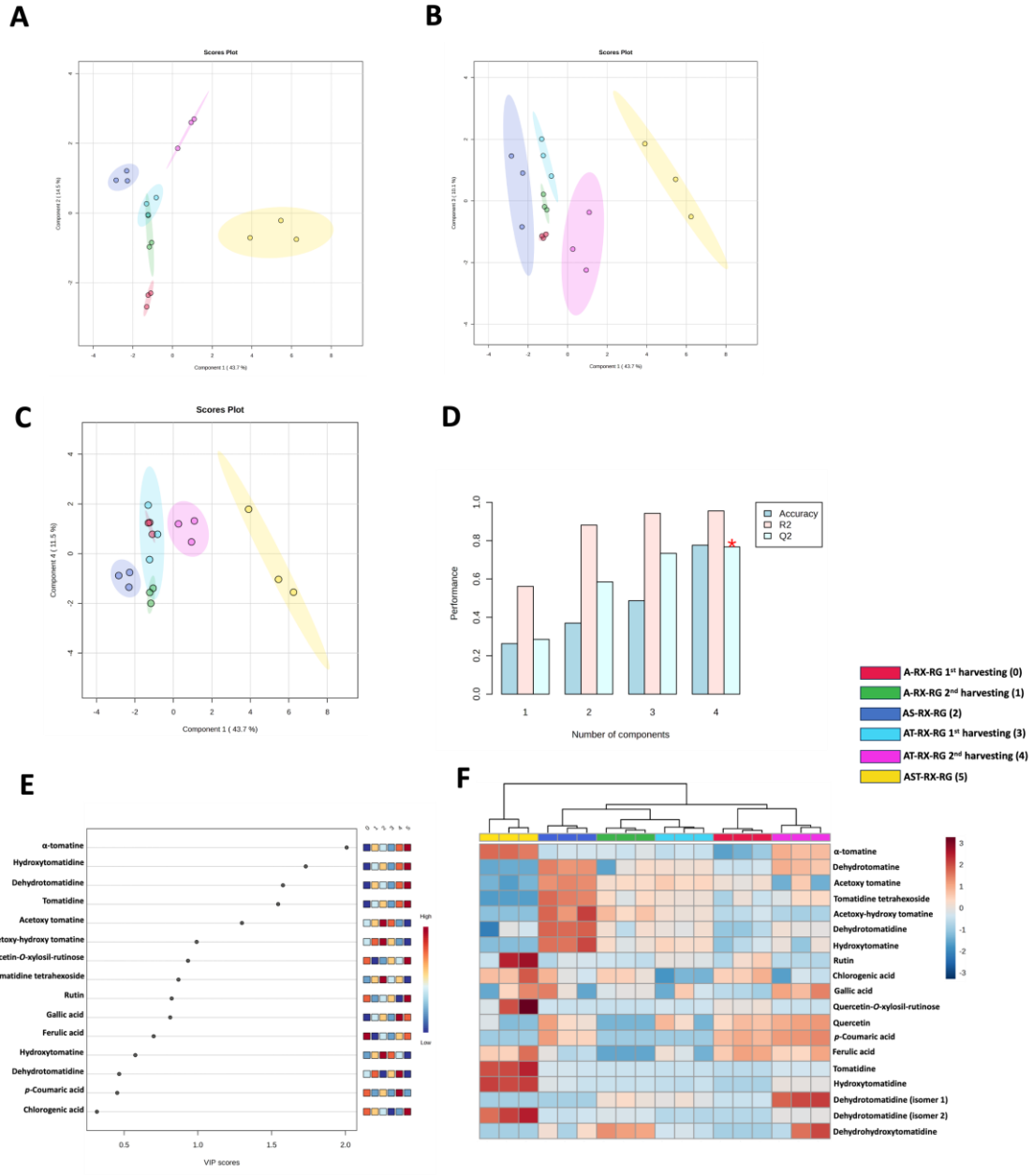


Figure 86: Multivariate analysis. (**A**), (**B**) and (**C**) Partial least square discriminant analysis (PLS-DA) scores plot, corresponding to a model aimed at the discrimination between treated and untreated roots (RG). The colored ellipses denote 95% confidence intervals for each group. (**D**) Cross-validation test, used to assess the correct number of Components to consider, according to the Q^2 value. (**E**) Variable importance on projection (VIP) scores from the PLS-DA model, indicating the most discriminating metabolites between samples in

descending order of importance and with relative levels of metabolites for each matrix. (**F**) Heatmap with Hierarchical clustering, illustrating the relative metabolite concentration among groups. The corresponding relative metabolite concentration is expressed as a color of different intensity from blue (lowest amount) to red (highest amount).

Sample	TD	Dehydrotomatidine (isomer 1)	Dehydrotomatidine (isomer 2)	Hydroxytomatidine	Dehydro-hydroxy tomatidine
	µg TD/g DW ± SD		µg TD eq/g DW ± SD		
A-RX-RG 1st harvesting	489.98 ± 8.16^{a}	0.07 ± 0.01^{a}	96.99 ± 0.53^{a}	142.55 ± 7.48^{a}	n.d.
AT-RX-RG 1st harvesting	1119.84 ± 319.23^{a}	0.14 ± 0.03^{a}	107.68 ± 40.41^{a}	271.74 ± 49.94^{b}	28.51 ± 9.53^{a}
A-RX-RG 2nd harvesting	1594.27 ± 40.07^{a}	0.17 ± 0.02^{a}	405.72 ± 28.00^{a}	339.87 ± 54.89^{b,c}	120.54 ± 7.65^{b}
AT-RX-RG 2nd harvesting	2192.48 ± 8.48^{a}	0.44 ± 0.03^{a}	532.31 ± 21.57^{a}	517.19 ± 20.37^{d}	157.85 ± 12.96^{c}
AS-RX-RG	1804.31 ± 647.14^{a}	267.88 ± 90.61^{b}	350.56 ± 138.35^{a}	379.24 ± 98.24^{c}	62.24 ± 9.53^{d}
AST-RX-RG	14986.99 ± 6929.48^{b}	3886.59 ± 680.61^{c}	1770.40 ± 858.14^{b}	1569.43 ± 47.50^{e}	n.d.

Table 78: Content of four selected steroidal alkaloids in treated and untreated roots (RG), indicated as µg/g dried matrix. Results are expressed as mean ± SD. Statistical significance was calculated by one-way ANOVA followed by Tukey's post-hoc test. Different letters in each bar reveal significant differences. "n.d." means "not detected".

Sample	α-TM	Dehydrotomatine	Acetoxytomatine	Tomatidine tetrahexoside	Acetoxyhydroxy tomatine	Dehydrotomatidine tetrahexoside	Hydroxytomatine
	mg α-TM/g DW ± SD			µg α-TM eq/g DW ± SD			
A-RX-RG 1st harvesting	1.37 ± 0.30^{a}	2985.68 ± 167.89^{a}	314.72 ± 20.30^{a}	150.11 ± 42.53^{a}	3.76 ± 1.00^{a,b}	24.15 ± 3.96^{a}	172.12 ± 39.88^{a}
AT-RX-RG 1st harvesting	2.07 ± 0.24^{b}	4231.08 ± 99.70^{b}	380.15 ± 21.80^{a,b}	198.92 ± 4.59^{a}	7.65 ± 0.47^{b,c}	39.44 ± 2.50^{a}	363.57 ± 23.89^{b,c}
A-RX-RG 2nd harvesting	2.34 ± 0.13^{b}	4145.51 ± 341.00^{b}	320.69 ± 53.11^{a}	202.64 ± 28.15^{a}	9.14 ± 3.63^{c}	37.87 ± 7.44^{a}	301.67 ± 54.66^{a,b}
AT-RX-RG 2nd harvesting	3.42 ± 0.10^{c}	5587.37 ± 376.43^{c}	432.41 ± 24.59^{b,c}	324.72 ± 10.16^{b}	2.06 ± 0.39^{a}	39.13 ± 1.93^{b}	302.03 ± 11.46^{a,b}
AS-RX-RG	2.57 ± 0.45^{b}	6787.16 ± 263.52^{d}	544.82 ± 10.50^{c}	328.61 ± 13.66^{b}	17.01 ± 2.72^{d}	57.58 ± 18.15^{b}	665.01 ± 102.50^{d}
AST-RX-RG	4.20 ± 0.09^{d}	4651.65 ± 313.53^{b}	329.52 ± 18.77^{a}	192.82 ± 11.26^{a}	13.57 ± 0.41^{c}	35.83 ± 2.10^{c}	454.45 ± 49.70^{c}

Table 79: content of five selected SGAs in treated and untreated roots (RG), indicated as µg/g dried matrix. Results are expressed as mean ± SD. Statistical significance was calculated by one-way ANOVA followed by Tukey's post-hoc test. Different letters in each bar reveal significant differences.

5.6.5.2.5. Metabolomic comparison between botanical parts

A comprehensive comparative study between different anatomical parts of tomato plants has been performed by considering two types of matrices, i.e., treated and untreated with *Trichoderma* spp., to perform two chemometric analyses. The aim was to evaluate the trend in the metabolic profile of each part, and which matrix displayed the best SGAs and polyphenols profile, both in the untreated and the treated group. Specifically, green fruits (FR), roots (RG), leaves (LG) and stem (SG) deriving from the 2nd harvesting in July ("AS" samples) and not treated with the *Trichoderma* spp. agent have been considered for this first comparison. The extracts of plant botanical parts were analyzed in triplicate for their SGAs and polyphenol content, and data obtained from the quantification were used to perform a

chemometric analysis, including the PLS-DA 2D analysis (**Figure 87A,** and **87B**), the cross-validation test (**Figure 87C**), the VIP score test (**Figure 87D**) and the Heatmap with hierarchical clustering (**Figure 87E**). According to the PLS-DA analysis (**Figure 87A** and **87B**), all these matrices are substantially dissimilar, as they are clearly spaced apart in the graphic. This variance is described mainly by Component 1 (51.4% of the variance) and Component 2 (25.6%) and partially by Component 3 (13.5%). The cross-validation test (**Figure 87C**) suggests considering only these three Components for a correct predictivity of the model, according to the Q^2 value. The VIP score test (**Figure 87D**) shows both polyphenols and SGAs as compounds responsible for this strong data variance. Among them, gallic acid (VIP score =2.5) is the only metabolite present at the highest level in the fruit, compared to the other anatomical parts. On the other hand, rutin (VIP score = 0.9), which is the most abundant polyphenol in the whole tomato plant, and α-TM (VIP score = 0.8), exhibit their highest level in the leaves. The heatmaps with Hierarchical clustering substantially confirm this difference among matrices (**Figure 87E**). In particular, as provided by the dendrogram, the AS-RX-RG matrix (represented by the roots) is remarkably different from all the other botanical parts. According to metabolites distribution, roots display the greatest SGAs content, as shown by the predominant red color in this region of the heatmap. Specifically, both glycosides and aglycon SGAs are present at the highest levels in the roots. The only exception is represented by the compound α-TM, whose highest content is provided by the leaves: in other words, the roots particularly accumulate α-TM catabolism products. Moreover, the roots are usually notoriously poor in polyphenols. Another interesting metabolite profile is those provided by leaves, which represent the best anatomical part of accumulation of almost all polyphenols, especially rutin and chlorogenic acid, as shown in **Table 80**. Specifically, rutin content (5.345 ± 0.441 mg of rutin/g of dry matrix) is seven times higher than that provided by fruits, while chlorogenic acid content (1076,88 ± 93,40 µg/g of dried matrix) is more than two times higher. On the other hand, leaves do not provide the best SGAs profile. As demonstrated by the Hierarchical clustering, stem and green unripe fruits deriving from the 2nd harvesting are partially similar and characterized overall by a low SGAs and polyphenols content. The only exception is represented by the phenolic compound gallic acid, whose fruits are particularly rich.

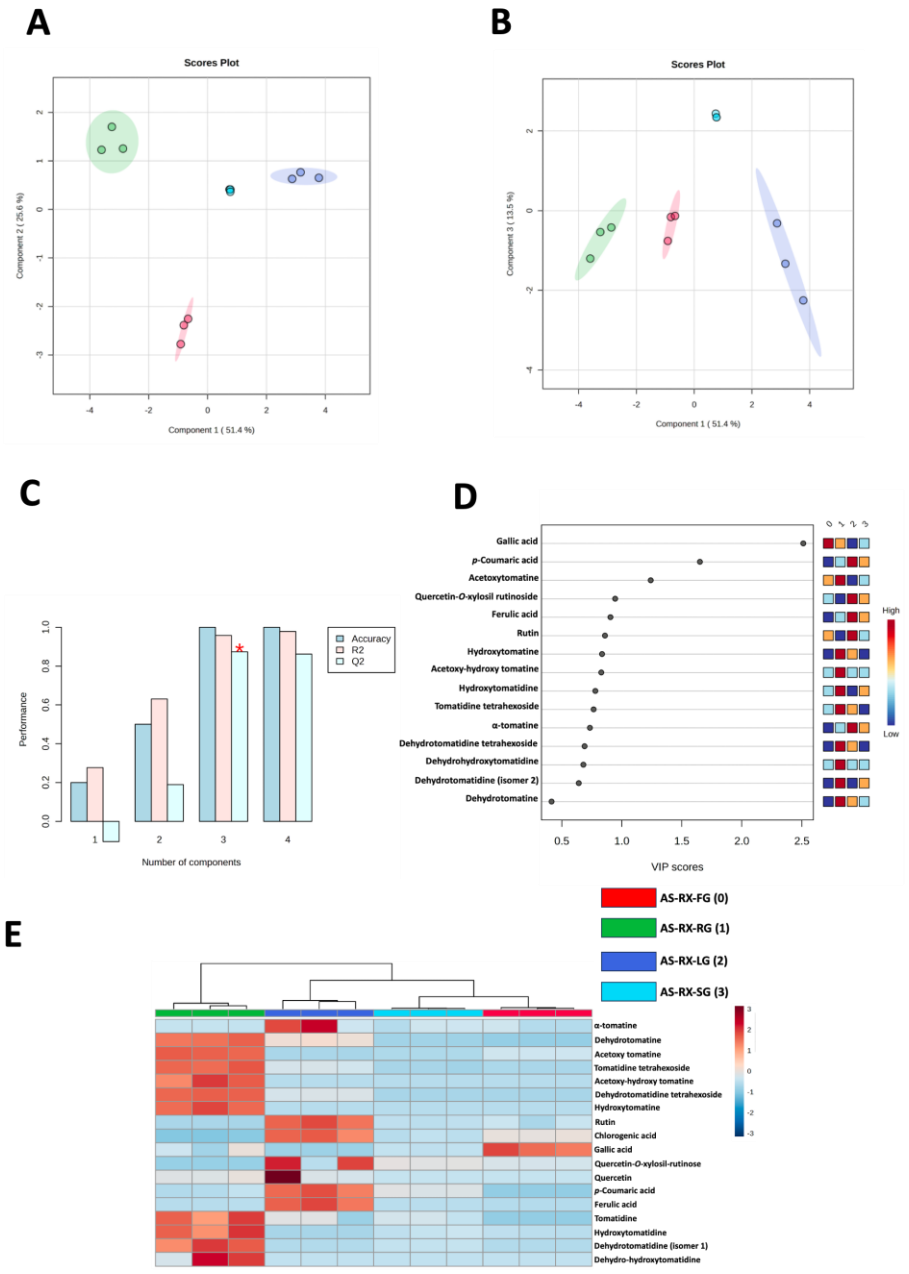


Figure 87: Multivariate analysis. (**A**) and (**B**) Partial least square discriminant analysis (PLS-DA) scores plot, corresponding to a model aimed at the discrimination between different botanical parts of Piennolo tomato plants. The colored ellipses denote 95% confidence intervals for each group. (**C**) Cross-validation test, used to assess the correct number of Components to consider, according to the Q^2 value. (**D**) Variable importance on projection (VIP) scores from the PLS-DA model, indicating the most discriminating metabolites between samples in descending order of importance and with relative levels of metabolites for each matrix. (**E**) Heatmap with Hierarchical clustering, illustrating the relative metabolite concentration among groups. The corresponding relative metabolite

concentration is expressed as a color of different intensity from blue (lowest amount) to red (highest amount).

Sample	Gallic acid	Quercetin	Chlorogenic acid	Quercetin 3-*O*-xylosylrutinoside	Rutin	*p*-coumaric acid	Ferulic acid
				µg/g DW± SD			
AS-RX-FG	120.32 ± 12.55^{a}	n.d.	451.19 ± 8.62^{a}	258.33 ± 11.65^{a}	765.62 ± 38.14^{a}	n.d.	n.d.
AS-RX-SG	$16.43 \pm 1.57^{b,c}$	n.d.	255.25 ± 27.52^{b}	322.23 ± 13.73^{a}	$488.37 \pm 23.50^{a,b}$	8.07 ± 0.56^{a}	8.87 ± 0.45^{a}
AS-RX-LG	n.d.	80.38 ± 28.79^{a}	1076.88 ± 93.40^{c}	1259.71 ± 97.25^{b}	5344.94 ± 440.64^{c}	26.93 ± 2.45^{b}	296.86 ± 30.89^{b}
AS-RX-RG	28.97 ± 9.88^{b}	9.41 ± 2.67^{b}	47.17 ± 15.45^{b}	2.58 ± 0.40^{c}	36.89 ± 11.10^{b}	3.87 ± 0.97	6.97 ± 2.26^{a}

Table 80: Content of seven selected polyphenols in different anatomical parts of tomato plants, deriving from the 2nd harvesting (AS- samples). Values are indicated as µg/g dried matrix. Results are expressed as mean ± SD. Statistical significance was calculated by one-way ANOVA followed by Tukey's post-hoc test. Different letters in each bar reveal significant differences. "n.d." means "not detected".

In a second step, different botanical parts deriving from the 2nd harvesting and treated with *Trichoderma* spp. (AST-RX samples) have been considered for a second comparative metanalysis analysis. These extracts were analyzed in triplicate for their SGAs and polyphenol content, and data obtained from the quantification were used to perform a chemometric analysis, including the PLS-DA 2D analysis (**Figure 88A,** and **88B**), the cross-validation test (**Figure 88C**), the VIP score test (**Figure 88D**) and the Heatmap with hierarchical clustering (**Figure 88E**). According to the PLS-DA 2D analysis (**Figure 88A** and **88B**) these matrices are clearly dissimilar according to Component 1 (39.6% of the data variance), Component 2 (38%) and partially Component 3 (7%). These three Components are sufficient to correctly describe the data variance, according to the Q^2 value provided by the cross-validation test (**Figure 88C**). Among the metabolites responsible for the difference among samples, TD is the most relevant (VIP score = 1.7), followed by dehydrotomatidine, hydroxytomatidine (VIP score = 1.7), and gallic acid (VIP score = 1.2). According to the VIP score test (**Figure 88D**), the leaves are confirmed as the matrix with the highest content of polyphenols, in particular rutin and chlorogenic acid (i.e., the most representative phenolic compounds of the tomato plant). In addition, leaves also show the highest α-TM and dehydrotomatine content, compared to all the other anatomical parts. On the other hand, the aglycon alkaloids (such as TD, dehydrotomatidine, and hydroxytomatidine) accumulate in the roots, which are the best source of these compounds. The dendrogram clustering method used in **Figure 88E** clearly allows the group of leaves to be separated from all the others, thus highlighting its different metabolic profile. As a matter of fact, this matrix

provides both the highest SGAs and polyphenols content, as shown by the predominant red color of the Heatmap. Few exceptions regard two glycosides (acetoxytomatine and dehydrotomatidine tetrahexoside) and the aglycones (TD, dehydrotomatidine and hydroxytomatidine), which are highest in the roots. Interestingly, the TD content clearly shows a progressive improvement by passing from the fruit (93.80 ± 29.07 µg of TD/g of dry matrix) to the leaves (189.06 ± 47.84 µg of TD/g of dry matrix), to the stem (326.44 ± 25.04 µg of TD/g of dry matrix) and finally to the roots (14.987 ± 6.929 mg of TD/g of dry matrix), as shown in **Table 81**. In other words, TD progressively increases in the anatomical parts closer to the site where the *Trichoderma* spp. formulation was inoculated. The stem (SG) and the immature green fruits (FG) are confirmed to be similar, as highlighted by the dendrogram and the color mapping on the graph. The only exceptions regard the compounds acetoxytomatine, chlorogenic acid, and gallic acid, which are clearly at higher levels in the fruits.

Sample	TD	Dehydrotomatidine (isomer 1)	Dehydrotomatidine (isomer 2)	Hydroxy tomatidine
	µg TD/g DW ± SD		µg TD eq/g DW ± SD	
AST-RX-FG	93.80 ± 29.07^{a}	n.d.	n.d.	27.85 ± 6.64^{a}
AST-RX-SG	326.44 ± 25.04^{b,c}	n.d.	n.d.	n.d.
AST-RX-LG	189.06 ± 47.84^{a,b}	n.d.	n.d.	n.d.
AST-RX-RG	14986 ± 6929.48^{c}	3886.59 ± 680.61	1770.40 ± 858.14	1569.43 ± 47.50^{b}

Table 81: Content of four selected steroidal alkaloids in treated roots (RG) stem (SG), leaves (LG) and green fruits (FG) deriving from the 2nd harvesting, indicated as µg/g dried matrix. Results are expressed as mean ± SD. Statistical significance was calculated by one-way ANOVA followed by Tukey's post-hoc test. Different letters in each bar reveal significant differences. "n.d." means "not detected".

All the other comparisons between different anatomical parts (considered at different treatment conditions and harvest periods) are provided in the section **Supplementary material**. These statistical analyses provided similar results. The **Figures** reported in **Supplementary material** describes the metabolic profile of different botanical parts, deriving from plants treated with *Trichoderma* spp. and harvested in July, after a 1st previous fruit harvest in June (AT-RX 2nd harvesting samples). The distribution trend of the different SGAs and polyphenols can be considered very similar to that just described for the AST-RX samples. However, the Heatmap clearly shows a more homogeneous distribution between leaves and roots. On the other hand, by comparing different anatomical parts deriving from untreated plants and harvested in June (A-RX 1st harvesting samples), the metabolites

distribution among groups seems to be similar to that provided by the corresponding treated matrices (i.e., AT-RX 1st harvesting samples). This statistical analysis confirms that the *Trichoderma* spp. treatment effect is strongly time-dependent and so it's still limited during the 1st harvesting (June), but it increases significantly during the 2nd harvesting (July).

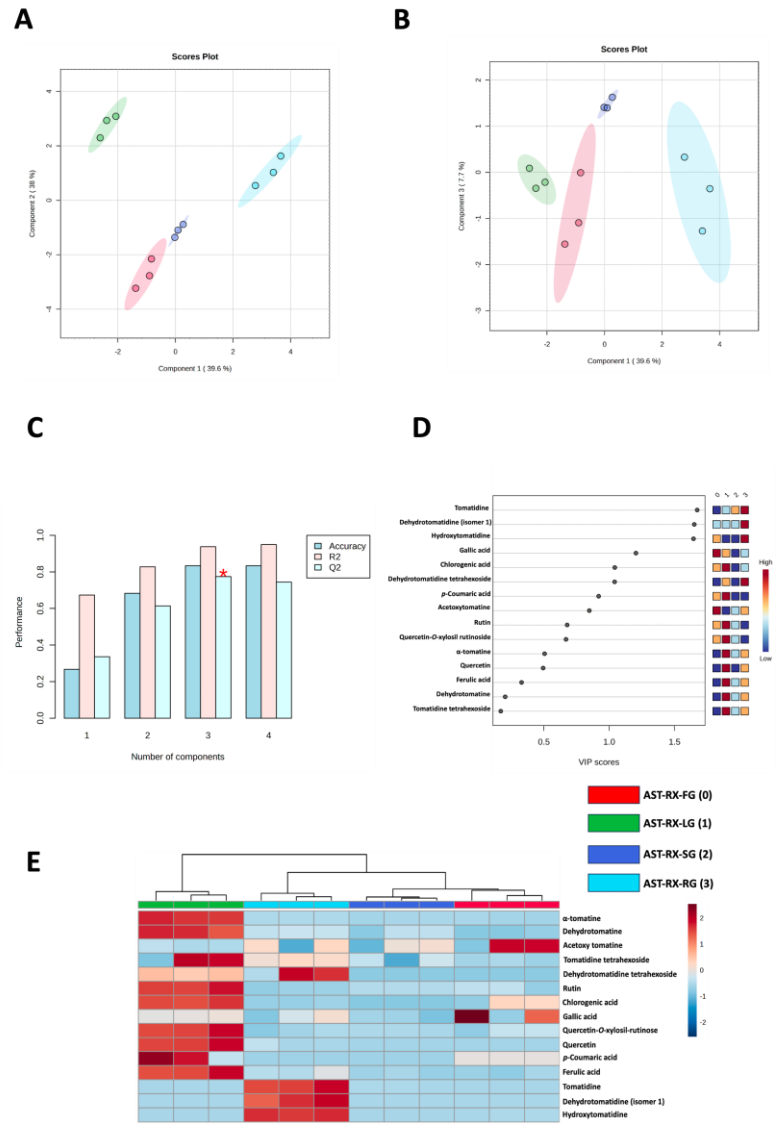


Figure 88: Multivariate analysis. (**A**) and (**B**) Partial least square discriminant analysis (PLS-DA) scores plot, corresponding to a model aimed at the discrimination between different botanical parts of Piennolo tomato plants. The colored ellipses denote 95% confidence intervals for each group. (**C**) Cross-validation test, used to assess the correct number of Components to consider, according to the Q^2 value. (**D**) Variable importance on

projection (VIP) scores from the PLS-DA model, indicating the most discriminating metabolites between samples in descending order of importance and with relative levels of metabolites for each matrix. (**E**) Heatmap with Hierarchical clustering, illustrating the relative metabolite concentration among groups. The corresponding relative metabolite concentration is expressed as a color of different intensity from blue (lowest amount) to red (highest amount).

5.6.6. Antioxidant activity of Piennolo tomato plant extracts

As a first screening of the antioxidant activity of tomato plant extracts, the Folin-Ciocalteau (FC) method, the FRAP assay, and the DPPH assay were performed on our 34 matrices, to obtain a first rapid indication of the *Trichoderma* spp. treatment and the harvesting period effect on the metabolic profile of the plant. Calibration curves and LODs and LOQs values of these assays were also reported and evaluated in **Figure 89** and **Table 82**.

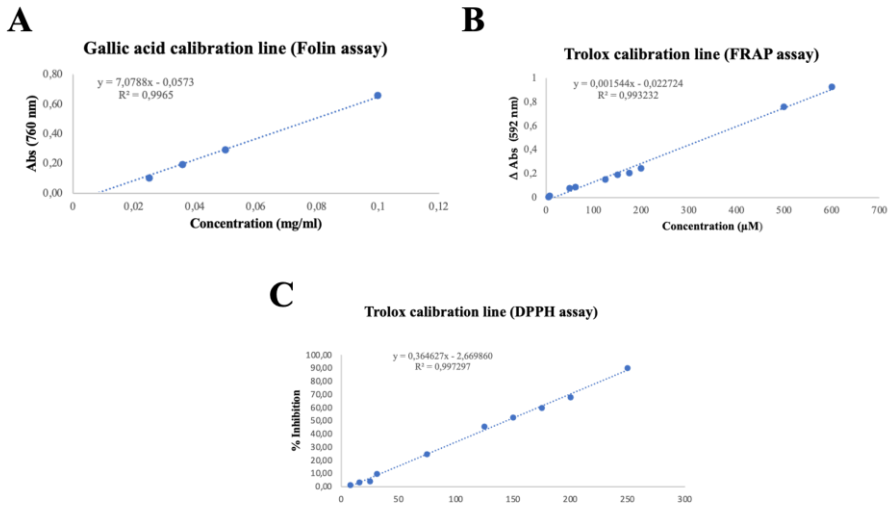


Figure 89: Gallic acid and Trolox calibration curves used for Folin-Ciocalteau (A), FRAP (B), and DPPH (C) assays.

Compound	Assay	LOD (µM)	LOQ (µM)
Trolox	DPPH	25.68	77.83
Gallic acid	FOLIN	0.018	0.055
Trolox	FRAP	84.18	255.09

Table 82: LODs and LOQs values (expressed as µM) for the calibration curves of Folin-Ciocalteau, DPPH, and FRAP assays. Abbreviations: DPPH: radical 2,2-diphenyl-1-picrylhydrazyl; FRAP: ferric reducing antioxidant power.

However, since these tests lack accuracy and specificity, the results obtained were not clear, in some cases, thus requiring a more robust HPLC-DAD analysis, to correctly evaluate the content of the single polyphenols in the extracts. For example, the FC assay made it possible to evaluate a statistically higher total phenolic content (expressed as mg GAE/g) in the *San Sebastiano* cultivar compared to the *Ercolano* cultivar (**Table 83**), although the FRAP and

DPPH assays did not confirm this difference (**Supplementary material**). This divergence could be explained by considered the different capacity of the single polyphenols to react in the antioxidant assays. Moreover, by considering these two cultivars, a statistical difference between green unripe tomatoes of the 1st harvesting (June) and those of the 2nd harvesting (July) was not described by these assays, in agreement with the previous metanalysis (Chapter **3.5.1. Comparison between green tomato cultivars)**.

Sample	mg GAE/g DW ± SD
San Sebastiano tomatoes, 1st harvesting	3.46 ± 0.13^{a}
San Sebastiano tomatoes, 2nd harvesting	3.95 ± 0.04^{a}
Ercolano tomatoes, 1st harvesting	2.98 ± 0.38^{b}
Ercolano tomatoes, 2nd harvesting	3.54 ± 0.08^{a}

Table 83: Results of FC method, expressed as mg of gallic acid equivalents on gram of dried matrix ± SD, for *San Sebastiano* and *Ercolano* cultivars. Statistical significance was calculated by one-way ANOVA followed by Tukey's post-hoc test. Different letters reveal significant differences ($p < 0.05$) between the samples.

A significant increase in the total phenolic content, linked to the treatment with *Trichoderma* spp., can be observed from the comparison between the A-RX-FG 1st harvesting fruit sample and its treated AT-RX-FG 1st harvesting, or between the AS- RX-FG and its corresponding treated, as provided in **Figure 84**.

Sample	mg GAE/g DW ± SD
A-RX-FG 1st harvesting	$3.47 \pm 0.32^{a,b}$
AT-RX-FG 1st harvesting	4.92 ± 0.56^{c}
A-RX-FG 2nd harvesting	$4.27 \pm 0.12^{b,c}$
AT-RX-FG 2nd harvesting	$3.77 \pm 0.21^{a,b}$
AS-RX-FG	3.00 ± 0.64^{a}
AST-RX-FG	$4.19 \pm 0.07^{b,c}$

Table 84: Results of FC method, expressed as mg of gallic acid equivalents on gram of dried matrix ± SD, for FG (i.e., green fruits) samples. Statistical significance was calculated by one-way ANOVA followed by Tukey's post-hoc test. Different letters reveal significant differences ($p < 0.05$) between the samples.

Moreover, the FRAP assay clearly shows a significant increase in the antiradical activity of stem extracts, by the *Trichoderma* spp. treatment, both during the 1st and the 2nd harvesting,

as reported in **Table 85**. A significant increase in the antiradical activity by this biological treatment is described also for the green unripe fruits, but only during the 2nd harvesting, as is evident by the comparison between A-FG 2nd harvesting, AS-FG and AS-RX-FG samples with their corresponding treated samples (**Tables 86** and **87**). However, all these three tests are not able to highlight a clear statistical difference between 1st harvesting and second-harvesting samples, although this difference has been found and described by the metanalysis (Chapter **3.5.2 Evaluation of harvesting period effects**)

Sample	mg TE/g DW ± SD
A-RX-SG 1st harvesting	11.24 ± 0.61^{a}
AT-RX-SG 1st harvesting	$31.00 \pm 5.97^{b,c}$
A-RX-SG 2nd harvesting	$30.85 \pm 1.69^{b,c}$
AT-RX-SG 2nd harvesting	59.81 ± 2.59^{d}
AS-RX-SG	35.08 ± 2.49^{c}
AST-RX-SG	$16.99 \pm 1.32^{a,b}$

Table 85: Results of FRAP method, expressed as µmol TE/g dried matrix ± SD, for SG (i.e., stem and branches) samples. Statistical significance was calculated by one-way ANOVA followed by Tukey's post-hoc test. Different letters reveal significant differences ($p < 0.05$) between the samples.

Sample	mg TE/g DW ± SD
A-RX-FG 1st harvesting	34.37 ± 1.79^{a}
AT-RX-FG 1st harvesting	$44.41 \pm 8.01^{a,b}$
A-RX-FG 2nd harvesting	35.08 ± 3.99^{b}
AT-RX-FG 2nd harvesting	29.27 ± 3.76^{a}
AS-RX-FG	27.38 ± 3.76^{a}
AST-RX-FG	117.35 ± 3.57^{c}

Table 86: Results of FRAP method, expressed as µmol TE/g dried matrix ± SD, for FG (i.e., green unripe fruits) samples. Statistical significance was calculated by one-way ANOVA followed by Tukey's post-hoc test. Different letters reveal significant differences ($p < 0.05$) between the samples.

Sample	mg TE/g DW ± SD
A-FG 1st harvesting	$23.48 \pm 2.38^{a,b}$
AT-FG 1st harvesting	19.44 ± 2.31^{b}
A-FG 2nd harvesting	25.49 ± 2.56^{a}
AT-FG 2nd harvesting	34.17 ± 0.03^{c}
AS-FG	26.52 ± 0.60^{b}
AST-FG	30.75 ± 0.40^{c}

Table 87: Results of FRAP method, expressed as µmol TE/g dried matrix ± SD, for FG (i.e., green unripe fruits) samples. Statistical significance was calculated by one-way ANOVA followed by Tukey's post-hoc test. Different letters reveal significant differences ($p < 0.05$) between the samples.

Overall, the increase in the antioxidant activity is not clearly explained by these assays, since the total phenolic content, the antiradical activity, and the iron-reducing activity do not follow a clear trend. More interesting is the comparison between different anatomical parts of the tomato plant. In this case, a remarkable statistical difference can be observed by comparing the leaves with all the other botanical parts. As a matter of fact, leaves clearly exhibit the greatest total phenolic content, the highest antiradical activity (DPPH test) and iron-reducing activity (FRAP test). For example, the AT-RX-LG 2nd harvesting sample (i.e., the treated leaves matrix deriving from the 2nd fruit harvest in July) displays a total phenolic content that is two times higher compared to the stems and more than three times higher than that of the roots and green unripe fruits (**Figure 88**). These data are substantially confirmed by the DPPH and FRAP tests. For example, treated leaves deriving from the 2nd harvesting exhibit the greatest antiradical activity, i.e., more than five times higher than those provided by green unripe fruits, which display the lowest value (**Table 89**). This trend is confirmed by the FRAP test, where the leaves are reported as the matrix with the highest ferric-reducing capability, followed by the stem sample. On the contrary, green unripe fruits display the lowest iron-reducing activity (**Table 90**). All these results are confirmed throughout the literature, where leaf extracts of tomato plants were reported as the matrix with the highest antioxidant activity (Silva-Beltrán et al., 2015). These great values provided both by FC, DPPH and FRAP tests, can be explained by considering the highest phenolic content of tomato leaves (Silva-Beltrán et al., 2015). Specifically, the most abundant polyphenols are rutin and chlorogenic acid, with a well-known and powerful antioxidant activity. As described by Silva-Beltrán et al., 2015, leaves are the plant section more exposed to light and heat: therefore, they greatly accumulate phenolic compounds as plant-defense molecules against abiotic stresses (i.e., heating and UV-light), by stimulating the biosynthetic pathway of these secondary metabolites (Silva-Beltrán et al., 2015). On the other hand, roots provide a significantly lower antioxidant activity and total phenolic content, since they're notoriously poor of polyphenols or other hydrophilic antioxidants (Silva-Beltrán et al., 2015) and rich in other secondary metabolites, such as terpenes (Tholl, 2006), which were not evaluated (Silva-Beltrán et al., 2015).

Sample	mg GAE/g DW ± SD
AT-RX-FG 2nd harvesting	17.35 ± 3.57[a]
AT-RX-SG 2nd harvesting	16.99 ± 1.32[a]
AT-RX-LG 2nd harvesting	101.17 ± 9.14[b]
AT-RX-RG 2nd harvesting	24.53 ± 0.92[a]

Table 88: Results of FC method, expressed as mg of gallic acid equivalents on gram of dried matrix ± SD, for treated 2nd harvesting samples. Statistical significance was calculated by one-way ANOVA followed by Tukey's post-hoc test. Different letters reveal significant differences ($p < 0.05$) between the samples.

Sample	mg TE/g DW ± SD
AT-RX-FG 2nd harvesting	35.80 ± 5.63[a]
AT-RX-SG 2nd harvesting	54.05 ± 3.03[a]
AT-RX-LG 2nd harvesting	198.11 ± 42.92[b]
AT-RX-RG 2nd harvesting	68.35 ± 7.50[a]

Table 89: Results of DPPH method, expressed as µmol TE/g dried matrix ± SD, for treated 2nd harvesting samples. Statistical significance was calculated by one-way ANOVA followed by Tukey's post-hoc test. Different letters reveal significant differences ($p < 0.05$) between the samples. Abbreviations: DPPH: radical 2,2-diphenyl-1-picrylhydrazyl; TE: Trolox equivalent

Sample	mg TE/g DW ± SD
AT-RX-FG 2nd harvesting	29.27 ± 3.76[a]
AT-RX-SG 2nd harvesting	59.81 ± 2.59[b]
AT-RX-LG 2nd harvesting	119.78 ± 4.86[c]
AT-RX-RG 2nd harvesting	31.35 ± 3.62[a]

Table 90: Results of FRAP method, expressed as µmol TE/g dried matrix ± SD, for treated 2nd harvesting samples. Statistical significance was calculated by one-way ANOVA followed by Tukey's post-hoc test. Different letters reveal significant differences ($p < 0.05$) between the samples. Abbreviations: FRAP: ferric reducing antioxidant power; TE: Trolox equivalent

However, these comparisons between anatomical parts do not consider only the polyphenolic content, but many other compounds with iron-reducing or anti-radical activity, which can lead to a final overestimation of the value. For example, green immature fruits are

well known for their content of ascorbic acid, tocopherol, reducing sugars and free amino acids (such as tyrosine and cysteine, among others) which can contribute to the positivity in these assays (Anton et al., 2017). Other compounds, such as carotenoids, may represent interferents since they are characterized by an absorbance spectrum that overlaps with that used in the FRAP test and DPPH test. Overall, these assays substantially confirmed the antioxidant activity of our green tomato extracts, making this matrix eligible for the development of a nutraceutical product, by combining the SGAs and polyphenol profile with other important lipophilic and hydrophilic antioxidants that characterize this fruit.

5.6.7. Development of a tomatidine-enriched food matrix: α-tomatine hydrolysis assay

Tomato plants and their immatire green fruits represent a great source of α-TM and TD, and therefore an eligible food matrix for the development of a potential food supplement or nutraceutical product. As a matter of fact, these compounds display some interesting pharmacological activities both *in vitro* and *in vivo*, by acting against several chronic human diseases, as described in the paragraph **2.4. Glycoalkaloids beneficial effects on human health**. For example, α-TM has been shown to lower blood cholesterol levels by forming a complex with cholesterol, thus inhibiting its oral absorption and bioavailability. On the other hand, TD may exhibit an antiobesity and cardioprotective activity, by acting as a vitamin D receptor agonist in fatty liver cells. This mechanism leads to a significant reduction in lipid accumulation and an increase in lipolysis and fatty acid beta-oxidation processes, as also demonstrated in an atherosclerosis rat model. Moreover, both these two compounds may exhibit a powerful anti-inflammatory activity, as demonstrated in a rat-powder edema model and in an osteoporosis-rat model. The anti-inflammatory action is due to the inhibition of the NFkB/JKN pathway, which results in a significant reduction in the expression of many inflammatory mediators, including TNF- α, NO, IL-1, IL-6, and PGE 2. Interestingly, the anti-aging activity is described only for the compound TD and is due to the activation of the mTORC pathway, involved in anabolic processes, in the promotion of skeletal muscle hypertrophy, and the associated loss of fat. TD may also activate the SNK-1/NrF2 pathway, involved in the antioxidant response and mitochondrial biogenesis. Furthermore, TD can reduce the expression of the ATF4 factor, involved in age-related muscle atrophy, and inhibit the formation and differentiation of osteoclasts, with a mechanism that is not yet fully elucidated (Bailly, 2021). These biological activities have been confirmed by a rat-aging model, where an overall improvement in musculoskeletal performance has been evaluated. Considering all these specific anti-aging activities, exhibited only by the compound TD, our aim was to develop suitable “food grade” conditions for the full conversion of α-TM into its aglycone, by directly using the vegetal matrix (i.e., the fresh green unripe tomatoes). As a matter of fact, green unripe fruits of *Solanum lycopersicum* L. represent a great source of α-TM and other steroidal SGAs. By considering the fresh fruit weight, they contain up to 500 mg/kg of α-TM, while red tomatoes have a maximum content of 5 mg/kg, due to the extensive catabolism that this compound undergoes during the ripening process (Bailly, 2021). Unfortunately, the fruits are poor in TD, which is the direct biosynthetic precursor of

α-TM. The biological treatment with the *Trichoderma* spp. agent has been positively evaluated for achieving a higher SGAs and polyphenols content and allowed to obtain the greatest TD amount in roots, especially during the 2nd harvesting. On the other hand, this treatment was less efficient in improving the TD content in green unripe tomatoes. Although the microbiological treatment is strongly effective in the increment of TD content, in the nutraceutical field the use of other botanical parts is generally avoid, preferring as source the fruits for the formulation development. Therefore, to achieve this goal and obtain a new TD-enriched matrix, a first acid treatment on the reference compound has been necessary to evaluate the α-TM stability profile under hot-acid conditions. In other words, the first experiment, described in the paragraph **5.5.15. α-tomatine acid hydrolysis**, was carried out to provide the best conditions, in terms of temperature and reaction time, for the successive experiment on the green unripe fruits. The graph below (**Figure 90**) provides the results obtained from the MS-MS analysis, performed with the method previously described in paragraph **5.5.8. Qualitative glycoalkaloids analysis**. The graph illustrates the stability profile for the reference compound, incubated at temperatures of 20°C, 40°C and 60°C, by monitoring different time-points in a range of 0-120 min.

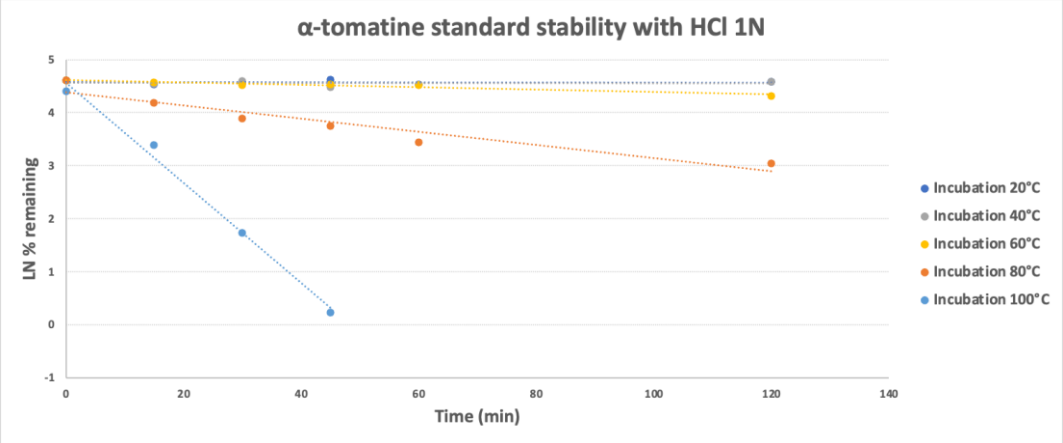


Figure 90: α-TM stability for each temperature, expressed as "ln % remaining", in the function of time (min).

The results at the first two temperatures are practically similar, thus indicating a negligible degradation. As a matter of fact, α-TM is practically stable at both 20°C and 40°C, while a slight degradation of 5% has been observed at a temperature of 60°C. On the other hand, a drastic decrease in the half-life value has been observed by progressively increasing

temperatures (80°C and 100°C), with 40% of degradation at 80°C and a complete degradation at 100°C (**Table 91**)

Temperature (°C)	Degradation (%)
20	Stable
40	Stable
60	5.0
80	40.0
100	100.0

Table 91: α-TM degradation percentages for each temperature.

	20 °C	40 °C	60 °C	80 °C	100 °C
Degradation constant K (min^{-1})	0.000019	0.000085	0.00226	0.012404	0.094192
t/2 (min)	35406.09	8137.42	306.75	55.88	7.35
t/2 (hour)	590.10	135.62	5.11		

Table 92: Degradation constants (*K*) and t/2 values for each temperature.

Table 92 also provides the degradation constant values, corresponding to the line slope for each temperature. As a matter of fact, extremely low values are provided at 20°C and 40°C (*K* = 0.0000195771 and *K* = 0.0000851802, respectively), thus confirming a significantly long half-life time for α-TM at these temperatures. Interstingly, in agreement with the literature, α-TM can be considered overall stable to the acidic conditions of the stomach (pH 2, 37°C) (Friedman, 2002). This data clearly suggests that the oral bioavailability values of α-TM are not affected by degradation processes caused by the acidic pH of the stomach. These data corroborate the results obtained by simulated gastro-intestinal digestion of LGT previously described in the paragraph **4.3.9. LGT gastro-intestinal digestion**, which demonstrated the stability of α-TM in the gastro-intestinal conditions. Furthermore, it's evident that higher temperature conditions are necessary to have an acceptable rate of α-TM hydrolysis and TD formation for our purposes. In fact, a slight increase in the constant value can be observed at a temperature of 60 °C. More remarkable is the increase of the *K* value at 80°C and 100°C, where significantly higher constant values are observed, thus indicating a rapid hydrolysis process of α-TM. As a matter of fact, at a temperature of 100°C, the highest constant value (*K* = 0.094192) and the greatest rate of α-TM degradation are provided.

As a second step of our project, the hot acid hydrolysis of α-TM was evaluated by directly considering the fresh food matrix. Since the temperature of 100°C provided the highest constant *K* value and the best t/2 value for the reference compound, the experiment was

repeated once again on fresh unripe green tomatoes deriving from the agricultural farmland "La Torrente". The experiment was performed in duplicate according to the procedure described in the paragraph **5.5.16 α-tomatine hydrolysis in green tomatoes matrix,** and α-TM was quantified via HPLC-MS/MS with the method described in the paragraph **5.5.8. Qualitative glycoalkaloids analysis**. Therefore, α-TM was quantified as "ln % remaining", by monitoring the peak area at different time points, at the sett temperature (100°C). Moreover, the α-TM stability profile was evaluated as well in water. This control was included in our experiment setting to evaluate the possibility of more "food grade" and inexpensive conditions for the hot treatment of the matrix, according to our nutraceutical purposes. Data obtained from the quantification were used to develop the α-TM degradation curve (**Figure 91**). Interestingly, 60 min of treatment at the set temperature of 100°C are sufficient to obtain a degradation rate of 98.8% in 1N HCl and 95.4% in water.

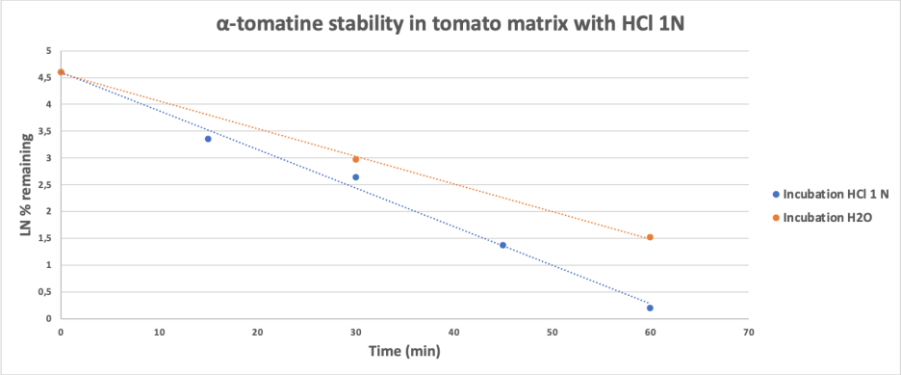


Figure 91: α-TM stability profile in fresh green tomatoes, at 100°C and two different pH conditions, expressed as “ln % remaining”, in the function of time (min).

The degradation kinetics seem to be very similar in the two conditions studied, as provided by the *K* constant value (0.071934627 and 0.051426 for acid and water incubation, respectively). Furthermore, very similar t/2 values (min) were obtained in the two incubations: as shown by **Table 93**, a time of approximately 9.6 min under acidic conditions (1N HCl) is sufficient to reduce the initial α-TM content by 50%, while a time of 13.5 min is required in the control conditions (i.e., in water).

Parameter	Incubation 1N HCl, 100 °C	Incubation H_2O, 100 °C
Degradation constant K (min^{-1})	0.071934627	0.051426
t/2 (min)	9.64	13.48
t/2 (hour)	0.16	0.25
Degradation rate (%)	98.8	95.4

Table 93: Degradation constants (*K*), t/2 values (min) and degradation rates (%) at two different incubation conditions.

The **Figure 92** provides the TD peak (rt = 9.06 min) in the MS_1 spectrum, obtained from the hydrolysis experiment in water at 0 min (**Figure 92A**) and 60 min (**Figure 92B**). The MS_1 spectrum obtained from the hydrolysis experiment after 0 min of treatment clearly shows the α-TM peak, with a retention time of 7.63 min. The comparison between these two spectra clearly demonstrates an increasing TD content with the hydrolysis process, whose identity is confirmed by observing the peak deriving from the analytical standard elution (**Figure 92C**).

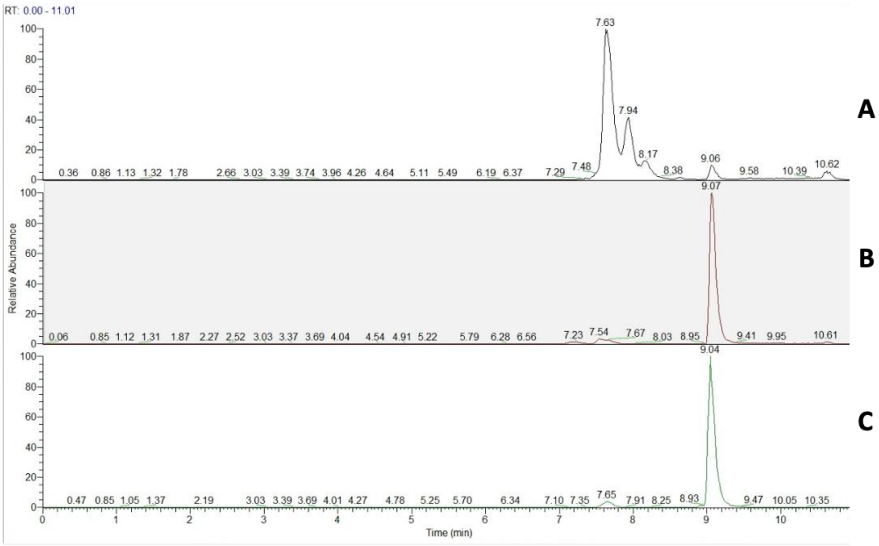


Figure 92: MS_1 spectrum of the hydrolysis experiment after 0 min of treatment (**A**) ad after 60 min (**B**); MS_1 spectrum of TD analytical standard (**C**).

Unfortunately, the α-TM compound did not provide only the aglycone of interest TD, but also other partial acid hydrolysis, which have been detected in the MS_1 spectrum of the sample (at different time points) by the LC-MS analysis in Full scan mode, as shown in **Figure 93**.

The MS spectrum of α-TM (**Figure 93A**) provides all the detected ions within a specific scan time, including both parent ion compounds and any ions or fragmentation ions formed in the ion source. Therefore, by comparing the MS_1 spectrum of t α-TM analytical standard

(**Figure 93A**) with the MS_1 spectrum deriving from the solution of the acid-hydrolysis experiment (**Figure 93B**), some fragment ions are clearly visible, including the ions 902 m/z, 876 m/z, 578 m/z, 416 m/z, and 318 m/z, but with a different relative intensity. For the solution deriving from the hydrolysis experiment, these ions are the result of the α-TM fragmentation in the ion source, on the one hand, and the hydrolysis process during the previous experiment, on the other hand. On the contrary, fragment ions obtained in the MS_1 spectrum of α-TM standard are the result of the only ion source fragmentation and, therefore, their relative intensity is lower.

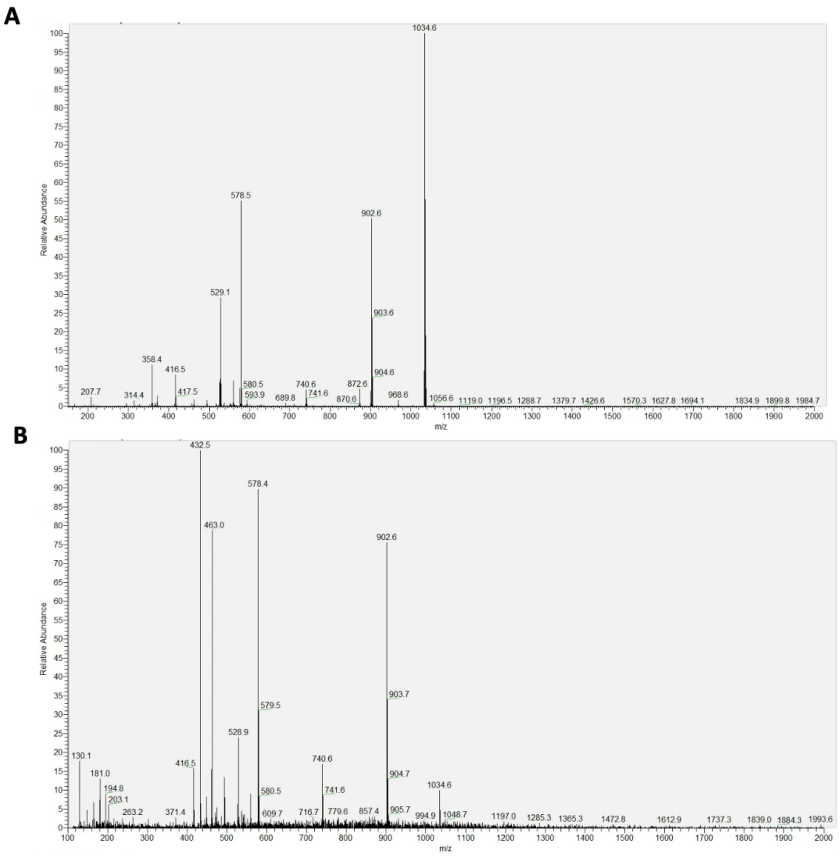


Figure 93: (**A**) MS^1 spectrum of α-TM (analytical standard) and (**B**) MS^1 spectrum of the solution deriving from the hydrolysis experiment (60 min, 100°C, 1 N HCl).

Therefore, the degradation rate of α-TM, evaluated in this study, does not necessarily correspond to TD formation rate. Moreover, these partial acid hydrolysis products are not well separated by using our MS-MS method, thus requiring the development of new suitable chromatographic conditions to correctly identify and quantify these compounds. Since the analytical standards of β1-TM, β2-TM, γ-TM, and δ-TM are not available, a chemical

synthesis or isolation with a preparative HPLC (for example coupled with a UV detector) could be necessary for a suitable quantification of these partial hydrolysis products. Moreover, untreated green tomatoes (enriched in the glycoside α-TM) could be integrated into a new formulation with chemically treated green tomatoes, which represents a TD-enriched matrix, to provide an innovative nutraceutical product that combines the advantages of both these two bioactive compounds.

Overall, these experiments open up to new interesting future applications. As widely demonstrated in our studies, it is possible to perform a hot water treatment directly on discarded green tomatoes to provide a new TD-enriched matrix and develop a nutraceutical product with a recognized anti-aging activity. On the other hand, these analytical limitations that have been found in these studies require to be overcome in the future.

5.7. Summary of chemical and microbiological effects on Piennolo tomato plant metabolome

The aim of this work was the characterization of polyphenolic and SGAs profile of Piennolo tomato plants, by considering biological variables that could increase this content in the different anatomical parts. Among them, the harvesting period of matrices (June and/or July), along with the presence or absence of the *Trichoderma* spp. treatment, were greatly useful in providing some important considerations. To achieve this goal, it was necessary to develop a suitable HPLC-MS/MS method in MRM acquisition mode for the analysis of glycosidic and aglycone alkaloids, and an HPLC-DAD method for the evaluation of polyphenols. Both these two methods were validated according to the ICH validation guideline (ICH.Q2[R2], 2022), by demonstrating their precision, accuracy, and sensitivity in the quantitative analysis. 34 matrices, accurately sampled to investigate the effect of these biological parameters, were extracted by using a hydroalcoholic mixture with a validated procedure, that demonstrated a high recovery rate and therefore a great efficiency of the process. The quantitative and statistical chemometric analysis have highlighted some remarkable evidence. Firstly, the *San Sebastiano* green tomatoes cultivar proved to be better, in terms of polyphenols and SGAs content, than the *Ercolano* cultivar. Therefore, it was chosen as the matrix on which to carry out further studies. Overall, a clear change due to the harvest period and the biological treatment has been found. The 1st harvesting green tomatoes, both treated and untreated, display a lower SGAs and polyphenols content, in particular for glycosides, than those belonging to the 2nd harvesting, thus demonstrating that the development of these secondary metabolites closely depends on the time of plant maturation and specifically on the fruits harvest period. *Trichoderma* spp. could strongly induce the development of glycosylated polyphenols (e.g., rutin) and SGAs (e.g., α-TM), by stimulating these biosynthetic pathways. The effects of this treatment are visible only by waiting for an appropriate time, i.e., until the period of 2nd harvesting (July). On the other hand, matrices sampled during the 1st harvesting (June) show a poor increase in metabolites due to the treatment, except for the aglycones quercetin and TD, which relatively accumulate and serve as biosynthetic precursors of the corresponding glycosides. The roots of the plant, which were the site of *Trichoderma* spp. inoculation, display the greatest effect due to the treatment, especially during the 2nd fruit harvesting (i.e., after waiting for an appropriate time). A remarkable increase in the SGAs content, including both glycosides and aglycones is observed, while the α-TM catabolism is inhibited by this treatment. By

comparing different anatomical parts (stem, leaves, green fruits and roots), leaves prove to be the matrix with the best SGAs and polyphenols content, especially after the *Trichoderma* spp. treatment. This excellent metabolic profile showed by leaves is confirmed by their greatest antioxidant activity, evaluated by the FC, DPPH and FRAP tests. Moreover, the good antioxidant activity provided by green fruits demonstrates and further validates their potential use as a nutraceutical product. However, the correlation between this biological treatment and the induction of secondary metabolites pathways, in a time-dependent way, should be better elucidated in the future. Since the *Trichoderma* spp. treatment is unable to enhance the TD content in green unripe fruits, the final step of our project was to develop suitable and inexpensive "food grade" conditions for the complete conversion of α-TM into its aglycone TD. Therefore, a first study of α-TM stability under acid conditions and heating demonstrated that a complete degradation is possible at 100°C. Subsequently, by repeating the experiment on the fresh green fruits, a drastic hydrolysis (rate of 95.4%) is observed at 100°C in water. This experiment was affected by analytical limitations, that should be overcome in the future, but strongly demonstrated that it is possible to treat green unripe fruits, an important waste of tomato crop, in water and under heating to obtain a new TD-rich matrix. This new matrix could be exploited for specific nutraceutical products, characterized by an anti-aging activity, and could be useful for the treatment of musculoskeletal atrophy and sarcopenia.

CHAPTER 6

DEVELOPMENT OF AN INNOVATIVE OIL FORMULATION FOR THE PREVENTION OF AGING RELATING SKIN DISEASES

6.1. Oleolytes: old remedies for modern diseases

Skin is a large and dynamic organ which is always in a flux state. Skin cells are constantly exfoliated and replenished with new skin cells. Most people have troublesome complexion flaws, such as rosacea, acne, fine wrinkles and lines, broken capillaries, age spots, scaly skin, and facial discolorations. Other skin damages include texture, tone, and loss of skin volume. A combination of cosmetic approaches and therapies are always necessary to obtain a satisfactory result. Generally, cosmetics are claimed not to have a therapeutic effect and have been labeled by the U.S. Federal Food, Drug, and Cosmetic Act (FD&C) as “an article intended to be applied to the human body for cleansing. beautifying, promoting attractiveness, or altering the appearance without affecting the body's structure or function.” A common feature of cosmetic product is that they are inert and have a primarily aesthetic effect. Instead, a different type of cosmetic product is represented by cosmeceuticals, which are a new breed of skin care products and represent a hybrid between cosmetics and pharmaceuticals. The word “cosmeceutical” was coined by Raymond Reed in 1961 to describe a product with a beneficial effect on the skin compared to an inert cosmetic. The term cosmeceutical is not recognized by the FDA and there are not specific criteria to include a product in this cosmetic category. Generally, cosmeceutical is referred to skin care products which contain active ingredients with beneficial effect to promote healthy skin. These effects can include the whitening, the protection, the tanning, the antiwrinkling, the antiaging, and the hair care.

Cosmetics and cosmeceutics products can be prepared with many types of natural extracts, such as aqueous, hydroalcoholic and alcoholic extracts and oils. Oleolytes, also known as macerated oils, have been used since antiquity in traditional medicine for the delivery of natural phytocomplexes by topical application. Oil formulations are used in cosmetics for the administration of natural apolar phytocomplexes by topical application. Therefore, they differ from mother tinctures and aqueous extracts, which are instead used for conveying polar active ingredients. In fact, oil is the best solvent for essences and other interesting lipophilic fractions such as phospholipids, sterols, carotenoids, and tocopherols, which are added to the eudermic substances which are normally present in plant oil. Moreover, for their chemical-physical characteristics, oils show a particular affinity with the skin, maintain its cellular balance and elasticity, and facilitate the passage of active molecules into the deepest layer of the skin by performing an occlusive activity that limits the exchange of water vapour with the environment, thus maintaining a sufficient state of hydration. The

most common oleolytes used in traditional medicine are obtained by *Hypericum perforatum*, *Calendula officinalis*, *Matricaria chamomilla*, and *Curcuma longa*. For example, an oleolyte widely used in traditional medicine is Oleum Hyperici, which was obtained from St. John's Wort (*Hypericum perforatum*), a European herb native whose flowers and leaves contain the active ingredients hypericin and hyperforin. This plant is used is used in the treatment of depression and its oil is used for the treatments of wounds and eczema by topic application on the skin. Oleolytes are obtained by macerating plant parts in an oily vehicle in order to extract the desired pharmacologically active compounds. Maceration is a process by which a series of components are extracted from a given matrix by prolonged immersion and eventual agitation in water or another solvent according to a standardised method for a specified time and at a controlled temperature, which varies depending on the matrix and the molecules to be extracted depending on their degradability. The maceration time is optimised for maximum extraction yield and can vary from a few hours up to 90 days. The matrix/solvent ratio may also vary, but generally the ideal proportions are 1:10, 1:5, and 1:2. After a suitable time for maceration, the preparation is filtered or centrifuged to obtain a clear oil. Oleolyte possess all beneficial properties of the oil used for extraction and those of the matrix that is macerated. A further advantage is the absence of potentially allergenic preservatives and thus the possibility of use in dermatitis sufferers, whereas this is not always true of all cosmetic preparations. The choice of oil to be used for maceration represents a critical parameter: the use of oils with a high content of unsaturated fatty acids can be a problem in formulation storage due to the high sensitivity of the double bonds to polyoxidation reactions, giving typical rancidity products. These products, represent reactive species that damage quality by affecting product shelf life. Therefore, the Official Pharmacopoeia recommends the use of specific oils that frequently undergo deacidification treatments to ensure a reduced and slower formation of these oxidation products. The active components contained in oleolytes are also often photosensitive and may degrade or alter in the light, which is why these preparations are stored in the dark or in darkened containers.

6.2. Annurca Apple as a promising food matrix for nutracosmeceutic applications

During this Ph.D. thesis, a study was performed to evaluate the preparation of an oleolyte with cosmeceutical properties from apple fruits from *Malus pumila* Miller named "Annurca" (family *Rosaceae*), an apple cultivar typical of Campania region in the south of Italy. This apple is listed as a PGI product with the name of "Mela Annurca Campana IGP" according to the European Council (Commission Regulation (EC) No. 417/2006). This apple cultivar was defined as "queen of the apples" for the white compact flesh and its peculiar organoleptic qualities, as the flavor, the taste, and the scent. The fruit has a minimal weight of 100 g and a dimension of 60 mm in diameter. It is an ancient cultivar originated in the area near Pozzuoli and its first documentation is in "*Naturalis Historia*" by Pliny the Elder. In this historical text, the authors referred to the cultivar as "Mala Oracula" for its growth near the Averno Lake. In the 1987, Giuseppe Antonio Pasquale published an agricultural manual in which he refers to the cultivar as "Annurca Apple" (AA), which is the name which is still used. Today, "Mela Annurca Campana" is referred as a PGI product, which represents a Protected Geographical Indication. The PGI represents "the name of an area, a specific place or, in exceptional cases, the name of a country, used as a description of an agricultural product or a foodstuff,

- Which comes from such an area, place or country;
- Which has a specific quality, goodwill or other characteristic property, attributable to its geographical origin;
- At least one of the stages of production, processing or preparation takes place in the area."

Therefore, the PGI recognition requires that the entire product is traditionally produced or manufactured for the preparation, the processing and the production within the recognition region. For the AA, the production region is the Campania region in the south of Italy. According to the traditional cultivation method, the harvesting period is handmaking in the middle of September. After the apple collection, they are reddened on the ground in some land plots called "melai" (**Figure 94**). They are land places smaller than 1.5 meters and they are covered by biodegradable and soft materials, such as pine needles, hemp, and other plant

materials. They protect the apples from water stagnation and the exposition to the sun. The fruits are positioned in rows and are sprayed daily with water. When the surface of the fruit becomes red, it is turned to redden its opposite side.



Figure 94: Fruits of “Mela Annurca Campana IGP” in the classical “melai” for the reddening post-harvesting period.

“Mela Annurca Campana” has been already studied for its nutraceutical potential in the management of metabolic syndrome for the reduction of cellular glucose levels and lipid uptake and in the control of hair growth (Tenore, Campiglia, Stiuso, et al., 2013; Tenore et al., 2014, 2018). These pharmacological activities have been mainly ascribed to polyphenols, which are part of the apple polar fraction. The polyphenols of the apples are mainly flavonoid derivatives and include flavonols (e.g., quercetin and its glycosides), flavanols (e.g., epicatechin, catechin and procyanidins), anthocyanins, dihydrocalcones (e.g., phloretin and phloridzin) and phenolic acids (e.g., chlorogenic acid) (Alonso-Salces et al., 2004). Some specific compounds of apple peel and apple pulp extracts have been identified as being responsible for these bioactivities. For example, phlorizin reduces cellular glucose uptake by inhibiting the sodium/glucose transport proteins SLGT1 and SLGT2 (Maisto et al., 2023), while the hypolipidemic effects have been attributed mainly to procyanidins. These compounds are accumulated in the intestinal lumen, inhibiting cholesterol uptake, and when they permeate into the bloodstream, they bind to HDL and regulate its transport and metabolism (Tenore, Campiglia, Ritieni, et al., 2013). Experimental data would also indicate a significantly higher polyphenol content in AA pulp than in other more common cultivars,

which further encourages its application (Tenore et al., 2014).

Although the polyphenols composition and the polar fraction of “Mela Annurca Campana” was extensively studied, the apolar fraction (e.g., essential oil and triterpenoid extract) composition of this apple cultivar was less investigated. The use of oils as extraction solvents allow to selectively extract the apolar components of the food matrix. Therefore, our attention was focused on the triterpenoid component, which represent a group of compounds with potential bioactivity and an application in cosmeceuticals preparation.

6.2.1. Triterpenoids: chemistry and botanical distribution

Triterpenoids represent a class of terpenes with a skeleton obtained by six isoprene units, with a great chemical diversity and can be found in nature both as aglycones called “saponins” and glycosylated derivatives. Triterpenoids constitute the plant cell membranes and are necessary in the physiology of the plant. Triterpenoids are widely spread in plant word and are identified in plants of different families, as *Leguminosae*, *Amaranthaceae*, *Apiaceae*, *Caryophyllaceae*, *Aquifoliaceae*, *Araliaceae*, *Cucurbitaceae*, *Berberidaceae*, *Chenopodiaceae*, *Myrsinaceae*, and *Zygophyllaceae*. Furthermore, they have been isolated in different botanical parts, such as fruits, leaves, roots, and branches. The triterpenoids distribution in the plant is selective. For example, glycyrrhizin was isolated in the roots of *Glycyrrhiza glabra*, while gymnemic acid and asiaticoside were isolated in the aerial parts of *Gymnema sylvestre* and *Centella asiatica*, respectively (T. Biswas & Dwivedi, 2019). Saponins synthesis and accumulation can depend on many factors which can be organ or tissue specific or can depend on environmental, genetic, and biological factors, supporting the hypothesis that these compounds have a physiological and a protective role in the plant (T. Biswas & Dwivedi, 2019).

The chemical diversity of triterpenoids derives from the key step of the cyclization of the precursor epoxide squalene through mevalonic acid pathway by different enzymes. The main triterpenoids class include the tetracyclic derivatives (e.g., protostanes, cycloartanes, dammaranes, eufans), and the pentacyclic derivatives (e.g., ursanes, gammaceranes, oleanes, lupanes, friedelanes, opanes). The fifth cycle in pentacyclic derivatives can be characterized by a cycle with six carbon atoms (e.g., ursanes, oleanes, gammaceranes) or by a cycle with five carbon atoms (e.g., lupanes, opanes) (Patocka et al., 2003).

The triterpenoids biosynthesis starts with the synthesis of mevalonate from acetyl-CoA and the subsequent phosphorylation and transport within the peroxisome in the cell, where it is

converted to isopentenyl phosphate (IPP), a 5-carbon atom isoprene derivative. IPP is a substrate of an isomerase that converts it into dimethylallyl pyrophosphate (DMAPP). IPP can be synthetized with the methylerythritol pathway in the plastids, where the biosynthesis of monoterpenes and diterpenes takes place. Within the peroxisome, a synthetase leads to the formation of farnesyl pyrophosphate (FPP) and the subsequent reaction of condensation of two FPP units generates squalene. This compound undergoes an epoxidation reaction with the formation of squalene 2,3-epoxide, which is the precursor of all triterpenoid scaffolds (T. Biswas & Dwivedi, 2019). A summary of triterpenoid biosynthetic pattern of squalene 2,3-epoxide is provided in the **Figure 95**. Finally, the triterpenoids aglycones can be glycosylated by reactions catalysed by enzymes of the class of UDP-glycosyltransferase (UGT) to obtain saponins. Glycosylation of these compounds can significantly alter their chemical and physical properties, such as solubility and the biological activity (T. Biswas & Dwivedi, 2019; Rahimi et al., 2019).

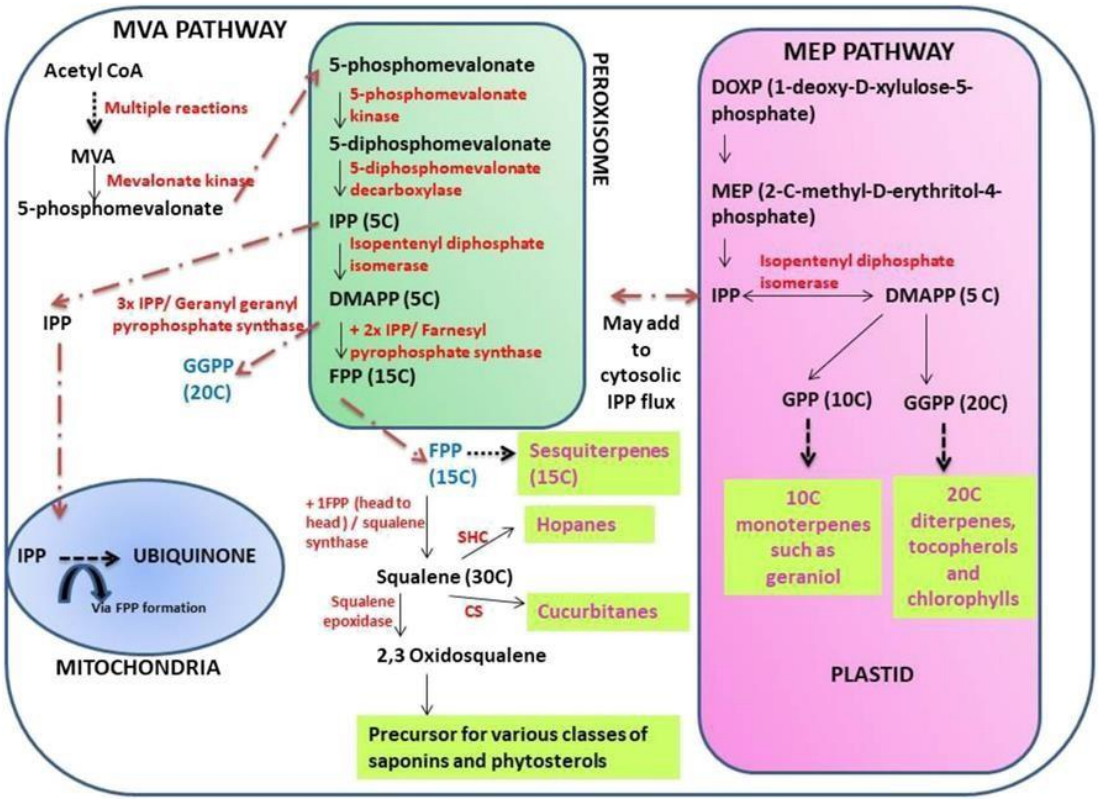


Figure 95: Biosynthetic pattern of squalene 2,3-epoxide (Picture from (T. Biswas & Dwivedi, 2019).

The chemical class of ursanes is one of the most representative of the triterpenoid class and

includes several metabolites, such as ursolic acid, oleanolic acid, α-amyrin, and β-amyrin. Ursolic acid (3-β-3-hydroxy-urs-12-en-28-oic acid) is a pentacyclic terpenic acid that can occur in free form or as a saponin complex in many matrices of natural origin, especially from the *Oleaceae*, *Rosaceae*, *Rubiaceae*, *Lamiaceae* and *Asteraceae* families. Its content varies greatly depending on the plant organ considered and the age of the plant (Kowalski, 2007). In addition, in some plants ursolic acid is synthesised in specific botanical parts, as in the bark of *Betula alba* (Jäger et al., 2009). Ursolic acid is biosynthesised in the mevalonate pathway from the precursor squalene epoxide, which is responsible for the formation of α-amyrin and β-amyrin with the characteristic ring system (**Figure 96**). These scaffolds represent the basic structures of ursolic acid and its isomer, oleanolic acid (3-β-hydroxy-olea-12-en-28-olic acid), respectively. They differ in the position of the methyl group at positions 19 and 20 of the steroid E-ring (Cui et al., 2006; Guinda et al., 2011; S. Guo et al., 2015; Kondo et al., 2011; López-Hortas et al., 2018; Yamaguchi et al., 2008).

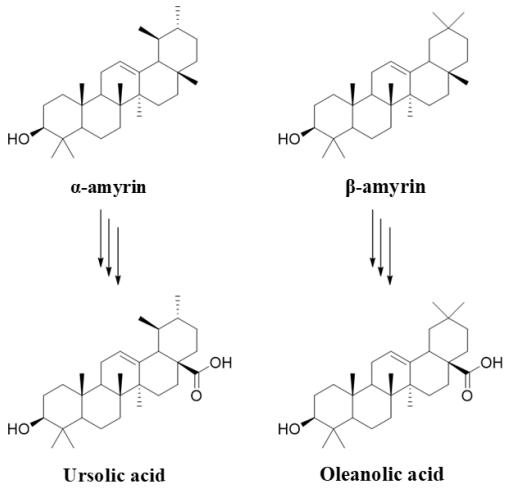
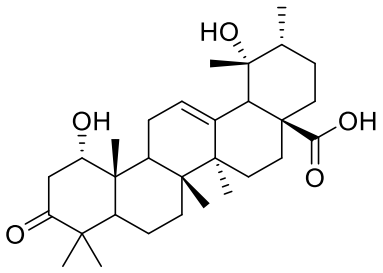


Figure 96: Biosynthetic pathway of ursanes.

The ursolic acid concentration was reported in many fruits, as the cranberry (7.09 mg/g dry fruit), jujube (0.53 mg/g dry fruit), apple peel (14.3 mg/g dry fruit), hawthorn (1.14 mg/g dry fruit), and argan (1.08 mg/g dry fruit) . In the fruit of many plants belonging to the Rosaceae family, a large number of triterpenes can be found, localised especially in the cuticular wax of the peel. In apple fruit, the total amount of triterpene compounds can reach high percentages, up to 75-95% of the total composition (Ludeña-Huaman & Ramos-Inquiltupa, 2019). Among these, ursolic acid is particularly abundant as it performs important functions in

preventing water loss and acting as the first defence barrier against pathogens. In fact, the epicuticular layer regulates a number of physiological phenomena in the plant, including transpiration and water loss, and it is precisely the lipophilic barrier constituted by the terpenes that regulates the transpiration level according to season and climatic conditions. Modern apple cultivations for commercial purposes are distinguished from older ones by a considerable increase of ursolic acid in the peels. In addition, the place where the plants are grown is also revealing for the accumulation of triterpenes (Sut et al., 2019). In this regard, apples grown in Northern regions have been shown to contain more ursolic acid than those grown in southern locations (Viškelis et al., 2019). The presence of ursolic acid has also been shown in some by-products of the agri-food industry. For example, it has been identified as a by-product of argan oil production from the leaves and the fruit and in waste such as those from juice production, unripe fruit, bark of *Eucalyptus* sp and persimmons (Gudoityte et al., 2021). AA cultivar represents not only a source of ursolic and oleanolic acid but provides also a distinctive ursane triterpenoid called annurcoic acid (acid 1α,19α-dihydroxyursan-28-oic) (**Figure 97**) (D'Abrosca et al., 2006).



Annurcoic acid

Figure 97: Chemical structure of annurcoic acid.

6.2.2. Triterpenoids: biological properties

Triterpenoids are characterized by a wide variety of biological properties with potential healthy activities, such as antitumoral, antiviral, antidiabetic, anti-inflammatory, antimicrobial, anti-parasitic, cardioprotective, hepatoprotective, and analgesic (**Figure 98**) (H. Sheng & Sun, 2011). The anti-inflammatory activities of triterpenoids have been studied in many experimental models. Many of these studies have confirmed the anti-inflammatory power of these compounds in both free and glycosylated forms, including oleanolic acid and

its saponins isolated from *Calendula officinalis*, escin from *Aesculus hippocastanum* (Sirtori, 2001) or glycyrrhizin extracted from the roots of *Glycirrhiza glabra* (Olukoga & Donaldson, 2000; Patocka & Patočka, 2003). Many pentacyclic triterpenoids have also shown an active role in regulating glucose and lipid metabolism. It has prompted research into their potential use in hypoglycaemic and hypolipidemic treatments, encouraged by the centuries-old use in traditional Chinese medicine of various drugs containing these compounds in antidiabetic and anti-obesity therapy. Pentacyclic triterpenoids may be regarded as multi-target regulators of lipid and glucose metabolism through their interaction with several receptor sites, resulting in a number of multi-organ synergistic effects which include:

- Increased glycogen synthesis and fatty acid oxidation;
- Decreased gluconeogenesis and glycogenolysis in the liver;
- Increased insulin secretion by the pancreas;
- Increased uptake and glycogenosynthesis in skeletal muscles;
- Decreased intestinal absorption of lipids and glucose;
- Increased HDL levels and decreased levels of LDL and VLDL in the vasculature (H. Sheng & Sun, 2011).

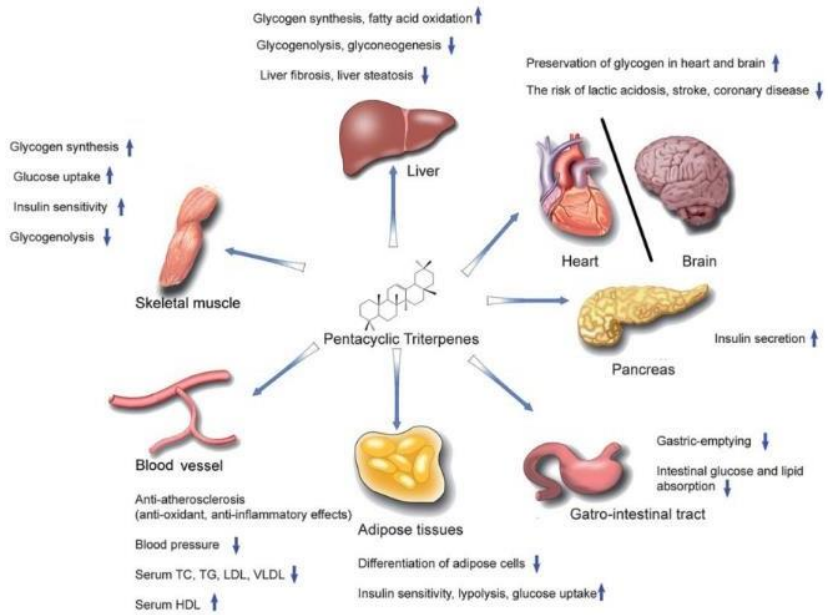


Figure 98: Biological effect of pentacyclic triterpenoids.

These observations show that pentacyclic triterpenoids are not only possible candidates in therapy but also possible natural scaffolds for the development of new drugs offering support in diseases involving lipid and glucose metabolism (H. Sheng & Sun, 2011). Metabolic disorders are closely correlated with cardiovascular diseases. Therefore, many studies investigated the potential of pentacyclic triterpenoids in the prevention and the treatment of cardiovascular diseases. The beneficial role of these compounds comes through interaction with specific molecular targets as well as through more indirect actions such as regulation of metabolism and antioxidant activity. An important interaction is certainly that with the growth factor TGF-β, a multifunctional cytokine involved in the pathogenesis of fibrotic processes, atherosclerosis and other diseases such as pancreatitis, nephritis, and cancer. Several members of the oleananes, ursanes and lupanes family have also been tested for inhibitory activity against endothelin receptors (ETa) and angiotensin II receptors (AT1), which are also involved in vascular homeostasis and thus in diseases such as hypertension and atherosclerosis. Among these, for example, Asiatic acid has shown inhibitory activity against ETa, oleanolic acid against AT1 and 18β-glycyrrhetinic acid against both receptors. Ursolic acid, betulinic acid and oleanolic acid also showed inhibitory activity against the nuclear factor NF-kB (Patocka & Patočka, 2003). Medicinal herbs containing pentacyclic triterpenoids have always been widely used in traditional medicine, especially on the Asian continent. However, their use in pharmaceutical and nutraceutical preparations is relatively recent and of growing interest, especially in the treatment of diabetes, hyperlipidaemia and cardiovascular diseases, as multi-target agents with low toxicity. Oleanolic acid, asiaticoside, glycyrrhizic acid and its derivative carbenoxolone are examples of compounds that have found use in registered prep(Patocka & Patočka, 2003)pe for several years (Patocka & Patočka, 2003). Some triterpenes have also long been used as adjuvants in vaccine formulations for their immunostimulating properties. A recent application of particular importance is that involving a Quillaja saponaria extract based on QS-21 (a quillaic acid saponin) used as an adjuvant in the Sars-Cov2 Novavax vaccine (P. Wang, 2021). A summary of the triterpenoids under study or in use with healthy potential properties on human health is provided in the **Table 94** (H. Sheng & Sun, 2011).

Name of active compound	Category	Indications	Current status	Region
CDDO (**246**)	Drug	Cancers	Phase I	America
CDDO-Me (**247**)	Drug	Cancers, kidney disease	Phase II	America
RTA 404	Drug	Multiple sclerosis	Pre-clinical study	America
Bevirimat (PA-457)	Drug	HIV infection	Phase II	America
S-0139 (**377**)	Drug	Cerebrovascular diseases	Phase II	Japan
Oleanolic acid (**10**)	Drug	Liver diseases	Registered (OTC drug)	China
Glycyrrhizic acid (**21**)	Drug	Liver diseases	Registered	China, Japan
Carbenoxolone (**321**)	Drug	Gastritis and peptic ulcers	Registered	Asia, Europe
Asiaticoside (**40**)	Drug	Wound-healing	Registered (OTC drug)	China, Europe
Corosolic acid (**30**)	Dietary supplement	Diabetes, obesity	Marketed	Asia, America
Gymnemic acids (**301**)	Dietary supplement	Diabetes	Marketed	Asia, America, Europe

Table 94: Summary of triterpenoids in study or in use with healthy potential properties on human health (Figure from ((H. Sheng & Sun, 2011)).

In the triterpenoids class, specific studies have been carried out to assess the possible biological properties of ursolic acid, which include anti-inflammatory, antioxidant, anticarcinogenic and neuroprotective activities. The mechanisms by which ursolic acid exerts its beneficial effects include the regulation of NF-kB factor in tumour cells, an increment of insulin signalling in adipose tissue, the control of the expression of endogenous substances involved in cardiac damage and inflammation, and antioxidant effects in the liver and brain (López-Hortas et al., 2018; Seo et al., 2018). Specifically, the beneficial effects of ursolic acid reported in literature are summarised as follows:

1) Anti-cancer effects, associated with cytotoxic activity verified on different cell lines. This property depends on promoting the scavenging of ROS, highly reactive radicals continuously produced in human cells that are the source of the DNA modifications underlying the carcinogenic process. Ursolic acid exerts different anti-tumoral activities, as the inhibition of angiogenesis, the antimetastatic activity, the induction of apoptosis in tumour cells, and the inhibition of glucose metabolism. This compound can inhibit the mutagenic processes and represent a chemoprotective agent in cytotoxic treatment for colon cancer, lymphoma, lung cancer and prostate cancer (López-Hortas et al., 2018).

2) Anti-obesity and anti-diabetic effects. Supplementation of ursolic acid within the diet showed a decrease in body weight by promoting the uptake and metabolism of free fatty acids by interaction with the UCP3/AMPK-dependent pathway (Chu et al., 2015). The decrease in postprandial blood glucose levels is due to the inhibition of α-amylase and α-glucosidase (S. Li et al., 2014). The potential of ursolic acid in antidiabetic therapy is mainly related to increased insulin levels and protective activity against β-pancreatic cells in association with immunomodulatory properties (T. Zhang et al., 2014).

3) Cardioprotective effects and prevention of hypertension. These effects are due to inhibition of apoptosis in cardiac muscle cells, antioxidant activity which is particularly important in the prevention of cardiovascular disease, anti-hyperlipidaemic, and hypoglycaemic properties .

4) Anti-inflammatory and analgesic effects. A key role in inflammation is played by the transcription factor NF-kB, which regulates the transcription of several genes involved in inflammation, cell proliferation and apoptosis. NF-kB is considered a critical factor in the pro-inflammatory signalling pathway, as it regulates the production of pro-inflammatory cytokines, such as TNF-α and several interleukins, in the macrophages and mast cells, which are crucial in the acute phases of inflammatory processes (Medzhitov, 2008). An important regulator of NF-kB activity is the factor IkB (Nuclear factor of kappa light polypeptide gene enhancer in B-cells inhibitor), a protein able to complex NF-kB thus inhibiting its activity and maintaining it in an inactive state. The release and nuclear transmigration of NF-kB occurs as a result of phosphorylation by certain kinases of factor IkB. Therefore, inhibition of NF-kB release represents a strategy for achieving the anti-inflammatory effect. Ursolic acid has been shown to act precisely on this cellular pathway, in particular by preventing the phosphorylation and degradation of IkB and thus the release of NF-kB at the nuclear level. The anti-inflammatory properties of ursolic acid have been confirmed by various preclinical *in vivo* experimental models such as the carrageenan and formalin tests in mice. Winter and Risley demonstrated the anti-inflammatory properties of ursolic acid with the carrageenan test, indicating a significant reduction of oedema in the paw induced by carrageenan. This effect was more pronounced than that achieved by indomethacin, a known cyclooxygenase inhibitor used in therapy. Analgesic properties were tested using experimental models such as the acetic acid-induced abdominal constriction test and the formalin test. Ursolic acid was shown to inhibit acetic acid-induced abdominal constriction, and the formalin test was performed to investigate the mechanism of action explaining this effect. Ursolic acid inhibited the second phase of formalin-induced pain, suggesting that the analgesic effect could be caused by a peripheral mechanism. Therefore, the mechanism of action could be due not only to the inhibition of inflammation mediators, such as prostaglandins, but also by blocking their receptor. *In vitro* studies have shown that this compound inhibits enzymes of the arachidonic acid cascade, in particular prostaglandin E2. These considerations suggest a

possible use of ursolic acid in combination with analgesic drugs to enhance their pharmacological activity.

5) Hepatoprotective effects against liver fibrosis. The mechanisms supporting this activity are related to inhibition of bile acid production, reduction of hepatic free radical levels through induction of transcription of Nrf2 factor target genes (S. R. Chen et al., 2015).

6) Antimicrobial effect, with an inhibition of the growth of both Gram-positive and Gram-negative bacteria and biofilm formation. Antimicrobial activity has been demonstrated against Gram-positive bacteria through *in vitro* tests with cultures of methicillin-resistant *Staphylococcus aureus*, vancomycin-resistant *Staphylococcus aureus,* and *Mycobacterium tuberculosis*. Anti-biofilm activity has been demonstrated against gram-positive bacteria through *in vitro* tests on cultures of *Streptococcus* spp, *Actinomyces* spp, and *Lysteria monocytogenes*. Finally, antimicrobial activity has also been demonstrated against various microorganisms belonging to the protozoan family such as *Plasmodium falciparum*, responsible for malaria.

7) Effects on the central nervous system in certain neurological diseases, also attributable to the antioxidant and anti-inflammatory power of triterpenoids. The brain function depends on the efficiency of neuronal signalling and the supporting activity of glial cells. Oxidative stress, and in particular increased levels of ROS and RNS are responsible for the progression of neuroinflammation underlying many brain diseases. Therefore, stimulation of cellular antioxidant systems and inactivation of ROS and RNS mediated by ursolic acid are absolutely beneficial in such disease states. The neuroprotective activity of the acid results in an increase in the size of the myelin area, the number of oligodendrocytes and the myelin basic protein (MBP) content, as it acts as an agonist of PPARy (peroxisome proliferator-activated receptor). In order to demonstrate the neuroprotective potential of ursolic acid, several studies have been conducted that have suggested its possible use in the prevention of neurodegenerative diseases such as Alzheimer's disease, Parkinson's disease and in the treatment of brain damage characteristic of pathological conditions such as ischaemia or cancerous lesions (Neimkhum et al., 2021).

8) Anti-aging effects in the skin, mainly related to the anti-inflammatory and antioxidant properties of the active ingredient. Ursolic acid has demonstrated a powerful inhibitory

action on DNA-damaging processes, particularly in scavenging ROS radicals. ROS play an essential role in the activation of transcription factors that determine the cellular senescence processes of aging skin layers in the epidermis and dermis through the release of pro-inflammatory cytokines and matrix metalloproteases (MPPs). Moreover, these oxygen radicals are implicated in the direct degradation of hyaluronic acid, a fundamental constituent of the skin matrix, and activate tyrosinase, an enzyme that converts tyrosine to dopachinone, a fundamental precursor for melanin synthesis, through an oxidation reaction. These effects lead to characteristic symptoms of skin aging, such as skin roughness, wrinkle formation and pigmentation abnormalities. On the basis of these pathophysiological phenomena, the prevention of oxidative stress, inflammation and remodelling of the extracellular matrix (ECM) have been proposed as strategies to combat skin aging (Feng et al., 2013). Several studies have demonstrated the properties of ursolic acid as an anti-aging agent for possible topical applications acting as an inhibitor of specific enzymes. One enzyme involved in wrinkle formation is elastase, which degrades the elastic fibres of connective tissue that produce the extracellular matrix responsible for skin elasticity. Ursolic acid has shown a strong inhibitory activity of this enzyme (IC_{50} = 5.51 μM), reducing the degradation of connective tissue fibres and consequently improving skin elasticity (Ying et al., 1991). Another key enzyme in skin physiology is hyaluronidase, which catalyses the hydrolysis of the 1,4-glycosidic bonds of hyaluronic acid. Hyaluronic acid is a hydrophilic polymer produced by epidermal keratinocytes and dermal fibroblasts to the skin its characteristic viscoelastic properties. Therefore, degradation of skin hyaluronic acid by hyaluronidase results in a loss of these properties, contributing to skin aging. Ursolic acid has demonstrated an inhibitory action on the hyaluronidase enzyme (IC_{50} = 103.18 μM), thus reducing the degradation of hyaluronic acid (Abdullah et al., 2016). Sensitive skin, associated with increased trans-epidermal water loss, penetrability and susceptibility to irritants, is subject to reduced permeability barrier function. This state may predispose to the development of various pathologies such as atopic dermatitis. Decreased levels of lipid components such as ceramides lead to a reduction in water retention in the stratum corneum, favoring the development of skin wrinkles and xerosis associated with aging. Ursolic acid is an excellent candidate as a moisturising agent as it stimulates ceramide synthesis and by increasing the expression of genes necessary for the differentiation of terminal keratinocytes, it improves skin permeability and recovery of the skin barrier function (Both et al., 2002). For its pharmacological properties, ursolic acid could represent a compound of interest for the development of new cosmetic and cosmeceutics formulations. This terpene,

as described above, can impart antioxidant, antimicrobial and anti-irritant functions to formulations. An example of use could be creams for external use or other cosmetics used for lip care or wrinkle treatment. Ursolic acid is also used to protect against the absorption of ultraviolet rays and prevent pigmentation induced by UV irradiation. In addition, it is used in the preparation of emulsions for wrinkle treatment, in anti-ageing moisturising gels in order to decrease water loss. For its antioxidant and anti-inflammatory properties, it is incorporated in preparations to improve and prevent skin roughness or in anti-acne formulations, in hand creams to promote healing, as a whitening agent to counteract tanning, in body creams and to regulate hair growth. Other uses include the formulation of soaps with skin care and disinfection functions, compositions for toothpastes or even preparations for the prevention of skin cancer for topical use. Ursolic acid has also found use in formulations for wound recovery, particularly in the formulation of ointments to promote skin regeneration. Cutaneous formulations based on extracts from pine branches, with titrated amounts of ursolic acid and flavonoids, have demonstrated efficacy in the treatment of mucosal changes due to radiation exposure, traumatic injuries, burns and surgical wounds. The cosmetic applications of ursolic acid that have already been patented are exhaustively summarised in the **Table 95**.

Cosmetic applications incorporating ursolic acid.

Objectives and products	Applicant	Patent number	Reference
Cosmetic composition containing *crataegi fructus* extract for preventing or delaying skin aging by removing free radicals	Coreana Cosmetics Co Ltd	KR 20000045576	Kim and Kim (2000)
Nano liposome composition containing ursolic acid or derivatives, with excellent bio-affinity and skin permeability, maximizing the inclusion of functional agents used in treating skin diseases	Aimsphil Co Ltd	KR 20040027829	Kim and Kim (2004)
Personal care compositions to regulate hair growth and the condition of mammalian skin, comprising at least one chronic skin care active, one acute skin care active, a carrier and a cationic thickener	Procter & Gmable and inventors	WO 2004078157 WO 2005110352 WO 2005110353	Oblong et al. (2004), Oblong, McPhail, Weitz, and Harris (2005), Oblong, McPhail, Weitz, Harris, and McIver (2005)
Enhancing stability of skin care preparations with ursolic acid and/or derivatives; the emulsion is constituted of at least two kinds of oil droplets to prevent crystal deposition at low temperatures	Pola Chem. Ind. Inc.	JP 2006036715 JP 2006036716	Sugiyama et al. (2006a), Sugiyama et al. (2006b)
Fragrant/flavorous formulation with hyaluronidase inhibitory action containing essential oil and either ursolic acid and oleanolic acid	Takasago Perfumery Co Ltd	JP 2006124322	Kawada (2006)
A composition for topical tanning application, comprising a liposome encapsulated ursolic acid, a tanning agent and a carrier	E L Management Corp. and inventors	WO 2006007487	Giacomoni and Maniruzman (2006)
Skin external composition comprising a microemulsion containing ursolic acid and xanthan gum and/or poloxamer	A & H Care Inst.	KR 20060126247	Jee and Park (2006)
Anti-wrinkle cosmetic composition with ursolic acid, an acidic salt, an alkaline salt, and ethanol, an oily phase liquid crystal composition and an aqueous phase liquid crystal composition	Kolmar Co Ltd	KR 20060118792	Jeong, Kang, Han, Jeong, and Han (2006)
Skin care preparation containing ursolic acid (or its salt, ester or dimer acid diester form) for lowering the transepidermal water loss	Pola Chem. Ind. Inc.	JP 2007161610 JP 2007161611	Akamatsu et al. (2007a), Akamatsu et al. (2007b)
Improving the solubility of ursolic acid in external preparations for preventing the skin roughness	Pola Chem. Ind. Inc.	JP 2007246459	Suenobe and Hitani (2007)
Technique to stabilize skin preparations in a water-in-oil emulsion, with low solubility ingredients, such as a phytosterol glycoside, sphingo glycolipid, ursolic acid or derivative	Pola Chem. Ind. Inc.	JP 2007308381	Akatsuka and Seto (2006)
Stably compounding low solubility ingredients in a water-in-oil emulsion using an organic-modified clay and ursolic acid	Pola Chem. Ind. Inc.	JP 2007308385	Akatsuka and Seto (2007)
Ursolic acid, its salt or its analog as an effective tyrosinase inhibitor	Nikko Chem. Co Ltd.; Cosmos Tech. CT KK	JP 2007332066	Kanjo and Okano (2007)
Cosmetic composition containing a cationic polymer nanocapsule with ursolic acid as active ingredients to enhance the skin penetration	AmorePacific Corp.	KR 100757043	Ryu et al. (2007)
Formula with excellent percutaneous absorption promoting action of an anti-inflammatory component in water or emulsion systems	Pola Chem. Ind. Inc.	JP 2008115109	Kobayashi et al. (2008)
A sheet-type cosmetic composition that includes a low-viscous nano-emulsion and a liposome insoluble material	AmorePacific Corp.	KR 20080038812	Kwon, An, Nam, Han, and Kang (2008)
Phosphorylated triterpenic acids and/or their salts for cosmetics and drugs with antiinflammatory action and inhibiting melanin production	Pola Kemikal Indastriz Ink	RU 2008100042	Otiai, Goto, Tokudome, and Khirokava (2008)
Hydrogel containing ursolic acid and providing moisturization and antiaging effects	Lee, G. W.; Seo, B. G.	KR 20090126048	Lee et al. (2009)
Technique for improving pharmaceutical compatibility and generality in an external skin preparation containing ursolic acid or derivative	Pola Chem. Ind. Inc.	JP 2009001502	Akatsuka, Sugiyama, Hatano, Imamura, and Fukuda (2009)
Technique for dissolving *Rosmarinus officinalis* extracts in stable creams or lotions	Sansho Seiyaku KK	JP 2009249306	Komiya and Iga (2009)
Use of ursolic acid and oleanolic acid for preparing a pharmaceutical composition useful for treating tuberculosis	Inst. Mexicano del Seguro Social	MXPA 06015160	López, Arellanes, Fischer, Pando, and Herrera (2009)
Skin external preparation containing a triterpenic acid having excellent storage stability by improving the dissolution stability	Kuraray Co. Ltd.; Pola Chem. Ind. INC and inventors	US 2009253663	Akamatsu, Suzuki, and Sakai (2009)
Water-in-oil emulsion skincare preparation for external use containing triterpenes, organomodified clays, ceramide and/or amino acid diester	Pola Chem. Ind. Inc.	JP 2009035512	Sugiyama et al. (2009)
Ursolic acid from plants used for the treatment of acne with no skin deformities left, side effects and combinations with other medicines	Kallimanis et al.	GR 1006399	Kallimanis et al. (2009)
A cosmetic composition for skin hydration and sedation effect by using *Prunella vulgaris* leaf extract, containing oleanolic acid and ursolic acid, extracts from *Aloe barbadensis* leaf and *Buddleja davidii*	AmorePacific Corp.	KR 20090038285	Jung et al. (2009)
Skin care compositions, comprising natural extracts and UA, with dual action for management of pathologies associated with skin insults	–	US 2009169651	Majeed (2009)
Skin preparation, containing either ursolic acid or a derivative and a hydroquinone derivative, to prevent pigmentation after UV irradiation	Pola Chem. Ind. Inc.	JP 2010030929	Fukuda (2010a)
Skin external preparation containing ursolic acid or derivative, and a water soluble derivative of ascorbic acid and/or its salt	Pola Chem. Ind. Inc.	JP 2010030928	Fukuda (2010b)
Anti-aging cosmetic composition to protect skin from stress and toxic factors and to activate skin cell regeneration, containing oleanolic acid, ursolic acid, betacarotene, or retinol	AmorePacific Corp.	KR 20100060753	Lim, Kim, Chang, Kim, and Cho (2010)
Skin anti-aging cosmetic composition containing a glutamylamidoethyl indole as an active ingredient and 0.001–10 wt% of oleanolic acid, ursolic acid, glycyrrhetinic acid, or retinol	AmorePacific Corp.	KR 20100058858	Kang, Lim, et al. (2010)

Table 95: Summary of patented cosmetic and cosmeceutic application of ursolic acid (López-Hortas et al., 2018).

The widely demonstrated activity of triterpenoids and ursolic acid has aroused great interest in their possible therapeutic use over the years. However, its use has often been discouraged

by the difficulty in formulating of hydrophobic compounds, a problem that translates into low water solubility and thus low bioavailability. In the Biopharmaceutics Classification System (BCS) of the drugs, which classify the compounds based on their solubility and permeability in the oral administration, ursolic acid is classify as a compound of class IV, with low permeability and low solubility. However, over the years, advances in pharmaceutical technology have made it possible to hypothese and develop formulation strategies that could also be applied to this type of compound to implement its pharmacokinetic properties. Strategies have recently been evaluated for ursolic acid, mainly involving the use of liposomal carriers, phospholipid carriers and nanoparticle polymeric complexes such as chitosan-modified polylactic acid (Antonio et al., 2021; S. Biswas et al., 2019; M. Wang et al., 2017). The main advantage of using these systems is in the possibility of improving the solubility and pharmacokinetic characteristics of apolar compounds and optimising the release profiles at the target district level. This makes it possible to drastically reduce the dose to be administered in order to have a therapeutic action, thus improving the safety profile of the active ingredient and reducing the risk of toxicity and side effects. *In vivo* experiments have shown a significant increase in oral bioavailability (Antonio et al., 2021; S. Biswas et al., 2019).

During this Ph.D. project, an approach of improvement of ursolic acid solubility and release using the oil as solvent was studied. The ursolic acid enriched oleolyte was studied as starting material for the development of a cosmeceutical formulation with potential anti-aging properties in skin diseases. To optimize ursolic acid extraction from the matrix AA, a statistical approach of response surface methodology (RSM) was applied to assess the optimum condition for the active ingredient extraction using sunflower oil as lipophilic extraction solvent. The extract obtained under the optimized RSM conditions, called Optimized Annurca Apple Oleolyte (OAAO), was chemically characterized and evaluated in some *in vitro* and *in vivo* assays to evaluate its cosmeceutical potential. The results of optimization were published as a scientific article entitled “Optimization of Ursolic acid Extraction in Oil from Annurca Apple to Obtain Oleolytes with Potential Cosmeceutical Application” in the international journal Antioxidant.

6.3. Materials and methods

6.3.1. Reagents

All chemicals, reagents, and standards used were analytical or LC-MS grade reagents. The water was treated in a Milli-Q water purification system (Millipore, Bedford, Burlington, MA, USA) before use. Sunflower oil was purchased in a local market. Ursolic acid (purity ≥ 98.5% HPLC), rutin (purity ≥ 94% HPLC), quercetin 3-O-glucoside (purity ≥ 98% HPLC), kaempferol 3-O-glucoside (purity ≥ 90% HPLC), kaempferol 3-O-rhamnoside (purity ≥ 98% HPLC), phloridzin (purity ≥ 99% HPLC), phloretin (purity ≥ 98.5% HPLC), gallic acid (purity ≥ 99% HPLC), 6-hydroxy-2,5,7,8-tetramethylchromane-2-carboxylic acid (purity > 97% HPLC) were purchased from Sigma-Aldrich (Milan, Italy).

6.3.2. Annurca apple collection and oleolyte preparation

6.3.2.1. Oleolyte preparation and experimental design

AA fruits (*Malus pumila* Miller cv Annurca) were collected in Valle di Maddaloni (41°04′44″N 14°24′53″E, Caserta, Italy) in October 2021 when the fruits had just been harvested (green peel). The fruits were reddened for about 30 days, and then analyzed (Lo Scalzo et al., 2001). After this time, the apples were washed, sliced, and then freeze-drying. The oleolyte formulation was performed by adding a defined weight of AA to a specific volume of a deacidified sunflower oil (g/mL) in a ratio of 1:4. At the end of matrix maceration in oil, the mixture was centrifuged at 9000 rpm for 10 min at different temperatures. The oil supernatant was collected and stored protected from light at 4 °C until analysis. As reported in **Table 96**, different extraction times (1h, 2h, 4h, 12h, 24h, 48h, and 96 h) and incubation temperatures (20 °C, 40 °C, 60 °C, and 80 °C) were opportunely combined to optimize ursolic acid incorporation in the oil. All optimization conditions were performed in triplicate.

Independent variables	Factor levels						
Time (hours)	1	2	4	12	24	48	96
Temperature (°C)	20	40	60	80			
Total runs	28						

Table 96: Experimental design for the independent variables used for the RSM optimization model.

6.3.2.2. Deacidification procedure of sunflower oil

Before the oleolyte preparation, the sunflower oil was previously deacidified with a liquid-liquid extraction with an alkaline solution. A volume of 250 mL of a sodium carbonate solution (Na_2CO_3 7.5%, *w*/*v*) was added to 250 mL of n-(Punathil Kannan & Ambale Gundappa, 2014) oil (Punathil Kannan & Ambale Gundappa, 2014). The solvent mixture was stirred for 10 min, and the organic phase was separated by liquid-liquid extraction. The organic phase was washed with 1000 mL of water to remove the alkaline solution traces. The mixture was left under stirring for 10 min, and the organic phase was recovered by liquid-liquid extraction. Finally, the hexane was evaporated under a vacuum at 35 °C to obtain a deacidified oil.

6.3.2.3. Oil samples acidity determination

Acidity determination was expressed as the weight percentage of oleic acid and was performed according to the Regulation (EU) No 2016/1227. A mixture of diethyl ether and ethanol (50:50 *v*/*v*) was neutralized with a potassium hydroxide 0.1 M solution and with 300 µL of a phenolphthalein 0.03 M ethanolic solution. An aliquot of oil (2.5 g) was dissolved with 50 mL of the neutralized solvent mixture. The mixture was titrated by stirring the mixture with an aqueous solution of potassium hydroxide 0.1 M till the pH indicator changes colour. All determinations were performed in triplicate. The acidity was calculated according to the following equation:

$$\textbf{Acidity (weight \% of oleic acid)} = \frac{V \times c \times M}{10 \times m}$$

where V is the volume (ml) of the titrated potassium hydroxide solution, c is the concentration (M) of titrated potassium hydroxide solution, M is the molar mass in grams per mole of oleic acid (282 g/mol), and m is the mass (g) of the oil sample.

6.3.3. Triterpenoid analysis of Annurca Apple oleolytes

6.3.3.1. Ursolic acid extraction of oil formulation

A volume of 120 mL of a solution of sodium carbonate Na_2CO_3 7.5% (*w/v*) was added to 60 mL of OAAO. The mixture was stirred for 10 min, and the aqueous phase was separated by liquid-liquid extraction. The aqueous phase was acidified with 2 N hydrochloride acid at pH = 3, frozen and then lyophilized. The solid residue was extracted with a volume of 20 mL of ethyl acetate was added. The mixture was vortexed for 1 min and sonicated in an ultrasonic bath (Branson Fisher Scientific 150 E Sonic Dismembrator) for 10 min. Samples were shaken on an orbital shaker (Sko-DXL, Argolab, Carpi, Italy) at 600 rpm for 10 min at room temperature and then centrifuged at 9000 rpm for 10 min at room temperature. The supernatants were collected and stored at 4 °C protected from the light. The obtained pellets were re-extracted with 10 mL of ethyl acetate using the same protocol. Finally, the extracts obtained were evaporated to dryness under a nitrogen light stream, reconstituted in dimethylsulfoxide (DMSO) at a concentration of 30 mg/mL, diluted with acetonitrile at a final concentration of 5 mg/mL, and stored at −20 °C until analysis. The preparation of the blank matrix sample for ursolic acid calibration curves and recovery and matrix effect experiments was performed by extracting the deacidificated sunflower oil without matrix with the same protocol described below.

6.3.3.2. Quantitative analysis of ursolic acid by HPLC-DAD

A Jasco Extrema LC-4000 HPLC system (Jasco Inc., Easton, MD, USA), coupled with an autosampler, a binary solvent pump, and a diode-array detector (DAD), was used for the analysis. Separation was performed according to the previously described method by (Kontogianni et al., 2013), with slight modifications. The column used was a Kinetex® C18 column (250 mm × 4.6 mm, 5 μm; Phenomenex, Torrance, CA, USA). Water with 0.1% formic acid (A) and acetonitrile (B) were used as mobile phases. The elution gradient was

performed under the following conditions: 0–3 min, isocratic on 60% phase B; 3–20 min, linear gradient from 60 to 90% B; 20–24 min, isocratic with 90% B; 24–29 min, isocratic on 60% B for column reconditioning (**Figure 97**). The injection volume was 20 µL, the column temperature was set at 30 °C, and the flow rate was set at 1 mL/min. The quantification of ursolic acid was performed at 205 nm.

Time (min)	% B
0	60.0
3.0	60.0
20.0	90.0
24.0	90.0
24.1	60.0
29.0	60.0

Table 97: HPLC-DAD method for ursolic acid analysis of Annurca apple oleolyte.

6.3.4. HPLD-DAD method validation for ursolic acid analysis

6.3.4.1. Linearity and sensitivity of ursolic acid HPLC-DAD analysis

Method validation was performed according to the ICH validation guideline (ICH.Q2[R2], 2022), which included the evaluation of a set of parameters, such as linearity range, the limit of detection (LOD), the limit of quantification (LOQ), precision and accuracy. Stock solutions of ursolic acid was prepared by dissolving the individual standards in acetonitrile to obtain a concentration of 1 mg/ml. The calibration curves ($R^2 \geq 0.99$) were obtained by diluting the individual stock solutions in the same solvent to obtain six ursolic acid concentrations (1 ppm, 5 ppm, 10 ppm, 50 ppm, 100 ppm, and 500 ppm) with dilution factors of 2 and 10. The standard dilutions were analyzed in triplicate injections at each concentration level. The calibration curves were constructed by plotting the peak area against the standard concentration to evaluate the linearity of the standard response. A 6-point calibration curve was constructed by plotting the peak area against the standard

concentration to evaluate the linearity of the method. Limits of detection (LODs) and limits of quantification (LOQs) were determined to evaluate the sensitivity of the method. Determination of the signal-to-noise ratio was performed by comparing measured signals from samples with known low concentrations of analyte with those of blank samples (Maisto et al., 2022). Evaluation of the signal-to-noise ratios was performed by comparing measured signals from samples with a known low concentration of 0.295 ppm of ursolic acid with those of blank matrix samples. The blank matrix sample was obtained by a sunflower oil extract at a concentration of 5 mg/ml with acetonitrile. LOD represents the minimum concentration at which the analyte can be reliably detected and is defined as the lowest detectable concentration of analyte that gives a response that the analytical system can distinguish from the background level (S (signal of compound)/N (signal of noise)) = 3. Instead, LOQ is defined as the lowest quantifiable concentration of analyte that can be measured with a standard level of confidence, and it is typically calculated using (S/N) = 10 (Maisto et al., 2022).

6.3.4.2. Precision and accuracy of ursolic acid HPLC-DAD analysis

As recommended by the ICH validation guideline (ICH.Q2[R2], 2022), the determination of accuracy (estimated by calculating the % bias) and precision (estimated by calculating the coefficient of variation CV %) was performed to validate the analytical method. Precision and accuracy were calculated by an intra-day and an inter-day analysis of individual ursolic acid standard solutions at 3 different concentration levels. The intra-day analysis was performed by injecting the standard solutions 3 times per day. Instead, the inter-day analysis.

6.3.5. Matrix effect and recovery of ursolic acid extraction from oil formulation

The matrix effect was calculated by comparing the slope of the calibration curves of the analytical standard in the presence of the matrix (blank matrix sample spiked with ursolic acid post extraction) and the calibration curves of the analytical standards in the absence of the matrix (ursolic acid in acetonitrile). The significance of the matrix effect comparison

was performed using the student t-test, with a significant difference accepted at the 95% of confidence level. An evaluation of the matrix effect (%) was obtained by calculating the ratio of the peak area in the spiked blank matrix samples and in the blank solvent. The matrix was spiked with the analyte in triplicate with 10 µg (low), 20 µg (medium), and 30 µg (high) of ursolic acid. The ratio was calculated as follows:

$$\boldsymbol{Matrix\ effect}\ \% = \frac{\textbf{Peak area}_{\boldsymbol{in\ presence\ of\ matrix}}}{\textbf{Peak area}_{\boldsymbol{in\ solvent}}} \cdot \mathbf{100}$$

The recovery was calculated by using the ratio of the peak area in the pre-extraction spiked samples (matrix spiked with known concentration of analytes pre-extraction) to the peak area in the post-extraction spiked samples (matrix spiked with known concentration of analytes post-extraction). The spiked ursolic acid concentrations used for the recovery experiments were the same reported for the matrix effect analysis. The ratio was calculated as follows:

$$\boldsymbol{Recovery}\ \% = \frac{\textbf{Peak area}_{\boldsymbol{pre-extraction\ spiked\ sample}}}{\textbf{Peak area}_{\boldsymbol{post-extraction\ spiked\ sample}}} \cdot \mathbf{100}$$

6.3.6. Polyphenols analysis of Annurca Apple oleolyte

6.3.6.1. Polyphenols extraction of Annurca Apple oleolyte

An aliquot of OAAO (8 g) was dissolved in n-hexane (8 mL) and mixed with 8 mL of a solution of 80% methanol with 1% formic acid, shaken for 10 min on an orbital shaker (Sko-DXL, Argolab, Carpi, Italy) at 600 rpm at room temperature (Assiri et al., 2016). The hydroalcoholic phase was separated with a liquid-liquid extraction and protected from light at 4 °C. The oil phase was re-extracted with the same procedure using 8 mL of the hydroalcoholic extraction mixture. Finally, the solution was evaporated to dryness under a gentle stream of nitrogen, reconstituted in a hydroalcoholic mixture (solution at 50% of methanol, *v/v*) at a concentration of 20 mg/mL, and stored at −20 °C until the analysis.

6.3.6.2. Quantitative analysis of polyphenols by HPLC-DAD

Polyphenolic quantitative analysis of the OAAO hydroalcoholic extract was performed with an HPLC Jasco Extrema LC-4000 system (Jasco Inc., Easton, MD, USA), equipped with an autosampler, a binary solvent pump, and a diode-array detector (DAD). Chromatographic analysis was performed according to the previously validated method (Maisto et al., 2022). Hydroxycinnamic acids, flavanols, flavanones, and chalcones were monitored at 280 nm, while flavonols were monitored at 360 nm. The mobile phases were water at 2% formic acid (solvent A) and a solution at 0.5% formic acid in acetonitrile and water 50:50, *v*/*v* (solvent B). Separation was performed using as column a Kinetex® C18 column (250 mm × 4.6 mm, 5 µm; Phenomenex, Torrance, CA, USA): 0-2, isocratic on 10% phase B; 2-52, linear gradient from 10 to 55% B; 52-62, linear gradient from 55 to 95% B; 62-70, isocratic on 10% B for column recondition (**Figure 98**). The injection volume was 20 µL, the column temperature was set at 30 °C, and the flow rate was set at 1 mL/min. Peak identification was based on a comparison of retention times with analytical standards and standard addition to the samples. Quantitative analyses were performed using the calibration curve calculated with 6 different concentrations in a concentration range of 0.1–1000 ppm and triplicate injections at each concentration level.

Time (min)	% B
0	10.0
2.0	10.0
52.0	55.0
62.0	95.0
62.1	10.0
70.0	10.0

Table 98: HPLC-DAD method for polyphenols analysis of Annurca apple oleolyte.

6.3.7. Qualitative analysis of Annurca Apple oleolyte

An HPLC DIONEX UltiMate 3000 (Thermo Fisher Scientific, San Jose, CA, USA) equipment, coupled with an autosampler, a binary solvent pump, a diode-array detector (DAD), and an LTQ XL mass spectrometer (Thermo Fisher Scientific, San Jose, CA, USA),

were used for the analysis. Separation was performed using as column a Kinetex® C18 column (75 mm × 2.1 mm, 2.6 µm; Phenomenex, Torrance, CA, USA). The mobile phases were water at 0.1% formic acid (A) and acetonitrile at 0.1% formic acid (B). Elution was performed according to the following conditions: 0–3 min hold at 5% solvent B, from 5% (B) to 95% (B) in 22 min, followed by 3 min of maintenance; for the remaining 3 min, the column was equilibrated to the initial conditions. The injection volume was 5 µL, the column temperature was set at 35 °C, and the flow rate was set at 0.35 mL/min. For the mass parameters, the source was a heated electrospray interface (HESI) operated in negative ionization with full scanning (FS) and data-dependent acquisition (DDA). Collision-induced fragmentation was made using argon, with a collision energy of 35.0 eV. The source operated in negative ionization mode for polyphenolic extract analysis and both in positive and negative ionization modes for triterpenoic extract analysis. The ion source was set for positive ionization mode using the following parameters: source heated temperature: 150 °C; sheath gas flow rate: 30 l/min; auxiliary gas flow rate: 10 l/min; capillary temperature: 320 °C; source voltage: 3.5 kV; source current: 100 µA; capillary voltage: 32 V; and tube lens: 80 V. The ion source was set for negative ionization mode using the following parameters: source heated temperature: 150 °C; sheath gas flow rate: 30 l/min; auxiliary gas flow rate: 10 l/min; capillary temperature: 320 °C; source voltage: 3.5 kV; source current: 100 µA; capillary voltage: 31 V; and tube lens: 90 V. The separation conditions are summarized in the **Table 99**. The source parameters of positive and negative acquisition mode are summarized in **Tables 100** and **101**, respectively.

Time (min)	% B
0	5.0
3.0	5.0
22.0	95.0
25.0	95.0
25.1	5.0
28.0	5.0

Table 99: HPLC-HESI-MS/MS method for polyphenols and triterpenoids analysis of Annurca apple oleolyte.

Column	Kinetex® C18 column (75 mm x 2.1 mm; 2.6 µm)
Phase A	Water at 0.1% HCOOH
Phase B	Acetonitrile at 0.1% HCOOH
Column Temperature	35 °C
Injection volume	5 µl
Flow rate	0.35 ml/min
Collision Energy	35 eV
Sheath gas flow rate	30 l/min
Auxiliary gas flow rate	10 l/min
Capillary temperature	320 °C
Source heated temperature	150 °C
Source voltage	3.5 kV
Source current	100.0 µA
Capillary voltage	32 V
Tube lens	80 V

Table 100. Summary of the chromatographic and source parameters of the HPLC-HESI-MS/MS method in positive acquisition mode for oleolyte qualitative analysis.

Column	Kinetex® C18 column (75 mm x 2.1 mm; 2.6 µm)
Phase A	Water at 0.1% HCOOH
Phase B	Acetonitrile at 0.1% HCOOH
Column Temperature	35 °C
Injection volume	5 µl
Flow rate	0.35 ml/min
Collision Energy	35 eV
Sheath gas flow rate	30 l/min
Auxiliary gas flow rate	10 l/min
Capillary temperature	320 °C
Source heated temperature	150 °C
Source voltage	3.5 kV
Source current	100.0 µA
Capillary voltage	31 V
Tube lens	90 V

Table 101. Summary of the chromatographic and source parameters of the HPLC-HESI-MS/MS method in positive acquisition mode for oleolyte qualitative analysis.

6.3.8. Total phenolic content (TPC)

The Folin-Ciocalteau method was used to determine the total phenolic content (TPC). The assay was performed according to Maisto et al. (2022), with slight modifications. Briefly, 0.125 ml of each sample hydroalcoholic extracts were diluted to the final volume of 3 ml by addition of 0.125 ml of Folin-Ciocalteau's reagent, 1.25 ml of an aqueous solution of Na_2CO_3 7.5 (*w/v*), and 1.5 ml of water. After mixing for 10 seconds, the samples were kept in the dark for 90 min. After the reaction time, the absorbance was measured at 760 nm with a V-730 UV-visible/NIR spectrophotometer operated by Spectra Manager™ Suite (Jasco Inc., Easton, MD, USA). Calibration curve was obtained using seven concentrations of gallic acid, in a concentration range from 7.5 to 250 ppm with a dilution factor of 4 and three replicates were performed at each concentration. Gallic acid stock solution was obtained by dissolving the analytical standard in methanol at a concentration of 1 mg/ml. The hydroalcoholic OAAO extracts were analysed in triplicate and the total phenolic content was calculated as mg gallic acid equivalents (GAE)/g dry weight (DW).

6.3.9. DPPH assay

The antioxidant activity of GE samples was measured using DPPH (radical 2,2-diphenyl-1-picrylhydrazyl) assay. The assay was performed according to Iannuzzo et al. (2022), with slight modifications. Briefly, 200 µl of OAAO hydroalcoholic extracts were added to 1000 µl of a methanol solution of DPPH 0.05 mM. After mixing, the solutions were kept in the dark for 10 min. After the reaction period, a decrease in the absorbance was measured at 517 nm with a V-730 UV-visible/NIR spectrophotometer operated by Spectra Manager™ Suite (Jasco Inc., Easton, MD, USA). The absorbance of methanolic solution of DPPH radical without sample, e.g., the control, was used as blank. Inhibition was calculated according to the following equation:

$$\% \, \boldsymbol{inhibition} = \left[\frac{\left(\boldsymbol{A_i} - \boldsymbol{A_f}\right)}{\boldsymbol{A_c}}\right] \boldsymbol{x} \, \mathbf{100}$$

where Ai is the absorbance of the sample at time zero, Af is the absorbance after 10 min, and Ac is the absorbance of the control at time zero. 6-hydroxy-2,5,7,8-tetramethylchroman-2-carboxylic acid (Trolox) was used as antioxidant standard. Calibration curve was performed using eight concentrations, with a concentration range of 5 – 250 µM with two dilution factors of 2 and 5 and three replicates at each concentration. Trolox stock solution was obtained by dissolving the analytical standard in methanol at a concentration of 1 mM. Hydroalcoholic OAAO extracts were analysed in triplicate and the results were expressed in µmol Trolox equivalent (TE)/g DW. Furthermore, the results were reported as EC_{50}, which is the amount of sample necessary to decrease the initial DPPH concentration by 50%.

6.3.10. ABTS assay

The antioxidant activity of GE samples was measured using ABTS (2,20-azinobis(3-ethylbenzotiazoline-6-sulfonate)] assay. The assay was performed according to Maisto et al., 2023, with slight modifications. ABTS solution was prepared by adding 2.5 ml of ABTS 7.0 mM solution to 44 µl of potassium persulfate 140 mM solution, and kept 7 h, at 5°C in the dark to react. The mixture was diluted with ethanol until an absorbance value of 0.70 ± 0.05 at 754 nm (Jasco Inc., Easton, MD). 100 µl of OAAO hydroalcoholic extracts was added to 1000 µl of ABTS ethanolic solution. After mixing, the solutions were kept in the dark for 2.5 min. After the reaction period, a decrease in the absorbance was measured at 517 nm (Jasco Inc., Easton, MD, USA). The control ABTS ethanolic solution absorbance was used as blank. Inhibition was calculated according to the following equation:

$$\%\ \boldsymbol{inhibition} = \left[\frac{\left(\boldsymbol{A_i} - \boldsymbol{A_f}\right)}{\boldsymbol{A_c}}\right] \boldsymbol{x}\ \mathbf{100}$$

where Ai is the absorbance of the sample at time zero, Af is the absorbance after 10 min, and Ac is the absorbance of the control at time zero. Trolox was used as antioxidant standard. The calibration curve was performed with eight different concentrations, with a concentration range of 5 – 200 µM with two dilution factors of 2 and 5 and three replicates at each concentration. Trolox stock solution was obtained by dissolving the analytical standard in methanol at a concentration of 1 mg/ml. Hydroalcoholic OAAO extracts were analysed in triplicate and the results were expressed in µmol TE/g DW. Furthermore, the

results were reported as EC_{50}, which is the amount of sample necessary to decrease the initial ABTS concentration by 50%.

6.3.11. FRAP assay

Ferric reducing activity of GE samples was measured using the ferric reducing antioxidant power (FRAP) assay. The assay was performed according to the methods proposed by Schiano et al. (2022) To prepare the FRAP reactive, a solution of 10 mM TPTZ (2,4,6-tris(2-pyridyl)-s-triazine) was prepared by dissolving 33.5 mg of the reagent in 10 ml of 40 mM HCl solution. FRAP working solution was prepared by mixing 1 ml of TPTZ solution with 10 ml of 0.3 M pH 3.6 acetate buffer and 1 ml of 20 mM ferric chloride solution. The mixture was pre-warmed at 37°C. 0.15 ml of OAAO hydroalcoholic extracts was added to 2.85 ml of FRAP working solution. After mixing, the solutions were incubated at 37°C for 4 min. After the reaction period, an increase in the absorbance was measured at 593 nm with a V-730 UV-visible/NIR spectrophotometer operated by Spectra Manager™ Suite (Jasco Inc., Easton, MD, USA). The absorbance of FRAP control solution without samples was used as blank and was subtracted from the absorbances of the samples. Trolox was used as antioxidant standard, and the results were expressed in µmol TE/g DW. Trolox calibration curve was performed with eight different concentrations, with a concentration range of 5 – 200 µM with two dilution factors of 2 and 5 and three replicates at each concentration. Trolox stock solution was obtained by dissolving the analytical standard in methanol at a concentration of 1 mg/ml.

6.3.12. Statistical analysis

Unless otherwise stated, all the experimental results were calculated as the mean ± standard deviation (SD) of 3 repetitions. Graphics and IC_{50} values results were plotted using GraphPad Prism 8 software. The optimization was performed with a RSM approach with Minitab software version 21.1.0. The RSM optimization was performed by applying the variance ANOVA analysis and the Pareto-chart graphic to verify the significant process parameters. These parameters were used in a multiple-response prediction analysis to identify a polynomial model to optimize UA concentration.

6.4. Results and discussion

6.4.1. Experimental design of oleolyte preparation

The extraction of ursolic acid with sunflower oil represents a green extraction system for the oleolyte preparation, which is able to extract lipophilic compounds as triterpenoids. In literature, ursolic acid extraction is provided by different organic solvents, such as ethyl acetate, hexane, and chloroform (López-Hortas et al., 2018). Organic solvents are not biocompatible and the extracts are not suitable for cosmetic applications. Therefore, the preparation of an oil formulation represents an apolar biocompatible solvent for the extraction of lipophilic compounds from AA. Since oil is a rich source of free fatty acid that can damage the shelf life of the C_{18} column during the HPLC-DAD analysis, a previously deacidificated oil was preferred for the oleolyte preparation. The evaluation of the free fatty acid in sunflower oil was performed with the evaluation of acidic index, as previously described in the paragraph **6.3.2.3. Oil samples acidity determination**. The result of the acidic index is expressed as grams of oleic acid equivalents/g of oil (g OAE/g oil). The preparation of deacidificated sunflower oil was performed with the method reported in the paragraph **6.3.2.2. Deacidification procedure of sunflower oil**. The deacidification procedure required the use of a solution 7.5 % (*w/v*) of sodium carbonate Na_2CO_3, which is a strong base for the ionization of free fatty acid without the hydrolysis of the triglycerides of the oil. The analysis demonstrated that sunflower oil has an acidic index of 1.64 g OAE/g oil, while deacidificated sunflower oil has an acidic index of 0.27 g OAE/g oil, proving that the deacidification procedure with the solution 7.5 % (*w/v*) of sodium carbonate Na_2CO_3 remove effectively the free fatty acid from the oil. For the deacidification method, 250 mL of a sodium carbonate solution (Na_2CO_3 7.5%, *w*/*v*) was added to 250 mL of n-hexane and mixed with 500 mL of sunflower oil (Punathil Kannan & Ambale Gundappa, 2014). The sunflower oil and the organic n-hexane are miscible, generating a binary immiscible system with the aqueous phase which can be separated by a liquid-liquid extraction. The n-hexane is removed by evaporation at 35 °C. obtaining an oil with a low content of free fatty acid suitable for the oleolyte preparation by maceration. After the maceration of the matrix AA in the deacidificated oil, a centrifugation was used for the separation of the matrix from the oil and the recovery of OAAO. Deacidificated oil doesn't represent an optimum extraction solvent for triterpenoids recovery. Therefore, an optimization of extraction time and temperatures was performed using a RSM statistical model. The response surface methodology (RSM) is a statistical method which is used to optimize some parameters by

minimizing the sources and the quantitative data. To perform the optimization of ursolic acid incorporation in the oil, a HPLC-DAD method and an extraction protocol were previously optimized and validated.

6.4.2. Optimization and validation of oleolyte extraction

Ursolic acid extraction of OAAO was optimized to selectively extract the triterpenoids from the oleolyte and avoid the extraction of phospholipid and triglycerides of sunflower oil. Therefore, the extraction was performed using an acid-base reaction with liquid-liquid extraction. Triterpenoids are characterized by a carboxylic acid group, which allows the solubilization in aqueous solution as sodic salt. For the extraction, a solution of sodium carbonate Na_2CO_3 7.5% (*w/v*) was added to 60 mL of OAAO. The obtained aqueous solution was enriched of triterpenoids, while phospholipid and triglycerides are selectively retained in the organic phase. The basic aqueous solution is acidified with a solution 2 N of hydrochloride acid to obtain a pH = 3, to protonate the carboxylic group of triterpenoids. After the lyophilization, the solid residue obtained by the aqueous solution is extracted with ethyl acetate by a solid-liquid extraction. The organic solvent allows to extract triterpenoids by cleaning-up the salts from the residue. The workflow of OAAO extraction is summarized in the **Figure 99**.

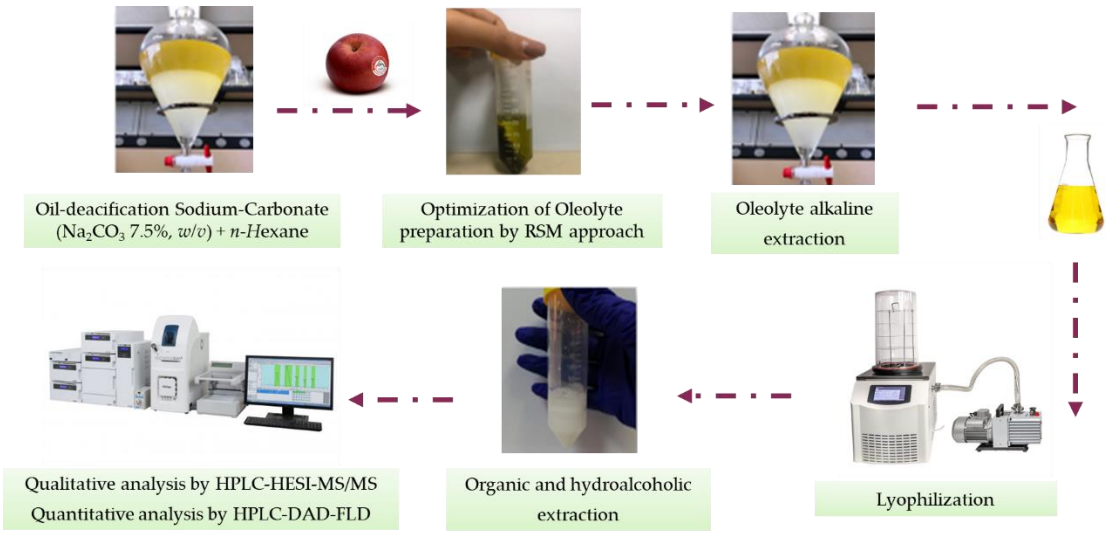


Figure 99: Workflow of OAAO extraction.

Recovery experiments of ursolic acid extraction has been performed following the procedure described in paragraph **6.3.5. Matrix effect and recovery of ursolic acid extraction from oil formulation**. The recovery is the closeness of agreement between the true value of the analyte concentration and the experimental results and represents the efficiency of the extraction method for that analyte. Therefore, recovery describes the amount actually recovered by the matrix and is expressed as the percentage (%) yield of the extraction method. According to FDA, a good recovery for the working analytes concentrations for this assay should be between 80-110% (Fda, 2011). For the experiment, the matrix was spiked in triplicate either before (pre-extraction spiked) or after (post-extraction spiked) extraction with the solution of the analyte, using three different concentrations according to the values obtained from the quantification. Ursolic acid standard concentrations (e.g., high: 30 µg; medium: 20 µg; low: 10 µg) have been selected in a way that even the lowest concentrations could have provided a statistically significant impact on the quantification of each compound for the evaluation of triterpenoid recovery. The recovery has been therefore investigated by calculating the ratio of the peak area in the pre-extraction spiked samples to the peak area in the post-extraction spiked samples. The ratio was calculated as follows:

$$\textbf{Recovery (\%)} = \left[\left(\frac{Peak\ area_{pre-extraction\ spiked\ sample}}{Peak\ area_{post-extraction\ spiked\ sample}}\right) x\ 100\right]$$

As shown in **Table 102**, the recovery values are close to 100% at three concentration levels, confirming the effectiveness of the procedure proposed for ursolic acid extraction by the combination of the liquid-liquid extraction and the solid-liquid extraction.

Spiked (µg)	Recovery (%)	Matrix effect (%)
10	91.21	6.86
20	89.42	1.42
30	89.65	2.29

Table 102. Recovery % and matrix effect % of ursolic acid extraction.

After ursolic acid quantification in OAAO extracts, the matrix effect has been investigated to evaluate the correctness and reliability of the quantification data provided by the HPLC-DAD method. As previously described in the paragraph **5.6.4.3. Recovery and matrix effect of polyphenols method**, the HPLC-DAD matrix effect is mainly due to the co-elution with other compounds which can generate an additive absorbance, enhancing the compound signal. Therefore, the aim of this assay was to assess the influence of all the other sample

components on ursolic acid response in quantitative analysis. Since the matrix may considerably affect the quality of analysis, to provide an accurate estimation of ursolic acid content in the matrix, the matrix effect had to be estimated. For the investigation of the matrix effect, ursolic acid analytical standard solutions at three different concentrations have been considered and the matrices chosen were the same used for the recovery experiment. The procedure for the evaluation of the matrix effect is accurately described in paragraphs **6.3.5. Matrix effect and recovery of ursolic acid extraction from oil formulation**. The matrix effect was calculated with this ratio:

$$\boldsymbol{Matrix\ effect}\ \% = \frac{\textbf{Peak area}_{\boldsymbol{in\ presence\ of\ matrix}}}{\textbf{Peak area}_{\boldsymbol{in\ solvent}}} \cdot \mathbf{100}$$

Matrix effect in ursolic acid analysis ranged from 1.42 % and 6.86 % (**Table 102**). These positive values can be explained by considering the co-elution of other compounds to ursolic acid peak. Although the matrix effect values are low, to avoid the signal enhancing which can overestimates the ursolic acid quantification in OAAO, quantification was performed using an ursolic acid calibration curve using a blank matrix solution of sunflower oil in acetonitrile at a concentration of 5 mg/ml. Therefore, these results allowed an accurate quantitative analysis of the metabolites of interest in the real samples.

6.4.3. HPLC-DAD method validation

6.4.3.1. Development of ursolic acid HPLC-DAD method

The method used for the quantitative analysis of ursolic acid is accurately described in the previous paragraph **6.3.3.2. Quantitative analysis of ursolic acid by HPLC-DAD**. For the quantitative analysis, a HPLC-DAD method was preferred to the use of other detectors. The diode-array detector is not the more sensitive detector for quantitative analysis. As matter of fact, ursolic acid is not responsive to other detectors, as the fluorimeter, and is poorly ionized during mass spectrometry analysis, reducing the sensitivity. Therefore, a HPLC-DAD analysis with a wavelength of 205 nm was selected for the quantitative analysis. The ursolic acid peak obtained with OAAO extract analysis is reported in the **Figure 100**.

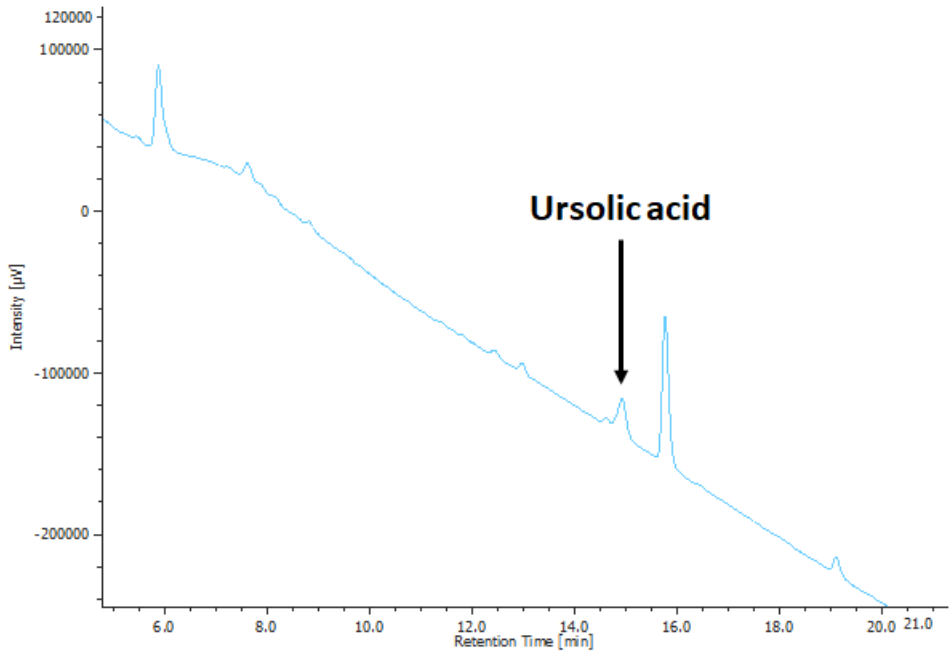


Figure 100: Ursolic acid peak in OAAO extract at a wavelength of 205 nm by HPLC-DAD analysis.

The wavelength of 205 nm was selected for the low UV-visibility, due to the absence of chromophore groups in the compound of interest. The UV spectrum of ursolic acid standard at a concentration of 50 ppm is reported in the **Figure 101**. The chromatographic analysis was performed by using water at 0.1% of formic acid and acetonitrile as phase B of the method. The use of an acidic pH for the phase A allow to ionize the carboxylic group, improving the peak shape.

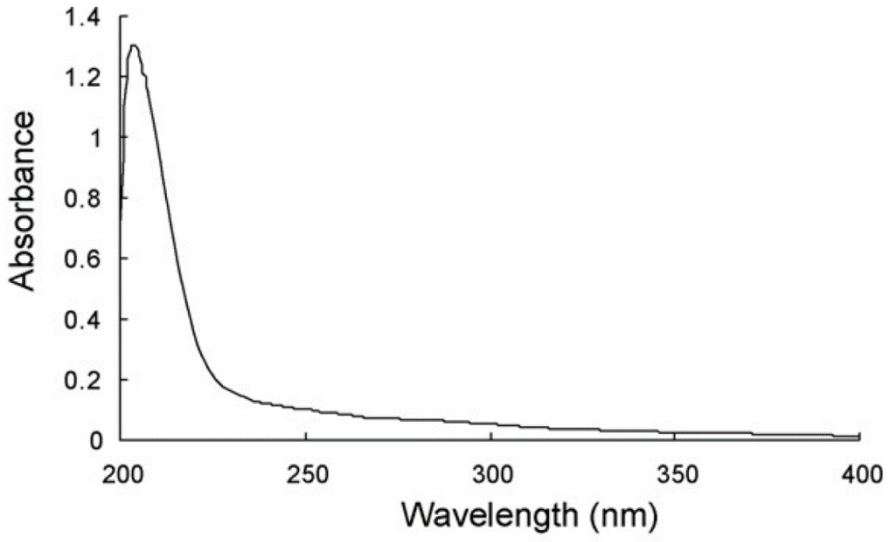


Figure 101: UV spectrum of ursolic acid standard.

6.4.3.2. Validation of ursolic acid method

The procedures described above in the paragraphs **3.2.11. Method validation according to ICH guidelines** were applied to the method reported in the paragraph **6.3.3.2. Quantitative analysis of ursolic acid by HPLC-DAD**. Ursolic acid calibration curve has been performed in a range of six concentration between 500 ppm and 1 ppm (**Figure 102**). For the calibration curve, one stock solution of ursolic acid analytical standard was prepared by dissolving it in acetonitrile to achieve a concentration of 1 mg/ml. According to literature, ursolic acid is soluble in organic solvents such as ethanol and acetonitrile, but not in more polar organic solvent such as methanol and in aqueous solution. The calibration curve displayed a favorable linear regression (R^2 > 0.99), thus demonstrating the linearity of the standard response in the range of concentrations analyzed. LODs and LOQs values were determined to evaluate the sensitivity of the method. Ursolic acid displayed a LOD value of 0.295 ppm and a LOQ value of 0.845 ppm (**Table 103**), which were above the compound values in the analysed matrices, confirming the efficiency of the method for the quantification in the real samples. These results are in according to the results obtained by other authors, which reported ursolic acid LOD and LOQ values of 0.15 ppm and 0.47, respectively (C. Xu et al., 2017).

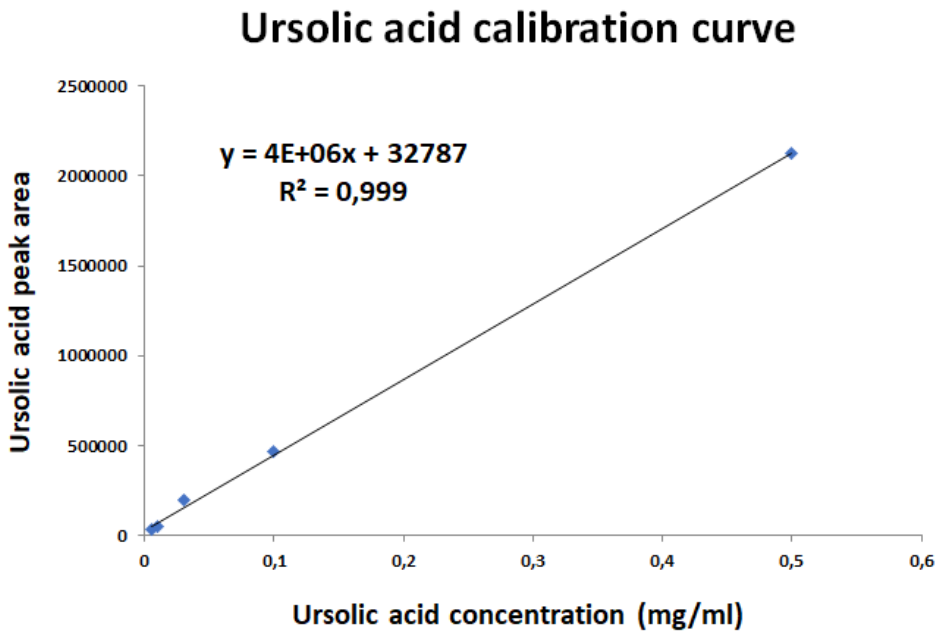


Figure 102: Ursolic acid calibration curve by HPLC-DAD analysis with a wavelength of 205 nm.

Compound	Linearity range (ppm)	Calibration curve	LOD (ppm)	LOQ (ppm)
Ursolic acid	1 – 500	y = 4E+06x + 32787	0.15	0.47

Table 103: Linearity range, calibration curves, limit of detection (LOD) and limit of quantification (LOQ) for ursolic acid analysis.

In agreement with the ICH validation guideline (ICH.Q2[R2], 2022), precision and accuracy were evaluated as well to validate the HPLC-DAD method, by considering that a measurement device for quantitative analysis should be both precise and accurate, providing measurements all close to and tightly clustered around the true value. Precision and accuracy were calculated by an intra-day and an inter-day analysis of ursolic acid standard solutions at 3 different concentrations (**Tables 104**). The 3 concentrations have been selected to represent the calibration levels (e.g., high, medium, low) included in the linearity range. The selection of these concentrations allowed to establish precision and accuracy of the entire calibration curves. The intra-day analysis was performed by injecting the two standard solutions three times per day. Instead, the inter-day analysis was performed by injecting the three selected standard solutions for 3 consecutive days. In the validation of the HPLC-DAD analysis, for the evaluation of intraday precision and accuracy, the RSD value ranged from 1.874 to 5.773 % ppm and from -0.534 to 3.142 %, respectively. Instead, for the evaluation of interday precision and accuracy, the RSD value ranged from 0.885 to 7.374 % ppm and from -0.521 to 1.386 %, respectively. These results assessed that the developed method was satisfactory with acceptable precision, accuracy, and reproducibility.

Analyte	Concentration (ppm)	Precision		Accuracy	
		Intra-day (CV %, *n=3*)	Inter-day (CV %, *n=3*)	Intra-day (bias %, *n=3*)	Inter-day (bias %, *n=3*)
Ursolic acid	500	1.874	1.720	3.142	1.386
	100	1.960	0.885	0.580	1.120
	5	5.773	7.374	-0.534	-0.521

Table 104: Intra- and inter-day precision and accuracy for ursolic acid analysis.

6.4.4. Ursolic acid quantification in oil formulations

After validating the extraction and analysis method of ursolic acid in OAAO, quantification was performed to perform the RSM optimization for the active ingredient incorporation in the oil. The optimization is performed with an appropriate experimental design with a multivariate equation . Three independent commonly modified factors, i.e., maceration time (seven times: 1h, 2h, 4h, 12h, 24h, 48h, and 96 h) and temperature (four temperatures: 20 °C, 40 °C, 60 °C, and 80 °C), combined with or without a single sonication cycle (30 min), were evaluated to optimize the UA yield in sunflower oil. The experimental design of RSM optimization was provided in the **Table 96** in the paragraph **6.3.2.1 Oleolyte preparation and experimental design**. For the selection of extraction temperature, this parameter was kept below 80 °C, considering that other authors reported that ursolic acid extraction decreases above 70 °C in the conventional extractions (G. Li et al., 2011) . A preliminary statistical evaluation of the quantitative results indicated that time and temperature represent significant parameters for ursolic acid incorporation in sunflower oil ($p < 0.05$), while the sonication is not a significant factor ($p > 0.05$). For example, for the OAAO preparation at 20 °C for 1 h of maceration, ursolic concentration was about 8.21 ± 0.41 µg of ursolic acid/ml of OAAO without sonication of the maceration mixture and 7.95 ± 0.63 µg of ursolic acid/ml of OAAO applying the sonication during the maceration of the food matrix in the sunflower oil. The significance of the value is provided by the Pareto Chart with α = 0.05 and is reported in the **figure 103**.

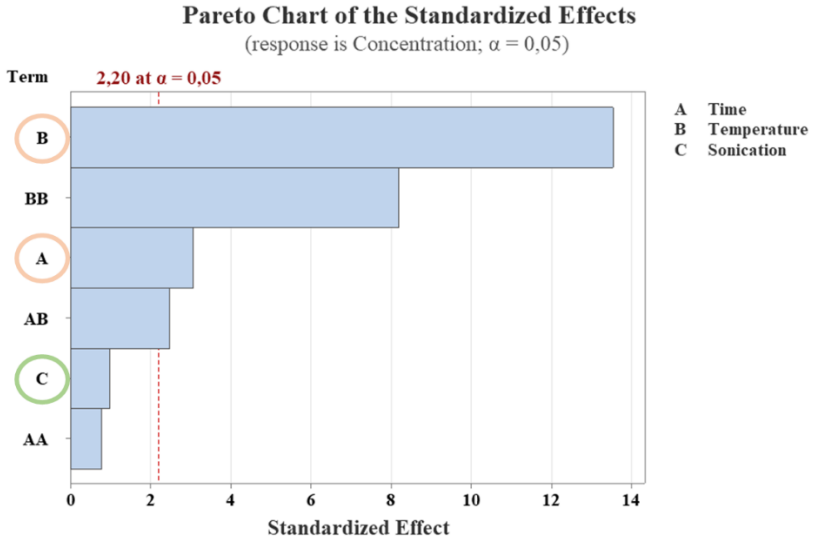


Figure 103: Pareto Chart of significant and not significant parameters of the RSM optimization, i.e., extraction time (A), temperature (B), and sonication (C).

The combination of the different time and temperature parameters was performed with 28 total extraction runs. The results of the quantification showed an ursolic acid concentration ranged from 8.21 ± 0.41 µg of ursolic acid/ml of OAAO (temperature: 20 °C; time: 1h) to 714.04 ± 3.29 µg of ursolic acid/ml of OAAO (temperature: 60 °C; time: 12h). A summary of the quantitative results obtained by the 28 extraction runs is provided in the **Table 105**.

Time (h)	20 °C	40 °C	60 °C	80 °C
		Ursolic acid concentration (µg/ml)		
1	8.21 ± 0.41	66.41 ± 0.66	416.85 ± 2.75	353.91 ± 0.53
2	13.00 ± 2.38	83.21 ± 1.13	529.93 ± 0.32	391.12 ± 1.45
4	23.88 ± 2.47	119.98 ± 0.72	689.00 ± 3.75	599.56 ± 1.94
12	21.16 ± 0.90	347.21 ± 5.74	714.04 ± 3.29	650.11 ± 3.55
24	86.48 ± 1.66	478.21 ± 9.64	700.34 ± 10.68	626.32 ± 11.90
48	201.24 ± 4.47	601.23 ± 11.51	689.87 ± 5.36	607.53 ± 14.91
96	233.60 ± 7.18	628.84 ± 5.96	692.11 ± 8.14	645.08 ± 6.40

Table 105: Ursolic acid quantification in the 28 extraction runs for the RSM optimization. Results are expressed as mean ± SD. “n.d.” means “not detected”.

Therefore, the statistical analysis by Pareto Chart was performed using only the results obtained by changing the significant parameters of the extraction time and the temperature, providing a statistical model for the RSM optimization. The significance of the value is provided by the Pareto Chart with α = 0.05 and is reported in the **Figure 104** and in the **Table 106**.

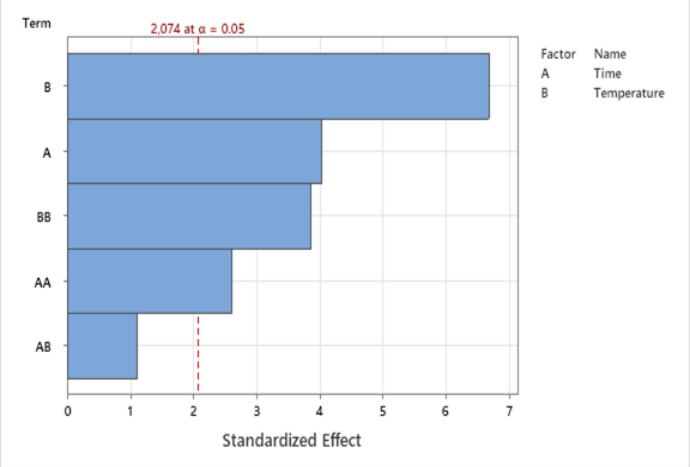


Figure 104: Pareto-chart of not-significant and significant parameters of the RSM optimization, i.e., extraction time (A), and temperature (B).

Term	Coefficient	SE Coefficient	t-value	p-value	VIF
Constant	671.6	53.6	12.52	0	
Time (A)	130.2	32.3	4.03	0.000565	1.01
Temperature (B)	235.8	35.3	6.68	0.000001	1.46
Time*Time (A^2)	-154.6	59.1	-2.61	0.015823	1.01
Temperature*Temperature (B^2)	-189.6	49.0	-3.87	0.000834	1.00
Time*Temperature (AB)	-47.9	43.1	1.11	0.278026	1.46

Table 106: Summary of parameters of significance in the RSM optimization model.

In agreement with the statistical results of the model fitting, the best model to optimize the ursolic acid yield is achieved by limiting the statistical analysis to two-variable, e.g., the extraction time (A) and the temperature (B). The multiple regression analysis of ursolic acid amounts indicated that the model was significant ($p < 0.0001$), didn't generate a lack of fit ($p = 0.182$), and the predictivity of the RSM model was 77.89% (R-sq = 84.47%; R-sq(adj) = 80.95%; R-sq(pred) = 77.89%). A second-order quadratic polynomial models were suitable to evaluate the effect of the two independent and significant variables on ursolic acid calculation, as the described by the following equation:

$$\textbf{Ursolic acid concentration (µg/ml)} = 11.07A + 30.55B - 0.0685A^2 - 0.2106B^2 - 0.0336AB - 624$$

This equation suggested that ursolic acid extraction in sunflower oil is both a time and a temperature dependent process. However, the two parameters influenced in a different way the ursolic acid incorporation in the oil. As matter of fact, the temperature (B) is associated to a high coefficient (30.55 and 0.278), indicating a greater role in the determination of ursolic acid extraction in oil than the extraction time (A). Since other studies about ursolic acid extraction with oils are not reported in literature, this is the first attempt to rationalize the phenomena which determine the active ingredient incorporation in sunflower oil. For example, according to the other authors which studied the optimization of ursolic acid extraction in ethanol from food sources, the optimum temperature values ranged between 40 °C and 50 °C (Fu et al., 2014; Vetal et al., 2013). The RSM model indicated an optimum temperature of 63 °C. This difference could be related to the use of a solvent with a higher viscosity as sunflower oil in comparison to conventional organic solvents generally employed for ursolic acid extraction, such as ethanol and ethyl acetate. As matter of fact, it's well established that high temperatures during the extraction decrease the viscosity of the medium, helping the penetration of the solvent in the plant matrix and resulting in a faster

and exhaustive kinetics of extraction (Miron et al., 2011). Moreover, the increase of the solvent temperature could reduce the surface tension, improving the permeability of the oil in the food matrix (Vergara-Salinas et al., 2012). However, the extraction temperature should be kept below the maximum values of 80 °C since higher temperature could cause ursolic acid degradation (G. Li et al., 2011). The results of the RSM optimization were provided in the multiple response prediction analysis (**Figure 105**), which correlated the independent variables of extraction time (A; hours) and temperature (B; °C) to the ursolic acid concentration in the oil (µg of ursolic acid/ml of OAAO). The predictive model estimated the theoretical conditions to optimize ursolic acid extraction with sunflower oil at 63 °C for 68.85 h, with a theorical ursolic acid concentration in OAAO of 761.50 ± 53.10 µg of ursolic acid/ml of OAAO. Therefore, OAAO was prepared under the optimized RSM conditions, obtaining an ursolic acid concentration of 784.40 ± 61.04 µg of ursolic acid/ml of OAAO, confirming the predictivity of the RSM model.

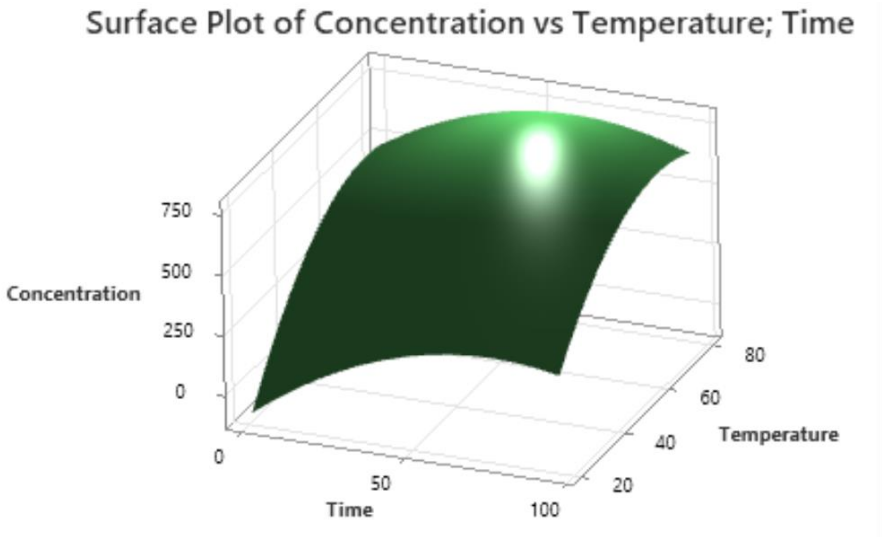


Figure 105: Multiple response prediction analysis provided by the RSM optimization of ursolic acid incorporation in sunflower oil.

6.4.5. Polyphenols quantification in oil formulations

The HPLD-DAD method for polyphenols quantification of the samples was accurately described in the previous paragraphs **3.3.3.2. Development of polyphenols HPLC-DAD-FLD method** and **6.3.6.2 Quantitative analysis of polyphenols by HPLC-DAD.** The method proved to be extremely valid for separating a large number of polyphenolic compounds in OAAO hydroalcoholic extract with a high resolution, high efficiency, and high selectivity, as shown in **Figure 106,** where peaks clearly appear to be sharp and well separated. The HPLC-DAD analysis allows to identify and quantify 7 phenolic compounds. Considering the great chemical diversity of AA polyphenolic composition, which ranged from polar compounds (e.g., phenolic acid) to lipophilic molecules (e.g., flavonols aglycones, only the AA lipophilic polyphenols was identified in OAAO. Specifically, rutin and quercetin 3-*O*-glucoside represent the most abundant polyphenols of OAAO hydroalcoholic extract. Moreover, dihydrochalcones represent the second most representative polyphenols class of OAAO hydroalcoholic extract, with phlorizin and phloretin values of 0.15 µg/ml of OAAO and 0.07 µg/ml of OAAO. Instead, the more hydrophilic AA polyphenols were not detected in OAAO hydroalcoholic extract. The selective abundance of lipophilic polyphenols in the OAAO is due to the high lipophilicity of sunflower oil. Instead, other lipophilic polyphenols as quercetin were not detected in OAAO hydroalcoholic extract despite its lipophilicity. This quantification is due to the low initial quercetin concentration in AA. The results of the polyphenols quantification in OAAO hydroalcoholic extract is reported in the **Table 107**. The values are expressed in µg/ml of OAAO ± standard deviation (SD) of three repetitions. “nd” represents compounds not detected in the analysis.

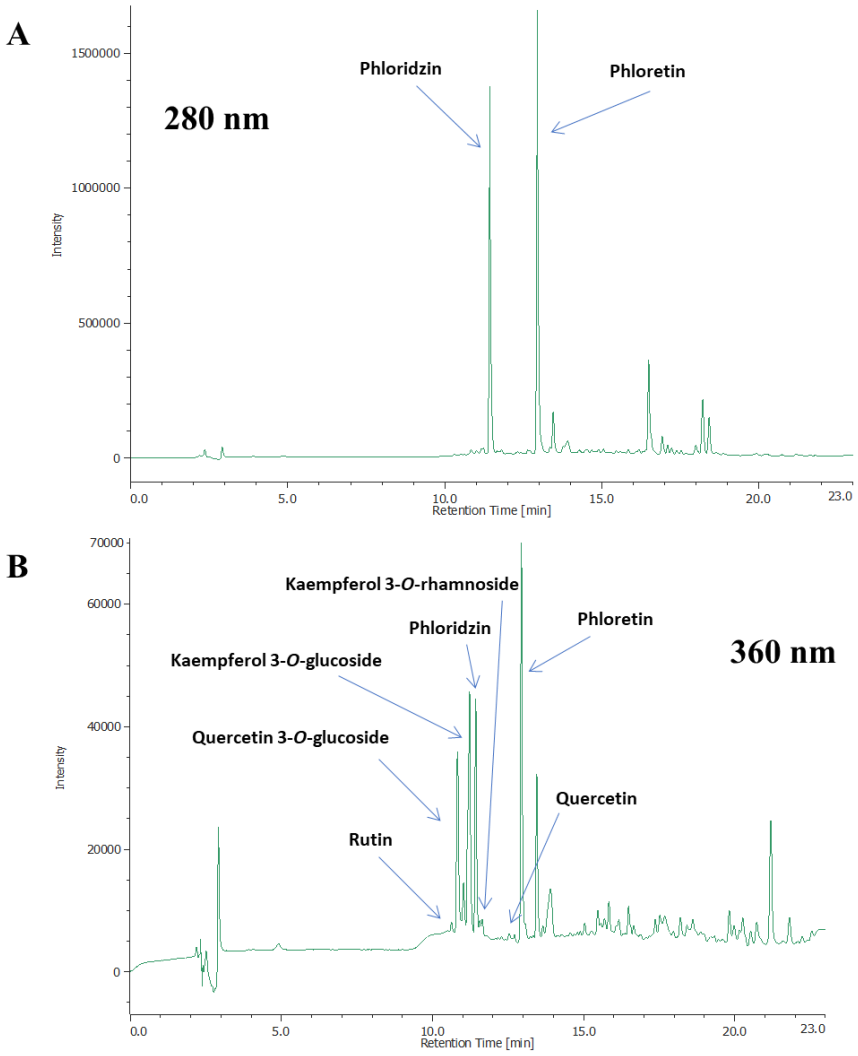


Figure 106: OAAO hydroalcoholic extract chromatogram at 280 nm (**A**) and 360 nm (**B**).

Compound	Mean value ± SD (µg/ml of OAAO)
Chlorogenic acid	n.d.
Caffeic acid	n.d.
p-coumaric acid	n.d.
Procyanidin B1 + B3	n.d.
Procyanidin B2	n.d.
Epicatechin	n.d.
Rutin	0.7684 ± 0.0132
Quercetin 3-*O*-glucoside	0.7173 ± 0.0173
Kaempferol 3-*O*-rhamnoside	0.1551 ± 0.0182
Kaempferol 3-*O*-glucoside	< LOQ
Apigenin 7-*O*-glucoside	0.0081 ± 0.0001
Phloridzin	0.1573 ± 0.0152
Quercetin	n.d.
Phloretin	0.0762 ± 0.0151

Table 107: Quantitative analysis of OAAO hydroalcoholic extract by HPLC-DAD analysis. Results are expressed as mean ± SD. “n.d.” means “not detected”.

6.4.6. Qualitative analysis of oil formulations

The analysis of OAAO extracts by HPLC-HESI-MS/MS allowed to putatively identify 18 compounds by comparison with literature data. The hydroalcoholic extract was analyzed to evaluate the qualitative OAAO polyphenols composition, while the ethyl acetate extract was analyzed to evaluate the qualitative OAAO triterpenoids composition. The analysis of polyphenols profile was performed in negative acquisition mode, while the analysis of triterpenoids composition was performed both in positive and in negative acquisition modes. The retention time, the quasi-molecular ion, the molecular formula, and the fragment ions were listed in the **Tables 108**. The base peak ion is bolded in the table. The molecular identity of 18 compounds (numbered as: **64**: rutin; **67**: quercetin 3-*O*-glucoside; **81**: ursolic acid; **82**: oleanolic acid; **83**: kaempferol 3-O-glucoside; **84**: phloridzin; **85**: kaempferol 3-*O*-rhamnoside; **86**: hydroxymethoxyursolic acid; **87**: phloretin; **88**: carboxyursolic acid; **89**: annurcoic acid; **90**: zanhic acid; **91**: medicagenic acid isomer 1; **92**: corosolic acid; **93**: arjunolic acid; **94**: medicagenic acid isomer 2; **95**: dihydroxy-{[(hydroxyphenyl)-propenoyl)]oxy}ursenoic acid; **96**: hydroxy-{[(hydroxyphenyl)-propenoyl)]oxy}ursenoic acid) was confirmed by comparison with analytical standards.

No.	Extraction solvent	Compound	R_t (min)	*m/z*	Diagnostic Fragment
64	Hydroalcoholic	Rutin *	8.05	609	591 $[M-H-H_2O]^-$, **301** [M-H-Glu-Rha]$^-$, 255 $[M-H-Rut-CO-H_2O]^-$, 179 $[M-H-Glu-Rha-C_7H_6O_2]^-$
67	Hydroalcoholic	Quercetin 3-*O*-glucoside *	8.16	463	445 $[M-H-H_2O]^-$, **301** [M-H-Glu]$^-$, 255 $[M-H-Glu-CO-CO-H_2O]^-$, 179 $[M-H-Glu-C_7H_6O_2]^-$
83	Hydroalcoholic	Kaempferol 3-*O*-glucoside *	8.73	447	429 $[M-H-H_2O]^-$, **285** [M-H-Glu]$^-$, 179 $[M-H-Glu-C_7H_6O]^-$, 151 $[M-H-Glu-C_8H_6O_3]^-$
84	Hydroalcoholic	Phloridzin *	9.41	435	417 $[M-H-H_2O]^-$, **273** [M-H-Glu]$^-$, 167 $[M-H-Glu-C_7H_6O]^-$
85	Hydroalcoholic	Kaempferol 3-*O*-rhamnoside *	9.78	431	413 $[M-H-H_2O]^-$, 327 $[M-H-C_4H_8O_3]^-$, **285** [M-H-Rha]$^-$, 179 $[M-H-Rha-C_7H_6O_2]^-$
86	Ethylacetate	Hydroxymethoxyursolic acid	11.49	503	485 $[M+H-H_2O]^+$, 467 $[M+H-2H_2O]^+$, **457** $[M+H-HCOOH]^+$, 439 $[M+H-HCOOH-H_2O]^+$
87	Hydroalcoholic	Phloretin *	11.61	273	**255** $[M-H-H_2O]^-$, 167 $[M-H-C_7H_6O]^-$, 125 $[M-H-C_9H_8O_2]^-$

88	Ethylacetate	Carboxyursolic acid	12.17	501	483 $[M+H-H_2O]^+$, **455** $[M+H-HCOOH]^+$, 437 $[M+H-HCOOH-H_2O]^+$, 419 $[M+H-HCOOH-2H_2O]^+$
89	Ethylacetate	Annurcoic acid	13.47	487	**469** $[M+H-H_2O]^+$, 451 $[M+H-2H_2O]^+$, 441 $[M+H-HCOOH]^+$, 423 $[M+H-HCOOH-H_2O]^+$
90	Ethylacetate	Zanhic acid	14.83	517	**499** $[M-H-H_2O]^-$, 473 $[M-H-CO_2]^-$, 455 $[M-H-CO_2-H_2O]^-$, 429 $[M-H-CO_2]^-$
91	Ethylacetate	Medicagenic acid isomer 1	15.09	501	**483** $[M-H-H_2O]^-$, 457 $[M-H-2CO_2]^-$, 409 $[M-H-2HCOOH]^-$, 391 $[M-H-2HCOOH-H_2O]^-$
92	Ethylacetate	Corosolic acid	15.19	473	455 $[M+H-H_2O]^+$, **427** $[M+H-HCOOH]^+$, 409 $[M+H-HCOOH-H_2O]^+$, 391 $[M+H-HCOOH-2H_2O]^+$
93	Ethylacetate	Arjunolic acid	15.75	487	**469** $[M-H-H_2O]^-$, 441 $[M-H-HCOOH]^-$, 425 $[M-H-CO_2-H_2O]^-$, 407 $[M-H-CO_2-2H_2O]^-$
82	Ethylacetate	Oleanolic acid	15.91	457	**439** $[M+H-H_2O]^+$, 411 $[M+H-HCOOH]^+$, 393 $[M+H-HCOOH-H_2O]^+$
81	Ethylacetate	Ursolic acid *	16.20	457	**439** $[M+H-H_2O]^+$, 411 $[M+H-HCOOH]^+$, 393 $[M+H-HCOOH-H_2O]^+$
94	Ethylacetate	Medicagenic acid isomer 2	16.67	501	**483** $[M-H-H_2O]^-$, 457 $[M-H-CO_2]^-$, 439 $[M-H-CO_2-H_2O]^-$, 391 $[M-H-HCOOH-H_2O]^-$
95	Ethylacetate	Dihydroxy-{[(hydroxyphenyl)-propenoyl)]oxy}ursenoic acid	18.79	633	615 $[M-H-H_2O]^-$, 589 $[M-H-CO_2]^-$, 571 $[M-H-CO_2-H_2O]^-$, **487** $[M-H-CA]^-$
96	Ethylacetate	Hydroxy-{[(hydroxyphenyl)-propenoyl)]oxy}ursenoic acid	20.89	617	599 $[M-H-H_2O]^-$, 573 $[M-H-CO_2]^-$, **453** $[M-H-CA-H_2O]^-$

Table 108. Triterpenoids and polyphenols putatively identified in AA oleolyte by their MS/MS spectra in agreement with literature by HPLC-MS analysis in positive and negative acquisition modes., Glu, Rha, Rut, and CA indicate glucose, rhamnose, rutinose, and coumaric acid groups, respectively. * The identification of this molecule was confirmed using commercial standard.

Rutin (**64**) showed a $[M-H]^-$ ion with *m/z* 609. The base peak ion at *m/z* 301 $[M-H-Rut]^-$ derived from the cleavage of the disaccharide moiety, and the fragment ions at *m/z* 255 $[M-H-Rut-CO-H_2O]^-$ and *m/z* 179 $[M-H-Rut-C_7H_6O_2]^-$ was obtained from the RDA fragmentation. This fragmentation pattern agreed with the literature results, was consistent

with the results obtained in the paragraphs **3.3.2.2. Polyphenolic profile of green tomatoes** and **4.3.7.2. Validation of rutin method** and was confirmed by comparison with an analytical standard (Z. H. Li et al., 2016b). Compound **67** displayed a $[M-H]^-$ ion with *m/z* 463. The base peak ion with *m/z* 301 $[M-H-Glu]^-$ derived from the neutral loss of the glucose group while the fragments with *m/z* 179 $[M-H-Glu-C_7H_6O_2]^-$ was obtained by the RDA fragmentation. This tandem mass spectrum agreed with the literature results of quercetin 3-*O*-glucoside, was consistent with the results obtained in the paragraph **3.3.2.2. Polyphenolic profile of green tomatoes** and was confirmed by comparison with an analytical standard (Z. H. Li et al., 2016b). Compound **81** displayed a $[M+H]^+$ ion with *m/z* 457 and a base peak ion with *m/z* 411 $[M+H-HCOOH]^+$. The tandem mass spectrum displayed a fragment ion with *m/z* 393 $[M+H-HCOOH-H_2O]^+$, confirming the presence of carboxylic acid and a hydroxy group. Based on the fragmentation mass spectrum and the comparison with an analytical standard, compound **81** was identify as ursolic acid (Y. P. Guo et al., 2021). Compound **82** displayed a $[M+H]^+$ ion with *m/z* 457 and was tentatively annotated as oleanolic acid. The tandem mass spectrum showed a base peak ion with *m/z* 439 $[M+H-H_2O]^+$ for the neutral loss of a water molecule, and the fragment ions with *m/z* 393 $[M+H-HCOOH-H_2O]^+$, confirming the presence of carboxylic acid and a hydroxy group (Y. P. Guo et al., 2021). Compound **83** showed a $[M-H]^-$ ion with *m/z* 447 and was annotated as kaempferol 3-*O*-glucoside. The tandem mass spectrum displayed a base peak ion with *m/z* 285 $[M-H-Glu]^-$ for the neutral loss of the glucose moiety, and the fragment ions with *m/z* 179 $[M-H-Glu-C_7H_6O_2]^-$ resulted by the RDA fragmentation. These results confirmed the linkage of the glucose group with the aglycone kaempferol. The kaempferol 3-*O*-glucoside identity was confirmed by comparison with an analytical standard and agreed with literature data (Kumar et al., 2017). Phloridzin (**84**) displayed a $[M-H]^-$ ion with *m/z* 435. The base peak ion with *m/z* 273 $[M-H-Glu]^-$ was due to the loss of the glucose unit and the fragment ion with *m/z* 167 $[M-H-Glu-C_7H_6O]^-$ confirmed the identity of the chalcone moiety and the linkage of the sugar group. The compound identity was confirmed by comparison of the tandem mass spectrum with an analytical standard (Z. H. Li et al., 2016b). Compound **85** showed a $[M-H]^-$ ion with *m/z* 431 and was annotated as kaempferol 3-*O*-rhamnoside. The base peak ion with *m/z* 285 $[M-H-Rha]^-$ derived from the neutral loss of the sugar group while the fragment ion with *m/z* 179 $[M-H-Rha-C_7H_6O_2]^-$ was due to the RDA fragmentation. Kaempferol 3-*O*-rhamnoside identity was confirmed by comparison with an analytical standard and agreed with literature data (Abdelaziz et al., 2020). Compound **86** displayed a $[M+H]^+$ ion with *m/z* 503. The base peak ion with *m/z* 485 $[M+H-H_2O]^+$ and the fragment

ions with *m/z* 467 $[M+H-2H_2O]^+$, with *m/z* 457 $[M+H-HCOOH]^+$, and with *m/z* 439 $[M+H-HCOOH-H_2O]^+$ confirmed the linkage of a carboxylic acid and a hydroxyl group to the triterpenoid scaffold. Based on the comparison with literature data, compound **86** was putatively identified as hydroxymethoxyursolic acid (Huhman et al., 2005). Phloretin (**87**) displayed a $[M-H]^-$ ion with *m/z* 273. The base peak ion with *m/z* 167 $[M-H-C_7H_6O]^-$ and the fragment ion *m/z* 125 $[M-H-C_9H_8O_2]^-$ suggested the presence of the chalcone moiety. The tandem mass spectrum and the comparison with analytical standard confirmed phloretin identity (Z. H. Li et al., 2016b). Compound **88** showed a $[M+H]^+$ ion with *m/z* 501, a base peak ion with *m/z* 455 $[M+H-HCOOH]^+$, and a fragment ion with *m/z* 419 $[M+H-HCOOH-2H_2O]^+$. By comparison with literature, compound **88** was putatively annotated as carboxyursolic acid (Z. H. Li et al., 2016b). Compound **89** displayed a $[M+H]^+$ ion with *m/z* 487 and was tentatively identified as annurcoic acid, a triterpenoid isolated exclusively in Annurca apple (Da Silva et al., 2013). The tandem mass spectrum showed a base peak ion with *m/z* 469 $[M+H-H_2O]^+$ and a fragment ion with *m/z* 423 $[M+H-HCOOH-H_2O]^+$, confirming the linkage of a hydroxy and a carboxylic acid groups. Compound **90** showed a $[M-H]^-$ ion with *m/z* 517. The base peak ion with *m/z* 455 $[M-H-CO_2-H_2O]^-$ and the fragment ion with *m/z* 429 $[M-H-2CO_2]^-$ suggested the presence of two carboxylic acid moieties and a hydroxy group. The tandem mass spectrum allowed to putatively annotate the compound **90** as zahnic acid (Zou et al., 2015). Compounds **91** and **94** were tentatively annotated as two isomers of medicagenic acid. The displayed a $[M-H]^-$ ion with *m/z* 501. The base peak ion with *m/z* 483 $[M-H-H_2O]^-$ and the fragment with *m/z* 391 $[M-H-2HCOOH-H_2O]^-$ confirmed the linkage of two carboxylic acid groups, in agreement with literature data (Huhman et al., 2005). Compound **92** displayed a $[M+H]^+$ ion with *m/z* 473 and was tentatively annotated as corosolic acid. The tandem mass spectrum showed a base peak ion with *m/z* 455 $[M+H-H_2O]^+$ and a fragment ion with *m/z* 391 $[M+H-HCOOH-2H_2O]^+$ for the neutral losses of a formic acid and two water molecules (Y. P. Guo et al., 2021). Compound **93** showed a $[M-H]^-$ ion with *m/z* 487 and is characterized by a tandem mass spectrum with a base peak ion with *m/z* 425 $[M-H-CO_2-H_2O]^-$ and the fragment ions with *m/z* 441 $[M-H-HCOOH]^-$ and with *m/z* 407 $[M-H-CO_2-2H_2O]^-$, which confirmed the linkage of the triterpenoid with a hydroxy and a carboxylic acid groups. Therefore, based on comparison with literature data, compound **93** was putatively annotated as arjunolic acid (Y. P. Guo et al., 2021). Compound **95** showed a $[M-H]^-$ ion with *m/z* 633. The base peak ion with *m/z* 589 $[M-H-CO_2]^-$ and the fragment ion with *m/z* 571 $[M-H-CO_2-H_2O]^-$ were obtained by the cleavage of the carboxy and the hydroxy groups. Instead, the fragment ion

with *m/z* 487 $[M-H-CA]^-$ confirmed the linkage of a coumaric acid group to the triterpenoid scaffold. The comparison with literature data allowed to annotate the compound **95** as dihydroxy-{[(hydroxyphenyl)-propenoyl)]oxy}ursenoic acid (C. Xu et al., 2017). Compound **96** displayed a $[M-H]^-$ ion with *m/z* 617. The base peak ion with *m/z* 573 $[M-H-CO_2]^-$ and the fragment ion with *m/z* 453 $[M-H-CA-H_2O]^-$ suggested the linkage of a carboxylic acid, a hydroxyl, and a coumaric acid groups. The comparison with literature data allowed to annotate the compound **96** as hydroxy-{[(hydroxyphenyl)-propenoyl)]oxy}ursenoic acid (C. Xu et al., 2017). Compound **95** and **96** represented an unusual example of triterpenoids linked with a polyphenolic moiety, which were not previously described in the apple fruits. The mass fragmentation pattern of triterpenoids is characterized by the fragmentation of the carboxylic group. The neutral loss obtained by this fragmentation varies in positive and negative acquisition mode. As matter of fact, in positive acquisition mode the neutral loss is represented by a formic acid group (-46 Da), while in negative acquisition mode the neutral loss is obtained by a dioxide carbon molecule (-44 Da).

6.4.7. Antioxidant properties of Annurca Apple oleolytes

As previously described in the paragraph **6.2.2. Triterpenoids: biological properties**, the UV irradiation and the oxidative stress can be causes of premature skin aging, generating skin cutaneous damages and diseases (Zillich et al., 2015). The reduction of ROS has been shown to reduce oxidative damage and improve and extend the tissues lifespan (Luo et al., 2021). Therefore, considering the role of oxidative stress in the skin aging-related diseases, an evaluation of total phenolic content (TPC) and the antioxidant properties of OAAO represent an interesting tool for the development of the cosmetic formulation. The Folin-Ciocalteau displayed a total polyphenolic content of OAAO hydroalcoholic extract of 5.56 ± 0.45 mg GAE/g of OAAO hydroalcoholic extract. Therefore, an evaluation of the antioxidant properties of OAAO hydroalcoholic extract was performed using the DPPH, the ABTS, and the FRAP assays. The antiradical activity of OAAO hydroalcoholic extracts displayed values of 14.63 ± 0.22 µmol TE/g of OAAO hydroalcoholic extract for DPPH assay, 5.90 ± 0.49 µmol TE/g of OAAO hydroalcoholic extract for ABTS assay, and 21.72 ± 0.68 µmol TE/g of OAAO hydroalcoholic extract for FRAP assay. Interestingly, the results agreed with the antiradical activity of AA hydroalcoholic extract previously reported in literature (15.59 ± 0.11 µmol TE/g of AA hydroalcoholic extract for DPPH assay, 40.98 ±

1.19 µmol TE/g of AA hydroalcoholic extract for ABTS assay, and 26.63 ± 0.70 µmol TE/g of AA hydroalcoholic extract for FRAP assay). A summary of the antiradical activity of OAAO and AA hydroalcoholic extracts provided by DPPH, ABTS, and FRAP assays is reported in **Table 109**.

Sample	DPPH assay	ABTS assay	FRAP assay
		µmol TE/g ± SD	
OAAO	14.63 ± 0.22	5.90 ± 0.49	21.72 ± 0.68
AA	15.59 ± 0.11	40.98 ± 1.19	26.63 ± 0.70

Table 109: Antiradical activity of OAAO and AA hydroalcoholic extracts provided by DDPH, ABTS, and FRAP assays. Abbreviations: DPPH: radical 2,2-diphenyl-1-picrylhydrazyl; ABTS: 2,20-azino-bis (3-ethylbenzothiazoline-6-sulfonic acid); FRAP: ferric reducing antioxidant power; TE: Trolox equivalent; OAAO: Optimized Annurca Apple Oleolyte; AA: Annurca Apple. Values are calculated as mean ± standard deviation (SD) of three repetitions.

The results of DPPH and ABTS assays were also calculated as IC_{50} values (**Figure 107**), which represent the amount of antioxidant required to reduce the initial concentration of the radical solution by 50%. The antiradical assays values of 10.21 mg/ml for the DPPH assay and 23.02 mg/ml for the ABTS assay confirmed the antioxidant properties of OAAO hydroalcoholic extract.

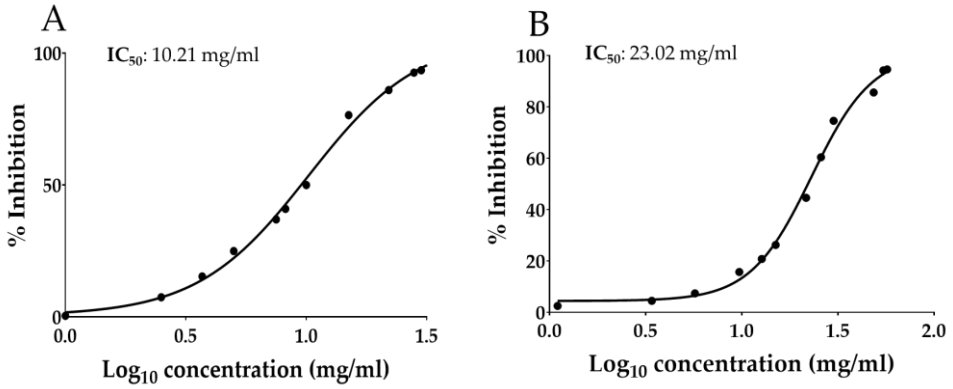


Figure 107: Antiradical activity of OAAO hydroalcoholic extracts expressed as IC50 of DPPH and ABTS assays. Values represent the mean ± standard deviation (SD) of three repetitions.

6.5. Summary of Annurca Apple oleolytes formulation

Annurca Apple fruits represent a potential source of bioactive compounds with nutraceutical and cosmeceutical potential. Although AA polyphenols fraction composition and pharmacological properties have been already investigated, the composition and the health beneficial effects of apolar triterpenoids fraction have been less studied. In addition, AA has never been considered as a material for the development of oil formulations and oleolytes preparations. Moreover, sunflower oil has never been used as an extractive solvent for ursolic acid extraction. Indeed, although the oil is not an effective solvent for triterpenoids extraction, it is food-grade and biocompatible for human application. In order to improve ursolic acid extraction in sunflower oil, a statistical optimization using the RSM approach was performed to increase the active ingredient extraction. This approach allowed to obtain an optimized oil formulation called OAAO with a high ursolic acid amount (784.40 ± 61.04 µg of ursolic acid/ml of OAAO). The analysis was performed with an HPLC-DAD method, which was validated to assess the reliability and reproducibility for the quantification of the active ingredient. Furthermore, the oleolyte was characterized to evaluate the chemical composition by HPLC-HESI-MS/MS analysis and to assess its *in vitro* biological potential. In particular, OAAO displayed an antioxidant activity (IC_{50} DPPH assay: 10.21 mg/ml; IC_{50} ABTS assay: 23.02 mg/ml)which could contribute to the pharmacological activity exerted by the triterpenoids fraction. Further studies are needed to assess the *in vitro* and *in vivo* efficacy of the oleolyte for the treatment of skin aging-related diseases.

CHAPTER 7

ANNURCA APPLE OLEOLYTE EFFICACY STUDY FOR NUTRACOSMECEUTIC APPLICATIONS

7.1. Introduction of the project

The development of a nutraceutical and a cosmeceutical formulation requires the use of appropriate *in vitro* and *in vivo* assay to evaluate its activity in the prevention and the treatment of a specific diseases. For the results of the chapter 6, the Optimized Annurca Apple Oleolyte OAAO was selected for its high ursolic acid concentration (784.40 ± 61.04 µg of ursolic acid/ml of OAAO) for a pharmacological study for the prevention of skin aging-related diseases. Both *in vitro* and *in vivo* assays were performed for the assessment of OAAO health benefits. These studies were carried out in collaboration with the research group of Prof. Angela Ianaro and the research group of Prof. Sonia Laneri of the Department of Pharmacy of the University of Naples Federico II.

In this context, the goals of this part of the thesis are as follows:

1) To demonstrate the potential of OAAO as a material for the preparation of cosmetical and cosmeceutical formulations.
2) To evaluate the skin-lighting activity of ursolic acid and OAAO for the treatment of skin aging-related diseases, such as hyperpigmentation, melasma, and age spots.
3) To demonstrate the potential of OAAO for the treatment of skin aging-related diseases linked to the loss of elastin content, such as the skin wrinkles, the roughness, and the loss of skin elasticity.

7.2. Materials and methods

7.2.1. Reagents

All chemicals, reagents, and standards used were analytical or LC-MS grade reagents. The water was treated in a Milli-Q water purification system (Millipore, Bedford, Burlington, MA, USA) before use. Sunflower oil was purchased in a local market. Ursolic acid (purity ≥ 98.5% HPLC), phloridzin (purity ≥ 99% HPLC), kojic acid (purity ≥ 98.5% HPLC), L-tyrosine (purity ≥ 98% HPLC), tyrosinase from mushroom (activity ≥ 1000 U/mg), human melanoma cells lines A375, MTT, TRI-Reagent, N-succinyl-(Ala)-3-p-nitroanilide, elastase from porcine pancreas Type I (Enzymatic activity ≥ 4.0 U/mg), Nanodrop were purchased from Sigma-Aldrich (Milan, Italy). DMEM medium, heat-inactivated fetal bovine serum, L-glutamine, penicillin, streptomycin, HEPES buffer were purchased from Gibco (New York, NY, USA). The iScript Reverse Transcription Supermix for RT-qPCR was purchased from Bio-Rad (Milan, Italy). H2DCFDHA, MitoTracker Green and TMRM were purchased from Thermo Fisher Waltham (MA, USA).

7.2.2. Franz's cell diffusion system

Four skin flaps of pig (age of 8-9 years) ears were excised from the outer part of a male pig ear, post-sacrifice, within 24 h from animal death, and left to settle at a controlled temperature and humidity of 24 °C and r.H. of 50.0% for approximately 30 min. Dial Calipers-0–4-Inch-001 Inch (52-008-704 SU, WESTport, Corporation, West Islip, New York 11795) was used to confirm skin thickness, and Tewameter TM Nano (C + K electronic GmbH, Köln, Germany) was employed to ensure skin integrity, accepted TEWL values were <15 g/mh^2. Then, skin samples were loaded in Franz's diffusion cell system. The diffusion cell system consists of two main chambers (the donor and the receptor), between the porcine skin flap, stripped of the subcutaneous tissue, is placed, with the epidermis facing the donor comportament and fixed with forceps. Triplicate Franz cells were fitted for each oleolyte to be analyzed, while one Franz cell was fitted for the blank. The donor compartment of each cell was loaded with 1 mL of oleolyte containing 211 µg/mL of UA. While the receptor was filled with 5 mL of PBS solution and a magnet to avoid the saturation of the first liquid layer in contact with the skin. After assembly, the cells are placed in a thermostatically controlled bath at 37.0 °C. A special cap is mounted on the

donor compartment to maintain a constant pressure (1 atm) inside the chamber. A total of 24 Franz cells were prepared, 12 with the oleolyte and 12 for blank. After placement, the time is monitored with a timer, and 1 mL of the receptor fluid is collected at set times. Finally, cells are disassembled, and the skin is collected for further extraction procedures. Skin flaps were rinsed with physiological saline solution (NaCl 0.9%) by dabbing with a cotton pad (Linea F, Angelini Acraf Spa, Aprilia, Italy), which was then cut into a 10 mm diameter piece. Before extractions, the epidermis and dermis were split by heating with a hair dryer for 30 secs, then by scraping with tweezers (Semken-Taylor Rette N. 1 Cm. 12, 5, Asa Dental Spa) and surgery (Pikdare Spa, Casnate con Bernate, Como, Italy) (Di Lorenzo et al., 2021; Neri et al., 2022). Afterward, the epidermis and dermis were placed in individual glass test tubes and kept in contact with 1 mL of an ethanolic solution containing PBS for 1 h. Subsequently, the solvent was gently evaporated under N_2 flow. The experiments were carried out employing 2 different concentrations, the higher of 50 µg/mL, out of iBuP, which was 100 µg/mL, and the lower of 5 µg/mL, out of iBuP, which was 10 µg/mL, respectively. Extraction from each skin layer (Epidermis and Dermis) was carried out using 1 mL of water: ethanol 50/50 (*v/v*) as an extraction solvent. The mixtures were sonicated for 30 min at 30 °C and finally left in agitation (600 rpm) at room temperature for 4 h. After the extraction time, skin samples were discharged, and the extraction solvent was transferred to plastic vials and then centrifuged at 12,000 rpm for 10 min. The supernatant was filtered using nylon syringe filters 0.22 µm (Phenomenex, Bologna, Italy) and analyzed by HPLC-MS.

7.2.3. Ursolic acid quantitative analysis in Franz's cell diffusion system

An HPLC Agilent 1200 coupled with an Agilent Technologies 6470-triple quadrupole mass spectrometer (Agilent Technologies, Palo Alto, CA, USA) was used for the analysis. Elution was performed on a Kinetex® XB-C18 column (50 mm × 3 mm, 2.6 µm; Phenomenex, Torrance, CA, USA). The mobile phases were water with 0.1% formic acid (A) and methanol with 0.1% formic acid (B). The elution gradient was performed according to the following conditions: 0–3 min, isocratic on 40% phase B; 3–13 min, linear gradient from 40 to 95% B; 13–18 min, isocratic on 95% B; 18–21 min, isocratic on 40% B for column recondition. The column temperature was set at 40 °C, inject volume was 5 µL, and the flow rate was set at 0.40 mL/min. The source was a heated electrospray interface (HESI) operated

in positive ionization with multiple reaction monitoring (MRM) scanning modes. One MRM transition was used as a quantifier transition and a second MRM transition served as a qualifier transition. The first transition (455.3–455.3) was performed with a collision energy of 20 eV, while the second transition (455.3–407.0) was made with a collision energy of 40 eV. The 2 transitions were made with a fragmentor of 135. Argon was used as a gas for collision-induced fragmentation. The MRM analyte parameters were optimized using a methanolic solution of ursolic acid at a concentration of 1 ppm. Ursolic acid was quantified according to a calibration curve ($R^2 \geq 0.99$) made with 9 different concentrations (5000, 1000, 500, 100, 50, 10, 5, 1, and 0.5 ppb) and triplicate injections at each concentration. The ion source was set using the following parameters: gas flow rate: 10 l/min; sheath gas flow rate: 12 l/min; gas temperature: 270 °C; nebulizer pressure: 40 psi; capillary voltage: 3500 V; and nozzle voltage: 1000 V. The separation conditions and the source parameters are summarized in the **Table 110** and **111**, respectively.

Time (min)	% B
0	40
3	40
13	95
18	95
18.1	40
21	40

Table 110: Summary of the gradient condition of the HPLC-HESI-MS/MS method for ursolic acid quantification in Franz's diffusion cell analysis.

Column	Kinetex® XB-C18 column (50 mm x 3.0 mm; 2.6 µm)
Phase A	Water at 0.1% HCOOH
Phase B	Methanol at 0.1% HCOOH
Column Temperature	40 °C
Injection volume	5 µl
Flow rate	0.40 ml/min
Collision energy transition quantifier	20 eV
Collision energy transition qualifier	40 eV
Gas flow rate	10 l/min
Sheath gas flow rate	12 l/min

Gas temperature	270 °C
Nebulizer pressure	40 psi
Capillary voltage	3500 V
Nozzle voltage	1000 V

Table 111: Summary of the chromatographic and source parameters of the HPLC-HESI-MS/MS method for ursolic acid quantification in Franz's diffusion cell analysis.

7.2.4. Tyrosinase inhibition assay

The tyrosinase inhibition assay was performed according to the modified dopachrome method (Kolakul & Sripanidkulchai, 2017). The enzyme inhibition was assessed by monitoring the enzymatic L-tyrosine metabolization using an HPLC assisted assay. 70 µL of different concentrations of the samples were added to a 96-well microplate. Then, 100 µL of 1 mM L-tyrosine and 30 µL of mushroom tyrosinase (500 U/ml) were added, mixed well, and incubated at room temperature for 30 min. For spectrophotometric optimization, absorbance was determined at 492 nm using a microplate reader. For the HPLC assay, 10 µL of the mixture was diluted with 90 µL of acetonitrile and centrifuged at 13000 rpm for 10 min. The supernatants were transferred to a vial and analyzed by HPLC-FLD. Different conditions of L-tyrosine concentration (11 concentrations: 0.01 mM, 0.025 mM, 0.05 mM, 0.1 mM, 0.25 mM, 0.4 mM, 0.5 mM, 1 mM, 2 mM, 3 mM, 4 mM; total range: 0 – 4 mM), enzymatic tyrosinase activity (11 tyrosinase activity values: 40 U/ml, 100 U/ml, 125 U/ml, 200 U/ml, 250 U/ml, 350 U/ml, 400 U/ml, 500 U/ml, 700 U/ml, 1000 U/ml, 1300 U/ml; total range: 0 – 1300 U/ml), incubation time (16 times: 0 min, 1 min, 2.5 min, 3.5 min, 5 min, 7.5 min, 10 min, 15 min, 20 min, 25 min, 30 min, 40 min, 50 min, 60 min, 70 min, 80 min; total range: 0 – 80 min), and DMSO content (7 DMSO %: 0%, 0.1%, 0.25%, 0.5%, 1%, 2.5%, 5%; total range: 0 – 5%) were selected to optimize the enzymatic activity and determine DMSO tolerance. 1 mM L-tyrosine and the mushroom tyrosinase (500 U/ml) were prepared in a 50 mM sodium phosphate buffer pH 6.5. Kojic acid was used as a positive control. The analyzed standards (e.g., kojic acid, ursolic acid, and phloridzin) and the triterpenoid extract of OAAO were dissolved in 100 % *v/v* DMSO and diluted with 50 mM sodium phosphate buffer pH 6.5 to obtain a final concentration of 1% *v/v* DMSO in the enzymatic mixture. In the spectrophotometric assay, enzymatic activity was evaluated as an increase in absorbance.

In the HPLC assay, enzymatic activity was evaluated as a decrease in the chromatographic L-tyrosine peak area for the tyrosinase reaction of the enzyme. The L-tyrosine peak area was normalized to the 1 mM L-tyrosine peak area. The inhibitory effect was expressed as the concentration required to inhibit L-tyrosine metabolism by 50% (IC_{50}).

7.2.5. HPLC-FLD assisted tyrosinase assay

A Jasco Extrema LC-4000 HPLC system (Jasco Inc., Easton, MD, USA), coupled with an autosampler, a binary solvent pump, and a fluorescence detector (FLD) was used for the analysis. The chromatographic analysis was performed according to Pan et al. (2014), with slight modifications. Elution was performed on a Luna HILIC column (150 mm x 3.0, 5 µm; Phenomenex, Torrance, CA, USA). The mobile phases were an ammonium acetate buffer 5 mM containing 0.1% formic acid (A) and acetonitrile (B). The elution gradient was performed under the following conditions: 0-5 min, isocratic on 90% phase B; 5-17 min, linear gradient from 90 to 70% B; 17-27 min, isocratic with 60% B; 24-29 min, isocratic with 90% B for column reconditioning. The separation parameters were as follows: column temperature was set at 35 °C, injection volume was 20 µl, and flow rate was set at 1 ml/min. The quantification of tyrosine was performed with an excitation wavelength of 272 nm and an emission wavelength of 312 nm. The separation conditions and the chromatographic conditions are summarized in the **Table 112** and **113**, respectively.

Time (min)	% B
0	90
5	90
17	70
17.1	60
24	60
24.1	90
29	90

Table 112: Summary of the gradient condition of the HPLC-FLD method for L-tyrosine quantification in tyrosinase assay.

Column	Luna HILIC column (150 mm x 3.0 mm; 5.0 µm)
Phase A	Ammonium acetate buffer 5 mM with 0.1% HCOOH
Phase B	Acetonitrile
Column Temperature	35 °C
Injection volume	20 µl
Flow rate	1.00 ml/min
Excitation FLD wavelength	272 nm
Emission FLD wavelength	312 nm

Table 113: Summary of the chromatographic and source parameters of the HPLC-FLD method for L-tyrosine quantification in tyrosinase assay.

7.2.6. HPLC-FLD method validation

7.2.6.1. Linearity and sensitivity of L-tyrosine HPLC-FLD method

Method validation was performed according to the ICH validation guideline (ICH.Q2[R2], 2022), which included the evaluation of a set of parameters, such as linearity range, the limit of detection (LOD), the limit of quantification (LOQ), precision and accuracy. Stock solutions of L-tyrosine was prepared by dissolving the individual standards in a solution of ammonium acetate buffer 5 mM with 0.1% of formic acid to obtain a concentration of 1 mM. The calibration curves ($R^2 \geq 0.99$) were obtained by diluting the individual stock solutions to obtain seven L-tyrosine concentrations (1.5 µM, 3 µM, 6.25 µM, 12.5 µM, 25 µM, 50 µM, 100 µM) with dilution factor of 2. These dilutions were prepared by diluting the stock solution of L-tyrosine 1 mM with acetonitrile to achieve a concentration of 100 µM with a dilution factor of 10. Therefore, the other six L-tyrosine concentrations were prepared by using a dilution solvent mixture of 9:1 acetonitrile/ammonium acetate buffer 5 mM with 0.1% of formic acid. The standard dilutions were analyzed in triplicate injections at each concentration level. The calibration curves were constructed by plotting the peak area against the standard concentration to evaluate the linearity of the standard response. A 7-point calibration curve was constructed by plotting the peak area against the standard

concentration to evaluate the linearity of the method. Limits of detection (LODs) and limits of quantification (LOQs) were determined to evaluate the sensitivity of the method. Determination of the signal-to-noise ratio was performed by comparing measured signals from samples with known low concentrations of analyte with those of blank samples (Maisto et al., 2022). Evaluation of the signal-to-noise ratios was performed by comparing measured signals from samples with a known low concentration of 1.5 µM of L-tyrosine with those of blank solvent of acetonitrile. LOD represents the minimum concentration at which the analyte can be reliably detected and is defined as the lowest detectable concentration of analyte that gives a response that the analytical system can distinguish from the background level (S (signal of compound)/N (signal of noise)) = 3. Instead, LOQ is defined as the lowest quantifiable concentration of analyte that can be measured with a standard level of confidence, and it is typically calculated using (S/N) = 10 (Maisto et al., 2022)

7.2.6.2. Precision and accuracy of L-tyrosine HPLC-FLD method

As recommended by the ICH validation guideline (ICH.Q2[R2], 2022), the determination of accuracy (estimated by calculating the % bias) and precision (estimated by calculating the coefficient of variation CV %) was performed to validate the analytical method. Precision and accuracy were calculated by an intra-day and an inter-day analysis of individual L-tyrosine standard solutions at 3 different concentration levels. The intra-day analysis was performed by injecting the standard solutions 3 times per day. Instead, the inter-day analysis.

7.2.7. Ultrafiltration assisted tyrosinase assay

The ultrafiltration HPLC-MS method was performed according to the method reported by Yang et al. (2012), with slight modifications. The method was performed with three subsequent steps of incubation, ultrafiltration, and characterization. The incubation step was performed by applying the same protocol of tyrosinase inhibition assay previously described in the paragraph **7.2.4. Tyrosinase inhibition assay**. The unbound low-mass compounds were separated from the ligand-enzyme complexes by ultrafiltration. After the incubation,

the enzymatic mixture was filtered with an Amicon Ultra-0.5 Centrifugal Filter 3 kD MWCO at 9000 rpm for 30 minutes at room temperature. The filter contained a regenerated cellulose ultrafiltration membrane with a 3000 molecular weight cut-off. The ultrafiltrates were analyzed by HPLC-MS/MS analysis for the evaluation of the chemical composition. Tyrosinase binding was determined by a decrease of the HPLC peak area of the detected compounds corresponding to incubation with active enzyme. Control experiment with a thermal denatured enzyme was carried out for comparison. The HPLC-MS/MS analysis was performed with the same method in negative acquisition mode reported in the paragraph **6.3.7. Qualitative analysis of Annurca Apple oleolyte**.

7.2.8. Elastase inhibition assay

The elastase inhibition assay was performed according to the spectrophotometric method reported in literature (Nema et al., 2013). The method is based on the activity of the enzyme elastase, which hydrolyzes the substrate N-succinyl-(Ala)-3-*p*-nitroanilide to *p*-nitroanilide, a colored compound which can be monitored at 410 nm. The assay was performed by mixing 1.3 ml of a solution 1.015 mM of N-succinyl-(Ala)-3-*p*-nitroanilide in 0.1232 M Tris-HCl buffer at pH 8.0 with 0.1 ml of the sample. The mixture was vortexed, pre-incubated at 25 °C for 10 minutes, and added to 0.1 ml of a solution of the enzyme elastase 0.0375 U/ml in 0.1232 M Tris-HCl buffer at pH 8.0. The mixture was incubated at 25 °C for 10 minutes, and then the absorbance is measured at 410 nm. Different conditions of enzymatic elastase activity (13 elastase activity values: 0 U/ml, 0.005 U/ml, 0.01 U/ml, 0.02 U/ml, 0.03 U/ml, 0.04 U/ml, 0.05 U/ml, 0.1 U/ml, 0.2 U/ml, 0.25 U/ml, 0.4 U/ml, 0.5 U/ml, 0.6 U/ml; total range: 0 – 0.6 U/ml), incubation time (13 times: 0 min, 2 min, 4 min, 6 min, 8 min, 10 min, 12 min, 14 min, 16 min, 18 min, 20 min, 25 min, 30 min; total range: 0 – 30 min), and DMSO content (10 DMSO %: 0%, 0.1%, 0.5%, 1%, 1.5%, 2%, 2.5%, 3%, 4%, 5%; total range: 0 – 5%) were selected to optimize the enzymatic activity and determine DMSO tolerance. Quercetin was used as a positive control. The analyzed standards (e.g., quercetin and ursolic acid) and the triterpenoid extract of OAAO were dissolved in 100 % *v/v* DMSO and diluted with 0.1232 M Tris-HCl buffer at pH 8.0 using a dilution factor of 2 to obtain a final concentration of 1.5% *v/v* DMSO in the enzymatic mixture. Triterpenoid extract of OAAO was diluted to prepare a calibration curve in a range of 700 µg/ml – 0 µg/ml (14 concentrations), ursolic acid was diluted to prepare a calibration curve in a range of 650 µg/ml – 0 µg/ml (18 concentrations), and quercetin was diluted to prepare a

calibration curve in a range of 800 µg/ml – 0 µg/ml (17 concentrations). The percentage of inhibition was calculated as follows:

$$\textbf{Inhibition (\%)} = \left(1 - \frac{B}{A}\right) x\ 100$$

where A is the enzymatic activity without the sample and B is the enzymatic activity in the presence of the sample.

7.2.9. Cell culture

The human melanoma cells lines A375 were cultured in DMEM medium supplemented with 10% heat-inactivated fetal bovine serum, 2 mmol/L L-glutamine, 100 U/mL penicillin, 100 µg/mL streptomycin and 10 mM HEPES buffer and grown at 37°C in a humidified incubator under 5% CO_2.

7.2.10. MTT assay

A375 cells (10^3 cells/well) were plated on a 96-well plate and treated with OAAO triterpenoids extract and ursolic acid, in a range of concentration of 0.01 µg/ml to 100 µg/ml for 72 hr. Next, 25 µL of MTT was added and incubated for 3 hr at 37°C. Thereafter, the dark blue crystals developed, were solubilized with DMSO and the absorbance was measured at 545 nm using Multiskan GO microplate reader (Thermo Fisher Scientific, MA, USA).

7.2.11. Measurement of melanin content

A375 cells ($3x10^5$/well) were plated in a 6-well plate and treated with OAAO triterpenoids extract and ursolic acid at a concentration of 30 µg/ml and 3 µg/ml, respectively. After 72 hours, cells were lysate in NaOH 1N, and incubated for 90 min at 37°C then centrifuged for 10 min at 10000 rpm. The optical density (OD) of supernatant was measured at 450 nm using Multiskan GO microplate reader (Thermo Fisher Scientific, Waltham, MA, USA).

7.2.12. RNA extraction and real time qPCR analysis

A375 human melanoma cells were treated with OAAO triterpenoids extract and ursolic acid standard at a concentration of 30 µg/ml and 3 µg/ml for 6 hours, respectively. Thereafter, total RNA was extracted by using TRI-Reagent, according to the manufacturer's instructions. After quantification with Nanodrop, 1 µg of total RNA was reverse-transcribed by using iScript Reverse Transcription Supermix for RT-qPCR. The $2^{\Delta DCt}$ formula was used for the analysis and ribosomal protein S16 (RPS16) was used as housekeeping gene. qPCR analysis was performed with Bio-Rad CFX384 real-time PCR detection system (Bio-Rad, Milan, Italy) by using the following primers:

TYR (Gene ID: 7299)**:** 5'- GCACAGATGAGTACATGGGAGG -3'; 5'- CTGATGGCTGTTGTACTCCTCC -3'

TYRP-1 (Gene ID: 7306)**:** 5'- TCTCAATGGCGAGTGGTCTGTG-3'; 5'- CCTGTGGTTCAGGAAGACGTTG-3'

TYRP-2 (Gene ID: 1638)**:** 5'- CTCAGACCAACTTGGCTACAGC-3'; 5'- CAACCAAAGCCACCAGTGTTCC-3'

MITF (Gene ID: 4286)**:** 5'- GGCTTGATGGATCCTGCTTTGC-3'; 5'- GAAGGTTGGCTGGACAGGAGTT-3'

GCLC (Gene ID: 2729)**:** 5'-GTTGGGGTTTGTCCTCTCCC-3'; 5'- GGGGTGACGAGGTGGAGTA-3'

GCLM (Gene ID: 2730)**:** 5'-AGGAGCTTCGGGACTGTATCC-3'; 5'- GGGACATGGTGCATTCCAAAA-3'

HMOX-1(Gene ID: 3162)**:** 5'-GCCGTGTAGATATGGTACAAGGA-3'; 5'- AAGCCGAGAATGCTGAGTTCA-3'

7.2.13. Flow cytometry analysis

A375 were treated for 48 hours with OAAO triterpenoids extract and ursolic acid at a concentration of 30 µg/ml and 3 µg/ml, respectively. Thereafter, ROS production was evaluated by using the H2DCFDHA probe. Likewise mitochondrial mass and membrane potential were evaluated by using MitoTracker Green and tetramethylrhodamine methyl

ester (TMRM) probes, as previously described. Samples were acquired on BriCyte E6 flow cytometer (Mindray Medical Italy S.r.l., Milan, Italy), and data were analyzed with FlowJo software (TreeStar V.10; Carrboro, NC, USA).

7.2.14. Preparation of a cosmetical OAAO cream for topical formulation

OAAO was used for the preparation of a cosmetic *o/w* emulsions with cosmetic grade ingredients by mixing an oil phase (Phase A) with an aqueous phase (Phase B). Phase A containing oily constituents, such as Caprylic/Capric Triglycerides (10.00% *w/w*), Glyceryl-Stearate (4.00% *w/w*), Cetyl Ricinoleate (2.00% *w/w*), and Cetearyl Alcohol (0.50 % *w/w*), were mixed using magnetic stirrer at 200 ± 25 rpm and heated up to 70 ± 5 °C. Once reached melting, Phase A was mixed with Phase B (aqueous phase), comprising deionized water (80.30% *w/w*), Carbomer (0.35% *w/w*), and Ethylenediaminetetraacetic acid (0.10% *w/w*), previously heated at the same temperature of Phase A. Phases mixing occurred using the mechanical stirrer Silverson L5T Laboratory Mixer (SBL, Shanghai, China), at 4500-5000 rpm until the 50 ± 2 °C temperature was reached, then at 2500-3000 rpm until the mix became supple and homogenous. Once reached 37 ± 2 °C, the final phase (Phase C) containing the active ingredient OAAO (2.50% *w/w*), and the preservative system, such as water solution of Methylisothiazolinone, Magnesium Nitrate, and Magnesium Chloride (0.15% *w/w*), was added to the mixture. Neutralization with a solution 2N NaOH was done once emulsions were cool. The placebo emulsions were prepared analogously and contained all cosmetic formulation ingredients, except for the OAAO ingredient. The quality control of the cream was assessed after 24 hours by evaluating the viscosity (29.145 – 30.633 mPa; L3, 20 rpm) with a Visco Basic Plus rheometer (Fungilab S.A., Barcelona, Spain), and the pH (5.0 ± 0.5) with GPL20 pH-Meter (Crison Instruments S.A., Barcelona, Spain). Once ready, cosmetic creams were placed in anonymous 30 mL jars, by a blind technician.

7.2.15. Study design and participants selection

This randomized, double-blind, efficacy study was done by the RD Cosmetics laboratory of the University of Naples Federico II - Pharmacy Department, which has a quality management system for cosmetic clinical trial certified by RINA S.p.A (Genova, Italy)

according to the UNI EN ISO 9001 standard. Patients aged 40–65 years (inclusive) with a diagnosis of relaxed skin tone and dermis thinning were eligible for inclusion.

Further inclusion criteria were discontinuation of all cosmetic products used to treat ageing phenomena from screening up until the final follow-up visit; however, cleansing preparations deemed acceptable by the investigator and makeups were permitted. Exclusion criteria included any dermatological disease, previous use of retinoids, and use of medical aesthetic procedures, such as bio-stimulations, filler or botox within 12 weeks or five half-lives of screening, face radiofrequencies within 8 weeks of screening, or anti-aging/antioxidant oral supplementation within 4 weeks of screening. Further exclusion criteria were presence of both topical and systemic pathologies or disease. After the enrollment visit, a mandatory washout period of 7 days was required before study entry. During the baseline (D0) and check-up visits, participants were assessed for the monitored skin parameters. The primary outcome of the study was the determination of the skin aging-related parameter improvement (skin elasticity, firmness and roughness), secondary outcomes were transepidermal water loss (TEWL) and corneometry assessment in accordance with literature findings with a short and long term test. All patients provided written informed consent. Since the cosmetic purpose of the present study and the involvement of adult healthy human subjects, a submission to the relevant ethics committee was not required. Nevertheless, the study was performed in accordance with the ICH GCP guidelines and the principles embodied by the Declaration of Helsinki, as applicable to cosmetic products. The timeline diagram of the study plan is reported in the **Figure 108**.

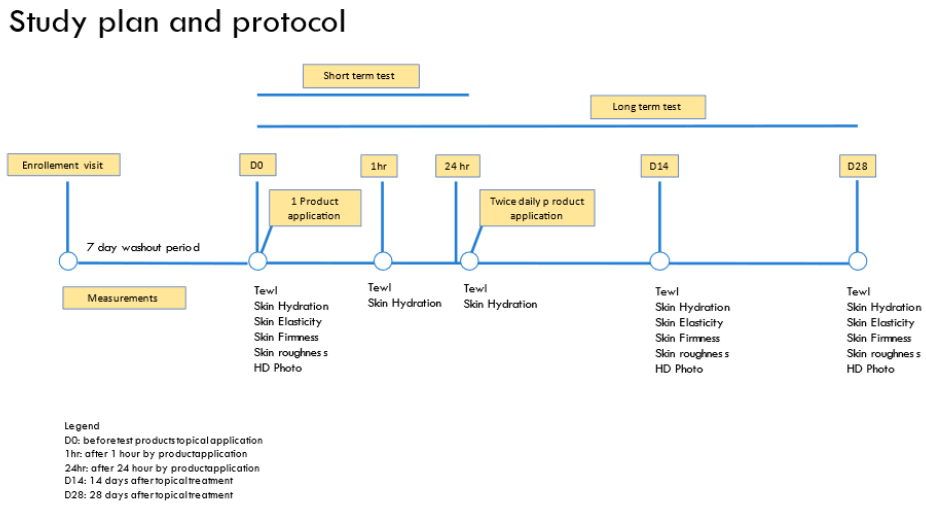


Figure 108. Timeline diagram of the study plan.

7.2.16. Randomization and masking

The laboratory staff used a system for the management of study enrolment and ensuring anonymity. The system assigned to the enrolled subjects a patient study number, randomized according to defined parameters drawing on a general panel where volunteers are recorded, and maintained treatment masking. Subjects came from all social categories, and they spontaneously participate in the study. Before admission, they received a clinical skin examination and a detailed cosmetic questionnaire. The system used a configurable buildable algorithm with limits set to patient age (≤ 40 and > 65 years) and skin type (thin dermis and relaxed face). Patients were randomly assigned to OAAO-based cream (2.5%$_{w/w}$ twice daily) or vehicle cream twice daily (placebo group) in a 1:1 ratio. Patients and investigators (except members of the primary endpoint analysis data monitoring teams) remained masked to each patient's treatment assignment throughout the study. Emergency unmasking was conducted in case of side effects that required the investigator's knowledge of the patient's treatment group. At the end of the study, the number of patients that respected the protocol with no significant deviation, which could influence the study results, had to be 20 for each treatment group. The flow diagram of participant recruitment and the exclusion criteria are summarized in the **Figure 109**.

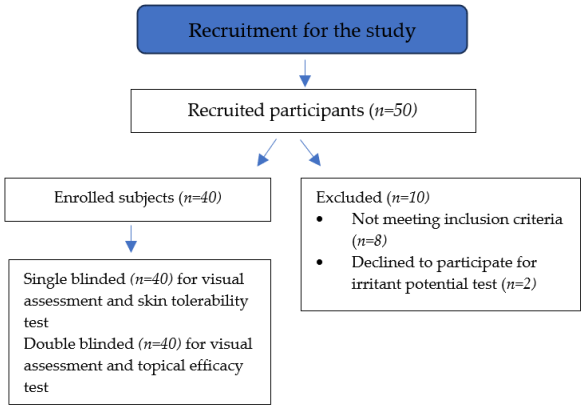


Figure 109. Flow diagram of participant recruitment for the study and clinical requirements (irritant potential and topical efficacy).

7.2.17. Skin tolerability test

In order to ensure the test product tolerability its potential irritant power was evaluated when it is applied in a single dose to intact human skin with an occlusive patch test for 72 hours. The irritancy patch test was conducted on the volar forearm due to its hairlessness, lower sebaceous gland count, and larger skin surface area. This test allowed for the evaluation of OAAO tolerability when transmitted in a topical formulation, through the identification and classification of its potential irritant power, as required by EEC Directive 76/768. The test is conducted using Finn Chambers® AQUA (Bio-Diagnostics Ltd, Worcester, United Kingdom) that is a patch delivery system and holding device to place allergens and allergen mixes in contact with the surface of the skin during allergen patch tests. The OAAO cream and placebo were displaced directly into different chamber and applied to healthy skin on upper forearm, which was clean, dry, and free of ointments or lotions. The panel was left *in situ* for 72 hours, then, the panel is removed, and skin reaction are recorded (PI48), and measured again after further 24 hours (PI72). Results to the patch test are measured by morphologic criteria recommended by the International Contact Dermatitis Research Group (Lazzarini et al., 2013), using a 2 × magnifying lamp for visual scoring using the following grading system: 0 = no evidence of reaction, 1 = minimal erythema, 2 = definite visible erythema and 3 = erythema and papules. The irritancy power was calculated using the average visual score + one standard deviation (SD) for 2.5%$_{w/w}$ OAAO formulation and the placebo – Irritancy levels for the sample were classified as follows: average clinical score + SD > 1.5 = sample is an irritant; average clinical score + SD ≤ 1.5 and > negative control = sample has low irritancy potential and a mean visual score + SD ≤ negative control = sample is not-irritant. The irritancy limit of 1.5 on a 0–3 scale for the visual score + one SD was used as the irritancy level threshold.

7.2.18. Statistics

GraphPad Prism software version 9 (San Diego, CA, USA) was used for statistical analysis. T test and ANOVA test were used for comparison of two groups or multiple groups respectively. The data were shown as mean ± SEM. A *p*-value < 0.05 was considered statistically significant and was labeled with *; *p*-values < 0.01, 0.001 or 0.0001 were labeled with **, *** or ****, respectively. In the cosmetic clinical trial a sample size of 40

randomly assigned patients (approximately 20 patients per group) was determined to provide sufficient statistical power to detect the difference between the OAAO cream twice daily and placebo**.** For the primary and key secondary endpoints, comparisons between the **O**AAO groups and placebo were done using ANOVA test (inter-groups differences), whereas average percentage variations compared to baseline for each group was controlled using the Student t-test (intra-groups differences) at an overall two-sided *p* of 0.05. Statistical analyses were done with SAS software version 9.4.

7.3. Results and discussion

7.3.1. Melanogenesis inhibition properties of Annurca Apple oleolytes

Melanin is the most important human pigment and is responsible for of skin, eyes, and hair pigmentation (D'Mello et al., 2016). It is produced by melanocytes in melanosome, a specific sub-cellular lysosome-like structure. Physiologically, synthesis and production of melanin protect human skin from UV radiation. However, melanin abnormal production can be related to several skin aging-related diseases, including acquired hyperpigmentation, age spots, and melasma. Specifically, melanogenesis is a multi-step process which involve the melanin synthesis and transport, and the subsequent release from the melanosomes. Chemically, the melanogenesis process begins with tyrosine oxidation to dopaquinone, catalyzing by the enzyme tyrosinase (TYR). Subsequently, dopaquinone is converted into dopachrome by an auto-oxidation reaction. The L-dopa produced is a tyrosinase substrate and is oxidized to dopaquinone by the enzyme tyrosinase. The resulting dopaquinone undergoes further oxidative polymerization steps that lead to melanin synthesis (N. Guo et al., 2020; L. Zhang et al., 2021). The reactions leading to melanin synthesis are summarized in the **Figure 110**.

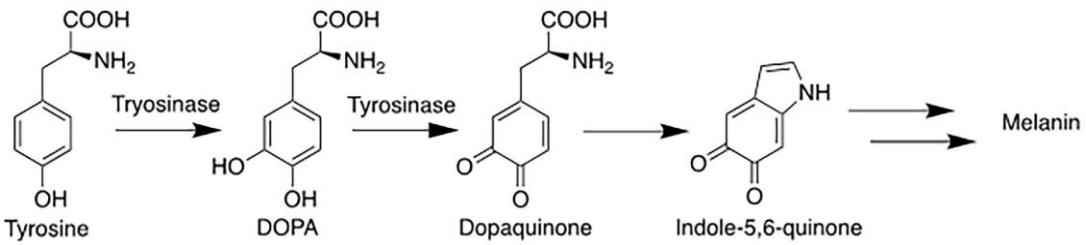


Figure 110: Biological synthesis of melanin.

Several molecular modulators are involved in the regulation of the melanogenesis process (D'Mello et al., 2016). Specifically, UV-irradiation induces α-melanocyte synthesis by stimulating α-melanocyte stimulating hormone (α-MSH) synthesis in melanocytes, which activates the melanocortin 1 receptor. The activation of the receptor leads to increase the expression of microphthalmia-associated transcription factor (MITF) through the activation

of the cyclic adenosine monophosphate pathway. The MITF factor can be considered a key protein that controls several melanogenesis-regulating protein factors synthesis, including tyrosinase and tyrosinase-related proteins (TRPs), which can be found as tyrosinase-related protein 1 (TRP1) and tyrosinase-related protein 2 (TRP2) (Nguyen & Fisher, 2019; Park et al., 2020). A summary of the biological role of enzymes TYR, TRP1 and TRP2 is summarized in the **Figure 111**.

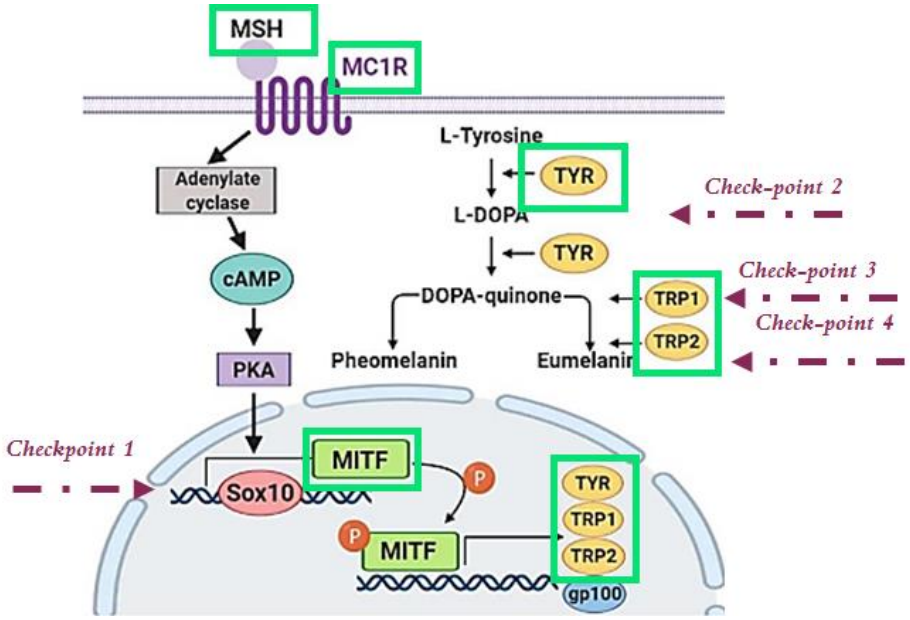


Figure 111: Description of the enzymes and the factors involved in melanin synthesis regulation.

Due to their pivotal role in melanin production, tyrosinase and tyrosinase-related proteins TRP1 and TRP2 represent the most important molecular targets for active compounds with skin bleaching and depigmenting effects. During the last years, a great attention has been given to natural and food-derived compounds identification as effective inhibitors of the tyrosinase enzyme. *In vitro* studies conducted using mushrooms tyrosinase have shown that some polyphenols, as chalcones (IC_{50} 0.07 µM) and hydroxystilbens are the most effective tyrosinase inhibitors (Bayrakçeken Güven et al., 2023). Instead, among lipophilic compounds, triterpenoids as ursolic acid have attracted great attention due to its reported potent *in vitro* tyrosinase inhibitory activity (IC_{50} 170.2 µM) (Bayrakçeken Güven et al., 2023) and its potentially favorable skin permeation ability ascribable to its high lipophilicity

(Maisto et al., 2023). To assess the capacity of ursolic acid and the triterpenoids extract of OAAO to inhibit the enzyme tyrosinase and to regulate the melanin production, an enzymatic assay of tyrosinase inhibition was validated.

7.3.1.1. Validation of the spectrophotometric tyrosinase inhibition assay

The tyrosinase inhibition assay is generally performed by a spectrophotometric assay to evaluate the oxidation reaction of L-tyrosinase to quinone, an oxidation product which is monitored at a wavelength of 492 nm (**Figure 112**) (Panzella & Napolitano, 2019).

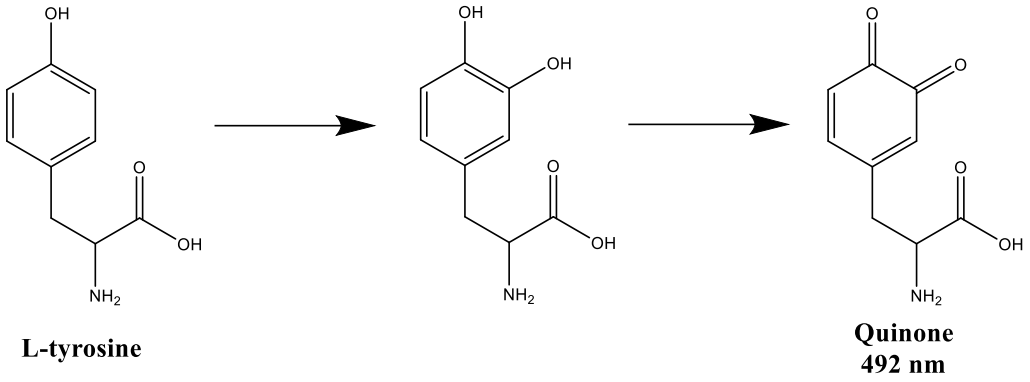


Figure 112: Oxidation reaction of L-tyrosinase to a quinone.

The validation of the tyrosinase inhibition assay requires the optimization of some parameters. Different conditions of L-tyrosine concentration (11 concentrations: 0.01 mM, 0.025 mM, 0.05 mM, 0.1 mM, 0.25 mM, 0.4 mM, 0.5 mM, 1 mM, 2 mM, 3 mM, 4 mM; total range: 0 – 4 mM), enzymatic tyrosinase activity (11 tyrosinase activity values: 40 U/ml, 100 U/ml, 125 U/ml, 200 U/ml, 250 U/ml, 350 U/ml, 400 U/ml, 500 U/ml, 700 U/ml, 1000 U/ml, 1300 U/ml; total range: 0 – 1300 U/ml), incubation time (16 times: 0 min, 1 min, 2.5 min, 3.5 min, 5 min, 7.5 min, 10 min, 15 min, 20 min, 25 min, 30 min, 40 min, 50 min, 60 min, 70 min, 80 min; total range: 0 – 80 min), and DMSO content (7 DMSO %: 0%, 0.1%, 0.25%, 0.5%, 1%, 2.5%, 5%; total range: 0 – 5%) were selected to optimize the enzymatic activity and determine DMSO tolerance. 1 mM L-tyrosine and the mushroom tyrosinase (500 U/ml) were prepared in a 50 mM sodium phosphate buffer pH 6.5. The composition of the buffer was not optimized but was extrapolated by the assay conditions reported in literature (Kolakul & Sripanidkulchai, 2017). Kojic acid was used as a positive

control as a well-known tyrosinase inhibitor. The optimization of DMSO % represents a critical point of enzymatic assay validation. DMSO is usually used to dissolve hydrophobic compounds but is employed at low concentrations to guarantee the intrinsic enzymatic activity. Over a critical concentration, DMSO perturbs the enzyme conformations, causing a gradual and reversible decrease of catalytic activity. Our results showed that the combination of parameters which guarantees a linear kinetics of response for quinone formation are as follows: L-tyrosine concentration of 1mM (**Figure 113A-A1**), tyrosinase concentration of 500 U/ml (**Figure 113B-B1**), and at a reaction time of 30 min (**Figure 113C-C1**). It's interesting to observe that the velocity of the enzymatic reaction, which is expressed as a difference of the absorbances of the reaction sample and the blank ($Abs_{quinone}$ - Abs_{blank}), is directly proportional to L-tyrosine concentration in a selective concentration range of 0 – 100 µM (**Figure 113A**). Therefore, tyrosinase (R^2 = 0.9939, y = 0.0007x + 0.0658) catalases a first order kinetics reaction, without enzymatic saturation. The first order kinetics displayed from the linearity of the reaction rate was also demonstrated for a selected range of L-tyrosine concentration (R^2 = 0.9902, y = 0.2662x + 0.1191) and reaction time (R^2 = 0.9903, y = 0.0118x + 0.0088). These optimized reaction conditions in the spectrophotometric assay were used as parameters for the development and validation of a HPLC-FLD assisted enzymatic assay. The analyzed standards (e.g., kojic acid, and phloridzin) were dissolved in 100 % *v/v* DMSO and diluted with 50 mM sodium phosphate buffer pH 6.5 to obtain a final concentration of 1% *v/v* DMSO in the enzymatic mixture.

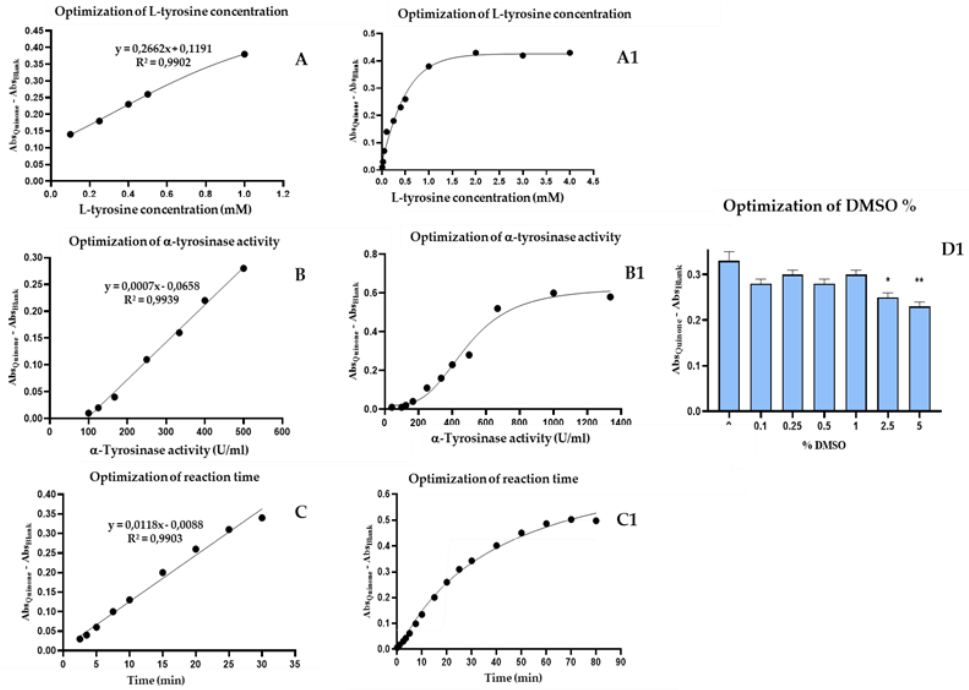


Figure 113: Optimization parameters of tyrosinase inhibition assay. **A**: optimization of L-tyrosinase concentration; **B**: optimization of tyrosinase activity; **C**: optimization of reaction time; **D**: optimization of DMSO %.

In a first moment, the tyrosinase inhibition assay was performed with the classical spectrophotometric method. Moreover, the analysis performed on the analytical standard demonstrated that polyphenols represent natural interferents of the assay acting as a suicidal enzyme inhibitor (J. Chen et al., 2020). The phenolic function represents an oxidation point for the enzyme tyrosinase, synthetizing a quinone with an absorbance similar to the absorbance of the L-tyrosine quinone. A dose-response curve for tyrosinase inhibition is reported in **Figure 114**, which allowed to calculate the IC_{50} of 21.48 µM for the standard of kojic acid, while phloridzin standard displayed a typical bell-shape. Therefore, to evaluate the capacity of the triterpenoids OAAO extract to inhibit the enzyme tyrosinase, which contains polyphenols which can interfere with the spectrophotometric assay, a HPLC-FLD assisted enzymatic assay was developed and validated.

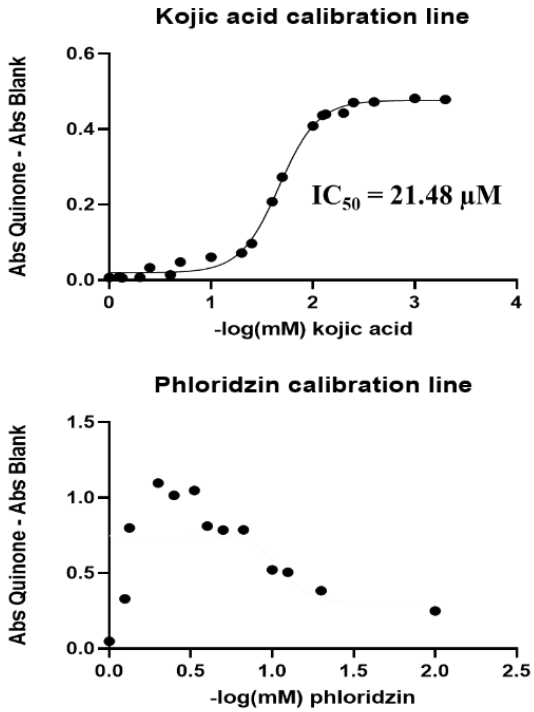


Figure 114: Dose-response curve of tyrosinase spectrophotometric inhibition assay for the standards of kojic acid and phloridzin.

7.3.1.2. Development and validation of the HPLC-FLD assisted tyrosinase assay

The method used for the HPLC-FLD tyrosinase inhibition assay is accurately described in the previous paragraph **7.2.5. HPLC-FLD analysis of tyrosinase assay**. The method was developed evaluating the reduction of L-tyrosine peak during the assay. L-tyrosine is an aminoacid, which is a compound with a great polarity which doesn't allow a corrected retention of the C_{18} column used in the reversed phase liquid chromatography (RP-LC). Therefore, the HPLC-FLD method was developed using the HILIC chromatography, which represents a valid approach for the separation of polar compounds. For the selection of the phases, the HILIC chromatography is usually employed using great percentages of apolar solvents, till a maximum % of water or aqueous buffer of 50-60%. The exact composition of phase A solution depends on the nature of the HILIC stationary phase. For example, the use of salt aqueous buffer in the phase A is usually applied to modify the ionization and the retention of polar compound to the stationary phase. Therefore, an ammonium acetate buffer 5 mM containing 0.1% formic acid (A) was selected as salt buffer of the phase A for L-tyrosine chromatographic method. To improve the sensitivity of the assay, a fluorimetric detector with an excitation wavelength of 272 nm and an emission wavelength of 312 nm was used for the analysis. The standards and samples solubilization was performed to obtain the same solvent composition of the initial chromatographic condition of the method (10:90 ammonium acetate buffer 5 mM containing 0.1% formic acid/acetonitrile). Therefore, the use of higher aqueous concentrations in the solubilization solvent could represent a problem in the interaction of the analytes with the stationary phase. The enzymatic assay is performed in an aqueous salt buffer without organic solvents. Therefore, at the end of the enzymatic incubation, 10 µL of the mixture was diluted with 90 µL of acetonitrile to achieve a final solvent composition of 10:90 ammonium acetate buffer 5 mM containing 0.1% formic acid/acetonitrile. The use of a great amount of organic solvent represents an efficient quenching system to completely inactivate the enzyme, avoiding the L-tyrosine oxidation in the vials during the working of the samples list. Since the addiction of acetonitrile also determines the precipitation of the salts and the enzyme, a centrifugation of 13000 rpm for 10 minutes is required to eliminate the contaminants from the mixture and recover the supernatant containing the L-tyrosine. The HPLC-FLD assisted tyrosinase assay was validated by monitoring the reduction of L-tyrosine chromatographic peak (**Figure 115**).

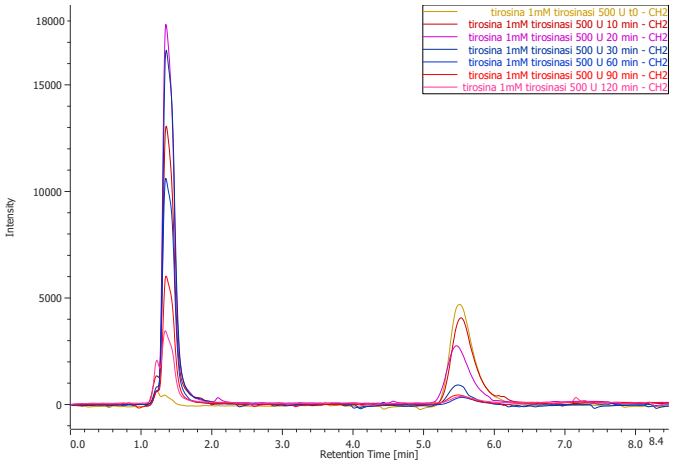


Figure 115: L-tyrosine chromatographic peak in different time points of the HPLC-FLD assisted tyrosinase inhibition assay.

For the validation of the chromatography of the HPLC-FLD assisted assay, the procedures described above in the paragraphs **3.1.11. Method validation according to ICH guidelines** were applied to the method reported in the paragraph **7.2.5. HPLC-FLD analysis of tyrosinase assay**. L-tyrosine calibration curve has been performed in a range of seven concentrations between 100 µM and 1.5 µM with a dilution factor of 2. The calibration curve displayed a favourable linear regression ($R^2 > 0.99$), thus demonstrating the linearity of the standard response in the range of concentrations analyzed (**Figure 116**). LOD and LOQ values were determined to evaluate the sensitivity of the method. L-tyrosine displayed a LOD value of 16.05 µM and a LOQ value of 5.30 µM (**Table 116**), which are above the compound values in the analysed real samples of the enzymatic mixtures, confirming the efficiency of the method for the quantification of L-tyrosine.

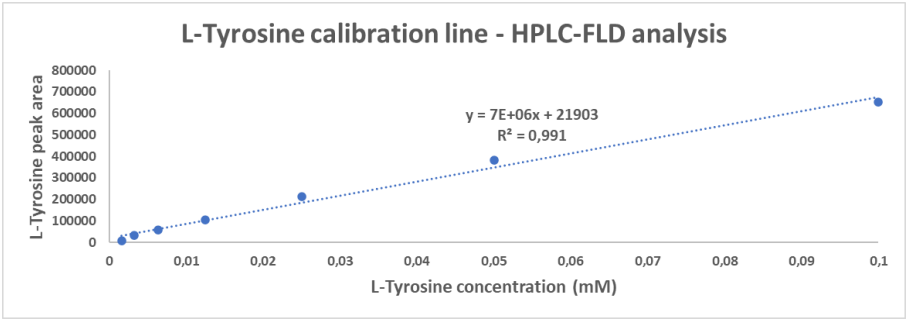


Figure 116. L-tyrosine calibration curve for the HPLC-FLD assisted tyrosinase inhibition assay.

Compound	Linearity range (µM)	Calibration curve	LOD (µM)	LOQ (µM)
L-tyrosine	1.5 - 100	y = 6537884x + 21903.27	16.05	5.30

Table 114. Linearity range, calibration curve, limit of detection (LOD) and limit of quantification (LOQ) for L-tyrosine.

In agreement with the ICH validation guideline (ICH.Q2[R2], 2022), precision and accuracy were evaluated to validate the HPLC-FLD method. Precision and accuracy were calculated by an intra-day and an inter-day analysis of L-tyrosine standard solutions at 3 different concentrations (**Table 115**). The 3 concentrations have been selected to represent the calibration level (e.g., high: 25 µM; medium: 6.25 µM; low: 1.55 µM) included in the linearity range. The selection of these concentrations allowed to establish precision and accuracy of the entire calibration curves. The intra-day analysis was performed by injecting L-tyrosine solutions three times per day. Instead, the inter-day analysis was performed by injecting the three selected standard solutions for 3 consecutive days. In the validation of the HPLC-FLD analysis, for the evaluation of intraday and interday precision and accuracy, the RSD value ranged from 1.080 to 4.375 % ppm and from -0.534 to 2.142 %, respectively. Therefore, all % CV and % bias values for precision and accuracy evaluation showed values lower than ± 5%. These results assessed that the developed method was satisfactory with acceptable precision, accuracy, and reproducibility for L-tyrosine analysis.

Compound	Concentration (µM)	Precision (CV %)		Accuracy (% bias)	
		Intraday	Interday	Intraday	Interday
L-tyrosine	25	1.882	1.754	-0.534	-0.521
	6.25	1.320	1.080	0.480	1.100
	1.55	4.321	4.375	2.142	1.583

Table 115. Intra-day and inter-day precision and accuracy of L-tyrosine analysis.

7.3.1.3. HPLC-FLD assisted tyrosinase assay: analysis of the real samples

After validating the enzymatic assay conditions and the HPLC-FLD method, quantification of L-tyrosine in the reaction mixtures was performed for the plotting of the dose-response curves and the calculation of the IC_{50} for the inhibition of the enzyme tyrosinase. The

analysis of the triterpenoids OAAO extract displayed a tyrosinase inhibition activity in a concentration dependent manner, with a IC_{50} value of 286.42 µg/ml (**Figure 117**).

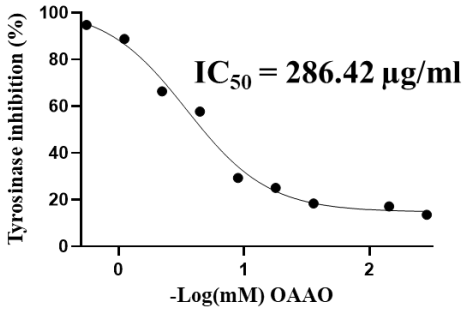


Figure 117: Evaluation of the IC_{50} for OAAO inhibition of tyrosinase enzyme.

To evaluate the activity of ursolic acid as the main bioactive compound of triterpenoids OAAO extract responsible for the inhibition of the enzyme tyrosinase, the ursolic acid standard was tested in the assay, calculating a IC_{50} value of 58.73 µM (**Figure 118**). Subsequently, to confirm the efficacy of the HPLC-FLD method for the evaluation of the tyrosinase inhibition assay, the assay was performed on phloridzin standard, calculating a IC_{50} value of 387.7 µM (**Figure 119**).

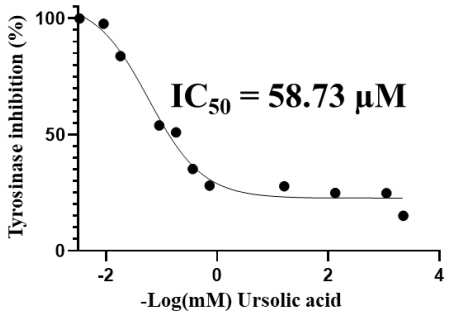


Figure 118: Evaluation of the IC_{50} for ursolic acid inhibition of tyrosinase enzyme.

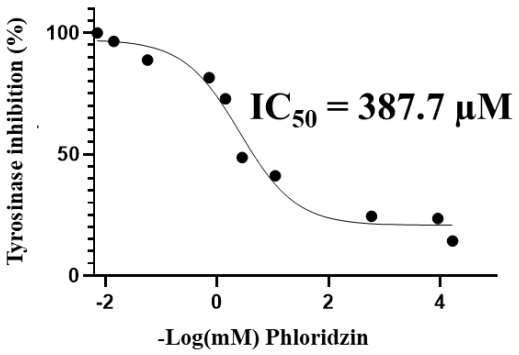


Figure 119: Evaluation of the IC_{50} for phloridzin inhibition of tyrosinase enzyme.

To validate the method for the tyrosinase inhibition assay, the efficiency of the method was confirmed by the positive control of kojic acid, a fungal metabolite with a well-known inhibitor activity of the enzyme for its strong chelating activity of the copper in the active site of the tyrosinase enzyme. Therefore, the assay was performed on kojic acid standard, calculating a IC_{50} value of 4.14 µM (**Figure 120**). This result is similar to the values calculated with the spectrophotometric assay at the paragraph **7.3.1.1. Validation of the spectrophotometric tyrosinase inhibition assay** (21.48 µM) and is in line with the value reported by other authors (Ashooriha et al. 2023), who reported an IC_{50} inhibition value in a range of 0.14 – 3.70 µM. The HPLC-FLD assisted tyrosinase inhibition assay represents the first attempt to develop a chromatographic application on the enzymatic assay.

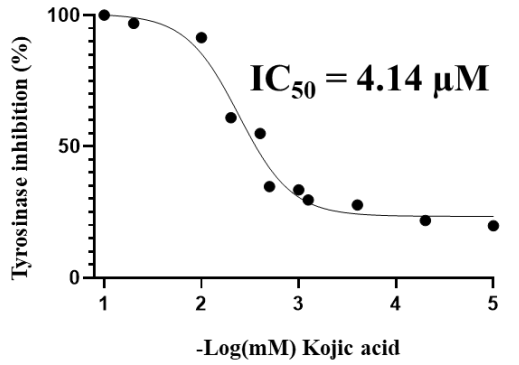


Figure 120: Evaluation of the IC_{50} for phloridzin inhibition of tyrosinase enzyme.

7.3.1.4. Ultrafiltration assisted tyrosinase assay

The evaluation of tyrosinase inhibition assay on triterpenoids OAAO extracts and on the analytical standards of ursolic acid and phloridzin represents an evaluable tool to indicate the bioactive compounds responsible of the enzyme inhibition. However, the confirming of the activity of these compounds as the main tyrosinase inhibitors of the extract require the evaluation of the bioactivity of the other molecules of the extract. In addition, the conventional procedure for the evaluation of enzymatic inhibition properties from plants requires procedures of bioassay-guided fractionation, purification, and structural identification. These procedures are time consuming and labour intensive. Therefore, an ultrafiltration approach coupled with HPLC-MS method represents an evaluable tool for the discover of biological active compounds from complex mixtures. This method requires the use of ultrafiltration system to evaluate the ability of the compounds to bind the enzyme. The ultrafiltration of the enzymatic mixture allows to separate the unbinding components of the extract from the mixture of the enzyme and the binding components of the extract. Therefore, the analysis of the two components indicates the compounds active as enzymatic inhibitor. The experiment is compared to a reaction mixture by using a thermally denaturated enzyme, to distinguish the compounds which bind the enzyme with a not-specific binding. A summary of the ultrafiltration HPLC-MS/MS method for the identification of enzymatic inhibitors is reported in **Figure 121** (Yang et al., 2012).

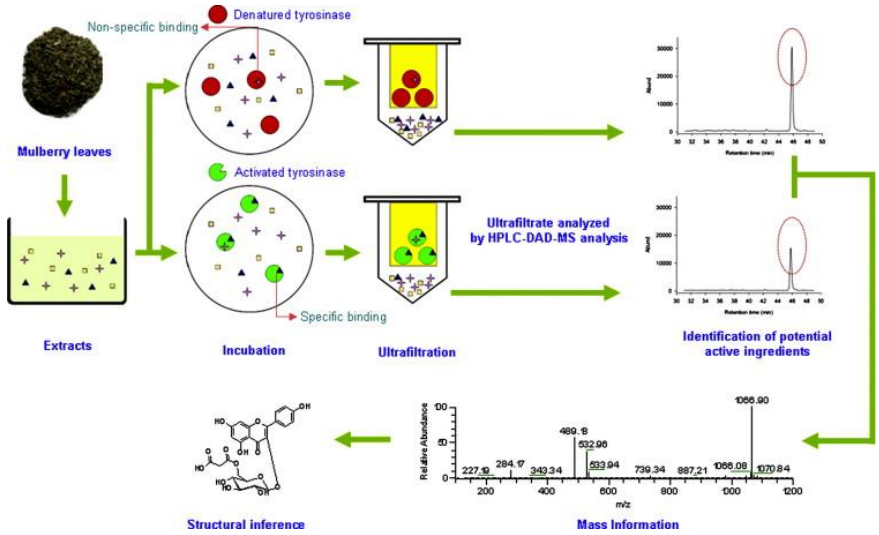


Figure 121: Summary of ultrafiltration HPLC-MS/MS method for the identification of enzymatic inhibitors (Picture from (Yang et al., 2012)).

The ultrafiltration HPLC-MS/MS method was applied for the identification of tyrosinase inhibitors screening on triterpenoids OAAO extracts. The comparison of the reaction mixture with the active tyrosinase enzyme with the thermally inactive enzyme displayed a strong binding of the phloridzin peak (**Figure 122**). This value agreed with the dose-response curve of phloridzin standard obtained in the HPLC-FLD assisted tyrosinase assay reported in the paragraph **7.3.1.3. HPLC-FLD tyrosinase inhibition assay: analysis of the real samples**.

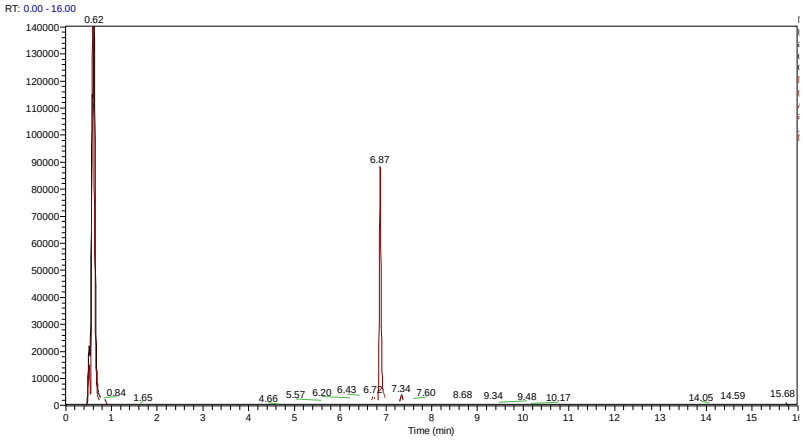


Figure 122: Ultrafiltration HPLC-MS/MS analysis of the triterpenoids OAAO extract.

7.3.1.5. Annurca Apple oleolytes activity on melanogenesis

For the evaluation of the anti-melanogenic OAAO effects, an evaluation of the effects on human melanoma cell line A375 was performed. As first step, the cytotoxicity of triterpenoids OAAO extract and ursolic acid standard on the cells was evaluated with the MTT assay. Cells were treated with increased concentration of the extract and the standard (0, 0.01, 0.1, 1, 10, and 100 µg/ml) for 72 hours, evaluating the cell viability. As shown in **Figure 123**, the triterpenoids OAAO extract impaired cell viability at a concentration of 100 µg/ml (**Figure 123A**: $p < 0.05$ *vs* CTR). Instead, ursolic acid standard displayed a cytotoxicity activity at a concentration of 10 µg/ml (**Figure 123B**: $p < 0.0001$ *vs* CTR). Therefore, the concentration of 30 µg/ml and 3 µg/ml were selected for the next experiments

on melanoma cell line A375 for triterpenoids OAAO extract and ursolic acid standard, respectively.

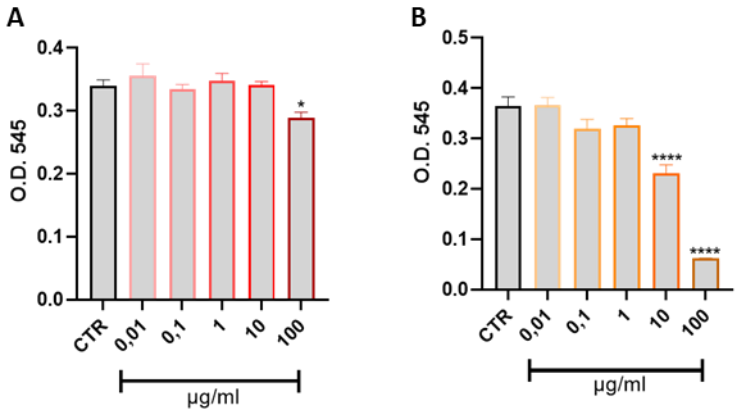


Figure 123: Cytotoxicity of triterpenoids OAAO extract (**A**) and ursolic acid (**B**) on A375 human melanoma cells after 72h, evaluated by the MTT assay. Data were shown as mean ± SEM of at least three independent experiments (* $p < 0.05$ *vs* CTR; **** $p < 0.0001$ *vs* CTR).

After the selection of the concentration of triterpenoids OAAO extract (30 µg/ml) and ursolic acid standard (3 µg/ml), the effects on melanin production in A375 human melanoma cells were evaluated (**Figure 124**). Both the extract and the standard displayed a significant reduction of melanin production after 72 hours of treatment (**Figure 124A**, **** $p < 0.0001$ *vs* CTR). Therefore, to evaluate the mechanism of action which lead the reduction of melanin content, a qPCR of A375 human melanoma cells after 6 hours of treatment with triterpenoids OAAO extract (30 µg/ml) and ursolic acid standard (3 µg/ml) was performed. This assay was performed to evaluate the mRNA expression of TYR, TRP1, TRP2 (**Figure 124B**), and MITF (**Figure 124C**). The triterpenoids OAAO extract displayed an inhibition of mRNA expression of the tyrosinase enzyme TYR (** $p < 0.01$ *vs* CTR), the related factor TRP2 (**** $p < 0.0001$ *vs* CTR), and the factor MITF (* $p < 0.05$ *vs* CTR). Instead, ursolic acid standard showed an inhibition of mRNA expression of the related factor TRP1 (* $p < 0.05$ *vs* CTR) and the related factor TRP2 (**** $p < 0.0001$ *vs* CTR). Both the extract and the standard displayed a strong inhibition activity on the related factor TRP2, highlighting the activity of the ursolic acid as the bioactive compound of triterpenoids OAAO extract responsible for tyrosinase inhibition. Instead, ursolic acid is not bioactive as inhibitor of

mRNA expression of the tyrosinase enzyme TYR and the factor MITF. Therefore, the inhibitor activity of the triterpenoids OAAO extract could be linked to other compounds.

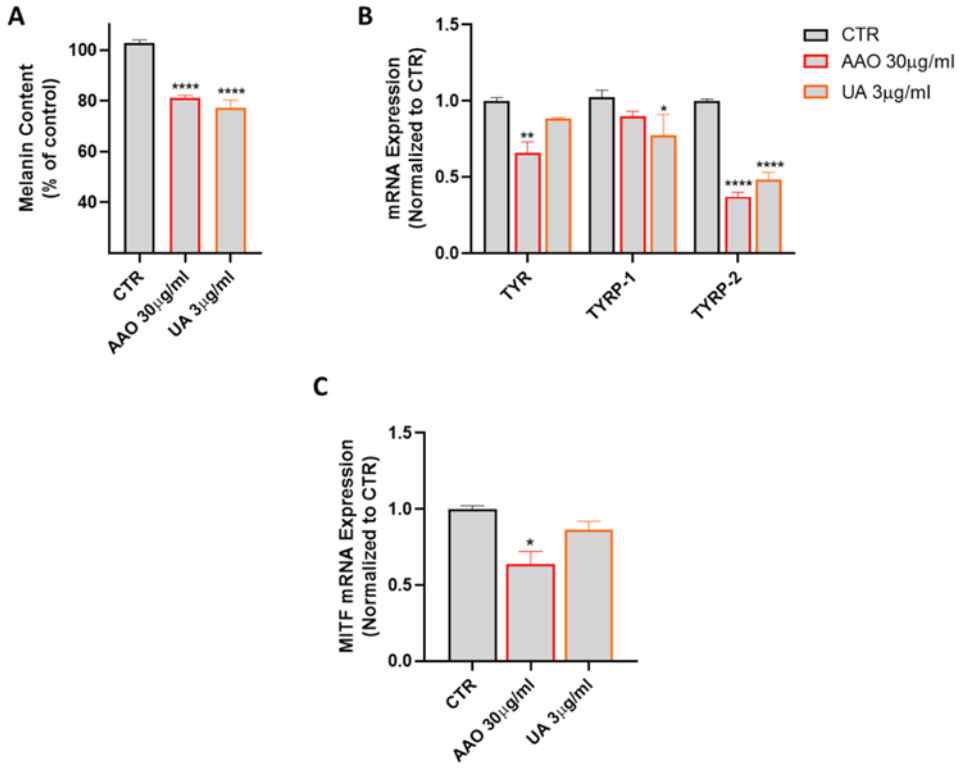


Figure 124: (**A**) Melanin content in A375 human melanoma cells after 72 hours of treatment with triterpenoids OAAO extract (30 µg/ml) and ursolic acid (3 µg/ml). (**B**) mRNA expression of TYR, TRP1, and TRP2 and (**C**) evaluated with qPCR on A375 human melanoma cells after 6 hours of triterpenoids OAAO extract (30 µg/ml) and ursolic acid (3 µg/ml). Data were shown as mean ± SEM of at least three independent experiments (* $p < 0.05$ *vs* CTR; ** $p < 0.01$ *vs* CTR; **** $p < 0.0001$ *vs* CTR).

To confirm the efficacy of triterpenois OAAO extract and ursolic acid standard in the regulation of melanin content production and the mRNA expression of the tyrosinase enzyme TYR and the factors TRP1, TRP2, and MITF, the experiments were repeated by evaluating the effect on the A375 human melanoma cells in the presence of the melanocyte stimulating hormone MSH (**Figure 125**). In fact, the hormone MSH stimulates the melanin production and the mRNA expression of all these factors. The treatment of A375 human melanoma cells with the hormone MSH increased melanin content, while both the extract

and the standard displayed a significant reduction of melanin production after 72 hours of treatment (**Figure 125A**, ** $p < 0.01$ *vs* CTR). Therefore, a qPCR of A375 human melanoma cells after 72 hours of treatment with triterpenoids OAAO extract (30 µg/ml) and ursolic acid standard (3 µg/ml) was performed. This assay was performed to evaluate the mRNA expression of the tyrosinase enzyme TYR, and the factors TRP1 and TRP2 (**Figure 125B**), and the factor MITF (**Figure 125C**). The treatment of A375 human melanoma cells with the hormone MSH increased the mRNA expression of the tyrosinase enzyme TYR, and the factors TRP1 and TRP2 (**Figure 125B**, ° $p < 0.05$ *vs* CTR; °° $p < 0.01$ *vs* CTR), and the factor MITF (**Figure 125C**, ° $p < 0.05$ *vs* CTR). Under treatment with the hormone MSH, the triterpenoids OAAO extract displayed an inhibition of mRNA expression of the tyrosinase enzyme TYR (**** $p < 0.0001$ *vs* CTR), the related factor TRP1 (* $p < 0.05$ *vs* CTR), the related factor TRP2 (**** $p < 0.0001$ *vs* CTR), and the factor MITF (* $p < 0.05$ *vs* CTR). Instead, under treatment with the hormone MSH, ursolic acid standard showed an inhibition of mRNA expression of the tyrosinase enzyme TYR (* $p < 0.05$ *vs* CTR), and the related factor TRP2 (* $p < 0.05$ *vs* CTR). As previously reported without the hormone MSH treatment, both the extract and the standard displayed a strong inhibition activity on the related factor TRP2, highlighting the activity of the ursolic acid as the bioactive compound of triterpenoids OAAO extract responsible for tyrosinase inhibition. Instead, ursolic acid is not bioactive as inhibitor of mRNA expression of the tyrosinase enzyme TYR and the factor MITF. Therefore, the inhibitor activity of the triterpenoids OAAO extract could be linked to other compounds. These results confirmed the capacity of the triterpenoids OAAO extract and ursolic acid standard to inhibit the melanogenesis and act as bioactive components for the treatment of skin aging-related diseases of hyperpigmentation, as the age spots. The anti-melanogenesis activity of triterpenoids OAAO extract and ursolic acid standard are both related to a direct inhibition of tyrosinase enzymatic activity, and the mRNA expression of the factors involved in melanin synthesis. Therefore, the OAAO could represent a valid active ingredient for the development of new cosmetic and cosmeceutical products with skin-lighting activity.

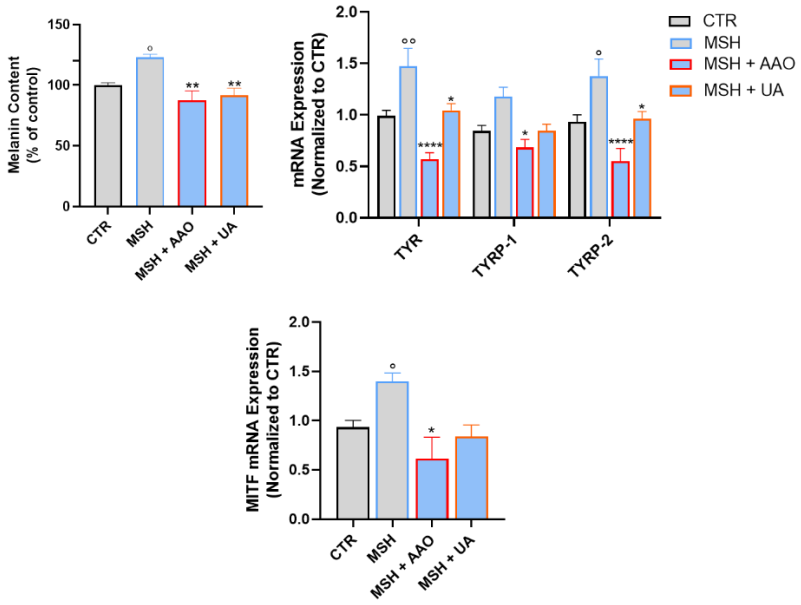


Figure 125: (**A**) Melanin content in A375 human melanoma cells after 72 hours of treatment with the hormone MSH and with triterpenoids OAAO extract (30 µg/ml) and ursolic acid (3 µg/ml). (**B**) mRNA expression of TYR, TRP1, and TRP2 and (**C**) evaluated with qPCR on A375 human melanoma cells after 72 hours of treatment with the hormone MSH and with triterpenoids OAAO extract (30 µg/ml) and ursolic acid (3 µg/ml). Data were shown as mean ± SEM of at least three independent experiments (° $p < 0.05$ *vs* CTR; °° $p < 0.01$ *vs* CTR; * $p < 0.05$ *vs* CTR; ** $p < 0.01$ *vs* CTR; **** $p < 0.0001$ *vs* CTR).

7.3.1.6. Antioxidant properties of Annurca Apple oleolytes on human melanoma cells

The melanin synthesis is a process which generate high levels of ROS (Urabe et al., 1994). Although the antioxidant properties of the hydroalcoholic OAAO extract was investigated and described in the paragraph **6.4.8. Antioxidant properties of Annurca apple oleolytes**, an evaluation of the ability of triterpenoids OAAO extract to regulate ROS production and the possible link with the anti-melanogenic properties on A375 human melanoma cells was performed (**Figure 126**). The ROS production is correlated with the development of the aging-related diseases, including skin aesthetic alterations as the skin spots and wrinkles. The melanin synthesis can generate high levels of ROS and the melanin is a modulator of the oxidative homeostasis at skin level (R´o˙ et al., 1999). The treatment for 48 hours with

the triterpenoids OAAO extract and the ursolic acid standard significantly reduced ROS production. The results are shown by the flow cytometry analysis of DCF-DHA probe and quantified as significant reduction of the mean fluorescence intensity (MFI) (**Figure 126A** and **126B**, * $p < 0.05$ *vs* CTR; ** $p < 0.01$ *vs* CTR). Mitochondria represent the main cell compartment of ROS production. Therefore, the mitochondrial functions were evaluated after treatment with triterpenoids OAAO extract (30 µg/ml) and ursolic acid standard (3 µg/ml). The evaluation of mitochondrial functions was performed by using the two cationic probes MitoTracker Green and tetramethylrhodamine methyl ester (TMRM), which measure the mitochondrial mass and the membrane potential after being sequestered in the mitochondrial matrix space (Gibellini et al., 2015). The MitoTracker Green dye uptake was significantly reduced in A375 human melanoma cells after the treatment, indicating a reduction of mitochondrial mass (**Figure 126C**, * $p < 0.05$ *vs* CTR). Therefore, the treatment with the probe TMRM was employed to evaluate the changes of mitochondrial membrane potential. As demonstrated by the MitoTracker Green results, the TMRM assay displayed a significant reduction of mitochondrial potential after the incubation of A375 human melanoma cells with triterpenoids OAAO extract (30 µg/ml) and ursolic acid standard (3 µg/ml) (**Figure 126D**, ** $p < 0.01$ *vs* CTR; *** $p < 0.001$ *vs* CTR). To confirm the results, the mRNA expression of three antioxidant enzymes (GCLC: glutamate-cysteine ligase catalytic subunit; GCLM: glutamate-cysteine ligase modifier subunit; HMOX-1: heme oxygenase-1-enzyme) was evaluated (**Figure 126E**). Both the triterpenoids OAAO extract and the ursolic acid standard displayed a strong increasing of HMOX-1 mRNA expression (**Figure 126E**, ** $p < 0.01$ *vs* CTR; **** $p < 0.0001$ *vs* CTR;), indicating an antioxidant activity which impaired the ROS production and the mitochondrial activity and corroborated the anti-melanogenic effect.

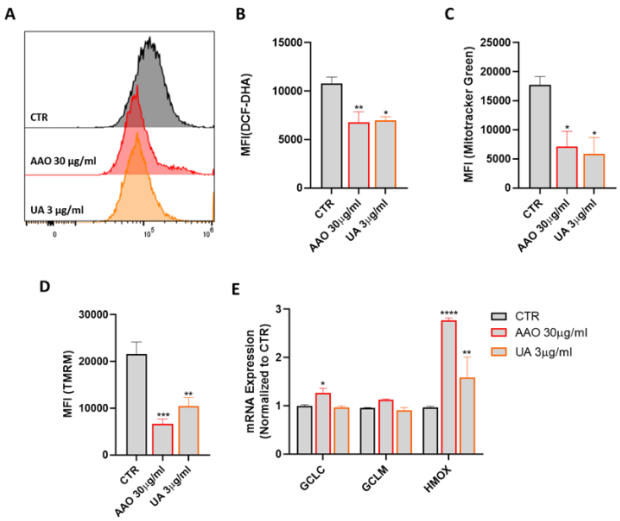


Figure 126: (**A**) Flow cytometry analysis of DCF-DHA and (**B**) quantification of mean fluorescence intensity (MFI). (**C**, **D**) Quantification of mean fluorescence intensity (MFI) of MitoTracker Green (**C**) and TMRM (**D**). (**E**) mRNA expression of GCLC, GCLM, HMOX-1 evaluated with qPCR on A375 human melanoma cells after 48 hours of treatment with triterpenoids OAAO extract (30 µg/ml) and ursolic acid (3 µg/ml). Data were shown as mean ± SEM of at least three independent experiments (* $p < 0.05$ *vs* CTR; ** $p < 0.01$ *vs* CTR; *** $p < 0.001$ *vs* CTR; **** $p < 0.0001$ *vs* CTR).

7.3.2. Ursolic acid skin permeation

A critical step for the development of a cosmetical or a cosmeceutical formulation is the determination of skin penetration of the active ingredient. The passage of a compound across the major the skin layers of epidermis and derma is a process which involves several steps:

1) The release of the molecule from the vehicle;
2) The penetration of the molecule into the stratum corneum;
3) The portioning between the stratum corneum and the sites of epidermis and dermis.

Therefore, to evaluate the penetration of ursolic acid in the skin layers for the application of Annurca Apple oleolyte, an analysis of the skin penetration rate was performed on a Franz's cell model. The results of the skin penetration assay were published as a scientific article entitled "Optimization of Ursolic acid Extraction in Oil from Annurca Apple to Obtain Oleolytes with Potential Cosmeceutical Application" in the international journal Antioxidant. The Franz's cell model is a simple and reproducible *in vitro* test for measuring the bioactive compound release from creams, gels, and oil formulations in skin topical applications. The system comprises a donor compartment for the application of the formulation, a compartment for the skin model, generally the pig ear, and a receiving liquid compartment, which mimic the blood of the skin model. A schematization of Franz's cell model is reported in the **Figure 127**. The mains difference between a drug for topical application and a cosmetic formulation is the ability of the bioactive compound to pass through the skin compartment and penetrate in the receiving compartment. As matter of fact, a drug can cross the skin layer and accumulates in the blood receiving compartment. Instead, in a cosmetical or cosmeceutical formulations the bioactive compound are accumulated in the skin model, without penetrating the receiving bloodstream compartment (Di Lorenzo et al., 2021). The Regulation (EC) No. 1223/2009 of the European Union defines a cosmetic

product as “any substance or mixture intended to come into contact with the external parts of the human body (epidermis, hair system, nails, lips, and external genital organs) or with the teeth and mucous membranes of the oral cavity with a view exclusively or mainly to cleaning them, perfuming them, changing their appearance, protecting them, keeping them in good condition or correcting body odors” (Di Lorenzo et al., 2021).

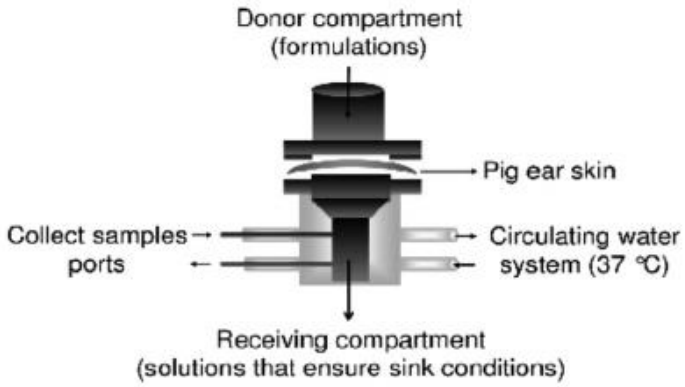


Figure 127: Schematization of Franz’s cell model for skin permeation study.

The procedure used for Franz’s cell diffusion assay is accurately described in the previous paragraph **7.2.2. Franz’s cell diffusion system**. To evaluate the skin penetration rate for the topical application of the Annurca Apple oleolyte, a quantification of ursolic acid was performed after 1 hour, 2 hours, and 4 hours of application. The quantification was performed on the two skin layers of epidermis and derma and on the blood receiving compartment. The Franz’s cell assay was performed with an Annurca Apple oleolyte with a concentration of ursolic acid of 211 µg/ml, which didn’t display edema and erythema after the administration on the porcine skin. After the Franz’s cell diffusion assay, each skin layer was extracted with a mixture of water:ethanol 50:50 (*v/v*). The use of an aqueous solution of ethanol represents the most efficient triterpenoids extraction system. The quantification analysis was performed by an HPLC-MS/MS method with a method accurately described in the previous paragraph **7.2.3. Ursolic acid quantitative analysis in Franz’s cell diffusion system by HPLC-HESI-MS/MS**. Among the HPLC methods, the LC-MS analysis in MRM acquisition mode was selected to provide the better conditions for ursolic acid quantification

in Franz's cell diffusion system. The transition 455.3 – 455.3 has been chosen as the quantifier transition, while the transition 455.3 – 407.0 has been chosen as the qualifier transition. The peak obtained by ursolic acid standard analysis with the MRM transition 455.3 – 455.3 at a concentration of 5 ppm was provided in **Figure 128**.

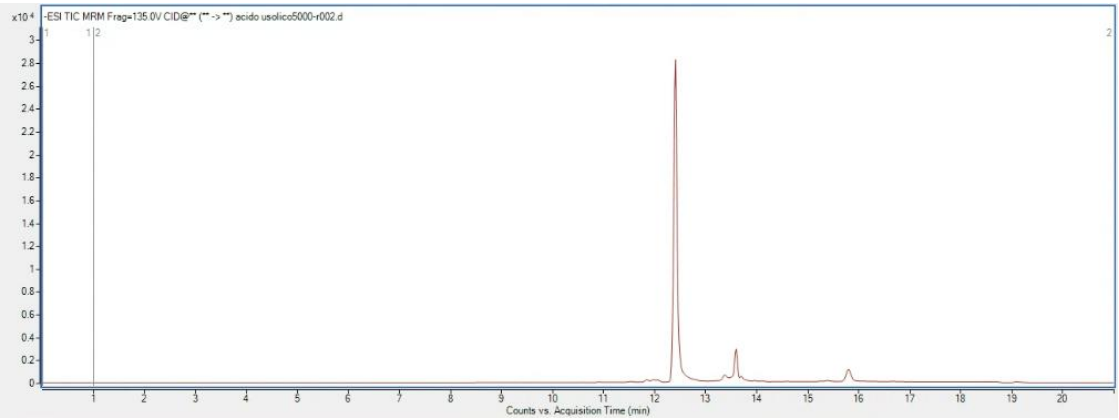


Figure 128. Ursolic acid standard at a concentration of 5 ppm, obtained by the MRM transition 455.3 – 455.3 with a CID of 20 eV.

The results of ursolic acid quantification displayed a linear compound distribution, with a progressive shift from the epidermis to the derma but without a significant absorbance in the bloodstream compartment (**Figure 129**). This result corroborates the potential of OAAO as a functional ingredient for the development of cosmetic and cosmeceutical formulations. This result could be linked to ursolic acid lipophilicity due to the triterpenoids scaffold, which is characterized by a XLogP3-AA of 7.3. Generally, the topically applied molecule penetrates the skin with two different routes, the transcellular and the intercellular, which depends on the polarity of the compound. Lipophilic compounds as triterpenoids generally cross the skin for intercellular passage (Thong et al., 2007).

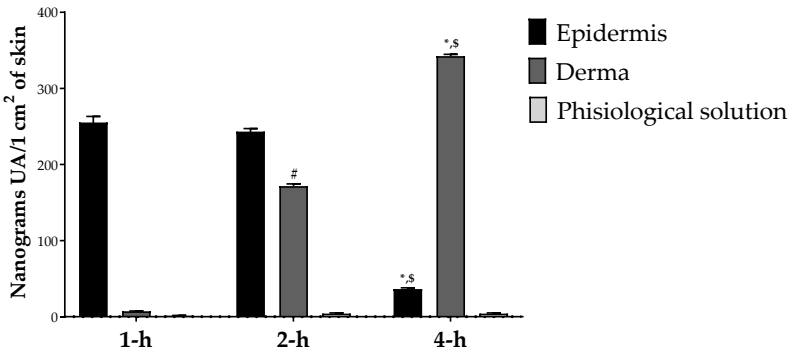


Figure 129. Ursolic acid penetration in the *in vitro* Franz's cell skin permeation study. Values are expressed as mean ± standard deviation of three repetitions. Data were analyzed with two-way ANOVA followed by Tukey's post-hoc test; * $p < 0.01$ 4h *vs* 1h, # $p < 0.01$ 2h *vs* 1h, $ $p < 0.01$ 4h *vs* 2h in the same group.

7.3.3. Elastase inhibition properties of Annurca Apple oleolytes

7.3.3.1. Validation of the spectrophotometric elastase inhibition assay

The elastase inhibition assay is generally performed by a spectrophotometric assay to evaluate the oxidation reaction of the peptide linkage of the substrate succinyl-(Ala)-3-*p*-nitroanilide (SANA) to *p*-ntroanilide, a cleavage product which is monitored at a wavelength of 410 nm (**Figure 130**).

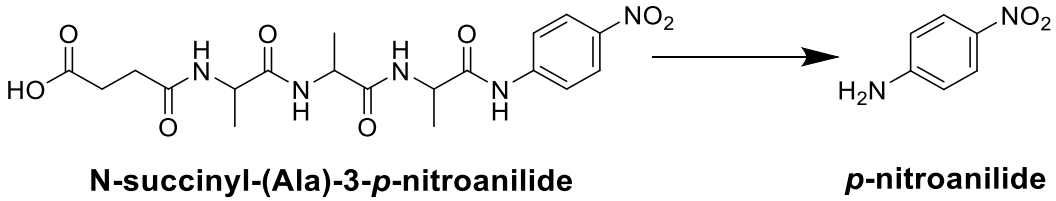


Figure 130: Peptide hydrolysis reaction of succinyl-(Ala)-3-*p*-nitroanilide (SANA) to *p*-ntroanilide.

The validation of the elastase inhibition assay requires the optimization of some parameters. Different conditions of enzymatic elastase activity (13 elastase activity values: 0 U/ml,

0.005 U/ml, 0.01 U/ml, 0.02 U/ml, 0.03 U/ml, 0.04 U/ml, 0.05 U/ml, 0.1 U/ml, 0.2 U/ml, 0.25 U/ml, 0.4 U/ml, 0.5 U/ml, 0.6 U/ml; total range: 0 – 0.6 U/ml), incubation time (13 times: 0 min, 2 min, 4 min, 6 min, 8 min, 10 min, 12 min, 14 min, 16 min, 18 min, 20 min, 25 min, 30 min; total range: 0 – 30 min), and DMSO content (10 DMSO %: 0%, 0.1%, 0.5%, 1%, 1.5%, 2%, 2.5%, 3%, 4%, 5%; total range: 0 – 5%) were selected to optimize the enzymatic activity and determine DMSO tolerance. 1.015 mM of N-succinyl-(Ala)-3-*p*-nitroanilide and the enzyme elastase (0.0375 U/ml) were prepared in a 0.1232 M Tris-HCl buffer at pH 8.0. The composition of the buffer was not optimized but was extrapolated by the assay conditions reported in literature. Quercetin was used as a positive control as a well-known elastase inhibitor. The optimization of DMSO % represents a critical point of enzymatic assay validation (Kolakul & Sripanidkulchai, 2017). Our results showed that the combination of parameters which guarantees a linear kinetics of response for quinone formation are as follows: SANA concentration of 1.015 mM, elastase concentration of 0.0375 U/ml (**Figures 131A** and **131B**), and at a reaction time of 10 min (**Figures 131C** and **131D**). It's interesting to observe that the velocity of the enzymatic reaction, which is expressed as follows, is directly proportional to L-tyrosine concentration in a selective elastase concentration range of 0 – 0.4 U/ml (**Figure 131B**) and in a selective reaction time range of 0 – 10 min (**Figure 131D**). Therefore, elastase (R^2 = 0.9917, y = 1.702x - 0.0064) and a direct reaction time (R^2 = 0.9900, y = 0.057x - 0.187) catalases a first order kinetics reaction, without enzymatic saturation (**Figures 131B** and **131D**). The analyzed standards (e.g., quercetin, and ursolic acid) were dissolved in 100 % *v/v* DMSO and diluted with 0.1232 M Tris HCl buffer at pH 8.0 to obtain a final concentration of 1.5 % *v/v* DMSO in the enzymatic mixture.

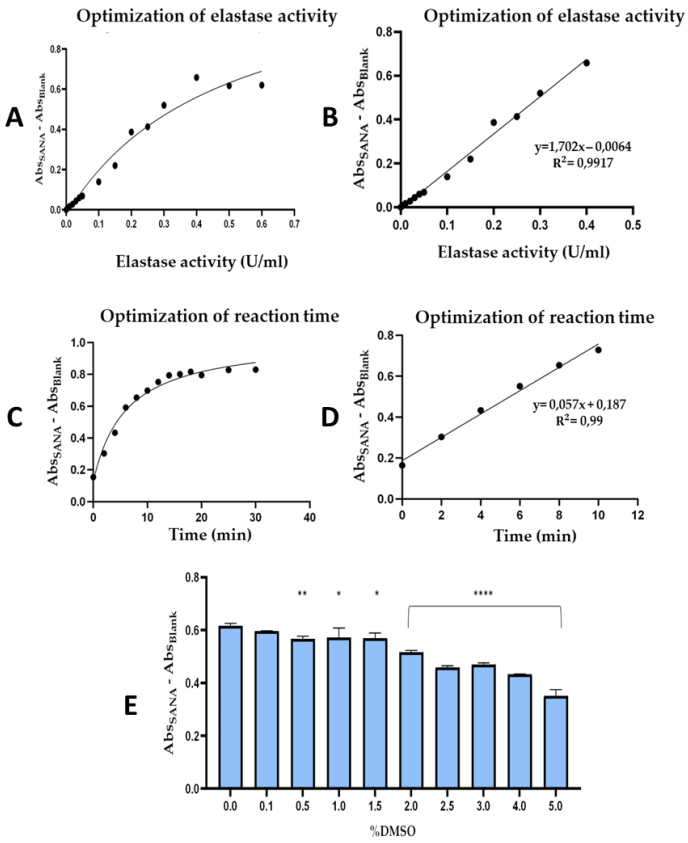


Figure 131: Optimization parameters of elastase inhibition assay. **A**, **B**: optimization of elastase activity; **C**, **D**: optimization of reaction time; **E**: optimization of DMSO %.

7.3.3.2. Elastase inhibition assay: analysis of the real samples

After validating the enzymatic assay conditions, the elastase inhibition assay was performed by plotting the dose-response curves and the calculation of the IC_{50} of the analytical standard and the real samples. The analysis of the triterpenoids OAAO extract displayed an elastase inhibition activity in a concentration dependent manner, with a IC_{50} value of 212.76 µg/ml (**Figure 132**).

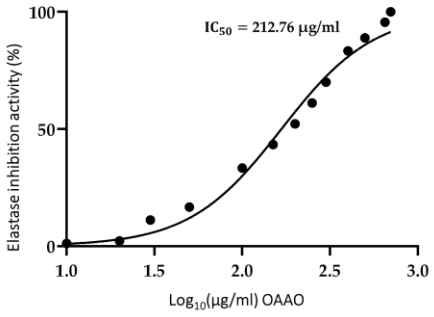


Figure 132: Evaluation of the IC_{50} for OAAO inhibition of elastase enzyme.

To evaluate the activity of ursolic acid as the main bioactive compound of triterpenoids OAAO extract responsible for the inhibition of the enzyme elastase, the ursolic acid standard was tested in the assay, calculating a IC_{50} value of 135.24 µg/ml (**Figure 133**). Subsequently, to confirm the efficacy of the assay for the evaluation of elastase inhibition, the assay was performed on the well-known inhibitor of the enzyme quercetin standard, calculating a IC_{50} value of 72.47 µg/ml (**Figure 134**).

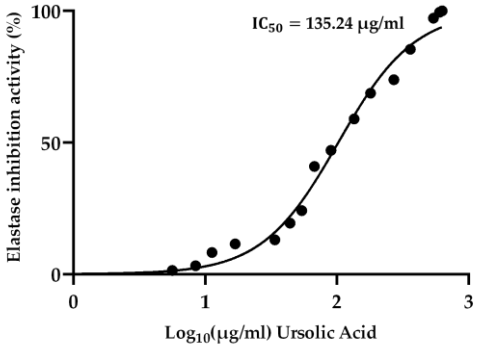


Figure 133: Evaluation of the IC_{50} for ursolic acid standard inhibition of elastase enzyme.

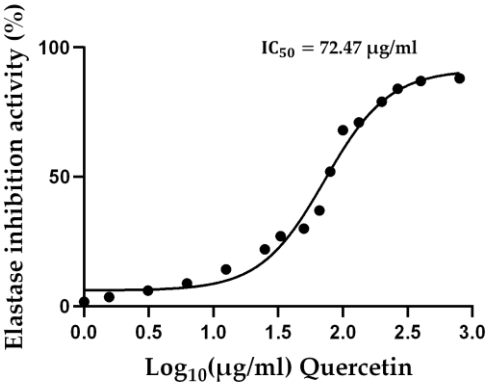


Figure 134: Evaluation of the IC_{50} for quercetin standard inhibition of elastase enzyme.

7.3.4. Efficacy study of OAAO cream for topical applications

7.3.4.1. Study design and skin tolerability test

The skin wrinkle and fine lines represent one of the most common phenotypic manifestations of skin aging (Matsumoto et al., 2010). Elastase is directly involved in wrinkle formation by degrading the elastic fibres and reducing the skin elasticity. As matter of fact, the inhibition of the enzyme represents a valuable cosmetical tool to improve the skin health quality. Based on the results of the in vitro elastase inhibition assay, the OAAO could represent a possible active ingredient for the development of new cosmeceutical to counteract the skin wrinkle formation. To confirm the efficacy of OAAO in wrinkle treatment by topical approach, a clinical trial was performed to evaluate the effectiveness of the product. The description of the design of the study and the exclusion criteria was accurately described in the paragraphs X. Instead, the OAAO cream preparation was reported in the paragraph X. The skin tolerability represented the first step of the clinical trial. It was verified with an occlusive patch test for 72 hours of treatment, confirming that OAAO cream at 2.5%$_{w/w}$ for topical application had not irritating power for application on the skin. The calculated values for the erythema and oedema index on 20 subjects of analysis displayed values lower than 1.5, which is the limit established to define as not-irritant a topical product (**Figure 135**) (Komane et al., 2017).

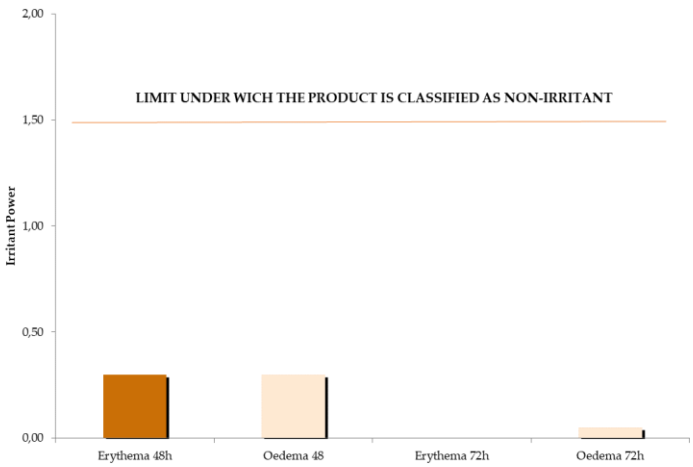


Figure 135. Results of skin tolerability test. The average of erythema and oedema index value at 48 and 72 hr compared to the established limit of 1.5.

7.3.4.2. Skin visco-elasticity test

The skin visco-elastic properties have been described with the cyclic suction/releasing method (Everett et al., 2013; Beatty et al., 2023). The evaluation of the skin biomechanical properties was performed with the *in vitro* models of controlled air depressor system and optical displacement measurement. The biomechanical properties include the factors R_0 and R_2, which indicate the skin pliability/firmness (mm) and the gross elasticity (%), respectively. As shown in **Table 116**, the application of OAAO cream displayed a significant improving of skin elasticity in a time-dependent manner at a topical concentration of 2.5%$_{w/w}$. The OAAO cream treatment determined a significant improvement of gross elasticity R_2, with an increment of 14.0% and 28.0% at D_{14} and D_{28} compared to the baseline D_0, respectively (*** $p < 0.001$ *vs* D_0), and a significant reduction of skin pliability/firmness R_0, with a decrement of -9.0% and -13.0% at D_{14} and D_{28} compared to the baseline D_0, respectively (*** $p < 0.001$ *vs* D_0). The placebo treatment didn't show the same effects in the regulation of skin biomechanics. For example, the skin pliability/firmness R_0 displayed a not-significant increment of 8.0% and 12.0% at D_{14} and D_{28} compared to the baseline D_0 for the placebo treatment, respectively. Instead, the gross elasticity R_2 displayed a not-significant increment of 3.0% and 4.0% at D_{14} and D_{28} compared to the baseline D_0 for the placebo treatment, respectively.

Formulation	Skin parameter	Visit day				
		Baseline (D_0) Mean ± SD	**Day 14 (D_{14}) Mean ± SD**	**Δ% *vs* D_0**	**Day 28 (D_{28}) Mean ± SD**	**Δ% *vs* D_0**
OAAO cream 2.5%$_{w/w}$	Skin pliability/firmness (R_0)	0.355 ± 0.024 mm	0.322 ± 0.014 mm	-9.0 % ***	0.308 ± 0.028 mm	-13.0 % ***
	Gross elasticity (R_2)	0.602 ± 0.066 %	0.676 ± 0.052 %	14.0 % ***	0.759 ± 0.071 %	28.0 % ***
Placebo	Skin pliability/firmness (R_0)	0.308 ± 0.047 mm	0.342 ± 0.037 mm	8.0 % n.s.	0.342 ± 0.037 mm	12.0 % *
	Gross elasticity (R_2)	0.507 ± 0.044 %	0.521 ± 0.041 %	3.0 % n.s.	0.526 ± 0.038 %	4.0 % n.s.

Table 116. Skin biomechanical properties (R_0: skin pliability/firmness (mm); R_2: gross elasticity (%)) before and after treatment with OAAO cream at 2.5%$_{w/w}$ or Placebo. The values are expressed as average ± SD. Differences between samples were assessed by the Student's two-tailed t-test for independent samples compared to the baseline D_0 (* $p < 0.05$ *vs* D_0 ** $p < 0.01$ *vs* D_0, *** $p < 0.001$ *vs* D_0).

7.3.4.3. Skin hydration and film repairing activity

To investigate the mechanism which determines the improvement of skin visco-elasticity, an evaluation of OAAO effects on hydration was performed. As matter of fact, a clear correlation between the hydration and the skin visco-elasticity is well known and some authors previously reported a potential activity of ursolic acid in the increment of ceramides production in skin cells, improving the hydration of the dermal layer (Both et al., 2002; Choi et al., 2013)). The skin hydration is usually evaluated by considering the conductance evaluated by the corneometry. Instead, the film repairing activity is assessed by evaluating the TEWL. Conductance results displayed a higher water content in the stratum corneum since the first application (short term treatment) of OAAO cream, with a significant improvement of 17.8% and 17.2% at T_{1h} and T_{24h} compared to the T_0, respectively (*** $p < 0.001$ *vs* D_0) (**Table 117**). This result was confirmed at the end of the 28 days of treatment with OAAO cream (long term treatment), with a significant increment of 20.0% and 25.0% at T_{14day} and T_{24day} compared to the T_0, respectively (*** $p < 0.001$ *vs* D_0) (**Table 118**). TEWL results displayed a higher recovery action of unpaired skin layer since the first application (short term treatment) of OAAO cream, with a significant decrement of -13.2% and -13.4% at T_{1h} and T_{24h} compared to the T_0, respectively (*** $p < 0.001$ *vs* D_0). This result was confirmed at the end of the 28 days of treatment with OAAO cream (long term treatment), with a significant reduction of -17.0% and -23.0% at T_{14day} and T_{24day} compared to the T_0, respectively (*** $p < 0.001$ *vs* D_0). The placebo treatment didn't show the same effects in the regulation of skin hydration and film repairing activity, with not-statistical variations both for short term and long-term treatments. These results demonstrated the ability of OAAO to ameliorate the skin barrier functions, promoting the skin hydration. OAAO properties were confirmed by the distribution profile of skin hydration and elasticity values. As matter of fact, the OAAO treatment displayed a difference from the basal condition for these two parameters. Interestingly, OAAO effects determined a linear tendency between hydration and elasticity (**Figure 136**). Instead, the placebo group and the baseline D_0 didn't show this distribution. Therefore, these indications confirmed the beneficial use of OAAO as active ingredient for the preparation of nutracosmeceutic formulations.

Formulation	Skin parameter	Check-up				
		Baseline (D_0) Mean ± SD	**1 hour (T_{1h}) Mean ± SD**	**Δ% *vs* D_0**	**24 hours (T_{24h}) Mean ± SD**	**Δ% *vs* D_0**
OAAO cream 2.5%$_{w/w}$	Skin conductance	29.6 ± 1.8 A.U.	34.8 ± 5.9 A.U.	17.8 % ***	34.6 ± 3.8 A.U.	17.2 % ***
	TEWL	9.0 ± 0.5 g/hm^2	7.8 ± 1.1 g/hm^2	-13.2 % ***	7.8 ± 1.1 g/hm^2	-13.4 % ***
Placebo	Skin conductance	32.0 ± 9.7 A.U.	33.3 ± 10.2 A.U.	4.8 % n.s.	32.0 ± 9.6 A.U.	1.3 % n.s.
	TEWL	7.7 ± 1.4 g/hm^2	7.8 ± 1.3 g/hm^2	3.5 % n.s.	7.9 ± 2.4 g/hm^2	4.1 % n.s.

Table 117. Skin hydration and film repairing activity (Corneometry and TEWL average value ± SD) before and after one application of OAAO cream at 2.5%$_{w/w}$ or Placebo (Short term test). Differences between samples were assessed by the Student's two-tailed t-test for independent samples compared to the baseline D_0 (*** $p < 0.001$ *vs* D_0).

Formulation	Skin parameter	Check-up				
		Baseline (D_0) Mean ± SD	**1 hour (T_{1h}) Mean ± SD**	**Δ% *vs* D_0**	**24 hours (T_{24h}) Mean ± SD**	**Δ% *vs* D_0**
OAAO cream 2.5%$_{w/w}$	Skin conductance	29.6 ± 1.8 A.U.	35.6 ± 3.7 A.U.	20.0 % ***	37.0 ± 3.2 A.U.	25.0 % ***
	TEWL	9.0 ± 0.5 g/hm^2	7.5 ± 0.8 g/hm^2	-17.0 % ***	6.9 ± 0.7 g/hm^2	-23.0 % ***
Placebo	Skin conductance	31.0 ± 4.4 A.U.	31.9 ± 4.4 A.U.	3.1 % n.s.	32.3 ± 4.9 A.U.	4.3 % n.s.
	TEWL	7.7 ± 1.4 g/hm^2	7.9 ± 1.1 g/hm^2	5.0 % n.s.	8.2 ± 1.3 g/hm^2	8.0 % n.s.

Table 118. Skin hydration and film repairing activity (Corneometry and TEWL average value ± SD) during the 28-day treatment with OAAO cream at 2.5%$_{w/w}$ or Placebo (Long term test). Differences between samples were assessed by the Student's two-tailed t-test for independent samples compared to the baseline D_0 (*** $p < 0.001$ *vs* D_0).

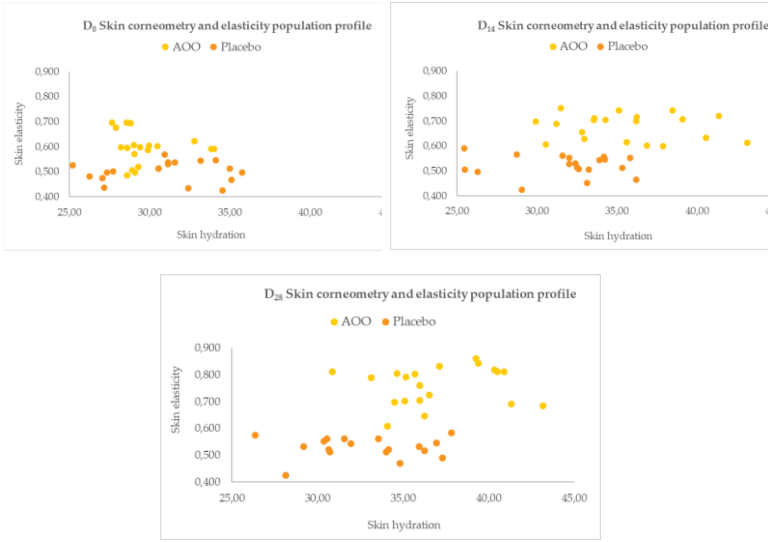


Figure 136. Distribution profile of skin hydration and elasticity values of the population under treatment with topical OAAO cream at 2.5%$_{w/w}$ or Placebo.

7.3.4.4. Evaluation of wrinkles and fine lines

After demonstrating the mechanisms of OAAO cream to improve the skin functions, the clinical effects on wrinkles and fine lines formation were evaluated. The clinical trial confirmed that OAAO decreased the frequency of facial wrinkles. Forehead and frown lines were evaluated by VISIA (Canfield Scientific, Inc.) in the forehead area, displaying a significant decrement of -6.1% at T_{14day} (** $p < 0.01$ *vs* D_0) and -7.2% at T_{24day} (*** $p < 0.001$ *vs* D_0) compared to the T_0, respectively. The placebo treatment didn't show the same effects in the frequency of forehead and frown lines formation, displaying a not-significant increment of 6.7% at T_{14day} (not-significant *vs* D_0) and 8.6% at T_{24day} (*** $p < 0.001$ *vs* D_0) compared to the T_0, respectively (**Figure 137**). In the same experimental protocol, the nasolabial lines were evaluated, displaying a significant decrement of 3.0% at T_{14day} (* $p < 0.05$ *vs* D_0) and -5.0% at T_{24day} (** $p < 0.01$ *vs* D_0) compared to the T_0, respectively. The placebo treatment didn't show the same effects in the frequency of nasolabial lines formation, displaying a not-significant increment of 4.0% at T_{14day} and 6.0% at T_{24day} compared to the T_0, respectively (not-significant *vs* D_0) (**Figure 138**). In both the analysis, the evaluation of frequency of forehead, frown, and nasolabial lines were performed by considering the smoothing effects on OAAO cream in treating expression lines, which are reported in the **Figures 137** and **138** as blue areas.

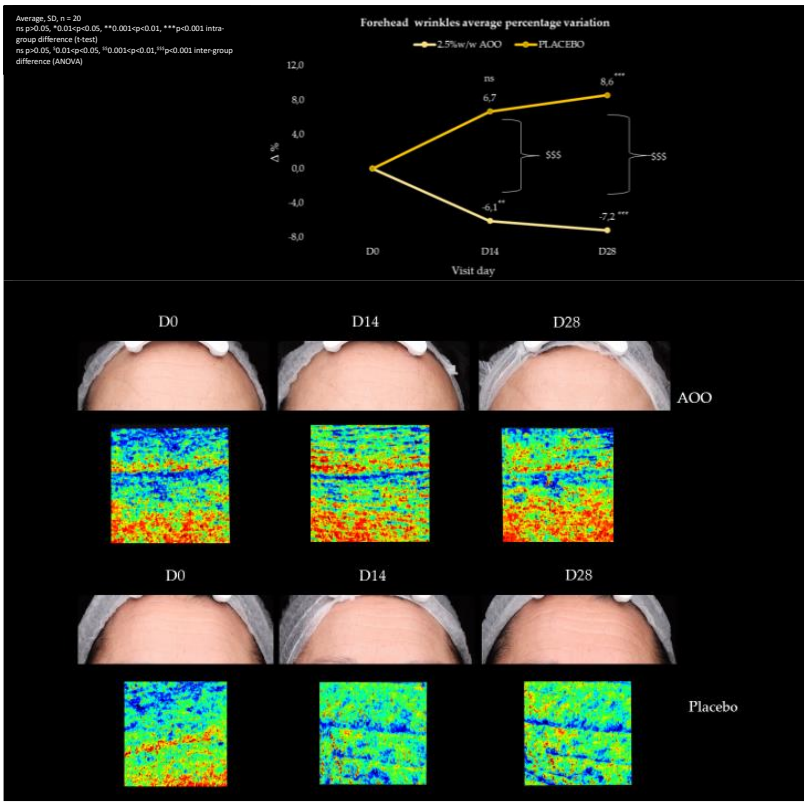


Figure 137. 2D and 3D Forehead wrinkles over 28-day treatment with OAAO cream at 2.5%$_{w/w}$ or Placebo. The 3D replica showed in blue skin furrows and in red hollows. The AOO group reduced blue area showing the smoothing ability of OAAO in treating expression lines.

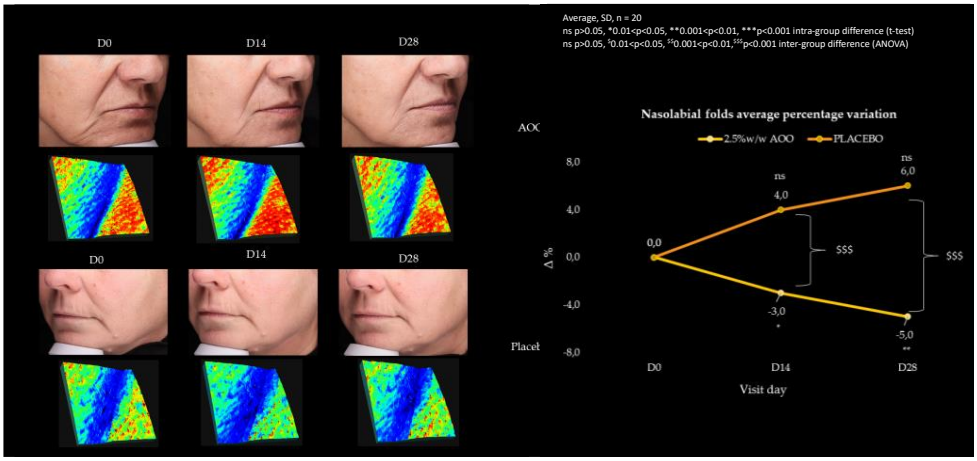


Figure 138. 2D and 3D Nasolabial folds over 28-day treatment with OAAO cream at 2.5%$_{w/w}$ or Placebo. The 3D replica showed in blue skin furrows and in red hollows. The AOO group reduced blue area showing the smoothing ability of OAAO in treating also gravitational lines.

7.4. Summary of Annurca apple oleolytes efficacy study

These results confirmed the capacity of the triterpenoids OAAO extract and ursolic acid standard to inhibit the melanogenesis and act as bioactive components for the treatment of skin aging-related diseases of hyperpigmentation, as the age spots. The anti-melanogenesis activity of triterpenoids OAAO extract and ursolic acid standard are both related to a direct inhibition of tyrosinase enzymatic activity, and the mRNA expression of the factors involved in melanin synthesis. Therefore, OAAO could represent a valid active ingredient for the development of new cosmetic and cosmeceutical products for skin-lighting and the treatment of hyperpigmentation diseases. In addition, ursolic acid and the triterpenoids OAAO extract were evaluated as inhibitors of the enzyme elastase. Elastase inhibition increases elastin content and improves the skin quality in some skin aging-related diseases, as the skin wrinkles and the loss of skin elasticity. Finally, a permability test of ursolic acid using Franz's cells was performed, which demonstrated the ability of the active ingredient to penetrate the skin layers without a systemic absorption. All these properties represent a clear demonstration of the potential of OAAO for the development of new cosmeceutical products for the prevention and the treatment of skin aging-related diseases.

CHAPTER 8

GENERAL CONCLUSION

Aging is a gradual process marked by the progressive decline in body functions, leading to a reduction of organism physical abilities. Recognizing aging as a significant risk factor for chronic diseases is crucial to identify new targets and developing future therapeutic approaches. The widespread of aging-related diseases represents a considerable challenge to the national health system. Therefore, nutraceuticals may offer a potential strategy for preventing aging-related diseases due to the health benefits associated with natural compounds found in food matrices. Therefore, this thesis focused on the development of novel nutraceutical formulations with health benefits in the prevention of sarcopenia and skin aging-related diseases. As first line of my thesis work, glycoalkaloids from unripe tomatoes, as α-TM, have been studied as potential bioactive compounds for sarcopenia prevention. The recover of unripe tomatoes, that are considered as industrial wastes, represents an opportunity for the development of innovative nutraceutical formulations rich in secondary metabolites. The chemical analysis of seven unripe tomatoes cultivars revealed a distinctive metabolic profile of Datterini tomatoes cultivar, showcasing its health potential benefits. In addition, the high α-TM content suggests its possible use as an anti-aging food matrix. After an in-depth chemical characterization, *in vitro* and *in vivo* studies have demonstrated the potential efficacy of Datterini tomatoes in sarcopenia prevention. TD molecular mechanisms were elucidated though *in vitro* studies on myoblast cells, showing health benefits effects by stimulating energy metabolism, protein synthesis, and modifying muscle fibers composition. In addition, the antisarcopenic properties of the nutraceutical product was confirmed by an *in vivo* study in an old mice model. The *in vivo* study showed the efficacy of Datterini tomatoes in the prevention of muscle atrophy and confirmed the safety of the product in a chronic administration. To increase the knowledge about the qualitative and quantitative profile of polyphenols and SGAs in tomato plants, an agronomic and microbiological study was performed on Piennolo tomato plants, a typical ecotype of Campania region (Southern Italy). The microbiological treatment with *Trichoderma* spp. proved a clear efficacy in enhancing glycosylated polyphenols and SGAs. Leaves emerged as the anatomical plant part with the highest metabolites content and antioxidant activity. Therefore, the study emphasized the correlation between biological treatments and the induction of secondary metabolite pathways, opening new possible contributions to the development of innovative nutraceuticals. Finally, a new food-grade method for the chemical conversion of α-TM to TD was investigated, obtaining a food matrix with a high TD content which could represent an innovative nutraceutical formulation with anti-sarcopenic properties.

As second line of my thesis work, the development of an innovative cosmeceutical formulation was investigated for the prevention and treatment of skin aging-related diseases, as age spots, fine wrinkles, and hyperpigmentation. For this goal, the study focused on ursolic acid, a natural compound of nutraceutical interest. Although this compound is reported in several food matrices, the study was carried out using the apples of "Annurca" variety, which are a typical cultivar of the Campania region (Southern Italy). In addition, in order to develop an ursolic acid enriched formulation for topical and cosmeceutical application, ursolic acid was delivered by the preparation of an oleolyte, an oil formulation obtained by maceration of the plant matrix in oil. Therefore, an oleolyte obtained by the "Annurca" apples was developed and optimized by a RSM approach using sunflower seed oil as oil vehicle. The oleolyte was chemically characterized for the evaluation of the qualitative and quantitative profile and the assessment of the antioxidant properties. After that, the skin-lighting properties of "Annurca" apple oleolyte and ursolic acid were evaluated. These results demonstrated the potential of this oleolyte for the development of new cosmeceutical formulations for the prevention and treatment of skin aging-related diseases. The study of these two formulations represents preliminary and interdisciplinary research for the development of innovative products of nutraceutical and cosmeceutical interest for the prevention of aging-related diseases.

CHAPTER 9

EXTERNAL PROJECT CONTRIBUTIONS

As part of my research activity, I collaborated on further projects partly related to my thesis work and which include the study of compound classes chemically correlated to those described in my doctoral project, in particular polyphenols. Therefore, a short summary of the scientific rationale and my contribution in these articles is described in this chapter.

The work published by Maisto et al. (2021) describes the nutraceutical potential of some functional snacks obtained with date fruits by enrichment with different *Lactobacillus* species. Indeed, the enzymatic activity of Lactobacilli can generate a fermentation of the food matrix during snack preparation, which remodels the polyphenolic composition and changes the nutritional values and the health benefits of the food matrix. The results showed a more pronounced fermentation activity by the strain of *Lactobacillus rhamnosus*. In order to demonstrate the beneficial role induced by matrix fermentation with *Lactobacillus* spp., I performed the qualitative and quantitative analysis of the polyphenols profile by using a HPLC-DAD method. This analysis confirmed the beneficial effect induced by lacto-fermentation, with a significant increase of some polyphenols. For example, gallic acid had a significant increment from 1.40 ± 0.03 of the control date fruits to 8.05 ± 0.03 (**** $p <$ 0.0001 *Lactobacillus rhamnosus* treated *vs* control), leading to a significant increase of its amount. This increase may be due to the tannase enzymes activity, which catalyse the hydrolysis of the gallic acid ester bonds of tannins. The resulting product can be considered a bi-functional snack, as it ensures both the intake of a higher polyphenols content with beneficial activity on human health and probiotics, which play a well-recognised role in gastrointestinal health.

The work published by Schiano et al. (2022) describes the nutraceutical activity of the thinned nectarines, an agro-food waste with a potential activity in the diabetes prevention and in the control of glycemic homeostasis. The antidiabetic potential of thinned nectarines is mainly attributable to abscisic acid, an isoprenoic plant hormone. However, polyphenols may also exert an anti-diabetic action that may contribute to the action of abscisic acid. Therefore, I performed the qualitative and quantitative analysis of the polyphenols profile by using a HPLC-DAD-FLD and HPLC-HESI-MS/MS methods. The analysis confirmed a high polyphenols content, with values of 1.456 ± 0.001 mg of neochlorogenic acid/g of DW and 1.496 ± 0.001 mg of chlorogenic acid/g of DW. In addition, in the paper we evaluated the inhibition of the advance glycation end-products formation (AGEs), which are strictly

correlated with the glycemic levels and are correlated with the development of diabetes complication. Since polyphenols have a well-known inhibition activity in the AGEs formation, their quantification represents a significant parameter for understanding the properties of thinned nectarines in the prevention of long-term diabetes complications.

The work published by Maisto et al. (2022) describes an innovative technological process based on an acidic treatment to increase the bioaccessibility of phenolic compounds in "Annurca" apples. In this project, I performed the validation of the HPLC-DAD-FLD method according to the ICH validation guideline (ICH.Q2[R2], 2022) and the quantification of polyphenols in the control and the treated samples with the previously validated method. The results assessed a significant increment of the food matrix polyphenols content after the acidic treatment, confirming the efficacy of the method for the development of a new nutraceutical formulations derived from "Annurca" apples.

The work published by Saviano et al. (2022) describes an assessment of the anti-inflammatory and immunomodulatory properties of a *Mangifera indica* L. extract in the regulation of the pathways COX-2/mPGES-1 and Th17/Treg. In this project, I performed the quantitative analysis of mangiferin, a polyphenol of the chemical class of xanthone, in the *Mangifera indica* L. extract by a quantitative NMR method. The method confirmed a high purity of the extract, with a content of mangiferin of 91.9%.

The work published by Maisto et al. (2022) describes an optimization of phlorizin extraction from "Annurca" apple leaves with the experimental design system of the RSM. Phlorizin represents an active ingredient with high content in the plant apple leaves and represent an active ingredient with anti-diabetic properties. The anti-diabetic activity is correlated with the reduction of glycemic levels for the inhibition of the glucose transporter sodium-glucose linked transporter 2 (SGLT2). SGLT2 is a transporter involved in the reabsorption of glucose in the kidneys. Therefore, its inhibition determines an increment of glucose excretion in the urines and a reduction of plasmatic glucose levels. The relevance of phloridzin in the anti-diabetic therapy is demonstrated by its use as lead compound for the discovery of the class of hypoglicemic agents of gliflozins, which are used in the diabetes therapy. In this project, I performed the qualitative and quantitative analysis of the polyphenols profile by using a HPLC-DAD-FLD and HPLC-HESI-MS/MS methods. After

that, I used the RSM model to optimize the extraction conditions for extracting phloridzin, with a quantification of the active compound in the optimized condition of 126.89 ± 7.58 mg of phloridzin/g of DW. To assess the anti-diabetic properties of the extract, I performed an evaluation of the inhibition activity of the AGEs formation, demonstrating the activity of the "Annurca" apple leaves in preventing even the long-term diabetes complications. These data represent a clear indication of the potential use of "Annurca" apple leaves an active ingredient for the development of new nutraceutical for the management of diabetes.

The work published by Iannuzzo et al. (2022a) describes an innovative technological process based on a basic treatment to chemical convert proanthocyanidins with a high molecular weight into low molecular weight procyanidins with a potential high intestinal bioavailability. For this study, the matrix selected was an extract of grape seed obtained by the plant *Vitis vinifera* L. In this project, I performed a qualitative analysis of the proanthocyanidins profile by using a HPLC-HESI-HRMS/MS method. To assess the effectiveness of the method, I asses a quali-quantitative analysis between the control and the treated groups assisted using a molecular networking approach. This approach demonstrated the potential of the method in the remodelling of proanthocyanidins profile, with a significant improvement of the amount of low molecular weight procyanidins with a higher bioavailability. These data represent a demonstration of the potential of this chemical approach to improve the composition of proanthocyanidins-enriched food matrix.

SUPPLEMENTARY MATERIAL

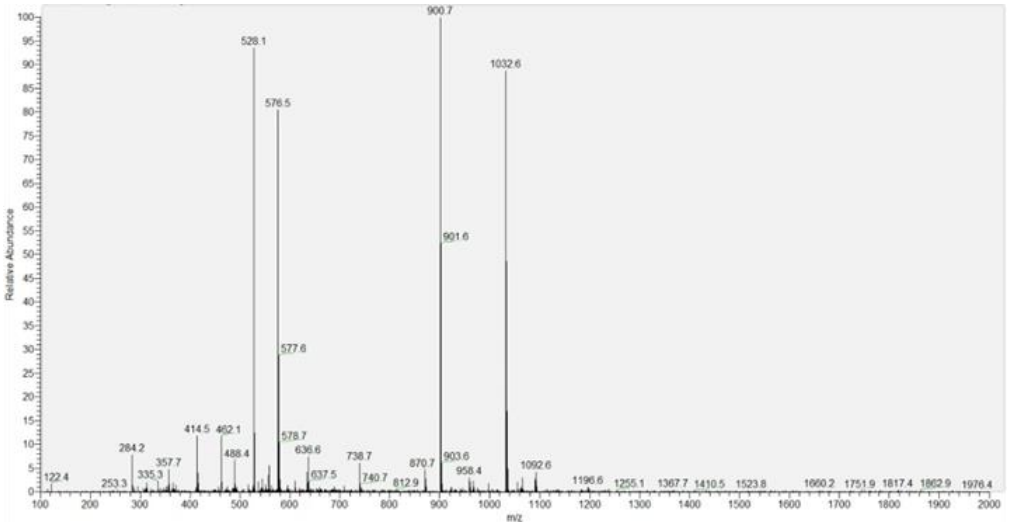


Figure S1: MS^1 spectrum of dehydrotomatine by an LC-MS analysis in Full scan mode.

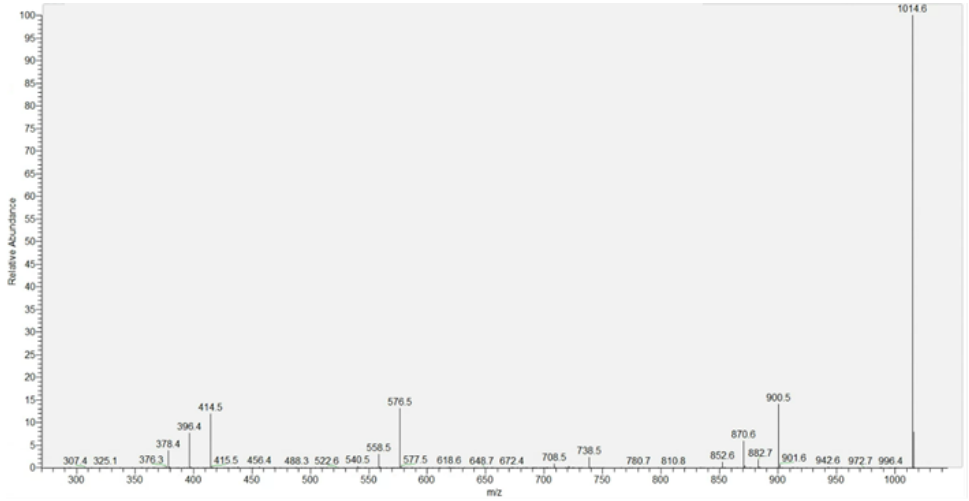


Figure S2: MS^2 spectrum of dehydrotomatine by using an MS/MS analysis mode.

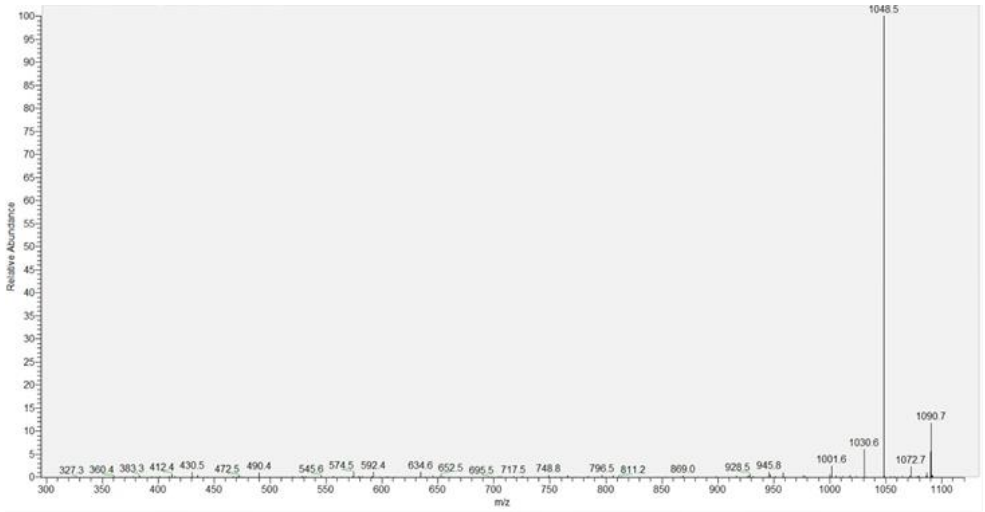


Figure S3: MS^2 spectrum of acetoxyhydroxytomatine by using an MS/MS analysis mode.

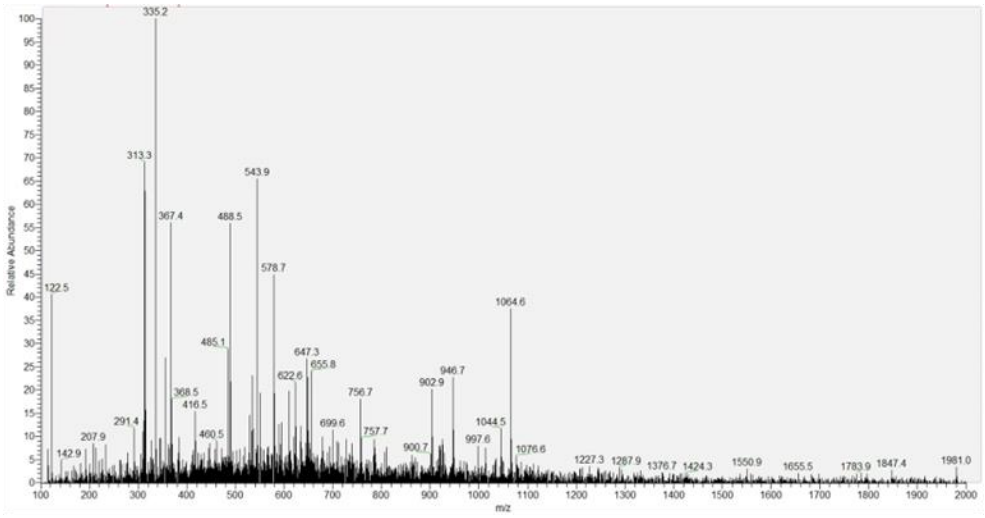


Figure S4: MS^1 spectrum of tomatidine tetrahexoside by an LC-MS analysis in Full scan mode.

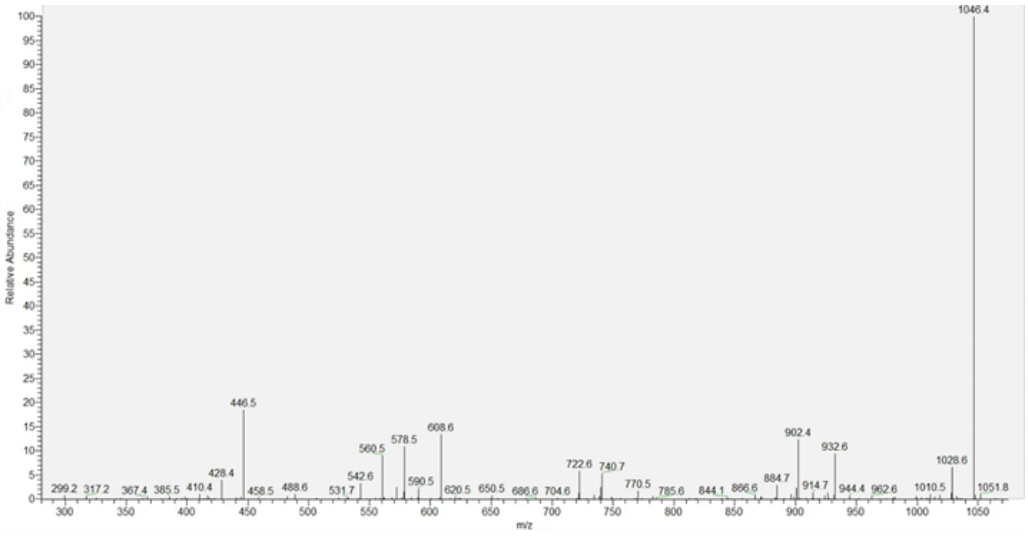


Figure S5: MS^2 spectrum of tomatidine tetrahexoside by using an MS/MS analysis mode.

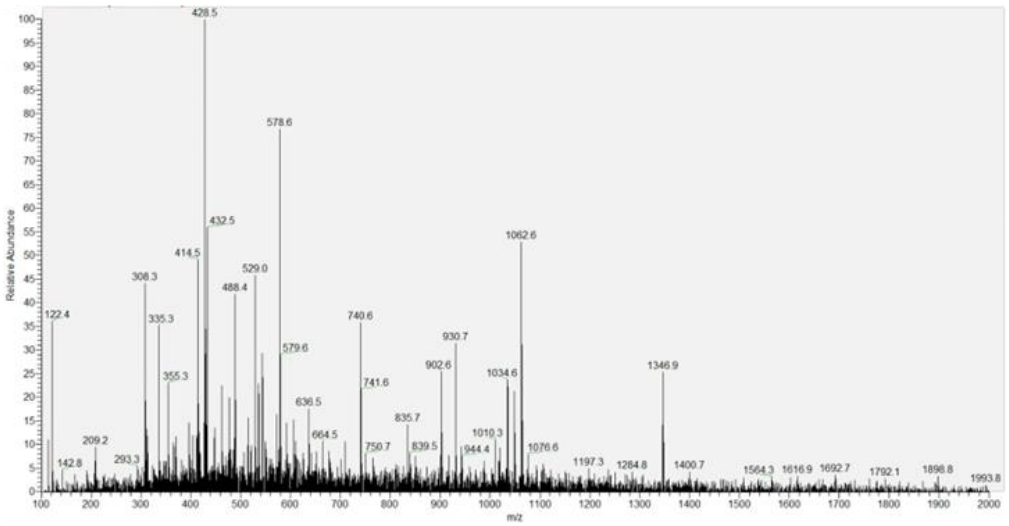


Figure S6: MS^1 spectrum of dehydrotomatidine tetrahexoside by an LC-MS analysis in Full scan mode.

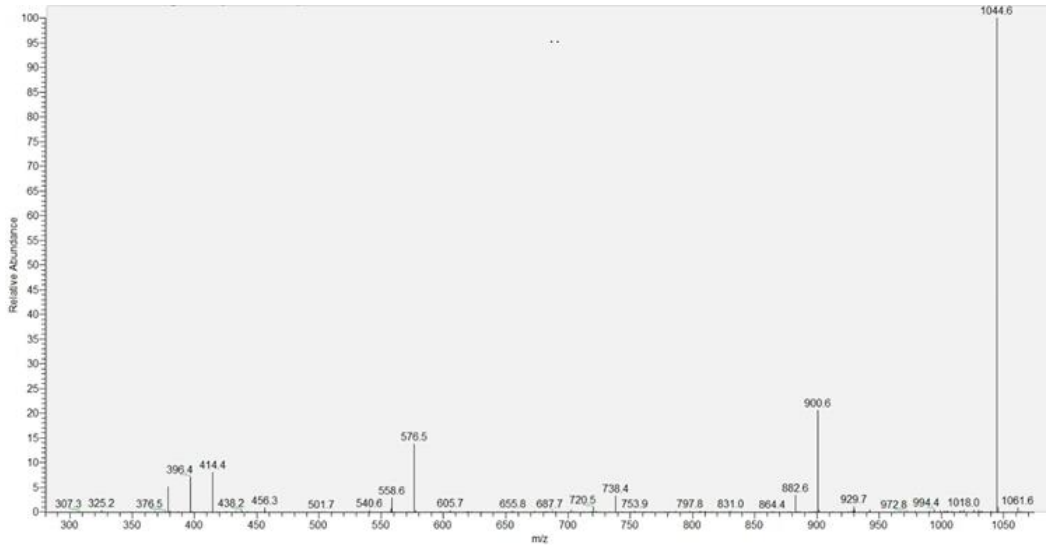


Figure S7: MS_2 spectrum of tomatidine dehydrotomatidine tetrahexoside by using an MS/MS analysis mode.

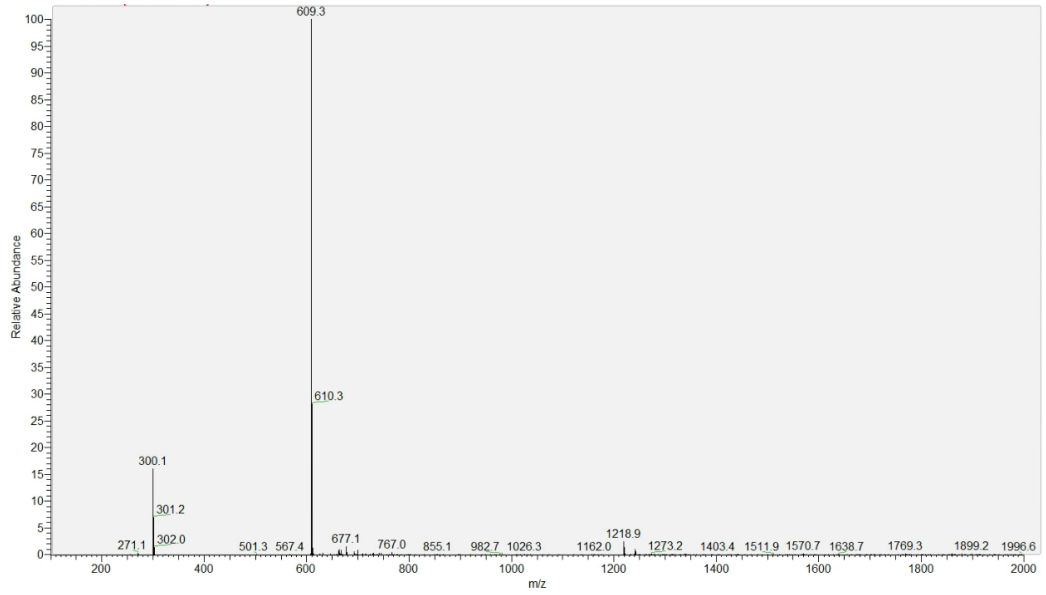


Figure S8: MS^1 spectrum of rutin by an LC-MS analysis in Full scan mode.

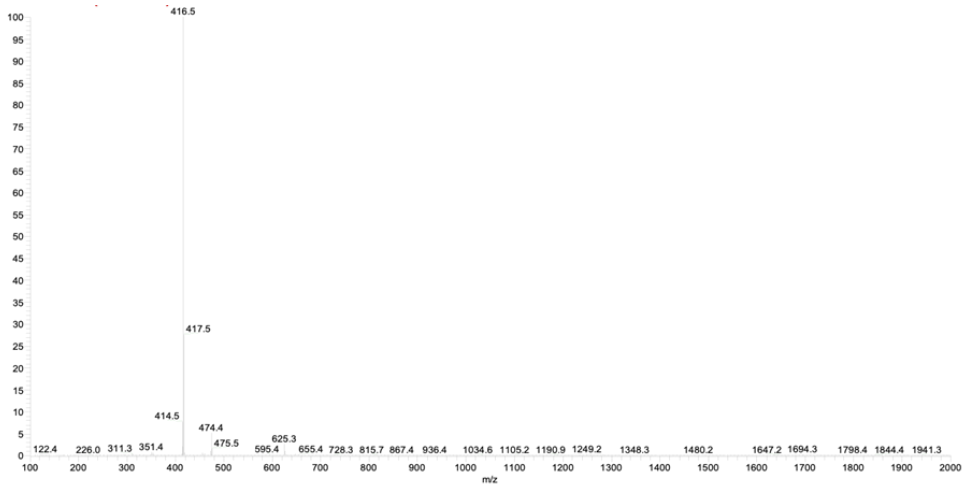


Figure S9: MS^1 spectrum of TD by an LC-MS analysis in Full scan mode.

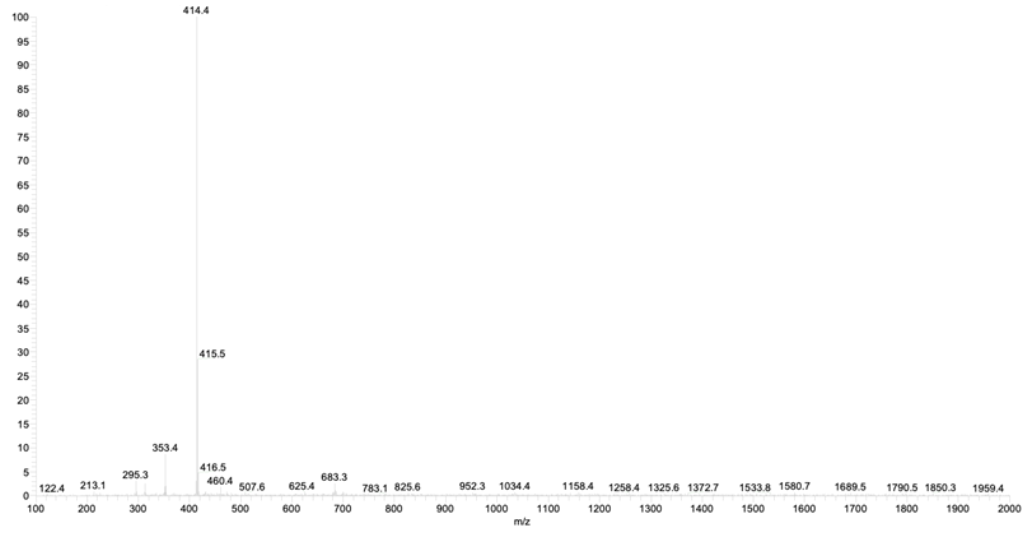


Figure S10: MS^1 spectrum of dehydrotomatidine by an LC-MS analysis in Full scan mode.

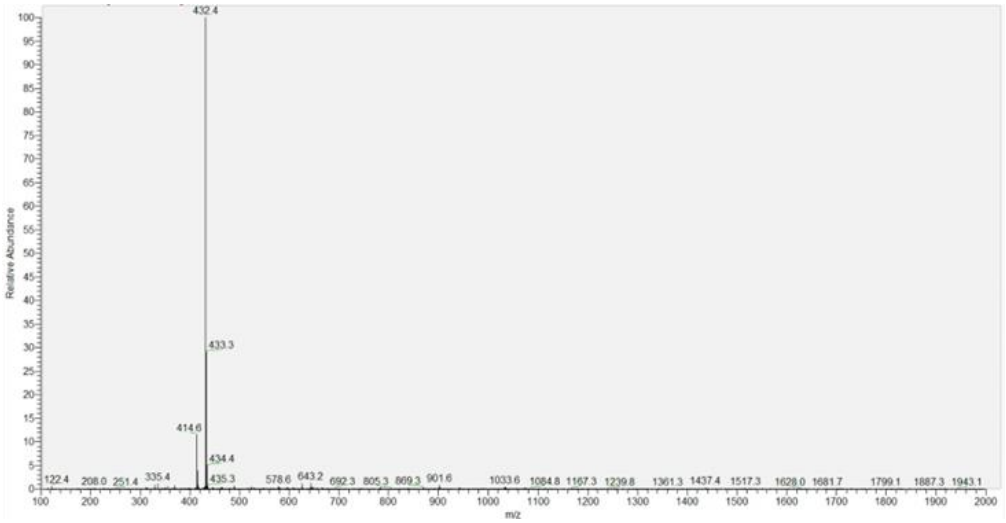


Figure S11: MS^1 spectrum of hydroxytomatidine by an LC-MS analysis in Full scan mode.

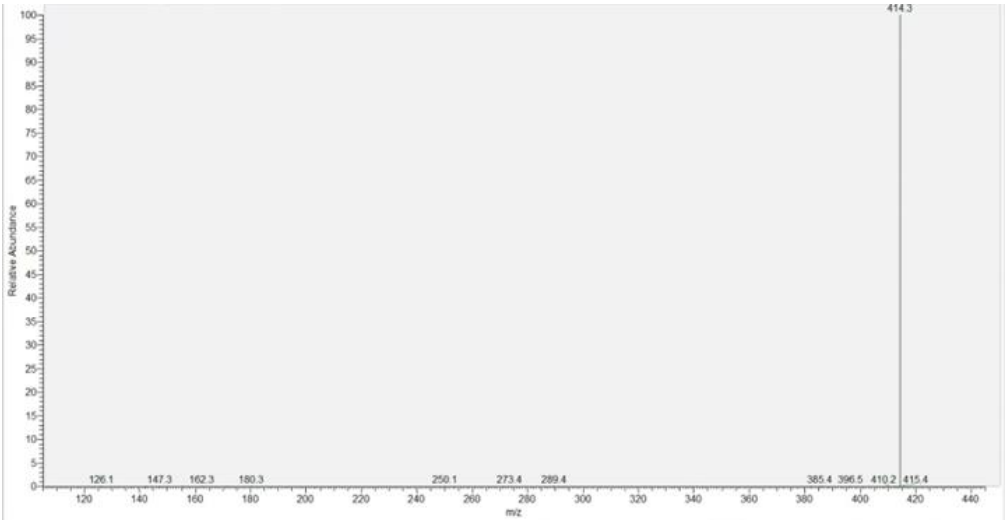


Figure S12: MS_2 spectrum of tomatidine hydroxytomatidine by using an MS/MS analysis mode.

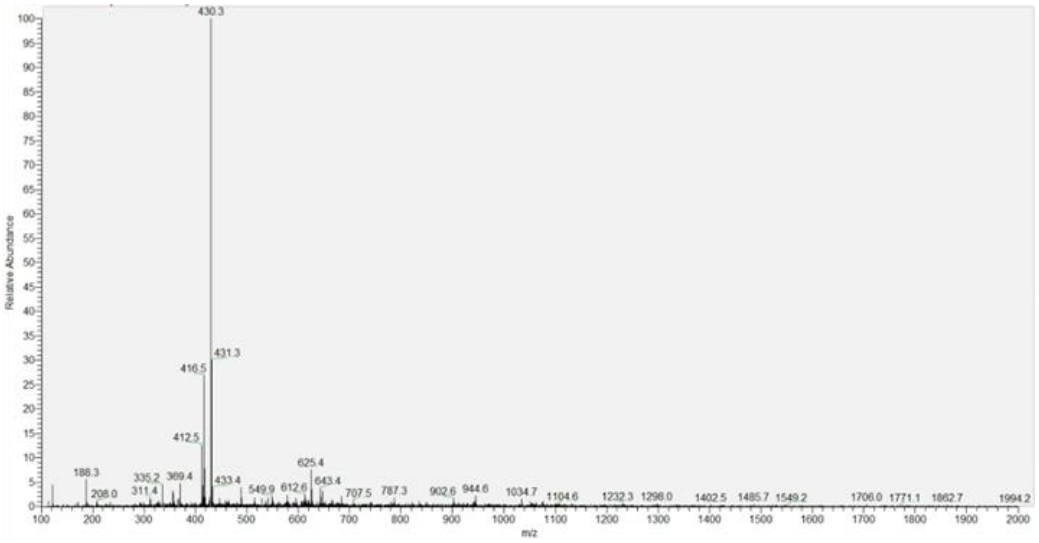


Figure S13: MS^1 spectrum of dehydro-hydroxytomatidine by an LC-MS analysis in Full scan mode.

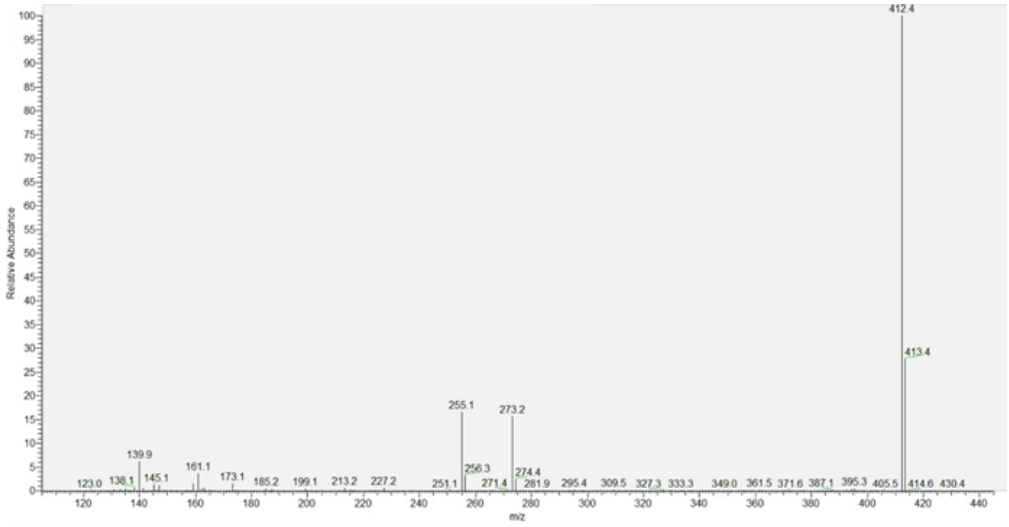


Figure S14: MS^2 spectrum of dehydro-hydroxytomatidine by using an MS/MS analysis mode.

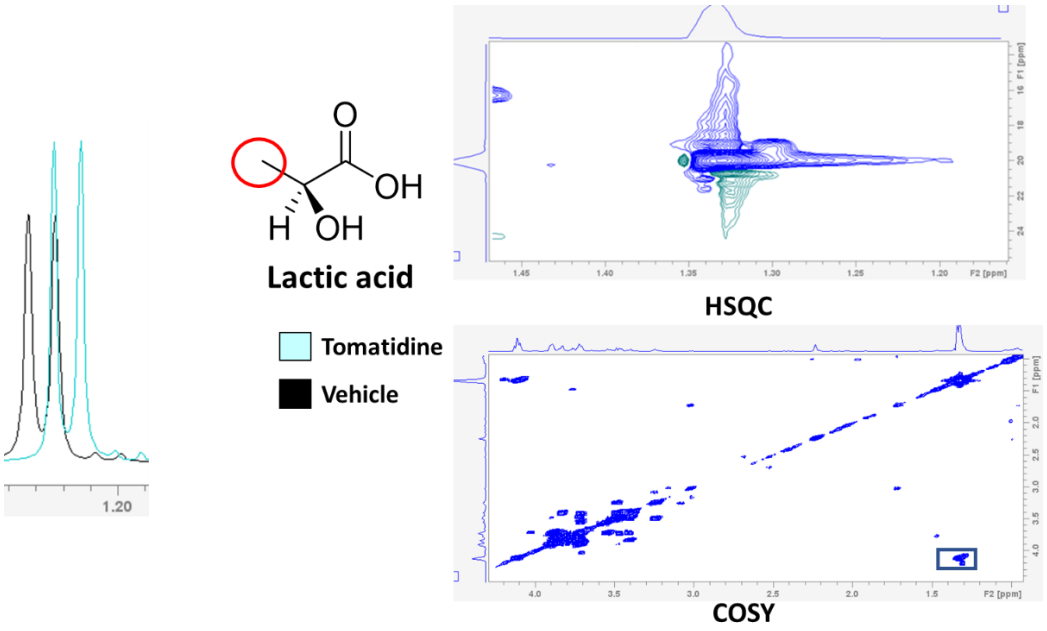


Figure S15: Overview of lactic acid methyl group signals in ^{1}H monodimensional and bidimensional HSQC and COSY NMR experiments of myoblast cells line C2C12 supernatants after TD and vehicle treatments.

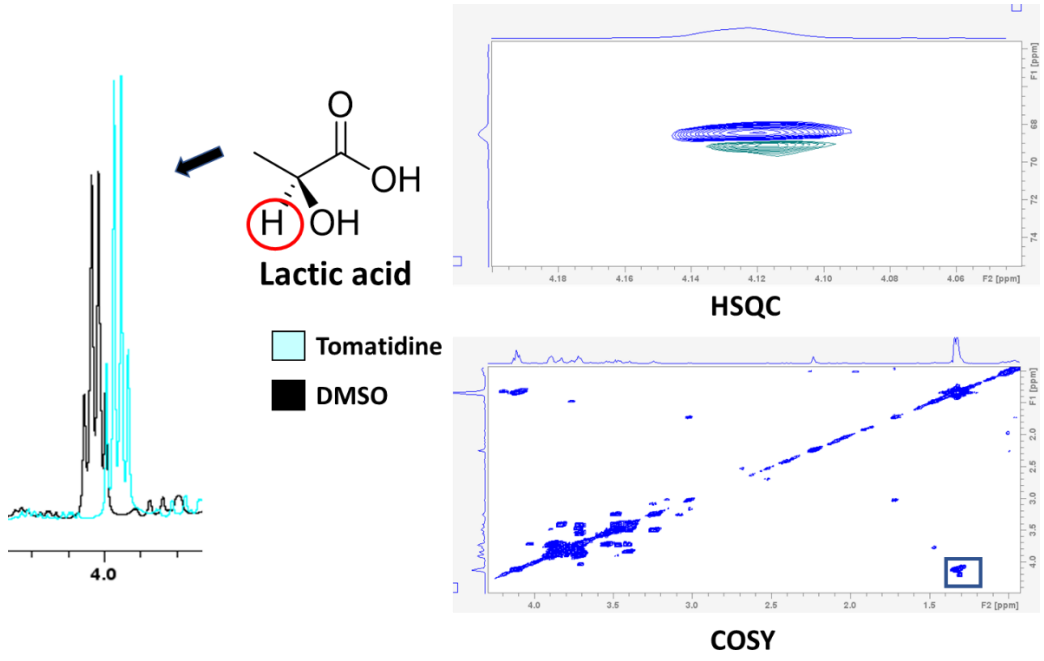


Figure S16: Overview of lactic acid methine group signals in ^{1}H monodimensional and bidimensional HSQC and COSY NMR experiments of myoblast cells line C2C12 supernatants after TD and vehicle treatments.

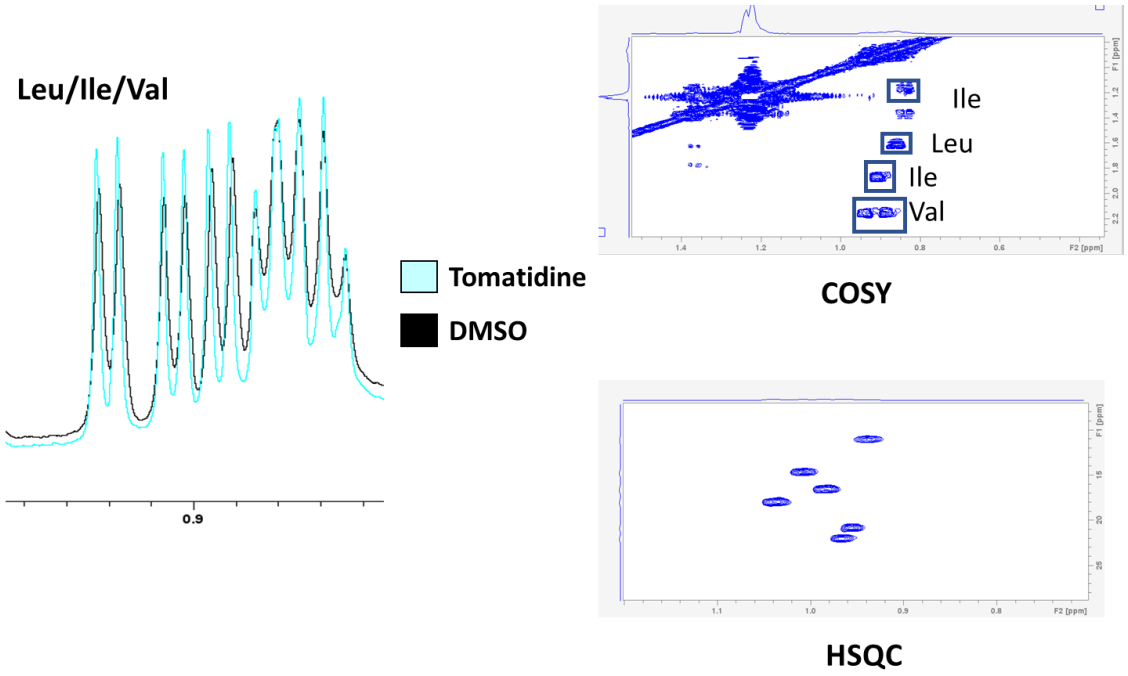


Figure S17: Overview of leucine, valine, and isoleucine methyl group signals in ^{1}H monodimensional and bidimensional HSQC and COSY NMR experiments of myoblast cells line C2C12 supernatants after TD and vehicle treatments.

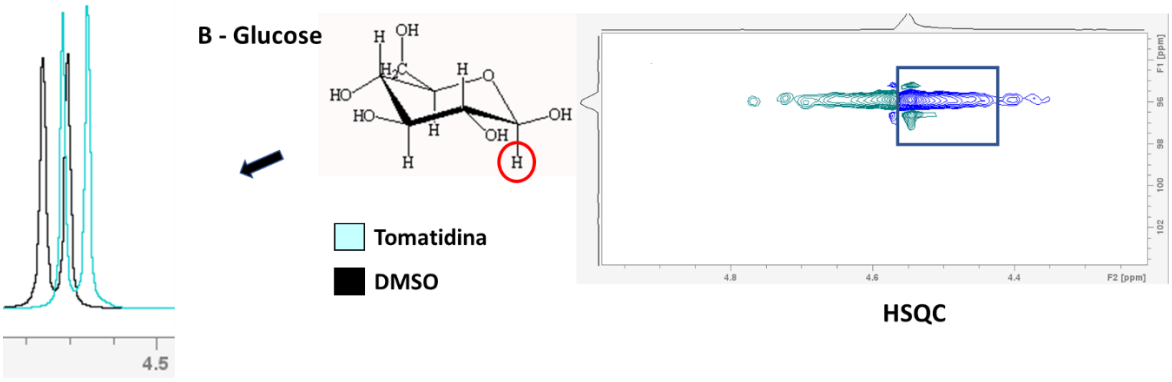


Figure S18: Overview of β-glucose anomeric signals in ^{1}H monodimensional and bidimensional HSQC NMR experiments of myoblast cells line C2C12 supernatants after TD and vehicle treatments.

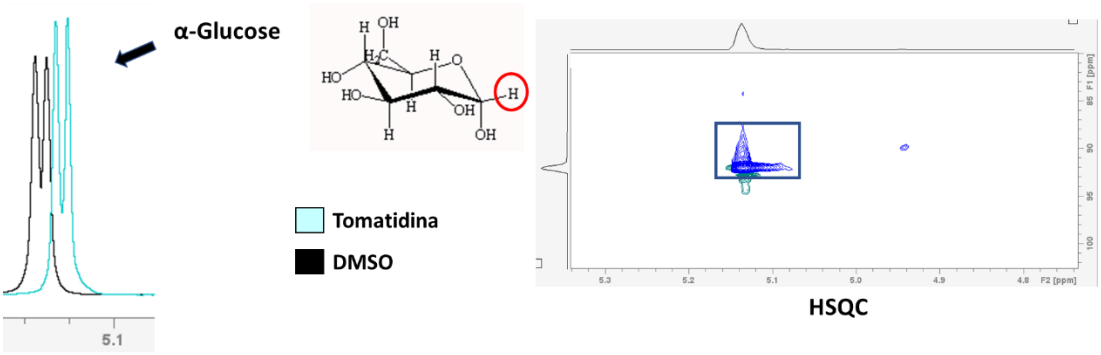


Figure S19: Overview of α-glucose anomeric signals in ^{1}H monodimensional and bidimensional HSQC NMR experiments of myoblast cells line C2C12 supernatants after TD and vehicle treatments.

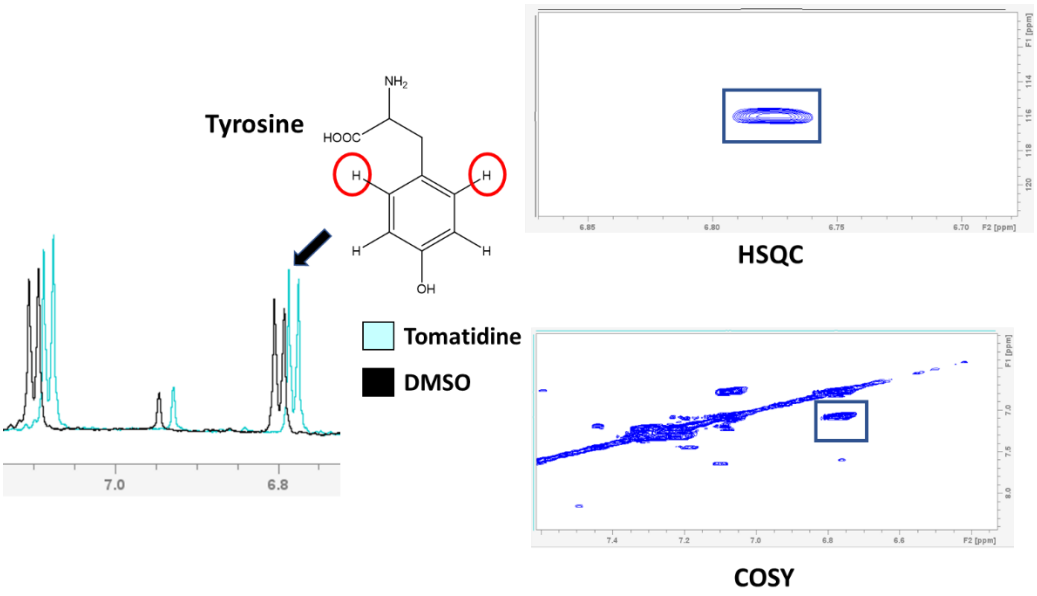


Figure S20: Overview of tyrosine 2,6 positions signals in ^{1}H monodimensional and bidimensional HSQC and COSY NMR experiments of myoblast cells line C2C12 supernatants after TD and vehicle treatments.

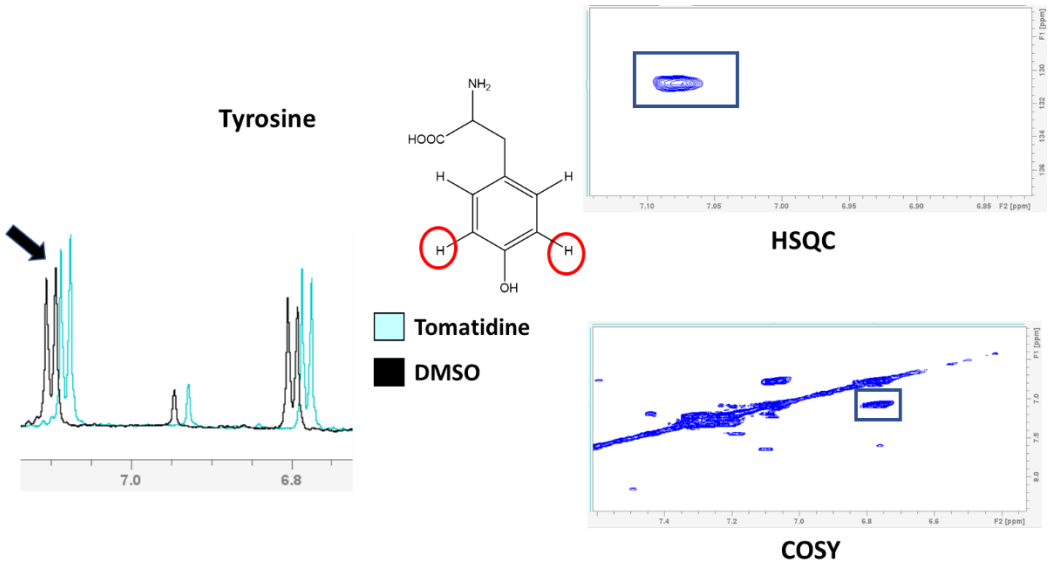


Figure S21: Overview of tyrosine 3,5 positions signals in ^{1}H monodimensional and bidimensional HSQC and COSY NMR experiments of myoblast cells line C2C12 supernatants after TD and vehicle treatments.

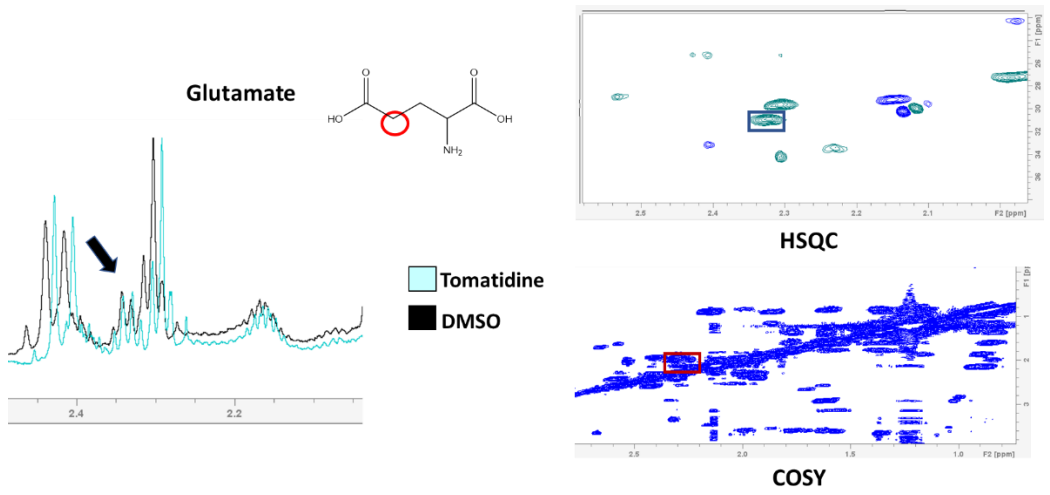


Figure S22: Overview of glutamate methylene group signals in ^{1}H monodimensional and bidimensional HSQC and COSY NMR experiments of myoblast cells line C2C12 supernatants after TD and vehicle treatments.

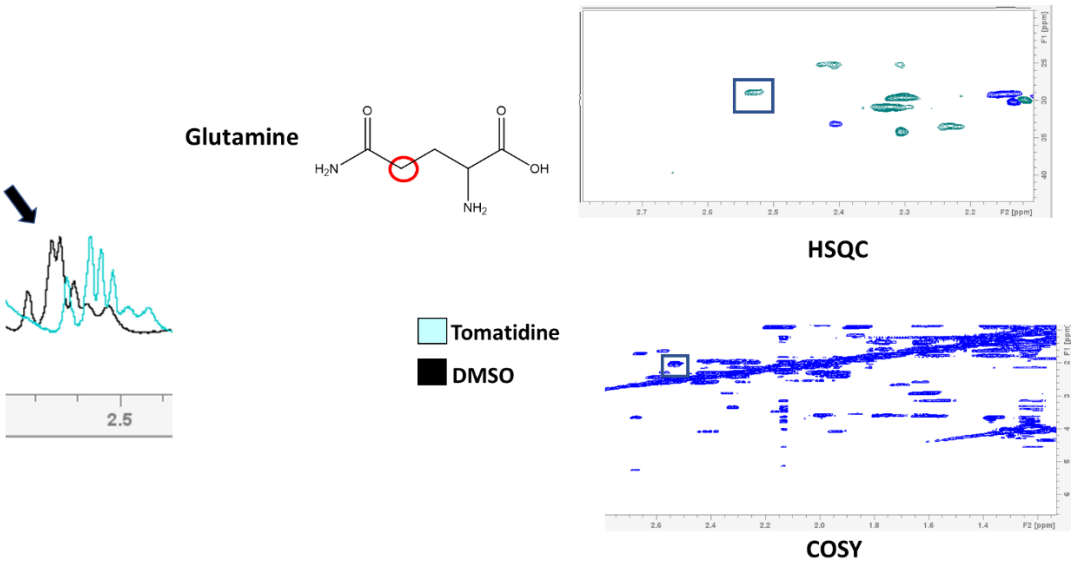


Figure S23: Overview of glutamine methylene group signals in ^{1}H monodimensional and bidimensional HSQC and COSY NMR experiments of myoblast cells line C2C12 supernatants after TD and vehicle treatments.

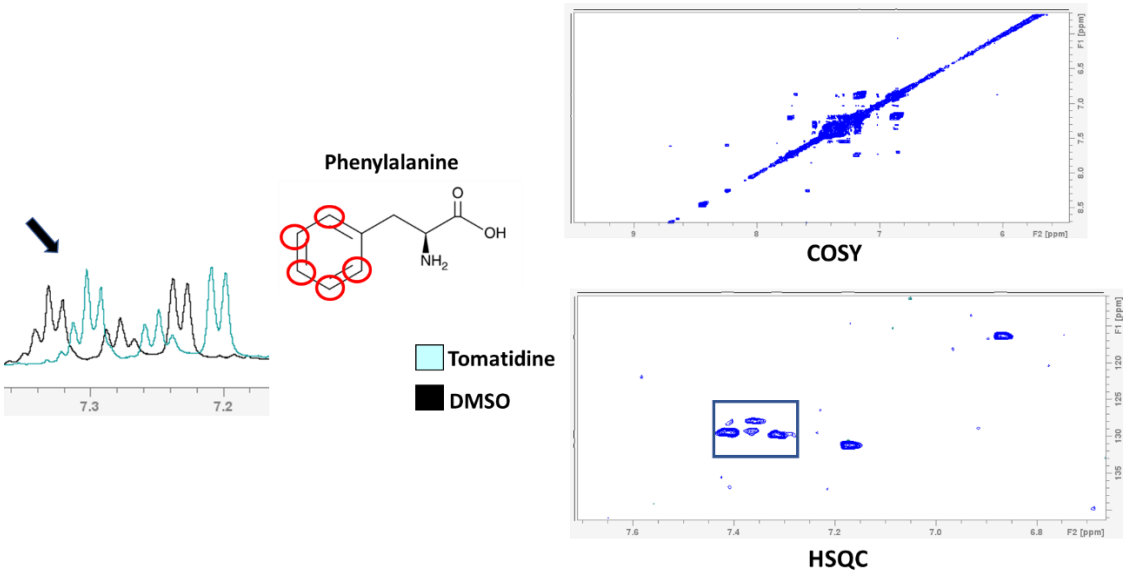


Figure S24: Overview of phenylalanine aromatic signals in ^{1}H monodimensional and bidimensional HSQC and COSY NMR experiments of myoblast cells line C2C12 supernatants after TD and vehicle treatments.

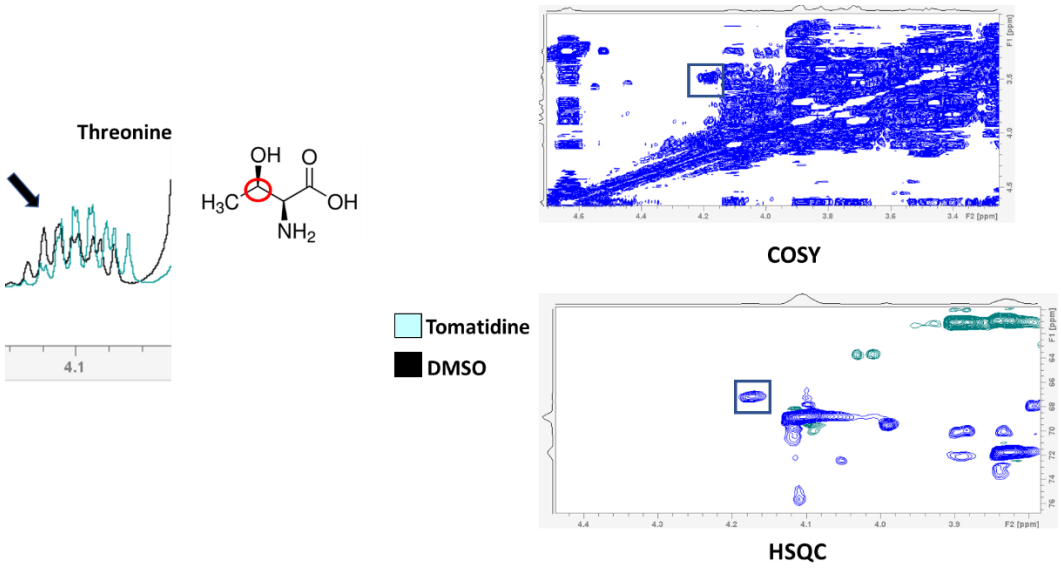


Figure S25: Overview of threonine methine group signals in ^{1}H monodimensional and bidimensional HSQC and COSY NMR experiments of myoblast cells line C2C12 supernatants after TD and vehicle treatments.

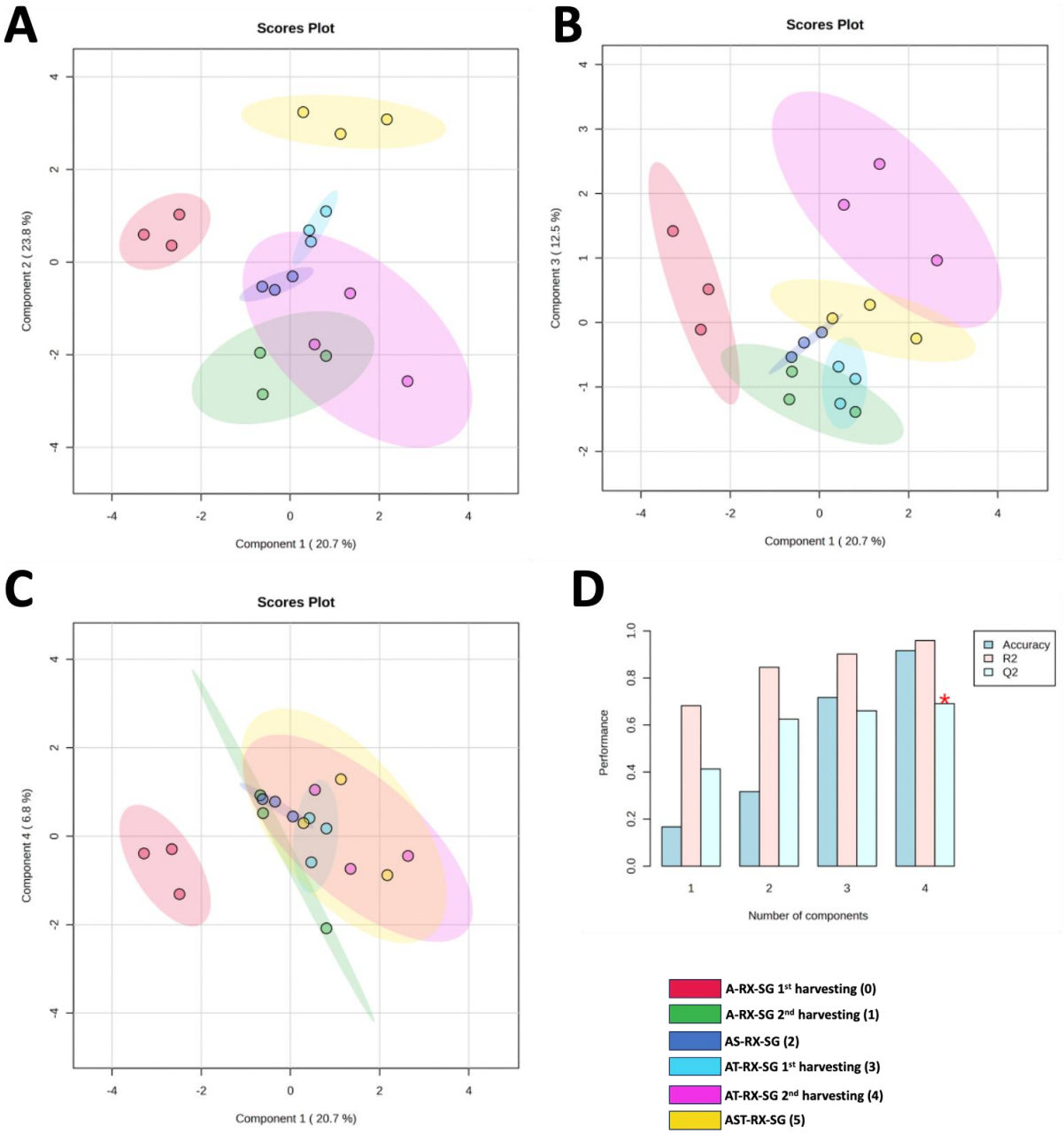


Figure S26: Multivariate analysis of treated and untreated stems (SG samples). (**A**), (**B**) and (**C**) Partial least square discriminant analysis (PLS-DA) scores plot, corresponding to a model aimed at the discrimination between treated and untreated stems. The colored ellipses denote 95% confidence intervals for each group. (**D**) Cross-validation test, used to assess the correct number of Components to consider, according to the Q2 value.

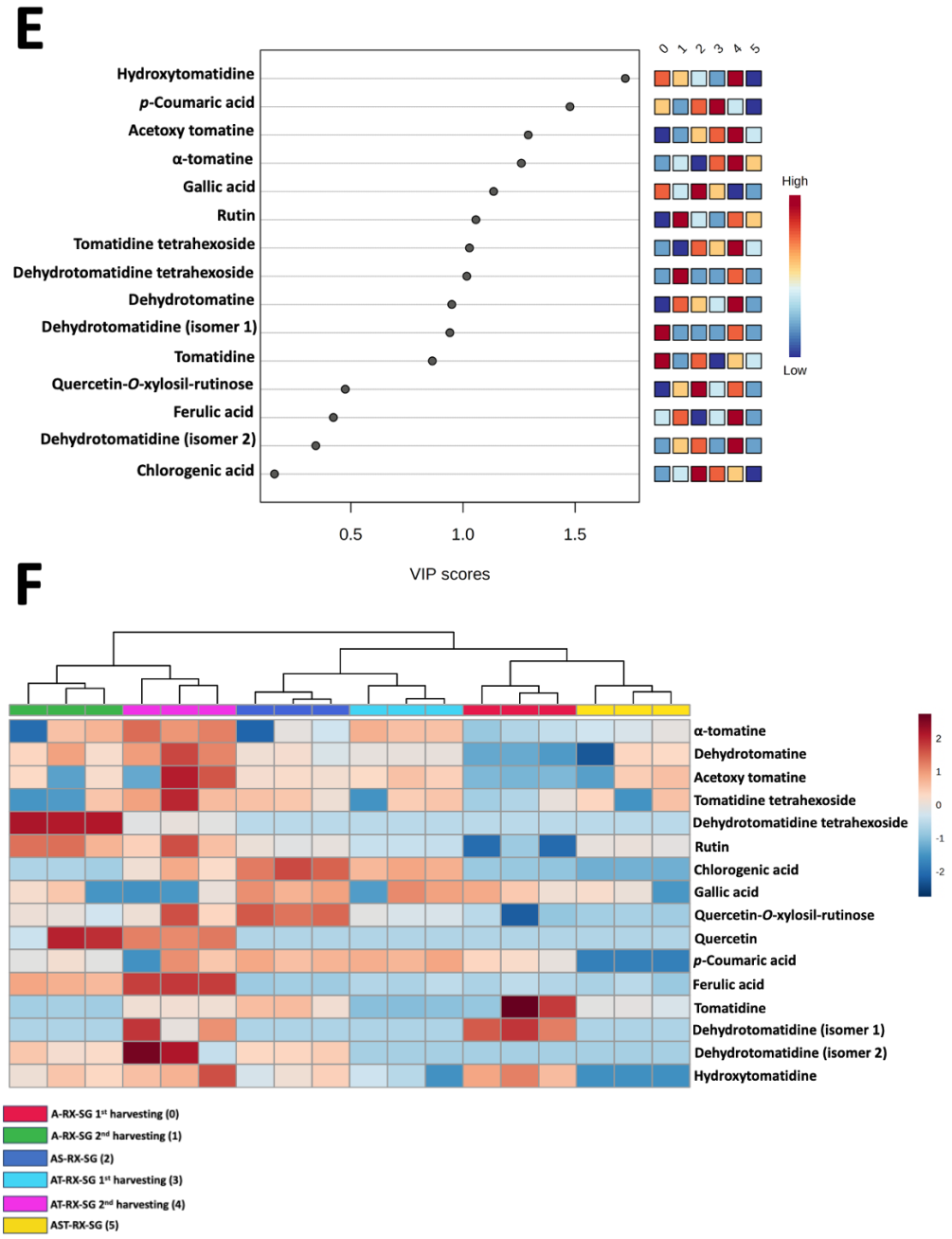


Figure S27: Multivariate analysis of treated and untreated stems (SG samples). (**E**) Variable importance on projection (VIP) scores from the PLS-DA model, indicating the most discriminating metabolites between samples in descending order of importance and with relative levels of metabolites for each matrix. (**F**) Heatmap with Hierarchical clustering, illustrating the relative metabolite concentration among groups. The corresponding relative metabolite concentration is expressed as a color of different intensity from blue (lowest amount) to red (highest amount).

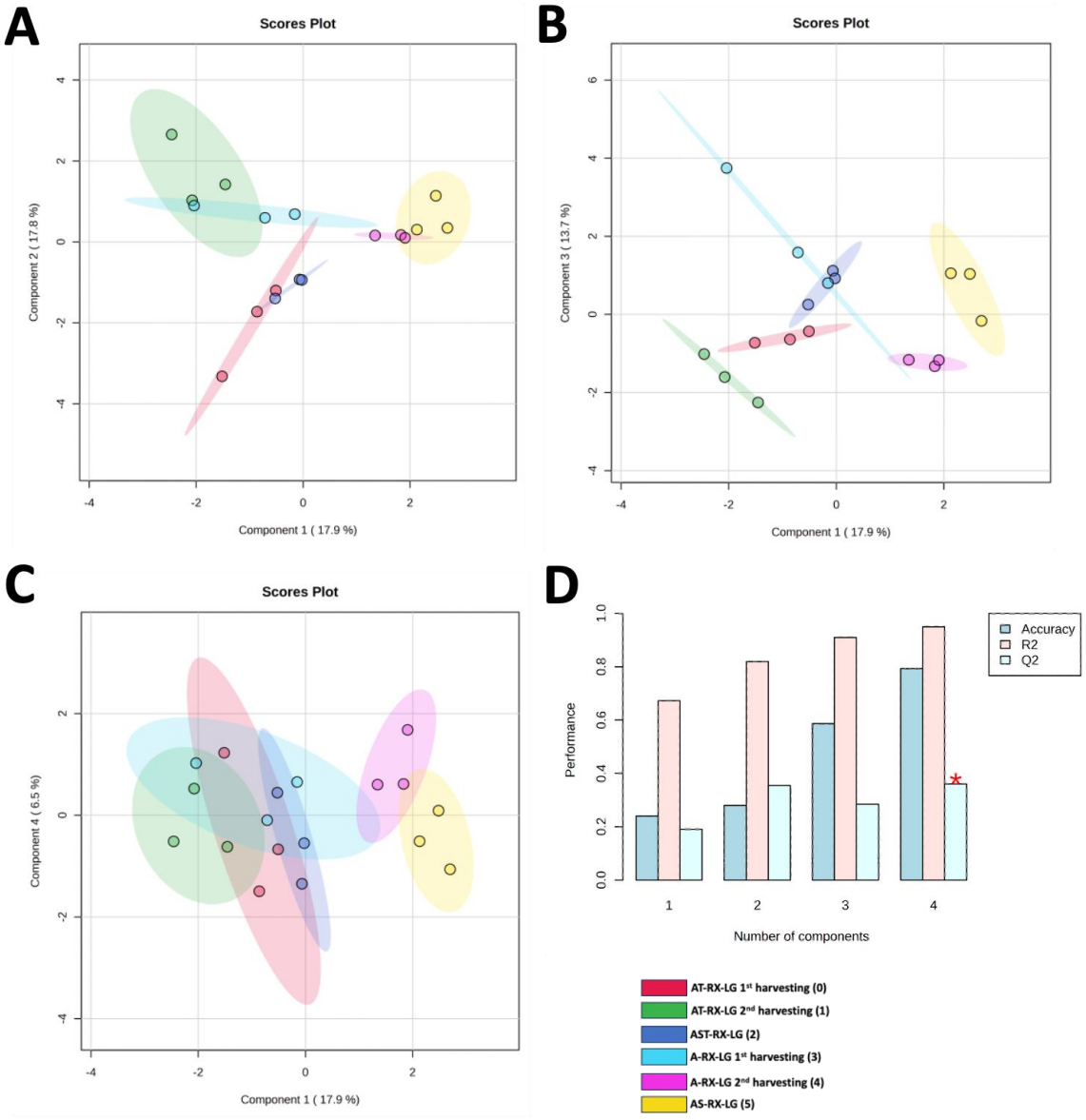


Figure S28: Multivariate analysis of treated and untreated leaves (LG samples). (**A**), (**B**) and (**C**) Partial least square discriminant analysis (PLS-DA) scores plot, corresponding to a model aimed at the discrimination between treated and untreated stems. The colored ellipses denote 95% confidence intervals for each group. (**D**) Cross-validation test, used to assess the correct number of Components to consider, according to the Q2 value.

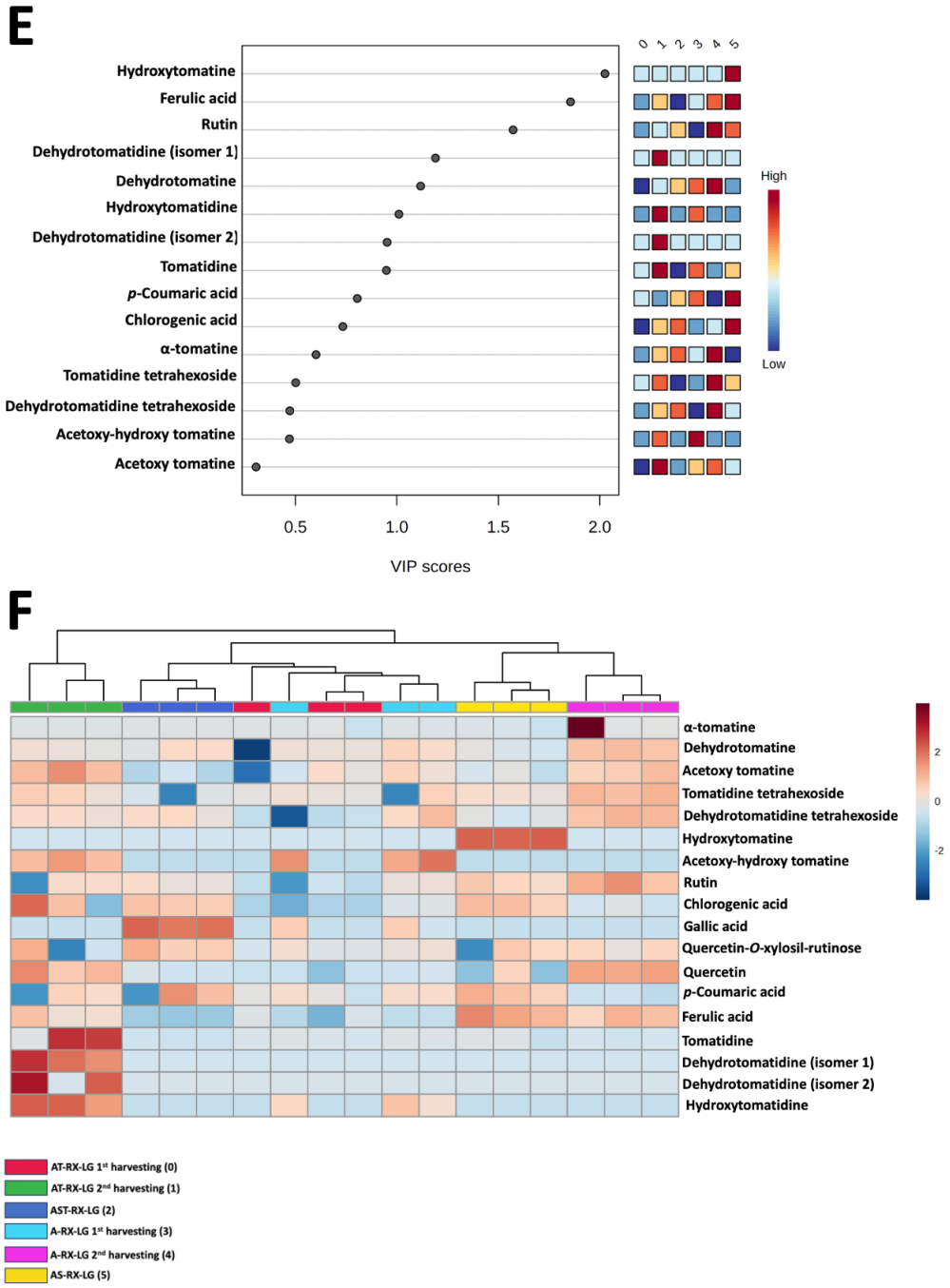


Figure S29: Multivariate analysis of treated and untreated leaves (LG samples). (**E**) Variable importance on projection (VIP) scores from the PLS-DA model, indicating the most discriminating metabolites between samples in descending order of importance and with relative levels of metabolites for each matrix. (**F**) Heatmap with Hierarchical clustering, illustrating the relative metabolite concentration among groups. The corresponding relative metabolite concentration is expressed as a color of different intensity from blue (lowest amount) to red (highest amount).

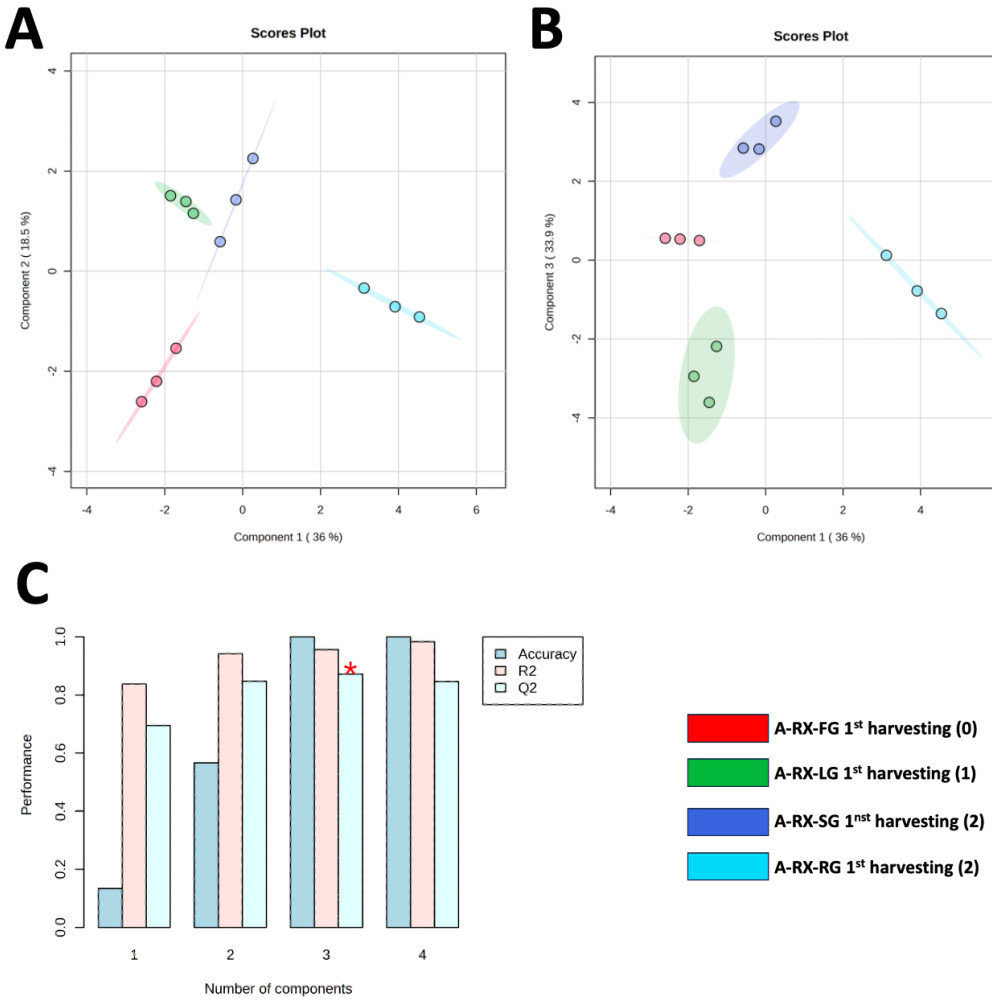


Figure S30: Multivariate analysis of different anatomical parts of Piennolo tomato plants in first-harvesting untreated samples. (**A**) and (**B**) Partial least square discriminant analysis (PLS-DA) scores plot, corresponding to a model aimed at the discrimination between different anatomical parts of Piennolo tomato plants. The colored ellipses denote 95% confidence intervals for each group. (**C**) Cross-validation test, used to assess the correct number of Components to consider, according to the Q2 value.

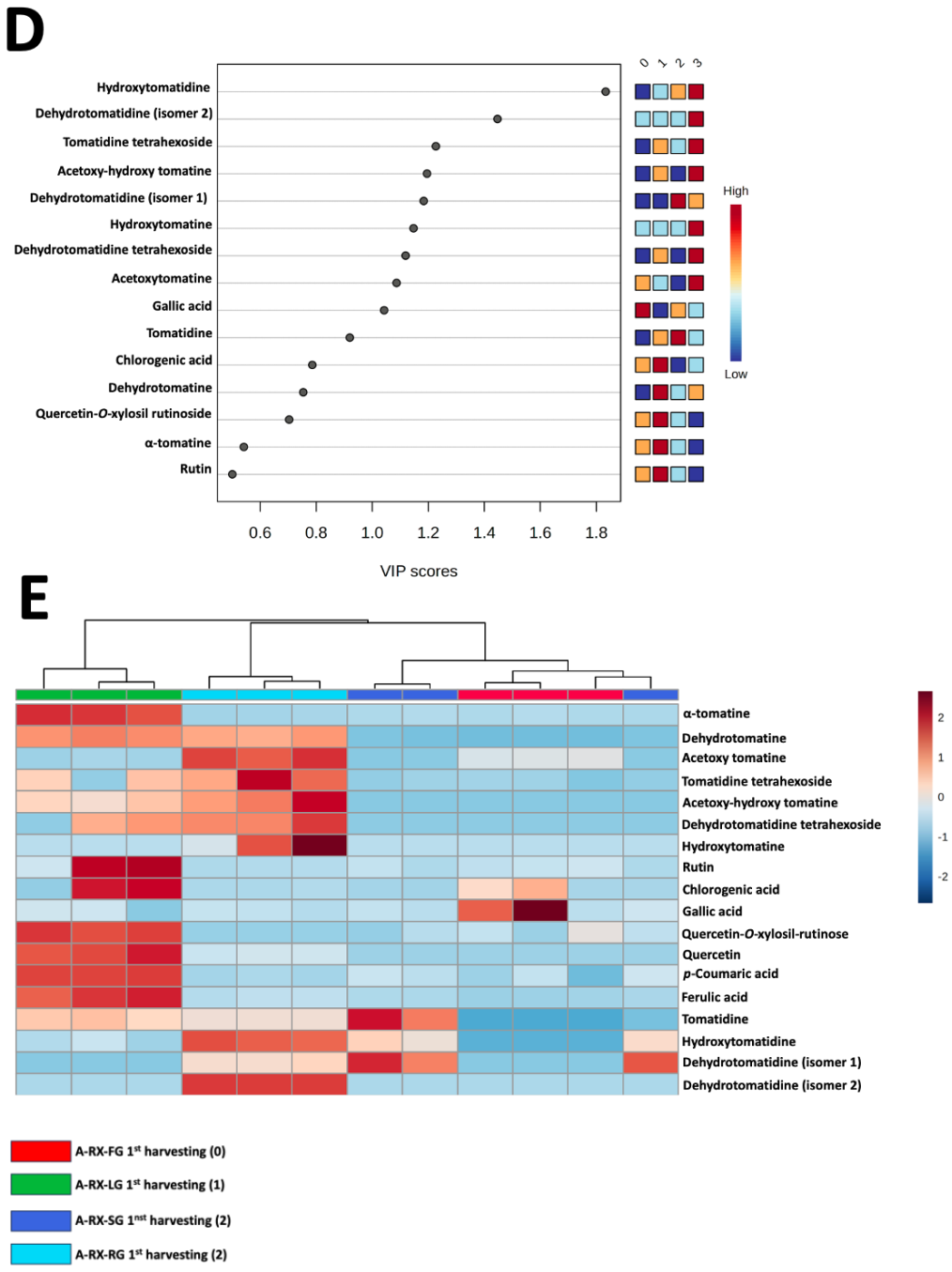


Figure S31: Multivariate analysis of different anatomical parts of Piennolo tomato plants in first-harvesting untreated samples. (**D**) Variable importance on projection (VIP) scores from the PLS-DA model, indicating the most discriminating metabolites between samples in descending order of importance and with relative levels of metabolites for each matrix. (**E**) Heatmap with Hierarchical clustering, illustrating the relative metabolite concentration among groups. The corresponding relative metabolite concentration is expressed as a color of different intensity from blue (lowest amount) to red (highest amount).

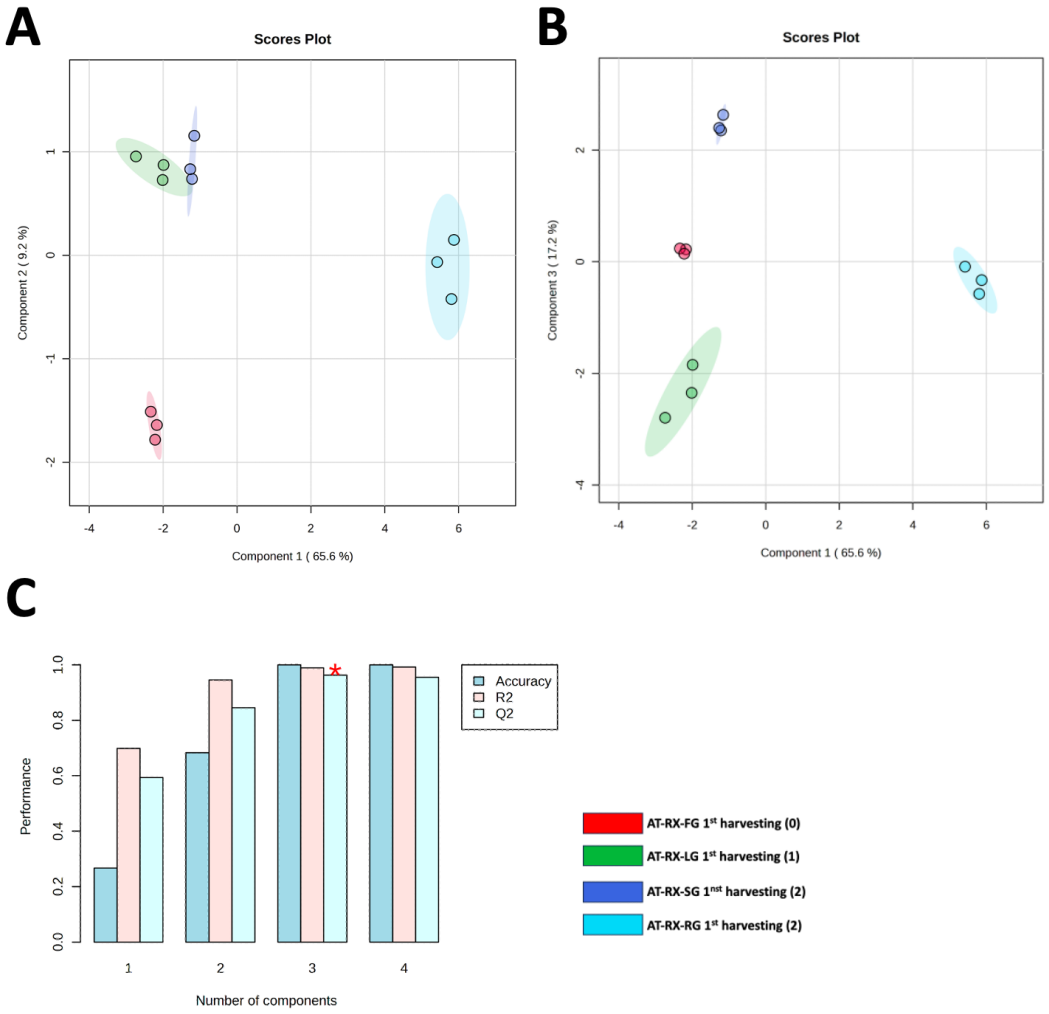


Figure S32: Multivariate analysis of different anatomical parts of Piennolo tomato plants in first-harvesting treated samples. (**A**) and (**B**) Partial least square discriminant analysis (PLS-DA) scores plot, corresponding to a model aimed at the discrimination between different anatomical parts of Piennolo tomato plants. The colored ellipses denote 95% confidence intervals for each group. (**C**) Cross-validation test, used to assess the correct number of Components to consider, according to the Q2 value.

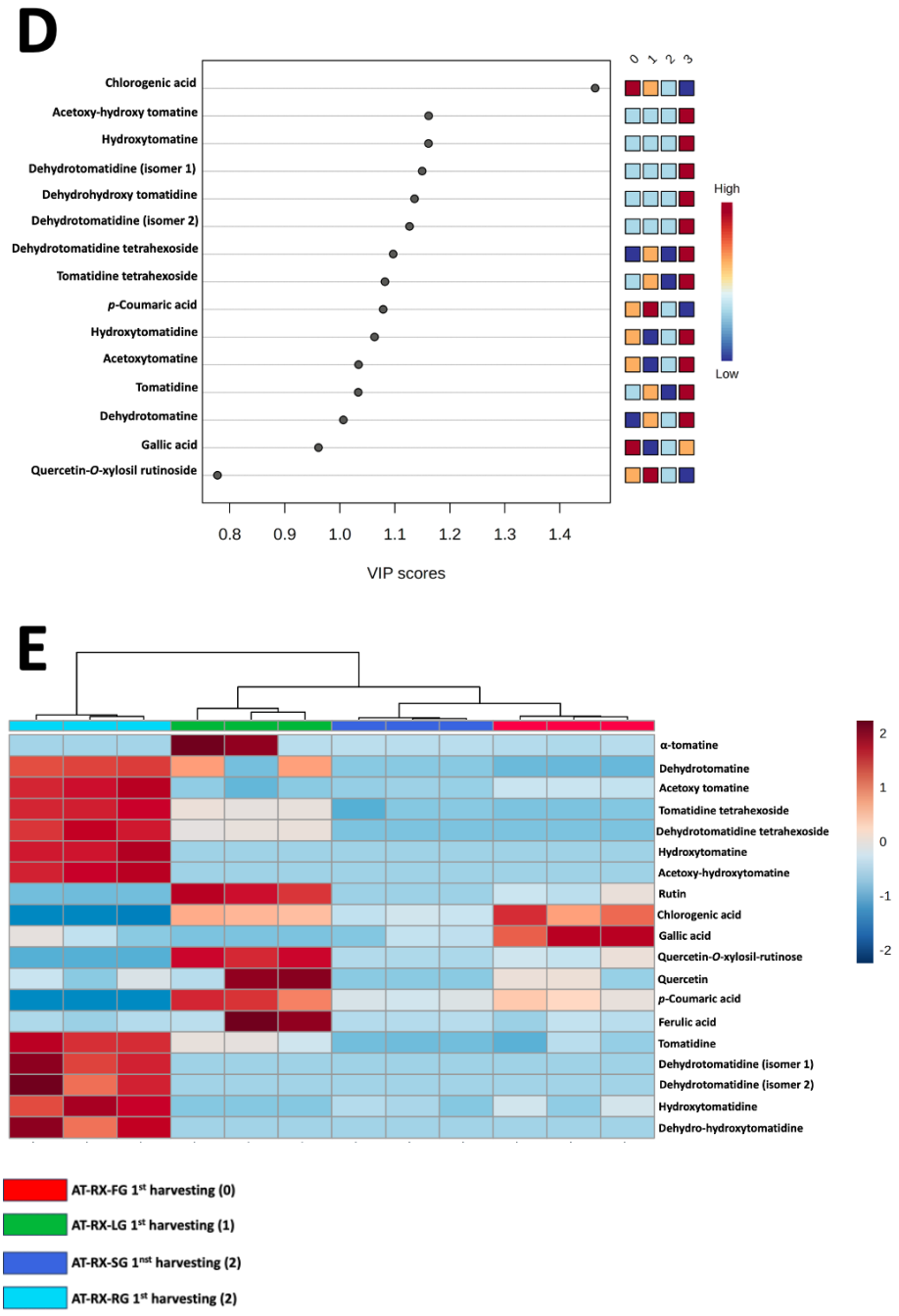


Figure S33: Multivariate analysis of different anatomical parts of Piennolo tomato plants in first-harvesting treated samples. (**D**) Variable importance on projection (VIP) scores from the PLS-DA model, indicating the most discriminating metabolites between samples in descending order of importance and with relative levels of metabolites for each matrix. (**E**) Heatmap with Hierarchical clustering, illustrating the relative metabolite concentration among groups. The corresponding relative metabolite concentration is expressed as a color of different intensity from blue (lowest amount) to red (highest amount).

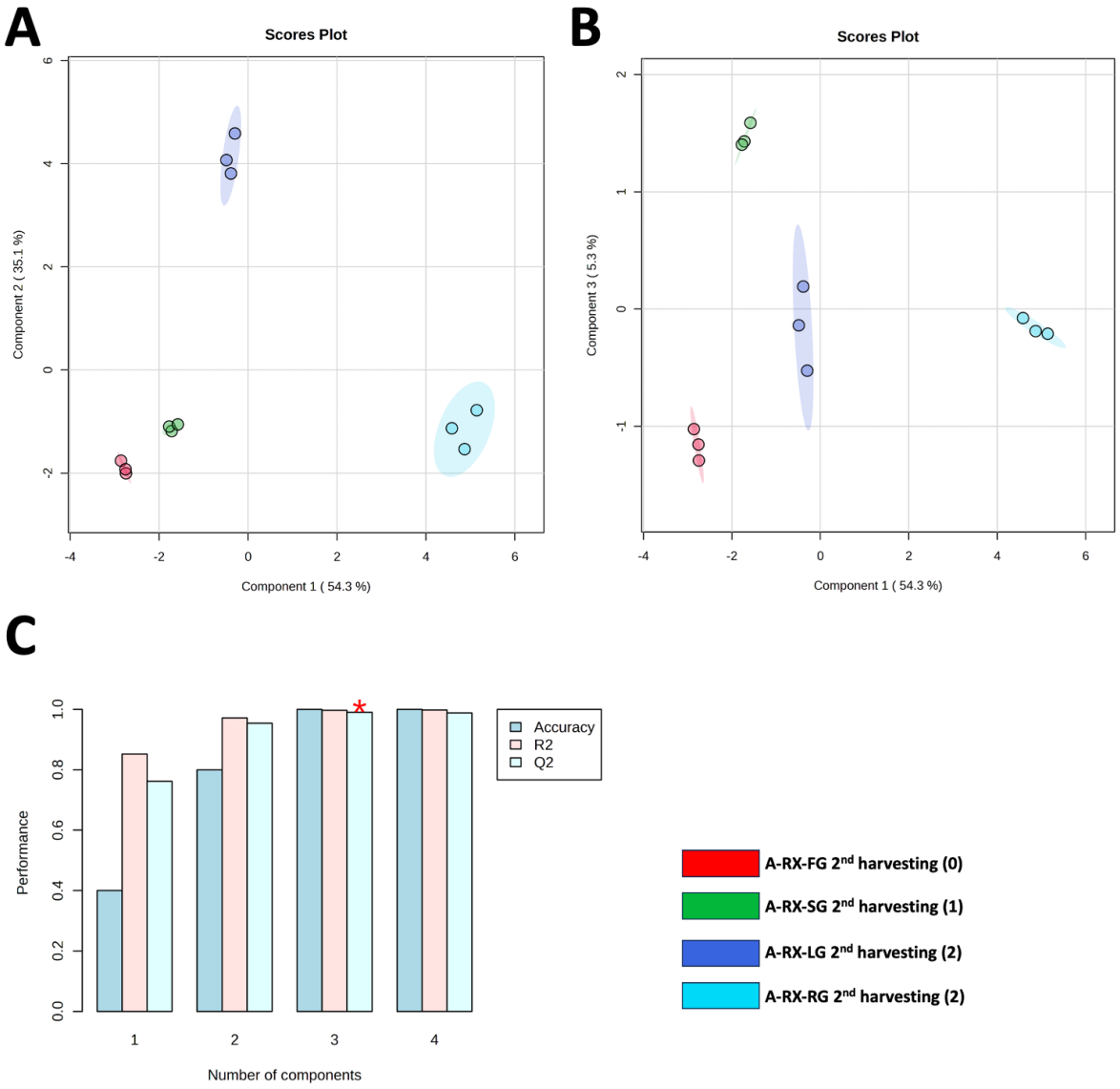


Figure S34: Multivariate analysis of different anatomical parts of Piennolo tomato plants in second-harvesting untreated samples. (**A**) and (**B**) Partial least square discriminant analysis (PLS-DA) scores plot, corresponding to a model aimed at the discrimination between different anatomical parts of Piennolo tomato plants. The colored ellipses denote 95% confidence intervals for each group. (**C**) Cross-validation test, used to assess the correct number of Components to consider, according to the Q2 value.

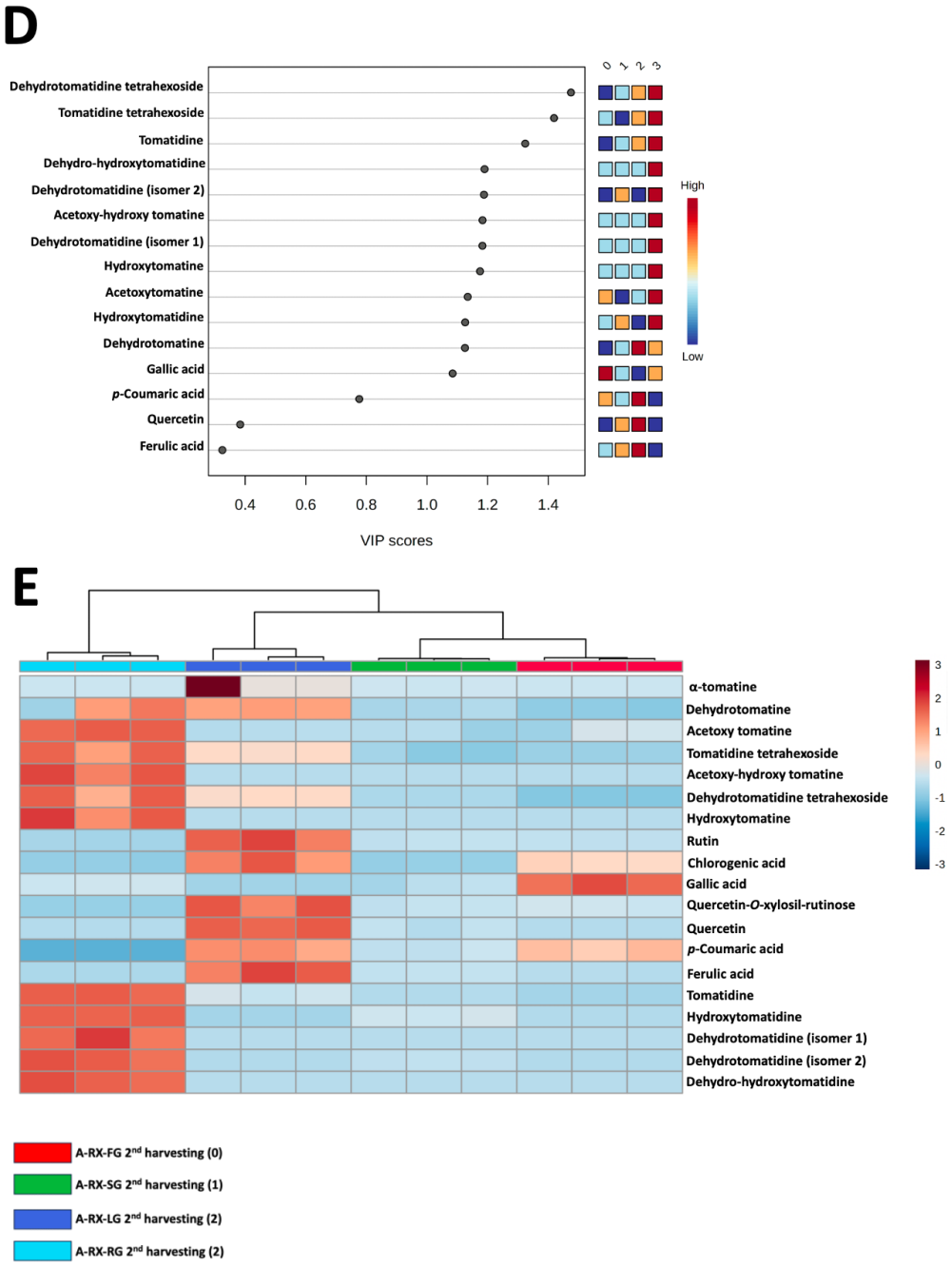


Figure S35: Multivariate analysis of different anatomical parts of Piennolo tomato plants in second-harvesting untreated samples. (**D**) Variable importance on projection (VIP) scores from the PLS-DA model, indicating the most discriminating metabolites between samples in descending order of importance and with relative levels of metabolites for each matrix. (**E**) Heatmap with Hierarchical clustering, illustrating the relative metabolite concentration among groups. The corresponding relative metabolite concentration is expressed as a color of different intensity from blue (lowest amount) to red (highest amount).

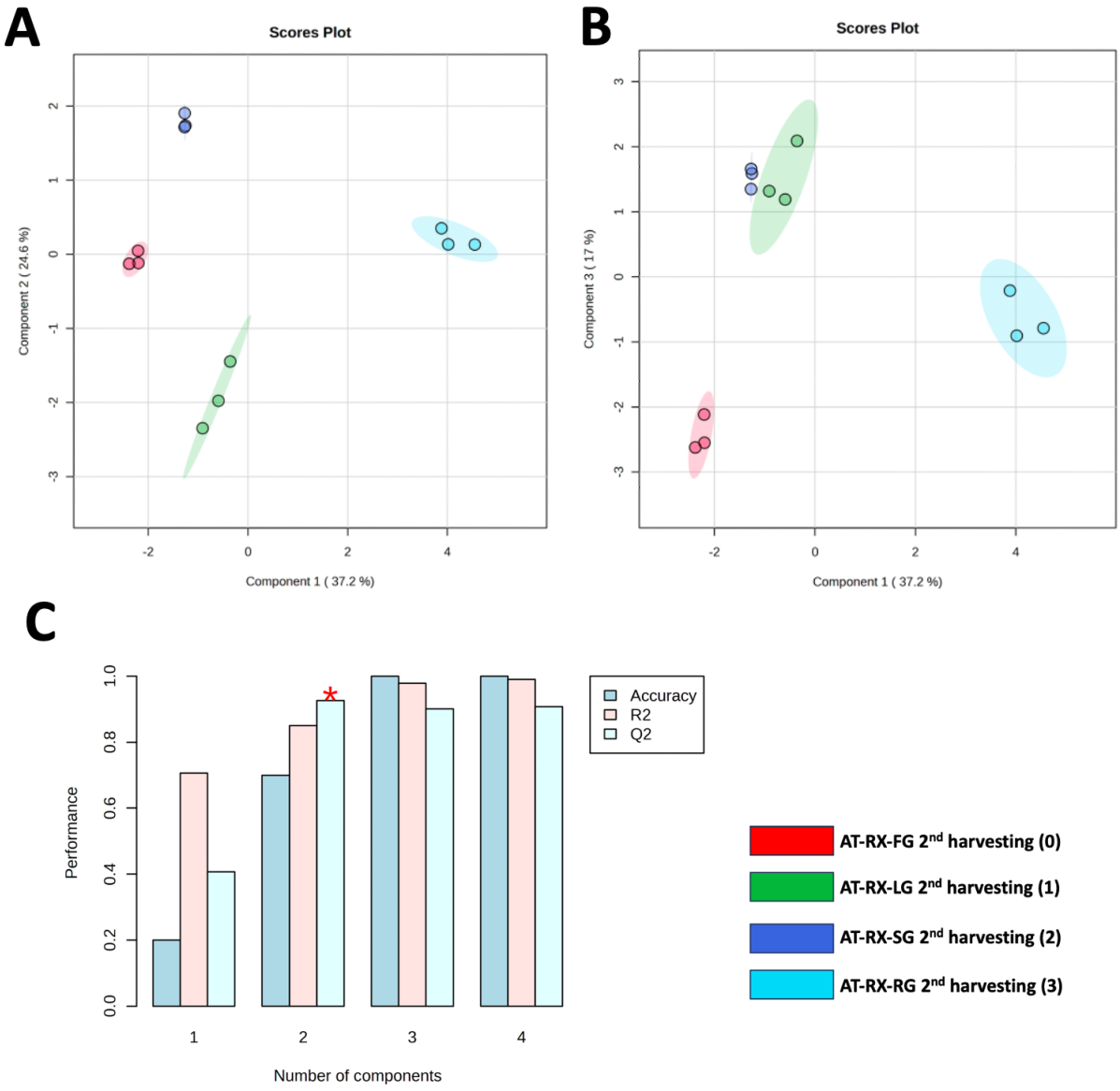


Figure S36: Multivariate analysis of different anatomical parts of Piennolo tomato plants in second-harvesting treated samples. (**A**) and (**B**) Partial least square discriminant analysis (PLS-DA) scores plot, corresponding to a model aimed at the discrimination between different anatomical parts of Piennolo tomato plants. The colored ellipses denote 95% confidence intervals for each group. (**C**) Cross-validation test, used to assess the correct number of Components to consider, according to the Q2 value.

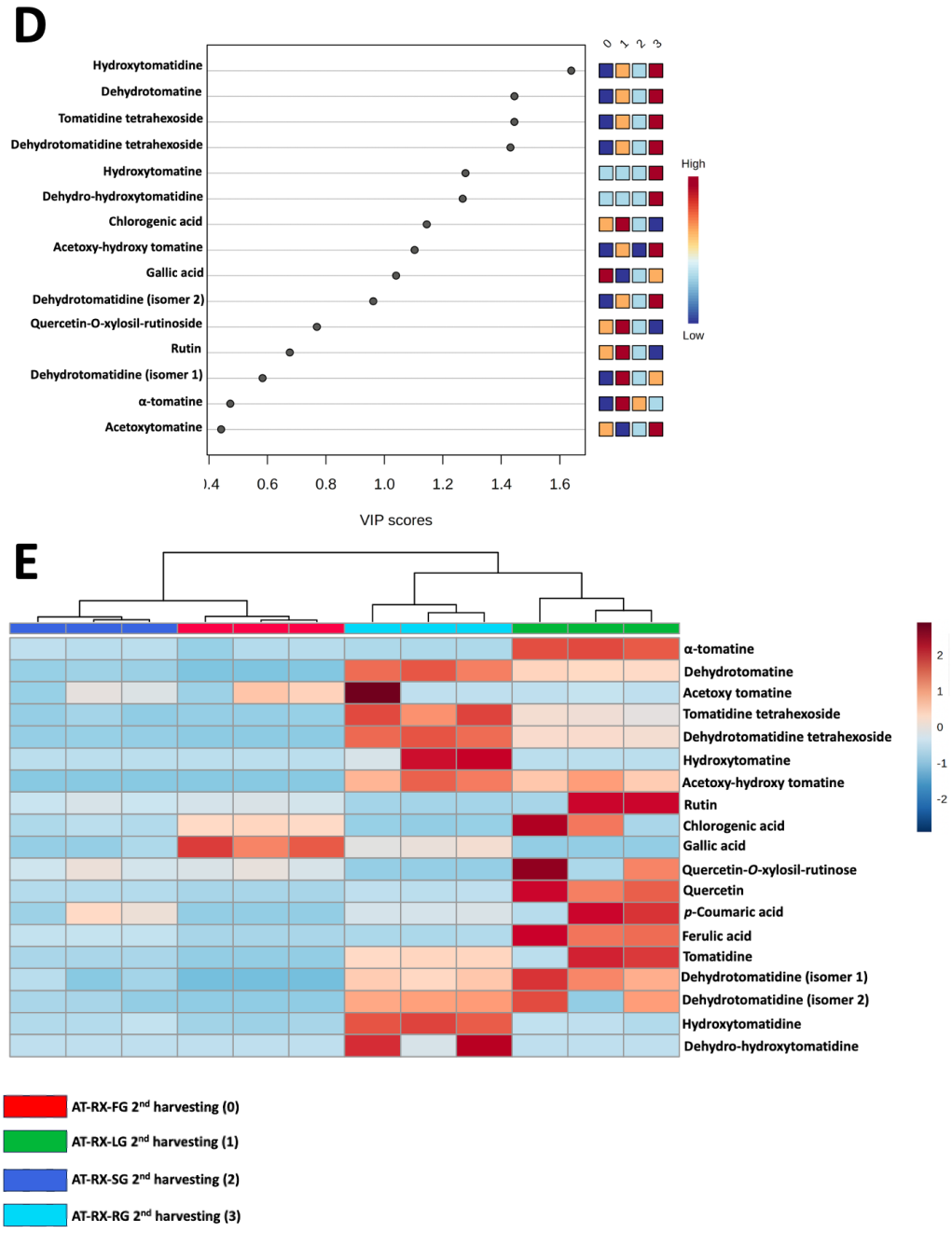


Figure S37: Multivariate analysis of different anatomical parts of Piennolo tomato plants in second-harvesting treated samples. (**D**) Variable importance on projection (VIP) scores from the PLS-DA model, indicating the most discriminating metabolites between samples in descending order of importance and with relative levels of metabolites for each matrix. (**E**) Heatmap with Hierarchical clustering, illustrating the relative metabolite concentration among groups. The corresponding relative metabolite concentration is expressed as a color of different intensity from blue (lowest amount) to red (highest amount).

Sample	α-tomatine	Dehydrotomatine	Acetoxytomatine	Tomatidine tetrahexoside	Acetoxy-hydroxy tomatine
	mg α-tomatine/ g DW	µg α-tomatine equivalents/ g DW			
A-RX-FG 1st harvesting	2,90 ± 0,41 ^{a,b}	161,11 ± 6,87 ^{a}	98,80 ± 4,60 ^{a,c}	18,00 ± 1,50 ^{a}	nd
AT-RX-FG 1st harvesting	3,76 ± 0,39 ^{b}	207,67 ± 11,59 ^{a}	93,75 ± 2,84 ^{a,b}	17,87 ± 1,55 ^{a}	nd
A-RX-FG 2nd harvesting	2,06 ± 0,19 ^{a}	143,19 ± 6,81 ^{a}	79,80 ± 9,22 ^{b}	15,53 ± 1,76 ^{a,b}	nd
AT-RX-FG 2nd harvesting	3,90 ± 0,55 ^{b}	258,81 ± 25,96 ^{b}	142,93 ± 8,88 ^{e}	26,11 ± 1,06 ^{c}	nd
AS-RX-FG	3,44 ± 0,02 ^{b}	233,90 ± 5,34 ^{b}	111,78 ± 5,06 ^{c,d}	27,36 ± 0,77 ^{c}	nd
AST-RX-FG	2,99 ± 0,49 ^{a,b}	173,35 ± 9,09 ^{a}	121,90 ± 1,88 ^{d}	14,68 ± 1,29 ^{b}	nd

Table S1: Content of five selected glycoalkaloids in treated and untreated green fruits (FG), indicated as mg α-tomatine/g dried matrix and µg α-tomatine equivalents/g dried matrix. Results are expressed as mean ± SD. Statistical significance was calculated by one-way ANOVA followed by Tukey's post-hoc test. Different letters in each bar reveal significant differences ($p < 0.05$). "nd" means "not detected".

Sample	Rutin	Chlorogenic acid	Gallic acid	Quercetin O-xylosylrutinoside	Quercetin	p-coumaric acid	Ferulic acid
	mg / g DW						
A-RX-FG 1st harvesting	333,62 ± 139,61^{a}	350,95 ± 164,82 ^{a}	90,66 ± 45,02 ^{a}	252,19 ± 104,48 ^{a}	nd ^{a}	6,23 ± 3,77 ^{a}	5,55 ± 2,23 ^{a}
AT-RX-FG 1st harvesting	874,92 ± 243,10 ^{b}	408,88 ± 81,45 ^{a}	97,12 ± 23,34 ^{a}	285,18 ± 57,63 ^{a}	15,65 ± 2,83 ^{b}	10,82 ± 1,39 ^{b}	12,44 ± 4,57 ^{c}
A-RX-FG 2nd harvesting	706,06 ± 33,29 ^{b}	337,92 ± 18,16 ^{a}	111,54 ± 8,822 ^{a}	242,71 ± 27,65 ^{a}	nd ^{a}	12,32 ± 0,85 ^{b}	9,69 ± 2,30 ^{a,c}
AT-RX-FG 2nd harvesting	849,22 ± 61,92 ^{b}	583,92 ± 24,3 ^{b}	97,64 ± 12,38 ^{a}	276,61 ± 42,03 ^{a}	nd ^{a}	nd ^{c}	9,24 ± 1,42 ^{a,c}
AS-RX-FG	765,62 ± 38,14 ^{b}	451,19 ± 8,62 ^{a,b}	120,32 ± 12,55 ^{a}	258,33 ± 11,65 ^{a}	nd ^{a}	nd ^{c}	nd ^{b}
AST-RX-FG	717,60 ± 24,05 ^{b}	479,55 ± 20,74 ^{a,b}	100,51 ± 27,18 ^{a}	245,32 ± 3,51 ^{a}	nd ^{a}	6,66 ± 0,00 ^{a}	8,86 ± 1,77 ^{a,c}

Table S2: Content of seven selected polyphenols in treated and untreated green fruits (FG), indicated as mg polyphenol/g dried matrix. Quercetin *O*-xylosylrutinoside is quantified as mg rutin/g dried matrix. Results are expressed as mean ± SD. Statistical significance was calculated by one-way ANOVA followed by Tukey's post-hoc test. Different letters in each bar reveal significant differences ($p < 0.05$). "nd" means "not detected".

Sample	Tomatidine	Dehydrotomatidine (isomer 1)	Dehydrotomatidine (isomer 2)	Hydroxy tomatidine	Dehydro-hydroxy tomatidine (isomer 1)	Dehydro-hydroxy tomatidine (isomer 2)
		µg / g DW				
A-RX-FG 1st harvesting	nd [a]	nd	nd	nd [a]	nd	nd
AT-RX-FG 1st harvesting	229,27 ± 60,37 [c]	nd	nd	71,97 ± 15,35 [c]	nd	nd
A-RX-FG 2nd harvesting	59,44 ± 8,40 [a,b]	nd	nd	17,81 ± 0,10 [b]	nd	nd
AT-RX-FG 2nd harvesting	nd [a]	nd	nd	36,47 ± 10,27 [b]	nd	nd
AS-RX-FG	nd [a]	nd	nd	34,75 ± 4,80 [b]	nd	nd
AST-RX-FG	93,80 ± 29,07 [b]	nd	nd	27,85 ± 6,64 [b]	nd	nd

Table S3: Content of six selected steroidal alkaloids in treated and untreated green fruits (FG), indicated as µg tomatidine/g dried matrix and µg tomatidine equivalents/g dried matrix. Results are expressed as mean ± SD. Statistical significance was calculated by one-way ANOVA followed by Tukey's post-hoc test. Different letters in each bar reveal significant differences ($p < 0.05$). "nd" means "not detected".

Sample	Rutin	Chlorogenic acid	Gallic acid	Quercetin-*O*-xylosylrutinoside	Quercetin	*p*-coumaric acid	Ferulic acid
	µg / g DW						
A-RX-RG 1st harvesting	67,67 ± 8,88 [a]	59,28 ± 5,79 [a,b]	12,56 ± 1,81 [a]	19,86 ± 2,89 [a]	9,80 ± 1,04 [a,c]	4,34 ± 0,29 [a,c]	15,56 ± 1,94 [a]
AT-RX-RG 1st harvesting	40,86 ± 5,28 [a,b]	12,68 ± 1,04 [c]	26,36 ± 7,98 [a,b]	5,42 ± 2,20 [a]	9,64 ± 1,40 [a,c]	nd [b]	9,45 ± 1,16 [a,c]
A-RX-RG 2nd harvesting	19,11 ± 4,78 [b]	52,72 ± 6,21 [a,b]	20,25 ± 1,15 [a,b]	nd [a]	nd [b]	nd [b]	nd [b]
AT-RX-RG 2nd harvesting	6,79 ± 1,65 [b]	38,91 ± 8,41 [a]	35,31 ± 4,27 [b]	nd [a]	12,19 ± 0,67 [c]	5,28 ± 0,25 [c]	13,78 ± 2,35 [a]
AS-RX-RG	36,89 ± 11,10 [a,b]	47,17 ± 15,45 [a,b]	28,97 ± 9,88 [b]	2,58 ± 0,40 [a]	9,41 ± 2,67 [a,c]	3,87 ± 0,97 [a]	6,97 ± 2,26 [c]
AST-RX-RG	211,78 ± 36,69 [c]	70,38 ± 15,82 [b]	31,01 ± 6,92 [b]	115,35 ± 28,51 [b]	6,45 ± 1,51 [a]	nd [b]	15,45 ± 4,23 [a]

Table S4: Content of seven selected polyphenols in treated and untreated roots (RG), indicated as µg polyphenol/g dried matrix. Quercetin *O*-xylosylrutinoside is quantified as mg rutin/g dried matrix. Results are expressed as mean ± SD. Statistical significance was calculated by one-way ANOVA followed by Tukey's post-hoc test. Different letters in each bar reveal significant differences ($p < 0.05$). "nd" means "not detected".

Sample	α-tomatine	Dehydro tomatine	Acetoxy tomatine	Tomatidine tetrahexoside	Dehydrotomatidine tetrahexoside	Hydroxy tomatine	Acetoxy-hydroxy tomatine
	mg α-tomatine/ g DW	µg α-tomatine equivalents/ g DW					
A-RX-LG 1st harvesting	36,86 ± 2,13 [d]	3355,73 ± 134,50 [a]	36,12 ± 5,44 [a,b]	92,58 ± 8,86 [a,c]	18,71 ± 1,41 [a,b]	nd	1,98 ± 0,32 [a]
AT-RX-LG 1st harvesting	43,09 ± 1,48 [a,b]	3120,54 ± 44,86 [a,c]	35,88 ± 2,52 [a,b]	77,25 ± 1,54 [a,b]	12,92 ± 0,05 [b]	nd	nd [b]
A-RX-LG 2nd harvesting	46,39 ± 0,58 [b]	3733,96 ± 55,29 [b]	42,84 ± 2,01 [b,c]	105,87 ± 2,64 [c]	20,32 ± 0,68 [c]	nd	nd [b]
AT-RX-LG 2nd harvesting	38,71 ± 1,04 [d]	3130,38 ± 120,12 [a,c]	47,59 ± 4,30 [c]	90,50 ± 7,56 [a,b]	17,18 ± 0,75 [a]	nd	1,55 ± 0,28 [a]
AS-RX-LG	30,92 ± 2,98 [c]	2899,37 ± 133,54 [c]	30,92 ± 2,98 [a]	83,39 ± 3,84 [a,b]	14,79 ± 0,76 [b]	0,66 ± 0,01	nd [b]
AST-RX-LG	41,09 ± 1,16 [a,d]	3252,74 ± 246,15 [a,c]	27,07 ± 2,83 [a]	75,97 ± 8,32 [b]	17,22 ± 1,06 [a]	nd	nd [b]

Table S5: Content of seven selected glycoalkaloids in treated and untreated leaves (LG), indicated as mg α-tomatine/g dried matrix and µg α-tomatine equivalents/g dried matrix. Results are expressed as mean ± SD. Statistical significance was calculated by one-way ANOVA followed by Tukey's post-hoc test. Different letters in each bar reveal significant differences ($p < 0.05$). "nd" means "not detected".

Sample	Rutin	Chlorogenic acid	Gallic acid	Quercetin-*O*-xylosylrutinoside	Quercetin	*p*-coumaric acid	Ferulic acid
		µg / g DW					
A-RX-LG 1st harvesting	4454,37 ± 195,13 [a,b]	619,84 ± 27,78 [a]	16,57 ± 0,98 [a]	1050,10 ± 34,59 [a]	56,84 ± 5,01 [a]	22,51 ± 0,19 [a,c]	102,64 ± 9,66 [a,b]
AT-RX-LG 1st harvesting	3243,87 ± 234,50 [a]	320,64 ± 13,04 [a]	nd [b]	895,65 ± 23,69 [a]	54,45 ± 2,72 [a]	18,30 ± 2,08 [a,b]	141,27 ± 8,40 [a]
A-RX-LG 2nd harvesting	6621,38 ± 748,58 [c]	579,15 ± 74,98 [a]	nd [b]	1166,45 ± 172,49 [a]	156,56 ± 4,01 [b]	16,03 ± 1,77 [b]	245,96 ± 29,72 [c,d]
AT-RX-LG 2nd harvesting	5814,35 ± 1409,63 [b,c]	1280,95 ± 315,05 [b]	nd [b]	1022,57 ± 336,73 [a]	146,90 ± 27,45 [b]	24,78 ± 2,28 [c]	207,74 ± 37,38 [c]
AS-RX-LG	5344,94 ± 440,64 [b,c]	1076,88 ± 93,40 [b]	nd [b]	1259,71 ± 97,25 [a]	80,38 ± 28,79 [a]	26,93 ± 2,45 [c,d]	296,86 ± 30,89 [d]
AST-RX-LG	4651,38 ± 307,39 [a,b]	1046,42 ± 39,66 [b]	34,11 ± 1,65 [c]	1288,45 ± 107,70 [a]	59,99 ± 5,25 [a]	30,03 ± 2,64 [d]	56,18 ± 5,45 [b]

Table S6: Content of seven selected polyphenols in treated and untreated leaves (LG), indicated as µg polyphenol/g dried matrix. Quercetin *O*-xylosylrutinoside is quantified as mg rutin/g dried matrix. Results are expressed as mean ± SD. Statistical significance was calculated by one-way ANOVA followed by Tukey's post-hoc test. Different letters in each bar reveal significant differences ($p < 0.05$). "nd" means "not detected".

Sample	Tomatidine	Dehydro tomatidine (isomer 1)	Dehydro tomatidine (isomer 2)	Hydroxy tomatidine	Dehydro-hydroxy tomatidine (isomer 1)	Dehydro-hydroxy tomatidine (isomer 2)
		µg / g DW				
A-RX-LG 1st harvesting	618,38 ± 59,92 [a]	nd [a]	nd [a]	35,63 ± 9,51 [a]	nd	nd
AT-RX-LG 1st harvesting	443,87 ± 58,70 [a]	nd [a]	nd [a]	nd [b]	nd	nd
A-RX-LG 2nd harvesting	326,67 ± 54,30 [a]	nd [a]	nd [a]	nd [b]	nd	nd
AT-RX-LG 2nd harvesting	5712,39 ± 909,61 [b]	0,69 ± 0,16 [b]	629,43 ± 108,23 [b]	80,88 ± 14,23 [c]	nd	nd
AS-RX-LG	658,09 ± 43,87 [a]	nd [a]	nd [a]	nd [b]	nd	nd
AST-RX-LG	189,06 ± 47,84 [a]	nd [a]	nd [a]	nd [b]	nd	nd

Table S7: Content of six selected steroidal alkaloids in treated and untreated leaves (LG), indicated as µg tomatidine/g dried matrix and µg tomatidine equivalents/g dried matrix. Results are expressed as mean ± SD. Statistical significance was calculated by one-way ANOVA followed by Tukey's post-hoc test. Different letters in each bar reveal significant differences ($p < 0.05$). "nd" means "not detected".

Sample	α-tomatine	Dehydrotomatine	Acetoxytomatine	Tomatidine tetrahexoside	Dehydrotomatidine tetrahexoside
	mg α-tomatine/ g DW	µg α-tomatine equivalents/ g DW			
A-RX-SG 1st harvesting	2,52 ± 0,30 [a]	257,02 ± 22,26 [a]	11,55 ± 0,70 [a]	12,35 ± 3,90 [a]	nd [a]
AT-RX-SG 1st harvesting	4,43 ± 0,15 [b]	523,80 ± 3,56 [b]	47,80 ± 3,71 [b]	21,36 ± 0,64 [a,b]	nd [a]
A-RX-SG 2nd harvesting	4,54 ± 0,20 [b]	624,59 ± 77,61 [b]	46,30 ± 4,71 [b]	24,63 ± 4,22 [b]	0,59 ± 0,01 [a]
AT-RX-SG 2nd harvesting	5,25 ± 0,36 [c]	787,68 ± 79,41 [c]	79,04 ± 7,43 [c]	28,45 ± 6,96 [b]	1,02 ± 0,13 [b]
AS-RX-SG	3,20 ± 0,21 [d]	530,12 ± 40,29 [b]	42,06 ± 1,08 [b]	20,71 ± 2,69 [a,b]	nd [a]
AST-RX-SG	4,49 ± 0,09 [b]	582,10 ± 14,09 [b]	49,79 ± 1,87 [b]	20,90 ± 1,31 [a,b]	nd [a]

Table S8: Content of five selected glycoalkaloids in treated and untreated stems (SG), indicated as mg α-tomatine/g dried matrix and µg α-tomatine equivalents/g dried matrix. Results are expressed as mean ± SD. Statistical significance was calculated by one-way ANOVA followed by Tukey's post-hoc test. Different letters in each bar reveal significant differences ($p < 0.05$). "nd" means "not detected".

Sample	Rutin	Chlorogenic acid	Gallic acid	Quercetin-*O*-xylosylrutinoside	Quercetin	*p*-coumaric acid	Ferulic Acid
	µg / g DW						
A-RX-SG 1st harvesting	296,05 ± 36,90 [a]	41,10 ± 4,23 [a,b]	13,67 ± 2,27 [a,b]	147,16 ± 17,5 [a]	nd [a]	6,29 ± 0,60 [a]	7,40 ± 1,06 [a]
AT-RX-SG 1st harvesting	400,20 ± 2,12 [a,b]	190,91 ± 9,26 [c]	17,28 ± 0,71 [c]	187,21 ± 6,48 [a,b]	nd [a]	8,27 ± 0,37 [b]	10,63 ± 0,80 [c]
A-RX-SG 2nd harvesting	756,54 ± 83,92 [c]	59,10 ± 5,29 [a]	12,87 ± 1,01 [a]	194,86 ± 16,38 [a,b]	10,64 ± 0,25 [b]	5,67 ± 0,43 [a]	22,64 ± 0,89 [b]
AT-RX-SG 2nd harvesting	696,93 ± 153,57 [c]	157,03 ± 35,51 [c]	11,18 ± 1,74 [a]	259,48 ± 70,30 [b,c]	7,51 ± 0,314 [c]	7,95 ± 1,14 [b]	31,72 ± 0,43 [d]
AS-RX-SG	488,37 ± 23,50 [b]	255,25 ± 27,52 [d]	16,43 ± 1,57 [b,c]	322,23 ± 13,73 [c]	nd [a]	8,07 ± 0,56 [b]	8,87 ± 0,45 [a,c]
AST-RX-SG	488,89 ± 13,29 [b]	14,11 ± 0,91 [b]	12,05 ± 1,63 [a]	139,54 ± 3,15 [a]	nd [a]	nd [c]	9,67 ± 1,86 [c]

Table S9: Content of seven selected polyphenols in treated and untreated stems (SG), indicated as µg polyphenol/g dried matrix. Quercetin *O*-xylosylrutinoside is quantified as mg rutin/g dried matrix. Results are expressed as mean ± SD. Statistical significance was calculated by one-way ANOVA followed by Tukey's post-hoc test. Different letters in each bar reveal significant differences ($p < 0.05$). "nd" means "not detected".

Sample	Tomatidine	Dehydrotomatidine (isomer 1)	Dehydro tomatidine (isomer 2)	Hydroxy tomatidine	Dehydro-hydroxy tomatidine (isomer 1)	Dehydro-hydroxy tomatidine (isomer 2)
		µg / g DW				
A-RX-SG 1st harvesting	1049,84 ± 138,43 [a]	0,15 ± 0,02 [a]	nd [a]	74,59 ± 8,69 [a]	nd	nd
AT-RX-SG 1st harvesting	74,67 ± 9,02 [b]	nd [b]	nd [a]	35,94 ± 5,57 [b]	nd	nd
A-RX-SG 2nd harvesting	141,57 ± 7,00 [b]	nd [b]	21,63 ± 3,62 [b]	56,47 ± 9,18 [a,b]	nd	nd
AT-RX-SG 2nd harvesting	397,35 ± 3,44 [c,d]	0,12 ± 0,06 [a]	63,60 ± 6,55 [c]	77,30 ± 16,91 [a]	nd	nd
AS-RX-SG	499,93 ± 87,42 [c]	nd [b]	22,66 ± 1,44 [b]	49,78 ± 9,80 [b]	nd	nd
AST-RX-SG	326,44 ± 25,04 [d]	nd [b]	nd [a]	nd [c]	nd	nd

Table S10: Content of six selected steroidal alkaloids in treated and untreated stems (SG), indicated as µg tomatidine/g dried matrix and µg tomatidine equivalents/g dried matrix. Results are expressed as mean ± SD. Statistical significance was calculated by one-way ANOVA followed by Tukey's post-hoc test. Different letters in each bar reveal significant differences ($p < 0.05$). "nd" means "not detected".

Sample	µmol TE/g dried matrix
S. Sebastiano discarded green tomatoes, 1st harvesting	24,89 ± 1,61 [a]
S. Sebastiano discarded green tomatoes, 2nd harvesting	28,14 ± 2,09 [a,b]
Ercolano discarded green tomatoes, 1st harvesting	30,42 ± 3,23 [b,c]
Ercolano discarded green tomatoes, 2nd harvesting	34,36 ± 1,08 [c]

Table S11: Results of the FRAP method for *S. Sebastiano* and *Ercolano* green tomato cultivars. The results are expressed as µmol TE/g dried matrix ± SD. Statistical significance was calculated by one-way ANOVA followed by Tukey's post-hoc test. Different letters in each bar reveal significant differences ($p < 0.05$). "nd" means "not detected".

Sample	µmol TE/ g dried matrix ± SD
S. Sebastiano discarded green tomatoes, 1st harvesting	21,21 ± 3,31 [a]
S. Sebastiano discarded green tomatoes, 2nd harvesting	24,12 ± 1,30 [a]
Ercolano discarded green tomatoes, 1st harvesting	27,67 ± 3,75 [a]
Ercolano discarded green tomatoes, 2nd harvesting	26,68 ± 2,63 [a]

Table S12: Results of the DPPH method for *S. Sebastiano* and *Ercolano* green tomato cultivars. The results are expressed as µmol TE/g dried matrix ± SD. Statistical significance was calculated by one-way ANOVA followed by Tukey's post-hoc test. Different letters in each bar reveal significant differences ($p < 0.05$). "nd" means "not detected".

Sample	mg AGE/ g dried matrix ± SD
A-FG 1st harvesting	3,35 ± 0,23 [a,b,c]
AT-FG 1st harvesting	3,82 ± 0,27 [b,c]
A-FG 2nd harvesting	2,82 ± 0,33 [a]
AT-FG 2nd harvesting	3,61 ± 0,24 [b,c]
AS-FG	3,98 ± 0,35 [c]
AST-FG	3,17 ± 0,07 [a,b]

Table S13: Results of the Folin-Ciocalteau method for treated and untreated green tomato (FG). The results are expressed as µmol GAE/g dried matrix ± SD. Statistical significance

was calculated by one-way ANOVA followed by Tukey's post-hoc test. Different letters in each bar reveal significant differences ($p < 0.05$). "nd" means "not detected".

Sample	µmol TE/ g dried matrix ± SD
A-FG 1st harvesting	22,20 ± 4,81 [a]
AT-FG 1st harvesting	22,02 ± 2,68 [a]
A-FG 2nd harvesting	29,32 ± 1,68 [a]
AT-FG 2nd harvesting	29,75 ± 4,92 [a]
AS-FG	26,33 ± 2,57 [a]
AST-FG	24,82 ± 1,71 [a]

Table S14: Results of the DPPH method for treated and untreated green tomato (FG). The results are expressed as µmol TE/g dried matrix ± SD. Statistical significance was calculated by one-way ANOVA followed by Tukey's post-hoc test. Different letters in each bar reveal significant differences ($p < 0.05$). "nd" means "not detected".

Sample	µmol TE/ g dried matrix ± SD
A-RX-FG 1st harvesting	61,18 ± 6,15 [a]
AT-RX-FG 1st harvesting	34,34 ± 5,20 [a,b]
A-RX-FG 2nd harvesting	30,55 ± 3,97 [a,b]
AT-RX-FG 2nd harvesting	35,80 ± 5,63 [a,b]
AS-RX-FG	40,81 ± 6,58 [a,b]
AST-RX-FG	48,97 ± 4,68 [a]

Table S15: Results of the DPPH method for treated and untreated green tomato (RX-FG). The results are expressed as µmol TE/g dried matrix ± SD. Statistical significance was calculated by one-way ANOVA followed by Tukey's post-hoc test. Different letters in each bar reveal significant differences ($p < 0.05$). "nd" means "not detected".

Sample	µmol TE/ g dried matrix ± SD
A-RX-SG 1st harvesting	28,63 ± 2,75 [a,b]
AT-RX-SG 1st harvesting	34,65 ± 1,71 [b]
A-RX-SG 2nd harvesting	32,49 ± 1,63 [a,b]
AT-RX-SG 2nd harvesting	54,05 ± 3,03 [c]
AS-RX-SG	35,18 ± 4,31 [b]
AST-RX-SG	26,95 ± 2,61 [a]

Table S16: Results of the DPPH method for treated and untreated stems (RX-SG). The results are expressed as µmol TE/g dried matrix ± SD. Statistical significance was calculated by one-way ANOVA followed by Tukey's post-hoc test. Different letters in each bar reveal significant differences ($p < 0.05$). "nd" means "not detected".

Sample	mg AGE/ g dried matrix ± SD
A-RX-SG 1st harvesting	2,72 ± 0,40 [a]
AT-RX-SG 1st harvesting	3,20 ± 0,25 [a,b]
A-RX-SG 2nd harvesting	3,55 ± 0,32 [b,c]
AT-RX-SG 2nd harvesting	4,07 ± 0,00 [c]
AS-RX-SG	3,07 ± 0,28 [a,b]
AST-RX-SG	2,47 ± 0,41 [a]

Table S17: Results of the Folin-Ciocalteau method for treated and untreated stems (RX-SG). The results are expressed as µmol GAE/g dried matrix ± SD. Statistical significance was calculated by one-way ANOVA followed by Tukey's post-hoc test. Different letters in each bar reveal significant differences ($p < 0.05$). "nd" means "not detected".

Sample	mg AGE/ g dried matrix ± SD
A-RX-LG 1st harvesting	4,90 ± 0,38 [a]
AT-RX-LG 1st harvesting	4,58 ± 0,14 [a]
A-RX-LG 2nd harvesting	6,52 ± 0,29 [b]
AT-RX-LG 2nd harvesting	6,80 ± 0,32 [b]
AS-RX-LG	6,17 ± 0,91 [b]
AST-RX-LG	5,99 ± 0,34 [b]

Table S18: Results of the Folin-Ciocalteau method for treated and untreated leaves (RX-LG). The results are expressed as µmol GAE/g dried matrix ± SD. Statistical significance

was calculated by one-way ANOVA followed by Tukey's post-hoc test. Different letters in each bar reveal significant differences ($p < 0.05$). "nd" means "not detected".

Sample	µmol TE/g dried matrix
A-RX-LG 1st harvesting	74,54 ± 6,84 [a,b]
A-RX-LG 2nd harvesting	101,45 ± 8,56 [b,c]
AT-RX-LG 1st harvesting	69,31 ± 5,55 [a]
AT-RX-LG 2nd harvesting	119,78 ± 4,86 [c]
AS-RX-LG	115,69 ± 23,91 [c]
AST-RX-LG	101,17 ± 9,14 [b,c]

Table S19: Results of the FRAP method for treated and untreated leaves (RX-LG). The results are expressed as µmol TE/g dried matrix ± SD. Statistical significance was calculated by one-way ANOVA followed by Tukey's post-hoc test. Different letters in each bar reveal significant differences ($p < 0.05$). "nd" means "not detected".

Sample	µmol TE/ g dried matrix ± SD
A-RX-LG 1st harvesting	162,64 ± 3,60 [a]
AT-RX-LG 1st harvesting	152,13 ± 5,54 [a]
A-RX-LG 2nd harvesting	198,35 ± 18,52 [a]
AT-RX-LG 2nd harvesting	198,11± 42,92 [a]
AS-RX-LG	154,12 ± 3,86 [a]
AST-RX-LG	172,23 ± 5,36 [a]

Table S20: Results of the DPPH method for treated and untreated leaves (RX-LG). The results are expressed as µmol TE/g dried matrix ± SD. Statistical significance was calculated by one-way ANOVA followed by Tukey's post-hoc test. Different letters in each bar reveal significant differences ($p < 0.05$). "nd" means "not detected".

Sample	mg AGE/ g dried matrix ± SD
A-RX-RG 1st harvesting	2,32 ± 0,12 [a]
AT-RX-RG 1st harvesting	2,58 ± 0,50 [a,b]
A-RX-RG 2nd harvesting	2,51 ± 0,42 [a,b]
AT-RX-RG 2nd harvesting	2,90 ± 0,17 [a,b]
AS-RX-RG	3,12 ± 0,04 [b]
AST-RX-RG	2,67 ± 0,12 [a,b]

Table S21: Results of the Folin-Ciocalteau method for treated and untreated roots (RX-RG). The results are expressed as µmol GAE/g dried matrix ± SD. Statistical significance was calculated by one-way ANOVA followed by Tukey's post-hoc test. Different letters in each bar reveal significant differences ($p < 0.05$). "nd" means "not detected".

Sample	µmol TE/ g dried matrix ± SD
A-RX-RG 1st harvesting	18,82 ± 3,90 [a]
AT-RX-RG 1st harvesting	47,53 ± 7,44 [b]
A-RX-RG 2nd harvesting	55,57 ± 4,61 [b,c]
AT-RX-RG 2nd harvesting	68,35 ± 7,50 [c]
AS-RX-RG	49,44 ± 8,05 [b,c]
AST-RX-RG	49,38 ± 12,22 [b,c]

Table S22: Results of the DPPH method for treated and untreated roots (RX-RG). The results are expressed as µmol TE/g dried matrix ± SD. Statistical significance was calculated by one-way ANOVA followed by Tukey's post-hoc test. Different letters in each bar reveal significant differences ($p < 0.05$). "nd" means "not detected".

Sample	µmol TE/g dried matrix
A-RX-RG 1st harvesting	25,15 ± 0,58 [a]
A-RX-RG 2nd harvesting	26,68 ± 0,42 [a]
AT-RX-RG 1st harvesting	25,78 ± 5,00 [a]
AT-RX-RG 2nd harvesting	31,35 ± 3,62 [a]
AS-RX-RG	23,05 ± 5,29 [a]
AST-RX-RG	24,53 ± 4,92 [a]

Table S23: Results of the FRAP method for treated and untreated roots (RX-RG). The results are expressed as µmol TE/g dried matrix ± SD. Statistical significance was calculated by one-way ANOVA followed by Tukey's post-hoc test. Different letters in each bar reveal significant differences ($p < 0.05$). "nd" means "not detected".

ABREVIATIONS AND ACRONYMS

AA	Annurca Apple
AcOH	Acetic acid
Agl	Aglycone
ABTS	2,20-azinobis(3-ethylbenzotiazoline-6-sulfonate)
AGEs	Advance glycation end-products
ANOVA	Analysis of Variance
AT	“Avellino” tomatoes
ATCC	American type Culture Collection
Akt	Protein kinase B
ATF4	Activating transcription factor 4
BCA	Biological control agent
BSA	Bovin Serum Albumin
BSTFA	N,O-Bis(trimethylsilyltrifluoroacetamide
CA	Caffeic acid
CD	Control diet
CE	Capillary electrophoresis
CT	“Cuore di bue” tomatoes
CHIKV	Chikungunya virus
COSY	^{1}H-^{1}H Correlated Spectroscopy
COX-2	Cyclooxygenase-2
CSA	Cross-sectional area
CTR	Control
CV%	Coefficient of variation %
DAD	Diode array detector
DAMPs	Damage-associated molecular patterns

DDA	Data dependent acquisition
DDVP	Dichlorvos
DEJ	Dermal-epidermal junction
DENV	Dengue virus
DMEM	Dulbecco's modifies Eagle medium
DMSO	Dimethylsulfoxide
DPPH	Radical 2,2-diphenyl-1-picrylhydrazyl
DT	"Datterini" tomatoes
DW	Dry weight
EC	European Council
ECM	Extracellular matrix
EC_{50}	Concentration require to obtain the 50% of the effect
EFSA	European Food Safety Authority
ELS	Evaporative light scattering
ERK	Extracellular signal regulated kinase
ESI	Electrospray ionization
EWGSOP	European Working Group on Sarcopenia in Older People
FAO STAT	Food and Agriculture Organization of the United Nations
FBS	Fetal Bovine Serum
FLD	Fluorimetric detector
FRAP	Ferric reducing antioxidant power
FS	Full scan
FTICR	Fourier transform ion cyclotron resonance
FOXO1	Forkhead box protein O1
GABA	γ-aminobutirric acid

Gadd45a	Growth arrest and DNA damage 45-α
GAE	Gallic acid equivalent
GC	Gas chromatography
GCLC	Glutamate-cysteine ligase catalytic subunit
GCLM	Glutamate-cysteine ligase modifier subunit
GT	Green tomatoes
GPT2	Glutamic-pyruvic aminotransferase
HAD	Hydrogen atom donor
HESI	Heated electrospray ionization
Hex	Hexoside
HILIC	Hydrophilic interaction liquid chromatography
HMOX-1	Heme oxygenase-1-enzyme
HPLC	High performance liquid chromatography
HRF	Heterocyclic ring fission
HTS	High Throughput Screening
HSQC	^{1}H-^{13}C Heteronuclear Single Quantum Coherence
HSV	Herpes simplex virus
H/E	Haematoxylin Eosin
IL	Interleukin
ISF	Isotopic fine distribution
i.v.	Intravenous
iNOS	Inducible nitric oxide synthase
JA	Jasmonic acid
LC	Liquid chromatography
LD_{50}	Lethal dose for 50% of population

LGT	Lyophilized green tomatoes
LLE	Liquid-liquid extraction
LOD	Limit of detection
LOQ	Limit of quantification
LS	Long-storage
MAFbx	E3-ubiquitin-ligase-atrogin-1
MAMPs	Microorganism-associated molecular patterns
MFI	Mean Fluorescence intensity
MHC	Myosin heavy chain
MITF	Microphtalmia-associated transcription factor
MRM	Multiple reaction monitoring
MS	Mass spectrometry
MS/MS	Tandem mass spectrometry
mTORC1	Mammalian target of rapamycin complex 1
MuRF-1	Muscle RING-finger protein-1
myoD	myoblast determination protein
NF-κB	Nuclear factor κB
NMR	Nuclear Magnetic Resonance
NOXs	NADPH oxidases
OAAO	Optimized Annurca Apple Oleolyte
OD	Optical density
PAD	Pulsed amperometry detector
PAHs	Polyclic aromatic hydrocarbons
Pax7	Paired box protein 7
PCA	Principal component analysis

Pent	Pentoside
PGC1-α	Peroxisome Proliferator Receptor γ Coactivator 1α
PGE2	Prostaglandin E2
PGPF	Plant growth-promoting fungi
PI3K	Phosphoinositide 3-kinase
PLS-DA	Partial Least Square Discriminant analysis
p.o.	Oral administration
POM	Polyoxymethylene
Ppb	Parts per billion
Ppm	Parts per million
PRRs	Pattern-recognition receptors
PDO	Protected designation of Origin
QA	Quinic acid
QM	Quinone methide cleavage
Q-TOF MS	Quadropole time-of-flight mass spectrometer
RDA	Retro Diels-Alder fission
RI	Refractive index
RP	Reverse phase
RNS	Reactive nitrogen species
RONS	Reactive oxygen and nitrogen species
ROS	Reactive oxygen species
RPS16	Ribosomal protein S16
RSM	Response Surface Methodology
Rut	Rutinoside
SAM	S-adenosyl-L-methionine

SANA	Succinyl-(Ala)-3-*p*-nitroanilide
SCVs	*Staphylococcus aureus* small-colony variants
SCX	Sulphonic acid cation exchanger
SD	Standard deviation
SEM	Standard error of mean
SET	Single Electron Transfer
SGA	Steroidal Glycoalkaloid
SGF	Simulated gastric fluid
SIF	Simulated intestinal fluid
SSF	Simulated salivary fluid
SGLT	Sodium Glucose Linked Transporter
SIM	Single Ion Monitoring
S/N	Signal to Noise
SPE	Solid Phase Extraction
sRNA	small RNA
ST	“Sorrento” tomatoes
S6K1	S6 kinase 1
T2DM	Type 2 Diabetes mellitus
TD	Tomatidine
TE	Trolox equivalent
TIC	Total current ion
TT	“Tondi” tomatoes
TEWL	Transepidermal water loss
TLC	Thin layer chromatography
TMRM	Tetramethylrhodamine methyl ester

TNF-α	Tumor necrosis factor α
TRPs	Tyrosinase-related proteins
TPC	Total phenolic content
TPS	Sodium 3-trimethylsilyl-tetradeuteriopropionate
TPTZ	2,4,6-tris(2-pyridyl)-s-triazine
TSS	Total soluble solid
TYR	Tyrosinase
t/2	Half time
UAE	Ultrasound assisted extraction
UDP-Glc	Glucose Uridine diphosphate
UV	Ultraviolet
VIP	Variable Important for Projection
Xyl	Xylose
α-MSH	α-Melanocyte stimulating hormone
α-TM	α-Tomatine
β1-TM	β1-Tomatine
β2-TM	β2-Tomatine
γ-TM	γ-Tomatine
δ-TM	δ-Tomatine
4EBP1	4E binding protein 1

LIST OF PUBLICATIONS

- Maisto M., Annunziata G., Schiano E., **Piccolo V.**, Iannuzzo F., Santangelo R., Ciampaglia R., Tenore G.C., Novellino E., Grieco P. Potential Functional Snacks: Date Fruit Bars Supplemented by Different Species of Lactobacillus spp. *Foods.* **2021**, 10(8),1760.

- Schiano E., **Piccolo V.**, Novellino E., Maisto M., Iannuzzo F., Summa V., Tenore G. C. Thinned Nectarines, an Agro-Food Waste with Antidiabetic Potential: HPLC-HESI-MS/MS Phenolic Characterization and In Vitro Evaluation of Their Beneficial Activities. *Foods.* **2022**, 11(7), 1010.

- Maisto M., Schiano E., Novellino E., **Piccolo V.**, Iannuzzo F., Salviati E., Summa V., Annunziata G., Tenore G.C. Application of a Rapid and Simple Technological Process to Increase Levels and Bioaccessibility of Free Phenolic Compounds in Annurca Apple Nutraceutical Product. *Foods.* **2022**, 11(10), 1453.

- Saviano A., Raucci F., Casillo G.M., Mansour A.A., **Piccolo V.**, Montesano C., Smimmo M., Vellecco V., Capasso G., Boscaino A., Summa V., Mascolo N., Iqbal A.J., Sorrentino R., d'Emmanuele R.V.B., Bucci M., Brancaleone V., Maione F. Anti-inflammatory and immunomodulatory activity of Mangifera indica L. reveals the modulation of COX-2/mPGES-1 axis and Th17/Treg ratio. *Pharmacological Research*. **2022**, 182(6):106283.

- D'Amelia V., Staiti A., D'Orso F., Maisto M., **Piccolo V**., Aversano R., Carputo D. Targeted mutagenesis of StISAC stabilizes the production of anthocyanins in potato cell culture. *Plant Direct*. **2022**, 6(8).

- Schiano E., Maisto M., **Piccolo V.**, Novellino E., Annunziata G., Ciampaglia R., Montesano C., Croce M., Caruso G., Iannuzzo F., Summa V., Tenore G.C. Beneficial Contribution to Glucose Homeostasis by an Agro-Food Waste Product Rich in Abscisic Acid: Results from a Randomized Controlled Trial. *Foods.* **2022**, 11(17), 2637.

- Maisto M., **Piccolo V.**, Novellino E., Schiano E., Iannuzzo F., Ciampaglia R., Summa V., Tenore G.C. Optimization of Phlorizin Extraction from Annurca Apple Tree Leaves Using Response Surface Methodology. *Antioxidants.* **2022**, 11(10), 1933.

- Maisto M., Iannuzzo F., Schiano E., Ciampaglia R., Labanca A., Montesano D., **Piccolo V.**, Rossi P., Tenore G.C. Effects of Fortified Laying Hen Diet with Moringa oleifera Leaves and Goji Berries on Cholesterol and Carotenoid Egg Content. *Foods.* **2022**, 11(20), 3156.

- Iannuzzo F., **Piccolo V.**, Novellino E., Schiano E., Salviati E., Summa V., Campiglia P., Tenore G.C., Maisto M. A Food-Grade Method for Enhancing the Levels of Low Molecular Weight Proanthocyanidins with Potentially High Intestinal Bioavailability. *International Journal of Molecular Sciences*. **2022**; 23(21).

- Maria M., **Piccolo V.**, Novellino E., Schiano E., Iannuzzo F., Ciampaglia R., Summa V., Tenore G.C. Optimization of Ursolic Acid Extraction in Oil from Annurca Apple to Obtain Oleolytes with Potential Cosmeceutical Application. *Antioxidants*. **2023**; 12(2):224.

- Schiano E., Neri I., Maisto M., Novellino E., Iannuzzo F., **Piccolo V.**, Summa V., Grumetto L., Tenore G.C. Validation of an LC-MS/MS Method for the Determination of Abscisic Acid Concentration in a Real-World Setting. *Foods*. **2023**; 12(5):1077.

- Maisto M., Marzocchi A., Keivani N., **Piccolo V.**, Summa V., Tenore G.C. Natural Chalcones for the Menagement of Obesity Disease. *International Journal of Molecular Sciences*. **2023**; 24(21):15929.

- **Piccolo V.**, Maisto M., Schiano E., Iannuzzo F., Keivani N., Rigano M.M., Santini A., Novellino E., Tenore G.C., Summa V. Phytochemical investigation and antioxidant properties of unripe tomato cultivars (Solanum lycopersicum L.). *Food Chemistry*. **2023**; 438(3):137863

BIBLIOGRAPHY

Abdelaziz, S., Hassan, W. H. B., Elhassanny, A. E. M., Al-Yousef, H. M., Elsayed, M. A., & Adel, R. (2020). Ultra performance liquid chromatography-tandem mass spectrometeric analysis of ethyl acetate fraction from saudi Lavandula coronopifolia Poir and evaluation of its cytotoxic and antioxidant activities. *Journal of HerbMed Pharmacology*, *9*(3), 268–276. https://doi.org/10.34172/jhp.2020.34

Abdullah, N. H., Thomas, N. F., Sivasothy, Y., Lee, V. S., Liew, S. Y., Noorbatcha, I. A., & Awang, K. (2016). Hyaluronidase inhibitory activity of pentacylic triterpenoids from prismatomeris tetrandra (Roxb.) K. schum: Isolation, synthesis and QSAR Study. *International Journal of Molecular Sciences*, *17*(2). https://doi.org/10.3390/ijms17020143

Adams, C. M., Ebert, S. M., & Dyle, M. C. (2017). Role of ATF4 in skeletal muscle atrophy. In *Current Opinion in Clinical Nutrition and Metabolic Care* (Vol. 20, Issue 3, pp. 164–168). Lippincott Williams and Wilkins. https://doi.org/10.1097/MCO.0000000000000362

Ak, G., Zengin, G., Mahomoodally, M. F., Llorent-mart, E., Orlando, G., Chiavaroli, A., Brunetti, L., Recinella, L., Leone, S., Cristina, S., Simone, D., Menghini, L., & Ferrante, C. (2021). *Shedding Light into the Connection between Chemical Components and Biological Effects of Extracts from Epilobium hirsutum : Is It a Potent Source of Bioactive Agents from Natural Treasure ?*

Alonso-Salces, R. M., Ndjoko, K., Queiroz, E. F., Ioset, J. R., Hostettmann, K., Berrueta, L. A., Gallo, B., & Vicente, F. (2004). On-line characterisation of apple polyphenols by liquid chromatography coupled with mass spectrometry and ultraviolet absorbance detection. *Journal of Chromatography A*, *1046*(1–2), 89–100. https://doi.org/10.1016/j.chroma.2004.06.077

Altria, K. D., Marsh, A., & Sänger-van de Griend, C. (2006). Capillary electrophoresis for the analysis of small-molecule pharmaceuticals. In *Electrophoresis* (Vol. 27, Issue 12, pp. 2263–2282). Wiley-VCH Verlag. https://doi.org/10.1002/elps.200600030

Aman, Y., Schmauck-Medina, T., Hansen, M., Morimoto, R. I., Simon, A. K., Bjedov, I., Palikaras, K., Simonsen, A., Johansen, T., Tavernarakis, N., Rubinsztein, D. C., Partridge, L., Kroemer, G., Labbadia, J., & Fang, E. F. (2021). Autophagy in healthy

aging and disease. In *Nature Aging* (Vol. 1, Issue 8, pp. 634–650). Springer. https://doi.org/10.1038/s43587-021-00098-4

Anton, D., Bender, I., Kaart, T., Roasto, M., Heinonen, M., Luik, A., & Püssa, T. (2017). Changes in Polyphenols Contents and Antioxidant Capacities of Organically and Conventionally Cultivated Tomato (Solanum lycopersicum L.) Fruits during Ripening. *International Journal of Analytical Chemistry*, *2017*. https://doi.org/10.1155/2017/2367453

Antonio, E., dos Reis Antunes Junior, O., Marcano, R. G. D. J. V., Diedrich, C., da Silva Santos, J., Machado, C. S., Khalil, N. M., & Mainardes, R. M. (2021). Chitosan modified poly (lactic acid) nanoparticles increased the ursolic acid oral bioavailability. *International Journal of Biological Macromolecules*, *172*, 133–142. https://doi.org/10.1016/j.ijbiomac.2021.01.041

Assiri, A. M. A., Elbanna, K., Abulreesh, H. H., & Ramadan, M. F. (2016). Bioactive compounds of cold-pressed thyme (Thymus vulgaris) oil with antioxidant and antimicrobial properties. *Journal of Oleo Science*, *65*(8), 629–640. https://doi.org/10.5650/jos.ess16042

Bailly, C. (2021). The steroidal alkaloids α-tomatine and tomatidine: Panorama of their mode of action and pharmacological properties. In *Steroids* (Vol. 176). Elsevier Inc. https://doi.org/10.1016/j.steroids.2021.108933

Barbosa-Filho, J. M., Piuvezam, M. R., Moura, M. D., Silva, M. S., Lima, K. V. B., Leitão Da-Cunha, E. V, Fechine, I. M., & Takemura, O. S. (n.d.). Anti-infl ammatory activity of alkaloids: A twenty-century review. In *Revista Brasileira de Farmacognosia Brazilian Journal of Pharmacognosy* (Vol. 16, Issue 1).

Barros, L., Dueñas, M., Pinela, J., Carvalho, A. M., Buelga, C. S., & Ferreira, I. C. F. R. (2012). Characterization and Quantification of Phenolic Compounds in Four Tomato (Lycopersicon esculentum L.) Farmers' Varieties in Northeastern Portugal Homegardens. *Plant Foods for Human Nutrition*, *67*(3), 229–234. https://doi.org/10.1007/s11130-012-0307-z

Baumgartner, R. N., Koehler, K. M., Gallagher, D., Romero, L., Heymstleld, S. B., Ross, R. R., Garry, P. J., & Lindeman, R. D. (1998). *Epidemiology of Sarcopenia among the Elderly in New Mexico* (Vol. 147, Issue 8).

Bayrakçeken Güven, Z., Saracoglu, I., Nagatsu, A., Yilmaz, M. A., & Basaran, A. A. (2023). Anti-tyrosinase and antimelanogenic effect of cinnamic acid derivatives from Prunus mahaleb L.: Phenolic composition, isolation, identification and inhibitory activity. *Journal of Ethnopharmacology*, *310*. https://doi.org/10.1016/j.jep.2023.116378

Bergamin, A., Mantzioris, E., Cross, G., Deo, P., Garg, S., & Hill, A. M. (2019). Nutraceuticals: Reviewing their Role in Chronic Disease Prevention and Management. In *Pharmaceutical Medicine* (Vol. 33, Issue 4, pp. 291–309). Springer International Publishing. https://doi.org/10.1007/s40290-019-00289-w

Bettonte, S., Berton, M., & Marzolini, C. (2022). Magnitude of Drug–Drug Interactions in Special Populations. In *Pharmaceutics* (Vol. 14, Issue 4). MDPI. https://doi.org/10.3390/pharmaceutics14040789

Bianco, G., Schmitt-Kopplin, P., De Benedetto, G., Kettrup, A., & Cataldi, T. R. I. (2002). Determination of glycoalkaloids and relative aglycones by nonaqueous capillary electrophoresis coupled with electrospray ionization-ion trap mass spectrometry. *Electrophoresis*, *23*(17), 2904–2912. https://doi.org/10.1002/1522-2683(200209)23:17<2904::AID-ELPS2904>3.0.CO;2-1

Biswas, S., Mukherjee, P. K., Harwansh, R. K., Bannerjee, S., & Bhattacharjee, P. (2019). Enhanced bioavailability and hepatoprotectivity of optimized ursolic acid–phospholipid complex. *Drug Development and Industrial Pharmacy*, *45*(6), 946–958. https://doi.org/10.1080/03639045.2019.1583755

Biswas, T., & Dwivedi, U. N. (2019). Plant triterpenoid saponins: biosynthesis, in vitro production, and pharmacological relevance. In *Protoplasma* (Vol. 256, Issue 6, pp. 1463–1486). Springer-Verlag Wien. https://doi.org/10.1007/s00709-019-01411-0

Blum, A., Monir, M., Wirsansky, I., & Ben-Arzi, S. (2005). The beneficial effects of tomatoes. In *European Journal of Internal Medicine* (Vol. 16, Issue 6, pp. 402–404). https://doi.org/10.1016/j.ejim.2005.02.017

Blume-Peytavi, U., Kottner, J., Sterry, W., Hodin, M. W., Griffiths, T. W., Watson, R. E. B., Hay, R. J., & Griffiths, C. E. M. (2016). Age-associated skin conditions and diseases: Current perspectives and future options. In *Gerontologist* (Vol. 56, pp. S230–S242). Gerontological Society of America. https://doi.org/10.1093/geront/gnw003

Bolognia, J., Murray, M., & Pawelek, J. (n.d.). *UVB-Induced Melanogenesis May Be Through the MSH-Receptor System Mediated*.

Both, D. M., Goodtzova, K., Yarosh, D. B., & Brown, D. A. (2002). Liposome-encapsulated ursolic acid increases ceramides and collagen in human skin cells. *Archives of Dermatological Research*, *293*(11), 569–575. https://doi.org/10.1007/s00403-001-0272-0

Brincat, M., Moniz, C. F., Studd, J. W. W., Darby, A. J., Magos, A., & Cooper, D. (1983). 12 Aitken RCB. A growing edge of measurement of feelings. In *Proceedings of the Royal Society of Medicine* (Vol. 287).

Brioche, T., & Lemoine-Morel, S. (2016). Oxidative Stress, Sarcopenia, Antioxidant Strategies and Exercise: Molecular Aspects. *Current Pharmaceutical Design*, *22*(18), 2664–2678. https://doi.org/10.2174/1381612822666160219120531

Brito, A., Ramirez, J. E., Areche, C., Sepúlveda, B., & Simirgiotis, M. J. (2014). HPLC-UV-MS profiles of phenolic compounds and antioxidant activity of fruits from three citrus species consumed in Northern Chile. *Molecules*, *19*(11), 17400–17421. https://doi.org/10.3390/molecules191117400

Broughton, P. M. G. (n.d.). Carry-over in automatic analysers. In *Journal of Automatic Chemistry* (Vol. 6, Issue 2). http://www.hindawi.com

Buford, T. W., Anton, S. D., Judge, A. R., Marzetti, E., Wohlgemuth, S. E., Carter, C. S., Leeuwenburgh, C., Pahor, M., & Manini, T. M. (2010). Models of accelerated sarcopenia: Critical pieces for solving the puzzle of age-related muscle atrophy. In *Ageing Research Reviews* (Vol. 9, Issue 4, pp. 369–383). Elsevier Ireland Ltd. https://doi.org/10.1016/j.arr.2010.04.004

Bushway, R. J., Lewis, ·+, Perkins, B., Paradis, L. R., & Vanderpan, S. (1994). *High-Performance Liquid Chromatographic Determination of the Tomato Glycoalkaloid, Tomatine, in Green and Red Tomatoes* (Vol. 42). https://pubs.acs.org/sharingguidelines

Bystrom, L. M., Lewis, B. A., Brown, D. L., Rodriguez, E., & Obendorf, R. L. (2008). *Characterisation of phenolics by LC – UV / Vis , LC – MS / MS and sugars by GC in Melicoccus bijugatus Jacq . ‘ Montgomery ’ fruits*. *111*, 1017–1024. https://doi.org/10.1016/j.foodchem.2008.04.058

Cai, F., Yu, G., Wang, P., Wei, Z., Fu, L., Shen, Q., & Chen, W. (2013). Harzianolide, a novel plant growth regulator and systemic resistance elicitor from Trichoderma harzianum. *Plant Physiology and Biochemistry*, *73*, 106–113. https://doi.org/10.1016/j.plaphy.2013.08.011

Calvano, C. D., Cataldi, T. R. I., Kögel, J. F., Monopoli, A., Palmisano, F., Sundermeyer, J., Chimica, D., Aldo, B., Interdipartimentale, R., & Aldo, B. (2017). *Structural Characterization of Neutral Saccharides by Negative Ion MALDI Mass Spectrometry Using a Superbasic Proton Sponge as Deprotonating Matrix*. 1666–1675. https://doi.org/10.1007/s13361-017-1679-y

Caprioli, G., Cahill, M. G., & James, K. J. (2014). Mass Fragmentation Studies of α-Tomatine and Validation of a Liquid Chromatography LTQ Orbitrap Mass Spectrometry Method for Its Quantification in Tomatoes. *Food Analytical Methods*, *7*(8). https://doi.org/10.1007/s12161-013-9771-9

Caprioli, G., Cahill, M., Logrippo, S., & James, K. (2015). Elucidation of the Mass Fragmentation Pathways of Tomatidine and β 1-Hydroxytomatine using Orbitrap Mass Spectrometry. In *NPC Natural Product Communications* (Vol. 10, Issue 4).

Carillo, P., D'Amelia, L., Dell'Aversana, E., Faiella, D., Cacace, D., Giuliano, B., & Morrone, B. (2018). Eco-friendly use of tomato processing residues for lactic acid production in campania. *Chemical Engineering Transactions*, *64*, 223–228. https://doi.org/10.3303/CET1864038

Casarrubias-Castillo, K., Montero-Vargas, J. M., Dabdoub-González, N., Winkler, R., Martinez-Gallardo, N. A., Zañudo-Hernández, J., Avilés-Arnaut, H., & Délano-Frier, J. P. (2020). Distinct gene expression and secondary metabolite profiles in suppressor of prosystemin-mediated responses2 (spr2) tomato mutants having impaired mycorrhizal colonization. *PeerJ*, *2020*(4). https://doi.org/10.7717/peerj.8888

Castro, E., & Llerena, W. (2020). *Extraction Strategies to Recover Bioactive Compounds , Incorporation into Food and Health Benefits* (Issue July).

Cataldi, T. R. I., Lelario, F., & Bufo, S. A. (2005). Analysis of tomato glycoalkaloids by liquid chromatography coupled with electrospray ionization tandem mass spectrometry. *Rapid Communications in Mass Spectrometry*, *19*(21), 3103–3110. https://doi.org/10.1002/rcm.2176

Cebadera, L., In, M., Barros, L., Fern, V., Mª, R., Pino, Á. Del, Santos-buelga, C., Ferreira, I. C. F. R., Morales, P., & Montaña, C. (2020). *Characterization of Extra Early Spanish Clementine Varieties (Citrus clementina Hort ex Tan) as a Relevant Source of Bioactive Compounds with Antioxidant Activity*. 1–16.

Chaudhary, P., Sharma, A., Singh, B., & Nagpal, A. K. (2018). Bioactivities of phytochemicals present in tomato. In *Journal of Food Science and Technology* (Vol. 55, Issue 8, pp. 2833–2849). Springer. https://doi.org/10.1007/s13197-018-3221-z

Chen, J., Li, Q., Ye, Y., Huang, Z., Ruan, Z., & Jin, N. (2020). Phloretin as both a substrate and inhibitor of tyrosinase: Inhibitory activity and mechanism. *Spectrochimica Acta - Part A: Molecular and Biomolecular Spectroscopy*, *226*. https://doi.org/10.1016/j.saa.2019.117642

Chen, S., Lu, C., & Zhao, R. (2014). *Qualitative and Quantitative Analysis of Rhizoma Smilacis glabrae by Ultra High Performance Liquid Chromatography Coupled with LTQ OrbitrapXL Hybrid Mass Spectrometry*. 10427–10439. https://doi.org/10.3390/molecules190710427

Chen, S. R., Chen, X. P., Lu, J. J., Wang, Y., & Wang, Y. T. (2015). Potent natural products and herbal medicines for treating liver fibrosis. In *Chinese Medicine (United Kingdom)* (Vol. 10, Issue 1). BioMed Central Ltd. https://doi.org/10.1186/s13020-015-0036-y

Chiriac, E. R., Chiţescu, C. L., Geană, E. I., Gird, C. E., Socoteanu, R. P., & Boscencu, R. (2021). Advanced analytical approaches for the analysis of polyphenols in plants matrices—a review. In *Separations* (Vol. 8, Issue 5). MDPI AG. https://doi.org/10.3390/separations8050065

Chiu, F. L., & Lin, J. K. (2008). Tomatidine inhibits iNOS and COX-2 through suppression of NF-κB and JNK pathways in LPS-stimulated mouse macrophages. *FEBS Letters*, *582*(16), 2407–2412. https://doi.org/10.1016/j.febslet.2008.05.049

Cho, C. W., Park, Y. S., Yan, X., Kim, H. J., Kim, Y. H., Kim, K. T., Men, C. Van, & Kang, J. S. (2020). *Quantitation of Phenolic Compounds Related to Antioxidant and Antiosteoporosis Activities in Ripe and Unripe Maesil (Prunus mume)*. *2020*.

Choi, E. H., Man, M. Q., Xu, P., Xin, S., Liu, Z., Crumrine, D. A., Jiang, Y. J., Fluhr, J. W., Feingold, K. R., Elias, P. M., & Mauro, T. M. (2007). Stratum corneum acidification is

impaired in moderately aged human and murine skin. *Journal of Investigative Dermatology*, *127*(12), 2847–2856. https://doi.org/10.1038/sj.jid.5700913

Chu, X., He, X., Shi, Z., Li, C., Guo, F., Li, S., Li, Y., Na, L., & Sun, C. (2015). Ursolic acid increases energy expenditure through enhancing free fatty acid uptake and β-oxidation via an UCP3/AMPK-dependent pathway in skeletal muscle. *Molecular Nutrition and Food Research*, *59*(8), 1491–1503. https://doi.org/10.1002/mnfr.201400670

Chuong, C. M., Nickoloff, B. J., M Elias, T.-P. P., Goldsmith, L. A., Macher, E., Maderson, P. A., Sundberg, J. P., Tagami, H., Plonka, P. M., Thestrup-Pedersen, K., Bernard, B. A., Schröder, J. M., Dotto, P., Chang, C. H., Williams, M. L., Feingold, K. R., King, L. E., Kligman, A. M., Rees, J. L., & Christophers, E. (2002). EXPERIMENTAL DERMATOLOGY What is the "true" function of skin? the "true" function of skin? Conventional textbook wisdom portrays the skin as an organ that individual member of the mammalian species, and has it that the skin primarily establishes, controls and transmits contacts with the. *Experimental Dermatology*, *11*, 349–367.

Cichon, M. J., Riedl, K. M., Wan, L., Thomas-Ahner, J. M., Francis, D. M., Clinton, S. K., & Schwartz, S. J. (2017). Plasma Metabolomics Reveals Steroidal Alkaloids as Novel Biomarkers of Tomato Intake in Mice. *Molecular Nutrition and Food Research*, *61*(12). https://doi.org/10.1002/mnfr.201700241

Clark, B. C., & Manini, T. M. (2008). *Sarcopenia 6 ¼ Dynapenia*.

Cooperstone, J. L., Tober, K. L., Riedl, K. M., Teegarden, M. D., Cichon, M. J., Francis, D. M., Schwartz, S. J., & Oberyszyn, T. M. (2017). Tomatoes protect against development of UV-induced keratinocyte carcinoma via metabolomic alterations. *Scientific Reports*, *7*(1). https://doi.org/10.1038/s41598-017-05568-7

Cruz-Jentoft, A. J., Baeyens, J. P., Bauer, J. M., Boirie, Y., Cederholm, T., Landi, F., Martin, F. C., Michel, J. P., Rolland, Y., Schneider, S. M., Topinková, E., Vandewoude, M., & Zamboni, M. (2010). Sarcopenia: European consensus on definition and diagnosis. *Age and Ageing*, *39*(4), 412–423. https://doi.org/10.1093/ageing/afq034

Cui, T., Li, J. Z., Kayahara, H., Ma, L., Wu, L. X., & Nakamura, K. (2006). Quantification of the polyphenols and triterpene acids in Chinese hawthorn fruit by high-performance

liquid chromatography. *Journal of Agricultural and Food Chemistry*, *54*(13), 4574–4581. https://doi.org/10.1021/jf060310m

Da Silva, G. N. S., Maria, N. R. G., Schuck, D. C., Cruz, L. N., De Moraes, M. S., Nakabashi, M., Graebin, C., Gosmann, G., Garcia, C. R. S., & Gnoatto, S. C. B. (2013). Two series of new semisynthetic triterpene derivatives: Differences in anti-malarial activity, cytotoxicity and mechanism of action. *Malaria Journal*, *12*(1). https://doi.org/10.1186/1475-2875-12-89

D'Abrosca, B., Fiorentino, A., Monaco, P., Oriano, P., & Pacifico, S. (2006). Annurcoic acid: A new antioxidant ursane triterpene from fruits of cv. Annurca apple. *Food Chemistry*, *98*(2), 285–290. https://doi.org/10.1016/j.foodchem.2005.05.072

Damiano, S., Muscariello, E., La Rosa, G., Di Maro, M., Mondola, P., & Santillo, M. (2019). Dual role of reactive oxygen species in muscle function: Can antioxidant dietary supplements counteract age-related sarcopenia? In *International Journal of Molecular Sciences* (Vol. 20, Issue 15). MDPI AG. https://doi.org/10.3390/ijms20153815

Daniell, H. W. (1971). Smoker's Wrinkles A Study in the Epidemiology of "Crow's Feet." In *Annals of Internal Medicine* (Vol. 75). http://annals.org/pdfaccess.ashx?url=/data/journals/aim/19456/

De Beer, D., Schulze, A. E., Joubert, E., Villiers, A., Malherbe, C. J., & Stander, M. A. (2012). Food ingredient extracts of cyclopia subternata (Honeybush): Variation in phenolic composition and antioxidant capacity. *Molecules*, *17*(12), 14602–14624. https://doi.org/10.3390/molecules171214602

Degeneve, A. (2004). *Antioxidants in fruits and vegetables*.

Delmonico, M. J., Harris, T. B., Lee, J. S., Visser, M., Nevitt, M., Kritchevsky, S. B., Tylavsky, F. A., & Newman, A. B. (2007). Alternative definitions of sarcopenia, lower extremity performance, and functional impairment with aging in older men and women. *Journal of the American Geriatrics Society*, *55*(5), 769–774. https://doi.org/10.1111/j.1532-5415.2007.01140.x

Di Lorenzo, R., Bernardi, A., Grumetto, L., Sacchi, A., Avagliano, C., Coppola, S., Severina, A. F. de G. di S., Bruno, C., Paparo, L., Laneri, S., & Dini, I. (2021).

Phenylalanine butyramide is a new cosmetic ingredient with soothing and anti-reddening potential. *Molecules*, *26*(21). https://doi.org/10.3390/molecules26216611

D'Mello, S. A. N., Finlay, G. J., Baguley, B. C., & Askarian-Amiri, M. E. (2016). Signaling pathways in melanogenesis. In *International Journal of Molecular Sciences* (Vol. 17, Issue 7). MDPI AG. https://doi.org/10.3390/ijms17071144

Dorais, M., Ehret, D. L., & Papadopoulos, A. P. (2008). Tomato (Solanum lycopersicum) health components: From the seed to the consumer. In *Phytochemistry Reviews* (Vol. 7, Issue 2, pp. 231–250). https://doi.org/10.1007/s11101-007-9085-x

Dutta, S., Ali, K. M., Dash, S. K., & Giri, B. (2018). ROLE OF NUTRACEUTICALS ON HEALTH PROMOTION AND DISEASE PREVENTION: A REVIEW. *Journal of Drug Delivery and Therapeutics*, *8*(4). https://doi.org/10.22270/jddt.v8i4.1759

Dyle, M. C., Ebert, S. M., Cook, D. P., Kunkel, S. D., Fox, D. K., Bongers, K. S., Bullard, S. A., Dierdorff, J. M., & Adams, C. M. (2014). Systems-based discovery of tomatidine as a natural small molecule inhibitor of skeletal muscle atrophy. *Journal of Biological Chemistry*, *289*(21), 14913–14924. https://doi.org/10.1074/jbc.M114.556241

Dzakovich, M. P., Goggans, M. L., Thomas-Ahner, J. M., Moran, N. E., Clinton, S. K., Francis, D. M., Cooperstone, J. L., & Cooperstone, J. (2023). *Title: Transcriptomics and Metabolomics Reveal Tomato Consumption Alters Hepatic Xenobiotic Metabolism and Induces Steroidal Alkaloid Metabolite Accumulation in Mice*. https://doi.org/10.1101/2023.04.18.536606

Dzakovich, M. P., Hartman, J. L., & Cooperstone, J. L. (2020). A High-Throughput Extraction and Analysis Method for Steroidal Glycoalkaloids in Tomato. *Frontiers in Plant Science*, *11*. https://doi.org/10.3389/fpls.2020.00767

El Mashad, H. M., Zhao, L., Zhang, R., & Pan, Z. (2019). Tomato. In *Integrated Processing Technologies for Food and Agricultural By-Products* (pp. 107–131). Elsevier. https://doi.org/10.1016/B978-0-12-814138-0.00005-8

Elsadig Karar, M. G., & Kuhnert, N. (2016). UPLC-ESI-Q-TOF-MS/MS Characterization of Phenolics from Crataegus monogyna and Crataegus laevigata (Hawthorn) Leaves, Fruits and their Herbal Derived Drops (Crataegutt Tropfen). *Journal of Chemical Biology & Therapeutics*, *01*(02), 1–23. https://doi.org/10.4172/2572-0406.1000102

Emmerson, E., & Hardman, M. J. (2012). The role of estrogen deficiency in skin ageing and wound healing. In *Biogerontology* (Vol. 13, Issue 1, pp. 3–20). https://doi.org/10.1007/s10522-011-9322-y

Fabre, N., Rustan, I., Hoffmann, E. de, & Quetin-Leclercq, J. (2001). Determination of Flavone, Flavonol, and Flavanone Aglycones by Negative Ion Liquid Chromatography Electrospray Ion Trap Mass Spectrometry. *J Am Soc Mass Spectrom*, *12*(6), 707–715. https://doi.org/https://doi.org/10.1016/S1044-0305(01)00226-4

Faria-Silva, C., de Sousa, M., Carvalheiro, M. C., Simões, P., & Simões, S. (2022). Alpha-tomatine and the two sides of the same coin: An anti-nutritional glycoalkaloid with potential in human health. In *Food Chemistry* (Vol. 391). Elsevier Ltd. https://doi.org/10.1016/j.foodchem.2022.133261

Fda. (2011). *Guidance for Industry Studies to Evaluate the Metabolism and Residue Kinetics of Veterinary Drugs in Food-Producing Animals: Validation of Analytical Methods Us ed in Res idue Depletion Studies*. http://www.regulations.gov.

Feng, L., Liu, X., Zhu, W., Guo, F., Wu, Y., Wang, R., Chen, K., Huang, C., & Li, Y. (2013). Inhibition of human neutrophil elastase by pentacyclic triterpenes. *PLoS ONE*, *8*(12). https://doi.org/10.1371/journal.pone.0082794

Fielding, R. A., Vellas, B., Evans, W. J., Bhasin, S., Morley, J. E., Newman, A. B., Abellan van Kan, G., Andrieu, S., Bauer, J., Breuille, D., Cederholm, T., Chandler, J., De Meynard, C., Donini, L., Harris, T., Kannt, A., Keime Guibert, F., Onder, G., Papanicolaou, D., … Zamboni, M. (2011). Sarcopenia: An Undiagnosed Condition in Older Adults. Current Consensus Definition: Prevalence, Etiology, and Consequences. International Working Group on Sarcopenia. *Journal of the American Medical Directors Association*, *12*(4), 249–256. https://doi.org/10.1016/j.jamda.2011.01.003

Fiorilli, V., Wang, J. Y., Bonfante, P., Lanfranco, L., & Al-Babili, S. (2019). Apocarotenoids: Old and New Mediators of the Arbuscular Mycorrhizal Symbiosis. *Frontiers in Plant Science*, *10*(September), 1–9. https://doi.org/10.3389/fpls.2019.01186

Fratianni, F., Cozzolino, A., D'acierno, A., Nazzaro, F., Riccardi, R., & Spigno, P. (2020). Qualitative aspects of some of some traditional landraces of the tomato "piennolo"

(Solanum lycopersicum L.) of the Campania Region, Southern Italy. *Antioxidants*, *9*(7), 1–14. https://doi.org/10.3390/antiox9070565

Friedman, M. (2002). Tomato glycoalkaloids: Role in the plant and in the diet. In *Journal of Agricultural and Food Chemistry* (Vol. 50, Issue 21, pp. 5751–5780). https://doi.org/10.1021/jf020560c

Friedman, M. (2013). Anticarcinogenic, cardioprotective, and other health benefits of tomato compounds lycopene, α-tomatine, and tomatidine in pure form and in fresh and processed tomatoes. In *Journal of Agricultural and Food Chemistry* (Vol. 61, Issue 40, pp. 9534–9550). American Chemical Society. https://doi.org/10.1021/jf402654e

Friedman, M., Kozukue, N., & Harden, L. A. (1998). *Preparation and Characterization of Acid Hydrolysis Products of the Tomato Glycoalkaloid r-Tomatine*. https://pubs.acs.org/sharingguidelines

Friedman, M., & Levin, C. E. (1995). Tomatine Content in Tomato and Tomato Products Determined by HPLC with Pulsed Amperometric Detection. In *J. Agrie. FoodChem* (Vol. 43). https://pubs.acs.org/sharingguidelines

Friedman, M., Levin, C. E., & Mcdonald, G. M. (1994). *Food Chem* (Vol. 42). https://pubs.acs.org/sharingguidelines

Fu, Q., Zhang, L., Cheng, N., Jia, M., & Zhang, Y. (2014). Extraction optimization of oleanolic and ursolic acids from pomegranate (Punica granatum L.) flowers. *Food and Bioproducts Processing*, *92*(3), 321–327. https://doi.org/10.1016/j.fbp.2012.12.006

Ghisalberti, E. L. (2006). *Steroidal Glycoalkaloids: Isolation, Structure, Analysis, and Biosynthesis*.

Gibellini, L., Bianchini, E., De Biasi, S., Nasi, M., Cossarizza, A., & Pinti, M. (2015). Natural Compounds Modulating Mitochondrial Functions. In *Evidence-based Complementary and Alternative Medicine* (Vol. 2015). Hindawi Limited. https://doi.org/10.1155/2015/527209

Gomes, M. J., Felippe Martinez, P., Pagan, L. U., Damatto, R. L., Diacardia, M., Cezar, M., Regina, A., Lima, R., Okoshi, K., & Okoshi, M. P. (2017). Skeletal muscle aging: influence of oxidative stress and physical exercise. In *Oncotarget* (Vol. 8, Issue 12). www.impactjournals.com/oncotarget/

González-Lamothe, R., Mitchell, G., Gattuso, M., Diarra, M. S., Malouin, F., & Bouarab, K. (2009). Plant antimicrobial agents and their effects on plant and human pathogens. In *International Journal of Molecular Sciences* (Vol. 10, Issue 8, pp. 3400–3419). https://doi.org/10.3390/ijms10083400

González-Sarrías, A., Larrosa, M., García-Conesa, M. T., Tomás-Barberán, F. A., & Espín, J. C. (2013). Nutraceuticals for older people: Facts, fictions and gaps in knowledge. In *Maturitas* (Vol. 75, Issue 4, pp. 313–334). https://doi.org/10.1016/j.maturitas.2013.05.006

Goodpaster, B. H., Park, S. W., Harris, T. B., Kritchevsky, S. B., Nevitt, M., Schwartz, A. V, Simonsick, E. M., Tylavsky, F. A., Visser, M., & Newman, A. B. (2006). *The Loss of Skeletal Muscle Strength, Mass, and Quality in Older Adults: The Health, Aging and Body Composition Study*. http://biomedgerontology.oxfordjournals.org/

Grieman, M. M., Greaves, J., & Saltzman, E. S. (2015). A method for analysis of vanillic acid in polar ice cores. *Climate of the Past*, *11*(2), 227–232. https://doi.org/10.5194/cp-11-227-2015

Gudoityte, E., Arandarcikaite, O., Mazeikiene, I., Bendokas, V., & Liobikas, J. (2021). Ursolic and oleanolic acids: Plant metabolites with neuroprotective potential. In *International Journal of Molecular Sciences* (Vol. 22, Issue 9). MDPI. https://doi.org/10.3390/ijms22094599

Guinda, A., Rada, M., Delgado, T., & Castellano, J. M. (2011). Pentacyclic triterpenic acids from Argania spinosa. *European Journal of Lipid Science and Technology*, *113*(2), 231–237. https://doi.org/10.1002/ejlt.201000342

Guo, J., Huang, X., Dou, L., Yan, M., Shen, T., Tang, W., & Li, J. (2022). Aging and aging-related diseases: from molecular mechanisms to interventions and treatments. In *Signal Transduction and Targeted Therapy* (Vol. 7, Issue 1). Springer Nature. https://doi.org/10.1038/s41392-022-01251-0

Guo, N., You, X., Wu, Y., Du, D., Zhang, L., Shang, Q., & Liu, W. (2020). Continuous Fluorometric Method for Determining the Monophenolase Activity of Tyrosinase on L-Tyrosine, through Quenching L-DOPA Fluorescence by Borate. *Analytical Chemistry*, *92*(8), 5780–5786. https://doi.org/10.1021/acs.analchem.9b05127

Guo, S., Duan, J. A., Qian, D., Tang, Y., Wu, D., Su, S., Wang, H., & Zhao, Y. (2015). Content variations of triterpenic acid, nucleoside, nucleobase, and sugar in jujube (Ziziphus jujuba) fruit during ripening. *Food Chemistry*, *167*, 468–474. https://doi.org/10.1016/j.foodchem.2014.07.013

Guo, Y. P., Yang, H., Wang, Y. L., Chen, X. X., Zhang, K., Wang, Y. L., Sun, Y. F., Huang, J., Yang, L., & Wang, J. H. (2021). Determination of flavonoids compounds of three species and different harvesting periods in crataegi folium based on lc-ms/ms. *Molecules*, *26*(6). https://doi.org/10.3390/molecules26061602

Harman, D. (n.d.). *AGING: A THEORY BASED ON FREE RADICAL AND RADIATION CHEMISTRY*. http://geronj.oxfordjournals.org/

Harvell, J. D., & Maibach, H. I. (1994). Percutaneous absorption and inflammation in aged skin: A review. *Journal of the American Academy of Dermatology*, *31*(6), 1015–1021. https://doi.org/10.1016/S0190-9622(94)70273-X

Hayflick, L., & Moorhead, P. S. (1961). THE SERIAL CULTIVATION OF HUMAN DIPLOID CELL STRAINS'. In *Experimental Cell Research* (Vol. 25).

Heinig, U., & Aharoni, A. (2014). Analysis of Steroidal Alkaloids and Saponins in Solanaceae Plant Extracts Using UPLC-qTOF Mass Spectrometry. *Methods in Molecular Biology*, *1153*, 171–185. https://doi.org/10.1007/978-1-4939-0606-2_12

Hong, Y., Wang, Z., Barrow, C. J., Dunshea, F. R., & Suleria, H. A. R. (2021). High-throughput screening and characterization of phenolic compounds in stone fruits waste by lc-esi-qtof-ms/ms and their potential antioxidant activities. *Antioxidants*, *10*(2), 1–22. https://doi.org/10.3390/antiox10020234

Hooshmand, K., & Fomsgaard, I. S. (2021). Analytical methods for quantification and identification of intact glucosinolates in arabidopsis roots using lc-qqq(Lit)-ms/ms. *Metabolites*, *11*(1), 1–18. https://doi.org/10.3390/metabo11010047

Hord, J. M., & Lawler, J. M. (2017). ROS and nNOS in the regulation of disuse-induced skeletal muscle atrophy. In *The Plasticity of Skeletal Muscle: From Molecular Mechanism to Clinical Applications* (pp. 231–250). Springer Singapore. https://doi.org/10.1007/978-981-10-3292-9_11

Hövelmann, Y., Jagels, A., Schmid, R., Hübner, F., & Humpf, H. U. (2020). Identification of potential human urinary biomarkers for tomato juice intake by mass spectrometry-based metabolomics. *European Journal of Nutrition*, *59*(2), 685–697. https://doi.org/10.1007/s00394-019-01935-4

Huhman, D. V., Berhow, M. A., & Sumner, L. W. (2005). Quantification of saponins in aerial and subterranean tissues of Medicago truncatula. *Journal of Agricultural and Food Chemistry*, *53*(6), 1914–1920. https://doi.org/10.1021/jf0482663

Iannuzzo, F., Piccolo, V., Novellino, E., Schiano, E., Salviati, E., Summa, V., Campiglia, P., Tenore, G. C., & Maisto, M. (2022). A Food-Grade Method for Enhancing the Levels of Low Molecular Weight Proanthocyanidins with Potentially High Intestinal Bioavailability. *International Journal of Molecular Sciences*, *23*(21). https://doi.org/10.3390/ijms232113557

Iijima, Y., Watanabe, B., Sasaki, R., Takenaka, M., Ono, H., Sakurai, N., Umemoto, N., Suzuki, H., Shibata, D., & Aoki, K. (2013). Steroidal glycoalkaloid profiling and structures of glycoalkaloids in wild tomato fruit. *Phytochemistry*, *95*, 145–157. https://doi.org/10.1016/j.phytochem.2013.07.016

Itkin, M., Rogachev, I., Alkan, N., Rosenberg, T., Malitsky, S., Masini, L., Meir, S., Iijima, Y., Aoki, K., de Vos, R., Prusky, D., Burdman, S., Beekwilder, J., & Aharoni, A. (2011). GLYCOALKALOID METABOLISM1 is required for steroidal alkaloid glycosylation and prevention of phytotoxicity in tomato. *Plant Cell*, *23*(12), 4507–4525. https://doi.org/10.1105/tpc.111.088732

Ito, S. ichi, Ihara, T., Tamura, H., Tanaka, S., Ikeda, T., Kajihara, H., Dissanayake, C., Abdel-Motaal, F. F., & El-Sayed, M. A. (2007). α-Tomatine, the major saponin in tomato, induces programmed cell death mediated by reactive oxygen species in the fungal pathogen Fusarium oxysporum. *FEBS Letters*, *581*(17), 3217–3222. https://doi.org/10.1016/j.febslet.2007.06.010

Izzo, L., Rodríguez-carrasco, Y., Pacifico, S., Castaldo, L., Narváez, A., & Ritieni, A. (2020). Colon bioaccessibility under in vitro gastrointestinal digestion of a red cabbage extract chemically profiled through UHPLC-Q-Orbitrap HRMS. *Antioxidants*, *9*(10), 1–18. https://doi.org/10.3390/antiox9100955

Jäger, S., Trojan, H., Kopp, T., Laszczyk, M. N., & Scheffler, A. (2009). Pentacyclic triterpene distribution in various plants - rich sources for a new group of multi-potent plant extracts. *Molecules*, *14*(6), 2016–2031. https://doi.org/10.3390/molecules14062016

Janssen, I., Baumgartner, R. N., Ross, R., Rosenberg, I. H., & Roubenoff, R. (2004). Skeletal Muscle Cutpoints Associated with Elevated Physical Disability Risk in Older Men and Women. In *American Journal of Epidemiology* (Vol. 159, Issue 4, pp. 413–421). https://doi.org/10.1093/aje/kwh058

Janssen, I., Heymsfield, S. B., & Ross, R. (2002). Low Relative Skeletal Muscle Mass (Sarcopenia) in Older Persons Is Associated with Functional Impairment and Physical Disability. In *J Am Geriatr Soc* (Vol. 50).

Jiang, Z., Kempinski, C., & Chappell, J. (2016). Extraction and Analysis of Terpenes/Terpenoids. *Current Protocols in Plant Biology*, *1*(2), 345–358. https://doi.org/10.1002/cppb.20024

J-m, J., Jensen, J.-M., Fo, M., Winoto-Morbach, S., Seite, S., Schunck, M., Proksch, E., Schu, S., & Schü tze, S. (n.d.). *Acid and neutral sphingomyelinase, ceramide synthase, and acid ceramidase activities in cutaneous aging*.

K McKEE, B. R. (1959). Affecting the Toxicity of Solanine and Related Alkaloids to Fusarium caeruleum. In *J. gen. Microbial* (Vol. 20).

Kadunce, D. P., Burr, R., Gress, R., Kanner, R., Lyon, J. L., & Zone, J. J. (1991). Cigarette Smoking: Risk Factor for Premature Facial Wrinkling. In *Annals of Internal Medicine* (Vol. 114). http://annals.org/

Kasimir, M., Wolbeck, A., Behrens, M., & Humpf, H. U. (2023). Intestinal Metabolism of Selected Steroidal Glycoalkaloids in the Pig Cecum Model. *ACS Omega*, *8*(20), 18266–18274. https://doi.org/10.1021/acsomega.3c01990

Kaya, G., & Saurat, J. H. (2007). Dermatoporosis: A chronic cutaneous insufficiency/fragility syndrome - Clinicopathological features, mechanisms, prevention and potential treatments. *Dermatology*, *215*(4), 284–294. https://doi.org/10.1159/000107621

Kaya, G., Tran, C., Sorg, O., Hotz, R., Grand, D., Carraux, P., Didierjean, L., Stamenkovic, I., & Saurat, J. H. (2006). Hyaluronate fragments reverse skin atrophy by a CD44-dependent mechanism. *PLoS Medicine*, *3*(12), 2291–2303. https://doi.org/10.1371/journal.pmed.0030493

Kedare, S. B., & Singh, R. P. (2011). Genesis and development of DPPH method of antioxidant assay. In *Journal of Food Science and Technology* (Vol. 48, Issue 4, pp. 412–422). https://doi.org/10.1007/s13197-011-0251-1

Keukens, E. A. J., De Vrije, T., Van Den Boom, C., De Waard, P., Plasman, H. H., Thiel, F., Chupin, V., Jongen, W. M. F., & De Kruijff, B. (1995). Biochi ~mi c~a et Biophysica A~ta Molecular basis of glycoalkaloid induced membrane disruption. In *Biochimica et Biophysica Acta* (Vol. 1240).

Kim, D. S., Na, H., Kwack, Y., & Chun, C. (2014). Secondary metabolite profiling in various parts of tomato plants. *Korean Journal of Horticultural Science and Technology*, *32*(2), 252–260. https://doi.org/10.7235/hort.2014.13165

Kimura, S., & Sinha, N. (2008). Tomato (Solanum lycopersicum): A model fruit-bearing crop. *Cold Spring Harbor Protocols*, *3*(11). https://doi.org/10.1101/pdb.emo105

Kiralan, M., & Ketenoglu, O. (2022). Utilization of Tomato (Solanum lycopersicum) by-Products: An Overview. In *Mediterranean Fruits Bio-wastes: Chemistry, Functionality and Technological Applications* (pp. 799–818). Springer International Publishing. https://doi.org/10.1007/978-3-030-84436-3_34

Koh, E., Kaffka, S., & Mitchell, A. E. (2013). A long-term comparison of the influence of organic and conventional crop management practices on the content of the glycoalkaloid α-tomatine in tomatoes. *Journal of the Science of Food and Agriculture*, *93*(7), 1537–1542. https://doi.org/10.1002/jsfa.5951

Kolakul, P., & Sripanidkulchai, B. (2017). Phytochemicals and anti-aging potentials of the extracts from Lagerstroemia speciosa and Lagerstroemia floribunda. *Industrial Crops and Products*, *109*, 707–716. https://doi.org/10.1016/j.indcrop.2017.09.026

Kondo, M., Mackinnon, S. L., Craft, C. C., Matchett, M. D., Hurta, R. A. R., & Neto, C. C. (2011). Ursolic acid and its esters: Occurrence in cranberries and other Vaccinium fruit and effects on matrix metalloproteinase activity in DU145 prostate tumor cells. *Journal*

of the Science of Food and Agriculture, *91*(5), 789–796. https://doi.org/10.1002/jsfa.4330

Kontogianni, V. G., Tomic, G., Nikolic, I., Nerantzaki, A. A., Sayyad, N., Stosic-Grujicic, S., Stojanovic, I., Gerothanassis, I. P., & Tzakos, A. G. (2013). Phytochemical profile of Rosmarinus officinalis and Salvia officinalis extracts and correlation to their antioxidant and anti-proliferative activity. *Food Chemistry*, *136*(1), 120–129. https://doi.org/10.1016/j.foodchem.2012.07.091

Kowalski, R. (2007). Studies of selected plant raw materials as alternative sources of triterpenes of oleanolic and ursolic acid types. *Journal of Agricultural and Food Chemistry*, *55*(3), 656–662. https://doi.org/10.1021/jf0625858

Kozukue, N., Han, J. S., Lee, K. R., & Friedman, M. (2004). Dehydrotomatine and α-Tomatine Content in Tomato Fruits and Vegetative Plant Tissues. *Journal of Agricultural and Food Chemistry*, *52*(7), 2079–2083. https://doi.org/10.1021/jf0306845

Kozukue, N., Kim, D. S., Choi, S. H., Mizuno, M., & Friedman, M. (2023). Isomers of the Tomato Glycoalkaloids α-Tomatine and Dehydrotomatine: Relationship to Health Benefits. *Molecules*, *28*(8). https://doi.org/10.3390/molecules28083621

Krutmann, J., Liu, W., Li, L., Pan, X., Crawford, M., Sore, G., & Seite, S. (2014). Pollution and skin: From epidemiological and mechanistic studies to clinical implications. In *Journal of Dermatological Science* (Vol. 76, Issue 3, pp. 163–168). Elsevier Ireland Ltd. https://doi.org/10.1016/j.jdermsci.2014.08.008

Kumar, S., Singh, A., & Kumar, B. (2017). Identification and characterization of phenolics and terpenoids from ethanolic extracts of Phyllanthus species by HPLC-ESI-QTOF-MS/MS. *Journal of Pharmaceutical Analysis*, *7*(4), 214–222. https://doi.org/10.1016/j.jpha.2017.01.005

Lanzuise, S., Manganiello, G., Guastaferro, V. M., Vincenzo, C., Vitaglione, P., Ferracane, R., Vecchi, A., Vinale, F., Kamau, S., Lorito, M., & Woo, S. L. (2022). Combined Biostimulant Applications of Trichoderma spp. with Fatty Acid Mixtures Improve Biocontrol Activity, Horticultural Crop Yield and Nutritional Quality. *Agronomy*, *12*(2). https://doi.org/10.3390/agronomy12020275

Lauretani, F., Russo, C. R., Bandinelli, S., Bartali, B., Cavazzini, C., Di Iorio, A., Corsi, A. M., Rantanen, T., Guralnik, J. M., & Ferrucci, L. (2003). Age-associated changes in skeletal muscles and their effect on mobility: An operational diagnosis of sarcopenia. *Journal of Applied Physiology*, *95*(5), 1851–1860. https://doi.org/10.1152/japplphysiol.00246.2003

Laurila, J., Laakso, I., Väänänen, T., Kuronen, P., Huopalahti, R., & Pehu, E. (1999). Determination of solanidine- and tomatidine-type glycoalkaloid aglycons by gas chromatography/mass spectrometry. *Journal of Agricultural and Food Chemistry*, *47*(7), 2738–2742. https://doi.org/10.1021/jf981009b

Lee, S. T., Wong, P. F., Hooper, J. D., & Mustafa, M. R. (2013). Alpha-tomatine synergises with paclitaxel to enhance apoptosis of androgen-independent human prostate cancer PC-3 cells in vitro and in vivo. *Phytomedicine*, *20*(14), 1297–1305. https://doi.org/10.1016/j.phymed.2013.07.002

Li, G., Zhang, X., You, J., Song, C., Sun, Z., Xia, L., & Suo, Y. (2011). Highly sensitive and selective pre-column derivatization high-performance liquid chromatography approach for rapid determination of triterpenes oleanolic and ursolic acids and application to Swertia species: Optimization of triterpenic acids extraction and pre-column derivatization using response surface methodology. *Analytica Chimica Acta*, *688*(2), 208–218. https://doi.org/10.1016/j.aca.2011.01.010

Li, S., Meng, F., Liao, X., Wang, Y., Sun, Z., Guo, F., Li, X., Meng, M., Li, Y., & Sun, C. (2014). Therapeutic role of ursolic acid on ameliorating hepatic steatosis and improving metabolic disorders in high-fat diet-induced non-alcoholic fatty liver disease rats. *PLoS ONE*, *9*(1). https://doi.org/10.1371/journal.pone.0086724

Li, Y., Liu, Y., Liu, R., Liu, S., Zhang, X., Wang, Z., Zhang, J., & Lu, J. (2015). HPLC-LTQ-orbitrap MSn profiling method to comprehensively characterize multiple chemical constituents in xiao-er-qing-jie granules. *Analytical Methods*, *7*(18), 7511–7526. https://doi.org/10.1039/c5ay00420a

Li, Z. H., Guo, H., Xu, W. Bin, Ge, J., Li, X., Alimu, M., & He, D. J. (2016a). Rapid Identification of Flavonoid Constituents Directly from PTP1B Inhibitive Extract of Raspberry (Rubus idaeus L.) Leaves by HPLC-ESI-QTOF-MS-MS. *Journal of Chromatographic Science*, *54*(5), 805–810. https://doi.org/10.1093/chromsci/bmw016

Li, Z. H., Guo, H., Xu, W. Bin, Ge, J., Li, X., Alimu, M., & He, D. J. (2016b). Rapid Identification of Flavonoid Constituents Directly from PTP1B Inhibitive Extract of Raspberry (Rubus idaeus L.) Leaves by HPLC-ESI-QTOF-MS-MS. *Journal of Chromatographic Science*, *54*(5), 805–810. https://doi.org/10.1093/chromsci/bmw016

Liguori, I., Russo, G., Aran, L., Bulli, G., Curcio, F., Della-Morte, D., Gargiulo, G., Testa, G., Cacciatore, F., Bonaduce, D., & Abete, P. (2018). Sarcopenia: Assessment of disease burden and strategies to improve outcomes. In *Clinical Interventions in Aging* (Vol. 13, pp. 913–927). Dove Medical Press Ltd. https://doi.org/10.2147/CIA.S149232

Lo Scalzo, R., Testoni, A., & Genna, A. (2001). *`Annurca' apple fruit, a southern Italy apple cultivar: textural properties and aroma composition*. www.elsevier.com/locate/foodchem

López-fernández, O., Domínguez, R., Pateiro, M., Munekata, P. E. S., Rocchetti, G., & Lorenzo, J. M. (2020). Determination of polyphenols using liquid chromatography–tandem mass spectrometry technique (LC–MS/MS): A review. *Antioxidants*, *9*(6), 1–27. https://doi.org/10.3390/antiox9060479

López-Hortas, L., Pérez-Larrán, P., González-Muñoz, M. J., Falqué, E., & Domínguez, H. (2018). Recent developments on the extraction and application of ursolic acid. A review. In *Food Research International* (Vol. 103, pp. 130–149). Elsevier Ltd. https://doi.org/10.1016/j.foodres.2017.10.028

Lorito, M., Farkas, V., Rebuffat, S., Bodo, B., & Kubicek, C. P. (1996). Cell Wall Synthesis Is a Major Target of Mycoparasitic Antagonism by Trichoderma harzianum. In *JOURNAL OF BACTERIOLOGY* (Vol. 178, Issue 21).

Lötsch, J., & Geisslinger, G. (2011). Low-dose drug combinations along molecular pathways could maximize therapeutic effectiveness while minimizing collateral adverse effects. In *Drug Discovery Today* (Vol. 16, Issues 23–24, pp. 1001–1006). Elsevier Ltd. https://doi.org/10.1016/j.drudis.2011.10.003

Lu, S., Chen, S., Li, H., Paengkoum, S., Taethaisong, N., Meethip, W., Surakhunthod, J., Sinpru, B., Sroichak, T., Archa, P., Thongpea, S., & Paengkoum, P. (2022). Sustainable Valorization of Tomato Pomace (Lycopersicon esculentum) in Animal Nutrition: A Review. In *Animals* (Vol. 12, Issue 23). MDPI. https://doi.org/10.3390/ani12233294

Ludeña-Huaman, M. A., & Ramos-Inquiltupa, D. A. (2019). Determination of the content of ursolic and oleanolic acid in the cuticular wax of fruits of different species of rosaceae. *Revista Colombiana de Quimica*, *48*(2), 15–20. https://doi.org/10.15446/rev.colomb.quim.v48n2.77046

Luo, J., Si, H., Jia, Z., & Liu, D. (2021). Dietary anti-aging polyphenols and potential mechanisms. In *Antioxidants* (Vol. 10, Issue 2, pp. 1–20). MDPI. https://doi.org/10.3390/antiox10020283

Lyu, X., Lee, J., & Chen, W. N. (2019). Potential Natural Food Preservatives and Their Sustainable Production in Yeast: Terpenoids and Polyphenols. *Journal of Agricultural and Food Chemistry*, *67*(16), 4397–4417. https://doi.org/10.1021/acs.jafc.8b07141

Madia, V. N., De Vita, D., Ialongo, D., Tudino, V., De Leo, A., Scipione, L., Di Santo, R., Costi, R., & Messore, A. (2021). Recent advances in recovery of lycopene from tomato waste: A potent antioxidant with endless benefits. In *Molecules* (Vol. 26, Issue 15). MDPI AG. https://doi.org/10.3390/molecules26154495

Maes, K., Smolders, I., Michotte, Y., & Van Eeckhaut, A. (2014). Strategies to reduce aspecific adsorption of peptides and proteins in liquid chromatography-mass spectrometry based bioanalyses: An overview. In *Journal of Chromatography A* (Vol. 1358, pp. 1–13). Elsevier. https://doi.org/10.1016/j.chroma.2014.06.072

Maisto, M., Annunziata, G., Schiano, E., Piccolo, V., Iannuzzo, F., Santangelo, R., Ciampaglia, R., Tenore, G. C., Novellino, E., & Grieco, P. (2021). Potential Functional Snacks: Date Fruit Bars Supplemented by Different Species of Lactobacillus spp. *Foods*, *10*(8), 1760. https://doi.org/10.3390/foods10081760

Maisto, M., Piccolo, V., Novellino, E., Schiano, E., Iannuzzo, F., Ciampaglia, R., Summa, V., & Tenore, G. C. (2022). Optimization of Phlorizin Extraction from Annurca Apple Tree Leaves Using Response Surface Methodology. *Antioxidants*, *11*(10), 1933. https://doi.org/10.3390/antiox11101933

Maisto, M., Piccolo, V., Novellino, E., Schiano, E., Iannuzzo, F., Ciampaglia, R., Summa, V., & Tenore, G. C. (2023). Optimization of Ursolic Acid Extraction in Oil from Annurca Apple to Obtain Oleolytes with Potential Cosmeceutical Application. *Antioxidants*, *12*(2). https://doi.org/10.3390/antiox12020224

Maisto, M., Schiano, E., Novellino, E., Piccolo, V., Iannuzzo, F., Salviati, E., Summa, V., Annunziata, G., & Tenore, G. C. (2022). Application of a Rapid and Simple Technological Process to Increase Levels and Bioccessibility of Free Phenolic Compounds in Annurca Apple Nutraceutical Product. *Foods*, *11*(10). https://doi.org/10.3390/foods11101453

Manzo, N., Pizzolongo, F., Meca, G., Aiello, A., Marchetti, N., & Romano, R. (2018). Comparative chemical compositions of fresh and stored vesuvian PDO "Pomodorino del Piennolo" tomato and the ciliegino variety. *Molecules*, *23*(11). https://doi.org/10.3390/molecules23112871

Marcolongo, P., Gamberucci, A., Tamasi, G., Pardini, A., Bonechi, C., Rossi, C., Giunti, R., Barone, V., Borghini, A., Fiorenzani, P., Frosini, M., Valoti, M., & Pessina, F. (2020). Chemical characterisation and antihypertensive effects of locular gel and serum of Lycopersicum esculentum L. var. "Camone" tomato in spontaneously hypertensive rats. *Molecules*, *25*(16). https://doi.org/10.3390/molecules25163758

Martínez Bueno, M. J., Díaz-Galiano, F. J., Rajski, Ł., Cutillas, V., & Fernández-Alba, A. R. (2018). A non-targeted metabolomic approach to identify food markers to support discrimination between organic and conventional tomato crops. *Journal of Chromatography A*, *1546*, 66–76. https://doi.org/10.1016/j.chroma.2018.03.002

Martires, K. J., Fu, P., Polster, A. M., Cooper, K. D., & Baron, E. D. (2009). Factors That Affect Skin Aging A Cohort-Based Survey on Twins. In *Arch Dermatol* (Vol. 145, Issue 12). https://jamanetwork.com/

Masike, K., Mhlongo, M. I., Mudau, S. P., Nobela, O., Ncube, E. N., Tugizimana, F., George, M. J., & Madala, N. E. (2017). Highlighting mass spectrometric fragmentation differences and similarities between hydroxycinnamoyl-quinic acids and hydroxycinnamoyl-isocitric acids. *Chemistry Central Journal*, *11*(1), 1–7. https://doi.org/10.1186/s13065-017-0262-8

Matei, E., Râpă, M., Predescu, A. M., Țurcanu, A. A., Vidu, R., Predescu, C., Bobirica, C., Bobirica, L., & Orbeci, C. (2021). Valorization of agri-food wastes as sustainable eco-materials for wastewater treatment: Current state and new perspectives. In *Materials* (Vol. 14, Issue 16). MDPI AG. https://doi.org/10.3390/ma14164581

Mcgraphery, K. (2021). *Functional and Comparative Analysis of Small Molecule Glycosyltransferases from Plants by High-Throughput Assays*.

Medzhitov, R. (2008). Origin and physiological roles of inflammation. In *Nature* (Vol. 454, Issue 7203, pp. 428–435). Nature Publishing Group. https://doi.org/10.1038/nature07201

Miron, T. L., Plaza, M., Bahrim, G., Ibáñez, E., & Herrero, M. (2011). Chemical composition of bioactive pressurized extracts of Romanian aromatic plants. *Journal of Chromatography A*, *1218*(30), 4918–4927. https://doi.org/10.1016/j.chroma.2010.11.055

Mitchell, G., Lafrance, M., Boulanger, S., Séguin, D. L., Guay, I., Gattuso, M., Marsault, É., Bouarab, K., & Malouin, F. (2012). Tomatidine acts in synergy with aminoglycoside antibiotics against multiresistant Staphylococcus aureus and prevents virulence gene expression. *Journal of Antimicrobial Chemotherapy*, *67*(3), 559–568. https://doi.org/10.1093/jac/dkr510

Moco, S., Bino, R. J., Vorst, O., Verhoeven, H. A., De Groot, J., Van Beek, T. A., Vervoort, J., & Ric De Vos, C. H. (2006). A liquid chromatography-mass spectrometry-based metabolome database for tomato. *Plant Physiology*, *141*(4), 1205–1218. https://doi.org/10.1104/pp.106.078428

Monteiro, T., & Pinheiro, M. A. (2013). *Lycopersicon esculentum Miller: from by-products towards neuroprotection*.

Montero-Vargas, J. M., Casarrubias-Castillo, K., Martínez-Gallardo, N., Ordaz-Ortiz, J. J., Délano-Frier, J. P., & Winkler, R. (2018). Modulation of steroidal glycoalkaloid biosynthesis in tomato (Solanum lycopersicum) by jasmonic acid. *Plant Science*, *277*, 155–165. https://doi.org/10.1016/j.plantsci.2018.08.020

Moro, T., Ebert, S. M., Adams, C. M., & Rasmussen, B. B. (2016). Amino Acid Sensing in Skeletal Muscle. In *Trends in Endocrinology and Metabolism* (Vol. 27, Issue 11, pp. 796–806). Elsevier Inc. https://doi.org/10.1016/j.tem.2016.06.010

Mossad, O., Batut, B., Yilmaz, B., Dokalis, N., Mezö, C., Nent, E., Nabavi, L. S., Mayer, M., Maron, F. J. M., Buescher, J. M., de Agüero, M. G., Szalay, A., Lämmermann, T., Macpherson, A. J., Ganal-Vonarburg, S. C., Backofen, R., Erny, D., Prinz, M., &

Blank, T. (2022). Gut microbiota drives age-related oxidative stress and mitochondrial damage in microglia via the metabolite N 6-carboxymethyllysine. *Nature Neuroscience*, *25*(3), 295–305. https://doi.org/10.1038/s41593-022-01027-3

Murofushi, N., & Yamane, H. (1999). *The University of Tokyo , Japan*.

Muscaritoli, M., Anker, S. D., Argilés, J., Aversa, Z., Bauer, J. M., Biolo, G., Boirie, Y., Bosaeus, I., Cederholm, T., Costelli, P., Fearon, K. C., Laviano, A., Maggio, M., Fanelli, F. R., Schneider, S. M., Schols, A., & Sieber, C. C. (2010). Consensus definition of sarcopenia, cachexia and pre-cachexia: Joint document elaborated by Special Interest Groups (SIG) " cachexia-anorexia in chronic wasting diseases" and " nutrition in geriatrics." *Clinical Nutrition*, *29*(2), 154–159. https://doi.org/10.1016/j.clnu.2009.12.004

Nagana Gowda, G. A., & Raftery, D. (2021). NMR-Based Metabolomics. In *Advances in Experimental Medicine and Biology* (Vol. 1280, pp. 19–37). Springer. https://doi.org/10.1007/978-3-030-51652-9_2

Neimkhum, W., Anuchapreeda, S., Lin, W. C., Lue, S. C., Lee, K. H., & Chaiyana, W. (2021). Effects of carissa carandas linn. Fruit, pulp, leaf, and seed on oxidation, inflammation, tyrosinase, matrix metalloproteinase, elastase, and hyaluronidase inhibition. *Antioxidants*, *10*(9). https://doi.org/10.3390/antiox10091345

Nema, N. K., Maity, N., Sarkar, B. K., & Mukherjee, P. K. (2013). Matrix metalloproteinase, hyaluronidase and elastase inhibitory potential of standardized extract of Centella asiatica. *Pharmaceutical Biology*, *51*(9), 1182–1187. https://doi.org/10.3109/13880209.2013.782505

Nepal, B., & Stine, K. J. (2019). Glycoalkaloids: Structure, properties, and interactions with model membrane systems. In *Processes* (Vol. 7, Issue 8). MDPI. https://doi.org/10.3390/PR7080513

Neri, I., Laneri, S., Di Lorenzo, R., Dini, I., Russo, G., & Grumetto, L. (2022). Parabens Permeation through Biological Membranes: A Comparative Study Using Franz Cell Diffusion System and Biomimetic Liquid Chromatography. *Molecules*, *27*(13). https://doi.org/10.3390/molecules27134263

Ngo, T. H., Park, J., Jo, Y. D., Jin, C. H., Jung, C. H., Nam, B., Han, A. R., & Nam, J. W. (2022). Content of Two Major Steroidal Glycoalkaloids in Tomato (Solanum lycopersicum cv. Micro-Tom) Mutant Lines at Different Ripening Stages. *Plants*, *11*(21). https://doi.org/10.3390/plants11212895

Nguyen, N. T., & Fisher, D. E. (2019). MITF and UV responses in skin: From pigmentation to addiction. In *Pigment Cell and Melanoma Research* (Vol. 32, Issue 2, pp. 224–236). Blackwell Publishing Ltd. https://doi.org/10.1111/pcmr.12726

Nirmala, F. S., Lee, H., Kim, J. S., Ha, T., Jung, C. H., & Ahn, J. (2020). Green tomato extract prevents bone loss in ovariectomized rats, a model of osteoporosis. *Nutrients*, *12*(10), 1–13. https://doi.org/10.3390/nu12103210

Olukoga, A., & Donaldson, D. (2000). Liquorice and its health implications. In *Journal of The Royal Society for the Promotion of Health* (Vol. 120, Issue 2, pp. 83–89). Royal Society for the Promotion of Health. https://doi.org/10.1177/146642400012000203

P. A. Silva, Y., Borba, B. C., Pereira, V. A., Reis, M. G., Caliari, M., Brooks, M. S. L., & Ferreira, T. A. P. C. (2019). Characterization of tomato processing by-product for use as a potential functional food ingredient: nutritional composition, antioxidant activity and bioactive compounds. *International Journal of Food Sciences and Nutrition*, *70*(2), 150–160. https://doi.org/10.1080/09637486.2018.1489530

Pan, Z., Li, Y., Deng, X., & Xiao, S. (2014). Non-targeted metabolomic analysis of orange (Citrus sinensis [L.] Osbeck) wild type and bud mutant fruits by direct analysis in real-time and HPLC-electrospray mass spectrometry. *Metabolomics*, *10*(3), 508–523. https://doi.org/10.1007/s11306-013-0597-7

Panzella, L., & Napolitano, A. (2019). Natural and bioinspired phenolic compounds as tyrosinase inhibitors for the treatment of skin hyperpigmentation: Recent advances. In *Cosmetics* (Vol. 6, Issue 4). MDPI AG. https://doi.org/10.3390/cosmetics6040057

Pardini, A., Consumi, M., Leone, G., Bonechi, C., Tamasi, G., Sangiorgio, P., Verardi, A., Rossi, C., & Magnani, A. (2021). Effect of different post-harvest storage conditions and heat treatment on tomatine content in commercial varieties of green tomatoes. *Journal of Food Composition and Analysis*, *96*. https://doi.org/10.1016/j.jfca.2020.103735

Park, J. U., Yang, S. Y., Guo, R. H., Li, H. X., Kim, Y. H., & Kim, Y. R. (2020). Anti-Melanogenic Effect of Dendropanax morbiferus and Its Active Components via Protein Kinase A/Cyclic Adenosine Monophosphate-Responsive Binding Protein- and p38 Mitogen-Activated Protein Kinase-Mediated Microphthalmia−Associated Transcription Factor Downregulation. *Frontiers in Pharmacology*, *11*. https://doi.org/10.3389/fphar.2020.00507

Patel, A. H., Sharma, H. P., & Vaishali. (2023). Physiological functions, pharmacological aspects and nutritional importance of green tomato- a future food. In *Critical Reviews in Food Science and Nutrition*. Taylor and Francis Ltd. https://doi.org/10.1080/10408398.2023.2212766

Patocka, J., & Patočka, J. (2003). Biologically active pentacyclic triterpenes and their current medicine signification. *Journal of Applied Biomedicine*, *1*(1), 7–12. https://www.researchgate.net/publication/26596773

Periago, M. J., Garcia-Alonso, J., Jacob, K., Olivares, A. B., Bernal, M. J., Iniesta, M. D., Martinez, C., & Ros, G. (2008). Bioactive compounds, folates and antioxidant properties of tomatoes (Lycopersicum esculentum) during vine ripening. *International Journal of Food Sciences and Nutrition*, 1–15. https://doi.org/10.1080/09637480701833457

Periago, M. J., Martínez-Valverde, I., Chesson, A., & Provan, G. (2002). Phenolic compounds, lycopene and antioxidant activity in commercial varieties of tomato (Lycopersicum esculentum). *Journal of the Science of Food and Agriculture*, *82*(3), 323–330. https://doi.org/10.1002/jsfa.1035

Perry, B. D., Caldow, M. K., Brennan-Speranza, T. C., Sbaraglia, M., Jerums, G., Garnham, A., Wong, C., Levinger, P., Asrar Ul Haq, M., Hare, D. L., Price, S. R., & Levinger, I. (2016). Muscle atrophy in patients with Type 2 Diabetes Mellitus: roles of inflammatory pathways, physical activity and exercise HHS Public Access. In *Exerc Immunol Rev* (Vol. 22).

Platzer, M., Kiese, S., Herfellner, T., Schweiggert-Weisz, U., & Eisner, P. (2021). How does the phenol structure influence the results of the folin-ciocalteu assay? *Antioxidants*, *10*(5). https://doi.org/10.3390/antiox10050811

Plotkin, D. L., Roberts, M. D., Haun, C. T., & Schoenfeld, B. J. (2021). Muscle fiber type transitions with exercise training: Shifting perspectives. In *Sports* (Vol. 9, Issue 9). MDPI. https://doi.org/10.3390/SPORTS9090127

Poprawski, T. J., Greenberg, S. M., & Ciomperlik, M. A. (2000). Effect of host plant on Beauveria bassiana- and Paecilomyces fumosoroseus-induced mortality of Trialeurodes vaporariorum (Homoptera: Aleyrodidae). *Environmental Entomology*, *29*(5), 1048–1053. https://doi.org/10.1603/0046-225X-29.5.1048

Prior, R. L., Wu, X., & Schaich, K. (2005). Standardized methods for the determination of antioxidant capacity and phenolics in foods and dietary supplements. In *Journal of Agricultural and Food Chemistry* (Vol. 53, Issue 10, pp. 4290–4302). https://doi.org/10.1021/jf0502698

Punathil Kannan, P. K., & Ambale Gundappa, G. K. (2014). Impact of different deacidifcation methods on quality characteristics and composition of olein and stearin in crude red palm oil. *Journal of Oleo Science*, *63*(12), 1209–1221. https://doi.org/10.5650/jos.ess14060

Quinet, M., Angosto, T., Yuste-Lisbona, F. J., Blanchard-Gros, R., Bigot, S., Martinez, J. P., & Lutts, S. (2019). Tomato Fruit Development and Metabolism. In *Frontiers in Plant Science* (Vol. 10). Frontiers Media S.A. https://doi.org/10.3389/fpls.2019.01554

R´o˙, M., Zanowska, R., Sarna, T., Land, E. J., & George Truscott, T. (1999). *Original Contribution FREE RADICAL SCAVENGING PROPERTIES OF MELANIN INTERACTION OF EU-AND PHEO-MELANIN MODELS WITH REDUCING AND OXIDISING RADICALS*.

Rahimi, S., Kim, J., Mijakovic, I., Jung, K. H., Choi, G., Kim, S. C., & Kim, Y. J. (2019). Triterpenoid-biosynthetic UDP-glycosyltransferases from plants. In *Biotechnology Advances* (Vol. 37, Issue 7). Elsevier Inc. https://doi.org/10.1016/j.biotechadv.2019.04.016

Rejczak, T., & Tuzimski, T. (2017). QuEChERS-based extraction with dispersive solid phase extraction clean-up using PSA and ZrO2-based sorbents for determination of pesticides in bovine milk samples by HPLC-DAD. *Food Chemistry*, *217*, 225–233. https://doi.org/10.1016/j.foodchem.2016.08.095

Ribas-Agustí, A., Cáceres, R., Gratacós-Cubarsí, M., Sárraga, C., & Castellari, M. (2012). A Validated HPLC-DAD Method for Routine Determination of Ten Phenolic Compounds in Tomato Fruits. *Food Analytical Methods*, *5*(5), 1137–1144. https://doi.org/10.1007/s12161-011-9355-5

Rick, C. M., Uhligt, J. W., & Jones, A. D. (1994). *High a-tomatine content in ripe fruit of Andean Lycopersicon esculentum var. cerasiforme: Developmental and genetic aspects* (Vol. 91).

Ripperger, H. (1996). STEROIDAL ALKALOIDS FROM ROOTS OF SOLANUM SPIRALE*. In *Phytochemistry* (Vol. 43, Issue 3).

Rockenbach, I. I., Jungfer, E., Ritter, C., Santiago-Schübel, B., Thiele, B., Fett, R., & Galensa, R. (2012). Characterization of flavan-3-ols in seeds of grape pomace by CE, HPLC-DAD-MS n and LC-ESI-FTICR-MS. *Food Research International*, *48*(2), 848–855. https://doi.org/10.1016/j.foodres.2012.07.001

Roddick, J. G. (1989). *THE ACETYLCHOLINESTERASE-INHIBITORY ACTIVITY OF STEROIDAL GLYCOALKALOIDS AND THEIR AGLYCONES* (Vol. 28, Issue 10).

Rosenberg, I. H. (n.d.). *Symposium: Sarcopenia: Diagnosis and Mechanisms Sarcopenia: Origins and Clinical Relevance 1*. https://academic.oup.com/jn/article-abstract/127/5/990S/4724144

Rubio-Ruiz, M. E., Guarner-Lans, V., Pérez-Torres, I., & Soto, M. E. (2019). Mechanisms underlying metabolic syndrome-related sarcopenia and possible therapeutic measures. In *International Journal of Molecular Sciences* (Vol. 20, Issue 3). MDPI AG. https://doi.org/10.3390/ijms20030647

Rue, E. A., Rush, M. D., & van Breemen, R. B. (2018). Procyanidins: a comprehensive review encompassing structure elucidation via mass spectrometry. *Phytochemistry Reviews*, *17*(1), 1–16. https://doi.org/10.1007/s11101-017-9507-3

Salas-Marina, M. A., Silva-Flores, M. A., Uresti-Rivera, E. E., Castro-Longoria, E., Herrera-Estrella, A., & Casas-Flores, S. (2011). Colonization of Arabidopsis roots by Trichoderma atroviride promotes growth and enhances systemic disease resistance through jasmonic acid/ethylene and salicylic acid pathways. *European Journal of Plant Pathology*, *131*(1), 15–26. https://doi.org/10.1007/s10658-011-9782-6

Šamec, D., Karalija, E., Šola, I., Vujčić Bok, V., & Salopek-Sondi, B. (2021). The role of polyphenols in abiotic stress response: The influence of molecular structure. In *Plants* (Vol. 10, Issue 1, pp. 1–24). MDPI AG. https://doi.org/10.3390/plants10010118

Sandrock, R. W., Vanetten, H. D., & Sandrock, W. (1998). *Biochemistry and Cell Biology Fungal Sensitivity to and Enzymatic Degradation of the Phytoanticipin α-Tomatine* (Vol. 88, Issue 2).

Santini, A., Cammarata, S. M., Capone, G., Ianaro, A., Tenore, G. C., Pani, L., & Novellino, E. (2018). Nutraceuticals: opening the debate for a regulatory framework. In *British Journal of Clinical Pharmacology* (Vol. 84, Issue 4, pp. 659–672). Blackwell Publishing Ltd. https://doi.org/10.1111/bcp.13496

Santini, A., & Novellino, E. (2013). *Send Orders for Reprints to reprints@benthamscience.ae Expert's Opinion Nutraceuticals: Beyond the Diet Before the Drugs*. http://www.fda.gov.

Saviano, A., Raucci, F., Casillo, G. M., Mansour, A. A., Piccolo, V., Montesano, C., Smimmo, M., Vellecco, V., Capasso, G., Boscaino, A., Summa, V., Mascolo, N., Iqbal, A. J., Sorrentino, R., d'Emmanuele di Villa Bianca, R., Bucci, M., Brancaleone, V., & Maione, F. (2022). Anti-inflammatory and immunomodulatory activity of Mangifera indica L. reveals the modulation of COX-2/mPGES-1 axis and Th17/Treg ratio. *Pharmacological Research*, *182*. https://doi.org/10.1016/j.phrs.2022.106283

Scalabrin, M., Adams, V., Labeit, S., & Bowen, T. S. (2020). Emerging strategies targeting catabolic muscle stress relief. In *International Journal of Molecular Sciences* (Vol. 21, Issue 13, pp. 1–18). MDPI AG. https://doi.org/10.3390/ijms21134681

Schiaffino, S., & Mammucari, C. (2011). Regulation of skeletal muscle growth by the IGF1-Akt/PKB pathway: Insights from genetic models. In *Skeletal Muscle* (Vol. 1, Issue 1). https://doi.org/10.1186/2044-5040-1-4

Schiano, E., Piccolo, V., Novellino, E., Maisto, M., Iannuzzo, F., Summa, V., & Tenore, G. C. (2022a). Thinned Nectarines, an Agro-Food Waste with Antidiabetic Potential: HPLC-HESI-MS/MS Phenolic Characterization and In Vitro Evaluation of Their Beneficial Activities. *Foods*, *11*(7). https://doi.org/10.3390/foods11071010

Schiano, E., Piccolo, V., Novellino, E., Maisto, M., Iannuzzo, F., Summa, V., & Tenore, G. C. (2022b). Thinned Nectarines, an Agro-Food Waste with Antidiabetic Potential: HPLC-HESI-MS/MS Phenolic Characterization and In Vitro Evaluation of Their Beneficial Activities. *Foods*, *11*(7).

Schrenk, D., Bignami, M., Bodin, L., Chipman, J. K., del Mazo, J., Hogstrand, C., Hoogenboom, L., Leblanc, J. C., Nebbia, C. S., Nielsen, E., Ntzani, E., Petersen, A., Sand, S., Schwerdtle, T., Vleminckx, C., Wallace, H., Brimer, L., Cottrill, B., Dusemund, B., … Grasl-Kraupp, B. (2020). Risk assessment of glycoalkaloids in feed and food, in particular in potatoes and potato-derived products. *EFSA Journal*, *18*(8). https://doi.org/10.2903/j.efsa.2020.6222

Seo, D. Y., Lee, S. R., Heo, J. W., No, M. H., Rhee, B. D., Ko, K. S., Kwak, H. B., & Han, J. (2018). Ursolic acid in health and disease. In *Korean Journal of Physiology and Pharmacology* (Vol. 22, Issue 3, pp. 235–248). Korean Physiological Soc. and Korean Soc. of Pharmacology. https://doi.org/10.4196/kjpp.2018.22.3.235

Shao, Y., Xu, F., Sun, X., Bao, J., & Beta, T. (2014). Phenolic acids, anthocyanins, and antioxidant capacity in rice (oryza sativa l.) grains at four stages of development after flowering. *Food Chemistry*, *143*, 90–96. https://doi.org/10.1016/j.foodchem.2013.07.042

Sheng, F., Hu, B., Jin, Q., Wang, J., Wu, C., & Luo, Z. (2021). The analysis of phenolic compounds in walnut husk and pellicle by uplc-q-orbitrap hrms and hplc. *Molecules*, *26*(10). https://doi.org/10.3390/molecules26103013

Sheng, H., & Sun, H. (2011). Synthesis, biology and clinical significance of pentacyclic triterpenes: A multi-target approach to prevention and treatment of metabolic and vascular diseases. In *Natural Product Reports* (Vol. 28, Issue 3, pp. 543–593). https://doi.org/10.1039/c0np00059k

Shih, Y. W., Shieh, J. M., Wu, P. F., Lee, Y. C., Chen, Y. Z., & Chiang, T. A. (2009). α-Tomatine inactivates PI3K/Akt and ERK signaling pathways in human lung adenocarcinoma A549 cells: Effect on metastasis. *Food and Chemical Toxicology*, *47*(8), 1985–1995. https://doi.org/10.1016/j.fct.2009.05.011

Shinde, B. A., Dholakia, B. B., Hussain, K., Panda, S., Meir, S., Rogachev, I., Aharoni, A., Giri, A. P., & Kamble, A. C. (2017). Dynamic metabolic reprogramming of steroidal

glycol-alkaloid and phenylpropanoid biosynthesis may impart early blight resistance in wild tomato (Solanum arcanum Peralta). *Plant Molecular Biology*, *95*(4–5), 411–423. https://doi.org/10.1007/s11103-017-0660-2

Silva-Beltrán, N. P., Ruiz-Cruz, S., Cira-Chávez, L. A., Estrada-Alvarado, M. I., Ornelas-Paz, J. D. J., López-Mata, M. A., Del-Toro-Sánchez, C. L., Ayala-Zavala, J. F., & Márquez-Ríos, E. (2015). Total Phenolic, Flavonoid, Tomatine, and Tomatidine Contents and Antioxidant and Antimicrobial Activities of Extracts of Tomato Plant. *International Journal of Analytical Chemistry*, *2015*. https://doi.org/10.1155/2015/284071

Sinosaki, N. B. M., Tonin, A. P. P., Ribeiro, M. A. S., Poliseli, C. B., Roberto, S. B., da Silveira, R., Visentainer, J. V., Santos, O. O., & Meurer, E. C. (2020). Structural study of phenolic acids by triple quadrupole mass spectrometry with electrospray ionization in negative mode and H/D isotopic exchange. *Journal of the Brazilian Chemical Society*, *31*(2), 402–408. https://doi.org/10.21577/0103-5053.20190197

Sirtori, C. R. (2001). Aescin: Pharmacology, pharmacokinetics and therapeutic profile. *Pharmacological Research*, *44*(3), 183–193. https://doi.org/10.1006/phrs.2001.0847

Slimestad, R., & Verheul, M. (2009). *Review of flavonoids and other phenolics from fruits of different tomato (Lycopersicon esculentum Mill .) cultivars Rune Slimestad a ∗ and Michel Verheul b*. *January*, 1255–1270. https://doi.org/10.1002/jsfa.3605

Soytong, K., Kanokmedhakul, S., Rattanacherdchai, K., & Charoenporn, C. (2014). Microbial elicitors to induce immunity for plant disease control in chilli and tomato. In *Basic and Applied Aspects of Biopesticides* (Vol. 9788132218777, pp. 99–125). Springer India. https://doi.org/10.1007/978-81-322-1877-7_6

Spínola, V., Pinto, J., & Castilho, P. C. (2015). *Identification and quantification of phenolic compounds of selected fruits from Madeira Island by HPLC-DAD – ESI-MS n and screening for their antioxidant activity*. *173*, 14–30. https://doi.org/10.1016/j.foodchem.2014.09.163

Steuer, R. (2006). Review: On the analysis and interpretation of correlations in metabolomic data. In *Briefings in Bioinformatics* (Vol. 7, Issue 2, pp. 151–158). https://doi.org/10.1093/bib/bbl009

Sueiro, R. A., Leiro, J. M., Blanco-Abad, V., Raaijmakers, J., de Bruijn, I., Dirks, R. P. H., & Lamas, J. (2022). Plant-and Bacteria-Derived Compounds with Anti-Philasterides dicentrarchi Activity. *Pathogens*, *11*(2). https://doi.org/10.3390/pathogens11020267

Surjadinata, B. B., Jacobo-Velázquez, D. A., & Cisneros-Zevallos, L. (2021). Physiological role of reactive oxygen species, ethylene, and jasmonic acid on UV light induced phenolic biosynthesis in wounded carrot tissue. *Postharvest Biology and Technology*, *172*. https://doi.org/10.1016/j.postharvbio.2020.111388

Sut, S., Zengin, G., Maggi, F., Malagoli, M., & Dall'Acqua, S. (2019). Triterpene acid and phenolics from ancient apples of Friuli Venezia Giulia as nutraceutical ingredients: LC-MS study and in vitro activities. *Molecules*, *24*(6). https://doi.org/10.3390/molecules24061109

Tam, C. C., Nguyen, K., Nguyen, D., Hamada, S., Kwon, O., Kuang, I., Gong, S., Escobar, S., Liu, M., Kim, J., Hou, T., Tam, J., Cheng, L. W., Kim, J. H., Land, K. M., & Friedman, M. (2021). Antimicrobial properties of tomato leaves, stems, and fruit and their relationship to chemical composition. *BMC Complementary Medicine and Therapies*, *21*(1). https://doi.org/10.1186/s12906-021-03391-2

Tamasi, G., Pardini, A., Croce, R., Consumi, M., Leone, G., Bonechi, C., Rossi, C., & Magnani, A. (2021). Combined experimental and multivariate model approaches for glycoalkaloid quantification in tomatoes. *Molecules*, *26*(11). https://doi.org/10.3390/molecules26113068

Tanksley, S. D. (2004). The genetic, developmental, and molecular bases of fruit size and shape variation in tomato. In *Plant Cell* (Vol. 16, Issue SUPPL.). American Society of Plant Biologists. https://doi.org/10.1105/tpc.018119

Tavarini, S., De Leo, M., Matteo, R., Lazzeri, L., Braca, A., & Angelini, L. G. (2021). Flaxseed and camelina meals as potential sources of health-beneficial compounds. *Plants*, *10*(1), 1–17. https://doi.org/10.3390/plants10010156

Taveira, M., Ferreres, F., Gil-Izquierdo, A., Oliveira, L., Valentão, P., & Andrade, P. B. (2012). Fast determination of bioactive compounds from Lycopersicon esculentum Mill. leaves. *Food Chemistry*, *135*(2), 748–755. https://doi.org/10.1016/j.foodchem.2012.05.016

Tenore, G. C., Calabrese, G., Stiuso, P., Ritieni, A., Giannetti, D., & Novellino, E. (2014). Effects of Annurca apple polyphenols on lipid metabolism in HepG2 cell lines: A source of nutraceuticals potentially indicated for the metabolic syndrome. *Food Research International*, *63*, 252–257. https://doi.org/10.1016/j.foodres.2014.05.024

Tenore, G. C., Campiglia, P., Ritieni, A., & Novellino, E. (2013). In vitro bioaccessibility, bioavailability and plasma protein interaction of polyphenols from Annurca apple (M. pumila Miller cv Annurca). *Food Chemistry*, *141*(4), 3519–3524. https://doi.org/10.1016/j.foodchem.2013.06.051

Tenore, G. C., Campiglia, P., Stiuso, P., Ritieni, A., & Novellino, E. (2013). Nutraceutical potential of polyphenolic fractions from Annurca apple (M. pumila Miller cv Annurca). *Food Chemistry*, *140*(4), 614–622. https://doi.org/10.1016/j.foodchem.2012.10.112

Tenore, G. C., Carotenuto, A., Caruso, D., Buonomo, G., D'Avino, M., Brancaccio, D., Ciampaglia, R., Maisto, M., Schisano, C., & Novellino, E. (2018). A nutraceutical formulation based on Annurca apple polyphenolic extract is effective on intestinal cholesterol absorption: A randomised, placebo-controlled, crossover study. *PharmaNutrition*, *6*(3), 85–94. https://doi.org/10.1016/j.phanu.2018.05.001

Tholl, D. (2006). Terpene synthases and the regulation, diversity and biological roles of terpene metabolism. In *Current Opinion in Plant Biology* (Vol. 9, Issue 3, pp. 297–304). https://doi.org/10.1016/j.pbi.2006.03.014

Thong, H. Y., Zhai, H., & Maibach, H. I. (2007). Percutaneous penetration enhancers: An overview. In *Skin Pharmacology and Physiology* (Vol. 20, Issue 6, pp. 272–282). https://doi.org/10.1159/000107575

Urabe, K., Aroca, P., Tsukamoto, K., Mascagna, D., Palumbo, A., Prota, G., & Hearing, V. J. (1994). Biochi ~mi c~a et Biophysica A~ta The inherent cytotoxicity of melanin precursors: a revision. In *Biochimica et Biophysica Acta* (Vol. 1221).

Vaananen, T., Kuronen, P., & Pehu, E. (2000). Comparison of commercial solid-phase extraction sorbents for the sample preparation of potato glycoalkaloids. In *Journal of Chromatography A* (Vol. 869). www.elsevier.com/locate/chroma

Vallverdú-Queralt, A., Jáuregui, O., Di Lecce, G., Andrés-Lacueva, C., & Lamuela-Raventós, R. M. (2011). Screening of the polyphenol content of tomato-based products

through accurate-mass spectrometry (HPLC-ESI-QTOF). *Food Chemistry*, *129*(3), 877–883. https://doi.org/10.1016/j.foodchem.2011.05.038

Vallverdú-Queralt, A., Jáuregui, O., Medina-Remón, A., & Lamuela-Raventós, R. M. (2012). Evaluation of a method to characterize the phenolic profile of organic and conventional tomatoes. *Journal of Agricultural and Food Chemistry*, *60*(13), 3373–3380. https://doi.org/10.1021/jf204702f

Velderrain-Rodríguez, G. R., Quero, J., Osada, J., Martín-Belloso, O., & Rodríguez-Yoldi, M. J. (2021). Phenolic-rich extracts from avocado fruit residues as functional food ingredients with antioxidant and antiproliferative properties. *Biomolecules*, *11*(7). https://doi.org/10.3390/biom11070977

Vergara-Salinas, J. R., Pérez-Jiménez, J., Torres, J. L., Agosin, E., & Pérez-Correa, J. R. (2012). Effects of temperature and time on polyphenolic content and antioxidant activity in the pressurized hot water extraction of deodorized thyme (Thymus vulgaris). *Journal of Agricultural and Food Chemistry*, *60*(44), 10920–10929. https://doi.org/10.1021/jf3027759

Verma, H. V. (2011). Skin 'fairness'-culturally embedded meaning and branding implications. *Global Business Review*, *12*(2), 193–211. https://doi.org/10.1177/097215091101200202

Vetal, M. D., Lade, V. G., & Rathod, V. K. (2013). Extraction of ursolic acid from Ocimum sanctum by ultrasound: Process intensification and kinetic studies. *Chemical Engineering and Processing: Process Intensification*, *69*, 24–30. https://doi.org/10.1016/j.cep.2013.01.011

Viškelis, J., Uselis, N., Liaudanskas, M., Lanauskas, J., Bielicki, P., Univer, T., Lepsis, J., & Kviklys, D. (2019). *Location effects across northeastern Europe on bioactive compounds in apple fruit* (Vol. 28).

Wang, M., Zhao, T., Liu, Y., Wang, Q., Xing, S., Li, L., Wang, L., Liu, L., & Gao, D. (2017). Ursolic acid liposomes with chitosan modification: Promising antitumor drug delivery and efficacy. In *Materials Science and Engineering C* (Vol. 71, pp. 1231–1240). Elsevier Ltd. https://doi.org/10.1016/j.msec.2016.11.014

Wang, P. (2021). *Natural and Synthetic Saponins as Vaccine Adjuvants*. https://doi.org/10.3390/vaccines

Werneck-De-Castro, J. P., Fonseca, T. L., Ignacio, D. L., Fernandes, G. W., Andrade-Feraud, C. M., Lartey, L. J., Ribeiro, M. B., Ribeiro, M. O., Gereben, B., & Bianco, A. C. (2015). Thyroid hormone signaling in male mouse skeletal muscle is largely independent of D2 in myocytes. *Endocrinology*, *156*(10), 3842–3852. https://doi.org/10.1210/en.2015-1246

Wilson, R. H., Poley, G. W., Deeds, F., & Fontaine, T. D. (1961). Some Pharmacologic and Toxicologic Properties of Tomatine and Its Derivatives. In *TOXICOLOGY AND APPLIED PHARMACOLOGY* (Vol. 3).

Wolfender, J. L. (2009). HPLC in natural product analysis: The detection issue. In *Planta Medica* (Vol. 75, Issue 7, pp. 719–734). https://doi.org/10.1055/s-0028-1088393

Woo, S. L., Hermosa, R., Lorito, M., & Monte, E. (2023). Trichoderma: a multipurpose, plant-beneficial microorganism for eco-sustainable agriculture. In *Nature Reviews Microbiology* (Vol. 21, Issue 5, pp. 312–326). Nature Research. https://doi.org/10.1038/s41579-022-00819-5

Xu, C., Liao, Y., Fang, C., Tsunoda, M., Zhang, Y., Song, Y., & Deng, S. (2017). Simultaneous Analysis of Ursolic Acid and Oleanolic Acid in Guava Leaves Using QuEChERS-Based Extraction Followed by High-Performance Liquid Chromatography. *Journal of Analytical Methods in Chemistry*, *2017*. https://doi.org/10.1155/2017/2984562

Xu, F., & Tian, Y. (2009). *Quasi-MSidentification of flavanone 7-glycoside isomers in Da Chengqi Tang by high performance liquid chromatography-tandem mass spectrometry*. *May 2014*. https://doi.org/10.1186/1749-8546-4-15

Yamaguchi, H., Noshita, T., Kidachi, Y., Umetsu, H., Hayashi, M., Komiyama, K., Funayama, S., & Ryoyama, K. (2008). Isolation of Ursolic Acid from Apple Peels and Its Specific Efficacy as a Potent Antitumor Agent. In *Journal of Health Science* (Vol. 54, Issue 6).

Yamashoji, S., & Onoda, E. (2016). Detoxification and function of immature tomato. *Food Chemistry*, *209*, 171–176. https://doi.org/10.1016/j.foodchem.2016.04.042

Yang, Z., Zhang, Y., Sun, L., Wang, Y., Gao, X., & Cheng, Y. (2012). An ultrafiltration high-performance liquid chromatography coupled with diode array detector and mass spectrometry approach for screening and characterising tyrosinase inhibitors from mulberry leaves. *Analytica Chimica Acta*, *719*, 87–95. https://doi.org/10.1016/j.aca.2012.01.018

Ying, Q.-L., Rinehart, A. R., Simon, S. R., & Cheronist, J. C. (1991). Inhibition of human leucocyte elastase by ursolic acid Evidence for a binding site for pentacyclic triterpenes. In *Biochem. J* (Vol. 277).

Yoon, M. S. (2017). mTOR as a key regulator in maintaining skeletal muscle mass. In *Frontiers in Physiology* (Vol. 8, Issue OCT). Frontiers Media S.A. https://doi.org/10.3389/fphys.2017.00788

Zammit, P. S., Relaix, F., Nagata, Y., Ruiz, A. P., Collins, C. A., Partridge, T. A., & Beauchamp, J. R. (2006). Pax7 and myogenic progression in skeletal muscle satellite cells. *Journal of Cell Science*, *119*(9), 1824–1832. https://doi.org/10.1242/jcs.02908

Zhang, J., Sasaki, T., Li, W., Nagata, K., Higai, K., Feng, F., Wang, J., Cheng, M., & Koike, K. (2018). Identification of caffeoylquinic acid derivatives as natural protein tyrosine phosphatase 1B inhibitors from Artemisia princeps. *Bioorganic and Medicinal Chemistry Letters*, *28*(7), 1194–1197. https://doi.org/10.1016/j.bmcl.2018.02.052

Zhang, L., Shang, Q., Chen, C., Tang, W., Xu, Y., & Liu, W. (2021). Synchronous fluorometric method for continuous assay of monophenolase activity. *Spectrochimica Acta - Part A: Molecular and Biomolecular Spectroscopy*, *252*. https://doi.org/10.1016/j.saa.2021.119486

Zhang, T., Su, J., Wang, K., Zhu, T., & Li, X. (2014). Ursolic acid reduces oxidative stress to alleviate early brain injury following experimental subarachnoid hemorrhage. *Neuroscience Letters*, *579*, 12–17. https://doi.org/10.1016/j.neulet.2014.07.005

Zhang, Y., Xiong, H., Xu, X., Xue, X., Liu, M., Xu, S., Liu, H., Gao, Y., Zhang, H., & Li, X. (2018). Compounds identification in semen cuscutae by ultra-high-performance liquid chromatography (uplcs) coupled to electrospray ionization mass spectrometry. *Molecules*, *23*(5). https://doi.org/10.3390/molecules23051199

Zhao, B., Zhou, B., Bao, L., Yang, Y., & Guo, K. (2015). Alpha-Tomatine Exhibits Anti-inflammatory Activity in Lipopolysaccharide-Activated Macrophages. *Inflammation*, *38*(5), 1769–1776. https://doi.org/10.1007/s10753-015-0154-9

Zhao, D. K., Zhao, Y., Chen, S. Y., & Kennelly, E. J. (2021). Solanum steroidal glycoalkaloids: Structural diversity, biological activities, and biosynthesis. In *Natural Product Reports* (Vol. 38, Issue 8, pp. 1423–1444). Royal Society of Chemistry. https://doi.org/10.1039/d1np00001b

Zillich, O. V., Schweiggert-Weisz, U., Eisner, P., & Kerscher, M. (2015). Polyphenols as active ingredients for cosmetic products. In *International Journal of Cosmetic Science* (Vol. 37, Issue 5, pp. 455–464). https://doi.org/10.1111/ics.12218

Zin, N. A., & Badaluddin, N. A. (2020). Biological functions of Trichoderma spp. for agriculture applications. In *Annals of Agricultural Sciences* (Vol. 65, Issue 2, pp. 168–178). Faculty of Agriculture, Ain-Shams University. https://doi.org/10.1016/j.aoas.2020.09.003

Zou, D., Wang, J., Zhang, B., Xie, S., Wang, Q., Xu, K., Lin, R., & Lam, C. W. K. (2015). Analysis of chemical constituents in Wuzi-Yanzong-Wan by UPLC-ESI-LTQ-Orbitrap-MS. *Molecules*, *20*(12), 21373–21404. https://doi.org/10.3390/molecules201219765